frontiers | Research Topics

IPPS - plant phenotyping for a sustainable future

2022

Edited by
Ulrich Schurr, Elias Kaiser, Jennifer Clarke and Philipp Von Gillhaussen

Published in
Frontiers in Plant Science

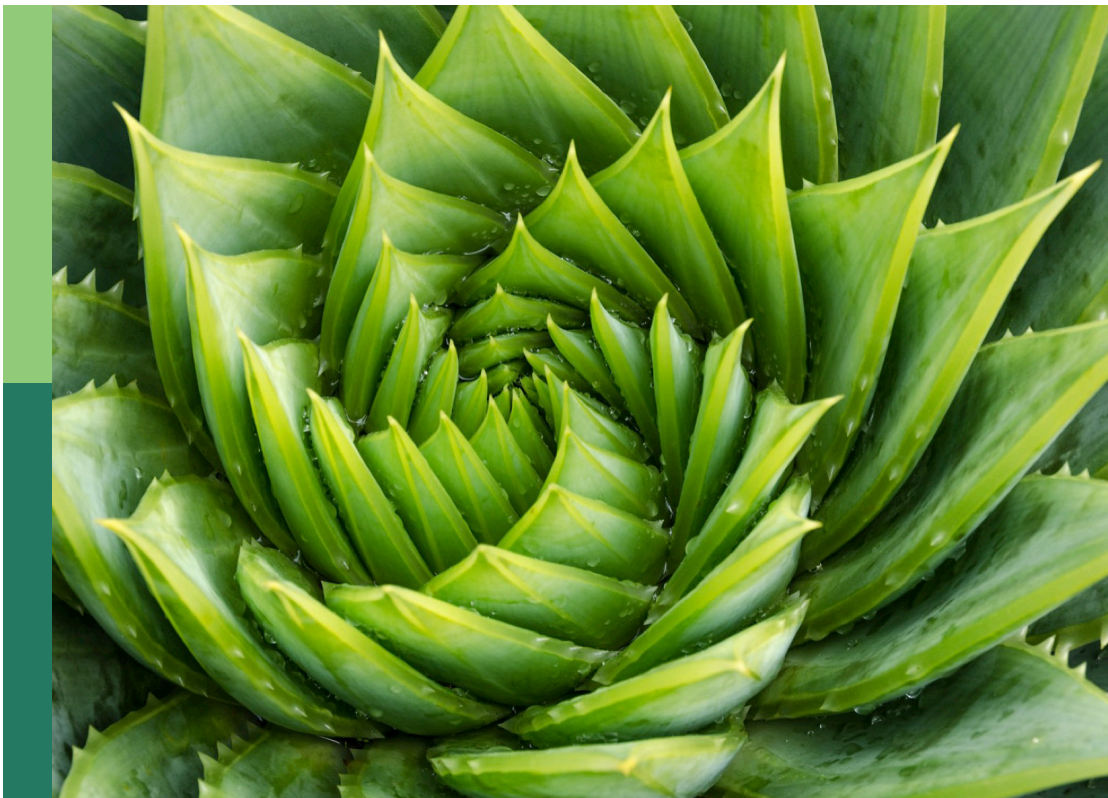

ISSN 1664-8714
ISBN 978-2-8325-4567-6
DOI 10.3389/978-2-8325-4567-6

About Frontiers

Frontiers is more than just an open access publisher of scholarly articles: it is a pioneering approach to the world of academia, radically improving the way scholarly research is managed. The grand vision of Frontiers is a world where all people have an equal opportunity to seek, share and generate knowledge. Frontiers provides immediate and permanent online open access to all its publications, but this alone is not enough to realize our grand goals.

Frontiers journal series

The Frontiers journal series is a multi-tier and interdisciplinary set of open-access, online journals, promising a paradigm shift from the current review, selection and dissemination processes in academic publishing. All Frontiers journals are driven by researchers for researchers; therefore, they constitute a service to the scholarly community. At the same time, the *Frontiers journal series* operates on a revolutionary invention, the tiered publishing system, initially addressing specific communities of scholars, and gradually climbing up to broader public understanding, thus serving the interests of the lay society, too.

Dedication to quality

Each Frontiers article is a landmark of the highest quality, thanks to genuinely collaborative interactions between authors and review editors, who include some of the world's best academicians. Research must be certified by peers before entering a stream of knowledge that may eventually reach the public - and shape society; therefore, Frontiers only applies the most rigorous and unbiased reviews. Frontiers revolutionizes research publishing by freely delivering the most outstanding research, evaluated with no bias from both the academic and social point of view. By applying the most advanced information technologies, Frontiers is catapulting scholarly publishing into a new generation.

What are Frontiers Research Topics?

Frontiers Research Topics are very popular trademarks of the *Frontiers journals series*: they are collections of at least ten articles, all centered on a particular subject. With their unique mix of varied contributions from Original Research to Review Articles, Frontiers Research Topics unify the most influential researchers, the latest key findings and historical advances in a hot research area.

Find out more on how to host your own Frontiers Research Topic or contribute to one as an author by contacting the Frontiers editorial office: frontiersin.org/about/contact

IPPS 2022 - plant phenotyping for a sustainable future

Topic editors

Ulrich Schurr — Plant Sciences (IBG-2), Institute of Bio- and Geosciences, Julich Research Center, Helmholtz Association of German Research Centres (HZ), Germany

Elias Kaiser — Wageningen University and Research, Netherlands

Jennifer Clarke — University of Nebraska-Lincoln, United States

Philipp Von Gillhaussen — Interantional Plant Phenotyping Network (IPPN), Germany

Citation

Schurr, U., Kaiser, E., Clarke, J., Von Gillhaussen, P., eds. (2024). *IPPS 2022 - plant phenotyping for a sustainable future*. Lausanne: Frontiers Media SA.

doi: 10.3389/978-2-8325-4567-6

Table of contents

frontiers | Frontiers in Plant Science

TYPE Editorial
PUBLISHED 27 February 2024
DOI 10.3389/fpls.2024.1383766

OPEN ACCESS

EDITED AND REVIEWED BY
Diego Rubiales,
Spanish National Research Council (CSIC), Spain

*CORRESPONDENCE
Elias Kaiser
elias.kaiser@wur.nl

RECEIVED 08 February 2024
ACCEPTED 19 February 2024
PUBLISHED 27 February 2024

CITATION
Kaiser E, Von Gillhaussen P, Clarke J and Schurr U (2024) Editorial: IPPS 2022 - plant phenotyping for a sustainable future. *Front. Plant Sci.* 15:1383766. doi: 10.3389/fpls.2024.1383766

Editorial: IPPS 2022 - plant phenotyping for a sustainable future

Elias Kaiser[1]*, Philipp Von Gillhaussen[2], Jennifer Clarke[3] and Ulrich Schurr[4]

[1]Horticulture and Product Physiology, Plant Sciences Group, Wageningen University and Research, Wageningen, Netherlands, [2]Forschungszentrum Jülich GmbH IBG-2: Plant Sciences, International Plant Phenotyping Network (IPPN), Juelich, Germany, [3]Quantative Life Sciences Initiative (Complex Biosystems), University of Nebraska-Lincoln, Lincoln, NE, United States, [4]Plant Sciences (IBG-2), Institute of Bio- and Geosciences, Julich Research Center, Helmholtz Association of German Research Centres (HZ), Juelich, Germany

KEYWORDS

plant phenotyping, image analysis, model, phenomics, plant-environment interaction

Editorial on the Research Topic
IPPS 2022 - plant phenotyping for a sustainable future

Plants are a venue for addressing the challenges facing humanity. The need for a reliable supply of food, feed, materials, chemicals and energy as well as ways to manage agroecology and climate change are among the challenges that we can address through the sustainable use of plants and plant ecosystems. The research community needs to integrate plant systems approaches, from molecular to organismal to applications in the field and ecosystems, to increase productivity sustainably while using fewer land, water, and nutrient resources. In the past two decades, plant phenotyping research has developed a highly valuable portfolio of technologies, processes and infrastructures to address these questions (Pieruschka and Schurr, 2019). In the past, the creation of datasets was limited by low throughput sensing and image analysis (Tsaftaris et al., 2016). However, through the development of digital image analysis the previous phenotyping "bottleneck" has shifted towards a capacity problem, making it difficult to interpret vast datasets (especially in the face of plant x environment interactions), leading to an "interpretation bottleneck" (Smith et al., 2021). Innovative plant phenotyping approaches that reveal and target relevant traits are thus still needed to identify and quantify key traits and processes and to understand the dynamic interactions between genetics, molecular and biochemical processes, and the physiological responses to changes in the environment that lead to the development of a phenotype.

The IPPS 2022 conference in Wageningen (the Netherlands) brought together a diverse phenotyping community from academia and industry to discuss and realize potentials to harness the power of plant phenotyping. In this Research Topic (RT), we have collected contributions from attendees of IPPS 2022, as well as from other scientists working on plant phenotyping. The RT comprises ten experimental and three review papers. It is noteworthy that eight out of ten research papers are devoted to field crops (including the major crops

wheat, maize, potato, sugarcane, and cotton), highlighting the community's increasing focus on the application of plant phenotyping for crop improvement and the understanding of physiological patterns in large populations of crops for food, feed, and energy security. Plant phenotyping is a highly interdisciplinary field, as it requires constant development and critical evaluation of methods in both data acquisition and analysis. The papers of this RT can be categorized broadly into those focused on data collection (7 papers), those focused on data analysis and/or modeling (5 papers), and one review paper on policy and governance that broadly deals with both aspects (Gerullis et al.).

Regarding data collection through rapid phenotyping, several authors applied existing methods to new problems, thereby expanding the tested range of these methods. Ma et al. successfully applied near-infrared spectroscopy to a diversity panel of sugarcane to detect differences in stalk crushing strength, a trait closely related to mechanical stability of sugarcane. Using this method, breeders may be able to breed for more lodging-resistant sugarcane. In a noteworthy example of phenotyping of growth and photosynthesis during the growing season in the field, Knopf et al. assessed the genotypic diversity of ten wheat cultivars under ambient and elevated (CO_2). Among other sensors, the light-induced fluorescence transient (LIFT) sensor was used, enabling the researchers to detect earlier onset of senescence under elevated (CO_2). Shi et al. provide an example of combined phenotyping of root and shoot growth in maize, an approach that is currently unusual and deserves more attention given the intimate connection of root and shoot functioning, as well as the importance of above- and belowground biomass allocation. Njane et al. assessed the effects of UAV height on imaging of potato, for traits including crop height and volume. They determined that a flying height of 15 m was preferable to that of 30 m, as it provided for better resolution. Dong et al. visually inspected seeds of several accessions of the leguminous plant *Sophora moorcroftiana*, identifying genetic variation in traits that in other species have been shown to correlate with fitness in the field, such as seed weight, providing implications for crop improvement in legumes, which contribute largely to global food security. In their review paper on Sainfoin (*Onobrychis* spp. Fabaceae), Karabulut et al. provide an overview of all traits (82 in total) which have so far been measured on this perennial forage legume, which is mostly used as livestock feed but could feed humans as well.

Although they are undoubtedly useful, large high-throughput phenotyping (HTP) facilities are subject to several pitfalls, as illustrated in the review by Poorter et al. For example, projected leaf area, which is often used to estimate biomass, can be underestimated by ~20% due to diurnal leaf movement. Also, Poorter et al. highlight the fact that the high degree of automation that HTP systems require results in reduced experimental flexibility (in terms of possible measurements and treatments) and a demand for expert knowledge (to run and fix such systems). Proxies generated by such systems often require calibration curves that are specific to a given crop. Given the inflexibility in the set of traits measured by many HTP systems, researchers using such systems may fall prey to the "if the only tool you have is a hammer, everything looks like a nail" problem. The importance of systemic approaches to regulation and governance in plant breeding is highlighted by Gerullis et al. The authors propose a new governance heuristic – a rule of thumb for decision makers – for evaluating plant breeding research that includes social systems feedback, along with genetics, environment and management.

Several publications report progress on the use of data analysis and modelling for trait estimation. One highlight is presented by Cantürk et al. who used 3D point clouds based on RGB and laser data acquired by UAVs to detect key morphological features of vine plants in the field, including plant height, plant volume and canopy width. Key to determining these features was correct identification of trunk location, which allowed for the identification of single plants. Carlier et al. tested several model types on RGB and multispectral data of wheat, identifying convolutional neural network (CNN) models to be superior to partial least squares regression (PLSr) models for trait extraction. Similarly, Renó et al. used two AI models – random forest and multilayer perceptron processing – to detect drought in cotton using thermography, thereby increasing the throughput of thermal image analysis.

The last two papers of this RT deal with the connection between phenomics data and genetics, a topic that is highly relevant for plant breeding. In a population of potato grown throughout several seasons and across various levels of heat stress, Martins et al. showed that including a family effect significantly improved the genetic selection of potato clones for subsequent breeding. Finally, Li et al. describe an interesting example of using phenomic rather than genomic selection to estimate genetic diversity in Scots pine. They performed phenomic selection using hyperspectral reflectance data acquired by UAVs, which in many cases is much easier and cheaper to obtain than molecular markers, especially in long-living woody plants. Phenomic selection may hold great promise in the future of plant breeding.

We believe that this RT is a nice representative sample of the state of the art of plant phenotyping. We hope that readers will thoroughly enjoy these articles and derive valuable knowledge from them.

Author contributions

EK: Writing – original draft, Writing – review & editing. PG: Writing – original draft, Writing – review & editing. JC: Writing – original draft, Writing – review & editing. US: Writing – original draft, Writing – review & editing.

Conflict of interest

The authors declare that the research was conducted in the absence of any commercial or financial relationships that could be construed as a potential conflict of interest.

The author(s) declared that they were an editorial board member of Frontiers, at the time of submission. This had no impact on the peer review process and the final decision.

Publisher's note

References

Pieruschka, R., and Schurr, U. (2019). Plant phenotyping: past, present, and future. *Plant Phenomics* 2019, 1–6. doi: 10.34133/2019/7507131

Smith, D. T., Potgieter, A. B., and Chapman, S. C. (2021). Scaling up high-throughput phenotyping for abiotic stress selection in the field. *Theor. Appl. Genet.* 134, 1845–1866. doi: 10.1007/s00122-021-03864-5

Tsaftaris, S. A., Minervini, M., and Scharr, H. (2016). Machine learning for plant phenotyping needs image processing. *Trends Plant Sci.* 21, 989–991. doi: 10.1016/j.tplants.2016.10.002

frontiers | Frontiers in Plant Science

TYPE Original Research
PUBLISHED 15 May 2023
DOI 10.3389/fpls.2023.1177406

OPEN ACCESS

EDITED BY
Philipp Von Gillhaussen,
Interantional Plant Phenotyping Network (IPPN), Germany

REVIEWED BY
Fabio Fiorani,
Helmholtz Association of German Research Centres (HZ), Germany
Dionysia Apostolos Fasoula,
Agricultural Research Insitute, Cyprus

*CORRESPONDENCE
Muhammet Şakiroğlu
msakiroglu@atu.edu.tr
Brandon Schlautman
schlautman@landinstitute.org

RECEIVED 01 March 2023
ACCEPTED 18 April 2023
PUBLISHED 15 May 2023

CITATION
Karabulut E, Erkoç K, Acı M, Aydın M, Barriball S, Braley J, Cassetta E, Craine EB, Diaz-Garcia L, Hershberger J, Meyering B, Miller AJ, Rubin MJ, Tesdell O, Schlautman B and Şakiroğlu M (2023) Sainfoin (*Onobrychis* spp.) crop ontology: supporting germplasm characterization and international research collaborations. *Front. Plant Sci.* 14:1177406. doi: 10.3389/fpls.2023.1177406

Sainfoin (*Onobrychis* spp.) crop ontology: supporting germplasm characterization and international research collaborations

Ebrar Karabulut[1], Kübra Erkoç[1], Murat Acı[1,2], Mahmut Aydın[3], Spencer Barriball[2], Jackson Braley[4], Eric Cassetta[2], Evan B. Craine[2], Luis Diaz-Garcia[5], Jenna Hershberger[6], Bo Meyering[2], Allison J. Miller[4,7], Matthew J. Rubin[4], Omar Tesdell[8], Brandon Schlautman[2*] and Muhammet Şakiroğlu[1*]

[1]Bioengineering Department, Adana Alparslan Türkeş Science and Technology University, Adana, Türkiye, [2]The Land Institute, Salina, KS, United States, [3]Department of Computer Engineering, Kafkas University, Kars, Türkiye, [4]Donald Danforth Plant Science Center, St. Louis, MO, United States, [5]Department of Viticulture and Enology, University of California Davis, Davis, CA, United States, [6]Plant and Environmental Sciences Department, Clemson University, Clemson, SC, United States, [7]Department. of Biology, Saint Louis University, St. Louis, MO, United States, [8]Department of Geography, Birzeit University, Birzeit, West Bank, Palestine

Sainfoin (*Onobrychis* spp.) is a perennial forage legume that is also attracting attention as a perennial pulse with potential for human consumption. The dual use of sainfoin underpins diverse research and breeding programs focused on improving sainfoin lines for forage and pulses, which is driving the generation of complex datasets describing high dimensional phenotypes in the post-omics era. To ensure that multiple user groups, for example, breeders selecting for forage and those selecting for edible seed, can utilize these rich datasets, it is necessary to develop common ontologies and accessible ontology platforms. One such platform, Crop Ontology, was created in 2008 by the Consortium of International Agricultural Research Centers (CGIAR) to host crop-specific trait ontologies that support standardized plant breeding databases. In the present study, we describe the sainfoin crop ontology (CO). An in-depth literature review was performed to develop a comprehensive list of traits measured and reported in sainfoin. Because the same traits can be measured in different ways, ultimately, a set of 98 variables (variable = plant trait + method of measurement + scale of measurement) used to describe variation in sainfoin were identified. Variables were formatted and standardized based on guidelines provided here for inclusion in the sainfoin CO. The 98 variables contained a total of 82 traits from four trait classes of which 24 were agronomic, 31 were morphological, 19 were seed and forage quality related, and 8 were phenological. In addition to the developed variables, we have provided a roadmap for developing and submission of new traits to the sainfoin CO.

KEYWORDS

sainfoin, *Onobrychis* spp., crop ontology, perennial grain, pulse, forage

1 Introduction

Sainfoin (*Onobrychis* spp. Fabaceae) has a long and rich history of cultivation across Asia, Europe, and North America where it is used to provide roughage for livestock and to maintain soil fertility (Frame et al., 1998). Sainfoin has been used as a perennial forage legume and in crop rotation regimes with major grains such as wheat and barley (Hayot Carbonero et al., 2011). Sainfoin use has been centered in Turkey, the Balkans, and Central and Southern Europe (Bennett et al., 2001), but historical evidence suggests it was also grown in Palestine, Syria, and Lebanon in the late 1800s (Tristram, 1885). The introduction of synthetic fertilizer-based production schemes led to a reduction in sainfoin cultivation in these regions (Hayot Carbonero et al., 2011), and a concomitant decline in research and breeding efforts. Recently, as concerns about synthetic fertilizers have grown, attention has refocused on the crucial role of legumes in agricultural systems, and as a result, interest in sainfoin has been revived (Şakiroğlu, 2021; Craine et al., 2023).

Agriculture and plant breeding are undergoing a revolution in response to calls for the development of more diverse, sustainable, agricultural systems. A key part of this is plant breeding, the improvement of existing crops and development of new ones that provide agronomic products and critical ecosystem services. For example, there is emerging interest in domesticating sainfoin as a potential novel, sustainable food source - a perennial pulse - for human consumption (Butkutė et al., 2018a; Butkutė et al., 2018b; Schlautman et al., 2018). Evidence from nutritional analyses and animal feeding studies suggest sainfoin seeds could be suitable for human and animal consumption (Ditterline, 1973; Tarasenko et al., 2015; Baldinger et al., 2016; Wijekoon et al., 2021; Craine et al., 2023). Thus, recent breeding efforts to develop sainfoin for dual-purpose perennial grain and forage production by selecting phenotypes related to grain yield and grain quality have begun at The Land Institute (Salina, KS, USA), Adana Alparslan Türkeş Science and Technology University (Adana, Turkey), and elsewhere.

As plant breeding programs expand and evolve to meet current and future agricultural needs, it is necessary to adapt existing frameworks for cataloging plant information. In the post-omics era (e.g. genomics, transcriptomics, proteomics, metabolomics, hormonomics, ionomics, and large-scale automated phenomics) the amount and complexity of data collected, stored, and shared within and among breeding and agriculture research programs has reached an all-time high (Langridge and Fleury, 2011; Leonelli et al., 2017; Li and Yan, 2020; Van Tassel et al., 2022). These post-omics era technologies promise to generate more data at lower costs than ever before, which could accelerate genetic gains in underutilized crops or even rapidly domesticate new ones. However, leveraging these technologies and large datasets when collaborating is only possible with available infrastructure to robustly store and access data. As such, there is a need for new frameworks that enable breeders to efficiently share and communicate about the multi-dimensional plant phenotypes characterized in their programs, for different breeding goals, in a broader diversity of current and emerging crop species like sainfoin.

As early as the 1990s, the need for designing databases serving multiple users with a robust set of common ontologies was recognized (Wieczorek et al., 2012). Numerous ontologies and ontology platforms have since been created to support and standardize data sharing within and among research fields such as Darwin Core (https://dwc.tdwg.org) as a standard for biodiversity data and the Planteome platform (https://www.planteome.org) and related Plant Ontology (PO), Plant Trait Ontology (TO), and Plant Experimental Conditions Ontology (PECO) frameworks, which provide a base for ontologies for plant and species-specific traits related to plant development, anatomy, physiology in the context of genomics data (Jaiswal et al., 2005; Pujar et al., 2006; Ilic et al., 2007; Avraham et al., 2008; Arnaud et al., 2012; Cooper et al., 2013; Cooper and Jaiswal, 2016; Cooper et al., 2018).

Crop Ontology (CO, https://cropontology.org, Matteis et al., 2013)) was created in 2008 by the CGIAR to provide a framework and common language to catalog crop-specific trait data, allowing traits to be easily interpretable and interoperable for further aggregation, analysis, and multidisciplinary communication (Gruber, 2009). CO currently supports the standardization of plant breeding databases such as the Integrated Breeding Platform's BMS (IBP; https://www.integratedbreeding.net/), the Boyce Thompson Institute's Breedbase (https://breedbase.org/, (Morales et al., 2022), and others (Arnaud et al., 2020) which allow the creation and management of annotated trial data (Crop Ontology 2022). The Minimum Information About a Plant Phenotype Experiment (MIAPPE https://www.miappe.org/; (Ćwiek-Kupczyńska et al., 2016; Papoutsoglou et al., 2020) and the Breeding Application Programming Interface (BrAPI; https://brapi.org/; (Selby et al., 2019) have both adopted the CO format, demonstrating the widespread acceptance and utility of the standard (Arnaud et al., 2020). The CO Application Programming Interface (API) is used by third-party websites and databases like the EMBL-EBI Ontology Lookup Service that replicates CO and provides term search access through its own portal. Agroportal, the registry of ontologies in agriculture and related domains, regularly synchronizes their files with CO.

Several different COs have since been developed and made accessible through the CO platform by research groups and crop specific consortiums for several commonly cultivated crops including apple, banana, cotton, corn, common bean, potato, rice, and wheat. We expect that the broader impacts made possible through international and transdisciplinary collaboration and germplasm characterization in sainfoin can be magnified through early efforts of a consortium of researchers, hereafter referred to as the "Sainfoin Consortium." In this current work, we describe the efforts of the Sainfoin Consortium to standardize the nomenclature and data storage systems used for sainfoin research to create a sainfoin CO - the first CO developed for a perennial forage legume and grain crop. We also include a roadmap for further expansion of

Abbreviations: Crop Ontology, CO; Plant Ontology, PO; Agronomy Ontology, AGRO; Plant Trait Ontology, TO; Plant Experimental Conditions Ontology, PECO; The Environment Ontology, ENVO; The Phenotype And Trait Ontology, PATO; The Consultative Group on International Agricultural Research, CGIAR.

the sainfoin CO through a set of guidelines for the development and suggestion of new traits.

2 The sainfoin ontology framework

2.1 Ontology construction methods

We used the Crop Ontology framework guidelines (version 2.1; Pietragalla et al., 2022) and trait dictionary template to build the first version of a sainfoin crop ontology. The online database software, Airtable, was used to create the first version of the ontology as it incorporates relational data structures that can be used to easily link ontology terms across tables in the database. Figures and entity relation diagrams were constructed in DrawIO (https://github.com/jgraph/drawio). The Crop Ontology CGIAR advisory board assigned the crop code CO_369 to sainfoin, which is prepended to Variable terms in the final sainfoin ontology. The sainfoin crop ontology is available to the public, can be browsed on the Crop Ontology website (https://cropontology.org/term/CO_369:ROOT), resides in a dedicated GitHub repository (https://github.com/Planteome/CO_369-sainfoin-traits), and is maintained by a group of community curators from the Sainfoin Consortium.

2.2 Term types and structure

The CO phenotype annotation model is based on three fundamental CO term types: Trait, Method, and Scale. These three fundamental types are then used in conjunction to construct a fourth term type, Variable, which formalizes how a given trait is collected. Each CO term in the sainfoin ontology was assigned a persistent unique identifier (PUID), which is composed of the sainfoin CO crop code and a seven-digit number in the form {CO crop code}:{#######}, e.g., CO_369:0000001. While the format of the ID system is constrained as shown above, the CO guidelines do not mandate a particular system for assigning PUIDs to Variables, Traits, Methods, or Scales within an individual ontology. To maintain an incremental, identifiable PUID system, we added constraints for each term type (Variable, Trait, Method, and Scale) shown in Table 1.

In addition to PUIDs, all terms in the ontology were given human-readable names and abbreviations that can be used in trait selection used in data collection. We avoided using acronyms within CO term names except where the term name would become unwieldy without its use or when the acronym is more widely known than the actual phrase which the acronym represents (e.g., 'SPAD' for soil plant analysis development). Term names were constrained to standard ASCII characters, and aside from acronyms, only the first letter of the first word in each name is capitalized.

2.3 Trait composition framework

A Trait in the Sainfoin CO is a subcomponent of a variable that defines what is observed. Traits are composed of a meaningful, two- to four-word phrase consisting of an Entity, the observed part of a plant, and an Attribute, a feature of an entity, in the form {Entity} {Attribute} such as {Plant} {height}. Traits are then assigned to one of the nine Trait classes specified in the CO guidelines for organizational purposes when viewing the ontology (Table 2). When possible, Entities and Attributes in the sainfoin ontology were cross referenced with terms in existing relevant ontologies such as PO, the Agronomy Ontology (AGRO, Aubert et al., 2017), The Environment Ontology (ENVO, Buttigieg et al., 2016) and The Phenotype And Trait Ontology (PATO, Gkoutos) to standardize term vocabulary across other ontology frameworks.

Extensive examination of ontologies from other species revealed inconsistent approaches for assigning Entities and Attributes, especially those that can have multiple states. This multiple state problem is common when a treatment or processing step is applied (e.g., drying, boiling, milling). Using the example of the Entity {Forage} and the attribute {mass}, which can be measured either in a fresh or dried state. The CO guidelines specify two distinct approaches for assigning the state "dry", but each has its own challenge.

1. The "dry" state is assigned to the Entity {Dry forage} rather than the Attribute{mass}.

a. This approach creates a hierarchy of entities with multiple states rather than treating entities as a single observed part of a plant.

2. The "dry" state is not assigned to either the Entity {Forage} or Attribute {mass} but is instead included in the Method describing how Forage mass was measured either fresh or dry.

b. This approach results in multiple traits with the same name, which can create downstream challenges for users in selecting the proper Variable in tools such as Field Book (Rife and Poland, 2014) or Gridscore (Raubach et al., 2022). This is especially important in

TABLE 1 Term type ID series composition and creation.

Term Type	Term PUID Base Series	Term PUID Constraints
Variable	CO_369:0000000	1-999
Trait	CO_369:0001000	1001-1999
Method	CO_369:0002000	2001-2999
Scale	CO_369:0003000	3001-3999

The Sainfoin Crop Ontology V1 increments each term type from the base series within the constraints of each term type. This allows for the development of 999 unique terms for each term type while enforcing strict identifiability for each term type.

TABLE 2 List of trait classes, descriptions, and corresponding frequencies in the Sainfoin Crop Ontology.

Trait class	Absolute frequency	Relative frequency	Class Description
Agronomic	24	0.29	All main traits contributing to yield and related to the agronomic performance of plants.
Morphological	31	0.38	All traits related to anatomical and morphological structure of the plant, its organs, and tissues.
Quality	19	0.23	All traits related to key characteristics that influence end-use quality of crop/plant products and sub-products.
Phenological	8	0.10	All traits related to growth/developmental stages and periods of crop/plants.
Abiotic Stress	0	0.0	All traits related to stress caused by non-living stressors.
Biochemical	0	0.0	All traits related to chemical components of a plant entity.
Biotic Stress	0	0.0	All traits related to stress caused by living stressors.
Fertility	0	0.0	Traits specifically related to fertility aspects of importance to breeding.
Physiological	0	0.0	All traits related to the functioning of the crop/plant and its response/adaptation to the environment.
Total	82	1.00	

the sainfoin ontology where only the Method class abbreviation is included in the Variable name.

We chose a third approach, which was to assign the state to the attribute instead of the entity or method. In this fashion, any traits with state(s) would be constructed as {Entity} {(state) attribute} as in Forage dry mass and Forage fresh mass. With this format, we can have Methods that simply describe the Method for a given Trait(s) without having to form specific Methods for each Trait that only differ in the state of a Trait.

Finally, when choosing Attribute words, we opted for words that were specific enough to be contextually correct, but general enough that they could be used in more than one context. For example, "mass" was used instead of "weight", and "mass" was chosen over "biomass" since the latter adds no further meaning when the context is already scoped to biological organisms.

2.4 Method composition framework

Methods are the component of a Variable that describes how an observation is made. The framework we followed for composing Methods was based on the outline specified in the CO guidelines, with some modifications that add clarity to the procedures and allow for some flexibility between different breeding programs' goals. Our modifications fall into three main categories: Method name, Method description, and Method abbreviation.

First, we constrain the Method name to be a succinct, human-readable name appended with the Method class abbreviation. In most cases this should be the trait name followed by the Method class the Method belongs to following the format of {Trait} {Method class}. For example, 'Leaflet SPAD measurement' tells us this Method describes how to measure SPAD values of a leaflet. However, exceptions were made when general Methods could be assigned to multiple traits, as in the case of 'Object equivalent diameter measurement', which describes a simple image processing technique that could be applied to many different objects in an image. Methods were categorized into one of the seven classes (measurement, counting, estimation, computation, prediction, description, or classification) defined in the CO Guidelines.

Second, the Method description should be structured according to the format shown in Figure 1. While the Method description is allowed to be a free text field in the CO guidelines, we constrained our descriptions to include at minimum the following structured information: ***Description***: A brief, one sentence description of the Method; ***Materials***: A semicolon separated list of materials or supplies needed for the Method; ***Dependent_on***: A semicolon separated list of Variables that the Method uses for computational purposes or for normalization. Variables can be specified either by the variable label (Raceme length msr [cm]), ID (CO_369:0000061), or name (RaL_RaLmsr_cm); ***Protocol***: A detailed, ordered list of steps in the protocol needed to complete the Method. When it is infeasible to write out a lengthy protocol, it is indicated by writing "See full protocol in {publication title, author, year}".

Many existing CO Method descriptions either present no added information beyond that which is already specified in the Method name or present methodology too vague to be followed without error. We developed our Method descriptions to be agnostic regarding the sampling procedure so that the employment of a given Method can be adapted to the end user's specific experimental design. This modification is not entirely in line with the CO guidelines which state that the sampling should specify whether the observation is collected on a single plant or an aggregation from multiple plants (an experimental group or plot). However, this poses an issue with the scope of sample sizes (e.g., number of samples aggregated) commonly seen in breeding or agronomic trials. Specifically, a trait collected in greenhouse studies using single plant reps should, according to this guideline, have a separate method from the same trait collected in a field trial with collections of plants in a plot or sward. This leads to, at most, doubling the number of variables in the ontology. Furthermore, while the guidelines state that the experimental protocol should be distinguished from the observational protocol, the authors realize that the sampling protocol is inevitably linked to the experimental design and informs the observation procedure. Various research groups have their preferred sampling methods, dependent on goals, scale of

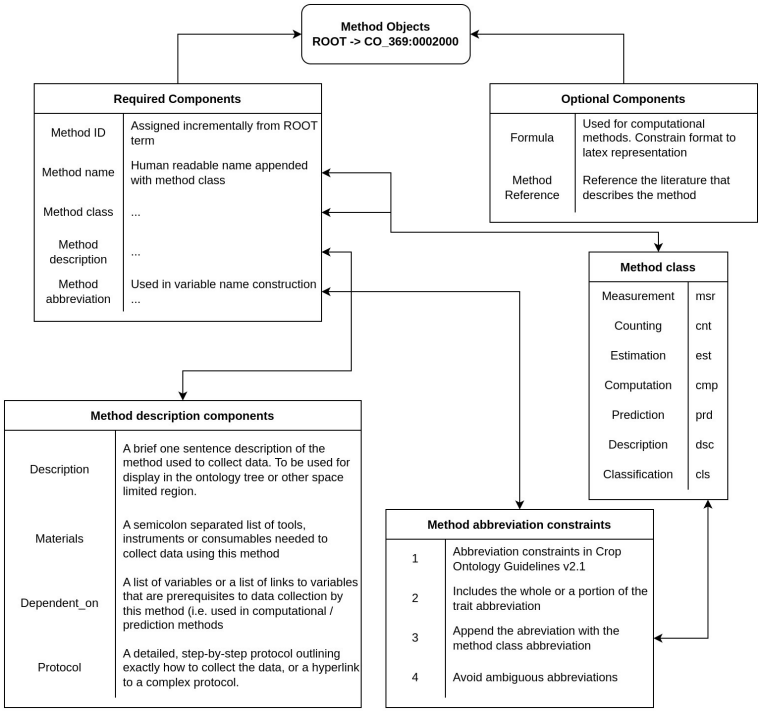

FIGURE 1
Schematic representation of the Method development for the Sainfoin Crop Ontology.

projects, funding, etc.; therefore, we leave the specific sampling procedure up to the individual researchers and only dictate that the trait value is represented *as-is* for data collected on one observational unit, or the mean/aggregated value for a collection of observational units.

Finally, we constrain the abbreviation of the Method used in Variable name construction to include the Trait abbreviation, or if not possible, at least a portion of the Trait abbreviation. Ambiguous abbreviations such as 'PH' for 'Plant height' or 'pH' were avoided. Additionally, the standard abbreviation of the Method class is appended at the end: msr, cnt, est, cmp, prd, dsc, or cls (See Supplemental Table 3). This is to avoid confusion about what type of methodology is being employed in a Variable.

New Methods are to be developed following the above guidelines as schematized in Figure 1. Briefly, there are five obligatory Method components: Method ID, Method name, Method class, Method description, and Method abbreviation. The Method ID is assigned automatically and incrementally. The Method class must be selected among the seven different Method classes (Figure 1).

2.5 Scale composition framework

Scales are the component of a variable that describes how the observation is expressed. Scales were composed of units in the International System of Units (SI) with their associated official abbreviations. Scales were cross referenced to the Units of measurement Ontology (Gkoutos et al., 2012) or other ontologies such as PO and AGRO when applicable. Units with a 'µ' prefix were included even though they are not a part of the ASCII standard character set, however, 'u' may be used in place of 'µ' when convenient. Scales were specified as either a Date, Duration, Nominal, Numerical, Ordinal, Text, or Code Scale class.

2.6 Variable composition framework

Variables are the breeder's or agronomist's observations or measurements. The CO model defines a Variable as a unique combination of a Trait, Method, and Scale (Variable = Trait + Method + Scale), which allows for standardized data collection, storage, and sharing. Variable labels are human readable: they are composed of a Trait name followed by an associated Method class abbreviation, and a Scale enclosed in square brackets (e.g., Seed length msr [mm]); and used in scientific discussions and publications. Variable abbreviations, also referred to as names in the CO guidelines, are composed of {Trait abbreviation}_{Method abbreviation}_{Scale abbreviation} with no further modifications, (e.g., 'SdL_Lmsr_mm'); and used as unique IDs in databases, analyses, and phenotyping applications. A detailed schematic of Variable composition is shown in Figure 2.

3 Populating the sainfoin ontology

3.1 Gathering a broad target list and shortlist of most used traits

Despite limited interest in sainfoin in the research community, a wealth of research targeting various aspects of the crop has been

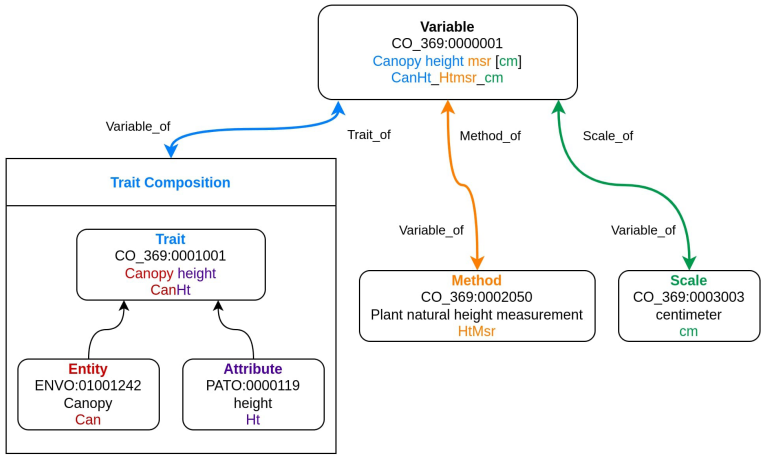

FIGURE 2
Schematic representation of Variable term composition in the Sainfoin Crop Ontology. In this example, the Variable 'Canopy height msr [cm]' is used to demonstrate how complex ontology terms are constructed of simpler terms and how the term identification number system functions. For each term type, (Variable, Trait, Method, and Scale) the PUID, term label and abbreviations are listed in order.

published in different languages. In addition to forage yield and quality traits, adaptability, resistance to biotic and abiotic stress factors, biochemical, physiological, morphological and phenological traits have been investigated. Research targeting cytogenetic, morphological, and molecular aspects along with taxonomic status of sainfoin and allied taxa have also been investigated and reported (Aktoklu, 1995; Hayot Carbonero et al., 2011; Kempf et al., 2017; Şakiroğlu, 2021).

We performed an in-depth literature review in the languages accessible to our consortium (English and Turkish) to develop a comprehensive list of Variables that have been previously measured and reported in sainfoin. The process of determining which of these variables to include, and the specific Trait, Method, and Scale terms to use, required many discussions, compromises, and decisions that spanned multiple months. The terms we included reflect the traits, methods, and scales currently being used in breeding and research programs led by the authors of this manuscript. In some instances, multiple variables are included for the same trait reflecting the differences in methods or scales used within the consortium. We selected 76 sainfoin Variables to include in sainfoin CO v1, of which the majority are from the agronomic, morphological, quality, and phenological trait classes (Table 2). We observed many traits from other classes (e.g. abiotic stress and biotic stress) during our literature review, but did not incorporate them into Variables in the first version of the sainfoin CO. We have included a list of 79 Traits that could be added to the sainfoin CO in the future as our community's expertise or interest in these other trait classes expands (Supplementary Table 1).

3.2 Adding quality traits relevant to sainfoin as a perennial grain crop

Developing sainfoin as a new perennial pulse will require measuring new traits that are typically relevant only to cereal and grain legume crops. We reviewed the ontologies for several grain crops, including wheat, barley, oat, and common bean, that are available on the CO platform, and we compiled a list of 258 Variables from multiple trait classes that have not been previously measured in sainfoin but might be applicable to sainfoin breeding as a perennial pulse crop (Supplemental Table 2). While cereals provide a broad frame for grain related traits, common bean traits are particularly relevant, serving as a source of legume specific traits.

A comprehensive understanding of the chemical composition and nutritional quality of sainfoin seeds is needed to determine the safety of this new food source and the nutritional value of sainfoin as a novel pulse crop. Some of these quality traits, such as crude protein, dietary fiber, and phytic acid content, were recently measured in sainfoin for the first time (Craine et al., 2023). Compared to other pulses, depodded sainfoin seeds have higher protein content, as reported by Baldinger et al. (2016) (38.8%), Woodman and Evans (1947) (36.6%), Craine et al. (2023) (38.78%), and Ditterline (1973) (36.0%), and comparable iron and zinc content, as reported by Craine et al. (2023) (Fe, 56.25 - 74.24 ppm; Zn, 54.78 - 79.05 ppm), each of which plays a vital role in human health.

Of the many potential "grain" related traits, we chose to create only 8 Variables related to seed quality in the initial sainfoin CO, which were recently profiled in a study evaluating sainfoin seed attributes (Craine et al., 2023). Creating Variables and appropriate terms for these eight seed quality Traits, namely, protein, crude fat, carbohydrates, total starch, dietary fiber, iron, zinc, and phytic acid content, was simplified by their common use across many crop species (Table 3). These quality Traits are measured using methods approved by the Association of Official Agricultural Chemists (AOAC) and/or American Association of Cereal Chemists (AACC), and the appropriate AOAC and AACC method codes are referenced in the related Method description in the sainfoin CO.

TABLE 3 Variables from Craine et al. (2023) that are included in the Sainfoin Crop Ontology V1.

Variable	Trait		Method		Scale	
	Name	Class	Protocol	Class	Name	Class
Seed protein content msr [DMB*]	Seed crude protein	Quality	AACC 46-30.01	Measurement	g/100g	Numerical
Seed crude fat content msr [DMB]	Seed crude fat content	Quality	AACC 30-25.01 (ETHER EXTRACTION)	Measurement	g/100g	Numerical
Seed carbohydrate content cmp [DMB]	Seed carbohydrates	Quality	100 - (ASH + MOISTURE + FAT + PROTEİN)	Computation	g/100g	Numerical
Seed total starch content msr [DMB]	Seed total starch content	Quality	AOAC 996.11	Measurement	g/100g	Numerical
Seed dietary fiber content msr [DMB]	Seed dietary fiber content	Quality	AACC 32-07.01/AOAC 991.43	Measurement	g/100g	Numerical
Seed iron content msr [DMB]	Seed iron content	Quality	AACC 40-70.01	Measurement	ppm	Numerical
Seed zinc content msr [DMB]	Seed zinc content	Quality	AACC 40-70.01	Measurement	ppm	Numerical
Seed phytic acid content msr [DMB]	Seed phytic acid content	Quality	HPLC RI	Measurement	mg	Numerical

*DMB, Dry matter basis.

4 Future perspectives

4.1 Guidelines for contributing to the sainfoin ontology

The sainfoin CO represents a necessary step towards making sainfoin research accessible and discernable to an international community of researchers. However, the sainfoin CO is far from complete. Sainfoin has tolerance to various biotic and abiotic stresses, and traits related to sainfoin drought and salinity tolerance would be of immense importance in agriculture (Heinrichs, 1972; Juan, 1982; Morrill et al., 1998; Meyer and Badaruddin, 2001; Irani et al., 2015; Kölliker et al., 2017). We encourage researchers with expertise and experience in areas not represented in the current sainfoin CO to contribute to expanding its scope and utility in the future.

Researchers can suggest and submit new sainfoin ontology terms (I.e., Variables, Traits, Methods, or Scales) through https://trait-requests.planteome.org/or a GitHub issues template form. Extant terms can be updated with sufficient rationale, or term synonyms can be suggested where two competing names are commonly used to describe that term. Any new terms should meet the baseline guidelines laid forth in the official CO Guidelines v2.1, and conform to the additional requirements and constraints set forth above. Such a system will aid in constructing a more helpful ontology. Two curators (English and Turkish native speakers) are actively maintaining and improving the sainfoin CO. The curators are notified upon any new term submission, and follow-up discussions about the term are handled through GitHub issues.

4.2 The roles of crop ontologies in developing new sustainable crops and cropping systems

In this manuscript, we share our experiences in building the sainfoin CO in hopes that we can continue improving research infrastructure for the international sainfoin community and to provide a template for future crop ontology development for other perennial grains, forages or minor pulse crops. There is global recognition for the growing need for agroecosystem sustainability and resilience to climate change (FAO (Food and Nations), A. O. of the United Nations, 2018; Tittonell, 2020). Sainfoin, as both a perennial pulse and perennial forage, has the potential to contribute towards these goals internationally; however, many other new and underutilized crops will be needed in various contexts. We expect that data infrastructure, such as the sainfoin CO presented herein, combined with technology to collect multi-dimensional data at scales and rates higher than ever before, will allow researchers from multiple languages and research disciplines to collaborate effectively to make rapid progress towards domesticating new perennial grains, developing new sustainable cropping systems, and preparing agriculture internationally for climate challenges in the future.

Data availability statement

The datasets presented in this study can be found in online repositories. The names of the repository/repositories and accession number(s) can be found below: https://cropontology.org/term/CO_369:ROOT https://github.com/Planteome/CO_369-sainfoin-traits.

Author contributions

Conceptualization: BS, MS. Data curation - EK, KE, ECr, MAc, MAy, SB, BM, JB. Funding acquisition - BS, MS, AM. Methodology- BM, SB, JH, EK, KE, ECr, SB, LD, OT. Project administration - BS, MS, BM. Software - MAy, BM. Supervision - MS, BS. Visualization – BM. Writing – original draft - MS, BM, BS, KE, EK, ECr, ECa, MR. Writing – review & editing - All authors. All authors contributed to the article and approved the submitted version.

Funding

The Scientific and Technological Research Council of Turkey (TUBITAK) Research Grant (number 120C136); The Foundation for Food & Agriculture Research Seeding Solutions Grant, The Perennial Agriculture Project, a joint venture between the Malone Family Foundation and The Land Institute; Clemson University Startup.

Conflict of interest

The authors declare that the research was conducted in the absence of any commercial or financial relationships that could be construed as a potential conflict of interest.

Publisher's note

All claims expressed in this article are solely those of the authors and do not necessarily represent those of their affiliated organizations, or those of the publisher, the editors and the reviewers. Any product that may be evaluated in this article, or claim that may be made by its manufacturer, is not guaranteed or endorsed by the publisher.

Supplementary material

The Supplementary Material for this article can be found online at: https://www.frontiersin.org/articles/10.3389/fpls.2023.1177406/full#supplementary-material

SUPPLEMENTARY TABLE 1
List of important Traits and Variables in sainfoin as determined by literature review.

SUPPLEMENTARY TABLE 2
Traits and variables from wheat, oat, barley, and common bean that might be relevant to sainfoin.

SUPPLEMENTARY TABLE 3
List of entities and descriptions in the ontology.

References

Agronomy Ontology. CGIAR *Platform for big data in agriculture*. Available at: https://bigdata.cgiar.org/resources/agronomy-ontology/ (Accessed August 23, 2022).

Aktoklu, E. (1995). *Revision of onobrychis miller (Fabaceae) species grown in Turkey*. (Malatya, Türkiye: PhD Dissertation. Inönü Univ.).

Arnaud, E., Cooper, L., Menda, N., Nelson, R., Matteis, L., Skofic, M., et al. (2012). Towards a Reference Plant Trait Ontology For Modeling Knowledge of Plant Traits and Phenotypes. *Proceedings of the International Conference on Knowledge Engineering and Ontology Development (KEOD-2012)*, 220–225. doi: 10.13140/2.1.2550.3525

Arnaud, E., Laporte, M.-A., Kim, S., Aubert, C., Leonelli, S., Miro, B., et al. (2020). The ontologies community of practice: a CGIAR initiative for big data in agrifood systems. *Patterns* 1, 100105. doi: 10.1016/j.patter.2020.100105

Aubert, C., Buttigieg, P., Laporte, M., Devare, M., and Arnaud, E. (2017) *CGIAR agronomy ontology*. Available at: http://purl.obolibrary.org/obo/agro.owl.

Avraham, S., Tung, C.-W., Ilic, K., Jaiswal, P., Kellogg, E. A., McCouch, S., et al. (2008). The plant ontology database: a community resource for plant structure and developmental stages controlled vocabulary and annotations. *Nucleic Acids Res.* 36, D449–D454. doi: 10.1093/nar/gkm908

Baldinger, L., Hagmüller, W., Minihuber, U., Matzner, M., and Zollitsch, W. (2016). Sainfoin seeds in organic diets for weaned piglets–utilizing the protein-rich grains of a long-known forage legume. *Renew. Agric. Food Syst.* 31, 12–21. doi: 10.1017/S1742170514000386

Bennett, S., Francis, C., and Reid, B. (2001). "Minor and under-utilised legumes," in *Plant genetic resources of legumes in the Mediterranean current plant science and biotechnology in agriculture*. Eds. N. Maxted and S. J. Bennett (Dordrecht: Springer Netherlands), 207–230. doi: 10.1007/978-94-015-9823-1_12

Butkutė, B., Padarauskas, A., Cesevičienė, J., Taujenis, L., and Norkevičienė, E. (2018a). Phytochemical composition of temperate perennial legumes. *Crop Pasture Sci.* 69, 1020. doi: 10.1071/CP18206

Butkutė, B., Taujenis, L., and Norkevičienė, E. (2018b). Small-seeded legumes as a novel food source. variation of nutritional, mineral and phytochemical profiles in the chain: raw seeds-sprouted seeds-microgreens. *Molecules* 24, 133. doi: 10.3390/molecules24010133

Buttigieg, P., Pafilis, E., Lewis, S., Schildhauer, M., Walls, R., and Mungall, C. (2016). The environment ontology in 2016: bridging domains with increased scope, semantic density, and interoperation. *J. BioMed. Semant* 7, 57. doi: 10.1186/s13326-016-0097-6

Cooper, L., and Jaiswal, P. (2016). The plant ontology: a tool for plant genomics. *Methods Mol. Biol.* 1374, 89–114. doi: 10.1007/978-1-4939-3167-5_5

Cooper, L., Meier, A., Laporte, M.-A., Elser, J. L., Mungall, C., Sinn, B. T., et al. (2018). The planteome database: an integrated resource for reference ontologies, plant genomics and phenomics. *Nucleic Acids Res.* 46, D1168–D1180. doi: 10.1093/nar/gkx1152

Cooper, L., Walls, R. L., Elser, J., Gandolfo, M. A., Stevenson, D. W., Smith, B., et al. (2013). The plant ontology as a tool for comparative plant anatomy and genomic analyses. *Plant Cell Physiol.* 54, e1. doi: 10.1093/pcp/pcs163

Craine, E. B., Şakiroğlu, M., Peters, T. E., Barriball, S., and Schlautman, B. (2023). Nutritional quality of onobrychis viciifolia (Scop.) seeds: a potentially novel perennial pulse crop for human use. *Legume Sci.* 2023, e189. doi: 10.1002/leg3.189

Ćwiek-Kupczyńska, H., Altmann, T., Arend, D., Arnaud, E., Chen, D., Cornut, G., et al. (2016). Measures for interoperability of phenotypic data: minimum information requirements and formatting. *Plant Methods* 12, 44. doi: 10.1186/s13007-016-0144-4

Ditterline, R. L. (1973) *Yield and yield components of sainfoin (Obobrychis viciaefolia scop.) seed and an evaluation of its use as a protein supplement* (ScholarWorks at Montana State University). Available at: https://scholarworks.montana.edu/xmlui/bitstream/handle/1/4295/31762100107232.pdf?sequence=1 (Accessed November 17, 2022).

FAO. (2018). *The 10 elements of agroecology: guiding the transition to sustainable food and agricultural systems* (Rome: Food and Agriculture Organization of the United Nations).

Frame, J., Charlton, J. F. L., and Laidlaw, A. S. (1998). *Temperate forage legumes* (Wallingford, Oxon, UK ; New York, NY, USA: CAB International).

Gkoutos, G. *Phenotype and trait ontology*. Available at: https://github.com/pato-ontology/pato/.

Gkoutos, G., Schofield, P., and Hoehndorf, R. (2012). The units ontology: a tool for integrating units of measurement int science. *Database*, bas033. doi: 10.1093/database/bas033

Gruber, T. (2009). *Ontology in encyclopedia of database systems*. Eds. L. Liu and M.T. Özsu. Springer-Verlag.

Hayot Carbonero, C., Mueller-Harvey, I., Brown, T. A., and Smith, L. (2011). Sainfoin (onobrychis viciifolia): a beneficial forage legume. *Plant Genet. Resour.* 9, 70–85. doi: 10.1017/S1479262110000328

Heinrichs, D. H. (1972). Root-zone temperature effects on flooding tolerance of legumes. *Can. J. Plant Sci.* 52, 985–990. doi: 10.4141/cjps72-169

Ilic, K., Kellogg, E. A., Jaiswal, P., Zapata, F., Stevens, P. F., Vincent, L. P., et al. (2007). The plant structure ontology, a unified vocabulary of anatomy and morphology of a flowering plant. *Plant Physiol.* 143, 587–599. doi: 10.1104/pp.106.092825

Irani, S., Majidi, M. M., and Mirlohi, A. (2015). Half-Sib matting and genetic analysis of agronomic, morphological, and physiological traits in sainfoin under nonstressed versus water-deficit conditions. *Crop Sci.* 55, 123–135. doi: 10.2135/cropsci2014.03.0235

Jaiswal, P., Avraham, S., Ilic, K., Kellogg, E. A., McCouch, S., Pujar, A., et al. (2005). Plant ontology (PO): a controlled vocabulary of plant structures and growth stages. *Comp. Funct. Genomics* 6, 388–397. doi: 10.1002/cfg.496

Juan, N. F. (1982) *Some effects of boron to the growth and chemical composition of sainfoin (Onobrychis viciaefolia scop.) : a thesis presented in partial fulfilment of the requirmeents for the degree of master of agricultural science in plant science at Massey university, palmerston north, new Zealand*. Available at: https://mro.massey.ac.nz/handle/10179/13712 (Accessed January 22, 2023).

Kempf, K., Malisch, C. S., Grieder, C., Widmer, F., and Kölliker, R. (2017). Marker-trait association analysis for agronomic and compositional traits in sainfoin (Onobrychis viciifolia). *Genet. Mol. Res.* 16 (1). doi: 10.4238/gmr16019483

Kölliker, R., Kempf, K., Malisch, C. S., and Lüscher, A. (2017). Promising options for improving performance and proanthocyanidins of the forage legume sainfoin (Onobrychis viciifolia scop.). *Euphytica* 213, 179. doi: 10.1007/s10681-017-1965-6

Langridge, P., and Fleury, D. (2011). Making the most of 'omics' for crop breeding. *Trends Biotechnol.* 29, 33–40. doi: 10.1016/j.tibtech.2010.09.006

Leonelli, S., Davey, R. P., Arnaud, E., Parry, G., and Bastow, R. (2017). Data management and best practice for plant science. *Nat. Plants* 3, 1–4. doi: 10.1038/nplants.2017.86

Li, Q., and Yan, J. (2020). Sustainable agriculture in the era of omics: knowledge-driven crop breeding. *Genome Biol.* 21, 1–5. doi: 10.1186/s13059-020-02073-5

Matteis, L., Chibon, P. Y., Espinosa, H., Skofic, M., Finkers, H. J., Bruskiewich, R., et al. (2013) *Crop ontology: vocabulary for crop-related concepts*. Available at: https://library.wur.nl/WebQuery/wurpubs/441015 (Accessed February 5, 2022).

Meyer, D. W., and Badaruddin, M. (2001). Frost tolerance of ten seedling legume species at four growth stages. *Crop Sci.* 41, 1838–1842. doi: 10.2135/cropsci2001.1838

Morales, N., Ogbonna, A. C., Ellerbrock, B. J., Bauchet, G. J., Tantikanjana, T., Tecle, I. Y., et al. (2022). Breedbase: a digital ecosystem for modern plant breeding. *G3 (Bethesda)* 12, jkac078. doi: 10.1093/g3journal/jkac078

Morrill, W. L., Ditterline, R. L., and Cash, S. D. (1998). Insect pests and associated root pathogens of sainfoin in western USA. *Field Crops Res.* 59, 129–134. doi: 10.1016/S0378-4290(98)00113-0

Papoutsoglou, E. A., Faria, D., Arend, D., Arnaud, E., Athanasiadis, I. N., Chaves, I., et al. (2020). Enabling reusability of plant phenomic datasets with MIAPPE 1.1. *New Phytol.* 227, 260–273. doi: 10.1111/nph.16544

Pietragalla, J., Valette, L., Shrestha, R., Laporte, M.-A., Hazekamp, T., and Arnaud, E. (2022) *Guidelines for creating crop-specific ontologies to annotate phenotypic data: version 2.1*. Available at: https://cgspace.cgiar.org/handle/10568/110906 (Accessed November 21, 2022).

Pujar, A., Jaiswal, P., Kellogg, E. A., Ilic, K., Vincent, L., Avraham, S., et al. (2006). Whole-plant growth stage ontology for angiosperms and its application in plant biology. *Plant Physiol.* 142, 414–428. doi: 10.1104/pp.106.085720

Raubach, S., Schreiber, M., and Shaw, P. D. (2022). GridScore: a tool for accurate, cross-platform phenotypic data collection and visualization. *BMC Bioinf.* 23, 214. doi: 10.1186/s12859-022-04755-2

Rife, T. W., and Poland, J. A. (2014). Field book: an open-source application for field data collection on android. *Crop Sci.* 54, 1624–1627. doi: 10.2135/cropsci2013.08.0579

Şakiroğlu, M. (2021). "Population genomics of perennial temperate forage legumes," in *Population genomics* (Cham: Springer International Publishing). doi: 10.1007/13836_2021_90

Schlautman, B., Barriball, S., Ciotir, C., Herron, S., and Miller, A. J. (2018). Perennial grain legume domestication phase I: criteria for candidate species selection. *Sustainability* 10, 730. doi: 10.3390/su10030730

Selby, P., Abbeloos, R., Backlund, J. E., Salido, M. B., Bauchet, G., Benites-Alfaro, O. E., et al. (2019). BrAPI–an application programming interface for plant breeding applications. *Bioinformatics* 35, 4147. doi: 10.1093/bioinformatics/btz190

Tarasenko, N., Butina, E., and Gerasimenko, E. (2015). Peculiarities of chemical composition of sainfoin seeds powder. *Orient. J. Chem.* 31, 1673–1682. doi: 10.13005/ojc/310346

Tittonell, P. (2020). Assessing resilience and adaptability in agroecological transitions. *Agric. Syst.* 184, 102862. doi: 10.1016/j.agsy.2020.102862

Tristram, H. B. (1885). *The survey of western Palestine: the fauna and flora of Palestine* (The Committee of the Palestine Exploration Fund: London).

Van Tassel, D. L., DeHaan, L. R., Diaz-Garcia, L., Hershberger, J., Rubin, M. J., Schlautman, B., et al. (2022). Re-imagining crop domestication in the era of high throughput phenomics. *Curr. Opin. Plant Biol.* 65, 102150. doi: 10.1016/j.pbi.2021.102150

Wieczorek, J., Bloom, D., Guralnick, R., Blum, S., Döring, M., Giovanni, R., et al. (2012). Darwin Core: an evolving community-developed biodiversity data standard. *PloS One* 7, e29715. doi: 10.1371/journal.pone.0029715

Wijekoon, C., Acharya, S. N., Siow, Y. L., Sura, S., Thandapilly, S., and Sabra, A. (2021). Canadian Sainfoin and fenugreek as forage and functional foods. *Crop Sci.* 61, 1–20. doi: 10.1002/csc2.20280

Woodman, H. E., and Evans, R. E. (1947). The chemical composition and nutritive value of ryegrass-seed meal, clover-seed meal, lucerne-seed meal and sainfoin-seed meal. *J. Agric. Sci.* 37, 311–315. doi: 10.1017/S0021859600008133

frontiers | Frontiers in Plant Science

TYPE Original Research
PUBLISHED 29 May 2023
DOI 10.3389/fpls.2023.1185393

OPEN ACCESS

EDITED BY
Philipp Von Gillhaussen,
Interantional Plant Phenotyping Network (IPPN), Germany

REVIEWED BY
Fiona R. Hay,
Aarhus University, Denmark
Rupesh Tayade,
Kyungpook National University, Republic of Korea

*CORRESPONDENCE
Huie Li
lihuiesh@126.com

RECEIVED 13 March 2023
ACCEPTED 02 May 2023
PUBLISHED 29 May 2023

CITATION
Dong R, Guo Q, Li H, Li J, Zuo W and Long C (2023) Estimation of morphological variation in seed traits of *Sophora moorcroftiana* using digital image analysis. *Front. Plant Sci.* 14:1185393. doi: 10.3389/fpls.2023.1185393

Estimation of morphological variation in seed traits of *Sophora moorcroftiana* using digital image analysis

Rui Dong[1], Qiqiang Guo[2], Huie Li[3]*, Jiangrong Li[4], Weiwei Zuo[3] and Cha Long[3]

[1]Department of Grassland Science, College of Animal Science, Guizhou University, Guiyang, China, [2]Institute for Forest Resources and Environment of Guizhou, Guizhou University, Guiyang, China, [3]College of Agriculture, Guizhou University, Guiyang, China, [4]Key Lab Forest Ecology Tibet Plateau, Ministry Education, Tibet Agriculture & Animal Husbandry University, Nyingchi, China

Sophora moorcroftiana is a leguminous plant endemic to the Qinghai-Tibet Plateau. It has excellent abiotic stress tolerance and is considered an ideal species for local ecological restoration. However, the lack of genetic diversity in the seed traits of *S. moorcroftiana* hinders its conservation and utilization on the plateau. Therefore, in this study, genotypic variation and phenotypic correlations were estimated for nine seed traits among 15 accessions of *S. moorcroftiana* over two years, 2014 and 2019, respectively from 15 sample points. All traits evaluated showed significant ($P< 0.05$) genotypic variation. In 2014, accession mean repeatability was high for seed perimeter, length, width, and thickness, and 100-seed weight. In 2019, mean repeatability for seed perimeter and thickness, and 100-seed weight were high. The estimates of mean repeatability for seed traits across the two years ranged from 0.382 for seed length to 0.781 for seed thickness. Pattern analysis showed that 100-seed weight was significantly positively correlated with traits such as seed perimeter, length, width, and thickness, and identified populations with breeding pool potential. In the biplot, principal components 1 and 2 explained 55.22% and 26.72% of the total variation in seed traits, respectively. These accessions could produce breeding populations for recurrent selection to develop *S. moorcroftiana* varieties suitable for restoring the fragile ecological environment of the Qinghai-Tibet Plateau.

KEYWORDS

***Sophora moorcroftiana*, seed traits, genotypic variation, image analysis, digital technologies**

1 Introduction

The Qinghai-Tibet Plateau, with an average altitude of more than 4,000 m above sea level (m a.s.l.), is called the "Roof of the World" or the "Third-Pole on Earth" (Chen et al., 2020). The area is approximately 2.5 million km^2, accounting for a fourth of China's total territorial land (Dong et al., 2020; Shi et al., 2021). Owing to its characteristics of high

terrain and low oxygen, the unique biological resources of the Qinghai-Tibet Plateau play a vital role in global biodiversity (Tao et al., 2020). At the same time, although different terrain and topography create a large number of diverse habitats for plants, the ecosystem in this region is fragile, and the vegetation is extremely sensitive to global climate change (Chen et al., 2020; Deng et al., 2020).

Sophora moorcroftiana (Benth.) Baker, is a perennial deciduous dwarf shrub of the legume family endemic to the Qinghai-Tibet Plateau. It has strong ecological adaptability, such as drought resistance, barren tolerance, and wind and sand resistance. It is mainly distributed in the valleys and hillsides of the Yarlung Zangbo River Basin at an altitude of 2,800–4,500 m above sea level (m a.s.l.) and is a dominant pioneer plant among drought-tolerant shrubs (Liu et al., 2020) and the preferred tree species for ecological restoration in the plateau. Further, low-polarity compounds contained in the seeds, such as matrine and sophocarpine, can be used to treat *Echinococcus granulosus* infections (Luo et al., 2018).

Seeds provide plants with an evolutionary advantage that allows them to survive and develop in drier places/times, store energy and nutrients to support initial development and growth, increase offspring fitness, and allow colonization and survival in adverse environments (Niklas et al., 2008; Lamont and Groom, 2013; Saatkamp et al., 2019). A range of seed morphological characteristics (e.g., seed size and epidermal characteristics) and physiological traits can coordinate the timing of seed germination under conditions suitable for seedling establishment (Saatkamp et al., 2019). In addition, both seed shape and size traits are useful for analyzing plant biodiversity and can be used to characterize intra- and inter-species variation as well as genotypic discrimination, and their correlation information is important for breeding, targeting seed yield and quality (Cervantes et al., 2016; Saatkamp et al., 2019; Khamassi et al., 2021). For example, seed mass has been identified as a key plant fitness-related trait, with larger seeds conferring advantages to plants in properties such as drought tolerance during seedling establishment, compared to small-seeded plants (Cochrane et al., 2015). This trait may reflect a trade-off for plants to develop short-term reductions in reproductive success (e.g., reduced seed production) with reduced long-term risk (Venable, 2007).

Compared to other plant organs such as flowers and leaves, using seed traits to characterize the genetic diversity of species has certain advantages because seeds are relatively easier to collect and store (Grillo et al., 2010). Pinna et al. (2014) used seed morphology parameters to analyze the interspecific, specific, and intraspecific levels of 10 *Juniperus* populations collected from the Mediterranean. Khamassi et al. (2021) characterized and evaluated the seed morphology of 24 local faba bean (*Vicia faba*) accessions and found that accessions with a white hilum were associated with lower mature grain content. Bacchetta et al. (2008) measured seed morphological characteristics for 220 accessions in the Sardinian Germplasm Bank using digital image analysis techniques and concluded that the method could be used to identify very similar taxa in these species with an accuracy of 83.7%–100%. At present, the precise quantification of seed morphological characteristics is facilitated by the development and use of digital techniques, quantification, and modeling methods (Cervantes et al., 2016).

Therefore, in this study, the variation in seed morphological characteristics of 15 *S. moorcroftiana* populations collected from different locations on the Qinghai-Tibet Plateau was studied using digital image analysis techniques. Our research focused on estimating the genetic variation within and among populations. In addition, a combination of potentially beneficial seed traits has been evaluated in breeding programs. This study aimed to provide data support for the genetic diversity and taxonomy of *S. moorcroftiana*, and to provide valuable parameters and information for the selection and breeding of strong adaptability *S. moorcroftiana* varieties.

2 Materials and methods

2.1 Germplasm

The seed resources of 15 accessions were evaluated in this study. *S. moorcroftiana* seeds were collected at 15 sampling points during October 1–7, 2014, and October 1–7, 2019 (Figure 1). The collected seeds were dried to a moisture content of 6%–8% and stored at 4°C and 30%–50% relative humidity. The climate data of the sampling points are provided by the meteorological data center of the China meteorological administration.

2.2 Trait measurements

Nine seed traits were measured: SL, seed length (mm); SW, seed width (mm); W/L, seed width to seed length ratio; HL, hilum length (mm); HW, hilum width (mm); HW/HL, hilum width to hilum length ratio; Pe, perimeter (mm); ST, seed thickness (mm) and SY, 100-seed weight (g). 100 seeds were manually counted. Use an electronic balance (Sartorius, BSA224S-CW, China) for weighing. Before trait measurements, a flatbed scanner (EPSON GT-15000) was used to obtain digital images of the seed samples. During the scan, the seeds were allowed to equilibrate before measurement (room temperature was maintained at 20 ± 3°C and 40 ± 5% relative humidity) (Grillo et al., 2010). The scanned image resolution was 200 dpi, and the number of pixels was 1024 × 1024.

Three replicates were scanned for each population and each replicate included 100 seeds. Seed samples were prepared and scanned according to methods described by Venora et al. (2007); Bacchetta et al. (2008), and Dong et al. (2016). A WinSEEDLE 2011 image analysis system was used to process the acquired images (Dong et al., 2016).

2.3 Data analysis

Data analysis was based on (1) variance component analysis to assess the magnitude and significance of genotypic variation between populations and (2) pattern analysis, including a

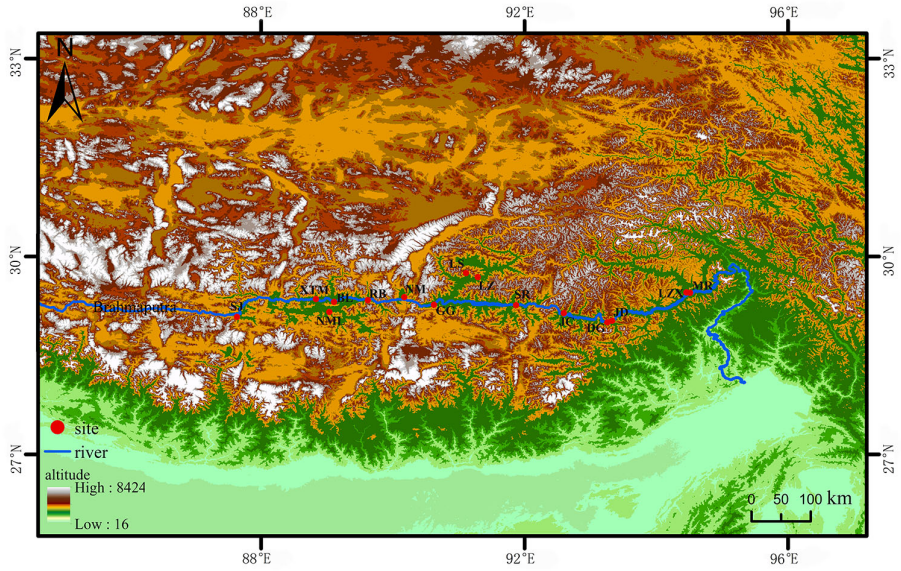

FIGURE 1
The distribution of 15 *S. moorcroftiana* accessions used in this study. The red dots represent the sampling points. LZX, Lin zhi; NML, Nan mu lin; GG, Gong ga; RB, Ren bu; JC, Jia cha; LS, La sa; JD, Jin dong; BL, Bai lang; XTM, Xie tong men; DG, Dong ga; SJ, Sa jia; NM, Ni mu; SR, Sang ri; MR, Mi rui; LZ, Lin zhou.

combination of clustering and principal component analysis (PCA) (Dong et al., 2016; Dong et al., 2019) to provide a graphical summary of the multi-trait data matrices.

Data on seed traits from 15 *S. moorcroftiana* population accessions were analyzed within and over two years (2014 and 2019). The analyses were conducted using the variance component analysis procedure, residual maximum likelihood (REML), in GenStat 7.1 (2003) (Dong et al., 2019). Analysis of data over the years was performed using a mixed linear model (Dong et al., 2019).

All seed trait means were derived from the best linear unbiased predictor (BLUP) analysis (White and Hodge 1989; Dong et al., 2019). These BLUP values were used to build a population × trait mean matrix adjusted for population × year interaction effects.

Referring to Fehr (1987) method, the estimated genotypic (σ_g^2), genotype × year interaction (σ_{gl}^2), experimental error (σ_ε^2), *nl* (number of years), and *nr* (number of replications) obtained from REML analysis were used to estimate the population accession mean repeatability (*R*).

Accession mean repeatability within a single year:

$$R_1 = \frac{\sigma_g^2}{\sigma_g^2 + \frac{\sigma_\varepsilon^2}{n_r}} \quad (1)$$

Accession mean repeatability across years:

$$R_2 = \frac{\sigma_g^2}{\sigma_g^2 + \frac{\sigma_{gl}^2}{n_l} + \frac{\sigma_\varepsilon^2}{n_l n_r}} \quad (2)$$

Phenotypic correlation (*rp*) analysis was performed using GenStat 7.1 (2003), and multivariate analysis of variance (MANOVA) was used to assess accessions for 15 populations over two years, resulting in the sum of the estimated cross-products of the multi-trait data matrix.

Pattern analysis is a combination of cluster analysis and principal component analysis (PCA): a) based on the variance components over the two years 2014 and 2019 to obtain an adjusted mean matrix of genotype × trait BLUP and finally obtain a graphical summary of accession traits for eight populations; and b) to analyze the type of association (positive or negative) among the nine seed traits in 2014 and 2019.

3 Results

3.1 Genotypic variance components and the mean repeatability of nine seed traits of *S. moorcroftiana*

The genotypic variance components of the nine seed traits in 2014 and 2019 showed significant differences ($P< 0.05$) for all the traits evaluated in the 15 *S. moorcroftiana* accessions (Tables 1, 2).

In 2014, accession mean repeatability (*R1*) was high for seed perimeter, length, width, and thickness, and 100-seed weight, ranging from 0.933 to 0.992 (Table 1; Supplementary Figure 1A). The *R1* values for the hilum length, width, and hilum length/width ratio were intermediate, ranging from 0.633 to 0.697. *R1* for seed width/seed length was the lowest at 0.058. In 2019, *R1* for seed perimeter and thickness, and 100-seed weight were high, ranging from 0.846 to 0.991 (Table 2; Supplementary Figure 1B). *R1* for seed length, hilum length and width, and hilum length/width ratio were intermediate, ranging from 0.604 to 0.767. *R1* values for seed width and seed width/length ratio were lower than those of the other traits (0.489 and 0.054, respectively).

Analysis of variance for over two years, 2014 and 2019, showed significant genotypic variation ($P< 0.05$) among the 15 *S.*

TABLE 1 Average, maximum, minimum, least significant differences ($l.s.d._{0.05}$), estimated genotypic (σ_g^2) and experimental error (σ_e^2) variance components and associated standard errors (± SE), and mean repeatability (R_1) estimated from the 15 *S. moorcroftiana* accessions, evaluated in 2014.

Traits	Perimeter	Seed Length	Seed Width	Seed width/ Seed Length	Hilum length	Hilum width	Hilum width/ Hilum length	Seed thickness	100-seed weight
Average	14.661	4.453	4.405	0.990	1.790	1.295	0.725	3.594	0.791
Min	13.626	4.157	4.066	0.951	1.612	1.171	0.683	3.305	0.553
Max	15.262	4.644	4.611	1.023	1.918	1.516	0.797	3.711	0.900
$l.s.d._{0.05}$	0.491*	0.157*	0.143*	0.044*	0.117*	0.093*	0.040*	0.107*	0.064*
σ_g^2	0.211 ± 0.091	0.016 ± 0.007	0.016 ± 0.007	0.001 ± 0.001	0.004 ± 0.002	0.133 ± 0.359	0.141 ± 0.097	0.010 ± 0.004	0.009 ± 0.004
σ_e^2	0.086 ± 0.023	0.007 ± 0.002	0.008 ± 0.002	0.007 ± 0.002	0.005 ± 0.001	0.152 ± 0.549	0.186 ± 0.016	0.004 ± 0.001	0.001 ± 0.003
R_1	0.948	0.939	0.933	0.058	0.688	0.697	0.633	0.949	0.992

* indicates significance at P< 0.05.

moorcroftiana accessions for nine seed traits (Table 3). The mean repeatability (*R2*) of hilum length/width and seed thickness was higher than that of the other traits (0.757 and 0.781, respectively). The *R2* values for the hilum length and width, and 100-seed weight were intermediate at 0.597, 0.643, and 0.626, respectively. *R2* for seed perimeter, length, width, and width/length ratio were lower than those for the other traits, ranging from 0.097 to 0.493.

3.2 Pattern analysis and phenotypic correlation of *S. moorcroftiana*

In 2014, based on phenotypic correlation analysis, there was a positive correlation between 100-seed weight and seed perimeter, length, width, and thickness (Table 4). Seed perimeter, length, and width also exhibited strong positive correlations at the phenotypic level. In the biplot, principal components 1 and 2 explained 53.88% and 24.26% of the total variation in seed traits, respectively (Figure 2). The BLUP mean matrix of nine seed traits was used for the cluster analysis grouping of 15 *S. moorcroftiana* accessions in 2014, truncated at the group three level. According to the trait means for each group, Group 1 had the highest mean seed perimeter, length, width, and width/length ratio, hilum length, width, and length/width ratio, and 100-seed weight and included two accessions (Supplementary Table 1).

In 2019, the phenotypic correlation analysis showed that 100-seed weight, seed perimeter, length, width, and thickness showed strong positive correlations at the phenotypic level (Table 5). In the

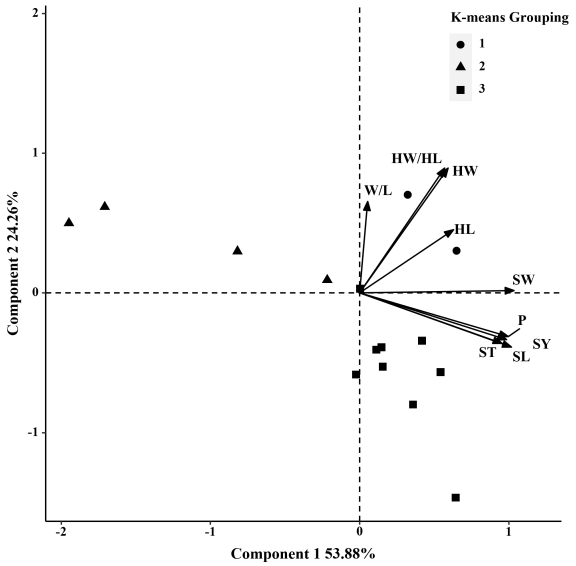

FIGURE 2
Biplot generated using standardized Best Linear Unbiased Predictor values for nine seed traits measured from 15 *S. moorcroftiana* accessions, evaluated in 2014. Components I and II account for 53.88% and 24.26% of total variation, respectively. The different symbols indicate progeny Groups 1 to 3 generated from cluster analysis.

TABLE 2 Average, maximum, minimum, least significant differences ($l.s.d._{0.05}$), estimated genotypic (σ_g^2) and experimental error (σ_e^2) variance components and associated standard errors (± SE), and mean repeatability (R_1) estimated from the 15 *S. moorcroftiana* accessions, evaluated in 2019.

Traits	Perimeter	Seed Length	Seed Width	Seed width/ Seed Length	Hilum length	Hilum width	Hilum width/ Hilum length	Seed thickness	100-seed weight
Average	14.959	4.592	4.554	0.992	1.773	1.307	0.738	3.730	0.876
Min	14.427	4.453	4.379	0.978	1.695	1.242	0.704	3.561	0.548
Max	15.340	4.706	4.720	1.010	1.856	1.368	0.806	3.846	0.995
$l.s.d._{0.05}$	0.851*	0.263*	0.214*	0.034*	0.110*	0.070*	0.045*	0.113*	0.094*
σ^2_g	0.327 ± 0.068	0.018 ± 0.006	0.009 ± 0.008	0.008 ± 0.001	0.002 ± 0.002	0.001 ± 0.001	0.007 ± 0.001	0.007 ± 0.005	0.020 ± 0.011
σ^2_e	0.242 ± 0.092	0.023 ± 0.009	0.017 ± 0.006	0.059 ± 0.001	0.003 ± 0.001	0.002 ± 0.001	0.007 ± 0.002	0.004 ± 0.002	0.003 ± 0.001
R_1	0.846	0.648	0.489	0.054	0.604	0.715	0.767	0.890	0.991

* indicates significance at P< 0.05.

biplot, principal component 1 explained 70.74% of the total seed trait variation and principal component two explained 15.39% (Figure 3). The 15 *S. moorcroftiana* accession groups generated from the cluster analysis were truncated at the two-group level. The results showed that the second group had a higher seed perimeter, length, width, thickness and width/length ratio, hilum length, and 100-seed weight (Supplementary Table 2).

In 2014 and 2019, based on the phenotypic correlation analysis, 100-seed weight showed a strong positive correlation with seed perimeter, length, width, and thickness at the phenotypic level and a strong negative correlation with hilum length/width ratio (Table 6). In the biplot, principal components 1 and 2 explained 55.22% and 26.72% of the total variation in seed traits, respectively (Figure 4). The 15 *S. moorcroftiana* accession groups generated from the cluster analysis were truncated at the three-group level. The third group of accessions had higher seed perimeter, seed length, width, width/length ratio, thickness, and 100-seed weight, including five accessions (Supplementary Table 3). Furthermore, in 2014 and 2019, the seed traits perimeter, hilum length/width ratio, seed thickness, and 100-seed weight were all significantly correlated with altitude, and hilum length/width ratio, seed thickness, and 100-seed were significantly correlated with the monthly average maximum temperature, monthly average minimum temperature, and monthly average temperature during the growing season (Supplementary Figure 2).

4 Discussion

Numerous studies have shown that structural diversity in seed traits helps characterize both intra- and inter-species variation. Therefore, the study of macro- and micro-seed traits is important in quantifying genetic diversity and plant taxonomy (Barthlott, 1981; Grillo et al., 2010).

Previous studies on *S. moorcroftiana* have mainly focused on its population distribution (Liu et al., 2020; Xin et al., 2021; Yang et al.,

TABLE 3 Average, maximum, minimum, least significant differences ($l.s.d._{0.05}$), estimated genotypic (σ_g^2), genotype × year interaction (σ_{gy}^2) and experimental error (σ_e^2) variance components and associated standard errors (± SE), and mean repeatability (R_2) estimated from the 15 *S. moorcroftiana* accessions, evaluated across two years, 2014 and 2019.

Traits	Perimeter	Seed Length	Seed Width	Seed width/ Seed Length	Hilum length	Hilum width	Hilum width/ Hilum length	Seed thickness	100-seed weight
Average	14.778	4.522	4.470	0.989	1.782	1.297	0.729	3.652	0.830
Min	13.626	4.157	4.066	0.951	1.612	1.171	0.683	3.305	0.548
Max	15.340	4.706	4.720	1.023	1.918	1.516	0.806	3.846	0.995
$l.s.d._{0.05}$	0.551*	0.182*	0.181*	0.025*	0.108*	0.083*	0.035*	0.136*	0.134*
σ^2_g	0.055 ± 0.017	0.043 ± 0.006	0.072 ± 0.005	0.068 ± 0.000	0.180 ± 0.002	0.260 ± 0.221	0.016 ± 0.062	0.058 ± 0.001	0.099 ± 0.006
σ^2_e	0.154 ± 0.054	0.016 ± 0.006	0.111 ± 0.004	0.042 ± 0.001	0.080 ± 0.003	0.450 ± 0.142	0.382 ± 0.135	0.004 ± 0.001	0.003 ± 0.001
σ^2_{gy}	0.005 ± 0.001	0.005 ± 0.002	0.008 ± 0.003	0.046 ± 0.001	0.052 ± 0.004	0.069 ± 0.030	0.003 ± 0.080	0.004 ± 0.003	0.015 ± 0.009
R_2	0.441	0.382	0.493	0.097	0.597	0.643	0.757	0.781	0.626

* indicates significance at P< 0.05.

TABLE 4 Phenotypic (r_p) correlation coefficients, between traits based on the 15 *S. moorcroftiana* accessions, evaluated in 2014.

Traits	Perimeter	Seed Length	Seed Width	Seed width/Seed Length	Hilum length	Hilum width	Hilum width/ Hilum length	Seed thickness
Seed Length	0.947**							
Seed Width	0.846**	0.825**						
Seed width/Seed Length	-0.220	-0.346*	0.245					
Hilum length	0.384**	0.388**	0.382**	-0.033				
Hilum width	0.017	-0.010	0.014	0.038	0.133			
Hilum width/ Hilum length	-0.006	-0.033	-0.010	0.040	0.072	0.998**		
Seed thickness	0.680**	0.725**	0.755**	0.009	0.288*	-0.176	-0.195	
100-seed weigh	0.668**	0.728**	0.764**	0.024	0.424**	-0.011	-0.038	0.833**

*, ** indicates significant at P< 0.05 and P< 0.01 levels, respectively.

2021), soil seed banks (Zhao et al., 2007), medicinal functions (Wang et al., 2014; Luo et al., 2018), analysis of transcriptome (Li et al., 2015) and verification of gene functions (Li et al., 2017). In this study, we report, for the first time, the phenotypic and genotypic variations in nine seed traits and the mean repeatability of 15 accessions of *S. moorcroftiana*.

In nature, plants growing in various environments have evolved adaptive traits related to seed morphology and physiology to cope with adverse environments, such as variability in seed size, seed dormancy characteristics, and a special structure that maintains the reproduction and spread of the population (Venable and Brown, 1988; Luzuriaga et al., 2006). These seed traits are mainly determined by the seed genotype and parental environment (Schmitt et al., 1992). At the same time, parental effects also include the result of the interaction of genotype and maternal environment. The influence of parents on offspring is partly determined by genes; therefore, they are evolvable (Lacey, 1998). In the present study, seed perimeter, seed thickness, and 100-seed weight all had high *R1* values in a single year, whereas hilum length/ hilum width and seed thickness had high *R2* values across years. The relatively high genotypic variation in these traits indicated potential genetic variation among the 15 *S. moorcroftiana* accessions that could be used for selection and breeding (Dong et al., 2019). Furthermore, these seed trait variation reflects the result of genetic variation and phenotypic plasticity in response to environmental variation (Wang et al., 2023). This information helps to understand the response mechanism and variation rules of plants to the environment, which is important for the collection, preservation and evaluation of germplasm resources.

The size and weight of seeds produced by different plant species vary widely. A previous study found that seed size showed different characteristics during the growth and development of plant offspring (Moles et al., 2005). Small-seeded plant species can produce more seeds than large-seeded plant species for a given amount of energy. However, seedlings of large-seeded plant species are more resilient to biotic and abiotic stresses during their establishment. Small-seeded plant species adopt another strategy for winning by quantity: producing as many offspring as possible to ensure their survival. This suggests that traits such as seed size and weight of different species grown in a specific environment can have

TABLE 5 Phenotypic (r_p) correlation coefficients, between traits based on the 15 *S. moorcroftiana* accessions, evaluated in 2019.

Traits	Perimeter	Seed Length	Seed Width	Seed width/Seed Length	Hilum length	Hilum width	Hilum width/ Hilum length	Seed thickness
Seed Length	0.865**							
Seed Width	0.811**	0.658**						
Seed width/Seed Length	-0.068	-0.419**	0.408**					
Hilum length	0.227	0.266	0.301*	0.040				
Hilum width	0.014	0.025	0.131	0.126	0.252			
Hilum width/ Hilum length	0.005	0.014	0.117	0.122	0.205	0.998**		
Seed thickness	0.622**	0.641**	0.636**	-0.006	0.377*	0.012	-0.012	
100-seed weigh	0.710**	0.793**	0.747**	-0.058	0.313*	0.062	0.047	0.762**

*, ** indicates significant at P< 0.05 and P< 0.01 levels, respectively.

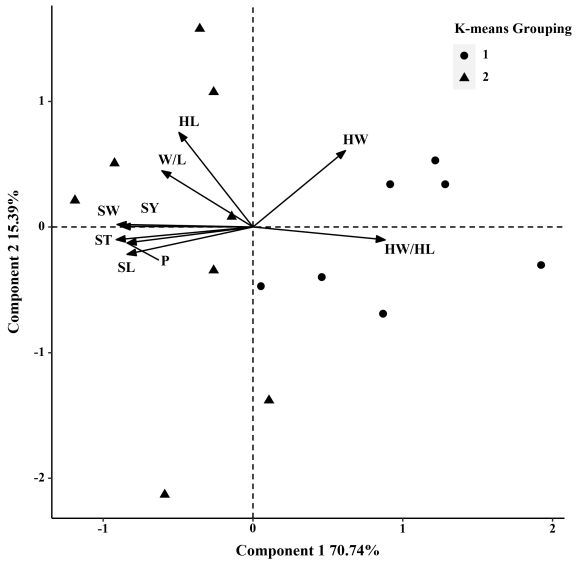

FIGURE 3
Biplot generated using standardized Best Linear Unbiased Predictor values for nine seed traits measured from 15 *S. moorcroftiana* accessions, evaluated in 2019. Components I and II account for 70.74% and 15.39% of total variation, respectively. The different symbols indicate progeny Groups 1 and 2 generated from cluster analysis.

a major impact on seedling establishment and survival (Dong et al., 2016). Therefore, information on the genetic variation in key seed-size traits in breeding materials will facilitate the execution of various developmental programs (Odiaka, 2005). In this study, the ranges of seed perimeter, seed thickness, and 100-seed weight reflecting seed size and quality were 13.626–15.262 mm, 3.305–3.711 mm, and 0.553–0.900 g in 2014 and 14.427–15.340 mm, 3.561–3.846 mm, and 0.548–0.995 g in 2019, respectively; the *R1* of these traits was higher than 0.8, and the *R2* of seed thickness and 100-seed weight were higher than 0.6. This suggests that these traits are mainly affected by the genotype and can provide valuable information for *S. moorcroftiana* breeding. In addition, seed thickness, length, width, and perimeter, and 100-seed weight showed extremely significant positive correlations between the two years, indicating that changes in any trait may significantly affect seed weight. This result indicated that these traits were mainly determined by seed genotype and that changes in either trait could significantly affect seed weight. This positive correlation has important commercial and practical implications for breeding programs (Amiri et al., 2010; Dong et al., 2019). At the same time, variability in seed size affects seed dispersal in a variety of ways. Because smaller seeds are usually dispersed further by abiotic factors such as water and wind. This is closely related to the external environment such as the altitude, slope, temperature and rainfall of the population (Liao et al., 2020; Yang et al., 2021). This was also supported by the correlations between seed traits and altitude and

TABLE 6 Phenotypic (r_p) correlation coefficients, between traits based on the 15 *S. moorcroftiana* accessions, evaluated across two years, 2014 and 2019.

Traits	Perimeter	Seed Length	Seed Width	Seed width/Seed Length	Hilum length	Hilum width	Hilum width/ Hilum length	Seed thickness
Seed Length	0.954**							
Seed Width	0.907**	0.834**						
Seed width/Seed Length	-0.081	-0.286	0.289					
Hilum length	0.466*	0.434*	0.467*	0.058				
Hilum width	-0.053	-0.079	-0.215	-0.242	0.299			
Hilum width/ Hilum length	-0.443*	-0.436*	-0.582**	-0.259	-0.610**	0.572**		
Seed thickness	0.599**	0.584**	0.755**	0.303	0.312	-0.554**	-0.735**	
100-seed weigh	0.562**	0.569**	0.717**	0.266	0.452*	-0.520**	-0.832**	0.859**

*, ** indicates significant at P< 0.05 and P< 0.01 levels, respectively.

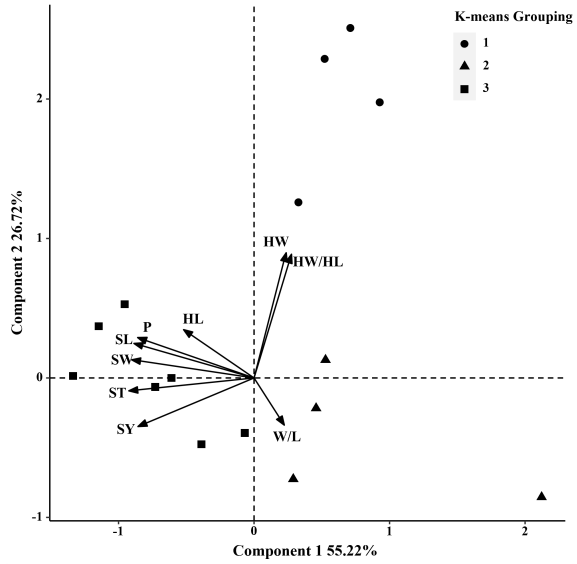

FIGURE 4
Biplot generated using standardized Best Linear Unbiased Predictor values for nine seed traits measured from 15 *S. moorcroftiana* accessions, evaluated across two years, 2014 and 2019. Components I and II account for 55.22% and 26.72% of total variation, respectively. The different symbols indicate progeny Groups 1 to 3 generated from cluster analysis.

temperature in this study. This phenomenon has important implications for individual reproductive success, community structure, and biodiversity patterns of plants (Snell et al., 2019).

In previous studies, pattern analysis has been successfully used to analyze nine environmental and nine genotype trait data matrices (Jahufer et al., 1997; Zhang et al., 2006; Luo et al., 2016). Jahufer et al. (1997) used pattern analysis to analyze 439 white clover germplasm resources and screened out germplasm populations characterized by large leaves, tall plants, and thick stolons, which could be used to develop varieties that can tolerate summer drought stress environments. Dong et al. (2019) analyzed the genotypic and phenotypic variation of 18 traits of 418 common vetch germplasms based on pattern analysis and obtained germplasm populations with low shattering rates, high seed yields, and high plant dry weights, which can be used for common vetch breeding programs with high seed yield and high dry plant weight. Similarly, in this study, we obtained germplasm populations with higher seed sizes and 100-seed weights using pattern analysis. These accessions could be used in *S. moorcroftiana* breeding programs with high seedling establishment success rates to adapt to the harsh natural conditions of the Qinghai-Tibet Plateau.

Seed size, shape, and epidermal surface characteristics of plants play important roles in plant morphological diversity, and these seed morphological characteristics can provide data for taxa at different taxonomic levels (Ocampo et al., 2014). In addition, the seed characteristics of plants are different from their floral features, which are generally considered to be more conserved and thus can provide valuable information on the evolutionary history of flowering plants (Barthlott, 1981). Becquer et al. (2014) studied seed shape and size, raphe shape and size, and seed coat surface morphology data of 47 Compositae species from the Antilles, providing information for phylogenetic reconstruction and trait evolution analysis. In this study, the genotypic variation in different seed traits of each accession was significantly different ($P < 0.05$), which may help to investigate their taxonomic relationships. Analysis of the seed morphological characteristics of *S. moorcroftiana* showed that the JC, JD, SR, and BL accessions were significantly different ($P < 0.05$) from the GG, RB, NML, XTM, NM, DG, and SJ accessions, which could be divided into two groups. Our study shows that these heterogeneous seed traits can provide valuable information on the evolutionary relationship of *S. moorcroftiana*, and the seed morphology database has the potential for taxonomic screening (Dell'Aquila, 2007).

Nondestructive studies based on the plant seed characterization have proven to be an informative, noninvasive, and suitable tool for differentiating germplasm resources (Sinkovič et al., 2019). The results obtained in this study are serving as the useful information on genetic diversity, plant classification and breeding of *S. moorcroftiana* accessions, which could be used for future research on the evolution, classification and population restoration of *S. moorcroftiana*.

5 Conclusion

This study estimated the phenotypic correlation, genotypic variation, and mean repeatability of nine seed traits in 15 *S. moorcroftiana* accessions. Seed perimeter, seed thickness, and 100-seed weight showed high mean repeatability over two years (2014 and 2019), indicating their potential for genetic improvement. Pattern analysis showed that the 100-seed weight was significantly and positively correlated with seed perimeter,

length, width, and thickness. The significant correlation between these traits provides key information for *S. moorcroftiana* breeding programs that focus on developing varieties with high seedling establishment success rates. This study not only deepens our understanding of the genetic diversity of *S. moorcroftiana* seed morphological traits but also provides important information for the development of breeding banks.

Data availability statement

The original contributions presented in the study are included in the article/Supplementary Material. Further inquiries can be directed to the corresponding author.

Author contributions

RD and HL conceived the experiment. QG and JL collected the seeds. WZ and CL carried out the experiment. RD and QG analyzed the data. RD and HL wrote the paper. All the authors contributed to the manuscript and approved the submitted version. All authors contributed to the article and approved the submitted version.

Funding

This research was supported by the National Natural Science Foundation of China (31960320 and 32060392) and the Guizhou Province Science and Technology Projects (Qian Ke He Zhi Cheng [2020]1Y074), Qian Ke He Cheng Guo ([2022] Zhong Dian 005), and the GZMARS-Forage Industry Technology System of Guizhou Province.

Acknowledgments

We thank Baocheng Jin and Jinping Zhang (Guizhou University, China) for their valuable help and advice on the GS figures.

Conflict of interest

The authors declare that the research was conducted in the absence of any commercial or financial relationships that could be construed as a potential conflict of interest.

Publisher's note

Supplementary material

The Supplementary Material for this article can be found online at: https://www.frontiersin.org/articles/10.3389/fpls.2023.1185393/full#supplementary-material

References

Amiri, R., Vahdati, K., Mohsenipoor, S., Mozaffari, M. R., and Leslie, C. (2010). Correlations between some horticultural traits in walnut. *HortScience* 45, 1690–1694. doi: 10.21273/HORTSCI.45.11.1690

Bacchetta, G., Grillo, O., Mattana, E., and Venora, G. (2008). Morpho-colorimetric characterisation by image analysis to identify diaspores of wild plant species. *Flora.* 203, 669–682. doi: 10.1016/j.flora.2007.11.00

Barthlott, W. (1981). Epidermal and seed surface characters of plants: systematic applicability and some evolutionary aspects. *Nord. J. Bot.* 1, 345–355. doi: 10.1111/j.1756-1051.1981.tb00704.x

Becquer, E. R., Michelangeli, F. A., and Borsch, T. (2014). Comparative seed morphology of the antillean genus *Calycogonium* (*Melastomataceae: miconieae*) as a source of characters to untangle its complex taxonomy. *Phytotaxa* 166, 241–258. doi: 10.11646/phytotaxa.166.4.1

Cervantes, E., Martín, J. J., and Saadaoui, E. (2016). Updated methods for seed shape analysis. *Scientifica* 2016, 5691825. doi: 10.1155/2016/5691825

Chen, F., Zhang, J., Liu, J., Cao, X., Hou, J., Zhu, L., et al. (2020). Climate change, vegetation history, and landscape responses on the Tibetan plateau during the Holocene: a comprehensive review. *Quat. Sci. Rev.* 243, 106444. doi: 10.1016/j.quascirev.2020.106444

Cochrane, A., Yates, C. J., Hoyle, G. L., and Nicotra, A. B. (2015). Will among-population variation in seed traits improve the chance of species persistence under climate change? *Glob. Ecol. Biogeogr.* 24, 12–24. doi: 10.1111/geb.12234

Dell'Aquila, A. (2007). Towards new computer imaging techniques applied to seed quality testing and sorting. *Seed Sci. Technol.* 35, 519–538. doi: 10.15258/sst.2007.35.3.01

Deng, T., Wu, F., Zhou, Z., and Su, T. (2020). Tibetan Plateau: an evolutionary junction for the history of modern biodiversity. *Sci. China Earth Sci.* 63, 172–187. doi: 10.1007/s11430-019-9507-5

Dong, R., Jahufer, M. Z. Z., Dong, D. K., Wang, Y. R., and Liu, Z. P. (2016). Characterisation of the morphological variation for seed traits among 537 germplasm accessions of common vetch (*Vicia sativa* l.) using digital image analysis. *New Z. J. Agric. Res.* 59, 422–435. doi: 10.1080/00288233.2016.1229682

Dong, S., Shang, Z., Gao, J., and Boone, R. B. (2020). Enhancing sustainability of grassland ecosystems through ecological restoration and grazing management in an era of climate change on qinghai-Tibetan plateau. *Agric. Ecosyst. Environ.* 287, 106684. doi: 10.1016/j.agee.2019.106684

Dong, R., Shen, S. H., Jahufer, M. Z., Dong, D. K., Luo, D., Zhou, Q., et al. (2019). Effect of genotype and environment on agronomical characters of common vetch (*Vicia sativa* l.). *Genet. Resour. Crop Evol.* 66, 1587–1599. doi: 10.1007/s10722-019-00789-3

Grillo, O., Mattana, E., Venora, G., and Bacchetta, G. (2010). Statistical seed classifiers of 10 plant families representative of the Mediterranean vascular flora. *Seed Sci. Technol.* 38, 455–476. doi: 10.15258/sst.2010.38.2.19

Jahufer, M. Z. Z., Cooper, M., and Harch, B. D. (1997). Pattern analysis of the diversity of morphological plant attributes and herbage yield in a world collection of white clover (*Trifolium repens* l.) germplasm characterised in a summer moisture stress environment of Australia. *Genet. Resour. Crop Evol.* 44, 289–300. doi: 10.1023/A:1008692629734

Khamassi, K., Babay, E., Rouissi, M., Dakhlaoui, A., Ben Ayed, R., and Hanana, M. (2021). Genetic variability of Tunisian faba beans (*Vicia faba* l.) based on seeds' morphophysical properties as assessed by statistical analysis. *J. Food Qual.* 2021, 1–10. doi: 10.1155/2021/9493607

Lacey, E. P. (1998). "What is an adaptive environmentally induced parental effect?," in *Maternal effects as adaptations*. Eds. T. A. Mousseau and C. W. Fox (New York: Oxford Univ. Press), 54–66.

Lamont, B., and Groom, P. (2013). Seeds as a source of carbon, nitrogen, and phosphorus for seedling establishment in temperate regions: a synthesis. *AJPS.* 4, 30–40. doi: 10.4236/ajps.2013.45A005

Li, H., Yao, W., Fu, Y., Li, S., and Guo, Q. (2015). *De novo* assembly and discovery of genes that are involved in drought tolerance in Tibetan sophora moorcroftiana. *PloS One* 10, e111054. doi: 10.1371/journal.pone.0111054

Li, H., Zhang, Y., Guo, Q., and Yao, W. (2017). Molecular characterisation of a DREB gene from sophora moorcroftiana, an endemic species of plateau. *Protoplasma* 254, 1735–1741. doi: 10.1007/s00709-016-1065-9

Liao, C., Li, H., Lv, G., Tian, M., Tian, J., Shi, H., et al (2020) Stability and micro-topography effects of sophora moorcroftiana community for fixation of sandy land under natural restoration, southern Tibetan plateau. *Authorea*. doi: 10.22541/au.158679907.75173603

Liu, Y., Yi, F., Yang, G., Wang, Y., Pubu, C., He, R., et al. (2020). Geographic population genetic structure and diversity of sophora moorcroftiana based on genotyping-by-sequencing (GBS). *PeerJ* 8, e9609. doi: 10.7717/peerj.9609

Luo, K., Jahufer, M. Z. Z., Wu, F., Di, H. Y., Zhang, D. Y., Meng, X. C., et al. (2016). Genotypic variation in a breeding population of yellow sweet clover (*Melilotus officinalis*). *Front. Plant Sci.* 7. doi: 10.3389/fpls.2016.00972

Luo, Y., Zhang, G., Liu, X., Yuan, M., Gao, Q., Gao, H., et al. (2018). Therapeutic and immunoregulatory effects of water-soluble alkaloids E2-a from sophora moorcroftiana seeds as a novel potential agent against echinococcosis in experimentally protoscolex-infected mice. *Vet. Res.* 49, 1–13. doi: 10.1186/s13567-018-0596-9

Luzuriaga, A. L., Escudero, A., and Pérez-García, F. (2006). Environmental maternal effects on seed morphology and germination in sinapis arvensis (Cruciferae). *Weed Res.* 46, 163–174. doi: 10.1111/j.1365-3180.2006.00496.x

Moles, A. T., Ackerly, D. D., Webb, C. O., Tweddle, J. C., Dickie, J. B., and Westoby, M. (2005). A brief history of seed size. *Sci.* 307, 576–580. doi: 10.2307/3840005

Niklas, K. J., Leck, M. A., Parker, V. T., and Simpson, R. L. (2008). *Embryo morphology and seedling evolution. seedling ecology and evolution*. Eds. M. A. Leck, V. T. Parker and R. L. Simpson (Cambridge: Cambridge University Press), 103–129.

Ocampo, G., Michelangeli, F. A., and Almeda, F. (2014). Seed diversity in the tribe miconieae (*Melastomataceae*): taxonomic, systematic, and evolutionary implications. *PloS One* 9, e100561. doi: 10.1371/journal.pone.0100561

Odiaka, N. (2005). Morphological diversity among local germplazm of fluted pumpkin collected in makurdi, Nigeria. *J. Food Agr Environ.* 3, 199–204.

Pinna, M. S., Grillo, O., Mattana, E., Cañadas, E. M., and Bacchetta, G. (2014). Inter- and intraspecific morphometric variability in *Juniperus* l. seeds (Cupressaceae). *System. Biodivers.* 12, 211–223. doi: 10.1080/14772000.2014.904827

Saatkamp, A., Cochrane, A., Commander, L., Guja, L. K., Jimenez-Alfaro, B., Larson, J., et al. (2019). A research agenda for seed-trait functional ecology. *New Phytol.* 221, 1764–1775. doi: 10.1111/nph.15502

Schmitt, J., Niles, J., and Wulff, R. D. (1992). Norms of reaction of seed traits to maternal environments in plantago lanceolata. *Am. Nat.* 139, 451–466. doi: 10.1086/285338

Shi, W., Qiao, F., and Zhou, L. (2021). Identification of ecological risk zoning on qinghai-tibet plateau from the perspective of ecosystem service supply and demand. *Sustainability* 13, 5366–466. doi: 10.3390/su13105366

Sinkovič, L., Pipan, B., Sinkovič, E., and Meglič, V. (2019). Morphological seed characterization of common (*Phaseolus vulgaris* l.) and runner (*Phaseolus coccineus* l.) bean germplasm: a Slovenian gene bank example. *BioMed. Res. Int.* 1-13, 6376948. doi: 10.1155/2019/6376948

Snell, R. S., Beckman, N. G., Fricke, E., Loiselle, B. A., Carvalho, C. S., Jones, L. R., et al. (2019). Consequences of intraspecific variation in seed dispersal for plant demography, communities, evolution and global change. *AoB Plants* 11, plz016. doi: 10.1093/aobpla/plz016

Tao, R., Xu, C., Wang, Y., Sun, X., Li, C., Ma, J., et al (2020). Spatiotemporal differentiation of alpine butterfly Parnassius glacialis (Papilionidae: Parnassiinae) in China: Evidence from mitochondrial DNA and nuclear single nucleotide polymorphisms. *Genes* 11, 188. doi: 10.3390/genes11020188

Venable, D. (2007). Bet hedging in a guild of desert annuals. *Ecology* 88, 1086–1090. doi: 10.1890/06-1495

Venable, D. L., and Brown, J. S. (1988). The selective interactions of dispersal, dormancy, and seed size as adaptations for reducing risk in variable environments. *Am. Nat.* 131, 360–383. doi: 10.1086/284795

Venora, G., Grillo, O., Shahin, M. A., and Symons, S. J. (2007). Identification of Sicilian landraces and Canadian cultivars of lentil using an image analysis system. *Food Res. Int.* 40, 161–166. doi: 10.1016/j.foodres.2006.09.001

Wang, C., Gong, H., Feng, M., and Tian, C. (2023). Phenotypic variation in leaf, fruit and seed traits in natural populations of *Eucommia ulmoides*, a relict chinese endemic tree. *Forests* 14, 462. doi: 10.3390/f14030462

Wang, S. Y., Sun, Z. L., Liu, T., Gibbons, S., Zhang, W. J., and Qing, M. (2014). Flavonoids from sophora moorcroftiana and their synergistic antibacterial effects on MRSA. *Phytother. Res.* 28, 1071–1076. doi: 10.1002/ptr.5098

White, T. L., and Hodge, G. R. (1989). *Predicting breeding values with applications in forest tree improvement* (Boston: Springer science business media).

Xin, F., Liu, J., Chang, C., Wang, Y., and Jia, L. (2021). Evaluating the influence of climate change on sophora moorcroftiana (Benth.) baker habitat distribution on the Tibetan plateau using maximum entropy model. *Forests* 12, 1230. doi: 10.3390/f12091230

Yang, L., Li, H., Li, Q., Guo, Q., and Li, J. (2021). Genetic diversity analysis and potential distribution prediction of *Sophora moorcroftiana* endemic to qinghai–Tibet plateau, China. *Forests* 12, 1106. doi: 10.3390/f12081106

Zhang, Y., He, Z., Zhang, A., van Ginkel, M., Peña, R. J., and Ye, G. (2006). Pattern analysis on protein properties of Chinese and CIMMYT spring wheat cultivars sown in China and CIMMYT. *Aust. J. Agr. Res.* 57, 811–822. doi: 10.1071/AR05372

Zhao, W., Zhang, Z., and Li, Q. (2007). Growth and reproduction of sophora moorcroftiana responding to altitude and sand burial in the middle Tibet. *Eng. Geol.* 53, 11–17. doi: 10.1007/s00254-006-0613-6

frontiers | Frontiers in Plant Science

TYPE Original Research
PUBLISHED 20 July 2023
DOI 10.3389/fpls.2023.1224268

OPEN ACCESS

EDITED BY
Philipp Von Gillhaussen,
Interantional Plant Phenotyping Network (IPPN), Germany

REVIEWED BY
Dong-Liang Huang,
Guangxi Academy of Agricultural Sciences, China
Meng Li,
Hunan Agricultural University, China

*CORRESPONDENCE
Jiangfeng Huang
hjfjiayoua@yeah.net;
supercane.hjf@gxu.edu.cn
Muqing Zhang
zmuqing@163.com

RECEIVED 17 May 2023
ACCEPTED 04 July 2023
PUBLISHED 20 July 2023

CITATION
Ma F, Shen Y, Su D, Adnan M, Wang M, Jiang F, Hu Q, Chen X, He G, Yao W, Zhang M and Huang J (2023) A high-throughput phenotyping assay for precisely determining stalk crushing strength in large-scale sugarcane germplasm. *Front. Plant Sci.* 14:1224268. doi: 10.3389/fpls.2023.1224268

A high-throughput phenotyping assay for precisely determining stalk crushing strength in large-scale sugarcane germplasm

Fumin Ma[1], Yinjuan Shen[1,2], De Su[1], Muhammad Adnan[1], Maoyao Wang[1], Fuhong Jiang[1], Qian Hu[1], Xiaoru Chen[1], Guanyong He[1], Wei Yao[1], Muqing Zhang[1]* and Jiangfeng Huang[1]*

[1]State Key Laboratory for Conservation and Utilization of Subtropical Agro-bioresources, Guangxi Key Laboratory of Sugarcane Biology, Ministry Co-sponsored Collaborative Innovation Center of Canesugar Industry, Academy of Sugarcane and Sugar Industry, College of Agriculture, Guangxi University, Nanning, Guangxi, China, [2]Guangxi China-ASEAN Youth Industrial Park, Chongzuo Agricultural Hi-tech Industry Demo Zone, Chongzuo, Guangxi, China

Sugarcane is a major industrial crop around the world. Lodging due to weak mechanical strength is one of the main problems leading to huge yield losses in sugarcane. However, due to the lack of high efficiency phenotyping methods for stalk mechanical strength characterization, genetic approaches for lodging-resistant improvement are severely restricted. This study attempted to apply near-infrared spectroscopy high-throughput assays for the first time to estimate the crushing strength of sugarcane stalks. A total of 335 sugarcane samples with huge variation in stalk crushing strength were collected for online NIRS modeling. A comprehensive analysis demonstrated that the calibration and validation sets were comparable. By applying a modified partial least squares method, we obtained high-performance equations that had large coefficients of determination (R^2 > 0.80) and high ratio performance deviations (RPD > 2.4). Particularly, when the calibration and external validation sets combined for an integrative modeling, we obtained the final equation with a coefficient of determination (R^2) and ratio performance deviation (RPD) above 0.9 and 3.0, respectively, demonstrating excellent prediction capacity. Additionally, the obtained model was applied for characterization of stalk crushing strength in large-scale sugarcane germplasm. In a three-year study, the genetic characteristics of stalk crushing strength were found to remain stable, and the optimal sugarcane genotypes were screened out consistently. In conclusion, this study offers a feasible option for a high-throughput analysis of sugarcane mechanical strength, which can be used for the breeding of lodging resistant sugarcane and beyond.

KEYWORDS

sugarcane, lodging resistance, mechanical strength, crushing strength, NIRS

Introduction

In crops, lodging is one of the major problems that affect growth and potential yield (Guo et al., 2021). Generally, stalk lodging and root lodging constitute the two most common forms of lodging (Zhang et al., 2016). The term root lodging refers to the entire plant falling to the ground without being bent by the stalk, whereas stalk lodging refers to the stalk inclines and bends at different angles (Berry et al., 2003).

As one of the most commonly grown C4-type industrial crops, sugarcane (*Saccharum* spp.) is known for its high photosynthesis efficiency and high yield (Swapna and Kumar, 2017). However, due to its stalk-harvesting nature, sugarcane faces a much higher risk of lodging, which results in a huge decrease in yield, as well as difficulties with mechanical harvesting, increasing the cost of production (van Heerden et al., 2015). It has been documented that sugarcane lodging is influenced by the environment and phenotype, as well as number of canopy leaves, planting depth, center of gravity height, and stalk hardness (Park et al., 2005; Babu et al., 2010; van Heerden et al., 2010). Specifically, from the perspective of genetic bias, mechanical strength appears to be the most important factor affecting stalk lodging resistance (Xie et al., 2022). It has been shown that stalk mechanical strength can be used as an important index to predict lodging risk, and that bending strength and rind penetrometer resistance (RPR) can reflect stalk mechanical strength (Zhang et al., 2019). A combination of crushing strength, rind penetrometer resistance (RPR), and bending strength has been used to determine the relationship between stalk mechanical strength and lodging (Stubbs et al., 2020; Wang et al., 2020; Shao et al., 2021). In a recent study, we have demonstrated that rind penetrometer resistance (RPR) and breaking force can be used to determine the mechanical strength of sugarcane stalks (Shen et al., 2021). However, it is important to realize that rind penetrometer resistance (RPR) alone cannot properly reflect stalk lodging resistance because it ignores the contributions from the stalk's cross-sectional area and vascular bundles (Robertson et al., 2016). Particularly, laboratory-based mechanical phenotyping requires a significant amount of time and therefore cannot be used for large-scale genetic screening projects. Hence, it is essential to develop high-throughput assays for measuring the stalk mechanical strength of sugarcane onto a global scale.

The near infrared spectroscopy (NIRS) is a very efficient method that has been widely used for high-throughput determine various chemical and biochemical structures of agricultural crop (Washburn et al., 2013). For instances, NIRS has been used for high-throughput predicting fiber and nutrient content of dryland cereal cultivars (Brenna and Berardo, 2004; Stubbs et al., 2010), phenotyping of moisture and amylose content in maize (Wang et al., 2019; Dong et al., 2021), evaluating the composition of carbohydrates in soybean (Leite et al., 2020; Singh et al., 2021), detecting biomass of plant root mixtures (Roumet et al., 2006), analyzing available P contents in soils to aid fertilization (Patzold et al., 2020), as well as determining the internal quality and physiological maturity in the fruit (Cunha et al., 2016; de Carvalho et al., 2019; Minas et al., 2021). In our previous studies, the NIRS has been successfully applied for stalk quality determination (Wang et al., 2021), cell wall features and lignocellulose digestibility characterization in sugarcane (Li et al., 2021; Adnan et al., 2022). Notably, in a recent study, we have also successfully implemented the NIRS for assessing the mechanical strength of sugarcane stalks by measuring the rind penetrometer resistance (RPR) and breaking force (Shen et al., 2022).

As a coupled complementary exploration, this study aimed to establish a set of methods for high-throughput phenotyping of sugarcane crushing strength. Due to the large number of diverse sugarcane germplasms collected, a precise online NIRS assay was developed using chemometric analysis. After three years of testing in large-scale sugarcane germplasm, the NIRS model exhibited stable and reliable performance, enabling the optimal germplasm to be selected. Therefore, this study provided a reliable strategy for crushing strength determination, which could be integrated with our previous studies for lodging resistant aimed precision breeding in sugarcane.

Materials and methods

Experimental site and sugarcane planting

This experiment was conducted at the Fusui experimental field located at Guangxi University (107° 47′17.66′′ E, 22° 31′ 5.85′′ N), and the soil type is loam. As a subtropical monsoon climate, there are 1050 - 1300 mm of precipitation annually, a mean annual temperature of 21.3 - 22.80°C, and a mean annual sunshine of 1693 hours (data source: http://www.gxcounty.com/pindao/112287/). We utilized a randomized block design to plant the sugarcane genotypes at three identical experimental field plots of 5 m row length, 2 m row spacing, and 0.6 m depth. A total of 860 sugarcane germplasm collected from all over China were planted in each planting plot, of which 416 core germplasm samples were selected for crushing strength characterization in this study. All sugarcane germplasm were planted in May 2019 with basal fertilizer (organic-inorganic fertilizer 12-6-7, 750 kg ha^{-1}), tillering fertilizer (NPK 20-10-10, 300 kg ha^{-1}) and jointing fertilizer (NPK 20-10-10, 1500 kg ha^{-1}). For the fertilization of ratoon sugarcane, urea (150 kg ha^{-1}) and KCl (150 kg ha^{-1}) were applied in April and August, and compound fertilizer (NPK 15-15-15, 1875kg ha^{-1}) was applied in May. Pest control was not applied throughout the growing period, but irrigation and weeding were performed as necessary.

Assay of stalk crushing strength in sugarcane population

An electronic universal testing machine, DNS-20 (Sinotest Equipment Co., Ltd, China), was used to measure the stalk crushing strength. For each sugarcane genotype, the 15^{th} internode was selected to measure stalk crushing strength (kN) (Shen et al., 2021). In summary, the sugarcane stalk was arranged horizontally on the stage to permit direct compression of the internodes by a circular probe of 90 mm diameter. The

movement of probe consisted of four processes (descent, gap elimination, compression, lifting). In order to maximize test efficiency and data accuracy, we set the speed of the four processes at 500 mm/min, 150 mm/min, 150 mm/min, 500 mm/min, respectively. The load cell collected force data every 100 ms. Three biological replicates were performed for each genotype planted in each experimental field plot. The mechanical data were recorded and analyzed using the TestExpert software (version 3.2).

Online NIRS data collection

During the maturity period, 383, 368, and 376 genotypes of sugarcane germplasm were collected from three planting plots in November 2021 for online NIRS modeling. The online NIRS data were collected by a well-established method previously described by Li et al. (2021) with minor modification. Briefly, for each genotype, three plants were randomly selected, and leaves and young tips were removed and immediately shredded using DM540 (IRBI Machines and Equipment Ltd, Brazil). The shredded sugarcane sample was blended and transmitted *via* CPS (Cane presentation system, Bruker Optik GmbH, Germany). The spectral was collected through MATRIX-F (Bruker Optik GmbH, Germany) online system. A full scanning mode was used to scan the shredded samples, with a wavelength range of 4000 to 10000 cm^{-1} in 4 cm^{-1} steps. The absorbance values of the spectra were recorded in log(1/R), where R is the reflectance of sample. To provide a more comprehensive analysis, the OPUS software automatically averaged the online reflectance values obtained. A standard equipped in Q413 sensor of MATRIX-F was scanned every one hour for instrument correction.

NIRS pretreatments and modeling

The spectral data were collected and analyzed using the OPUS software. Before modeling, the samples were randomly divided into calibration and validation sets in a roughly 4:1 ratio, which was used for modeling and external validation, respectively. Pretreatment of spectral data was performed in order to minimize the risk of physical disturbance. To obtain the optimal spectral region for modeling, OPUS software used ten spectral pretreatment methods in combination to divide the NIRS spectrum into multiple sections (Wang et al., 2021), including constant offset elimination (COE), straight-line subtraction (SSL), standard normal variate (SNV), Min-Max normalization (MMN), multivariate scattering correction (MSC), first derivative (FD), second derivative (SED), combination of the first derivative and straight-line subtraction (FD+SSL), standard normal variate (FD+SNV), and multiplicative scattering correction (FD+MSC). A principal component analysis (PCA) of the raw spectral data was conducted to determine the distribution of spectral groups, and outlier samples were excluded based on GH values (> 3.0). Based on the partial least squares (PLS) method, the calibration equations were generated by combining the selected samples with the optimal parameters. A default setting in OPUS software was used to select the wavelength range. A combination in terms of wavelength range selection and spectrum pretreatment was made to obtain calibration models in PLS analysis (Li et al., 2021; Adnan et al., 2022). Internal cross-validation and external validation of the equations were used to evaluate the performance of the model (Williams and Sobering, 1996). Finally, the optimal equation was selected based on high coefficient of determination ($R^2_c/R^2_{cv}/R^2_{ev}$), ratio of prediction to deviation (RPD), and low root mean square error (RMSEC/RMSECV/RMSEP) from calibration/internal cross-validation/external validation.

Application of the model in sugarcane population

A total of 336 samples of sugarcane were harvested at maturation in three years (2019, 2020, and 2021), the NIR spectra were online collected as described above. Based on our established model in the year of 2021, the acquired spectral data was analyzed with the help of the OPUS software to obtain the predicted stalk crushing strength across these three years. Samples with GH > 3.0 were considered outlier based on principal component analysis. After excluding all outliers, sugarcane germplasm with high and low stalk crushing strength was screened out.

Results

Accurate determination of stalk crushing strength in sugarcane

For a precise and reliable determination of stalk mechanical strength, the 15th internode of the sugarcane stalk was selected to determine crushing strength at maturity. In detail, the selected internode was placed horizontally in the middle of the stage and compressed by a probe with a threshold force of 4 kN (Figure 1A). As illustrated in Figure 1B, when a certain amount of pressure is applied to the cane stem, cracks begin to appear along its axis. The internodes ruptured when a continuous compressive force was applied to the internodes up to the threshold, causing irreversible morphological changes (Figure 1C). In the course of this process, TestExpert software generated a compression force curve with multiple peaks (Figure 1D). Remarkably, the curve showed three compressive states (elasticity, yield, compaction strengthening) (Sun et al., 2022). For the purpose of verifying the reliability of each peak, ten randomly selected sugarcane samples were tested for compressive force. A similar fluctuating change in the compressive force between the same samples was observed (Figure S1), consistent with the results observed in maize (Kovacs and Kerenyi, 2019; Zhang et al., 2020). Noteworthy, the relative standard deviation (RSD) value of the first peak was significantly less than that of the other peaks (Figure 1E; Table S1).

Further tests were conducted on two representative groups of ten representative sugarcane genotypes, and the differences in compressive force was clearly observed between them (Figure S2). Particularly, a comparison of the first peak of compressive force in

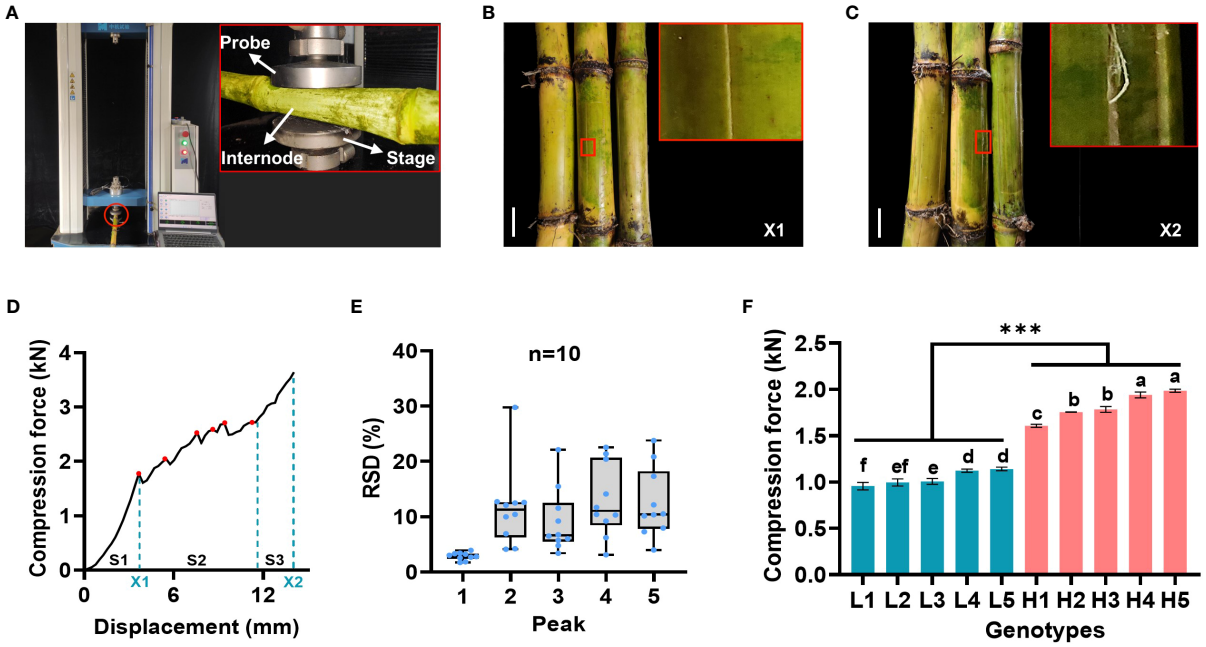

FIGURE 1
Laboratory analytical method for stalk crushing strength determination in sugarcane. **(A)** Schematic diagram of sugarcane crushing strength determination. **(B, C)** Morphological changes of internode at the moment of cracks appeared **(B)** and complete ruptured **(C)**, bars = 3 cm. **(D)** Compression force curve with multiple peaks for crushing strength determination. S1-S3: three compressive states (elasticity, yield, compaction strengthening); Red dots represent the detected peaks; X1 and X2 represent the key steps as described in B and C, respectively; **(E)** Comparative analysis of each detected peaks in the compressive force curves in ten representative sugarcane samples. RSD: relative standard deviation. **(F)** Comparative analysis of the first peak between two groups of ten representative sugarcane genotypes. Different letters indicated statistically significant differences among these genotypes *via* one-way ANOVA and LSD test at $\alpha \leq 0.05$ level; *** indicated statistically significant different between the two groups at $p < 0.001$ level. H1-H5 and L1-L5 represented five sugarcane genotypes with high (H) and low (L) mechanical strength, respectively. Each sample contained three biological replicates.

the two groups revealed that there was a significant difference between them (Figure 1F), indicating that the first peak was sufficient to identify the high and low samples. Therefore, it was appropriate to assess the crushing strength of sugarcane stalks based on the first peak.

Diversity of stalk crushing strength in sugarcane population

Sugarcane germplasm planted in three experimental field plots were applied for the stalk crushing strength determination by DNS-20 electronic universal testing machine. In detail, 383, 368, and 376 sugarcane samples were harvested at maturity in each of the three planting plots and the first peak from the compressive force curves was recorded (Figure 2A). Among these samples, 306 were common to all three plots and they displayed a wide range of agronomic trait variability (Table S2). Specifically, their crushing strength exhibited considerable variation, although some genotypes varied across three planting plots (Figures 2B, C; Table S3). An analysis of correlations revealed that stalk crushing strength was negatively correlated with internode length, but positively correlated with stalk diameter and internode number (Table S4), suggesting that the stalk crushing strength should be affected by the physiological morphology of sugarcane stalks. Besides, the frequency distribution statistics showed that stalk crushing strength exhibited a normal distribution in all three planting plots (Figure 2D), implying that stalk crushing strength of sugarcane should be a quantitative trait. Notably, upon a correlation analysis of the stalk crushing strengths between the three planting plots, a highly significant ($P < 0.001$) correlation was observed (Figure 2D), indicating that stalk crushing strength should be a genetically controlled characteristic that could be stably applied for stalk mechanical strength characterization in sugarcane. Therefore, the observed genetically stable large variation of crushing strengths in the collected sugarcane germplasm population allows for reliable NIR modeling and applications.

Characterization of sugarcane samples by online near-infrared spectroscopy

A total of 335 sugarcane samples from three planting plots were used for NIRS modeling. The NIR spectral data of collected sugarcane samples showed continuous fluctuations with a normal range (Figure 3A), indicating a high level of genetic diversity in the germplasm for biochemical traits (Wang et al., 2021). The principal component analysis (PCA) was employed to identify and classify the samples based on their spectrum (Martin-Tornero et al., 2020). To characterize 335 sugarcane samples, the first ten principal components were extracted from the raw NIRS data. Notably, the first three principal components showed a greater contribution rate to the variable explanation (Figure 3B; Table S5), which explained

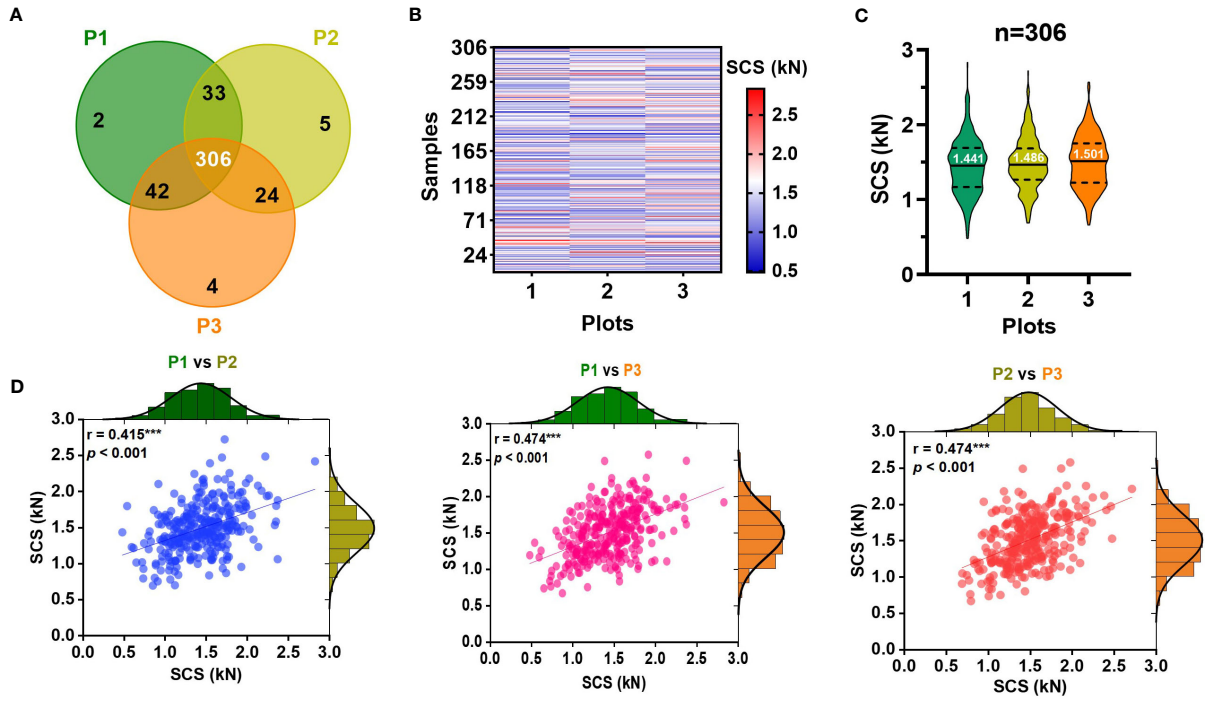

FIGURE 2
Diversity of stalk crushing strength (SCS) in collected sugarcane samples. **(A)** Venn diagram of sugarcane samples collected from three identical experimental field plots. **(B)** Heatmap and **(C)** violin chart displaying the stalk crushing strengths in collected sugarcane genotypes. **(D)** Distribution and correlation analysis of stalk crushing strength of 306 sugarcane genotypes in three planting plots. *** indicated significant correlations at $p < 0.001$ level. P1-P3: three planting plots.

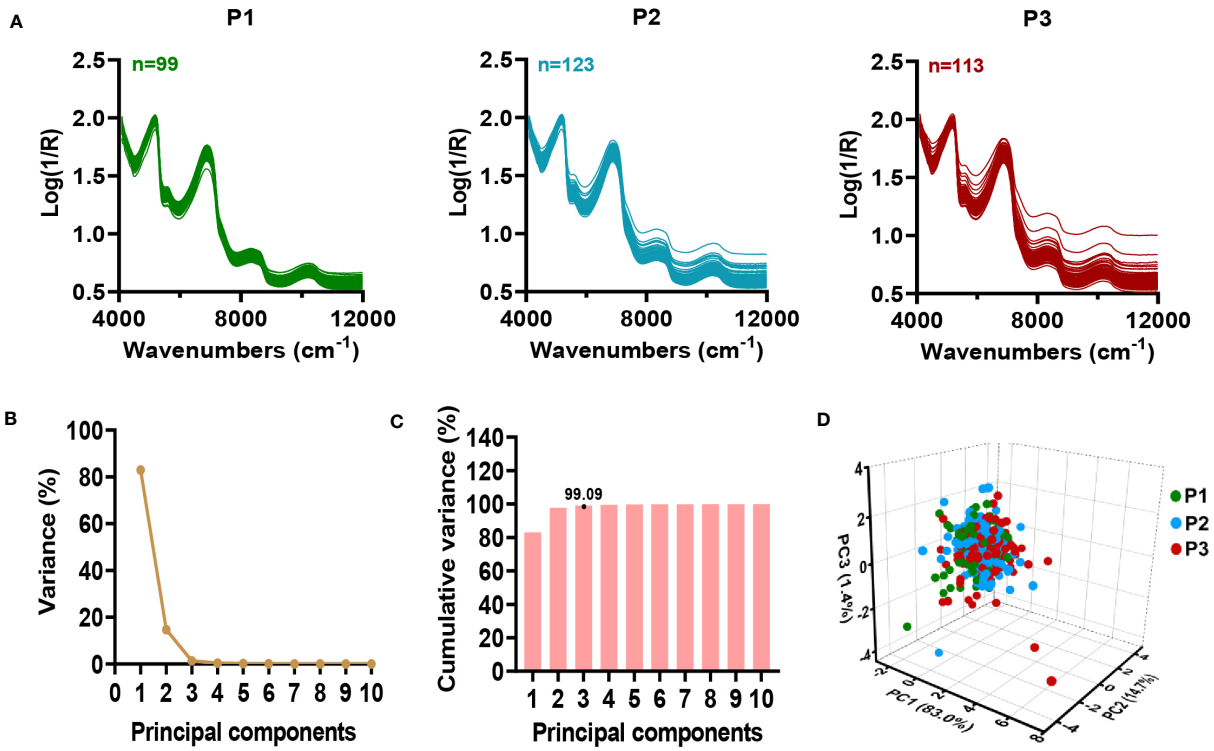

FIGURE 3
Characterization of near-infrared spectral in 335 sugarcane samples. **(A)** Original spectra of sugarcane samples in three planting plots. **(B-D)** Principal component analysis of NIRS data. **(B)** Contribution of each principal component to variable explanation. **(C)** Cumulative contribution of principal components to variable explanation. **(D)** 3D score view of sugarcane samples by PCA. P1-P3: three planting plots.

99.09% of the variance (Figure 3C; Table S5). As a means of better observing the distribution of the samples, the first three principal components were selected in order to generate the 3D scores plot of all samples. Consequently, we observed a relatively symmetrical distribution of sugarcane samples from different planting plots in the 3D plot (Figure 3D), with no obvious differences between the planting plots. According to the results, a quantitative analysis model for stalk crushing strength of sugarcane can be developed using online NIRS.

Online NIRS modeling for stalk crushing strength in sugarcane

In order to ensure accurate and stable NIRS modeling, sugarcane samples were allocated into critical calibration and validation sets (Payne and Wolfrum, 2015). In detail, a total of 262 sugarcane samples were used for calibration, whereas 73 samples were used for external validation. A wide variation range and continuous normal distribution were observed in all samples used for calibration and external validation (Figure 4A). Meanwhile, calibration set contained the range of the external validation set (Table S6), preventing the predicted value from exceeding the prediction range of model. Since the calibration and external validation sets were comparable, the NIRS model could be calibrated as well as externally validated.

With the assistance of OPUS software, the prediction equation of NIRS model was established through a partial least squares analysis (PLS) (Li et al., 2021). A pretreatment of raw spectral data was carried out before calibration in order to minimize the detrimental effect of the baseline (Devos et al., 2014). A series of complex eliminating modeling processes were applied by the OPUS software to optimize the prediction capability of the obtained equation. Performance of equations were measured by the coefficient of determination (R^2), the root mean square error (RMSE) and the ratio performance deviation (RPD) (Yang et al., 2016). As the calibration result, the coefficient of determination (R^2c) and RPD values were obtained as high as 0.92 and 3.58, respectively (Figure 4B; Table S7). Besides, cross-validation and external validation of the model were applied for model evaluation, resulting in constant high R^2cv/R^2ev values of over 0.8, RPD values of over 2.4, as well as low root mean square errors of 0.09 and 0.11 kN (Figure 4B; Table S7).

For the purpose of improving the prediction performance of the equation, external validation and calibration sets were combined to generate the final calibration equation (Windley and Foley, 2015). Although the R^2c value of the equation did not increased significantly during the calibration process (Figure 4C; Table S8), a higher correlation was observed between the measured value and the predicted value during the internal cross-validation. Accordingly, the R^2cv value increased from 0.89 to 0.90, and the RPD value increased from 3.06 to 3.16 (Figure 4C; Table S8), indicating that the new equation was capable of making even better predictions.

Model-based evaluation of stalk crushing strength in sugarcane germplasm

In an effort to evaluate the performance of our model developed for predicting stalk crushing strength in large-scale sugarcane germplasm, the model was applied to 336 sugarcane genotypes

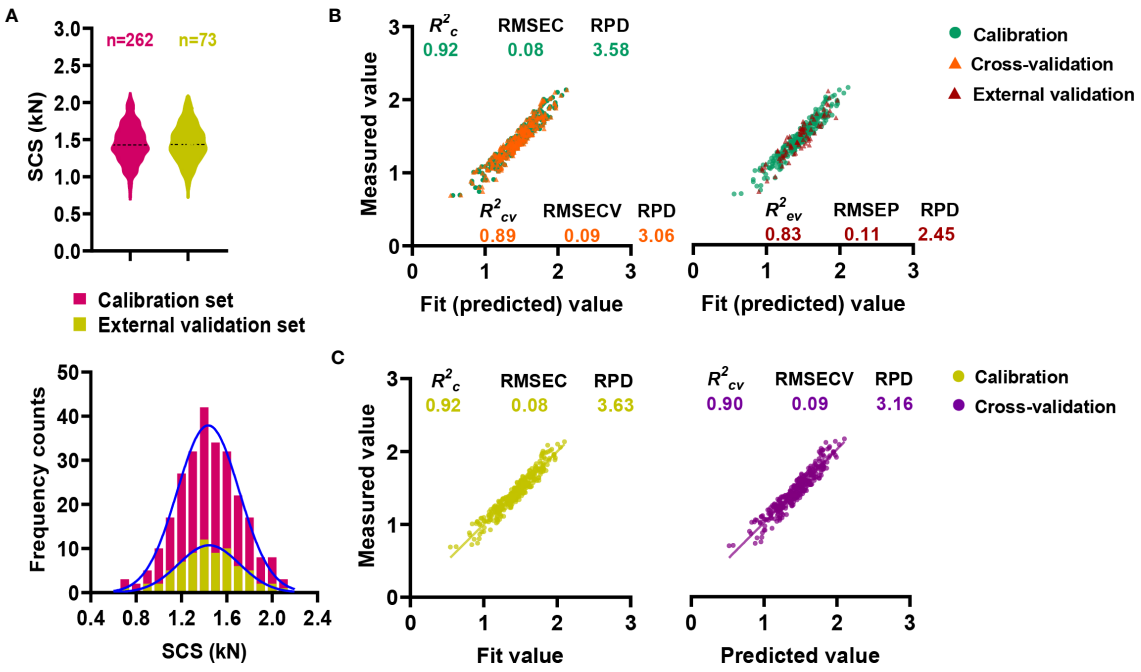

FIGURE 4
Online NIRS modeling for stalk crushing strength. **(A)** Distribution characteristics of calibration and validation sets. **(B)** Online NIRS calibration and external validation. **(C)** Performance of the integrative final NIRS equation.

planted in three planting plots over a period of three years (2019, 2020, 2021). As can be seen from the sample data, a limited number of outliers were observed, providing evidence that the model is robust and may be applied widely (Table S9). In either of all three planting plots for the same planting year or across different planting years, stalk crushing strength exhibited a similar range of variation (Figure 5A). In 2019, the sugarcane population appeared to have a slight lower in mean value and a substantial variation in crushing strength, which may be a result of the rainy climate in that year. Specifically, in 2020 and 2021, stalk crushing strengths were observed ranging from 0.69-2.13 kN and 0.69-2.10 kN, respectively, whereas in 2019 they ranged between 0.69-1.85 kN (Figure 5A).

Moreover, we conducted a correlation analysis of the predicted crushing strength of sugarcane samples across different years. It was observed that stalk crushing strength was highly correlated across all three years at a $p < 0.001$ significant level (Figure 5B), confirming the findings in NIRS calibration sets (Figure 2D), demonstrating

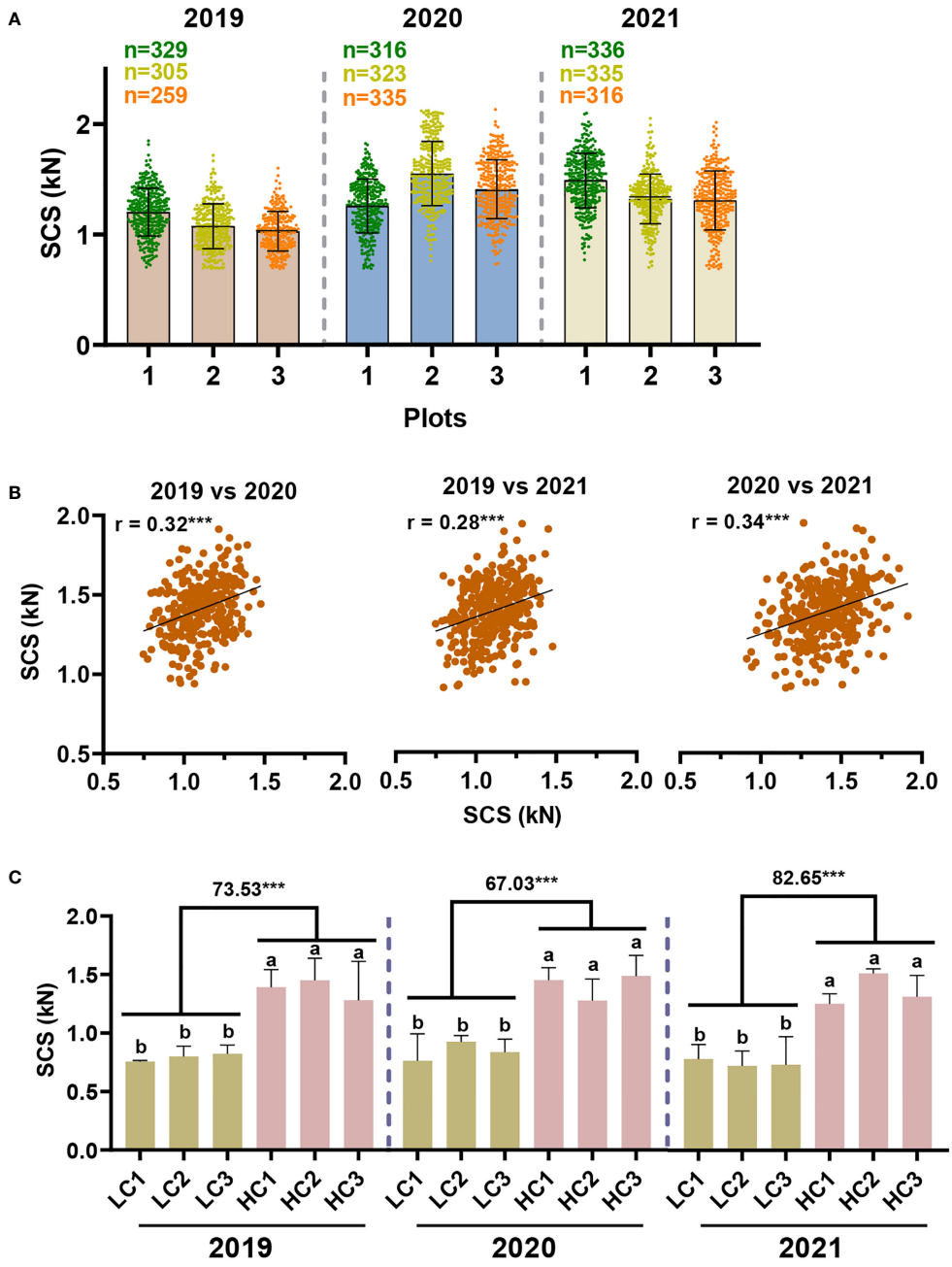

FIGURE 5
Model-based evaluation of stalk crushing strength in sugarcane germplasm. **(A)** Distribution of stalk crushing strength in sugarcane population. **(B)** Correlation analysis of stalk crushing strength between three years. *** indicated significant correlations at $p < 0.001$ level. **(C)** Comparative analysis of stalk crushing strength in the screened sugarcane germplasm. LC/HC: representing the sugarcane samples with low and high crushing strength, respectively. Different letters indicated statistically significant differences between the groups using one-way ANOVA and LSD test at $\alpha \leq 0.05$; *** indicated statistically significant different at $p < 0.001$ levels, respectively.

that sugarcane stalk crushing strength should have a steady inheritance pattern. It also proved that the model-based characterization of sugarcane crushing strength by means of NIRS is both accurate and stable. Accordingly, sugarcane germplasm with high and low stalk crushing strengths were successfully screened out according to the results predicted by the model. Notably, these screened sugarcane genotypes maintained significant differences in stalk crushing strengths over three years, consistent with the correlation results, further demonstrating that the NIRS model-based method of sugarcane crushing strength analysis is accurate and repeatable (Figure 5C). Overall, these findings suggest that the model is practical and can be used to rapidly identify ideal sugarcane germplasm from large-scale populations of sugarcane.

Discussion

Lodging is one of the major problems that affect the growth and potential yield of agricultural crops (Guo et al., 2021). However, it is challenging to accurately identify the lodging resistance of crops as it is a complex trait affected by a variety of factors (Khobra et al., 2019; Shah et al., 2019). Stem mechanical properties indicate the load-bearing capacity of plants, and therefore can be used as an indirect criterion for selecting lodging-resistant varieties (Yang et al., 2020). Studies have evaluated lodging resistance of stems by measuring their mechanical strength, and it has been found that improving the mechanical strength of stems can reduce lodging risks (Xue et al., 2016; Zhan et al., 2022). In spite of this, it remains a serious problem that there is currently no method of measuring mechanical strength in crops that is both accurate and high-throughput. In our latest study, a precise and high-throughput mechanical strength characterization assay was developed in terms of measuring rind penetrometer resistance (RPR) and breaking force by NIRS modeling in sugarcane (Shen et al., 2022), providing a framework for high-throughput phenotyping of crop stalk mechanical properties. Through a combination of complementary explorations, this study aimed to establish high-throughput phenotyping methods for sugarcane crushing strength.

As a first step toward an effective NIRS calibration, a laboratory analytical method was performed in an effort to ensure accuracy. Owing to an electronic universal testing machine packed with TestExpert software, we were able to obtain the curves of the changes in mechanical properties of sugarcane during crushing (Figure S1; Figure 1D). A comparative analysis revealed that the first peak of the sugarcane crushing mechanics curve provides a stable assessment of the sugarcane crushing strength (Figures 1E, F; Figure S2), which was consistent with the findings in maize (Xu et al., 2017). According to our established laboratory analysis method for sugarcane stalk crushing strength determination, a collection of 306 sugarcane germplasms revealed considerable genetic variability (Figure 2), which provides a significant basis for NIRS modeling. It should be noted that a total of 416 sugarcane genotypes planted in three test plots (with some samples missing in each plot) were tested for crushing strength characterization (Figure 2). However, only 335 of those that showed the best biological replicates across three test plots were selected for NIRS modelling to ensure an accurate calibration (Figure 3). As we expected, a high-performance NIRS model for sugarcane crushing strength characterization was obtained based on our established NIRS modeling method. In particular, the model exhibits stable and reliable prediction parameters in both internal cross-validation and external tests (Figure 4), indicating excellent performance in practice. In spite of this, it may be possible to improve the model further by adding more reliable data.

Besides, the model was applied to a large-scale phenotypic analysis of sugarcane crushing strength over a period of three consecutive years. Accordingly, the model demonstrated good robustness in its application, with only a few samples being detected as out of range (Table S9). In particular, we found that model-based predictions of sugarcane crushing strength showed significant correlations between years (Figure 5B). Material with high and low crushing strengths were consistently screened out from sugarcane population for three consecutive years (Figure 5C). It was further confirmed that the developed model has excellent predictive performance and can be applied to high-throughput phenotyping of sugarcane crushing strength in sugarcane population.

Notably, in our study, significant correlations were found between sugarcane crushing strength and internode length, stem diameter, and internode number (Table S4). This suggests that sugarcane crushing strength is a complex trait that is closely related to the biological properties of sugarcane stalks. This is different from the pattern of rind penetrometer resistance (RPR) and breaking force that characterized in our previous study (Shen et al., 2022). It implies that the application of a single indicator in assessing the mechanical strength of sugarcane stalks to determine the lodging resistant is not desirable. Therefore, the high-throughput phenotypic analysis assay for sugarcane crushing strength determination established in this study, combined with our previously established rapid assays for sugarcane rind penetrometer resistance (RPR) and breaking force characterization (Shen et al., 2021; Shen et al., 2022), can provide a more comprehensive and systematic technical support for lodging resistance targeted sugarcane breeding and beyond.

Conclusions

Using the established accurate laboratory method for crushing strength characterization as well as effective NIR modeling, this study developed a precise and high-throughput phenotyping assay for the determination of mechanical strength in sugarcane. The obtained final equation *via* integrative modeling exhibited a coefficient of determination (R^2) and ratio performance deviation (RPD) as high as over 0.9 and 3.0, respectively, reflecting excellent prediction capacity. Model-based application provided a stable and effective approach for crushing strength trait evaluation in large-scale sugarcane germplasm screening tasks. This study suggests that the NIRS assay could be applied as a highly reliable tool for lodging-resistant targeted phenotyping jobs.

Data availability statement

The raw data supporting the conclusions of this article will be made available by the authors, without undue reservation.

Author contributions

FM completed the major experiment, analyzed the data, and completed the first draft of manuscript. YS and DS participated in crushing strength determination. MW, FJ, MA, QH, XC, GH participated in sugarcane samples preparation and NIRS data collection. WY revised the manuscript. JH and MZ designed the project, supervised the experiments, interpreted the data, and finalized the manuscript. All authors contributed to the article and approved the submitted version.

Funding

This work was supported by National Key R&D Program of China [2022YFD2301100]; Guangxi Science and Technology Major Projects [Gui Ke AA22117001]; Guangxi Natural Science Foundation [2022GXNSFAA035547]; Sugarcane Research Foundation of Guangxi University [2022GZB005]; Guangxi Science and Technology Talent Special Project [Gui Ke AD20297067]; Academy of Sugarcane and Sugar Industry [ASSI-2022006] and Innovation Project of Guangxi Graduate Education [YCSW2023023].

Conflict of interest

The authors declare that the research was conducted in the absence of any commercial or financial relationships that could be construed as a potential conflict of interest.

Publisher's note

All claims expressed in this article are solely those of the authors and do not necessarily represent those of their affiliated organizations, or those of the publisher, the editors and the reviewers. Any product that may be evaluated in this article, or claim that may be made by its manufacturer, is not guaranteed or endorsed by the publisher.

Supplementary material

The Supplementary Material for this article can be found online at: https://www.frontiersin.org/articles/10.3389/fpls.2023.1224268/full#supplementary-material

References

Adnan, M., Shen, Y., Ma, F., Wang, M., Jiang, F., Hu, Q., et al. (2022). A quick and precise online near-infrared spectroscopy assay for high-throughput screening biomass digestibility in large scale sugarcane germplasm. *Ind. Crops Prod.* 189, 115814. doi: 10.1016/j.indcrop.2022.115814

Babu, C., Koodalingam, K., Natarajan, U. S., Shanthi, R. M., and Govindaraj, P. (2010). Genetic enhancement of sugarcane (*Saccharum* sp. hybrids) for resistance to red rot disease and economic traits. *J. Agric. Sci.* 4, 97–107. doi: 10.4038/jas.v4i3.1648

Berry, P. M., Spink, J. H., Gay, A. P., and Craigon, J. (2003). A comparison of root and stem lodging risks among winter wheat cultivars. *J. Agric. Sci.* 141, 191–202. doi: 10.1017/S002185960300354X

Brenna, O. V., and Berardo, N. (2004). Application of near-infrared reflectance spectroscopy (NIRS) to the evaluation of carotenoids content in maize. *J. Agric. Food Chem.* 52, 5577–5582. doi: 10.1021/jf0495082

Cunha, L. C., Teixeira, G. H. D., Nardini, V., and Walsh, K. B. (2016). Quality evaluation of intact acai and jucara fruit by means of near infrared spectroscopy. *Postharvest Biol. Technol.* 112, 64–74. doi: 10.1016/j.postharvbio.2015.10.001

de Carvalho, L. C., Pereira, F. M. V., de Morais, C. D. M., de Lima, K. M. G., and Teixeira, G. H. D. (2019). Assessment of macadamia kernel quality defects by means of near infrared spectroscopy (NIRS) and nuclear magnetic resonance (NMR). *Food Control* 106, 106695. doi: 10.1016/j.foodcont.2019.06.021

Devos, O., Downey, G., and Duponchel, L. (2014). Simultaneous data pre-processing and SVM classification model selection based on a parallel genetic algorithm applied to spectroscopic data of olive oils. *Food Chem.* 148, 124–130. doi: 10.1016/j.foodchem.2013.10.020

Dong, Q., Xu, Q., Wu, J., Cheng, B., and Jiang, H. (2021). Applicability of near infrared reflectance spectroscopy to predict amylose contents of single-grain maize. *Agronomy-Basel* 11, 2463. doi: 10.3390/agronomy11122463

Guo, Y., Hu, Y., Chen, H., Yan, P., Du, Q., Wang, Y., et al. (2021). Identification of traits and genes associated with lodging resistance in maize. *Crop J.* 9, 1408–1417. doi: 10.1016/j.cj.2021.01.002

Khobra, R., Sareen, S., Meena, B. K., Kumar, A., Tiwari, V., and Singh, G. P. (2019). Exploring the traits for lodging tolerance in wheat genotypes: a review. *Physiol. Mol. Biol. Plants* 25, 589–600. doi: 10.1007/s12298-018-0629-x

Kovacs, A., and Kerenyi, G. (2019). Physical characteristics and mechanical behaviour of maize stalks for machine development. *Int. Agrophys.* 33, 427–436. doi: 10.31545/intagr/113335

Leite, D. C., Correa, A. A. P., Cunha, L. C., de Lima, K. M. G., de Morais, C. D. M., Vianna, V. F., et al. (2020). Non-destructive genotypes classification and oil content prediction using near-infrared spectroscopy and chemometric tools in soybean breeding program. *J. Food Compost. Anal.* 91, 103536. doi: 10.1016/j.jfca.2020.103536

Li, X., Ma, F., Liang, C., Wang, M., Zhang, Y., Shen, Y., et al. (2021). Precise high-throughput online near-infrared spectroscopy assay to determine key cell wall features associated with sugarcane bagasse digestibility. *Biotechnol. Biofuels* 14, 1–12. doi: 10.1186/s13068-021-01979-x

Martin-Tornero, E., de Jorge Pascoa, R. N. M., Espinosa-Mansilla, A., Martin-Meras, I. D., and Lopes, J. A. (2020). Comparative quantification of chlorophyll and polyphenol levels in grapevine leaves sampled from different geographical locations. *Sci. Rep.* 10, 1–13. doi: 10.1038/s41598-020-63407-8

Minas, I. S., Blanco-Cipollone, F., and Sterle, D. (2021). Accurate non-destructive prediction of peach fruit internal quality and physiological maturity with a single scan using near infrared spectroscopy. *Food Chem.* 335, 127626. doi: 10.1016/j.foodchem.2020.127626

Park, S. E., Robertson, M., and Inman-Bamber, N. G. (2005). Decline in the growth of a sugarcane crop with age under high input conditions. *Field Crops Res.* 92, 305–320. doi: 10.1016/j.fcr.2005.01.025

Patzold, S., Leenen, M., Frizen, P., Heggemann, T., Wagner, P., and Rodionov, A. (2020). Predicting plant available phosphorus using infrared spectroscopy with consideration for future mobile sensing applications in precision farming. *Precis. Agric.* 21, 737–761. doi: 10.1007/s11119-019-09693-3

Payne, C. E., and Wolfrum, E. J. (2015). Rapid analysis of composition and reactivity in cellulosic biomass feedstocks with near-infrared spectroscopy. *Biotechnol. Biofuels* 8, 1–14. doi: 10.1186/s13068-015-0222-2

Robertson, D. J., Lee, S. Y., Julias, M., and Cook, D. D. (2016). Maize stalk lodging: flexural stiffness predicts strength. *Crop Sci.* 56, 1711–1718. doi: 10.2135/cropsci2015.11.0665

Roumet, C., Picon-Cochard, C., Dawson, L. A., Joffre, R., Mayes, R., Blanchard, A., et al. (2006). Quantifying species composition in root mixtures using two methods:

near-infrared reflectance spectroscopy and plant wax markers. *New Phytol.* 170, 631–638. doi: 10.1111/j.1469-8137.2006.01698.x

Shah, L., Yahya, M., Shah, S. M. A., Nadeem, M., Ali, A., Ali, A., et al. (2019). Improving lodging resistance: using wheat and rice as classical examples. *Int. J. Mol. Sci.* 20, 4211. doi: 10.3390/ijms20174211

Shao, H., Shi, D. F., Shi, W. J., Ban, X. B., Chen, Y. C., Ren, W., et al. (2021). The impact of high plant density on dry matter remobilization and stalk lodging in maize genotypes with a different stay-green degree. *Arch. Agron. Soil Sci.* 67, 504–518. doi: 10.1080/03650340.2020.1737679

Shen, Y., Adnan, M., Ma, F., Kong, L., Wang, M., Jiang, F., et al. (2022). A high-throughput method for precise phenotyping sugarcane stalk mechanical strength using near-infrared spectroscopy. *Research Square [Preprint]*. Available at: https://doi.org/10.21203/rs.3.rs-2248978/v1 (Accessed November 09, 2022).

Shen, Y., Ma, F., Wang, M., Li, X., Zhang, M., and Huang, J. (2021). Accurate evaluation and mechanism analysis of mechanical strength of sugarcane stalk. *Chin. J. Trop. Crops* 43, 207–215. doi: 10.3969/j.issn.1000-2561.2022.01.025

Singh, M., Bowman, M. J., Berhow, M. A., Price, N. P. J., and Liu, S. X. (2021). Application of near infrared spectroscopy for determination of relationship between crop year, maturity group, location, and carbohydrate composition in soybeans. *Crop Sci.* 61, 2409–2422. doi: 10.1002/csc2.20503

Stubbs, T. L., Kennedy, A. C., and Fortuna, A. M. (2010). Using NIRS to predict fiber and nutrient content of dryland cereal cultivars. *J. Agric. Food Chem.* 58, 398–403. doi: 10.1021/jf9025844

Stubbs, C., McMahan, C., Seegmiller, W., Cook, D. D., and Robertson, D. J. (2020). Integrated puncture score: force-displacement weighted rind penetration tests improve stalk lodging resistance estimations in maize. *Plant Methods* 16, 1–12. doi: 10.1186/s13007-020-00654-w

Sun, J. C., Zhao, R. J., Zhong, Y., and Chen, Y. P. (2022). Compressive mechanical properties of larch wood in different grain orientations. *Polymers* 14, 3771. doi: 10.3390/polym14183771

Swapna, M., and Kumar, S. (2017). MicroRNAs and their regulatory role in sugarcane. *Front. Plant Sci.* 8, 997. doi: 10.3389/fpls.2017.00997

van Heerden, P. D. R., Donaldson, R. A., Watt, D. A., and Singels, A. (2010). Biomass accumulation in sugarcane: unravelling the factors underpinning reduced growth phenomena. *J. Exp. Bot.* 61, 2877–2887. doi: 10.1093/jxb/erq144

van Heerden, P. D. R., Singels, A., Paraskevopoulos, A., and Rossler, R. (2015). Negative effects of lodging on irrigated sugarcane productivity-An experimental and crop modelling assessment. *Field Crops Res.* 180, 135–142. doi: 10.1016/j.fcr.2015.05.019

Wang, M., Li, X., Shen, Y., Adnan, M., Mao, L., Lu, P., et al. (2021). A systematic high-throughput phenotyping assay for sugarcane stalk quality characterization by near-infrared spectroscopy. *Plant Methods* 17, 1–14. doi: 10.1186/s13007-021-00777-8

Wang, X., Ma, T. M., Yang, T., Song, P., Chen, Z. G., and Xie, H. (2019). Monitoring model for predicting maize grain moisture at the filling stage using NIRS and a small sample size. *Int. J. Agric. Biol. Eng.* 12, 132–140. doi: 10.25165/j.ijabe.20191202.4708

Wang, Q., Xue, J., Zhang, G. Q., Chen, J. L., Xie, R. Z., Ming, B., et al. (2020). Nitrogen split application can improve the stalk lodging resistance of maize planted at high density. *Agriculture-Basel* 10, 364. doi: 10.3390/agriculture10080364

Washburn, J. D., Whitmire, D. K., Murray, S. C., Burson, B. L., Wickersham, T. A., Heitholt, J. J., et al. (2013). Estimation of rhizome composition and overwintering ability in perennial sorghum spp. using near-infrared spectroscopy (NIRS). *Bioenergy Res.* 6, 822–829. doi: 10.1007/s12155-013-9305-8

Williams, P. C., and Sobering, D. C. (1996). "How do we do it: a brief summary of the methods we use in developing near infrared calibration," in *Near Infrared Spectroscopy: The Future Waves*. Eds. A. M. C. Davies and P. Williams (Chichester, UK: NIR Publications), 185–188.

Windley, H. R., and Foley, W. J. (2015). Landscape-scale analysis of nutritional traits of New Zealand tree foliage using near-infrared spectroscopy. *For. Ecol. Manage.* 357, 161–170. doi: 10.1016/j.foreco.2015.08.018

Xie, L. Y., Wen, D. X., Wu, C. L., and Zhang, C. Q. (2022). Transcriptome analysis reveals the mechanism of internode development affecting maize stalk strength. *BMC Plant Biol.* 22, 1–16. doi: 10.1186/s12870-022-03435-w

Xu, X., Ren, X., Luan, Y., Su, Y., Li, R., and Yang, W. (2017). Genetic study on stalk crushing strength of improved maize inbred lines. *J. Jilin Agric. Univ.* 39, 648–654. doi: 10.13327/j.jjlau.2017.3153

Xue, J., Gou, L., Zhao, Y. S., Yao, M. N., Yao, H. S., Tian, J. S., et al. (2016). Effects of light intensity within the canopy on maize lodging. *Field Crops Res.* 188, 133–141. doi: 10.1016/j.fcr.2016.01.003

Yang, Y. S., Guo, X. X., Hou, P., Xue, J., Liu, G. Z., Liu, W. M., et al. (2020). Quantitative effects of solar radiation on maize lodging resistance mechanical properties. *Field Crops Res.* 255, 107906. doi: 10.1016/j.fcr.2020.107906

Yang, Z., Li, K., Zhang, M., Xin, D., and Zhang, J. (2016). Rapid determination of chemical composition and classification of bamboo fractions using visible-near infrared spectroscopy coupled with multivariate data analysis. *Biotechnol. Biofuels* 9, 1–18. doi: 10.1186/s13068-016-0443-z

Zhan, X. X., Kong, F. L., Liu, Q. L., Lan, T. Q., Liu, Y. Q., Xu, J. Z., et al. (2022). Maize basal internode development significantly affects stalk lodging resistance. *Field Crops Res.* 286, 108611. doi: 10.1016/j.fcr.2022.108611

Zhang, Y., Liang, T., Chen, M., Zhang, Y., Wang, T., Lin, H., et al. (2019). Genetic dissection of stalk lodging-related traits using an IBM Syn10 DH population in maize across three plots (*Zea mays* L.). *Mol. Genet. Genom.* 294, 1277–1288. doi: 10.1007/s00438-019-01576-6

Zhang, W., Wu, L., Wu, X., Ding, Y., Li, G., Li, J., et al. (2016). Lodging resistance of Japonica rice (*Oryza sativa* L.): morphological and anatomical traits due to top-dressing nitrogen application rates. *Rice* 9, 1–11. doi: 10.1186/s12284-016-0103-8

Zhang, T., Zhao, M. Q., Liu, F., Tian, H. Q., Wulan, T. Y., Yue, Y., et al. (2020). A discrete element method model of corn stalk and its mechanical characteristic parameters. *Bioresources* 15, 9337–9350. doi: 10.15376/biores.15.4.9337-9350

frontiers | Frontiers in Plant Science

TYPE Original Research
PUBLISHED 17 August 2023
DOI 10.3389/fpls.2023.1233349

OPEN ACCESS

EDITED BY
Philipp Von Gillhaussen,
International Plant Phenotyping Network (IPPN), Germany

REVIEWED BY
Patrick Sebastian,
University of Technology Petronas, Malaysia
Liang Wan,
Zhejiang University, China

*CORRESPONDENCE
Stephen Njehia Njane
njanes492@affrc.go.jp

RECEIVED 02 June 2023
ACCEPTED 27 July 2023
PUBLISHED 17 August 2023

CITATION
Njane SN, Tsuda S, van Marrewijk BM, Polder G, Katayama K and Tsuji H (2023) Effect of varying UAV height on the precise estimation of potato crop growth. *Front. Plant Sci.* 14:1233349. doi: 10.3389/fpls.2023.1233349

Effect of varying UAV height on the precise estimation of potato crop growth

Stephen Njehia Njane[1]*, Shogo Tsuda[1], Bart M. van Marrewijk[2], Gerrit Polder[2], Kenji Katayama[1] and Hiroyuki Tsuji[1]

[1]Hokkaido Agricultural Research Center, National Agriculture and Food Research Organization, Memurocho, Kasaigun, Hokkaido, Japan, [2]Wageningen Greenhouse Horticulture, Wageningen University and Research, Wageningen, Netherlands

A phenotyping pipeline utilising DeepLab was developed for precisely estimating the height, volume, coverage and vegetation indices of European and Japanese varieties. Using this pipeline, the effect of varying UAV height on the precise estimation of potato crop growth properties was evaluated. A UAV fitted with a multispectral camera was flown at a height of 15 m and 30 m in an experimental field where various varieties of potatoes were grown. The properties of plant height, volume and NDVI were evaluated and compared with the manually obtained parameters. Strong linear correlations with R^2 of 0.803 and 0.745 were obtained between the UAV obtained plant heights and manually estimated plant height when the UAV was flown at 15 m and 30 m respectively. Furthermore, high linear correlations with an R^2 of 0.839 and 0.754 were obtained between the UAV-estimated volume and manually estimated volume when the UAV was flown at 15 m and 30 m respectively. For the vegetation indices, there were no observable differences in the NDVI values obtained from the UAV flown at the two heights. Furthermore, high linear correlations with R^2 of 0.930 and 0.931 were obtained between UAV-estimated and manually measured NDVI at 15 m and 30 m respectively. It was found that UAV flown at the lower height had a higher ground sampling distance thus increased resolution leading to more precise estimation of both the height and volume of crops. For vegetation indices, flying the UAV at a higher height had no effect on the precision of NDVI estimates.

KEYWORDS

UAV, Potatoes, volume, vegetation indices, multispectral

1 Introduction

The precise monitoring of the phenotypic properties of potatoes is important for the development of new potato varieties for high quality and improved yield. Not only are some varieties susceptible to disease infestation such as early blight disease but also, their growth properties affect the yield of potatoes. Until today, monitoring of the growth of crops has relied on manual physical sampling where height of potato crops is sampled in

the plots containing the phenotypes. However, this is not only limited to a small area and several crops within the plots, but also the estimation of the height of the crops is difficult, especially due to the complex canopy of potato crops.

Recently the utilisation of remote sensing techniques together with image processing has enabled the precise estimation of the phenotypic properties of potatoes. Especially, the utilisation of UAV's has revolutionized phenotyping not only due to their low cost, but also a large area can be sampled in a short time. The emergence of potato crops was estimated using UAV thus reducing the time required for manual sampling of potato crops to determine their emergence (Li et al., 2019). The disease severity on potato crop field was estimated using an RGB camera mounted on a UAV (Sugiura et al., 2016) and while Jindo et al. (2023) utilised UAV to detect the damage caused by potato cyst nematode, Van De Vijver et al. (2022) utilised UAV to detect early blight disease. Furthermore, a multispectral camera mounted on a UAV could estimate SPAD values of barley leaves as demonstrated by Liu et al. (2021). The prediction of yield has also been made possible by utilisation of UAV in combination with machine learning (Sun et al., 2020), and also by combining cultivar information (Li et al., 2021).

Hitherto, parameters of plant height and canopy cover estimates have been used to measure the ability of crops to intercept radiation and also as a representation of the activity of the crop that relate to growth and development. Stewart et al. (2007) found a high correlation between canopy cover and leaf area index (LAI). Using non-linear models, Bojacá et al (2011) could estimate potato crop canopy coverage on different fields. However, only a small area could be sampled hence limiting observation in the whole field. de la Casa et al. (2007) found that there was a high linear correlation between potato crop coverage and the fraction of light interception. However, (Boyd et al., 2002) found that such a correlation of crop coverage with LAI, although linear, it varies with management of the field. Furthermore, (Bojacá et al., 2011) found that applying a non-linear model to characterise potato canopy coverage could yield more precise simulation results. Using crop canopy, Li et al. (2019) investigated the rate of emergence of various varieties and assessed the differences in the uniformity of their emergence from the soil. However, the penetration of light is affected not only by the crop surface cover, but also the architecture of the canopy, leaf size, angle, and the number of leaves. Photosynthesis activity is highly related to the light intensity within the leaf canopy, which is depended on the leaf size, distribution, and volume of the canopy. Therefore, it is important to estimate not only the surface crop cover but also the 3D properties of the potato canopies for informed decision making.

To generate such values, Structure from Motion (SfM) is utilised to reconstruct the images to form a 3D model. This is normally used in UAV imagery since special active illumination is not required. Furthermore, the resolution of the constructed model depends not only on the number of images, but also on the ground sampling distance and the resolution of the acquired images (Paulus, 2019). While, the combination of crop height and coverage was used to determine the spraying volume on potato (Xie et al., 2022), it was found that the point cloud data was unreliable especially during low coverage. Burgess et al. (2017) utilised individual plants extracted from a field grown plot to generate 3D representation of crops. However, this is difficult to apply in phenotyping in the actual field. Furthermore, due to the complex canopy of the potato crops and the ridges planted on them, it is imperative to develop an improved technique for extracting phenotypic properties of potato crops.

Hitherto, an easy-to-use automatic system for generating important crop properties like height, volume, crop coverage and vegetation indices has not been developed. This has limited such analysis to either commercial software or complicated programming skills which not only require fundamental understanding, but also complex computer environmental settings. Guo et al. (2017) developed a python-based tool for phenotyping. However, this could only estimate ground coverage ratio. Tresch et al. (2019) developed an automatic technique for generation of plots in the field thus making it easier to divide the field into plots. It is imperative to estimate not only the coverage but also the height and the volume of potato crops during growth. Especially during emergence, it is important to determine these parameters to precisely determine the sprout rate and their traits. It has been shown that increased flight altitude results in decreased resolution of the densified surface model (DSM) which is used to extract height and related parameters (Abou Chakra et al., 2020). While increasing the UAV flight height reduces the time taken to take mages in the same field, the lesser number of images captured reduces the processing time. This results in reduced time taken during the SfM (Structure from Motion) reprocessing to produce densified surface model and orthomosaic which are used to extract the parameters of height and coverage respectively. However, the increased UAV flight height results in decreased resolution, and this might affect the accuracy of extraction of the parameters of plant height, volume, and coverage. The effect of varying UAV height on seedling rapeseed found that higher GSD resulted in lower precision of NDRE vegetation index when estimating LAI (Zhang et al., 2020). While the effect of varied resolution by resampling the orthomosaic found that high resolution had higher correlation with potato's above ground biomass, however, this was only limited to a fixed UAV height of 20 m height (Liu et al., 2022). Therefore, it is paramount to determine the best UAV flight conditions that reduce processing time without compromising on the quality of the crop parameters to be estimated. Furthermore, for precise phenotyping properties, it is required to estimate the height, volume and crop coverage of potato varieties with high precision.

In this study, we will develop a new system for estimating the potato varieties traits. Firstly, a new automatic system for processing UAV-obtained DSM and orthomosaic will be developed. Secondly, using this new system, the crop properties of height, volume and coverage of both European and Japanese varieties will be estimated. As a lead on determining the ideal flight parameters for precisely obtain these phenotypic traits, we will compare the accuracy of UAV-obtained data by comparing the precision effect when UAV is flown at two different heights over the same area while analysing the growth parameters of plant height, volume, crop coverage and vegetation indices.

10.3389/fpls.2023.1233349

2 Materials and methodology

2.1 Experimental field set up

Eight varieties of potatoes were planted in an experimental plot in Memuro Hokkaido, Japan inside the National Agricultural and Research Centre (NARO) experimental field station as shown in Figure 1 on the 7th of May 2021. The experimental field measured 23.1 m by 19.5 m and three replications were planted with each plot measuring 4.5 m by 2.25 m. The potato varieties consisted of 5 European varieties, Euroviva, Etana, Priska, Sorentina and Montana, and 3 Japanese varieties, Toyoshiro, Konahime and Irish cobbler (locally known as Danshaku-imo). The potatoes which were hand planted were firstly cut into two and the half-cut potatoes whose sprout faced upward were placed at a crop spacing of 30 cm and each row was spaced at 75 cm from each other. After planting, the rows were covered with soil using a tractor-driven hiller thus ensuring a ridge of 30 cm height and a spacing of 75 cm between the ridges.

2.2 UAV images acquisition

For obtaining images on the experimental field from both 15 m and 30 m heights, a DJI P4 Multispectral UAV (SZ DJI Technology Co., Ltd) was utilised. The UAV has a camera consisting of 1 RGB camera and a 5-band multispectral camera. The multispectral camera consists of the Blue (450 ± 16nm), Green (560 ± 16nm), Red (650 ± 16nm), Red-edge (730 ± 16nm) and Near-infrared bands (840 ± 26nm). The UAV which also has an integrated RTK module was set at a FIXED GNSS position thus ensuring precise positioning when taking images. Furthermore, four ground control points were set at the four corners of the experimental field and their coordinates measured thus ensuring the project was georeferenced. The flight plan consisted of taking images in a grid system both at 15 m and 30 m. The time series images when the UAV is at 15 m and 30 m is as shown in Figure 2. For both heights, the RGB camera and the multispectral cameras ISO was set to AUTO mode with the shutter speed set at 1/1000 and shooting interval of 2 seconds with a front and side overlap of 80%. The camera was set such that the shooting angle was perpendicular to the course, and the cameras were set at Nadir (facing downwards) at an angle of 90 degrees with the horizontal field plane.

2.3 Pre-processing of the UAV images

The images were aligned and processed using a SfM (Structure from Motion) technique where the DSM was generated from the two-dimensional images obtained from the UAV. To do this, Pix4D mapper (Pix4D SA) software was utilised. In order to increase the accuracy of the map, the pre-measured GCP (Ground Control Points) were imported and marked in the ray cloud. Finally, re-optimisation was carried out, resulting in a calibration error of ± 2 cm. This error is equal to the absolute error of the RTK measurement of the GCP's. The point cloud was processed after which the orthomosaic and the Digital Surface Model (DSM), the Orthomosaic (RGB) and the reflectance maps (for each sensors' wavelength) were generated.

The parameters for obtaining UAV images and processing time when processing using a GPU NVIDIA Quadro RTX 6000 with an intel core i9 and a CPU processing speed of 3.31GHz are compared as shown in Table 1 below.

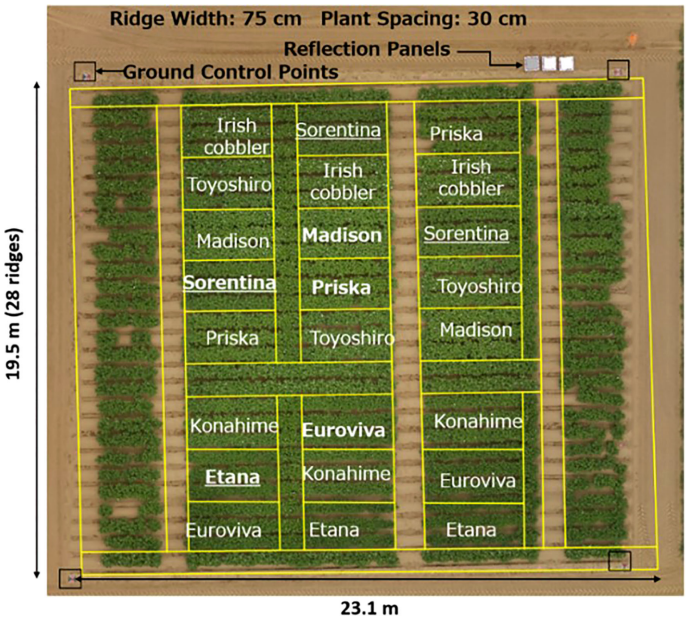

FIGURE 1
Set up of the field with the varieties planted on plots with three replications and ground control points were placed as shown with a black and red two-tone marker.

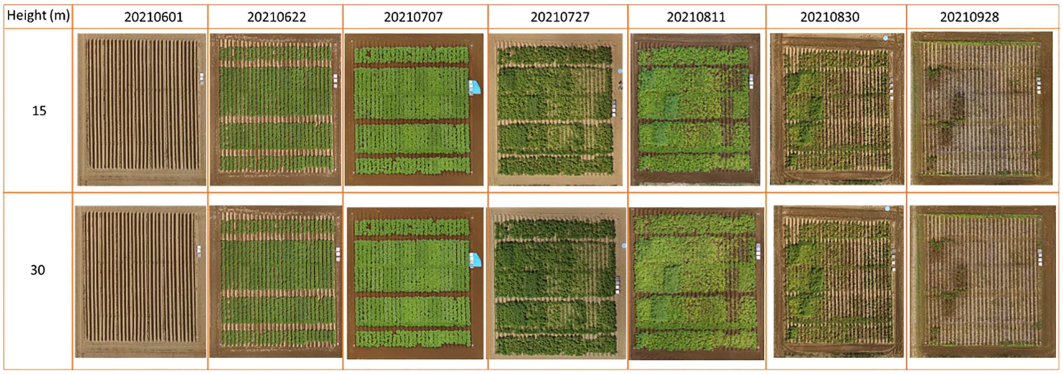

FIGURE 2
Time series orthomosaic images of the potato varieties plots for both UAV heights of 15 m and 30 m.

2.4 Plant segmentation

To do determine the crop properties, the crop parameters must be segmented from the bare soil. In this research segmentation is done by using DeeplabV3+ implemented in detectron2 (Chen et al., 2018). DeepLab is a deep learning based semantic segmentation method (Wu et al., 2023). In this research we used the pretrained weights available from the detectron2 framework. Transfer learning was applied by annotating 48 potato images. Since the dataset was quite small the number of iterations was set to 1000. Image size was set to 384 x 384. All the other parameters were similar as those mentioned by Wu et al. (2023). An example of the segmentation on an independent test image is shown Figure 3. Other segmentation methods like Otsu thresholding (Li et al., 2019) would fail at sunny condition or when the image is fully covered by crops.

2.5 Plant height measurement

A densified surface model with a resolution of 0.833 cm/pixel and 1.667 cm/pixel was generated from the densified point cloud for images taken at 15 m and 30 m respectively. To determine the height of crops from each plot, shapefiles measuring 3 m by 0.75 m were generated as representatives of each variety's plot's area (using QGIS software). To ensure precise height estimation, a plane surface on the top of the ridge was generated for each plot. This was done by determining the height of the bare soil 10 days after planting. Noise was removed by sorting the height array and selecting the height at 90% of the data. This base altitude ($Zplane_i$) was determined for each plot as shown in Figure 4.

TABLE 1 Comparison of flight parameters for both flight altitudes.

Height (m)	Camera angle	Mission type	Flight Time (min)	Processing time DSM and Orthomosaic
15	Nadir	Parallel	15	3 hours
30	Nadir	Parallel	7	1 hour

In the successive days as the crops grew, the height of the crops increased. The height was calculated by segmenting the background from the image and subsequently the difference between the base altitude and the terrain altitude of each segmented plot (Z_y) was used to determine the height, as shown in Eq. 1. Where *i*ndicates the plot number and *j* indicates the pixel number.

$$H_{ij} = Z_{ij} - Zplane_i \quad (1)$$

The height of the crops in each plot was extracted by determining the average of the total number of pixels.

As a proof of concept, the height of crops from each crop was measured manually on a weekly basis. This was done by placing the meter rule at the top of the ridge and measuring the height of the crop close to the apex. Taking care to prevent injuring the potato crops foliage, the height of the 5 sample crops in each plot were measured recorded from which the average height with growth period was calculated.

2.6 Volume measurement

The volume of the crops from each plot was determined by summation of the total volume of the pixels from the densified surface model. Each pixel consisted of length L_{ij} (cm), the width W_{ij} (cm), and the height H_{ij} (cm). The height was obtained using Eq. 1 (section 2.4). By multiplying the height with the length and width of each cell the volume was calculated as shown in Eq. 2 below.

$$V_{ij} = L_{ij} \times W_{ij} \times H_{ij} \quad (2)$$

The length and width of each pixel is equidistant and is equal to the ground sampling distance (GSD). Therefore, the length and width of each pixel obtained from the UAV's height, i.e., 15 m and 30 m was 0.833 cm/pixel and 1.667 cm/pixel respectively. Although the grid of the higher GSD i.e., 30 m would be larger than the grid with a smaller GSD, however, since the total volume was limited to the plot area of each variety, then the total area utilised for estimating volume would be similar despite their different GSD.

10.3389/fpls.2023.1233349

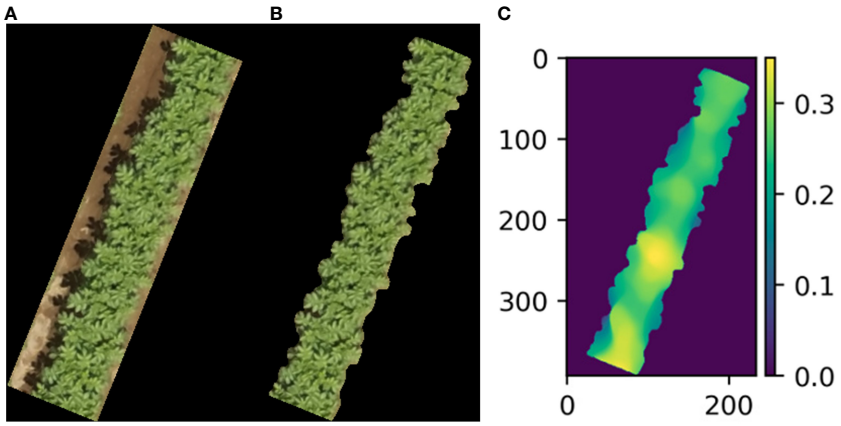

FIGURE 3
Example image of input image **(A)**, segmented image **(B)** and visualized height map, with height in meters **(C)** obtained on 46th day after planting.

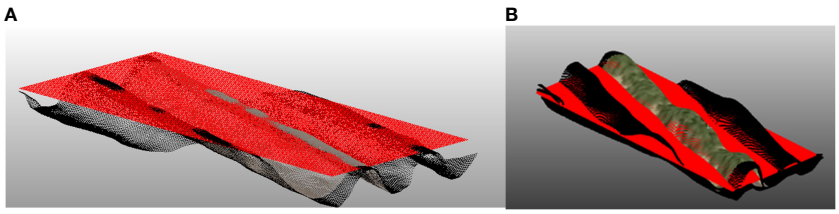

FIGURE 4
(A) plot with the fitted plane (red) on bare soil (day 5 after planting) and **(B)** 36 days after planting.

In order to compare the accuracy of estimation, the volume of the crops was also estimated by hand. This was done by manually measuring the width, breadth, and height of four samples from each plot. The average volume per plot was estimated from the four samples and used as the ground truth values for the volume of the crops.

2.7 Vegetation indices measurement

To determine the health of the potato crops during growth, each plot's average Normalised Difference Vegetation Index (NDVI) was estimated (Datt, 1999) from the NIR and Red reflectance maps generated from the processing of images in these respective wavelengths. In the mid to late stages when the chlorophyll concentration was relatively high, the Normalised Difference RedEdge (NDRE) was utilised to estimate the health of the potato crops. Both the NDVI and NDRE are popularly used to map the variability of nitrogen and hence determine the fertilizer requirement. The ratio of the reflectivity in the NIR and red-edge bands were used to estimate the chlorophyll content in the leaves using the Chlorophyll index -Red-Edge (Clre). Leaf Chlorophyll Index (LCI) was used to determine the change in chlorophyll content by estimating the spectral reflectance properties of both the near-infrared and the red reflectance wavelengths. The indices are shown in Table 2.

To compare the estimated NDVI values obtained from the reflectance maps generated by the UAV images, a handheld crop sensor, GreenSeeker (Trimble Inc.) was utilised to measure NDVI. The sensor had sensitivity of measurement at the wavelengths of

TABLE 2 Vegetation indices generated from the respective reflectance maps.

Vegetation index	Equation	Reference
Normalised Difference Vegetation Index (NDVI)	$\frac{NIR - Green}{NIR + Green}$	(Datt, 1999)
Normalised Difference Red Edge (NDRE)	$\frac{NIR - \mathrm{Re}\, dEdge}{NIR + \mathrm{Re}\, dEdge}$	(Barnes et al., 2000)
Chlorophyl Red Edge (Clre)	$\frac{NIR}{\mathrm{Re}\, dEdge} - 1$	(Gitelson, 2005)
Leaf Chlorophyll Index (LCI)	$\frac{NIR - \mathrm{Re}\, dEdge}{NIR + \mathrm{Re}\, d}$	(Rouse et al., 1974)

10.3389/fpls.2023.1233349

Red 660 ± 10 nm (full-width half-magnitude) and near-infrared 780 ± 15 nm (full-width half-magnitude). The sensor emits both of these wavelengths and measures the amount of each wavelength reflected from the surface of the crops. Measurements were taken by engaging the trigger and scanning the potato field crops' plots at height of about 50 cm from the surface of the crops. In each plot, the reading was taken three times and the average value was calculated.

3 Results

3.1 Potato crop height estimation

The orthomosaic images and the height of the potato crops was obtained after processing the densified surface model obtained when the UAV was flown at 15 m and 30 m as shown in Figures 5A, B below. During the early growth stages, there was a gradual increase in the height of the crops especially after emergence. However, 30 days after emergence, there was a sporadic increase in the height of all the potato varieties. The growth peaked between 60-67 days after planting from which the plant height decreased as the potato crops matured and senescence started. However, for the Euroviva variety, the plant height continued to increase with a prolonged growth period with the growth peaking at 102 days after planting after which maturity and senescence occurred.

For both UAV-heights, the plant height peaked between day 61 day 67. However, during the senescence stage, it was observed that plant heights obtained when the UAV was at 30 m showed a gradual increase in plant height at day 102 while the plant height obtained when the UAV was at 15 m showed a slight or no increase in plant height during the senescence stage. At days 81 and 102 where a large

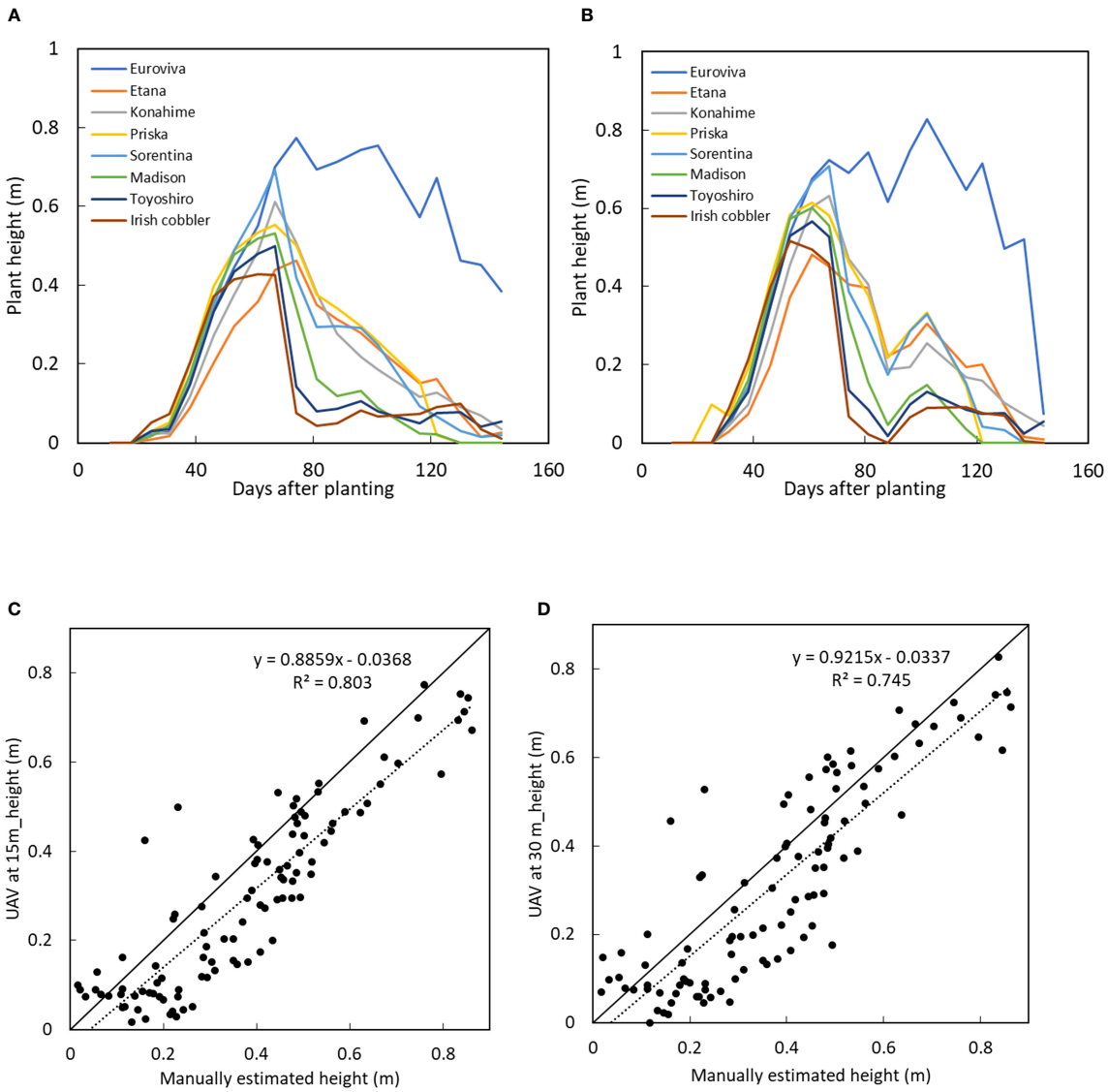

FIGURE 5
Plant height of 8 varieties with growth time when the UAV was at **(B)** 15 m and **(C)** at 30 m and comparison between manually measured plant height with the UAV-obtained height when the UAV was at **(C)** 15 m and **(D)** at 30 m.

10.3389/fpls.2023.1233349

decrease followed by a rapid increase in crop was observed, the standard deviation showed that a larger error was observed in the height values obtained when the UAV was at 30 compared to at 15 m as shown in Tables 3, 4.

There was a high correlation between the plant height obtained when the UAV was at 15 m and at 30 m as shown in Figure 6 below.

It was clear that especially during the early growth (plant height 0 - 0.1 m), the plant height obtained from images taken at 30 m showed no change in the height of the crops while there was observable change and differences in the height of potato crops when the UAV was at 15 m as shown in Figure 5C. The differences in the plant height were also compared with the manually obtained plant height obtained by sampling in the plots of the respective varieties. It was observed that while the plant height obtained from the UAV at 15 m showed a high linear correlation with the manually obtained values, the plant height obtained when the UAV was flown at 30 m as shown in Figure 5D. had a slightly lower correlation with the manually obtained plant height.

3.2 Plant volume estimation

The potato varieties' volume was compared between those estimated when the UAV was at 15 m from those obtained when the UAV was at 30 m as shown in Figures 7A, B. A similar tendency of growth was obtained when the UAV was at both heights. During the early stages of sprout emergence, there was little or no observable change in the volume of the potato varieties, until day 30, after which a rapid increase in the volume of the potato varieties was observed. From the volume estimated when the UAV was at 15 m, it was observed that the volume of all the varieties peaked at day 67 while the volume estimated when the UAV was at 30 m peaked at day 61. A similar growth curve tendency was obtained in both data sets when the UAV was flown at 15 m and at 30 m.

A high linear correlation was obtained between the volume of all the varieties when the UAV was at 15 m and at 30 m as shown in Figure 8. While it takes less time to obtain images at a higher altitude (30 m in this case), resulting in higher ground sampling distance and thus lower sampling resolution, it would, however, still have sufficient accuracy for precise estimation of the volume of potatoes with similar precision as that obtained when the UAV is flown at half the height (15 m).

A comparison was made between the UAV estimated volume and the manually estimated volume. From the manual measurement, the height, width and length of the potato crops was measured as a representative of the volume of crops. While a high linear correlation was obtained between the UAV estimated volume when the UAV was at 15 m, a slightly lower correlation was obtained from the volume estimated when the UAV was at 30 m as shown in Figures 7C, D respectively. However, in both cases, the manually estimated volume was higher than the UAV estimated volume.

It was considered that during the early stages of growth, at days 31, there was a low correlation with an R^2 of 0.67 between the UAV-estimated volume and the manually estimated volume as shown in Figure 9A. With successive growth, a high linear correlation of 0.9 was obtained between the UAV-estimated and the manually estimated volume as shown in Figure 9B.

3.3 Vegetation indices

From the multispectral bands, the reflection maps of NIR and Red bands were utilised to estimate the NDVI values of all the varieties of potato crops and a comparison was made between the NDVI values obtained when the UAV was at 15 m and 30 m as shown in Figures 10A, B respectively. A similar tendency of change in NDVI was obtained between the two datasets where the NDVI value increased rapidly from 30 days after planting to about 74 days after planting after which the values decreased, except for Euroviva variety which had a prolonged stable NDVI value from day 74 to day 116 after which NDVI values decreased.

A high linear correlation with a coefficient of variation close to 1 was obtained between the NDVI values obtained when the UAV was at 15 m and at 30 m as shown in Figure 11.

A comparison was made between the UAV estimated NDVI and the manually estimated NDVI. A similar high linear correlation with a coefficient of variation of 0.97 was obtained between the

TABLE 3 STDEV comparing plant heights on day 88.

Variety name	15 m	30 m
Euroviva	0.005	0.033
Etana	0.073	0.079
Konahime	0.069	0.097
Priska	0.010	0.035
Sorentina	0.036	0.045
Madison	0.033	0.030
Toyoshiro	0.029	0.032
Irish cobbler	0.018	0.00

TABLE 4 STDEV comparing plant heights on day 102.

Variety name	15 m	30 m
Euroviva	0.005	0.055
Etana	0.038	0.051
Konahime	0.021	0.063
Priska	0.019	0.054
Sorentina	0.020	0.060
Madison	0.025	0.048
Toyoshiro	0.029	0.043
Irish cobbler	0.012	0.018

10.3389/fpls.2023.1233349

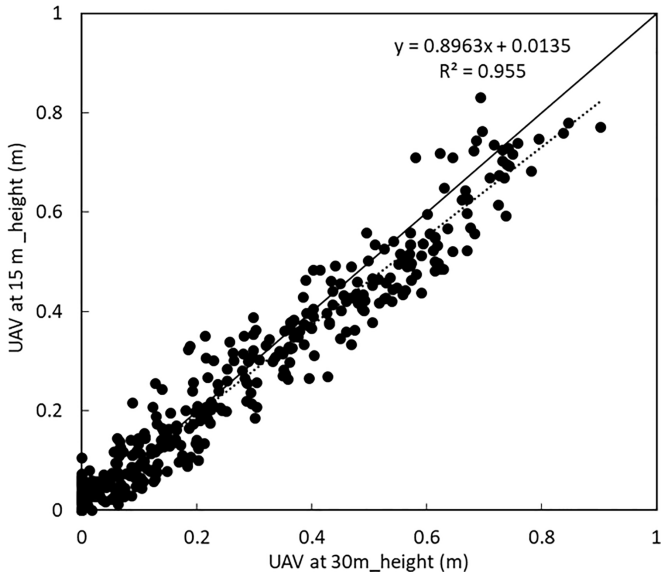

FIGURE 6
Comparison between plant height of all varieties when the UAV was at 15 m and at 30 m. A linear correlation with a coefficient of variation of 0.947 was obtained.

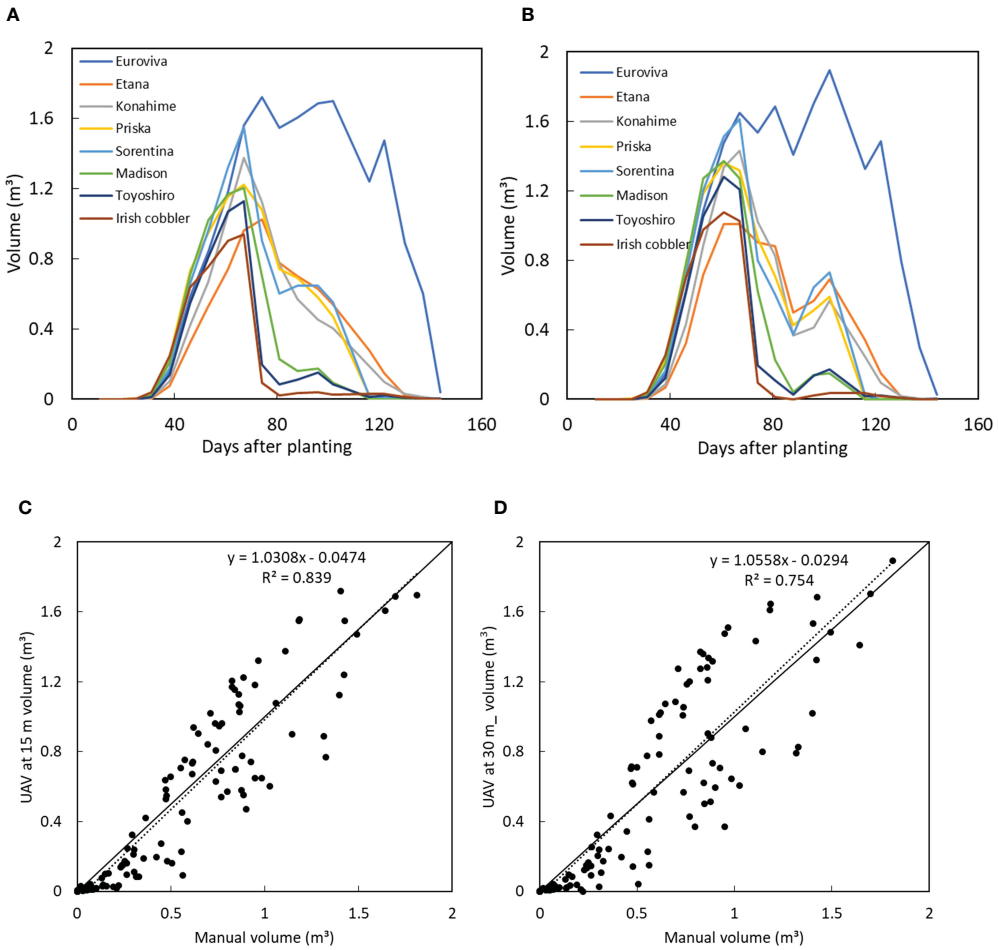

FIGURE 7
Plant volume of 8 varieties when the UAV was at **(A)** 15 m and **(B)** at 30 m and comparison between manually measured plant volume with the UAV-obtained volume when the UAV was at **(C)** 15 m and **(D)** at 30 m.

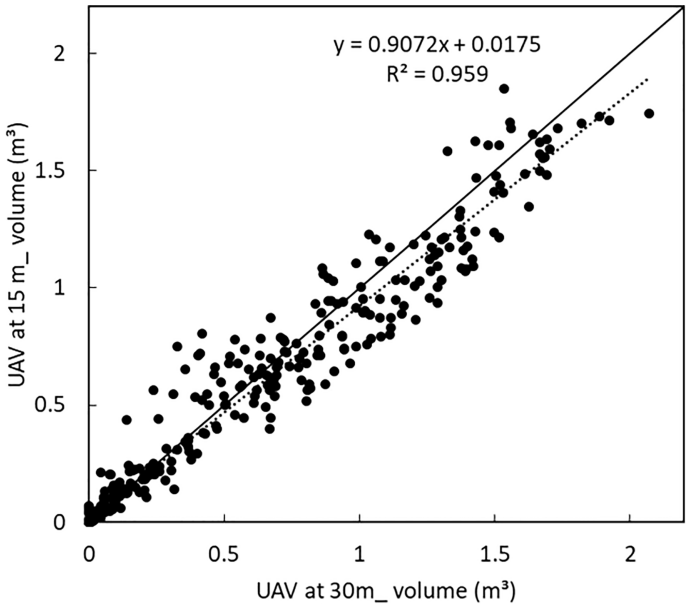

FIGURE 8
Comparison between plant volume of all varieties when the UAV was at 15 m and at 30 m. A linear correlation with a coefficient of variation of 0.956 was obtained.

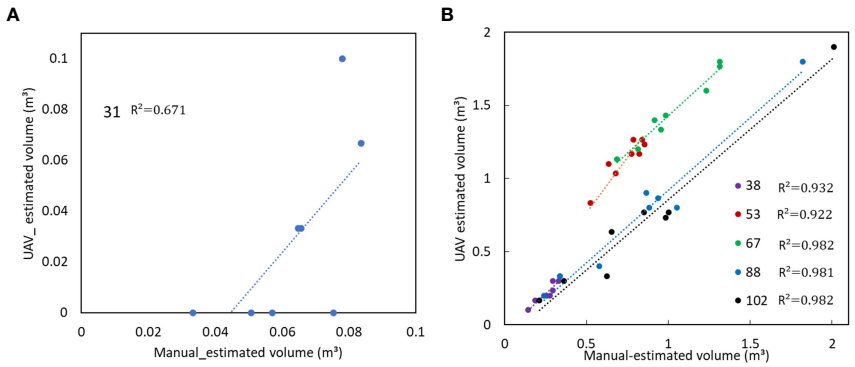

FIGURE 9
Early stages of growth **(A)** 31st day after planting and successive days **(B)** 38 to 102 days after planting showing the comparison between UAV estimated and manually estimated volume.

manually estimated and the UAV estimated NDVI when the UAV was at 15 m and at 30 m as shown in Figures 10C, D.

A high coefficient of determination was obtained for all parameters of height, volume and NDVI when the UAV was flown at both heights as shown in Table 5.

While both UAV-heights can be used to obtain the parameters of height, volume and NDVI, a comparison between manually estimated values of height, volume and NDVI with those when the UAV was at 15 m and 30m was obtained as shown in Tables 6, 7 showed that higher precision was obtained when the UAV was flown at a lower height. A high linear coefficient of determination with a lower RMSE was obtained when the UAV was at a lower height of 15 m than when flown at 30 m.

4 Discussion

Although there was a high correlation between the height of the varieties at both UAV heights, the potato crops height obtained when the UAV was flown at a higher height showed slightly higher errors especially at day 88 and day 102. This was as a result of noise in the densified point cloud as a result of reduced spatial resolution leading to inaccuracies in plant height extraction during the early stages (Moeckel et al., 2018). When the images were obtained at a lower height of 15 m this increased resolution, thus indicating that the plant height increased gradually according to the growth period as shown in Figure 12. There was no effect of downwash form the propellers of the UAV at both 15 m and 30 m height. While flying

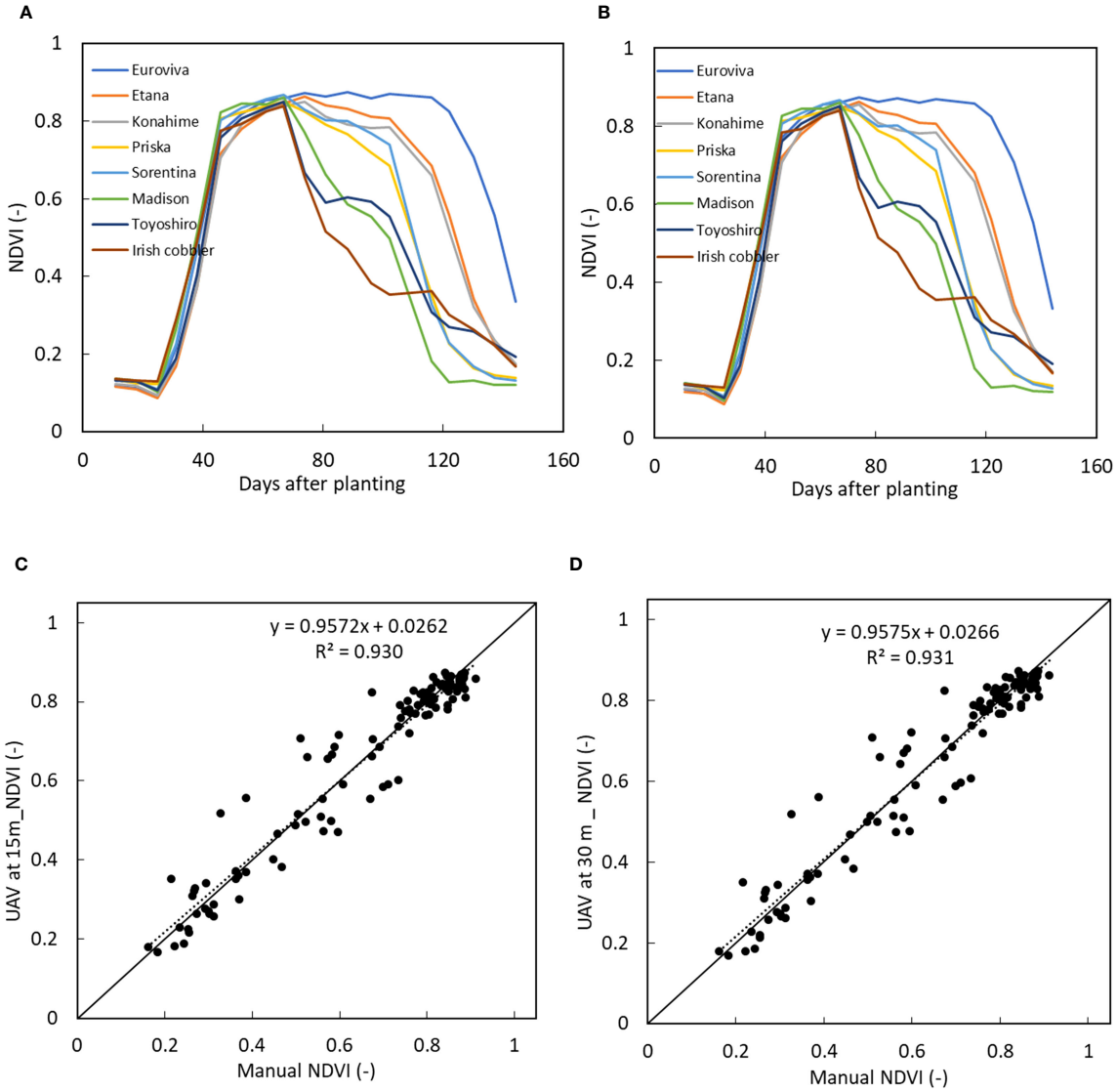

FIGURE 10
Time series NDVI values of 8 varieties when the UAV was at **(A)** 15 m and **(B)** at 30 m and comparison between manually measured NDVI with the UAV estimated NDVI when the UAV was at **(C)** 15 m and **(D)** at 30 m.

lower than 15 m would increase the ground sampling distance, however, this would also lead to more images and thus lengthening the processing time. Furthermore, for larger fields, this would mean that due to lower ground sampling distance, images would have to be taken at a hover-and-capture mode which takes much longer time as the UAV would have to stop while taking images before proceeding. While flying at higher heights such as 30 m would lead to fewer images and shorter processing time, however increased ground sampling distance leads to lower resolution, thus not ideal especially when estimating the crop traits at the initial stages of growth. Further studies exploring larger phenotypic fields would utilise higher UAV heights in order to cover such large areas.

From the images obtained when the UAV was both at 15 m and at 30 m, Euroviva had the highest height due to its prolonged maturity period. Thus Euroviva plant height remained relatively high even after flowering and the beginning of senescence period. Euroviva which has a late maturity, it continues to grow even after other varieties start to senescence. This was equally translated to the yield as Euroviva has been reported to have higher yields (Seed potatoes of the highest quality, 2021). Due to the prolonged growth period, the light interception area also increased as the height and volume of Euroviva varieties increased. This resulted in increased height and volume of the canopy thus leading to increased light penetration and providing higher sinks for photosynthesis leading to increased photosynthetic activities at the leaves level (Burgess et al., 2017). The sudden decrease in the plant height from day 67 to day 81 for the other varieties during the growth period was a result of senescence where the leaves begin to wither thus leading stems of the potatoes weakening thus decreased height. There was a sudden slight increase in the crops height from day 81 to day 96 as a result of sudden increased precipitation thus leading to the stems vigour increasing and thus increased height, but it was short-lived as

10.3389/fpls.2023.1233349

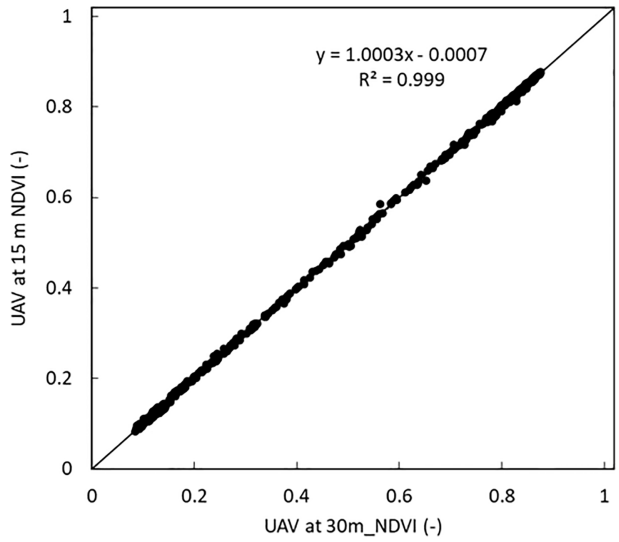

FIGURE 11
Comparison between NDVI volume of all the potato varieties when the UAV was at 15 m and at 30 m. A linear correlation with a coefficient of variation of 1 was obtained.

TABLE 5 Correlation between UAV parameters between UV flown at 15 m and 30 m.

Parameters	R^2	Adjusted R^2	RSME	*p* value
Height	0.955	0.955	0.046	0
Volume	0.959	0.959	0.100	0
Coverage	0.992	0.992	0.037	0
NDVI	0.999	0.999	0.004	0

TABLE 6 Comparison between manually estimated and UAV-estimated values at 15 m height.

Parameters	R^2	Adjusted R^2	RMSE	*p*value
Height	0.803	0.801	0.0919	<0.001
Volume	0.828	0.825	0.209	<0.001
NDVI	0.939	0.929	0.060	<0.001

TABLE 7 Comparison between manually estimated and UAV-estimated values at 30 m height.

Parameters	R^2	Adjusted R^2	RMSE	*p*value
Height	0.745	0.742	0.113	<0.001
Volume	0.735	0.732	0.280	<0.001
NDVI	0.931	0.930	0.060	<0.001

withering continued due to senescence and decreased height was obtained until near harvesting period.

Similarly, there was a high correlation between the volume of the potato varieties when the UAV was flown at both heights. It was observed that even during the early stages, since volume estimated not only the vertical elongation but also the horizontal elongation of the canopy, a normal growth curve was observed at both heights. The manual estimated volume was higher than the UAV estimated volume. This is because the manual measurement assumes that the vegetation block is cuboid thus estimates volume using the

10.3389/fpls.2023.1233349

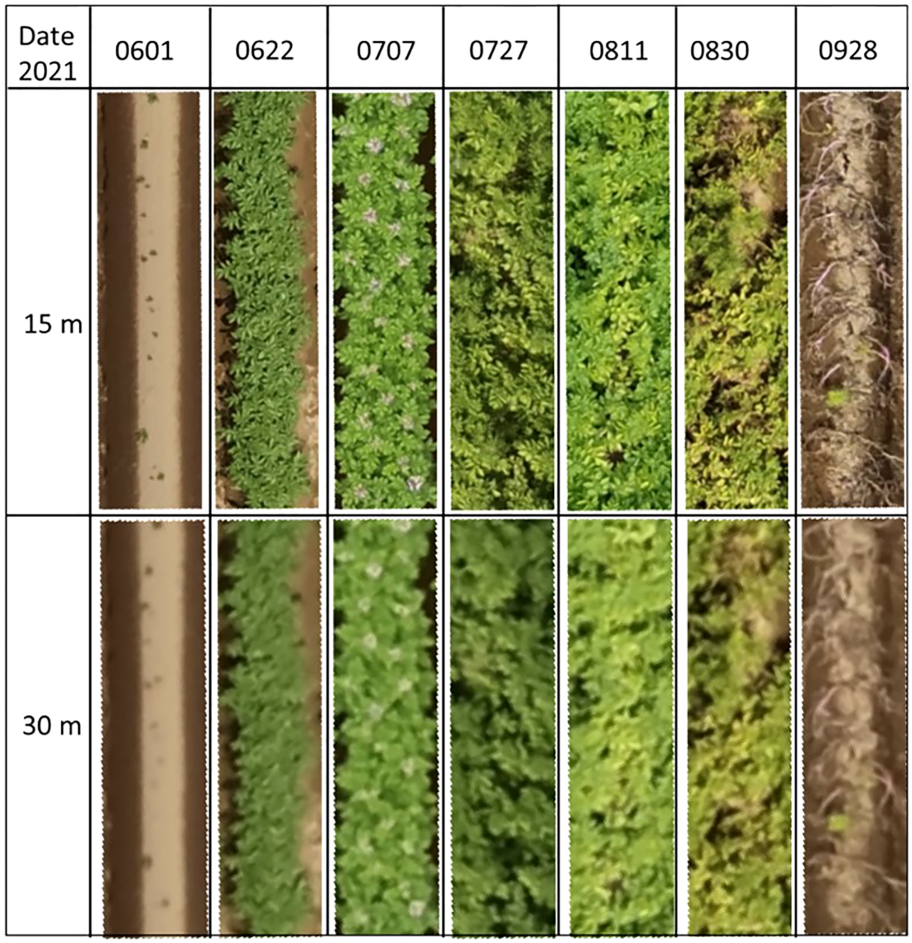

FIGURE 12
Time series orthomosaic images of one of the plots showing the difference between 15 m and 30 UAV processed orthomosaic files.

measurements of height, length and volume, unlike potato canopy, which is not only irregular in shape, but also has air spaces in between the vegetation foliage, thus resulting in overestimation when measured manually. Secondly, in the first days, the potatoes are relatively small. Deep learning networks like DeepLabv3+ are capable of detecting objects, but small objects ten to disappear in the large networks. Small plants are consequently not always recognized causing an underestimation of the volume compared to the manual measurements (Figure 10A). In the successive days, a higher correlation was obtained between the UAV and the manually obtained data (Figure 10B).

Furthermore, volume would be ideal in monitoring the growth of mixed varieties in large breeding fields since a similar precision for volume estimation would be obtained when the UAV was flown at a higher height thus ideal for obtaining phenotypic properties. Sun et al. (2018) observed that large differences in the volume of the cultivars could be obtained, in comparison to canopy area. Furthermore, while it is erroneous to measure the volume of crops manually due to their irregularity in both shape and structure, volume estimation using the densified surface model was precise and added a new trait for varietal differentiation. A similar tendency in the growth curve NDVI was obtained when the UAV was flown at both heights. This is because the reflectance map was not easily affected by the difference in the UAV height since clear reflectance values were obtained. This shows that the NDVI values are not affected by the changes in the ground sampling distance hence a higher UAV height would be ideal as it saves time and battery when taking images in the field. Furthermore, a similar high precision would be obtained thus enabling faster return and monitoring of potato varieties in the field.

However, because of the difference in the NIR bands between the UAV -multispectral camera (840 ± 26 nm) and the GreenSeeker (780 ± 15 nm) the sensitivity of measurement of NDVI varied between the former from that of the latter. Since the UAV utilises the sunshine sensor to correct for the irradiation, it is ideal in extracting the reflectance values on different days where the radiation would vary. Furthermore, since sampling using the GreenSeeker can only be done in a single plot, then utilisation of the UAV would be ideal in determining the change in the vegetation indices over the whole plot. Therefore, not only would it be faster to monitor a larger field using UAV compared to manual sampling of NDVI which can only be done in a small area and take a lot of time for sampling measurement, NDVI can be estimated using UAV at a faster rate, lesser time and the whole field can be estimated thus

ensuring precise monitoring of the growth of potato varieties in the field. A combination of these parameters of plant height, volume and NDVI would be ideal for predicting yield of potato crops or estimating nitrogen content (Lu et al., 2021).

5 Conclusion

A precise phenotyping pipeline using DeepLab was developed for estimating the potato crop traits from both the European and Japanese potato varieties. Using this pipeline, the precise estimates of height, volume and vegetation indices of potato varieties was compared with UAV-images taken at 15 am and 30 m altitude. There was a high correlation between the potato varieties at both heights with an R^2 of 0.947, 0.956 and 1 for crop varieties height, volume and NDVI respectively. While a high correlation was obtained, it was found that in the early stages of growth, higher resolution obtained from 15 m would be ideal for determining the volume and height of the potato crops after emergence. Furthermore, for NDVI, there was no difference between images obtained at the two heights of the UAV. As a proof of concept, it was found that there was a high correlation between the UAV obtained parameters of height, volume and NDVI with those measured manually with R^2 of 0.856, 0.845 and 0.968 respectively when the UAV was flown at a height of 15 m thus confirming the preciseness of the parameters obtained by the UAV. In the future, it is expected that these parameters would not only be useful for yield prediction but also provide breeders with more information about the varieties in the field thus saving time compared to manual measurements.

Data availability statement

The original contributions presented in the study are included in the article/supplementary material. Further inquiries can be directed to the corresponding author.

Author contributions

SN wrote the first draft of the manuscript. ST contributed to statistical analysis. BM and GP contributed to data analysis. KT and HT contributed to conception and design of the study. All authors contributed to the article and approved the submitted version.

Funding

This research was jointly funded by Wageningen University and Research and National Agriculture and Food Research Organisation, Hokkaido under the TTADDA project.

Acknowledgments

We would like to specially thank TADDA project members from Wageningen University and Research for their continuous collaboration in the joint research with NARO. We would also like to thank Dr. David Sprague for proofreading our manuscript.

Conflict of interest

The authors declare that the research was conducted in the absence of any commercial or financial relationships that could be construed as a potential conflict of interest.

Publisher's note

References

Abou Chakra, C., Somma, J., Gascoin, S., Fanise, P., and Drapeau, L. (2020). Impact of flight altitude on unmanned aerial photogrammetric survey of the snow height on mount Lebanon. *ISPRS - Int. Arch. Photogramm. Remote Sens. Spat. Inf. Sci.* XLIII-B2-2020, 119–125. doi: 10.5194/isprs-archives-xliii-b2-2020-119-2020

Barnes, E. M., Clarke, T. R., and Richards, S. E (2000). Coincident detection of crop water stress, nitrogen status and canopy density using ground based multispectral data. *Proceedings of the 5th International Conference on precision agriculture* (Madison, WI, USA).

Bojacá, C., Garcia, S., and Schrevens, E. (2011). Analysis of potato canopy coverage as assessed through digital imagery by nonlinear mixed effects models. *Potato Res.* 54, 237–252. doi: 10.1007/s11540-011-9189-y

Boyd, N. S., Gordon, R., and Martin, R. C. (2002). Relationship between leaf area index and ground cover in potato under different management conditions. *Potato Res.* 45, 117–129. doi: 10.1007/BF02736107

Burgess, A. J., Retkute, R., Herman, T., and Murchie, E. H. (2017). Exploring relationships between canopy architecture, light distribution, and photosynthesis in contrasting rice genotypes using 3D canopy reconstruction. *Front. Plant Sci.* 8. doi: 10.3389/fpls.2017.00734

Chen, L.-C., Zhu, Y., Papandreou, G., Schroff, F., and Adam, H. (2018). "Encoder-decoder with atrous separable convolution for semantic image segmentation," in *Computer vision – ECCV 2018, lecture notes in computer science*. Eds. V. Ferrari, M. Hebert, C. Sminchisescu and Y. Weiss (Cham: Springer International Publishing), 833–851. doi: 10.1007/978-3-030-01234-2_49

Datt, B. (1999). A new reflectance index for remote sensing of chlorophyll content in higher plants: tests using eucalyptus leaves. *J. Plant Physiol.* 154, 30–36. doi: 10.1016/S0176-1617(99)80314-9

de la Casa, A., Ovando, G., Bressanini, L., Rodríguez, A., and Martinez, J. (2007). Use of leaf area index and ground cover to estimate intercepted radiation in potato. *Agric. Tec.* 67, 78–85.

Gitelson, A. A., Viña, A., Ciganda, V., Rundquist, D. C., and Arkebauer, T. J. (2005). Remote estimation of canopy chlorophyll content in crops. *Geophysical Research Letters* 32. doi: 10.1029/2005GL022688

Guo, W., Zheng, B., Duan, T., Fukatsu, T., Chapman, S., and Ninomiya, S. (2017). EasyPCC: benchmark datasets and tools for high-throughput measurement of the plant canopy coverage ratio under field conditions. *Sensors* 17, 798. doi: 10.3390/s17040798

Jindo, K., Teklu, M. G., van Boheeman, K., Njehia, N. S., Narabu, T., Kempenaar, C., et al. (2023). Unmanned aerial vehicle (UAV) for detection and prediction of damage caused by potato cyst nematode G. pallida on selected potato cultivars. *Remote Sens.* 15, 1429. doi: 10.3390/rs15051429

Li, D., Miao, Y., Gupta, S. K., Rosen, C. J., Yuan, F., Wang, C., et al. (2021). Improving potato yield prediction by combining cultivar information and UAV remote sensing data using machine learning. *Remote Sens.* 13, 3322. doi: 10.3390/rs13163322

Li, B., Xu, X., Han, J., Zhang, L., Bian, C., Jin, L., et al. (2019). The estimation of crop emergence in potatoes by UAV RGB imagery. *Plant Methods* 15, 15. doi: 10.1186/s13007-019-0399-7

Liu, Y., Feng, H., Yue, J., Jin, X., Li, Z., and Yang, G. (2022). Estimation of potato above-ground biomass based on unmanned aerial vehicle red-green-blue images with different texture features and crop height. *Front. Plant Sci.* 13. doi: 10.3389/fpls.2022.938216

Liu, Y., Hatou, K., Aihara, T., Kurose, S., Akiyama, T., Kohno, Y., et al. (2021). A robust vegetation index based on different UAV RGB images to estimate SPAD values of naked barley leaves. *Remote Sens.* 13, 686. doi: 10.3390/rs13040686

Lu, J., Cheng, D., Geng, C., Zhang, Z., Xiang, Y., and Hu, T. (2021). Combining plant height, canopy coverage and vegetation index from UAV-based RGB images to estimate leaf nitrogen concentration of summer maize. *Biosyst. Eng.* 202, 42–54. doi: 10.1016/j.biosystemseng.2020.11.010

Moeckel, T., Dayananda, S., Nidamanuri, R. R., Nautiyal, S., Hanumaiah, N., Buerkert, A., et al. (2018). Estimation of vegetable crop parameter by multi-temporal UAV-borne images. *Remote Sens.* 10, 805. doi: 10.3390/rs10050805

Paulus, S. (2019). Measuring crops in 3D: using geometry for plant phenotyping. *Plant Methods* 15, 103. doi: 10.1186/s13007-019-0490-0

Rouse, J. W., Haas, R. H., Schel, J. A., and Deering, D. W (1974). Monitoring vegetation systems in the Great Plains with ERTS. In S. C. Freden, E. P. Mercanti and D. W. Becker (eds) *Third Earth Resources Technology Satellite–1 Syposium*. (NASA SP-351, NASA, Washington, D.C.: Volume I: Technical Presentations). pp. 309-317.

Seed potatoes of the highest quality - EUROPLANT Pflanzenzucht GmbH. Available at: https://www.europlant.biz/en/list-of-varieties/ (Accessed 9.25.21).

Stewart, A. M., Edmisten, K. L., Wells, R., and Collins, G. D. (2007). Measuring canopy coverage with digital imaging. *Commun. Soil Sci. Plant Anal.* 38, 895–902. doi: 10.1080/00103620701277718

Sugiura, R., Tsuda, S., Tamiya, S., Itoh, A., Nishiwaki, K., Murakami, N., et al. (2016). Field phenotyping system for the assessment of potato late blight resistance using RGB imagery from an unmanned aerial vehicle. *Biosyst. Eng.* 148, 1–10. doi: 10.1016/j.biosystemseng.2016.04.010

Sun, C., Feng, L., Zhang, Z., Ma, Y., Crosby, T., Naber, M., et al. (2020). Prediction of end-of-season tuber yield and tuber set in potatoes using in-season UAV-based hyperspectral imagery and machine learning. *Sensors* 20, 5293. doi: 10.3390/s20185293

Sun, S., Li, C., Paterson, A. H., Jiang, Y., Xu, R., Robertson, J. S., et al. (2018). In-field high throughput phenotyping and cotton plant growth analysis using liDAR. *Front. Plant Sci.* 9. doi: 10.3389/fpls.2018.00016

Tresch, L., Mu, Y., Itoh, A., Kaga, A., Taguchi, K., Hirafuji, M., et al. (2019). Easy MPE: Extraction of quality microplot images for UAV-based high-throughput field phenotyping. *Plant Phenomics* 2019 (2591849), 9. doi: 10.1101/745752

Van De Vijver, R., Mertens, K., Heungens, K., Nuyttens, D., Wieme, J., Maes, W. H., et al. (2022). Ultra-high-resolution UAV-based detection of alternaria solani infections in potato fields. *Remote Sens.* 14, 6232. doi: 10.3390/rs14246232

Wu, Y., Kirillov, A., Massa, F., Lo, W.-Y., and Girshick, R. (2023). Facebook research Detectron2. Available at: https://github.com/facebookresearch/detectron2.

Xie, J., Zhou, Z., Zhang, H., Zhang, L., and Li, M. (2022). Combining canopy coverage and plant height from UAV-based RGB images to estimate spraying volume on potato. *Sustainability* 14, 6473. doi: 10.3390/su14116473

Zhang, J., Wang, C., Yang, C., Xie, T., Jiang, Z., Hu, T., et al. (2020). Assessing the effect of real spatial resolution of *in situ* UAV multispectral images on seedling rapeseed growth monitoring. *Remote Sens.* 12, 1207. doi: 10.3390/rs12071207

frontiers | Frontiers in Plant Science

TYPE Original Research
PUBLISHED 21 August 2023
DOI 10.3389/fpls.2023.1156430

OPEN ACCESS

EDITED BY
Philipp Von Gillhaussen,
Interantional Plant Phenotyping Network (IPPN), Germany

REVIEWED BY
Huichun Zhang,
Nanjing Forestry University, China
Jennifer Clarke,
University of Nebraska-Lincoln, United States

*CORRESPONDENCE
Qifu Luan
qifu.luan@caf.ac.cn

RECEIVED 01 February 2023
ACCEPTED 02 August 2023
PUBLISHED 21 August 2023

CITATION
Li Y, Yang X, Tong L, Wang L, Xue L, Luan Q and Jiang J (2023) Phenomic selection in slash pine multi-temporally using UAV-multispectral imagery. *Front. Plant Sci.* 14:1156430. doi: 10.3389/fpls.2023.1156430

Phenomic selection in slash pine multi-temporally using UAV-multispectral imagery

Yanjie Li[1,2,3,4], Xinyu Yang[5], Long Tong[6], Lingling Wang[7], Liang Xue[1,2,3,4], Qifu Luan[1,2,3,4]* and Jingmin Jiang[2,3,4]

[1]State Key Laboratory of Tree Genetics and Breeding, Chinese Academy of Forestry, Beijing, China, [2]Research Institute of Subtropical Forestry, Chinese Academy of Forestry, Fuyang, Hangzhou, Zhejiang, China, [3]Key Laboratory of State Forestry and Grassland Administration on Subtropical Forest Cultivation, Fuyang, Hangzhou, Zhejiang, China, [4]Key Laboratory of Tree Breeding of Zhejiang Province, Fuyang, Hangzhou, Zhejiang, China, [5]Soybean Research Institute, National Center for Soybean Improvement, Key Laboratory of Biology and Genetic Improvement of Soybean (General, Ministry of Agriculture), State Key Laboratory of Crop Genetics and Germplasm Enhancement, Jiangsu Collaborative Innovation Center for Modern Crop Production, College of Agriculture, Nanjing Agricultural University, Nanjing, China, [6]Chongqing Academy of Forestry, Chongqing, China, [7]Forestry and Water Conservancy Bureau of Fuyang District in Hangzhou, Hangzhou, China

Genomic selection (GS) is an option for plant domestication that offers high efficiency in improving genetics. However, GS is often not feasible for long-lived tree species with large and complex genomes. In this paper, we investigated UAV multispectral imagery in time series to evaluate genetic variation in tree growth and developed a new predictive approach that is independent of sequencing or pedigrees based on multispectral imagery plus vegetation indices (VIs) for slash pine. Results show that temporal factors have a strong influence on the h^2 of tree growth traits. High genetic correlations were found in most months, and genetic gain also showed a slight influence on the time series. Using a consistent ranking of family breeding values, optimal slash pine families were selected, obtaining a promising and reliable predictive ability based on multispectral+VIs (MV) alone or on the combination of pedigree and MV. The highest predictive value, ranging from 0.52 to 0.56, was found in July. The methods described in this paper provide new approaches for phenotypic selection (PS) using high-throughput multispectral unmanned aerial vehicle (UAV) technology, which could potentially be used to reduce the generation time for conifer species and increase the genetic granularity independent of sequencing or pedigrees.

KEYWORDS

phenomic selection, forest phenomics, PBWAS, high throughput, time-series

1 Introduction

Tree breeding primarily mimics the natural selection of breeding domestication based on cycles of selection, mating, and testing that have successfully increased tree productivity and genetically improved tree materials for multiple traits (Pâques, 2013). However, forest trees typically have long breeding cycles and large physical sizes, making breeding and

progeny testing complex and expensive (Isik, 2014). Compared to crop breeding, forest tree breeding is still in its infancy (Lyzenga et al., 2021). The development of molecular genetic methods has greatly improved selection efficiency. Many available molecular markers are colocalized with functional genetic variation, and breeders can use these markers to aid breeding (Lande and Thompson, 1990; Wang et al., 2018). The goal of molecular genetics is to identify the polymorphic markers or genes associated with phenotypic variation in target traits (Rasmussen, 2020). However, most target traits are complex and influenced by numerous genes, but each effect is small. Low-throughput marker selection methods, such as microsatellites (Jarne and Lagoda, 1996) and marker-assisted selection (MAS) (Ribaut and Hoisington, 1998), are outdated and not as successful as expected. Therefore, genomic selection (GS) using genome-wide markers has been proposed in breeding (Jannink et al., 2010). GS mainly aims to calculate the genomic estimated breeding value (GEBV) of target traits by estimating the effects of all loci using single nucleotide polymorphism (SNP) markers, resulting in more comprehensive and reliable selection (Newell and Jannink, 2014). GS has been successfully applied in crop breeding, which can greatly improve the prediction of breeding value (BV) and reduce the recurrent cycles of selection. GS is becoming the most popular and successful strategy for predicting breeding values of target traits for selection (Crossa et al., 2017; O'Connor et al., 2021). As high-throughput sequencing becomes more efficient and affordable, interest in GS has increased in forest tree breeding (Grattapaglia et al., 2018; Ukrainetz and Mansfield, 2020). However, GS may not always be appropriate for tree species, especially conifers that have not been whole-genome sequenced, such as slash pine (Scott et al., 2020), because these candidates often have large, uncharacterized, and complex genomes, making rapid assembly of reference genomes difficult; without sufficient funding or prior genome characterization, GS seems out of reach (Rincent et al., 2018).

There are two important kernel functions that have been used primarily in GS, including the Gaussian kernel (GK) and the genomic best linear unbiased predictor (GB) (Cuevas et al., 2016). GB is a linear kernel that uses the marker matrix to compute the genomic relationship matrix, also called the kinship matrix, while GK is a covariance matrix that reveals the complex marker effects and the possible interactions (Cuevas et al., 2019). The prediction of GK usually performs better than GB in a single environmental condition (Bandeira e Sousa et al., 2017). All these kernel functions use a large number of molecular markers to predict the target traits, which is similar to predictive models built using machine or deep learning methods based on near-infrared spectroscopy (NIRS) or hyperspectral data (Yoosefzadeh-Najafabadi et al., 2021; Li et al., 2022). Therefore, it is plausible to use spectral data to estimate the kinship matrix, similar to the use of markers (Van Tassel et al., 2022).

Recently, phenomic selection (PS) has emerged to address these issues by using high-dimensional secondary traits (HDSTs) (e.g., individual sample near-infrared (NIR) spectra or hyperspectral imaging) instead of SNPs to estimate the realized genomic relationship matrix (kinship matrix) between individuals, taking advantage of algorithms and workflows developed for GS (Krause et al., 2019; Adak et al., 2021). PS was first proposed by Rincent et al. (2018), who compared the predictive ability of both NIRS and molecular markers with two types of GS models, including the GB and Bayesian LASSO (BL) models, respectively, and the results showed that using NIRS provided similar or even better predictive results than using molecular markers, depending on the trait of interest and the different types of NIRS. Similar results have been consistently shown in maize and soybean, where the use of NIRS or hyperspectral imaging could generate competitive estimated breeding values, called phenomic estimated breeding values (PEBVs), rather than genomic estimated breeding values (GEBVs) (Adak et al., 2021; Zhu et al., 2021; Weiß et al., 2022). However, phenomic selection using unmanned aerial vehicle (UAV)-based imagery has been less studied.

UAV-based remote sensing has been greatly facilitated for data acquisition by advances in sensor technology, which has the potential to increase fieldwork efficiency with less time to collect spatial information than ground-based spectroscopy and to cover large areas while maintaining accuracy and resolution.

UAVs can acquire various types of data, including spectral, structural, thermal, and feature data, which have been widely used in plant science to estimate various traits (Tsouros et al., 2019). For example, UAV-based multispectral or hyperspectral imagery could be used to estimate leaf chlorophyll content and nitrogen concentration (Zheng et al., 2018), canopy structure information such as height and canopy area from the Light Detection and Ranging (LiDAR) system (Maesano et al., 2020) and real-time kinematic (RTK) positioning system (Tao et al., 2021) for plant biomass (Masjedi and Crawford, 2020; Nik Effendi et al., 2021) and grain yield prediction (Li et al., 2020).

In addition, UAV-based imagery also provides a high-precision, high-throughput method for field-based multitemporal phenotyping data collection in the context of plant breeding. This allows for the provision of dynamic information on plant growth and performance (Díaz-Varela et al., 2015; Song et al., 2022). For example, the height data of sorghum and maize from different groups of breeding material estimated by UAV-based imagery have been used to detect the different growth stages (Han et al., 2018; Pugh et al., 2018). UAV-based thermal imagery has been used for high-throughput field phenotyping of black poplar response to drought (Ludovisi et al., 2017). Therefore, UAV-based imagery is very helpful for forest inventories because traditional measurements of tree height and crown growth are difficult due to the difficulty in determining the top of the tree crown and the two cross-crown diameters to simplify the calculation of crown area (Guerra-Hernández et al., 2017). With the specific wavelengths and the RTK system, UAV-based multispectral imagery allows us to obtain the growth parameters as well as the content of physiological and photosynthetic pigments in the leaves.

Although there are achievements in growth trait detection and leaf physiological prediction for plant breeding based on UAV-based imagery, no research has been found on the use of multitemporal HDSTs to perform phenomic selection of growth traits in slash pine. In previous studies (Tao et al., 2021; Song et al., 2022), we developed a UAV-based multispectral imagery phenotyping method that successfully detected growth parameters

such as tree height, crown area, and biomass, which were combined to estimate genetic variation with various vegetation indices (VIs) in slash pine (*Pinus elliottii*). However, previous studies did not consider using the multispectral as an indicator to predict the genetic parameter. Here, we further combined this methodology with multitemporal growth and multispectral data in a slash pine breeding plantation to evaluate the potential of linking high-throughput phenotyping with growth parameters to perform phenomic selection.

Slash pine is a typical conifer with a large, uncharacterized, and complex genome, and the reference genome of slash pine is still unavailable; therefore, genetic studies of slash pine are mainly based on the transcriptome (Diao et al., 2019; Ding et al., 2022).

Therefore, we used slash pine breeding populations as model materials to evaluate a novel approach for low-cost, high-throughput phenomic selection of growth trait-based multispectral images. Our objectives were to 1) estimate genetic variation in growth traits in time series using UAV multispectral imagery; 2) evaluate the predictive ability of the GB and GK models using time series multispectral data for phenomic selection; and 3) develop new predictive selection approaches that are independent of sequencing or pedigrees in trees, especially in conifer breeding programs.

2 Methods and materials

2.1 Site description

The study was conducted on a slash pine population in a national forest farm in Anhui, China; details can be found in Song et al. (2022). There were twenty open-pollinated families with a lattice incomplete block single-tree plot design planted in 2013 within two sites. Each block contained 20 trees, and the spacing between each tree per block was 2 m×3 m. Each tree represented a single family, with no replications within a block. There were 2 sites, and each site contained 20 blocks. 30% of the trees died (240/800) during these years. In total, there were 560 remaining individual trees. Tree canopies did not overlap. This region has a subtropical temperate climate with an average temperature of 15°C.

2.2 UAV flights and field data collection

Flights were performed monthly in 2021 (at the age of 8 years) using DJI Phantom 4 Multispectral (DJI, Shenzhen, China), which has 1 RGB camera and 5 wavelengths (450 nm ± 16 nm, 560 nm ± 16 nm, 650 nm ± 16 nm, 730 nm ± 16 nm, 840 nm ± 16 nm). This UAV is equipped with an RTK system that can reduce the horizontal and vertical positioning errors to 0.03 m and 0.06 m, respectively. The output images from each multispectral camera are in TIF format with a resolution of 1600×1300 pixels.

Flights were conducted at a fixed height of 35 m above ground level during a sunny and less windy day in each month to ensure high accuracy requirements and to reduce any systematic bias caused by environmental factors. A standard reflectance panel was used during each flight to improve the consistency of the spectral data. The operation was set to 80% overlap between images and a forward speed of 5 m/s during the flights. The original images were normalized to adjust the data and align the spectral information across the images. The total area covered was 4.5 ha and the duration of each flight was 1 hour. During the Covid-19, the field trip was strictly restricted in February 2021, so data were not available. To validate the accuracy of tree height and crown area (CA) measurement by UAV images, the ground truth data of tree height and CA were measured by randomly selected 100 trees in July of 2021, with the high accuracy of RTK system, the UAV-based tree height and CA have a high correlation with the ground truth, with the R2 value higher than 0.85 (Song et al., 2022).

2.3 Image processing

In this study, the image processing methodology employed a series of steps to extract essential information from the original multispectral images of the plantation. The initial data processing involved the use of DJI Terra software (version 3.3.0, Shenzhen, China) to generate multispectral orthomosaics and dense 3D point clouds of the entire plantation. These orthomosaic images, along with the 3D point clouds, served as the basis for further analysis.

The orthomosaic images and 3D point clouds were then further processed using the R software version 4.2.0 and the *lidR* package version 4.0.0 (Roussel et al., 2020). The first step in data analysis was the classification of ground points within the 3D point clouds using the cloth simulation filtering (CSF) function, as proposed by Zhang et al. (2016).This step was critical for creating a digital terrain model (DTM) that accurately represented the bare ground surface.

With the classified ground points, the next step was to create digital surface models (DSM) using a point-to-grid algorithm. The resolution of both the DTM and the DSM was set at 0.5 m, ensuring a high level of detail in the representation of terrain and surface objects. The difference between the DSM and the DTM provided the canopy height models (CHM), which indicate the height of vegetation above the ground surface.

Using the CHM, individual trees were detected using the *dalponte2016* function with specific criteria, including a minimum height threshold of 2.6 m and a maximum crown diameter of 2.5 m. This step allowed for the identification and delineation of individual trees within the study area.

For each detected individual tree, tree-level attributes such as tree height and crown area were manually labeled. In addition, relevant family, site, and block information was associated with each tree to improve the accuracy and context of the tree-level data.

To represent the spatial extent of individual tree canopies, tree crown polygons were generated from the manually labeled crown areas using the raster package (Hijmans et al., 2015). Finally, the spectra of each individual tree were extracted using the tree crown polygons. This extraction involved collecting spectral information from the multispectral orthomosaic images for all pixels within the boundary of each tree crown.

Similar to previous studies (Tao et al., 2021; Song et al., 2022), fifteen vegetation indices (VIs) were calculated for each pixel from all

extracted tree images (Table 1). These VIs were then averaged at the tree level based on the red, green, blue, red edge, and near-infrared (NIR) spectra, providing valuable insights into the vegetation health and other biophysical characteristics of the individual trees. The comprehensive image processing methodology described above ensured accurate data extraction and analysis, allowing researchers to gain valuable information about the structure, health, and vegetation dynamics of the plantation.

2.4 Genetic parameters

Estimates of genetic parameters for slash pine growth traits in each month of the year were collected by fitting a general multiple mixed linear model using restricted maximum likelihood (REML); details can be found in (Li et al., 2018; Cuevas et al., 2019). A brief description can be expressed as:

$$y_i = x_i m + b_i + f_i + e_i \quad (1)$$

y_i is a vector containing the phenotypic values for both traits (tree height and crown area) for the individual. $x_i$is a vector linking the fixed effects m to the observations for the individual. m is a vector of fixed effect coefficients for the traits. b_i is a vector representing the random block effects for the individual. f_i is a vector representing the random family effects for the individual. e_i is a vector representing the random residual effects for the individual. By stacking these vectors for all trees, we can represent the overall model equation as:

$$Y = Xm + Z_1 b + Z_2 f + e \quad (2)$$

where $Y$is a vector of phenotypic observations (containing measurements for both traits). m is a vector of fixed effects, representing the overall mean. b , f , and e are vectors of bivariate random effects for block, family, and residual effects, respectively.X is the incidence matrix linking observations to the fixed effects. Z_1 and Z_2 are incidence matrices linking observations to the appropriate random effects for block and family, respectively. In this model, the fixed effects represented by m(overall mean) are connected to the phenotypic observations through the incidence matrix X. Similarly, the random effects for block and family, represented by b and f respectively, are linked to the observations through the incidence matrices Z_1 and Z_2. The vector e accounts for the residual effects, which are not explained by the fixed or random effects. For each month, the equation can be:

$$Y_i = X_i m + Z_{i_1} b_i + Z_{i_2} f_i + e_i \quad (3)$$

Where Y_i is the vector of bivariate phenotypic observations for the i_{th}month. m is the vector of fixed effects, representing the overall mean. b_i , f_i, and e_i are the vectors of bivariate random effects for block, family, and residual effects, respectively, specific to the i_{th} month. $X_i$is the incidence matrix linking observations to the fixed effects for the ith month. Z_i1and Z_i2are the incidence matrices linking observations to the appropriate random effects for block and family, respectively, for the i_{th}month. The variance components were used to estimate the temporal narrow sense of h^2 for trait i and the genetic correlations ($r_{g_{ij}}$) between trait $i$and trait j,

$$h_i^2 = \frac{2.5\sigma_{fi}^2}{\sigma_{fi}^2 + \sigma_{bi}^2 + \sigma_{ei}^2} \quad (2)$$

TABLE 1 The spectral indices used in this study.λ_r, λ_b and $\lambda_g$are the reflectances at wavelength λ.

Name	Abbrev.	Equation	Reference
Normalized difference vegetation index	NDVI	$(NIR - R)/(NIR + R)$	Peñuelas et al. (1993)
Optimized soil adjusted vegetation index	OSAVI	$((NIR - R)(1 + 0.16))/((NIR + R + 0.16))$	Rondeaux et al. (1996)
Green normalized difference vegetation index	GNDVI	$(NIR - G)/(NIR + G)$	Gitelson et al. (1996)
Soil adjusted vegetation index	SAVI	$((NIR - R)(1 + 0.5))/((NIR + R + 0.5))$	Huete (1988)
Modified soil adjusted vegetation index	MSAVI	$(2NIR + 1 - \sqrt{((2NIR + 1)\ 2 - 8(NIR - R)\ ))/2}$	Qi et al. (1994)
Triangular greenness index	TGI	$-0.5[(\lambda_r - \lambda_b)(R - G) - (\lambda_r - \lambda_g)(R - B)]$	(Hunt et al., 2011)
Green leaf index	GLI	$(2G - R - B)/(2G + R + B)$	(Louhaichi et al., 2001)
Triangular vegetation index	TVI	0.5[120(N-G)-200(R-G)]	(Broge and Leblanc, 2001)
Red edge chlorophyll index	RECI	$NIR/E - 1$	Gitelson et al. (2003)
Leaf chlorophyll index	LCI	$(NIR - E)/(NIR + R)$	Pu et al. (2008)
Anthocyanin reflectance index	ARI	G/NIR	van den Berg and Perkins (2005)
Modified green red vegetation index	MGRVI	$(G\ 2 - R\ 2)/(G\ 2 + R\ 2\ )$	Bendig et al. (2015)
Modified anthocyanin reflectance index	MARI	$(G\ (\ -1) - E\ (\ -1))/NIR$	Gitelson et al. (2006)
Normalized difference red edge index	NDRE	$(NIR - E)/(NIR + E)$	Barnes et al. (2000)
Red green blue vegetation index	RGBVI	$(G\ 2 - R \times B)/(G\ 2 + R \times B)$	Bendig et al. (2015)

R: red bands, G: green bands, B: blue bands, E: red edge bands, NIR: near infrared bands.

$$r_{g_{ij}=}\frac{\sigma_{f_{ij}}}{\sqrt{\sigma_{f_i}^2+\sigma_{f_j}^2}} \quad (3)$$

where σ_{fi}^2, σ_{bi}^2 and σ_{ei}^2 are the temporal family, block and residual variance for trait *i*, respectively, and $\sigma_{f_{ij}}$ is the estimated family covariance between trait *i*and trait *j*. The genetic gain represents the effectiveness of tree improvement and is measured by the change in the mean breeding value of each trait population. In this study, genetic gain (ΔG_R) of each trait for each month was calculated by subtracting the mean breeding value of selected ratio growth traits from the total mean of growth traits by breeding value.

$$\Delta G_R = M_{BV} \times r \ - T_{BV}$$

Where $T_{BV}$is the total mean of the growth traits determined by breeding value, $M_{BV}$is the mean breeding value of the top selected proportions (r) of the growth traits in descending order. The variable *r*denotes the proportion of growth traits selected as top performers.

2.5 Kernel methods

We performed two important GS methods, including GB and GK kernels (Cuevas et al., 2019), to compare the phenomic prediction accuracy, and we used multispectral as input instead of SNP data. GB is a standard linear kernel, usually referred to as the genomic relationship matrix (Cuevas et al., 2016). GB is described as $GB = \frac{XX'}{p}$, where X in our study is the kernel matrix formed based on the multispectral and VIs matrix (M BLUP). GK, defined as $GK = \exp(-hd_{ii}^2/q)$, is different from GB, which is defined as the semiparametric model reproducing kernel Hilbert spaces (RKHS) and appears as a reproducing kernel(González-Camacho et al., 2012), where q and h are the median of the Euclidean squared distance and the bandwidth parameter affecting the covariance decay rate between genotypes, respectively. Specifically, for each month, we randomly divided the data into an 80% training set for model training and a 20% validation set for model validation. To evaluate model stability, the data were randomly divided 100 times for model training.

2.6 Phenotyping-based Wide Association Analysis (PBWAS)

The PBWAS in our study was conducted according to the principles of GWAS (Genome-Wide Association Study) methodology. We considered each temporal month as a chromosome, and a genome-wide association analysis (GWAS) was applied to detect the multispectral and VIs (20 variables) related to the growth traits at each temporal month level. Thresholds of P< 10^-3 were used as the significance level to identify associations between variables and traits. While a typical threshold for GWAS is usually around 10^-4 to 10^-5, we chose a relatively lower threshold given the smaller size and scope of our study compared to traditional GWAS studies with larger genomic datasets. The lower threshold allowed us to identify potentially meaningful associations between the multispectral and VIs traits and tree growth traits in the context of our specific study using spectral data.

All statistical analyses were performed in R software. The *BGGE* package (Granato et al., 2018) was used for GB and GK model calibration, the *sommer* package was used for genetic parameter analysis (Covarrubias-Pazaran, 2016), the *statgenGWAS* package (van Rossum and Kruijer, 2020) was used for PBWAS analysis, and the *ggtree* (Yu et al., 2017; Yu, 2020), *ggplot2* (Wickham, 2011) and *CMplot* packages (LiLin-Yin, 2022) were used for data visualization.

3 Results

3.1 The growth of height and CA in different months

The average growth trait performance of 20 families is shown in Figure 1. Since the growth rate can reflect the percentage change in the indicator over a given time horizon, it can be seen that the growth rate varies considerably among the families during the one-year growth period according to Figure 1. The NDVI shows that all trees have a high growth rate from April to September and a slow growth rate from December to March, and families 3, 5, 10, 13, 14, 16, and 19 have a higher mean tree height than other families. However, not all families had high mean tree height followed by high mean CA; only three families, including 3, 10, 16, had both high tree height and CA. Families 7 and 12 had relatively lower mean tree height and CA than the other families, but their growth rate (NDVI) from April to September was high. In general, the total amount of tree height and CA started to increase in summer and slowed down in winter (Figures 2A, B).

3.2 Genetic variation, correlations and family selection

The variation of the estimate h^2 for tree height, CA, VIs and the spectral bands over 11 months is shown in Figure 3. A range of h^2 from 0 to 0.41 was found for all traits. Temporal phenotypes have a strong influence on the h^2 estimates for all traits. All spectral bands including red, blue, green and NIR had relatively low h^2 in all months with a range of 0 to 0.25. RGBVI, MGRVI, and LCI had moderate h^2 in March, with h^2 values of 0.35, 0.31, and 0.31, respectively, but low h^2 values in all other months. The h^2 values of ARI, MACI, NDRE, GCI, GNDVI, LCI and RECI in the month of October also showed relatively high values compared to other months, with a range of 0.26 to 0.36. Tree height showed a strong stable h^2 in all months except Dec, ranging from 0.26 to 0.41. The highest h^2 for tree height was found in September, with a value of 0.41, but all spectral and VIs in September were low, with a range from 0 to 0.19. The months had a strong influence on the h^2 of CA; the highest h^2 of CA was found in January, June and July, and the lowest h^2 was found in April, with a value of 0.09.

Figure 4 shows the estimated genetic correlations between multispectral, VIs and tree growth traits (height and CA) in

10.3389/fpls.2023.1156430

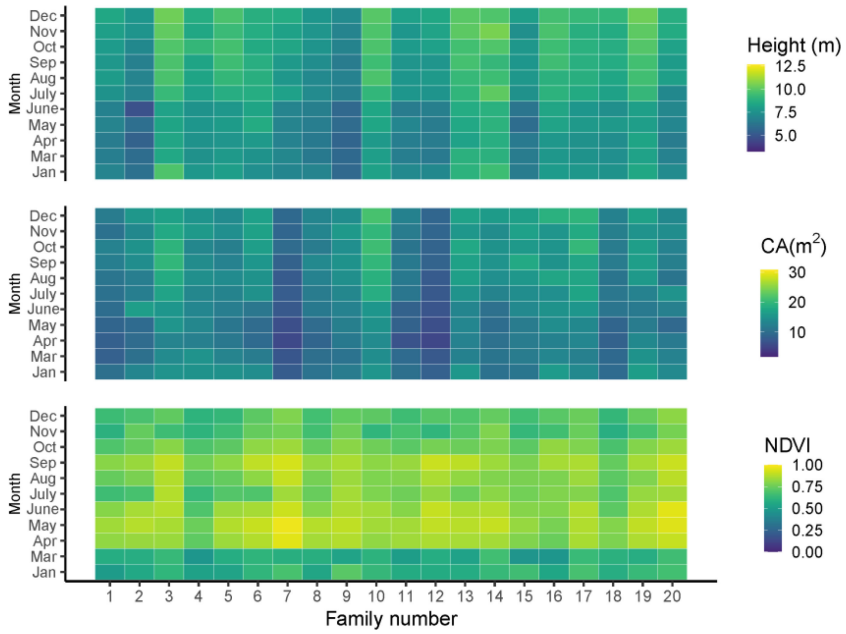

FIGURE 1
The growth traits of tree height, CA and NDVI in different months. Jan, Mar, Apr, May, June, July, Aug, Sep, Oct, Nov, Dec are represented as January, March, April, May, June, July, August, September, November, December, respectively.

different months. High genetic correlations were found from January and July to December. Multispectral and VIs have no significant genetic correlation with tree height or CA in March, April and June, and the highest genetic correlations between tree height and CA were found in October, with an rg value of 0.99. A large number of correlations between multispectral, VIs and tree growth traits (height and CA) were found in January, and red edge, blue and green spectra had a significant positive correlation with

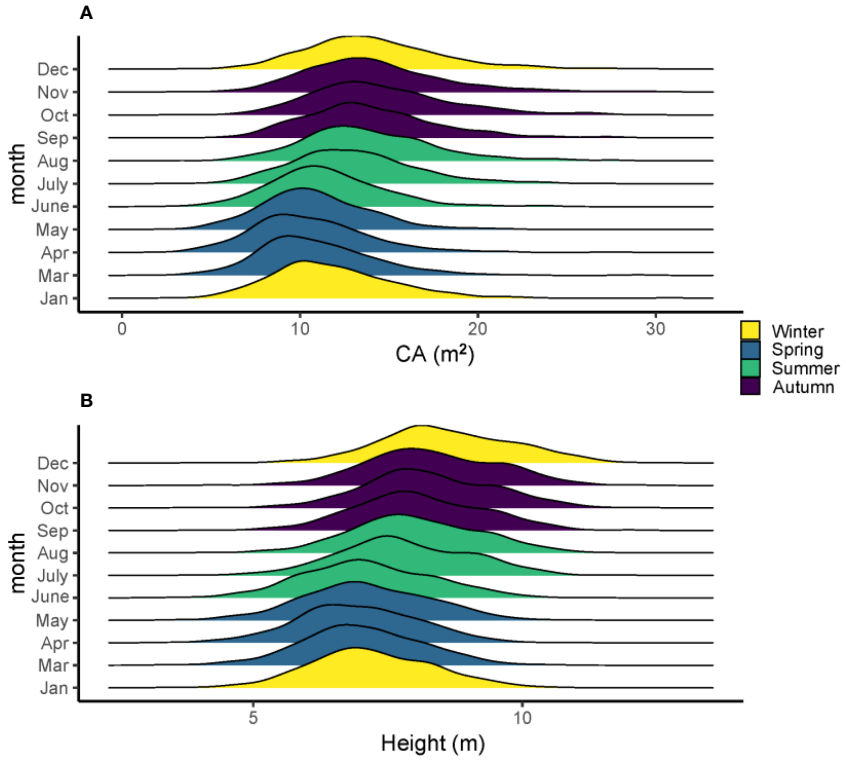

FIGURE 2
The density mean of tree height **(A)** and CA **(B)** in different months and seasons of the 560 slash pines in 2021.

10.3389/fpls.2023.1156430

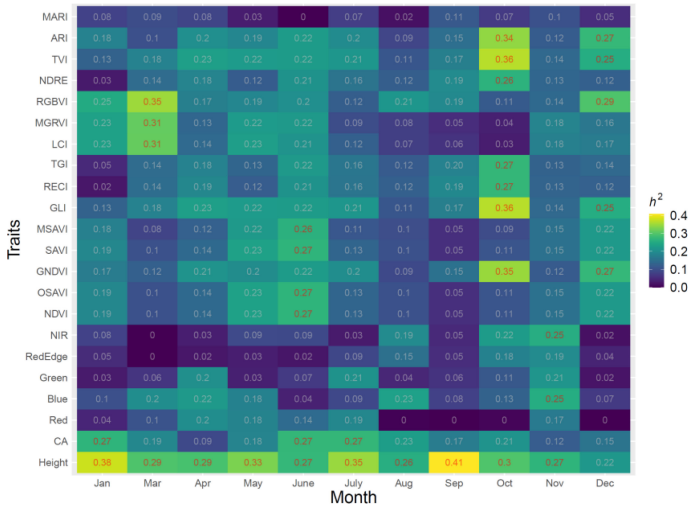

FIGURE 3
Estimates of h^2 from 11 months in 2021 for all traits, including five spectral bands, vegetation indices (VIs), and growth traits.

CA, with rg values of 0.79, 0.75 and 0.94, respectively. SAVI has a significant positive correlation with height in December (rg=0.77) and CA in May (rg=0.78), and the red spectra also have a strong positive correlation with CA (rg=0.89). In addition, a strong negative correlation was found between the blue spectra and CA in May (rg=-0.82).

The breeding values ranked between multitemporal of all families for tree height, CA, are shown in Figure 5. Although each family has variable breeding values in different months, most of the families are consistent between each month, and breeding selection is possible for high tree height and CA families in certain months. For tree height, family 19 had the highest breeding values, in addition to families 6 and 10, which also had the highest breeding values in most months. For CA, families 6, 10 and 19 were found to have the highest breeding values for month influence. Family 19 was also selected in January, March, May, November, and December. Families 6, 10 and 19 show the highest breeding value for tree height and CA.

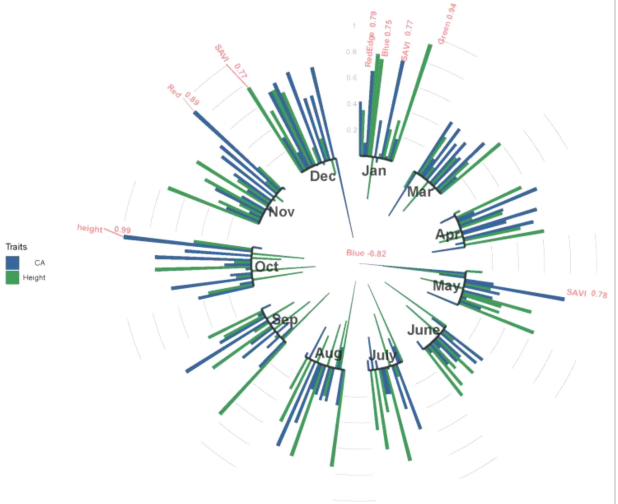

FIGURE 4
The genetic correlations between tree height and CA and multispectral and VIs at 11 months in 2021. Red indicates genetic correlations above 0.75 in absolute value. Blue color indicates CA; green color indicates height.

3.3 Genetic gain

The top 10%, 20% and 30% genetic gains of the families for tree height and crown in different months are shown in Figure 6. The highest and lowest genetic gains for tree height and CA with strong selection rates (top 10% and 20%) were found in September, July, and December, April, with values of 0.35, 0.25, 0.8, and 0.53 for the highest and 0.23, 0.18, 0.32, and 0.23 for the lowest, respectively. In general, genetic gains increased as stronger selection rates were applied to tree height and CA.

3.4 Phenomic selection using the GB and GK kernels

The phenomic selection based only on multispectral+VIs (MV) and the combination of MV and pedigree (MV+P) using the GB and GK models is shown in Figure 7. Temporal time influenced the predictive ability of PS, with a range from 0.13 to 0.56 for all traits using two kernels (GB, GK). The average prediction of GB is similar to that of the nonlinear kernel GK in all cases. Pedigree does not improve the prediction ability compared to the kernels using MV +P. Interestingly, the combination of pedigree with MV shows similar prediction accuracy compared to the prediction using MV only for the two kernels in some months (December, October, June, May), but similar in January, March, and April. The highest prediction ability for tree height and CA using GB and GK was found in July, with a prediction ability value ranging from 0.52 to 0.56, followed by Dec. The lowest prediction ability for tree height

10.3389/fpls.2023.1156430

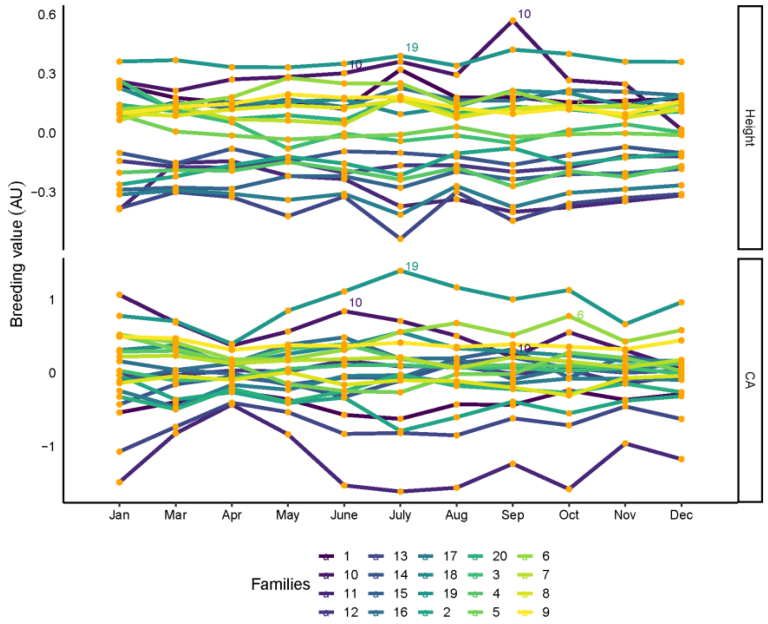

FIGURE 5
Family rankings for tree height and CA in slash pine in different months. Each line represent one family. Family values are expressed as deviation from each trait mean. AU: arbitrary units.

and CA was found in June using GB and March and June using GK, respectively.

3.5 PBWAS

PBWAS reveals 15 associations between significant multispectral, VIs and tree height and CA with P< 10^{-3} in these 11 months (Figure 8). Tree height was associated with 9 VIs from Jan to Dec, including TGI in May and Sep, GLI in June, NIR in Aug, GNDVI in Sep and ARI, MSAVI, and OSAVI in Oct. Six significant associations emerged between multispectral, VIs and tree CA, including MARI in Mar, Rededge and NIR in Apr, GLI in June and GNDVI in Sep. Among those, the GLI in June and GNDVI in Sep were associated with both tree height and CA. Time series significantly influence the association between multispectral, VIs and tree growth traits. No associations were found to emerge with tree height in Jan, Mar, Apr, July, Nov and Dec and Jan, May, July, Aug, Oct, Nov and Dec for tree CA.

4 Discussion

UAV-based imagery has been shown to predict tree growth traits at high throughput and to be used for breeding selection in various tree species (Ota et al., 2017; Jang et al., 2020; Jones et al.,

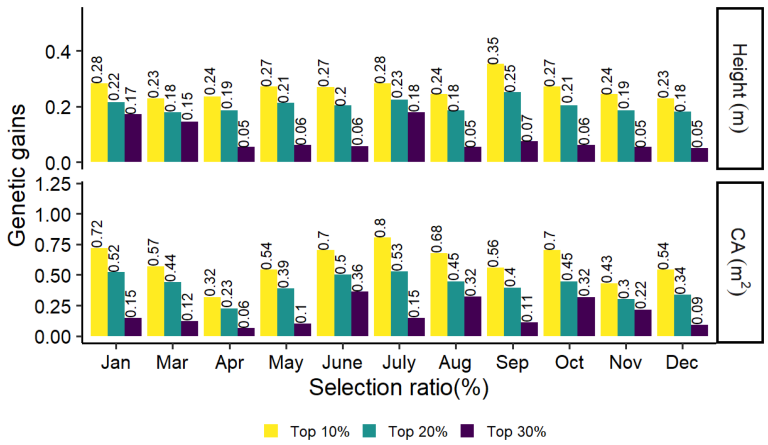

FIGURE 6
Realized genetic gains of tree height and CA traits at age 8 for slash pine at different months in 2021.

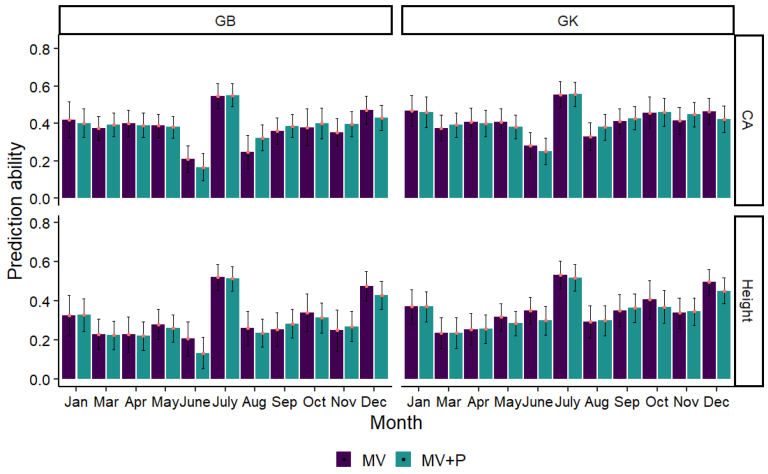

FIGURE 7
Average Pearson's correlations between observed and predicted values with standard deviation for 2 methods with 80% of the families in the training set and 20% of the families in the test set. Methods GB and GK are GBLUP and Gaussian Kernel, respectively. The black line in each bar represents the standard deviation (SD). The SD was calculated by training the model on 100 randomly divided subsets of the data and obtaining the standard deviation of the predicted values across these subsets.

2020; Rallo et al., 2020). Equipped with the RTK system, UAV multispectral imagery provided high accuracy of 3D point cloud data and spectral data for individual trees in forest plantations (Tao et al., 2021). Supportive results were reported by Volpato et al. (2021), who found that postprocessed kinematic (PPK) corrections are an affordable method for plant height, and that PPK or RTK corrections could greatly increase the accuracy of image georeferencing and provide a promising method for plant height. Therefore, UAV imagery is well suited to monitor plant growth traits in a long time series, and successful studies have been conducted in agriculture to estimate growth and yield for breeding selection purposes, including soybean (Borra-Serrano et al., 2020), cotton (Ashapure et al., 2020), sorghum (Masjedi et al., 2020) and tomato (Chang et al., 2021). However, there is limited research on monitoring tree growth in time series for breeding selection purposes (Guerra-Hernández et al., 2017; Solvin et al., 2020). Our study is the first to apply UAVs for tree growth trait identification and the use of multispectral data to perform multitemporal phenomic selection for tree growth traits in a slash pine breeding plantation. This comprehensive approach integrating UAV, multispectral data and multi-temporal analysis represents a unique contribution to the field of tree growth trait identification and phenomic selection in a breeding program. UAV imagery provides a cost- and time-saving phenotyping method for individual tree estimation of growth-related traits, greatly improving data collection over different months or years and characterization of the genetic basis underlying phenotypic differentiation (Masjedi and Crawford, 2020). Our approach collected growth information through multitemporal flights (n=11), each with low computational time, using a low-cost UAV device. This approach has been shown to provide accurate estimates of growth characteristics and VIs in slash pine plantations (Tao et al., 2021). Similar indices have been widely used in many studies at the individual tree level (Santini et al., 2019b; Santini et al., 2021).

Tree height and CA differences were detected among families and increased during spring (March, April, May) and summer (June, July and August) with the increase of tree growth characteristics. However, with the limitation of low quality of

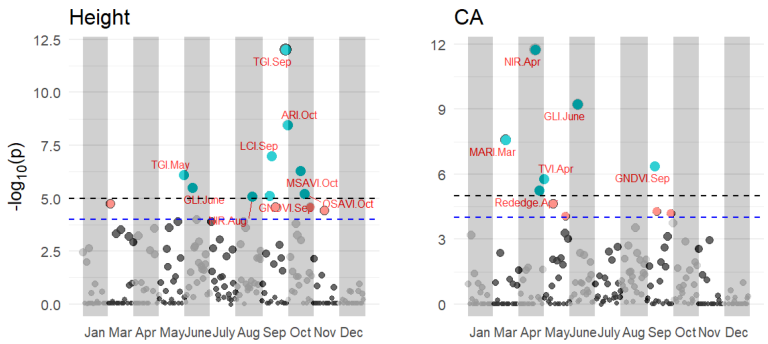

FIGURE 8
Results of the PBWAS using GWAS methodology based on multispectral and VIs for tree height and CA in 11 months in 2021. Each dot in a different month is a representation of that multispectral or VIs.

RGB camera, there are some tree height and CA do not extract correctly. which occurred that the tree height and CA for some trees from January to May have a trend of decreasing. The h^2 of tree height remained relatively stable during the whole growth year in 2021, with a range from 0.22 to 0.41, and tree CA did not have a stable h^2. The highest h^2 for CA was found in June and July. These results are consistent with our previous study in which tree height and CA had moderate h^2 values of 0.37 and 0.30, respectively, in July (Zhaoying Song et al., 2022). Moderate genetic variability in tree growth traits has also been found in other tree species, for example, a range of 0.21 to 0.30 and 0.19 to 0.28 h^2 for tree height in different ages of Norway spruce (*Picea abies* L. Karst.) were found by Solvin et al. (2020) using UAV imagery. The consistency of the families ranked in different months, and the moderate h^2, selected families with high genetic gains for both tree height and CA at different selection ratios. In addition, the best month of selection for tree height and CA was also found in our study.

Most multispectral and VIs in this paper have a large positive or negative genetic correlation with tree height and CA in different months, and multispectral and VIs have been shown to have a strong correlation with plant photosynthetic status, which has the potential to be used in plant phenomics approaches. Santini et al. (2021) proposed that VIs show a strong relationship with aboveground growth traits, whereas leaf biochemistry has no significant effect on tree growth (Santini et al., 2019a). The strong genetic correlation between VIs and tree growth traits suggests that a PS based on these factors is possible. In this paper, we aim to apply a PS approach similar to that first reported by Rincent et al. (2018), who used NIRS as a low-cost, high-throughput phenotype to make predictions instead of genetic markers. The only difference in our study is that we use five spectral bands and many VIs as inputs instead of markers to perform PS. Most of the canopy spectrum and VIs showed genetic variability in different months, which is consistent with the results of Rincent et al. (2018), who found that VIS-NIR wavelengths between 400-2500 nm mostly showed genetic variability. Therefore, Vis, like NIRS, should be used to process PS instead of genetic markers. We collected the spectrum and VIs from different growth months to determine the temporal influence on PS performance. Since we do not have marker data, the GB and GK models were performed based on MV and the combination of MV and pedigree data. Although the growth time influences the PS prediction, we still obtained the highest PS prediction ability in July with a range of 0.52 to 0.56. A supported study was reported by Rincent et al. (2018), who used NIRs and obtained moderate PS predictive abilities ranging from 0.34 to 0.53 for wood properties in black poplar, but slightly lower predictive abilities than those with SNPs. There were no significant differences in the accuracy of the PS models generated by GB and GK in our study. Moreover, the accuracy of both models was higher than the range reported by Cuevas et al. (2019), for wheat data, where GB and GK yielded a range between 0.349 and 0.367 for grain yield prediction using NIR spectroscopy. The PS models generated in our study also outperformed models using only genomic markers or a combination of genomic markers, pedigrees, and NIRS, which had predictive abilities ranging from 0.40 to 0.47. Cuevas et al. (2019) also reported that the markers obtained slightly higher correlations between observed and predicted values than pedigree + NIRS, indicating that even if PS is less accurate than GS in some cases, it could be a feasible alternative and reliable method for filtering the poor performing germplasm when markers are not available, which could be a low-cost and high-throughput method independent of sequencing or pedigrees for tree breeding selection, especially for tree species with large and complex genomes without prior genome characterization, GS is often costly and inaccessible.

We used GWAS methodology to reveal the significant VIs and spectra associated with growth traits at different growth times, which we call PBWAS. The results demonstrated the effectiveness of combining phenomic information with UAV imagery to characterize growth differentiation at different growth times in slash pine. We identified relevant VI phenotypic associations for tree height and CA in several months. These associations were inconsistent across months for tree height and CA, as reported by Roberts et al. (2016). NDVI, OSAVI, and GNDVI were found to be saturated at high leaf area and may not capture individual differences in tree growth. These indices were also found in our work to be highly associated with tree growth in different months. The strongest correlations between VIs and tree growth traits were TGI and LCI in Sep, ARI in Oct, GLI in June, and NIR spectra in Apr and Aug, respectively. TGI, LCI and GLI are the optimal spectral indices for leaf nitrogen detection, which are highly related to leaf chlorophyll content (Hunt et al., 2013; Lima et al., 2021). The anthocyanin reflectance index (ARI) can be used to estimate anthocyanin concentration (Kior et al., 2021). Santini et al. (2021) found four SNPs associated with anthocyanin content in P. halepensis, suggesting that VIs are associated with genomic information. Some VIs, such as GLI in June and GNDVI in September, showed associations with both tree height and crown area (CA), suggesting the possibility of pleiotropy where these VIs simultaneously influence both growth traits within the same month. These results suggest that the detected spectrum and VIs across different months deserve further attention in exploring their potential adaptive role for slash pine.

In discussing the limitations of our study, it is important to acknowledge the lack of a propagation of error analysis in our current manuscript. We recognize the importance of such an analysis in determining the reliability and applicability of our findings. However, several factors prevented us from including a comprehensive error propagation analysis in this study. First, the limitations of our experimental design and data collection process, including sample size limitations and measurement precision, may have affected the feasibility of conducting a robust error propagation analysis. Second, the selected data analysis methods, which rely on model-based estimation and prediction, have inherent limitations with respect to error propagation. Finally, given the scope and objectives of this study, we faced time and resource constraints, as well as limitations in data availability. As a result, a comprehensive analysis of error propagation was beyond the scope of this study.

5 Conclusion

With the development of UAV technology, the collection of multispectral or NIR spectra has greatly increased and conversely

decreased in cost. In this paper, we use this technology to reinforce the advantages of using the PS approach in Scots pine to estimate the ability of PS used in conifers independent of sequencing or pedigrees. The heritable variation of growth traits in time series was evaluated, temporal growth strongly influenced the genetic variation of growth traits, and the optimal breeding selection time for tree growth traits was suggested. Two types of GS kernels, including GB and GK, showed satisfactory prediction ability based on the tree growth traits at different months using the pedigree and MV instead of genomic markers, indicating that with high-throughput UAV imagery, phenomic selection using multispectral and VIs was possible and reliable. Our study provides insight into the spectral processes reflecting phenotypic differentiation (in our case, tree growth traits) in a time series of UAV technology. Our new PS approach in slash pine bridges the gap between high-dimensional secondary traits (in our study, multispectral imaging) and individual phenotypes.

Data availability statement

The original contributions presented in the study are included in the article/supplementary material. Further inquiries can be directed to the corresponding author.

Author contributions

YL designed the study, conducted the experiment and wrote the manuscript. XY, LT, LW, and LX revised the manuscript. JJ supported the data collection and field experiments and supervised the experiments. QL supervised experiments and performed revisions of the manuscript. All authors contributed to the article and approved the submitted version.

Funding

This research was supported by the cooperation projects between the People's Government of Zhejiang Province and the Chinese Academy of Forestry, No. 2023SY10 and the Zhejiang Science and Technology Major Program on Agricultural New Variety Breeding, No. 2021C02070-7-3.

Conflict of interest

The authors declare that the research was conducted in the absence of any commercial or financial relationships that could be construed as a potential conflict of interest.

Publisher's note

References

Adak, A., Murray, S. C., Božinović, S., Lindsey, R., Nakasagga, S., Chatterjee, S., et al. (2021). Temporal vegetation indices and plant height from remotely sensed imagery can predict grain yield and flowering time breeding value in maize *via* machine learning regression. *Remote Sens.* 13, 2141. doi: 10.3390/rs13112141

Ashapure, A., Jung, J., Chang, A., Oh, S., Yeom, J., Maeda, M., et al. (2020). Developing a machine learning based cotton yield estimation framework using multi-temporal UAS data. *ISPRS J. Photogrammetry Remote Sens.* 169, 180–194. doi: 10.1016/j.isprsjprs.2020.09.015

Bandeira e Sousa, M., Cuevas, J., de Oliveira Couto, E. G., Pérez-Rodríguez, P., Jarquín, D., Fritsche-Neto, R., et al. (2017). Genomic-enabled prediction in maize using kernel models with genotype× environment interaction. *G3: Genes Genomes Genet.* 7, 1995–2014. doi: 10.1534/g3.117.042341

Barnes, E. M., Clarke, T. R., Richards, S. E., Colaizzi, P. D., Haberland, J., Kostrzewski, M., et al. (2000). "Coincident detection of crop water stress, nitrogen status and canopy density using ground-based multispectral data," in *Proceedings of the 5th International Conference on Precision Agriculture* (Bloomington, MN,USA), 1–15.

Bendig, J., Yu, K., Aasen, H., Bolten, A., Bennertz, S., Broscheit, J., et al. (2015). Combining UAV-based plant height from crop surface models, visible, and near infrared vegetation indices for biomass monitoring in barley. *Int. J. Appl. Earth Observation Geoinformation* 39, 79–87. doi: 10.1016/j.jag.2015.02.012

Borra-Serrano, I., De Swaef, T., Quataert, P., Aper, J., Saleem, A., Saeys, W., et al. (2020). Closing the phenotyping gap: High resolution UAV time series for soybean growth analysis provides objective data from field trials. *Remote Sensing* 12:1644. doi: 10.3390/rs12101644

Broge, N. H., and Leblanc, E. (2001). Comparing prediction power and stability of broadband and hyperspectral vegetation indices for estimation of green leaf area index and canopy chlorophyll density. *Remote Sens. Environ.* 76, 156–172. doi: 10.1016/S0034-4257(00)00197-8

Chang, A. J., Jung, J. H., Yeom, J., Maeda, M. M., Landivar, J. A., Enciso, J. M., et al. (2021). Unmanned aircraft system-(UAS-) based high-throughput phenotyping (HTP) for tomato yield estimation. *J. Sens.* 2021, 8875606. doi: 10.1155/2021/8875606

Covarrubias-Pazaran, G. (2016). Genome-assisted prediction of quantitative traits using the R package sommer. *PloS One* 11, e0156744. doi: 10.1371/journal.pone.0156744

Crossa, J., Pérez-Rodríguez, P., Cuevas, J., Montesinos-López, O., Jarquín, D., De Los Campos, G., et al. (2017). Genomic selection in plant breeding: methods, models, and perspectives. *Trends Plant Sci.* 22, 961–975. doi: 10.1016/j.tplants.2017.08.011

Cuevas, J., Crossa, J., Soberanis, V., Pérez-Elizalde, S., Pérez-Rodríguez, P., De los Campos, G., et al. (2016). Genomic prediction of genotype× environment interaction kernel regression models. *Plant Genome* 9, 1–20. doi: 10.3835/plantgenome2016.03.0024

Cuevas, J., Montesinos-López, O., Juliana, P., Guzmán, C., Pérez-Rodríguez, P., González-Bucio, J., et al. (2019). Deep Kernel for genomic and near infrared predictions in multi-environment breeding trials. *G3: Genes Genomes Genet.* 9, 2913–2924. doi: 10.1534/g3.119.400493

Diao, S., Ding, X., Luan, Q., and Jiang, J. (2019). A complete transcriptional landscape analysis of Pinus elliottii Engelm. Using third-generation sequencing and comparative analysis in the Pinus phylogeny. *Forests* 10 (11), 942. doi: 10.3390/f10110942

Díaz-Varela, R. A., de la Rosa, R., León, L., and Zarco-Tejada, P. J. (2015). High-resolution airborne UAV imagery to assess olive tree crown parameters using 3D photo reconstruction: application in breeding trials. *Remote Sens.* 7, 4213–4232. doi: 10.3390/rs70404213

Ding, X., Diao, S., Luan, Q., Wu, H. X., Zhang, Y., and Jiang, J. (2022). A transcriptome-based association study of growth, wood quality, and oleoresin traits in a slash pine breeding population. *PloS Genet.* 18, e1010017. doi: 10.1371/journal.pgen.1010017

Gitelson, A. A., Gritz, Y., and Merzlyak, M. N. (2003). Relationships between leaf chlorophyll content and spectral reflectance and algorithms for non-destructive chlorophyll assessment in higher plant leaves. *J. Plant Physiol.* 160, 271–282. doi: 10.1078/0176-1617-00887

Gitelson, A. A., Kaufman, Y. J., and Merzlyak, M. N. (1996). Use of a green channel in remote sensing of global. *Remote Sens. Environ.* 58, 289–298. doi: 10.1016/S0034-4257(96)00072-7

Gitelson, A. A., Keydan, G. P., and Merzlyak, M. N. (2006). Three-band model for noninvasive estimation of chlorophyll, carotenoids, and anthocyanin contents in higher plant leaves. *Geophysical Res. Lett.* 33, 431–433. doi: 10.1029/2006GL026457

González-Camacho, J., de Los Campos, G., Pérez, P., Gianola, D., Cairns, J., Mahuku, G., et al. (2012). Genome-enabled prediction of genetic values using radial basis function neural networks. *Theor. Appl. Genet.* 125, 759–771. doi: 10.1007/s00122-012-1868-9

Granato, I., Cuevas, J., Luna-Vazquez, F., Cuevas, J., Montesinos-López, O., Burgueño, J., et al. (2018). *BGGE: a new package for genomic-enabled prediction incorporating genotype × environment interaction models*. G3 8, 3039–3047. doi: 10.1534/g3.118.200435

Grattapaglia, D., Silva-Junior, O. B., Resende, R. T., Cappa, E. P., Müller, B. S., Tan, B., et al. (2018). Quantitative genetics and genomics converge to accelerate forest tree breeding. *Front. Plant Sci.* 1693. doi: 10.3389/fpls.2018.01693

Guerra-Hernández, J., González-Ferreiro, E., Monleón, V. J., Faias, S. P., Tomé, M., and Díaz-Varela, R. A. (2017). Use of multi-temporal UAV-derived imagery for estimating individual tree growth in Pinus pinea stands. *Forests* 8, 300. doi: 10.3390/f8080300

Han, L., Yang, G., Yang, H., Xu, B., Li, Z., and Yang, X. (2018). Clustering field-based maize phenotyping of plant-height growth and canopy spectral dynamics using a UAV remote-sensing approach. *Front. Plant Sci.* 9, 1638. doi: 10.3389/fpls.2018.01638

Hijmans, R. J., Van Etten, J., Cheng, J., Mattiuzzi, M., Sumner, M., Greenberg, J. A., et al. (2015). Package 'raster'. R package 734. Available online at: https://cran.r-project.org/web/packages/raster/raster.pdf.

Huete, A. (1988). Huete, AR A soil-adjusted vegetation index (SAVI). Remote Sensing of Environment. *Remote Sens. Environ.* 25, 295–309. doi: 10.1016/0034-4257(88)90106-X

Hunt, E. R., Daughtry, C., Eitel, J. U., and Long, D. S. (2011). Remote sensing leaf chlorophyll content using a visible band index. *Agron. J.* 103, 1090–1099. doi: 10.2134/agronj2010.0395

Hunt, J. E. R., Doraiswamy, P. C., McMurtrey, J. E., Daughtry, C. S., Perry, E. M., and Akhmedov, B. (2013). A visible band index for remote sensing leaf chlorophyll content at the canopy scale. *Int. J. Appl. Earth observation Geoinformation* 21, 103–112. doi: 10.1016/j.jag.2012.07.020

Isik, F. (2014). Genomic selection in forest tree breeding: the concept and an outlook to the future. *New Forests 45*, 379–401. doi: 10.1007/s11056-014-9422-z

Jang, G., Kim, J., Yu, J.-K., Kim, H.-J., Kim, Y., Kim, D.-W., et al. (2020). Cost-effective unmanned aerial vehicle (UAV) platform for field plant breeding application. *Remote Sens.* 12, 998. doi: 10.3390/rs12060998

Jannink, J.-L., Lorenz, A. J., and Iwata, H. (2010). Genomic selection in plant breeding: from theory to practice. *Briefings Funct. Genomics* 9, 166–177. doi: 10.1093/bfgp/elq001

Jarne, P., and Lagoda, P. J. (1996). Microsatellites, from molecules to populations and back. *Trends Ecol. Evol.* 11, 424–429. doi: 10.1016/0169-5347(96)10049-5

Jones, A. R., Raja Segaran, R., Clarke, K. D., Waycott, M., Goh, W. S., and Gillanders, B. M. (2020). Estimating mangrove tree biomass and carbon content: a comparison of forest inventory techniques and drone imagery. *Front. Mar. Sci.* 6784. doi: 10.3389/fmars.2019.00784

Kior, A., Sukhov, V., and Sukhova, E. (2021). Application of Reflectance Indices for Remote Sensing of Plants and Revealing Actions of Stressors. *Photonics*. 8 (12), 582. doi: 10.3390/photonics8120582

Krause, M. R., González-Pérez, L., Crossa, J., Pérez-Rodríguez, P., Montesinos-López, O., Singh, R. P., et al. (2019). Hyperspectral reflectance-derived relationship matrices for genomic prediction of grain yield in wheat. *G3: Genes Genomes Genet.* 9, 1231–1247. doi: 10.1534/g3.118.200856

Lande, R., and Thompson, R. (1990). Efficiency of marker-assisted selection in the improvement of quantitative traits. *Genetics* 124, 743–756. doi: 10.1093/genetics/124.3.743

Li, Y., Apiolaza, L. A., and Altaner, C. (2018). Genetic variation in heartwood properties and growth traits of Eucalyptus bosistoana. *Eur. J. For. Res.* 137, 565–572. doi: 10.1007/s10342-018-1125-0

Li, Y., Sun, H., Tomasetto, F., Jiang, J., and Luan, Q. (2022). Spectrometric prediction of nitrogen content in different tissues of slash pine trees. *Plant Phenomics* 2022, 9892728. doi: 10.34133/2022/9892728

Li, B., Xu, X., Zhang, L., Han, J., Bian, C., Li, G., et al. (2020). Above-ground biomass estimation and yield prediction in potato by using UAV-based RGB and hyperspectral imaging. *ISPRS J. Photogrammetry Remote Sens.* 162, 161–172. doi: 10.1016/j.isprsjprs.2020.02.013

LiLin-Yin, (2022). *CMplot: Circle Manhattan Plot* (R package version 4.0.0.). Available at: https://CRAN.R-project.org/package=CMplot.

Lima, J. S., Altoe, M. S., Silva, S. A., Fonseca, A. S., and Medauar, C. C. (2021). Spatial variability of the nutritional status and the leaf chlorophyll index of from rubber tree. *Anais da Academia Bras. Ciências* 93, e20191336. doi: 10.1590/0001-3765202120191336

Louhaichi, M., Borman, M. M., and Johnson, D. E. (2001). Spatially located platform and aerial photography for documentation of grazing impacts on wheat. *Geocarto Int.* 16, 65–70. doi: 10.1080/10106040108542184

Ludovisi, R., Tauro, F., Salvati, R., Khoury, S., Mugnozza Scarascia, G., and Harfouche, A. (2017). UAV-based thermal imaging for high-throughput field phenotyping of black poplar response to drought. *Front. Plant Sci.* 8, 1681. doi: 10.3389/fpls.2017.01681

Lyzenga, W. J., Pozniak, C. J., and Kagale, S. (2021). Advanced domestication: harnessing the precision of gene editing in crop breeding. *Plant Biotechnol. J.* 19, 660–670. doi: 10.1111/pbi.13576

Maesano, M., Khoury, S., Nakhle, F., Firrincieli, A., Gay, A., Tauro, F., et al. (2020). UAV-based LiDAR for high-throughput determination of plant height and above-ground biomass of the bioenergy grass Arundo donax. *Remote Sens.* 12, 3464. doi: 10.3390/rs12203464

Masjedi, A., and Crawford, M. (2020). "Prediction of sorghum biomass using time series uav-based hyperspectral and lidar data," in *IGARSS 2020-2020 IEEE International Geoscience and Remote Sensing Symposium*, Waikoloa, HI, USA. 3912–3915.

Masjedi, A., Crawford, M. M., Carpenter, N. R., and Tuinstra, M. R. (2020). Multi-temporal predictive modelling of sorghum biomass using UAV-based hyperspectral and lidar data. *Remote Sens.* 12, 3587. doi: 10.3390/rs12213587

Newell, M. A., and Jannink, J. L. (2014). Genomic selection in plant breeding. *Methods Mol. Biol.* 1145, 117–130. doi: 10.1007/978-1-4939-0446-4_10

Nik Effendi, N. A. F., Mohd Zaki, N. A., Abd Latif, Z., Suratman, M. N., Bohari, S. N., Zainal, M. Z., et al. (2021). Unlocking the potential of hyperspectral and LiDAR for above-ground biomass (AGB) and tree species classification in tropical forests. *Geocarto Int.* 37 (25), 8036–8061. doi: 10.1080/10106049.2021.1990419

O'Connor, K. M., Hayes, B. J., Hardner, C. M., Alam, M., Henry, R. J., and Topp, B. L. (2021). Genomic selection and genetic gain for nut yield in an Australian macadamia breeding population. *BMC Genomics* 22, 1–12. doi: 10.1186/s12864-021-07694-z

Ota, T., Ogawa, M., Mizoue, N., Fukumoto, K., and Yoshida, S. (2017). Forest structure estimation from a UAV-based photogrammetric point cloud in managed temperate coniferous forests. *Forests* 8, 343. doi: 10.3390/f8090343

Pâques, L. E. (2013). Forest tree breeding in Europe. *Current State-of-the-Art and Perspectives*. Dordrecht: Springer Science+Business Media Dordrecht. doi: 10.1007/978-94-007-6146-9

Peñuelas, J., Filella, I., Biel, C., Serrano, L., and Save, R. (1993). The reflectance at the 950–970 nm region as an indicator of plant water status. *Int. J. Remote Sens.* 14, 1887–1905. doi: 10.1080/01431169308954010

Pu, R., Gong, P., and Yu, Q. (2008). Comparative analysis of EO-1 ALI and Hyperion, and Landsat ETM+ data for mapping forest crown closure and leaf area index. *Sensors* 8, 3744–3766. doi: 10.3390/s8063744

Pugh, N. A., Horne, D. W., Murray, S. C., Carvalho, G.Jr., Malambo, L., Jung, J., et al. (2018). Temporal estimates of crop growth in sorghum and maize breeding enabled by unmanned aerial systems. *Plant Phenome J.* 1, 1–10. doi: 10.2135/tppj2017.08.0006

Qi, J., Chehbouni, A., Huete, A. R., Kerr, Y. H., and Sorooshian, S. (1994). A modified soil adjusted vegetation index. *Remote Sens. Environ.* 48, 119–126. doi: 10.1016/0034-4257(94)90134-1

Rallo, P., de Castro, A. I., López-Granados, F., Morales-Sillero, A., Torres-Sánchez, J., Jiménez, M. R., et al. (2020). Exploring UAV-imagery to support genotype selection in olive breeding programs. *Scientia Hortic.* 273, 109615. doi: 10.1016/j.scienta.2020.109615

Rasmussen, S. K. (2020). Molecular genetics, genomics, and biotechnology in crop plant breeding. *Agronomy* 10 (3), 439. doi: 10.3390/agronomy10030439

Ribaut, J.-M., and Hoisington, D. (1998). Marker-assisted selection: new tools and strategies. *Trends Plant Science* 3 (6), 236–239. doi: 10.1016/S1360-1385(98)01240-0

Rincent, R., Charpentier, J.-P., Faivre-Rampant, P., Paux, E., Le Gouis, J., and Bastien, C.. (2018). Phenomic selection is a low-cost and high-throughput method based on indirect predictions: proof of concept on wheat and poplar. *G3: Genes Genomes Genet.* 8, 3961–3972. doi: 10.1534/g3.118.200760

Roberts, D. A., Roth, K. L., and Perroy, R. L. (2016). "Chapter 14: Hyperspectral vegetation indices," in *Hyperspectral Remote Sensing of Vegetation*, eds P. S. Thenkabail, J. G. Lyon and A. Huete (Boca Raton, FL: CRC Press), 309–328.

Rondeaux, G., Steven, M., and Baret, F. (1996). Optimization of soil-adjusted vegetation indices. *Remote Sens. Environ.* 55, 95–107. doi: 10.1016/0034-4257(95)00186-7

Roussel, J.-R., Auty, D., Coops, N. C., Tompalski, P., Goodbody, T. R., Meador, A. S., et al. (2020). lidR: An R package for analysis of Airborne Laser Scanning (ALS) data. *Remote Sens. Environ.* 251, 112061. doi: 10.1016/j.rse.2020.112061

Santini, F., Kefauver, S. C., Araus, J. L., Resco de Dios, V., Martin Garcia, S., Grivet, D., et al. (2021). Bridging the genotype–phenotype gap for a Mediterranean pine by semi-automatic crown identification and multispectral imagery. *New Phytol.* 229, 245–258. doi: 10.1111/nph.16862

Santini, F., Kefauver, S. C., Resco de Dios, V., Araus, J. L., and Voltas, J. (2019a). Using unmanned aerial vehicle-based multispectral, RGB and thermal imagery for phenotyping of forest genetic trials: A case study in Pinus halepensis. *Ann. Appl. Biol.* 174, 262–276. doi: 10.1111/aab.12484

Santini, F., Serrano, L., Kefauver, S. C., Abdullah-Al, M., Aguilera, M., Sin, E., et al. (2019b). Morpho-physiological variability of Pinus nigra populations reveals climate-

driven local adaptation but weak water use differentiation. *Environ. Exp. Bot.* 166, 103828. doi: 10.1016/j.envexpbot.2019.103828

Scott, A. D., Zimin, A. V., Puiu, D., Workman, R., Britton, M., Zaman, S., et al. (2020). A reference genome sequence for giant sequoia. *G3: Genes Genomes Genet.* 10, 3907–3919. doi: 10.1534/g3.120.401612

Solvin, T. M., Puliti, S., and Steffenrem, A. (2020). Use of UAV photogrammetric data in forest genetic trials: Measuring tree height, growth, and phenology in Norway spruce (Picea abies L. Karst.). *Scandinavian J. For. Res.* 35, 322–333. doi: 10.1080/02827581.2020.1806350

Song, Z., Tomasetto, F., Niu, X., Yan, W. Q., Jiang, J., and Li, Y. (2022). Enabling breeding selection for biomass in slash pine using UAV-based imaging. *Plant Phenomics* 2022, 9783785. doi: 10.34133/2022/9783785

Tao, X., Li, Y., Yan, W., Wang, M., Tan, Z., Jiang, J., et al. (2021). Heritable variation in tree growth and needle vegetation indices of slash pine (Pinus elliottii) using unmanned aerial vehicles (UAVs). *Ind. Crops Products* 173, 114073. doi: 10.1016/j.indcrop.2021.114073

Tsouros, D. C., Bibi, S., and Sarigiannidis, P. G. (2019). A review on UAV-based applications for precision agriculture. *Information* 10, 349. doi: 10.3390/info10110349

Ukrainetz, N. K., and Mansfield, S. D. (2020). Assessing the sensitivities of genomic selection for growth and wood quality traits in lodgepole pine using Bayesian models. *Tree Genet. Genomes* 16, 1–19. doi: 10.1007/s11295-019-1404-z

van den Berg, A. K., and Perkins, T. D. (2005). Nondestructive estimation of anthocyanin content in autumn sugar maple leaves. *HortScience* 40, 685–686. doi: 10.21273/HORTSCI.40.3.685

van Rossum, B.-J., Kruijer, W., Fv, E., Boer, M., Malosetti, M., Bustos-Korts, D., et al. (2020). statgenGWAS: Genome wide association studies. Available at: https://CRAN.R-project.org/package=statgenGWAS.

Van Tassel, D. L., DeHaan, L. R., Diaz-Garcia, L., Hershberger, J., Rubin, M. J., Schlautman, B., et al. (2022). Re-imagining crop domestication in the era of high throughput phenomics. *Curr. Opin. Plant Biol.* 65, 102150. doi: 10.1016/j.pbi.2021.102150

Volpato, L., Pinto, F., González-Pérez, L., Thompson, I. G., Borém, A., Reynolds, M., et al. (2021). High throughput field phenotyping for plant height using UAV-based RGB imagery in wheat breeding lines: feasibility and validation. *Front. Plant Sci.* 12. doi: 10.3389/fpls.2021.591587

Wang, X., Xu, Y., Hu, Z., and Xu, C. (2018). Genomic selection methods for crop improvement: Current status and prospects. *Crop J.* 6, 330–340. doi: 10.1016/j.cj.2018.03.001

Weiß, T. M., Zhu, X., Leiser, W. L., Li, D., Liu, W., Schipprack, W., et al. (2022). Unraveling the potential of phenomic selection within and among diverse breeding material of maize (Zea mays L.). *G3 Genes, Genomes, Genet.* 12, jkab445. doi: 10.1093/g3journal/jkab445

Wickham, H. (2011). ggplot2. *Wiley Interdiscipl. Rev. Comput. Statist.* 3, 180–185. doi: 10.1002/wics.147

Yoosefzadeh-Najafabadi, M., Earl, H. J., Tulpan, D., Sulik, J., and Eskandari, M. (2021). Application of machine learning algorithms in plant breeding: predicting yield from hyperspectral reflectance in soybean. *Front. Plant Sci.* 11, 2169. doi: 10.3389/fpls.2020.624273

Yu, G. (2020). Using ggtree to visualize data on tree-like structures. *Curr. Protoc. Bioinf.* 69, e96. doi: 10.1002/cpbi.96

Yu, G., Smith, D. K., Zhu, H., Guan, Y., and Lam, T. T. Y. (2017). ggtree: an R package for visualization and annotation of phylogenetic trees with their covariates and other associated data. *Methods Ecol. Evol.* 8, 28–36. doi: 10.1111/2041-210X.12628

Zhang, W., Qi, J., Wan, P., Wang, H., Xie, D., Wang, X., et al. (2016). An easy-to-use airborne LiDAR data filtering method based on cloth simulation. *Remote Sens.* 8, 501. doi: 10.3390/rs8060501

Zhaoying Song, F. T., Niu, X., Yan, W., Jiang, J., and Li, Y. (2022). Enabling breeding selection for biomass in slash pine using UAV-based imaging. *Plant Phenomics* 2022, 9783785. doi: 10.34133/2022/9783785

Zheng, H., Cheng, T., Li, D., Zhou, X., Yao, X., Tian, Y., et al. (2018). Evaluation of RGB, color-infrared and multispectral images acquired from unmanned aerial systems for the estimation of nitrogen accumulation in rice. *Remote Sens.* 10, 824. doi: 10.3390/rs10060824

Zhu, X., Leiser, W. L., Hahn, V., and Würschum, T. (2021). Phenomic selection is competitive with genomic selection for breeding of complex traits. *Plant Phenome J.* 4, e20027. doi: 10.1002/ppj2.20027

frontiers | Frontiers in Plant Science

TYPE Methods
PUBLISHED 23 August 2023
DOI 10.3389/fpls.2023.1233794

OPEN ACCESS

EDITED BY
Hanwei Mei,
Shanghai Agrobiological Gene Center, China

REVIEWED BY
Joaquim Miguel Costa,
University of Lisbon, Portugal
Dimitrios Fanourakis,
Technological Educational Institute of Crete, Greece

*CORRESPONDENCE
Hendrik Poorter
h.poorter@fz-juelich.de

RECEIVED 02 June 2023
ACCEPTED 01 August 2023
PUBLISHED 23 August 2023

CITATION
Poorter H, Hummel GM, Nagel KA, Fiorani F, von Gillhaussen P, Virnich O, Schurr U, Postma JA, van de Zedde R and Wiese-Klinkenberg A (2023) Pitfalls and potential of high-throughput plant phenotyping platforms. *Front. Plant Sci.* 14:1233794. doi: 10.3389/fpls.2023.1233794

Pitfalls and potential of high-throughput plant phenotyping platforms

Hendrik Poorter [1,2*], Grégoire M. Hummel [3], Kerstin A. Nagel [1], Fabio Fiorani [1], Philipp von Gillhaussen [4], Olivia Virnich[1], Ulrich Schurr [1], Johannes A. Postma [1], Rick van de Zedde [5] and Anika Wiese-Klinkenberg [1,6]

[1]Plant Sciences (IBG-2), Forschungszentrum Jülich GmbH, Jülich, Germany, [2]Department of Natural Sciences, Macquarie University, North Ryde, NSW, Australia, [3]Phenospex, Heerlen, Netherlands, [4]International Plant Phenotyping Network e.V. (IPPN), Jülich, Germany, [5]Plant Sciences Group, Wageningen University & Research, Wageningen, Netherlands, [6]Bioinformatics (IBG-4), Forschungszentrum Jülich GmbH, Jülich, Germany

Automated high-throughput plant phenotyping (HTPP) enables non-invasive, fast and standardized evaluations of a large number of plants for size, development, and certain physiological variables. Many research groups recognize the potential of HTPP and have made significant investments in HTPP infrastructure, or are considering doing so. To make optimal use of limited resources, it is important to plan and use these facilities prudently and to interpret the results carefully. Here we present a number of points that users should consider before purchasing, building or utilizing such equipment. They relate to (1) the financial and time investment for acquisition, operation, and maintenance, (2) the constraints associated with such machines in terms of flexibility and growth conditions, (3) the pros and cons of frequent non-destructive measurements, (4) the level of information provided by proxy traits, and (5) the utilization of calibration curves. Using data from an Arabidopsis experiment, we demonstrate how diurnal changes in leaf angle can impact plant size estimates from top-view cameras, causing deviations of more than 20% over the day. Growth analysis data from another rosette species showed that there was a curvilinear relationship between total and projected leaf area. Neglecting this curvilinearity resulted in linear calibration curves that, although having a high r^2 (> 0.92), also exhibited large relative errors. Another important consideration we discussed is the frequency at which calibration curves need to be generated and whether different treatments, seasons, or genotypes require distinct calibration curves. In conclusion, HTPP systems have become a valuable addition to the toolbox of plant biologists, provided that these systems are tailored to the research questions of interest, and users are aware of both the possible pitfalls and potential involved.

KEYWORDS

calibration curve, digital biomass, high-throughput plant phenotyping, leaf mass per area, sensors

1 Introduction

For decades, plant growth has been studied by taking non-destructive measurements such as plant height, along with destructive measurements such as plant dry mass. Typically, these assessments involved serial measurements over time, or comparisons of plants or plots at a 'final' harvest (Evans, 1972). Usually, 3-8 plants per treatment were harvested, or 2-30 genotypes compared, in a process that could easily take a full day or more for a single person. However, In the past 15 years, there has been a significant shift towards high-throughput plant phenotyping (HTPP). Fully automated systems now screen up to hundreds of genotypes and thousands of individual plants or field plots using non-destructive sensors, with the collected data automatically processed and stored for later use. (Furbank and Tester, 2011; Fiorani and Schurr, 2013; Tardieu et al., 2017; Lorence and Jimenez, 2022). In controlled conditions, automated phenotyping is often achieved by bringing individual plants to sensors (Yang et al., 2014; Al-Tamimi et al., 2016), or by moving sensors to or over the plants (Granier et al., 2006; Nagel et al., 2012). In the field, sensors are also brought to plants, either through mobile vehicles (White and Conley, 2013; Deery et al., 2014) or via drones or other aerial platforms that fly over field trials (Vargas et al., 2020; Roth et al., 2022). In all of these cases, automation has enabled a significant increase in the number of individual plants or plots that can be processed daily, often by an order of magnitude.

An important driver for the development of HTPP systems has been the rapid progress in the field of molecular biology. The extensive expansion and utilization of molecular tools at continuously decreasing costs have enabled thorough genotypic characterization of many plant species, cultivars, and genotypes. Phenotypic characterization, however, still lags behind, first because it is a time-consuming and often still manual measurement process, and second because plants of the same genotype can exhibit a range of different phenotypes, depending on environmental conditions (Furbank and Tester, 2011; Zavafer et al., 2023). This phenotyping bottleneck is particularly pronounced when studying traits that are controlled by multiple genes. In such cases, top-down approaches like Quantitative Trait Loci (QTL) analysis or Genome-Wide Association Studies (GWAS), are necessary to identify regions of the genome that are determining these traits (Gibson, 2018). However, conducting these analyses requires phenotyping hundreds of different genotypes, preferably all grown simultaneously in a common environment. Such analyses greatly benefit from the automation and standardization provided by HTPP systems (reviewed in Xiao et al., 2022).

Various technological advancements have facilitated the development of automated HTPP systems. A wide range of non-destructive sensors, including digital RGB cameras, hyperspectral, thermal, and fluorescence cameras, laser scanners, and LIDARs (Liu et al, 2020) enable repeated measurements of individual plants over time. This provides a higher resolution for capturing time-related phenotypic changes compared to experimental designs where new plants need to be harvested destructively for each time point (Poorter and Garnier, 1996; Walter et al., 2007). The use of automated gantries and transportation systems as well as drones allow us to minimize the distance between sensors and plants. Another significant factor is the increased computational power and improved algorithms that enable efficient image processing, with or without machine learning (Walter et al., 2015; Dobrescu et al., 2020).

As mentioned above, HTPP systems encompass a diverse range of approaches, all centered around non-destructive measurements. In the years ahead, more and more of these systems will be built to effectively screen a large number of plants for their size, growth trajectory, and other traits. However, like any complex equipment, the use of these platforms also presents challenges and limitations that may be overlooked by those who have not yet utilized them. Therefore, before investing in the purchase, construction, and utilization of these platforms, it is crucial to consider potential issues that may arise, and how they can be addressed. In the Results and Discussion section, we share insights gained from our experience in developing and deploying HTPP systems over the past 15 years. While our focus is primarily on systems operating in (semi-)controlled environments, several of the issues discussed will apply to field phenotyping as well.

2 Materials and methods

Part of the discussion that follows will address the relationship between non-destructive measurements, such as projected leaf area, and variables that require destructive analysis, including total leaf area, shoot biomass, and total plant biomass. We illustrate this part of the discussion with data from two experiments. In the first experiment, *Arabidopsis thaliana* (Col-0) plants were cultivated in a growth room using a rack equipped with neon tubes (Fluora, Osram, Munich). The plants were grown in soil (ED73, Einheitserde, Uetersen, Germany) in a cultivation tray with adjacent 80 ml cells. After incubating the seeds in the dark at 4°C, they germinated in the tray. The plants were then subjected to a 12-hour day length, a photosynthetic photon flux density (PPFD) of 40-50 µmol m^{-2} s^{-1}, a day/night temperature of 23/20°C and a relative humidity (RH) of ca. 55%. Plants were watered from below when the top-soil was fully dry. Thirty-nine days after sowing, the plants were imaged six times during the day, with 2-hour intervals. Screening and image analysis were performed following Walter et al. (2007). The data from this experiment can be found in Supplementary Data Sheet A1.

The second experiment involved studying *Plantago major*, another rosette-forming species, throughout a significant part of its growth cycle and included a large number of replicates per harvest (n=12). The plants were grown hydroponically under two different CO_2 concentrations (350 and 700 µmol mol^{-1}), in growth chambers with a 12-hour day length, a PPFD of 230-270 µmol m^{-2} s^{-1}, a day/night temperature of 20/18°C and a day/night RH of 60/90%. Plants from both treatments were monitored weekly over a 7-week growth period. Projected leaf area (PLA) was determined by capturing

Abbreviations: HTPP, High-Throughput Plant Phenotyping; MAPE, Mean Absolute Percentage Error; MdAPE, Median Absolute Percentage Error; RMSE, Root Mean Square Error; PLA, Projected Leaf Area; TLA, Total Leaf Area.

slides with an analogue camera placed at a height of 2 meters. The slides were projected, plant outlines traced on papers, and those were subsequently digitized semi-manually using a digitizer (model 9874a, Hewlett Packard, Stanford, CA, USA). Total leaf area per plant (TLA) was determined using a leaf area meter (LiCor 3100, Li-Cor Inc, Lincoln, NE, USA) equipped with a conveyor belt system. The determination of the total dry mass of shoots and roots was done manually, with plant size varying >300-fold throughout the course of the experiment. The data for this experiment is sourced from a previously published study by Poorter et al. (1988) and can be found in Supplementary Data Sheet 2.

Data were analyzed using R version 4.1 (R Core Team, 2022). Various calibration curves were established by employing the function lm, with or without a ln-transformation of the relevant variables, and with or without a quadratic term for the explanatory variable.

3 Results and discussion

Before proceeding with the design and implementation of a high-throughput plant phenotyping (HTPP) system, it is essential to consider the following questions. Figure 1 shows a schematic overview of the relevant aspects to be considered.

3.1 What is the specific research need?

HTPP systems are designed based on principles of automation and standardization. However, several critical aspects must be considered and discussed in order to effectively design and implement these systems. These include the required scale of the experiments, the selection of sensors that will be installed, the necessary software infrastructure, and the expected return on investment in terms of financial and human resources. These aspects can only be fruitfully discussed if guided by the question what purpose the system should serve and what goal(s) one would like to achieve through this platform. This is even more important in the case where multiple research groups with diverse interests are involved, as there is a risk that the intended platform becomes a compromise that in the end does not satisfy any.

3.2 What are the costs of investment and maintenance for a phenotyping platform?

HTPP systems involve a complex combination of logistics and technology, particularly when plants need to be moved to sensors. Such machines require the use of conveyor belts, gantries, or mobile robots to transport plants through growth chambers or glasshouses to an imaging station. At the imaging station, plants are generally subjected to controlled conditions, such as a consistent light spectrum and intensity, allowing for a consistent acquisition of images or other sensor-based data. Additionally, plants in pots or carriers can be automatically weighed and watered. Measurement equipment must be linked to large-scale data storage facilities and databases, in order to store and retrieve the collected measurement information and other metadata. Clearly, expert knowledge of automation, logistics, error control, fine mechanics, non-destructive sensing, image analysis, and database management is required to build and operate these systems properly. Companies specializing in these different fields offer to construct customized machines on-site. The costs of these systems can be substantial. Prices typically range from approximately €60,000 to €120,000 for small systems with a lower degree of automation and throughput, €350,000 – €500,000 for fully automated sensor-to-plant or plant-to-sensor systems, and up to €3,000,000 for high-end systems with extensive optimization and automation of the workflow. The costs vary depending on factors such as the types and number of sensors used, system size, quality of the product and service provided by the

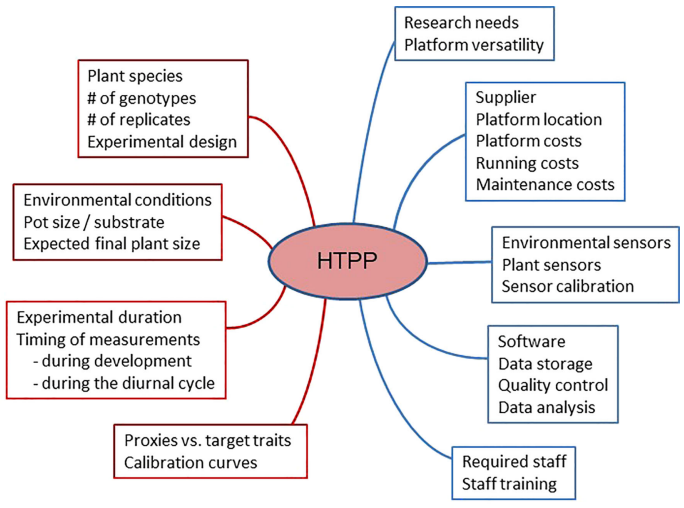

FIGURE 1
A schematic diagram indicating different aspects of high-throughput plant phenotyping (HTPP) systems that should be considered before purchasing such a system (in blue) and using it (in brown).

supplier. In addition, these custom-built facilities require expert maintenance, including sensor calibration, replacement of worn-out parts and preventive check-ups. Yearly servicing contracts often amount to 5-10% of the acquisition price and are necessary for the duration of system usage.

Given the above considerations, certain laboratories opt to construct HTPP systems themselves, either utilizing off-the-shelf products or with the support of robotics companies (Bagley et al., 2020). Building customized platforms can allow for increased flexibility (as discussed in section 3.4) and better fit the specific requirements of the involved labs. However, it is important to acknowledge that the path to a fully functional machine is challenging and time-consuming. While the direct hardware costs may be lower than those of commercial HTPP systems, the substantial human resources required for the development and maintenance of such automated systems should not be underestimated (Reynolds et al., 2019).

There are two additional points to consider regarding personnel investment. Firstly, it is advisable to involve expert users, project managers, and engineers throughout the planning and building phase. This ensures that any necessary compromises that almost inevitably have to be made during the whole process do not strongly constrain the desired goals of the end-users. Secondly, operating these systems can be complex, particularly when troubleshooting errors, as there are numerous variables to consider within the platform software, platform mechanics and network communications. Therefore, it is recommended to have an operational team led by an expert who is responsible for the platform. This lead expert can receive training from the supplier or the constructors, and subsequently train all other individuals who will be utilizing this platform. Clearly, such a person requires both technological as well as plant biological expertise to effectively manage and operate the HTPP system.

3.3 What other logistical and infrastructural adjustments are necessary?

An HTPP platform allows researchers to significantly scale up their experiments, often by an order of magnitude. This implies that also an order of magnitude more plants are processed, more containers have to be filled, more consumables are used, more electricity and irrigation are required, and additional cleaning has to be done at the end of the experiment. While these aspects are not part of the phenotyping platform *per se*, they contribute to a significant workload. As a result, there is often a need for subsequent adjustments to the workflow's ergonomics, such as automating tasks like pot filling, seed sowing (Jahnke et al., 2016) or plant transplantation. Together with the sampling for further physiological characterization and disinfection or disposal of used components, they bring about additional planning and investments on top of those for the platform itself.

Another aspect to consider is the data infrastructure. Given the massive amount of data generated by HTPP systems, effective storage and accessibility of data for both short-term and long-term use are essential. Such utilization of data requires a good documentation of data and metadata, as described in the 'Minimal Information About Plant Phenotyping Experiments' (MIAPPE) guidelines (Krajewski et al., 2015; Papoutsoglou et al., 2020). Also, data and metadata should be stored in accordance with the FAIR principle (findable, accessible, interoperable, and reusable; Wilkinson et al., 2016) as in GnpIS (Pommier et al., 2019) and as currently established in research data management infrastructures like DataPLANT (www.nfdi4plants.de).

Remote support by the different suppliers requires a safe, secure, and reliable access policy. Moreover, in the analysis of data from such platforms, there is a growing emphasis on integrating genotypic and phenotypic data, as well as incorporating detailed environmental characterization of the experiments. Bringing all these data together often requires a considerable *a-posteriori* effort from trained personnel, which also needs to be budgeted in advance to make full use of the potential of these HTPP systems (Reynolds et al., 2019).

3.4 How flexible can or should the system be?

Automation can replace a considerable amount of tedious repetitive manual labor, especially when routine operations are customized to the research question and species of interest. However, this increased automation often comes at the cost of reduced flexibility. For instance, a system that is perfectly fit for small rosette plants like *Arabidopsis thaliana*, may not be as suitable for a large species with different architecture, such as *Zea mays*. Increased flexibility of the system can be achieved by planning for modular components that can be interchanged depending on the prevailing research question. However, increased flexibility to accommodate the needs of a variety of researchers also implies that the system becomes increasingly complicated, with a higher likelihood of failures and more efforts to solve these problems. A 'jack-of-all-trades' system will hardly provide the same level of detail and raw data resolution across the entire range of plant sizes and architectures as a dedicated high-resolution system designed specifically for either small or big plants, due to limitations imposed by the optical properties of the sensor and system layout. In those cases, a potential solution could be to have two smaller and targeted systems, rather than relying on a one-size-fits-all solution.

Another aspect of flexibility is the expected lifespan of system components. Technological advancements occur rapidly, and new sensors, for example, will generally be more powerful and informative than their predecessors. However, owners of commercially-acquired phenotyping systems often face problems in that the software to run the whole system is proprietary to the company, and therefore not accessible for further development. In such cases, it is complicated or impossible to integrate new sensors or apply other modifications to existing HTPP systems. New buyers are advised to discuss with their suppliers what support they can get in that respect. Self-builders are suggested to set up their software interfaces as flexible as possible, to easier adjust their system when new sensors or updates become available.

3.5 What constraints does the system impose on growth conditions?

Plants are strongly influenced by their environment and different genotypes or species may show varying degrees of genotype x environment interactions for many of their phenotypic traits. This becomes particularly critical, because in most (semi-)controlled environments we impose abiotic conditions that significantly deviate from the natural conditions plants experience outdoors (Poorter et al., 2016; Chiang et al., 2020). Considerations about the location of the HTPP system (growth chamber, glasshouse, or field) and the range of environmental conditions provided to the plants are therefore an integral part of the design process.

Compared to traditional experiments, the use of high-throughput phenotyping systems often introduces additional constraints, that can impact the growth environment of the plants and, consequently, the outcomes of experiments. For instance, in a typical plant-to-sensor system, the combined weight of plants plus pots is limited by the strength of the conveyor belt used, as well as the scales used for gravimetric measurements. This limitation results in experiments being confined to plants in relatively small pots with substrates of low specific mass, which clearly affects plant growth and experimental outcomes (Passioura, 2002; Poorter et al., 2012). Transportation may also have other consequences. Tall plants, such as *Zea mays*, may topple over if the conveyor belts move too quickly. During transport, leaves of sensitive species (e.g. *Brassica rapa*, *Hordeum vulgare*) can get damaged, causing them to droop downwards along the pot. To mitigate damage, researchers may choose to place suitable support structures next to or around each plant, except in cases where wilting would be a phenotypic trait of interest. Apart from direct damage, one would also expect thigmo-morphogenetic responses to occur as a reaction to the mechanical perturbations during transport of plants, such as thicker and shorter stems (Anten et al., 2005). However, plant height was not negatively affected in the experiment of Brien et al. (2013), and neither was shoot biomass or leaf area in various experiments (Table 1).

Fixed distances between cameras/sensors and plants may restrict the range of plant sizes that can be investigated, thereby limiting the developmental stages that can be studied in such HTPP systems to young vegetative plants. A last example pertains to the watering of the plants. Well-watered containers, especially with peat substrate, often show algal growth on the soil surface, which hampers the non-destructive derivation of plant size through image analysis (Figure 2A). To avoid this complication, researchers may opt to cover the top of the pots with a plastic sheet of contrasting color (Junker et al., 2015). Alternatively, for small rosette species like *Arabidopsis*, reducing the volume and/or frequency of watering can keep the topsoil dry for a longer duration. Although this suppresses algal growth, it also has unknown consequences for the growth rate and phenotype of the plants. It is recommended to consider *a-priori* whether the additional constraints imposed by an HTPP system are acceptable within the scope of the research question.

3.6 When and how often should the plants be measured?

Once an operational HTPP system is in place, attention can shift to the performance of experiments. Given their typical large scale, careful consideration of experimental design is essential. For a comprehensive discussion on this topic, the reader is referred to Thompson et al. (2022). One notable advantage of high-throughput phenotyping systems is that individual plants (or microplots) can be measured frequently and non-destructively. This allows for the repeated measurements of the same plants, enabling the tracking of their growth and development over time. Such analyses can yield valuable insights, with a good example discussed in Box 1. However, in cases where the research question focuses on identifying the best-performing genotype at the end of the experiment, repeated measurements may be unnecessary. In those cases, researchers could also opt for one final destructive harvest, which might be more simple, cheaper, and more informative, as also illustrated in Box 1. A lower measurement frequency may also be advantageous if the measurements have the potential to interfere with plant growth.

TABLE 1 Effect of plant-to-sensor transport on shoot biomass, as based on various experiments carried out in glasshouses.

Reference	Mode of transport	Species	Measured variable	Size ratio of shoots (moving vs. non-moving plants)	P
Nagel et al. (2020)	pneumatically	*Arabidopsis thaliana*	LA	0.96	ns
F. Fiorani & N. Körber (unpubl.)	gantry system	*Hordeum vulgare*	FM	0.97	ns
F. Fiorani & N. Körber (unpubl.)	gantry system	*Brassica napus*	FM	1.02	ns
Brien et al. (2013)	conveyor belt	*Triticum aestivum*	FM	1.03	ns
Junker et al. (2015)	conveyor belt	*Arabidopsis thaliana*	DM	1.08	*

LA, Leaf area; FM, Fresh mass of the shoot; DM, Dry mass of the shoot. Statistical significance: *, $P < 0.05$; ns, non-significant. Included are the mode of transport of the plants, the species investigated, variable measured, the size ratio of shoots of plants that were moved relative to control plants that were not moved, and the statistical significance of these differences in plant mass. The experiments are ranked based on the observed effect size.

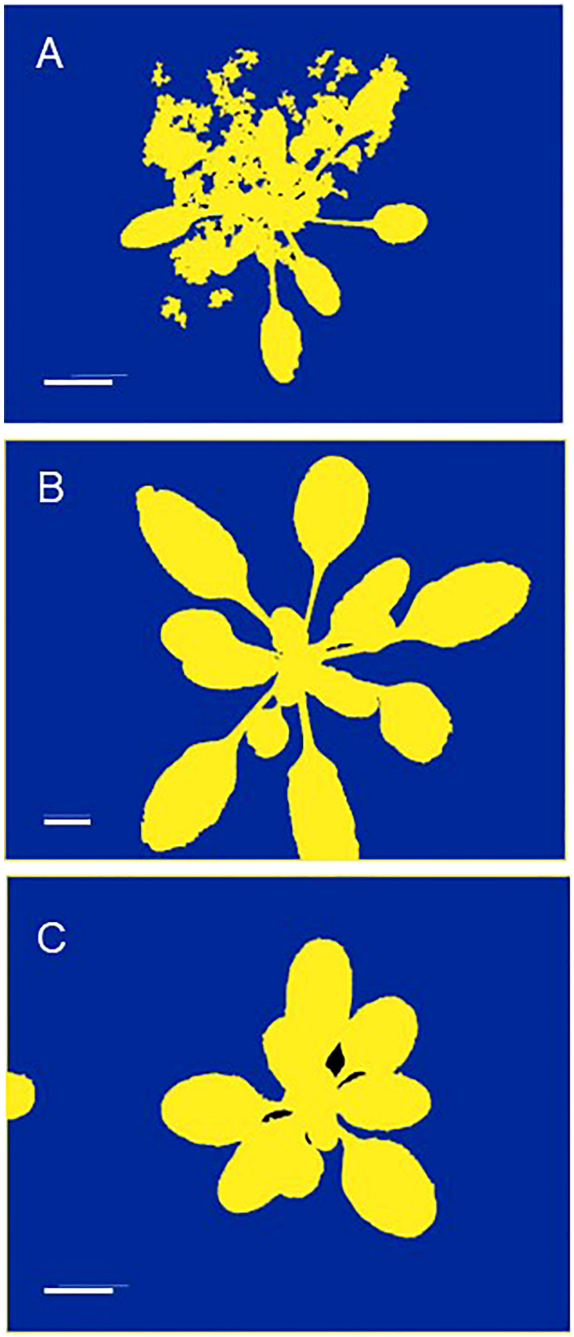

FIGURE 2
Examples where unsupervised automated high-throughput phenotyping may lead to incorrect results. **(A)** Algal growth resulting in a mask that is too broad and yields an overestimation of projected leaf area (PLA). **(B)** A plant grown out of the image acquisition area, resulting in an underestimation of PLA. **(C)** A neighboring plant growing into the image acquisition area, resulting in an overestimation of PLA. All pictures depict *Arabidopsis thaliana* plants and are masked images, used for measuring PLA by counting the number of green pixels. These images are for illustrative purposes only. The scale indicates a length of 1 cm.

This is particularly relevant when plants are taken out of their growth environment for longer-duration measurements, such as magnetic resonance imaging (MRI) or computer tomography (CT) scans. A higher measurement frequency then provides better insight into plant development, but may also have a stronger negative effect on plant growth.

A second point to consider is the time of day when plants will be measured. When using a drone to fly over an experimental field, it can capture images of many microplots simultaneously. Acquiring images or other data for these plots using sensors mounted on vehicles will take longer. Depending on the type of measurements taken, it may require minutes or more per microplot. With plant-to-sensor systems within a glasshouse, where it takes minutes to move a plant through the imaging station and measure its characteristics, phenotyping all plants in one experiment could take a full day. During that period, large changes in environmental variables, such as light intensity and temperature, may occur, likely resulting in large variation in physiological variables such as stomatal conductance and photosynthesis as well. One morphological trait that can exhibit considerable diurnal variation is leaf angle (Rosa and Forseth, 1996), which has obvious implications for the projected leaf area (PLA; Dobrescu et al., 2017) as used in many HTPP systems. For example, during the diurnal part of the diel cycle, *Arabidopsis* plants may *increase* their leaf area and biomass by 20% (Wiese et al., 2007). However, in a similar experiment, PLA values were found to *decrease* by 18-35% during the light period (Figures 4A, B, 5), due to upward movements of leaves and petioles. Consequently, when conducting consecutive 2D measurements of plants day after day, it is important to measure them at the same time of day, to avoid bias caused by the diurnal rhythm of leaf movements. Moreover, different genotypes or treatments should be blocked into the same time window, to ensure that no confounding effects occur. One fast alternative approach is to perform a 3D laser scan (Dornbusch et al., 2012). Other options include using multiple imaging stations, or employing a gantry system where sensors are brought to the plants, enabling parallel measurements of many plants in short time.

In some cases, the research question requires a high frequency of measurements on the same plants. Examples are physiological responses of plants following the application of a compound, exposure to a pathogen, or exposure to abiotic stress (Jansen et al., 2009; Mahlein et al., 2019). In some species, capturing images at higher frequencies and analyzing them in almost real-time can be used to detect the onset of potentially undesired drought stress during the experiment (Figures 4C, D; Eberius and Lima-Guerra, 2009; Janni et al., 2019).

3.7 How adequate is the quality control and data handling?

The amount of information collected from a single experiment can be substantial, especially when imaging of any kind is involved. The question is how well we, as experimenters, can handle this vast quantity of data (Eberius and Lima-Guerra, 2009; Tardieu et al., 2017). Based on our own experience, we have observed several issues that can arise during an experiment. Sensors, especially environmental sensors that are deployed throughout the year, may have not been calibrated for a long time or show failures of various kinds during the experimental period. With larger amounts of plants,

BOX 1 Example of the trade-off between measuring with higher frequency or higher precision.

Here we provide two examples of experiments focusing on root distribution. The first one followed root development non-destructively over time (Nabel et al., 2018). Seedlings of a woody shrub (*Sida hermaphrodita*) were grown for 90 days in rhizotrons of 36 x 75 x 2.6 cm in size, where one side consists of transparent acrylic glass. The researchers placed digestate, which is a residue remaining after anaerobic digestion of biomass to methane, at a specific location in the rhizobox. This location is indicated by the brown circles in Figures 3A–C. Root growth of the part of the root system close to the transparent side of the rhizobox was monitored by regularly capturing images (Nagel et al., 2012). These images showed that plants strongly avoided the digestate patch in the first 60 days of the experiment (Figures 3A, B). However, roots strongly proliferated into this patch of nutrients later in time (Figure 3C). In this case, the timing proved to be an essential aspect of how these plants reacted to the treatment. Although these analyses of root distribution are still challenging for computers and often need human supervision, the effort in this case proved worthwhile for understanding the timing of root responses.

An alternative approach was followed by Singh et al. (2010; Figure 3D). They grew two *Sorghum* genotypes in rhizotrons measuring 120 x 240 x 10 cm. When it comes to selecting, for example, the best-performing genotypes of a panel of genotypes, an evaluation at the end of the experiment could be as informative as a complete analysis over time. If this is the case, researchers may also opt for alternative and cheaper set-ups, such as rhizoboxes that are not integrated into automated HTPP systems. Those rhizoboxes could have larger dimensions and allow a wider range of root substrates. By pushing a pinboard into one of the sides before washing away the soil with water, the distribution of a *whole* root system can be characterized, rather than only those roots close to the acrylic glass (Singh et al., 2010; Figures 3D, E).

The dilemma faced by researchers in these cases is whether it is more informative to have estimated data over the course of the experiment for only a portion of the root system, as provided by automated rhizotron systems, or to have more precise data capturing the entire root system but only at the end of the experiment.

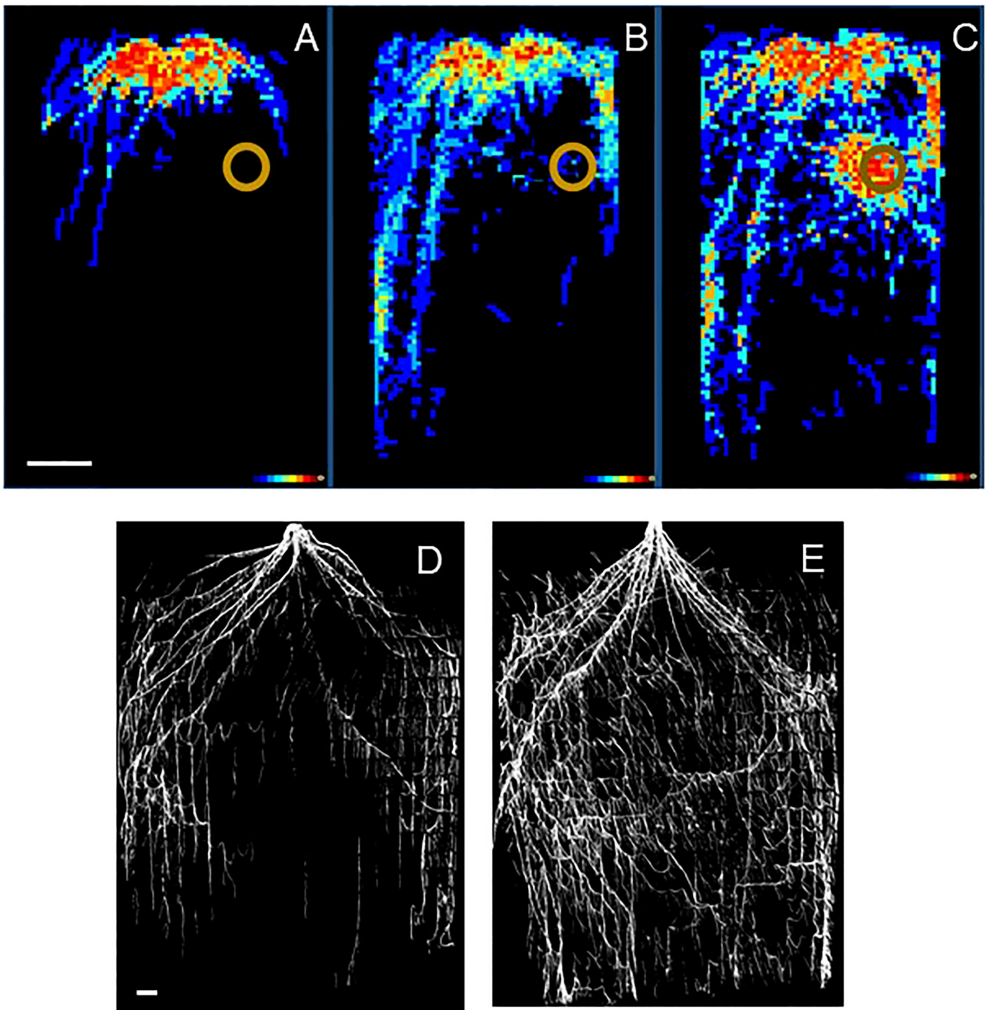

FIGURE 3
(A–C) Root distribution of *Sida hermaphrodita* plants in rhizotron boxes with a localized depot of digestate, indicated by the brown circle. **(D)** Root distribution in a rhizobox at the end of an experiment after the soil has been removed. Figures **(A–C)** are adapted from Nabel et al. (2018) and show in false colors ranging from dark blue to bright red the number of rhizotrons (out of 10 in total) where roots were observed for each x-y location in the rhizotron. **(A)** 30 days, **(B)** 60 days and **(C)** 90 days after the start of the experiment. Figures **(D, E)** show the root systems of two *Sorghum bicolor* genotypes at the 12th-leaf stage (ca. 6-8 weeks after germination) in an experiment similar to that described in Singh et al. (2010). The white bars indicate a length of 10 cm. Picture credits Figures **(A–C)**: Moritz Nabel, Forschungszentrum Jülich, Germany. **(D, E)**: Vijaya Singh, University of Queensland, Australia.

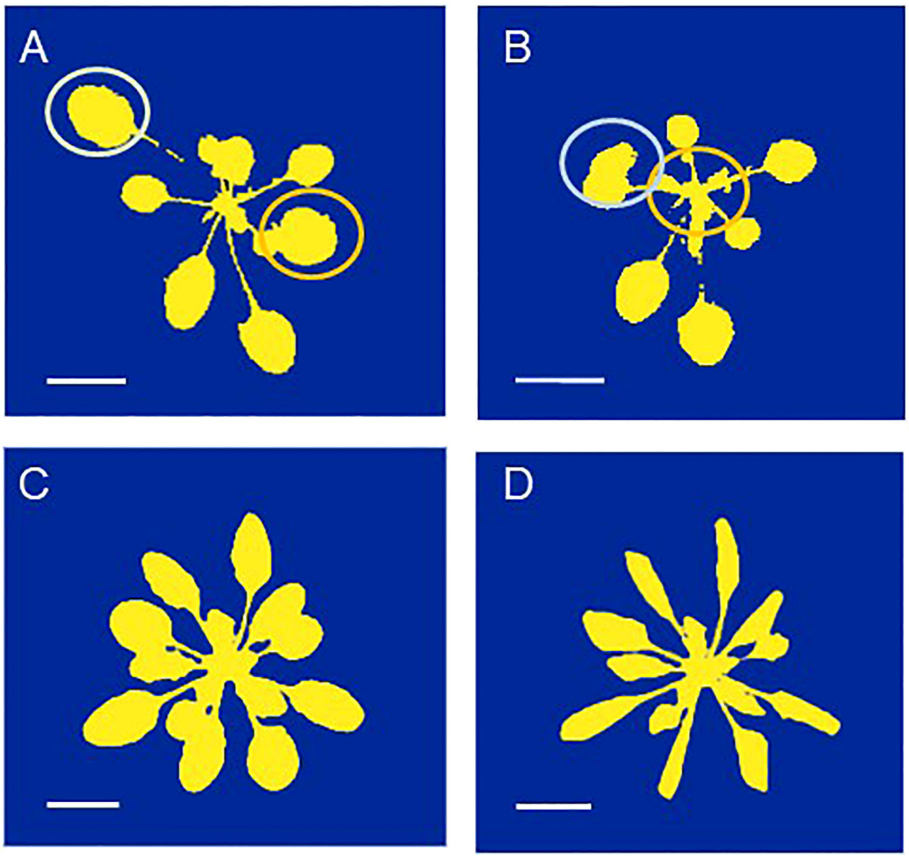

FIGURE 4
(A, B) The same *Arabidopsis thaliana* plant photographed **(A)** in the morning, with a low leaf angle and **(B)** at the end of the day with a much higher leaf angle. The yellow and orange circles indicate the positions of the youngest full-grown leaves which exhibit the largest change in leaf angle. **(C, D)**. The same plant photographed **(C)** before and **(D)** after the onset of water stress, which resulted in leaf wilting. These images are for illustrational purposes only. The scale indicates a length of 1 cm.

problems might more easily go undetected. For example, some plants could topple over or do not receive adequate watering. In image analysis systems, leaves from neighboring plants might appear in pictures taken, photos might not cover the full plant, or masking might not function properly (Figures 2B, C). These errors are easily noticed if they occur frequently, but in the midst of hundreds of plants, thousands of pictures, and tens of thousands of other collected data points, such errors can easily go unnoticed. Thorough data inspection and double-checking for mistakes are therefore crucial, but can be cumbersome without the assistance of digital tools. Dedicated software programs for data visualization and targeted image retrieval, such as Azure, iRods, PHIS, Fairdom, Zegami, or similar solutions, enable fast selection of images of specific plants over time, aiding in the identification of potential outlier data. Automated quality control procedures should routinely flag instances where parts of leaves are outside the picture, or leaves of neighboring plants are distorting the results. Graphical analysis of data distribution, time courses, or dose-response curves can provide insights into potential issues with specific plants or entire groups of plants (Xu et al., 2015). This is particularly useful in ongoing experiments, when possible problems can be detected and solved by data analysis at an early stage. Real-time reporting, along with easy and user-friendly (remote) access to visualizations and resulting analyses, facilitates early detection and problem-solving.

3.8 How informative are the selected proxies for the actual variables of interest?

For decades, scientists have relied on spectrophotometric measurements to asses enzyme activity, wet digestion or pyrolysis for leaf nitrogen determination, infra-red gas analyzers to determine photosynthesis, and manual harvesting to measure plant biomass. However, these conventional measurements all require significant manual effort, and are therefore not suitable for high-throughput phenotyping. Efforts have been made to automate such measurements (e.g. Gibon et al., 2004; Gomez et al., 2010), but challenges remain in automating processes such as grinding and weighing, particularly under low-temperature conditions to prevent chemical degradation (Hall et al., 2022). In search of alternatives, scientists have explored measurements that are easier to perform, yet still provide valuable information. For example, leaf nitrogen content can be estimated non-destructively using multispectral analysis (Ye et al., 2020), photosynthesis can be

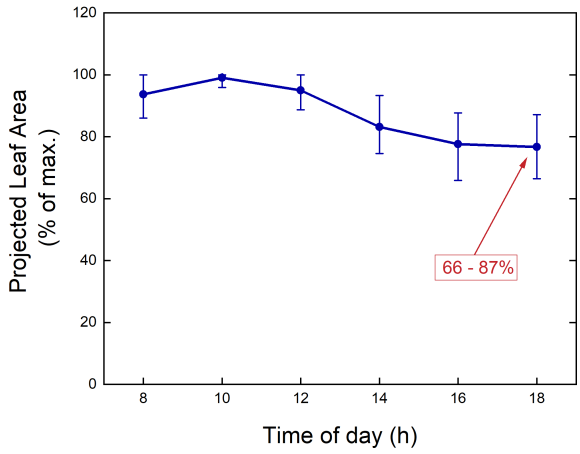

FIGURE 5
Measured Projected Leaf Area (PLA) over a day for *Arabidopsis thaliana* plants grown in a growth chamber. The values for each plant are normalized to the maximum value measured during the diurnal part of the day-night cycle. The dots indicate mean values, and the 'error bars' represent the 5% and 95% percentiles (n = 44).

assessed through fluorescence, and biomass by counting green pixels in plant images.

Are these proxies informative enough? The chlorophyll fluorescence parameter (F_v/F_m), for instance, is often measured, but in many cases variation in F_v/F_m does not reflect variation in the actual rate of photosynthesis (Poorter et al., 2019). The electron transport rate offers a better approximation, but still does not capture the true rate of C-fixation (Kalaji et al., 2014). Similarly, estimating digital biomass based on the number of green pixels in an image can provide an indication of plant size, but does not give the actual biomass, or information on biomass allocation to leaves, stems, and roots. This lack of information hampers comparisons across experiments, platforms, and the published literature. However, advancements in machine learning techniques now enable the segmentation of 2D or 3D images into leaves and stems (Golbach et al., 2016; Jin et al., 2019; Shi et al., 2019), so far only for smaller and/or specific species. Moreover, combined shoot and root phenotyping is feasible in rhizotron or agar-based platforms (Nagel et al., 2012; Nagel et al., 2020). These developments hold the potential to extract more comprehensive information from these photographs or raw sensor data.

In all cases, users must maintain a critical approach to their data, particularly when changes in plant morphology occur. A clear example is observed in drought-stressed plants where a loss in turgor can result in leaf rolling or wilting, leading to a noticeable decrease in projected leaf area (PLA; Figures 4C, D), while actual dry biomass is little affected. Even when the variable of interest is directly provided by sensors, it is wise to verify the definitions used. For one researcher, plant height may be the distance from the shoot basis to the highest plant part, for another it could be the distance from the basis to the apical meristem. In some non-destructive systems, a more statistical approach is taken, where this variable is defined as the average value of the pixels (or voxels) from the 80th till the 90th percentile with respect to height (Kjaer and Ottosen, 2015). Ideally, these definitions are included in the meta-data provided by the HTPP system.

3.9 Are non-destructive measurements sufficient?

The phenotype of plants is multifaceted, composed of hundreds of variables related to anatomy, morphology, chemical composition, carbon and water economy, growth, as well as reproduction (Lambers and Oliveira, 2019; Poorter et al., 2022; Zafaver et al., 2023). While some of these variables can be estimated non-destructively, the majority of plant traits require destructive sampling or harvesting. Consequently, HTPP systems, which are primarily non-destructive by nature, can only cover a subset of the phenotypic traits that researchers would ideally like to measure. However, by bringing sensors to the plant, additional measurements may become feasible. For example, continuous monitoring of transpiration over a plant's lifespan in real time can be achieved by placing plants on a balance (Tardieu et al., 2017; Dalal et al., 2020). Nevertheless, many other traits can only be measured through destructive sampling or harvesting, which necessitates additional planning and manpower.

A highly promising advancement is the development of robots capable of approaching a plant and taking a leaf punch from a specific leaf blade (Alenyà et al., 2013; Foix et al., 2018). By promptly storing these samples in liquid nitrogen, a broad array of relevant biochemical analyses can be conducted, including the assessment of key metabolites and RNA expression levels (Hall et al., 2022).

3.10 What calibration curve is required?

In certain cases, well-calibrated phenotyping equipment can directly provide data on physiologically relevant variables of interest. For instance, measurements such as leaf temperature or F_v/F_m yield output that is readily biologically interpretable and can be easily related to published work in the literature. In other cases, however, additional calibration is required to transform acquired

data (e.g., number of green pixels) into biological meaningful variables (e.g., shoot dry mass). In such cases, a common procedure involves periodic measurements of a subset of plants, initially through non-destructive imaging, and subsequently destructively by determining leaf area, shoot dry mass or other traits of interest. An example is shown in Figure 6, where the projected leaf area of *Plantago major* plants grown under different [CO_2] levels was assessed non-destructively through imaging, followed by destructive measurement of total leaf area and shoot biomass (see Material & Methods).

The first step in establishing a calibration curve involves plotting the variable of interest against the measured variable. We illustrate this process with a graph that depicts the relationship between total leaf area (TLA) and projected leaf area (PLA). The graph demonstrates that for small plants (< 30 cm^2 in this case, for plants up to 4 weeks old), TLA and PLA exhibit largely similar values. However, in larger plants, TLA increases at a faster rate than PLA, as newly-grown leaves will inevitably overlap partially or even fully with older leaves. In the experiment presented here, the TLA at the final harvest was approximately 2.3 times larger than the corresponding PLA, with no clear difference between plants of the two treatments.

The second step in constructing the calibration curve involves computing a regression line. Taken over both treatments, a linear regression yielded highly significant results ($P < 0.001$). Based on the calculated r^2, we found that variation in PLA accounted for 92% of the variation in TLA. While this initial outcome may appear very satisfactory, further examination showed that the regression line *underestimated* TLA at very small and high TLA values, while *overestimating* TLA at intermediate PLA values. Given the gradual increase in leaf overlap with plant size, a curved relationship appears to be a more appropriate model. Subsequent analysis with a second-order polynomial confirmed the high significance ($P<0.001$) of the quadratic term, resulting in a slightly improved r^2 (Table 2).

Although many users are satisfied with the aforementioned correlative approach and the high r^2 values (e.g. Nagel et al., 2012; Vadez et al., 2015; Banerjee et al., 2020), certain aspects warrant further inspection. For instance, the growth of young plants often follows an exponential pattern, characterized by smaller absolute size increases in small plants, and larger increases as plants grow bigger. As a consequence, in the experiment we are discussing with weekly harvests, the first half of the calibration curve is determined by 82% of the observations, while the remaining 18% contribute to the second half. To achieve a more balanced distribution, we could log-transform both PLA and TLA. In our experiment, this log-transformation resulted in the first half of the curve containing 32% of the data, with the remaining 68% in the second half (Figure 6B). Although the distribution is still not perfectly equal, it improved considerably compared to the non-transformed dataset. Performing a linear regression on the log-transformed data yielded a highly significant fit, with an r^2 of 0.986. However, it is important to acknowledge the biological phenomenon of overlapping leaves. Incorporating a quadratic term into the equation further improved the fit, resulting in an r^2 value of 0.989. Clearly, it pays to analyze which function is most appropriate, and whether log-transformation of the data and/or non-linear fits can provide a more robust basis for the calibration curve than a standard linear regression on non-transformed data.

3.11 How accurate is the calibration curve?

The coefficient of determination (r^2) is a convenient parameter to describe the goodness of fit of a statistical relationship between variables, and because it (generally) scales between 0 and 1, it allows easy comparisons across various experiments (Chicco et al., 2021). The calibration curves discussed in the previous section all exhibit relatively high r^2 values (Table 2), but does this r^2 truly represent the desired accuracy? Different expressions of plant size, such as leaf number, leaf area, and total biomass, are generally well correlated. How well the calibration curve works depends partly on the appropriateness of the chosen proxy trait. For instance: a top-view picture might provide more information for a rosette plant, while side views or views from different angles could be more informative for species with a single stem. Furthermore, it is important to note that r^2 provides information on the total variation in the y-variable that can be explained by the total variation in the x-variable. Hence, in monotonically increasing relationships like the one depicted in Figure 6, the larger the span in size in both x and y, the higher the r^2 will be. If we restrict the calculation to plants with a PLA >100 cm^2 instead of considering all data, the r^2 value decreases from 0.92 to 0.76. Consequently, a high r^2 for a calibration curve like the one shown in Figure 6, indicates that we are able to effectively distinguish between small and large plants. However, if a researcher's prime interest lies in understanding the variation in final size across genotypes, relying solely on the r^2 of the full calibration curve may provide a somewhat misleading sense of accuracy.

An alternative measure to assess the goodness of fit is the root mean square error (RMSE), which quantifies the average distance in the y-direction between the observed data points and the fitted line. It gives more weight to points that are further away from the line, compared to those that are closer (Hodson, 2022). The advantage of RMSE is that, all else being equal, it is not influenced by the total variation range in x and y, as is the case with r^2. Additionally, RMSE provides an absolute error in the units of the Y-axis. If the residuals follow a normal distribution, it informs the researcher that there is a 68% probability that the estimated total leaf area (TLA) deviates by less than the RMSE from the true TLA. However, RMSE may not be suitable for calibration curves that cover a wider range of plant sizes, as the error is not equal for plants of all sizes. For instance, an RMSE of 5 cm^2 may represent a minor deviation for a plant of 1000 cm^2, but a huge variation for a plant with a leaf area of 1 cm^2.

To assess the accuracy of the estimates, we calculated for each plant the absolute percentage error. This involved determining the absolute difference between the actual TLA, and the TLA value

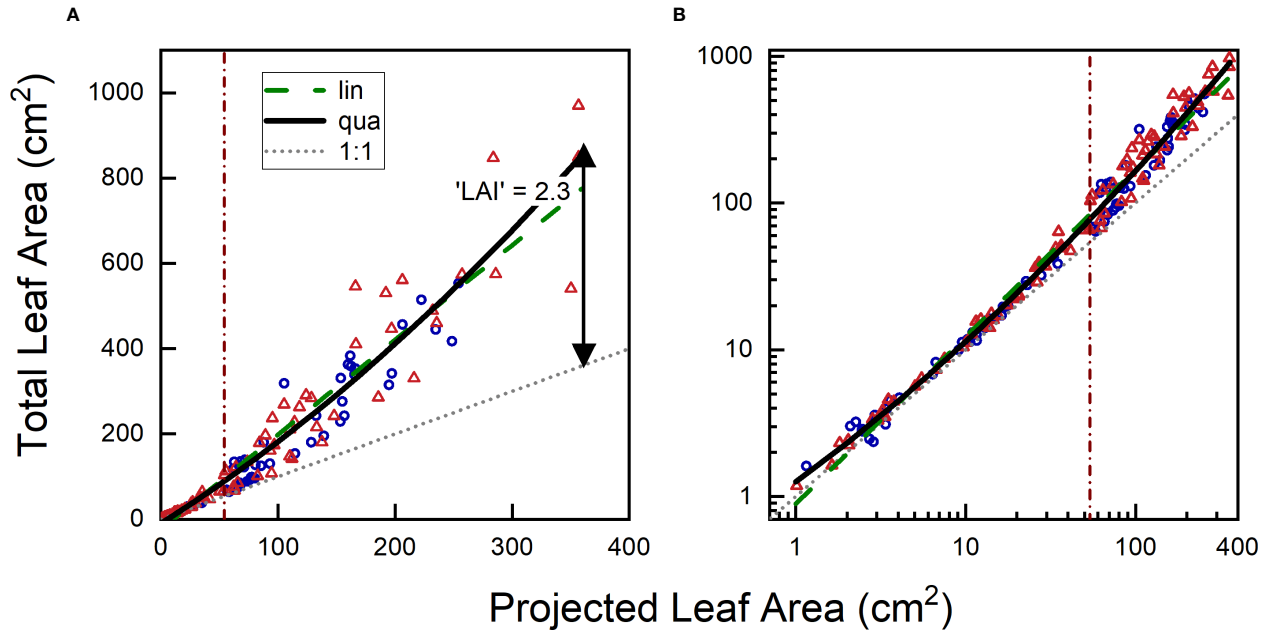

FIGURE 6
Relationship between projected leaf area and total leaf area of *Plantago major* plants harvested over an 8-week period and plotted on **(A)** linear or **(B)** logarithmic scales. Blue circles represent plants grown at low [CO_2] (350 μL L^{-1}), and orange triangles representplants grown at high [CO_2] (700 μL L^{-1}). The grey dotted line represents the 1:1 relationship between TLA (Total Leaf Area) and PLA (Projected Leaf Area), the green dashed line represents the linear fit through the data, and the black continuous line shows the quadratic fit. The vertical brown line indicates where the divide is between the 50% smaller and 50% larger plants, based on PLA.

estimated from the calibration curve, normalized to the actual TLA measured. These values ranged from nearly 0%, indicating a highly accurate estimate, to over 1000% in the specific case of very young plants where TLA was fitted with a straight line across all plant sizes (Figure 7A). In the last case, the actual TLA value was 1 cm^2, whereas the estimated TLA value was calculated to be -10 cm^2. This illustrates that even an r^2 value exceeding 0.90 does not necessarily guarantee accurate estimates for every individual plant. The median absolute percentage error (MdAPE) serves as a useful summary descriptor for non-normally distributed data. For the linear calibration curve, MdAPE was approximately 37% (Table 2; Figure 7A), indicating that the accuracy fell short of our expectations. However, when utilizing a quadratic fit with log-log transformed values, the MdAPE decreased to 11%, signifying a substantial improvement in accuracy. Additionally, in the quadratic fit, MdAPE values were lower for smaller compared to larger ones (Figure 7B), which is logical given the increased leaf overlap in larger plants.

The mean absolute percentage error (MAPE) is increasingly utilized in the field of high-throughput plant phenotyping (e.g. Paproki et al., 2012; Paulus, 2019; Rossi et al., 2022). However, given the log-normal distribution of these data, we advocate for the use of the median absolute percentage error (MdAPE) as a more informative measure of the general accuracy. By employing the MdAPE, we aim to capture a representative summary of the actual accuracy, rather than relying solely on the r^2 of a calibration curve.

TABLE 2 Characterization of different calibration curves for estimating total leaf area (TLA) from projected leaf area (PLA).

	lin	qua	Log(lin)	Log(qua)
P-value for a	***	ns	***	***
P-value for b	***	***	***	***
P-value for c	–	***	–	***
Adj. r^2	0.920	0.926	0.986	0.989
Df for the error term	162	161	162	161
RMSE (cm^2)	53.9	51.6	29.9 †	27.3 †
MdAPE (%)	38	25	17 †	12 †

Adj. r^2: adjusted r^2; df: degrees of freedom; RMSE: Root Mean Square Error; MdAPE: the Median values of the Absolute Percentage Error. Significance levels: ***, $P < 0.001$. Equations are of the form $y = a + bx$ for a linear polynomial (lin) or $y = a + bx + cx^2$ for a quadratic polynomial (qua). The last two columns are for x and y data that were log_{10}-transformed, with the fields marked by a † calculated after back-transformation to the original scale.

10.3389/fpls.2023.1233794

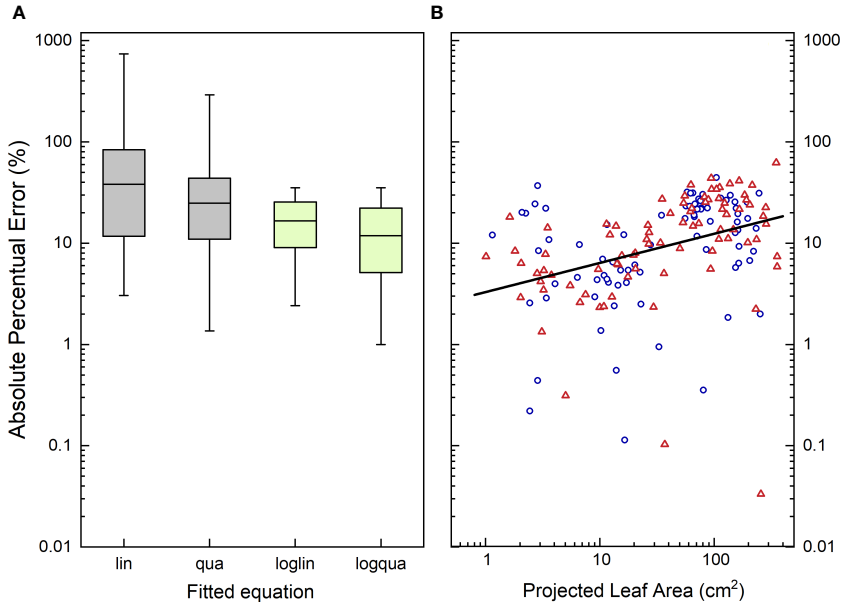

FIGURE 7
(A) Boxplot characterizing the distribution of the Absolute Percentage Error (APE) in the estimate of Total Leaf Area (TLA) from the measurements of Projected Leaf Area (PLA), using four different calibration curves. **(B)** Absolute Percentage Error in the estimate of Total Leaf Area using a log-quadratic calibration curve plotted against Projected Leaf Area. In **(A)**, boxplots indicate the 5th, 25th, 50th, 75th and 95th percentile of the APE values, taken over all plants and treatments. lin, linear regression; qua, quadratic regression; loglin, linear regression through the log_{10}-transormed value of TLA and PLA; logqua, quadratic regression through the log_{10}-transformed values. In **(B)**, blue circles represent plants grown at low [CO_2] (350 µL L^{-1}), and orange triangles represent high [CO_2]-grown plants (700 µL L^{-1}). The regression line passes through all points, and is significantly (P<0.001) different from zero, with an adjusted r^2 of 0.15.

3.12 How many calibration curves are required?

So far, we have considered a common calibration curve for both low and high CO_2 plants. For the relationship between projected leaf area (PLA) and total leaf area (TLA), this approach may seem reasonable as long as the treatment does not influence leaf angle or any other aspect of leaf display. However, what would happen if we aim to use PLA to estimate shoot biomass (Figure 8A)? The relationship between leaf dry mass and leaf area is known to shift, as plants exposed to elevated CO_2 almost invariably exhibit higher leaf mass per area (LMA; Poorter et al., 2022). Using quadratic polynomials on log-transformed PLA and shoot dry mass, we indeed found different curves (Figure 8B). They indicated that for a given PLA, elevated CO_2 plants were 20-30% heavier, although not for the smallest or largest plants. These findings align with the LMA data, which also showed LMA averages to be 20-30% heavier, except for the first and last harvest (cf. Figure 8B in Poorter et al., 1988). However, statistically, this did not show up as a significant effect, neither for CO_2 as a main factor nor for the interaction of CO_2 with the linear and quadratic components of PLA.

Having different calibration curves for different treatments, or maybe for different genotypes, can be quite inconvenient, as it requires more manual harvesting, partially nullifying the intended savings in human effort. What could we do about that? A well-cited method paper by Golzarian et al. (2011) discussed the phenotyping aspects of calibration curves, using the example of an experiment where plants were exposed to salinity or to control conditions. The study found that the two calibration curves were significantly different, with salt-stressed plants exhibiting higher biomass estimates for a given number of pixels compared to control plants. That would fit with the general understanding that salt stress increases leaf mass per area (LMA; Poorter et al., 2009; Kamanga et al., 2023). Golzarian et al. (2011), however, reasoned that salt-stressed plants were smaller, and considered them to be of 'younger' age. By adding the factor age to the equation, a single calibration function could be achieved for plants of both treatments. However, this approach mixes plant ontogeny with the direct effects of salinity, and is likely not broadly valid, especially when multiple treatments with varying salinity concentrations would be involved. Consequently, if the treatment of interest affects LMA, leaf angle, or other relevant morphological parameters, different calibration curves for different treatments may indeed be unavoidable.

Another important question to consider is the validity of a calibration curve that has been developed for a particular species, and whether it can be applied to other experiments involving the same species. In growth chambers, where light and temperature stay fixed to the same level, the transferability of a calibration curve seems more likely compared to glasshouses or field settings, where seasonal variation in light and temperature may strongly impact both LMA and stem thickness (and consequently stem mass per projected area). To use HTPP systems more effectively, calibration curves deserve more attention than they got so far. As is custom in many other laboratory methods, it might be good to regularly validate the measuring pipeline with a couple of reference samples that are measured using destructive methods.

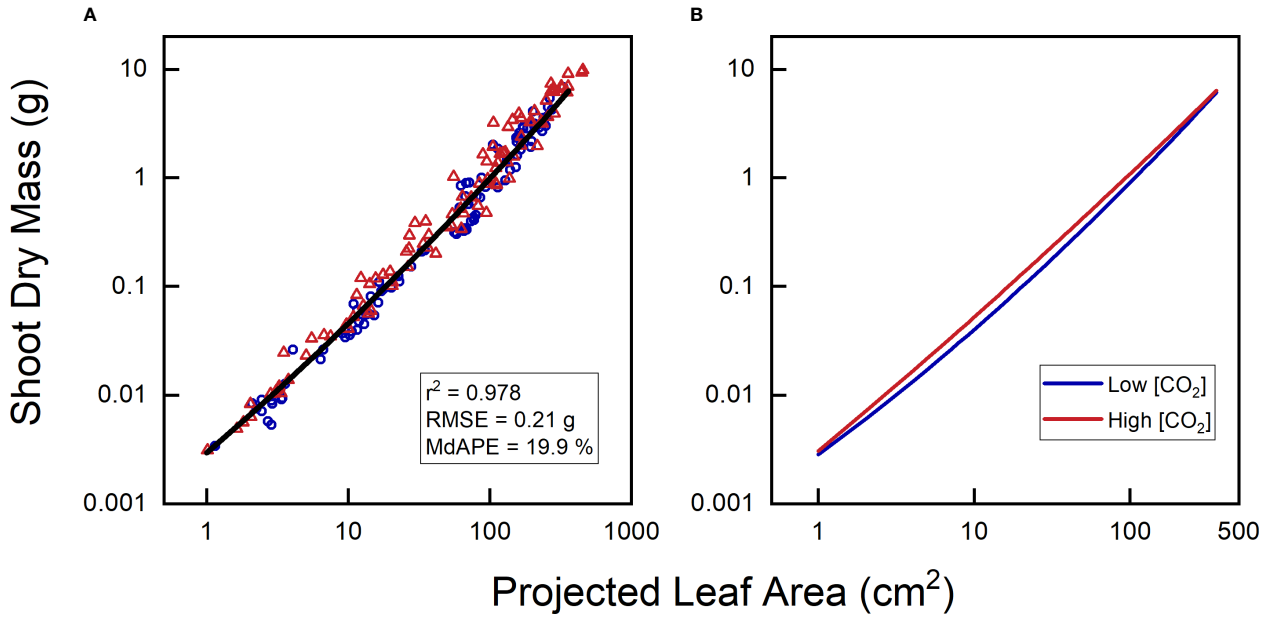

FIGURE 8
Relationship between projected leaf area and shoot dry mass of *Plantago major*, grown at low (CO_2] (350 µL L^{-1}) and high [CO_2] (700 µL L^{-1}). **(A)** Combined data for plants of both treatments; **(B)** calibration curves separately calculated for plants from each [CO_2]. All curves exhibited highly significant linear and quadratic components ($P < 0.001$) and $r^2 > 0.978$.

3.13 How many replicates per genotype or treatment?

Plants grown singly in pots may show quite some variability in plant mass or other traits, which can negatively impact the statistical power to detect differences between genotypes or treatments (Poorter and Garnier, 1996). When planning the size of an HTPP system, it is important to consider not only the number of species or genotypes to be tested, but also the number of replicates per genotype that will be required. Genome-wide association studies (GWAS) or Quantitative Trait Loci (QTL) experiments often benefit more from including additional genotypes rather than increasing the number of replicates per genotype (Zou et al., 2006). If treatments are compared across many genotypes, the large number of plants grown in HTPP systems will provide sufficient statistical power for general conclusions. However, when researchers are also interested in testing specific differences between individual genotypes, the number of replicates becomes more critical. This is particularly true when a calibration curve is used to estimate the values of the trait of interest. Calibration curves with low r^2 and high MdAPE introduce additional variability on top of the inherent variation that will already be present among plants. In the case of the CO_2 experiment, a t-test conducted at the final harvest revealed that the actual shoot dry mass for the two treatments was only marginally significant ($P = 0.10$). However, the difference was far further from significance when the shoot dry mass estimates based on PLA values were used ($P = 0.24$). In situations where HTPP system users are interested in specific contrasts, the utilization of calibration curves implies that they may need to include more replicates than in traditional experiments to achieve the same level of statistical power.

3.14 How often do you need to repeat an experiment?

Despite the robotized and computerized systems, HTPP experiments often push limits and compare large amounts of genotypes in a standardized manner. In as far as these experiments have a background in (eco)physiological approaches, with single plants growing in pots under controlled conditions, data from a single experiment is often considered sufficient for publication. However, in agriculture it is generally regarded as the gold standard to repeat an experiment in multiple years or locations, before any importance is attached to the results.

Possibly, HTPP in controlled conditions can be seen as the initial, important step in a two-phase approach. During this first step, a wide range of genotypes or species can be tested, either in their own right or in combination with specific treatment factors. Without being overly concerned about genotypic effects on calibration curves (as mentioned in point 12), this step can be used to identify the worst-performing and best-performing genotypes, simply based on green pixel counts or similar proxy traits ('forward phenomics' *sensu* Mir et al., 2019; cf. Merlot et al., 2002). The most extreme and interesting genotypes, for example those carrying contrasting alleles for important QTLs can then be further investigated in a targeted experiment. This subsequent phase would involve non-destructive phenotyping complemented by more labor-intensive physiological analyses such as gas exchange and chemical characterization on the one hand, and destructive harvesting of both shoot and root biomass on the other hand (Poudyal et al., 2018). Such a two-step approach would also be helpful in screening a wide range of germplasm for contrasting genotypes.

4 Conclusions and outlook

In this paper, we discussed a number of issues relevant to consider during the design and implementation phases of high-throughput plant phenotyping (HTPP) systems. A crucial aspect of an HTPP platform is its alignment with the specific research questions of interest and its careful design, both from the hardware and the workflow perspective. Different treatments applied to the shoot environment (such as light, CO_2, temperature) are often more complicated to implement, as this requires various growth environments all integrated into one HTPP system, or replicated HTPP systems, which is feasible but expensive. Treatments that can be applied to separate pots in the same location (such as drought, nutrients, salinity) are relatively easier to implement and amenable to computerized control. Additionally, efforts must be made to effectively address unforeseen problems and errors.

Regardless of the treatment approach, it is important to acknowledge that investment costs and maintenance requirements for most phenotyping systems are substantial. This is in part because the systems build now are often highly customized. If over time researchers will settle for more standardized systems and sensors, platform costs and time spend on complications will hopefully decrease.

Obtaining meaningful information from HTPP experiments requires to carefully consider the selection of meaningful proxy traits that enable us to answer the research questions at hand. Attention should also be paid to well-designed and regularly validated calibration curves, if necessary. An alternative strategy is to use HTPP systems as a good opportunity for prescreening. Such a prescreening would then be followed by an experiment focusing on a limited number of the most interesting genotypes. It allows to measure not only the proxy variables easily acquired by the phenotyping system ('soft' traits), but also the physiological 'hard-to-get' traits that provide valuable insights and a more comprehensive understanding of observed differences in plant performance.

Data availability statement

The original contributions presented in the study are included in the article/Supplementary Material. Further inquiries can be directed to the corresponding author.

Author contributions

HP and PvG initiated the idea, HP, OV and AWK collected data/images. HP wrote the ms. All authors contributed their experiences and viewpoints on phenotyping and commented on the ms. All authors contributed to the article and approved the submitted version.

Funding

This paper was partially funded by the Helmholtz Association of Germany and the European Union Grant agreement No. 101059784 (CROPINNO). Open access was partly funded by the Deutsche Forschungsgemeinschaft (DFG, German Research Foundation) – 491111487.

Acknowledgments

We thank Erik van Oosterom, Vijaya Singh and Nicolai Jablonowski for providing illustrative pictures for Box 1. Trevor Garnett and Ewaut Kissel commented on previous versions of this ms. We also appreciated the constructive comments of the reviewers. Open access was enabled by the DEAL project agreement. ChatGPT was used to check the language of the written text.

Conflict of interest

One of the authors (GMH) is co-founder of a company in high-throughput phenotyping and contributed valuable experience to this paper.

The remaining authors declare that the research was conducted in the absence of any commercial or financial relationships that could be construed as a potential conflict of interest.

Publisher's note

Supplementary material

The Supplementary Material for this article can be found online at: https://www.frontiersin.org/articles/10.3389/fpls.2023.1233794/full#supplementary-material

References

Alenyà, G., Dellen, B., Foix, S., and Torras, C. (2013). Robotized plant probing: Leaf segmentation utilizing time-of-flight data. *IEEE Robotics Autom. Magaz.* 20, 50–59. doi: 10.1109/MRA.2012.2230118

Al-Tamimi, N., Brien, C., Oakey, H., Berger, B., Saade, S., Ho, Y. S., et al. (2016). Salinity tolerance loci revealed in rice using high-throughput non-invasive phenotyping. *Nat. Commun.* 7, 13342. doi: 10.1038/ncomms13342

Anten, N. P., Casado-Garcia, R., and Nagashima, H. (2005). Effects of mechanical stress and plant density on mechanical characteristics, growth, and lifetime reproduction of tobacco plants. *Amer. Nat.* 166, 650–660. doi: 10.1086/497442

Bagley, S. A., Atkinson, J. A., Hunt, H., Wilson, M. H., Pridmore, T. P., and Wells, D. M. (2020). Low-cost automated vectors and modular environmental sensors for plant phenotyping. *Sensors* 20, 3319. doi: 10.3390/s20113319

Banerjee, B. P., Joshi, S., Thoday-Kennedy, E., Pasam, R. K., Tibbits, J., Hayden, M., et al. (2020). High-throughput phenotyping using digital and hyperspectral imaging-derived biomarkers for genotypic nitrogen response. *J. Exp. Bot.* 71, 4604–4615. doi: 10.1093/jxb/eraa143

Brien, C. J., Berger, B., Rabie, H., and Tester, M. (2013). Accounting for variation in designing greenhouse experiments with special reference to greenhouses containing plants on conveyor systems. *Plant Meth.* 9, 1–22. doi: 10.1186/1746-4811-9-5

Chiang, C., Bånkestad, D., and Hoch, G. (2020). Reaching natural growth: The significance of light and temperature fluctuations in plant performance in indoor growth facilities. *Plants* 9, 1312. doi: 10.3390/plants9101312

Chicco, D., Warrens, M. J., and Jurman, G. (2021). The coefficient of determination R-squared is more informative than SMAPE, MAE, MAPE, MSE and RMSE in regression analysis evaluation. *PeerJ. Comp. Sci.* 7, e623. doi: 10.7717/peerj-cs.623

Dalal, A., Shenhar, I., Bourstein, R., Mayo, A., Grunwald, Y., Averbuch, N., et al. (2020). A telemetric, gravimetric platform for real-time physiological phenotyping of plant–environment interactions. *J. Visual. Experim.* 162, e61280. doi: 10.3791/61280

Deery, D., Jimenez-Berni, J., Jones, H., Sirault, X., and Furbank, R. (2014). Proximal remote sensing buggies and potential applications for field-based phenotyping. *Agronomy* 4, 349–379. doi: 10.3390/agronomy4030349

Dobrescu, A., Giuffrida, M. V., and Tsaftaris, S. A. (2020). Doing more with less: a multitask deep learning approach in plant phenotyping. *Front. Plant Sci.* 11. doi: 10.3389/fpls.2020.00141

Dobrescu, A., Scorza, L. C., Tsaftaris, S. A., and McCormick, A. J. (2017). A "Do-It-Yourself" phenotyping system: measuring growth and morphology throughout the diel cycle in rosette shaped plants. *Plant Meth.* 13, 1–12. doi: 10.1186/s13007-017-0247-6

Dornbusch, T., Lorrain, S., Kuznetsov, D., Fortier, A., Liechti, R., Xenarios, I., et al. (2012). Measuring the diurnal pattern of leaf hyponasty and growth in Arabidopsis–a novel phenotyping approach using laser scanning. *Funct. Plant Biol.* 39, 860–869. doi: 10.1071/FP12018

Eberius, M., and Lima-Guerra, J. (2009). "High-throughput plant phenotyping–data acquisition, transformation, and analysis," in *Bioinformatics: tools and applications* eds Edwards, D., Stajich, J., and Hansen, D., (New York, NY: Springer), 259–278. doi: 10.1007/978-0-387-92738-1_13

Evans, G. C. (1972). The quantitative analysis of plant growth. Berkeley and Los Angeles: Univ. California Press.

Fiorani, F., and Schurr, U. (2013). Future scenarios for plant phenotyping. *Annu. Rev. Plant Biol.* 64, 267–291. doi: 10.1146/annurev-arplant-050312-120137

Foix, S., Alenyà, G., and Torras, C. (2018). Task-driven active sensing framework applied to leaf probing. *Comp. Electr. Agric.* 147, 166–175. doi: 10.1016/j.compag.2018.01.020

Furbank, R. T., and Tester, M. (2011). Phenomics–technologies to relieve the phenotyping bottleneck. *Trends Plant Sci.* 16, 635–644. doi: 10.1016/j.tplants.2011.09.005

Gibon, Y., Blaesing, O. E., Hannemann, J., Carillo, P., Hohne, M., Hendriks, J. H., et al. (2004). A robot-based platform to measure multiple enzyme activities in *Arabidopsis* using a set of cycling assays: comparison of changes of enzyme activities and transcript levels during diurnal cycles and in prolonged darkness. *Plant Cell* 16, 3304–3325. doi: 10.1105/tpc.104.025973

Gibson, G. (2018). Population genetics and GWAS: a primer. *PloS Biol.* 16, e2005485. doi: 10.1371/journal.pbio.2005485

Golbach, F., Kootstra, G., Damjanovic, S., Otten, G., and van de Zedde, R. (2016). Validation of plant part measurements using a 3D reconstruction method suitable for high-throughput seedling phenotyping. *Mach. Vision Appl.* 27, 663–680. doi: 10.1007/s00138-015-0727-5

Golzarian, M. R., Frick, R. A., Rajendran, K., Berger, B., Roy, S., Tester, M., et al. (2011). Accurate inference of shoot biomass from high-throughput images of cereal plants. *Plant Meth.* 7, 1–11. doi: 10.1186/1746-4811-7-2

Gomez, L. D., Whitehead, C., Barakate, A., Halpin, C., and McQueen-Mason, S. J. (2010). Automated saccharification assay for determination of digestibility in plant materials. *Biotechn. Biofuels* 3, 1–12. doi: 10.1186/1754-6834-3-23

Granier, C., Aguirrezabal, L., Chenu, K., Cookson, S. J., Dauzat, M., Hamard, P., et al. (2006). PHENOPSIS, an automated platform for reproducible phenotyping of plant responses to soil water deficit in *Arabidopsis thaliana* permitted the identification of an accession with low sensitivity to soil water deficit. *New Phytol.* 169, 623–635. doi: 10.1111/j.1469-8137.2005.01609.x

Hall, R. D., D'Auria, J. C., Ferreira, A. C. S., Gibon, Y., Kruszka, D., Mishra, P., et al. (2022). High-throughput plant phenotyping: a role for metabolomics? *Trends Plant Sci.* 27, 549–563. doi: 10.1016/j.tplants.2022.02.001

Hodson, T. O. (2022). Root-mean-square error (RMSE) or mean absolute error (MAE): when to use them or not. *Geosci. Model. Dev.* 15, 5481–5487. doi: 10.5194/gmd-15-5481-2022

Jahnke, S., Roussel, J., Hombach, T., Kochs, J., Fischbach, A., Huber, G., et al. (2016). Pheno seeder-a robot system for automated handling and phenotyping of individual seeds. *Plant Physiol.* 172, 1358–1370. doi: 10.1104/pp.16.01122

Janni, M., Coppede, N., Bettelli, M., Briglia, N., Petrozza, A., Summerer, S., et al. (2019). *In vivo* phenotyping for the early detection of drought stress in tomato. *Plant Phenom.* 2019, 6168209. doi: 10.34133/2019/6168209

Jansen, M., Gilmer, F., Biskup, B., Nagel, K. A., Rascher, U., Fischbach, A., et al. (2009). Simultaneous phenotyping of leaf growth and chlorophyll fluorescence via GROWSCREEN FLUORO allows detection of stress tolerance in Arabidopsis thaliana and other rosette plants. *Funct. Plant Biol.* 36, 902–914. doi: 10.1071/FP09095

Jin, S., Su, Y., Gao, S., Wu, F., Ma, Q., Xu, K., et al. (2019). Separating the structural components of maize for field phenotyping using terrestrial LiDAR data and deep convolutional neural networks. *IEEE T. Geosci. Remote Sens.* 58, 2644–2658. doi: 10.1109/TGRS.2019.2953092

Junker, A., Muraya, M. M., Weigelt-Fischer, K., Arana-Ceballos, F., Klukas, C., Melchinger, A. E., et al. (2015). Optimizing experimental procedures for quantitative evaluation of crop plant performance in high throughput phenotyping systems. *Front. Plant Sci.* 5. doi: 10.3389/fpls.2014.00770

Kalaji, H. M., Schansker, G., Ladle, R. J., Goltsev, V., Bosa, K., Allakhverdiev, S. I., et al. (2014). Frequently asked questions about in *vivo* chlorophyll fluorescence: practical issues. *Photosynth. Res.* 122, 121–158. doi: 10.1007/s11120-014-0024-6

Kamanga, R. M., Kopa, F., Kamala, F. D., Sefasi, A., and Ndakidemi, P. A. (2023). Screening and evaluation of salinity stress tolerance in local Malawian tomato cultivars. *Plant Physiol. Rep.* 28, 259–271. doi: 10.1007/s40502-023-00718-8

Kjaer, K. H., and Ottosen, C. O. (2015). 3D laser triangulation for plant phenotyping in challenging environments. *Sensors* 15, 13533–13547. doi: 10.3390/s150613533

Krajewski, P., Chen, D., Ćwiek, H., van Dijk, A. D., Fiorani, F., Kersey, P., et al. (2015). Towards recommendations for metadata and data handling in plant phenotyping. *J. Exp. Bot.* 66, 5417–5427. doi: 10.1093/jxb/erv271

Lambers, J. T., and Oliveira, R. S. (2019). *Plant physiological ecology* (Cham: Springer).

Liu, H., Bruning, B., Garnett, T., and Berger, B. (2020). The performances of hyperspectral sensors for proximal sensing of nitrogen levels in wheat. *Sensors* 20, 4550. doi: 10.3390/s20164550

Lorence, A., and Jimenez, K. M. (2022). *High-throughput plant phenotyping: methods and protocols (Methods in molecular biology vol. 2539)* (New York: Humana Press), ISBN: .

Mahlein, A. K., Kuska, M. T., Thomas, S., Wahabzada, M., Behmann, J., Rascher, U., et al. (2019). Quantitative and qualitative phenotyping of disease resistance of crops by hyperspectral sensors: seamless interlocking of phytopathology, sensors, and machine learning is needed! *Curr. Opin. Plant Biol.* 50, 156–162. doi: 10.1016/j.pbi.2019.06.007

Merlot, S., Mustilli, A. C., Genty, B., North, H., Lefebvre, V., Sotta, B., et al. (2002). Use of infrared thermal imaging to isolate Arabidopsis mutants defective in stomatal regulation. *Plant J.* 30, 601–609. doi: 10.1046/j.1365-313X.2002.01322.x

Mir, R. R., Reynolds, M., Pinto, F., Khan, M. A., and Bhat, M. A. (2019). High-throughput phenotyping for crop improvement in the genomics era. *Plant Sci.* 282, 60–72. doi: 10.1016/j.plantsci.2019.01.007

Nabel, M., Schrey, S. D., Poorter, H., Koller, R., Nagel, K. A., Temperton, V. M., et al. (2018). Coming late for dinner: Localized digestate depot fertilization for extensive cultivation of marginal soil with *Sida hermaphrodita*. *Front. Plant Sci.* 9. doi: 10.3389/fpls.2018.01095

Nagel, K. A., Lenz, H., Kastenholz, B., Gilmer, F., Averesch, A., Putz, A., et al. (2020). The platform *GrowScreen-Agar* enables identification of phenotypic diversity in root and shoot growth traits of agar grown plants. *Plant Meth.* 16, 89. doi: 10.1186/s13007-020-00631-3

Nagel, K. A., Putz, A., Gilmer, F., Heinz, K., Fischbach, A., Pfeifer, J., et al. (2012). GROWSCREEN-Rhizo is a novel phenotyping robot enabling simultaneous measurements of root and shoot growth for plants grown in soil-filled rhizotrons. *Funct. Plant Biol.* 39, 891–904. doi: 10.1071/FP12023

Papoutsoglou, E. A., Faria, D., Arend, D., Arnaud, E., Athanasiadis, I. N., Chaves, I., et al. (2020). Enabling reusability of plant phenomic datasets with MIAPPE 1.1. *New Phytol.* 227, 260–273. doi: 10.1111/nph.16544

Paproki, A., Sirault, X., Berry, S., Furbank, R., and Fripp, J. (2012). A novel mesh processing-based technique for 3D plant analysis. *BMC Plant Biol.* 12, 1–13. doi: 10.1186/1471-2229-12-63

Passioura, J. B. (2002). Soil conditions and plant growth. *Plant Cell Environ.* 25, 311–318. doi: 10.1046/j.0016-8025.2001.00802.x

Paulus, S. (2019). Measuring crops in 3D: using geometry for plant phenotyping. *Plant Meth.* 15, 1–13. doi: 10.1186/s13007-019-0490-0

Pommier, C., Michotey, C., Cornut, G., Roumet, P., Duchêne, E., Flores, R., et al. (2019). Applying FAIR principles to plant phenotypic data management in GnpIS. *Plant Phenom.* 2019, 1671403. doi: 10.34133/2019/1671403

Poorter, H., Bühler, J., van Dusschoten, D., Climent, J., and Postma, J. A. (2012). Pot size matters: a meta-analysis of the effects of rooting volume on plant growth. *Funct. Plant Biol.* 39, 839–850. doi: 10.1071/FP12049

Poorter, H., Fiorani, F., Pieruschka, R., Wojciechowski, T., van der Putten, W. H., Kleyer, M., et al. (2016). Pampered inside, pestered outside? Differences and similarities between plants growing in controlled conditions and in the field. *New Phytol.* 212, 838–855. doi: 10.1111/nph.14243

Poorter, H., and Garnier, E. (1996). Plant growth analysis: an evaluation of experimental design and computational methods. *J. Exp. Bot.* 47, 1343–1351. doi: 10.1093/jxb/47.12.1969

Poorter, H., Knopf, O., Wright, I. J., Temme, A. A., Hogewoning, S. W., Graf, A., et al. (2022). A meta-analysis of responses of C3 plants to atmospheric CO2: dose–response curves for 85 traits ranging from the molecular to the whole-plant level. *New Phytol.* 233, 1560–1596. doi: 10.1111/nph.17802

Poorter, H., Niinemets, Ü., Ntagkas, N., Siebenkäs, A., Mäenpää, M., Matsubara, S., et al. (2019). A meta-analysis of plant responses to light intensity for 70 traits ranging from molecules to whole plant performance. *New Phytol.* 223, 1073–1105. doi: 10.1111/nph.15754

Poorter, H., Niinemets, Ü., Poorter, L., Wright, I. J., and Villar, R. (2009). Causes and consequences of variation in leaf mass per area (LMA): a meta-analysis. *New Phytol.* 182, 565–588. doi: 10.1111/j.1469-8137.2009.02830.x

Poorter, H., Pot, S., and Lambers, H. (1988). The effect of an elevated atmospheric CO_2 concentration on growth, photosynthesis and respiration of *Plantago major*. *Physiol. Plant* 73, 553–559. doi: 10.1111/j.1399-3054.1988.tb05440.x

Poudyal, D., Rosenqvist, E., and Ottosen, C. O. (2018). Phenotyping from lab to field–tomato lines screened for heat stress using Fv/Fm maintain high fruit yield during thermal stress in the field. *Funct. Plant Biol.* 46, 44–55. doi: 10.1071/FP17317

R Core Team (2022). *R: A language and environment for statistical computing* (Vienna, Austria: R Foundation for Statistical Computing). Available at: https://www.R-project.org/.

Reynolds, D., Baret, F., Welcker, C., Bostrom, A., Ball, J., Cellini, F., et al. (2019). What is cost-efficient phenotyping? Optimizing costs for different scenarios. *Plant Sci.* 282, 14–22. doi: 10.1016/j.plantsci.2018.06.015

Rosa, L. M., and Forseth, I. N. (1996). Diurnal patterns of soybean leaf inclination angles and azimuthal orientation under different levels of ultraviolet-B radiation. *Agric. For. Meteor.* 78, 107–119. doi: 10.1016/0168-1923(95)02249-X

Rossi, R., Costafreda-Aumedes, S., Leolini, L., Leolini, C., Bindi, M., and Moriondo, M. (2022). Implementation of an algorithm for automated phenotyping through plant 3D-modeling: A practical application on the early detection of water stress. *Comput. Electron. Agric.* 197, 106937. doi: 10.1016/j.compag.2022.106937

Roth, L., Barendregt, C., Bétrix, C. A., Hund, A., and Walter, A. (2022). High-throughput field phenotyping of soybean: Spotting an ideotype. *Remote Sens. Environ.* 269, 112797. doi: 10.1016/j.rse.2021.112797

Shi, W., van de Zedde, R., Jiang, H., and Kootstra, G. (2019). Plant-part segmentation using deep learning and multi-view vision. *Biosyst. Eng.* 187, 81–95. doi: 10.1016/j.biosystemseng.2019.08.014

Singh, V., van Oosterom, E. J., Jordan, D. R., Messina, C. D., Cooper, M., and Hammer, G. L. (2010). Morphological and architectural development of root systems in sorghum and maize. *Plant Soil* 333, 287–299. doi: 10.1007/s11104-010-0343-0

Tardieu, F., Cabrera-Bosquet, L., Pridmore, T., and Bennett, M. (2017). Plant phenomics, from sensors to knowledge. *Curr. Biol.* 27, R770–R783. doi: 10.1016/j.cub.2017.05.055

Thompson, A., Kantar, M., and Rainey, K. (2022). "Designing experiments for physiological phenomics," in *High-throughput plant phenotyping: methods and protocols* (New York, NY: Springer US), 159–170.

Vadez, V., Kholová, J., Hummel, G., Zhokhavets, U., Gupta, S. K., and Hash, C. T. (2015). LeasyScan: a novel concept combining 3D imaging and lysimetry for high-throughput phenotyping of traits controlling plant water budget. *J. Exp. Bot.* 66, 5581–5593. doi: 10.1093/jxb/erv251

Vargas, J. Q., Bendig, J., Mac Arthur, A., Burkart, A., Julitta, T., Maseyk, K., et al. (2020). Unmanned aerial systems (UAS)-based methods for solar induced chlorophyll fluorescence (SIF) retrieval with non-imaging spectrometers: state of the art. *Remote Sens.* 12, 1624. doi: 10.3390/rs12101624

Walter, A., Liebisch, F., and Hund, A. (2015). Plant phenotyping: from bean weighing to image analysis. *Plant Meth.* 11, 1–11. doi: 10.1186/s13007-015-0056-8

Walter, A., Scharr, H., Gilmer, F., Zierer, R., Nagel, K. A., Ernst, M., et al. (2007). Dynamics of seedling growth acclimation towards altered light conditions can be quantified via GROWSCREEN: a setup and procedure designed for rapid optical phenotyping of different plant species. *New Phytol.* 174, 447–455. doi: 10.1111/j.1469-8137.2007.02002.x

White, J. W., and Conley, M. M. (2013). A flexible, low-cost cart for proximal sensing. *Crop Sci.* 53, 1646–1649. doi: 10.2135/cropsci2013.01.0054

Wiese, A., Christ, M. M., Virnich, O., Schurr, U., and Walter, A. (2007). Spatio-temporal leaf growth patterns of Arabidopsis thaliana and evidence for sugar control of the diel leaf growth cycle. *New Phytol.* 174, 752–761. doi: 10.1111/j.1469-8137.2007.02053.x

Wilkinson, M. D., Dumontier, M., Aalbersberg, I. J., Appleton, G., Axton, M., Baak, A., et al. (2016). The FAIR Guiding Principles for scientific data management and stewardship. *Sci. Data* 3, 1–9. doi: 10.1038/sdata.2016.18

Xiao, Q., Bai, X., Zhang, C., and He, Y. (2022). Advanced high-throughput plant phenotyping techniques for genome-wide association studies: A review. *J. Adv. Res.* 35, 215–230. doi: 10.1016/j.jare.2021.05.002

Xu, L., Cruz, J. A., Savage, L. J., Kramer, D. M., and Chen, J. (2015). Plant photosynthesis phenomics data quality control. *Bioinformatics* 31, 1796–1804. doi: 10.1093/bioinformatics/btu854

Yang, W., Guo, Z., Huang, C., Duan, L., Chen, G., Jiang, N., et al. (2014). Combining high-throughput phenotyping and genome-wide association studies to reveal natural genetic variation in rice. *Nat. Commun.* 5, 5087. doi: 10.1038/ncomms6087

Ye, X., Abe, S., and Zhang, S. (2020). Estimation and mapping of nitrogen content in apple trees at leaf and canopy levels using hyperspectral imaging. *Precis. Agric.* 21, 198–225. doi: 10.1007/s11119-019-09661-x

Zavafer, A., Bates, H., Mancilla, C., and Ralph, P. J. (2023). Phenomics: conceptualization and importance for plant physiology. *Trends Plant Sci.* 28, 1004-1013. doi: 10.1016/j.tplants.2023.03.023

Zou, F., Xu, Z., and Vision, T. (2006). Assessing the significance of quantitative trait loci in replicable mapping populations. *Genetics* 174, 1063–1068. doi: 10.1534/genetics.106.059469

frontiers | Frontiers in Plant Science

TYPE Original Research
PUBLISHED 01 September 2023
DOI 10.3389/fpls.2023.1233553

OPEN ACCESS

EDITED BY
Elias Kaiser,
Wageningen University and Research, Netherlands

REVIEWED BY
Hannah Schneider,
Wageningen University and Research, Netherlands
Hafiz Muhammad Ahmad,
Government College University, Pakistan

*CORRESPONDENCE
Thomas Altmann
altmann@ipk-gatersleben.de
Rongli Shi
shi@ipk-gatersleben.de

†PRESENT ADDRESS
Astrid Junker,
Phenomics Department, Syngenta Seeds GmbH, Bad Salzuflen, Germany

RECEIVED 02 June 2023
ACCEPTED 07 August 2023
PUBLISHED 01 September 2023

CITATION
Shi R, Seiler C, Knoch D, Junker A and Altmann T (2023) Integrated phenotyping of root and shoot growth dynamics in maize reveals specific interaction patterns in inbreds and hybrids and in response to drought.
Front. Plant Sci. 14:1233553.
doi: 10.3389/fpls.2023.1233553

Integrated phenotyping of root and shoot growth dynamics in maize reveals specific interaction patterns in inbreds and hybrids and in response to drought

Rongli Shi[1*], Christiane Seiler[2], Dominic Knoch[1], Astrid Junker[1†] and Thomas Altmann[1*]

[1]Department of Molecular Genetics, Leibniz Institute of Plant Genetics and Crop Plant Research (IPK), Seeland, Germany, [2]Federal Research Centre for Cultivated Plants, Institute for Resistance Research and Stress Tolerance, Julius Kühn Institute (JKI), Quedlinburg, Germany

In recent years, various automated methods for plant phenotyping addressing roots or shoots have been developed and corresponding platforms have been established to meet the diverse requirements of plant research and breeding. However, most platforms are only either able to phenotype shoots or roots of plants but not both simultaneously. This substantially limits the opportunities offered by a joint assessment of the growth and development dynamics of both organ systems, which are highly interdependent. In order to overcome these limitations, a root phenotyping installation was integrated into an existing automated non-invasive high-throughput shoot phenotyping platform. Thus, the amended platform is now capable of conducting high-throughput phenotyping at the whole-plant level, and it was used to assess the vegetative root and shoot growth dynamics of five maize inbred lines and four hybrids thereof, as well as the responses of five inbred lines to progressive drought stress. The results showed that hybrid vigour (heterosis) occurred simultaneously in roots and shoots and was detectable as early as 4 days after transplanting (4 DAT; i.e., 8 days after seed imbibition) for estimated plant height (EPH), total root length (TRL), and total root volume (TRV). On the other hand, growth dynamics responses to progressive drought were different in roots and shoots. While TRV was significantly reduced 10 days after the onset of the water deficit treatment, the estimated shoot biovolume was significantly reduced about 6 days later, and EPH showed a significant decrease even 2 days later (8 days later than TRV) compared with the control treatment. In contrast to TRV, TRL initially increased in the water deficit period and decreased much later (not earlier than 16 days after the start of the water deficit treatment) compared with the well-watered plants. This may indicate an initial response of the plants to water deficit by forming longer but thinner roots before growth was inhibited by the overall water deficit. The magnitude and the dynamics of the responses were genotype-dependent, as well as under the influence of the water consumption, which was related to plant size.

KEYWORDS

maize, whole-plant phenotyping, root imaging, dynamic growth, hybrid, inbred, drought stress

Introduction

Plant phenotyping is essential for genetic mapping approaches as well as selecting elite lines from diverse germplasms in breeding. About half of the improvements in grain yield observed over the past seventy years have been attributed to improvements in cultivar genetics (Hauck et al., 2014). In maize, hybrids contribute greatly to increased yield and play an important role in breeding (Duvick, 2005; Li C. et al., 2022). With rapid technological advancements, modern plant phenotyping has been widely applied in plant research during recent decades (Costa et al., 2019). It is mainly performed using non-invasive methods to measure complex plant traits, such as growth and physiology dynamics over time (Walter et al., 2015; Costa et al., 2019). Plant phenotyping is considered a key tool for understanding plant growth and development and plant–environment interactions across different scales of resolution, from the cellular to the whole plant or plant stand level (Janni and Pieruschka, 2022). It supports fundamental plant research towards the elucidation of biological processes and mechanisms leading from genetic variation and interaction with the environment to the expression of important traits (Langstroff et al., 2022). Furthermore, it can speed up the characterization and improvement of agronomic traits enabling more sustainable agriculture as well as the development of new industrial products, such as biostimulants (De Diego and Spíchal, 2022).

Initially, most phenotypic analyses have focused on the aboveground parts of plants. Many desirable agronomic traits, hybrid performance-related traits, or stress adaption-related traits were assessed via imaging-based high-throughput shoot phenotyping (Junker et al., 2015; Neumann et al., 2015; Knoch et al., 2020). Adaptation to stress mainly involves morphological and physiological changes. These changes are controlled by molecular mechanisms that regulate the expressions of genes. Plant phenotyping helps identify genomic regions associated with trait and ultimately causal genes and genetic variants (Janni et al., 2019). For example, Wu et al. (2021) identified 1,529 QTL and 2,318 candidate genes related to drought responses by using a high-throughput system to study 368 maize genotypes, and further validated the functions of two candidate genes.

In recent years, the importance of roots has been increasingly appreciated by researchers. Roots display strong plasticity and are able to respond dynamically to local gradients of moisture and nutrients and shape their architecture to explore the heterogeneous soil according to the plant's needs (López-Bucio et al., 2003; Hauck et al., 2015). Roots show plastic developmental responses to differences in nitrogen or other nutrients (Giehl et al., 2014; Jia et al., 2019) or water availability (Orman-Ligeza et al., 2018; Orosa-Puente et al., 2018; von Wangenheim et al., 2020) or to soil compaction (Pandey et al., 2021). The alteration of the root system architecture (RSA) by the *DEEPER ROOTING 1* (*DRO1*) gene, which was identified within a quantitative trait locus controlling root growth angle, improves drought avoidance in rice (Uga et al., 2013). Moreover, heterosis, the enhanced performance of hybrids compared to their inbred parents, is also manifested in roots (Hoecker et al., 2006) and Hauck et al. (2015) detected high variation and heterosis in traits of RSA and root complexity (the degree of branching) among 12 parental maize inbred lines and 66 F1 hybrids thereof using the excavated roots of field grown plants and a high-throughput imaging device. In order to support the assessment of root traits and thus to accelerate genetic analyses and investigations of mechanisms controlling root growth and development, as well as programs addressing the improvement of root traits important for plant performance, various root phenotyping facilities have been established. These include systems with artificial growth substrates such as agar or other media and platforms to monitor roots growing in soil (Iyer-Pascuzzi et al., 2010; Downie et al., 2012; Gioia et al., 2017; Shi et al., 2018), which offer different degrees of accessibility of the root in terms of visualizing the entire root system and in terms of the size to which the root system can grow.

At the whole plant level, the close interaction between the shoot and the root and their strong interdependence should be considered. When studying maize inbred lines released in different years, Ren and colleagues (2022) found that newly released inbred lines had steeper root angles. The results suggest that root traits were indirectly selected during modern breeding as breeders aimed at improving aboveground agronomic traits. By selecting shoot and root traits simultaneously and directly, it is possible to achieve genetic gain for the whole plant more quickly than selecting shoot or root traits alone (Tracy et al., 2020). However, to date, phenotyping studies have mostly focused on only the shoot or root system; there are quite limited platforms able to phenotype at the whole plant level (Nagel et al., 2012; Jeudy et al., 2016). With the GROWSCREEN-Rhizo, Nagel et al. (2012) presented a phenotyping system capable of automatic and simultaneous imaging of roots and shoots using soil-filled rhizotrons. However, the work focused mainly on characterizing root systems, and very few shoot phenotypic traits, such as the leaf area, were quantified. Shoot architecture-related traits or colour-related traits were not included. On the other hand, the relationship between shoot and root traits shows different patterns under various environmental conditions. Some researchers pointed out that altering the relationship among root and shoot traits is part of the strategies of plants to cope with drought (Lozano et al., 2020). Therefore, whole plant phenotyping covering both roots and shoots is required to gain a better understanding of the fundamental biological processes governing plant growth and development and ultimately plant performance.

The Leibniz Institute of Plant Genetics and Crop Plant Research (IPK), Gatersleben, operates and uses several automatic non-invasive high-throughput phenotyping platforms for different plant sizes in controlled-environment growth facilities, including a system suitable for large plants [described in Junker et al. (2015)]. The system facilitated the analysis of shoot phenotypes of diverse plant species such as maize (Muraya et al., 2017; Dodig et al., 2021) and rapeseed (Knoch et al., 2020). Increasing recognition of the importance of root system adaptation prompted us to extend our established shoot phenotyping platform for large plants with root phenotyping units based on a previously validated concept (Shi et al., 2018). In the following, we present two case studies illustrating the applicability of the platform: the vegetative root and shoot growth dynamics of 1) five maize inbred lines and four

hybrids and 2) the assessment of the responses of five inbred lines to progressive drought stress. The upgraded phenotyping system will facilitate future research on different environmental cues and in different plant species by simultaneously analysing the dynamics of root and shoot growth.

Materials and methods

Plant materials and growth conditions

Four maize (Zea mays L.) hybrids: B73xUH007, N22xUH007, P148xUH007, and PHT77xUH007 and their parental inbred lines B73, N22, P148, PHT77, and UH007 were used for the first case study. Four of these inbred lines, B73, N22, P148, and PHT77, and one additional inbred line, S052, were used for the second case study. Each line had nine replicates (individual pots/plants). All the lines are part of the EPPN/EPPN2020 reference maize panel and were selected for the present study according to results of a previous investigation on the genetics of shoot growth (Muraya et al., 2017). The lines B73, N22, and PHT77 were initially provided by Alain Charcosset and Cyril Bauland, INRA(E) Mulon, France (see Rincent et al., 2014) and lines S052, P148, and UH007 were made available by Albrecht Melchinger, University of Hohenheim, Germany, and were propagated at IPK Gatersleben. Seeds of the hybrids B73xUH007, N22xUH007, P148xUH007, and PHT77xUH007 were supplied by Claude Welcker, INRA(E), LEPSE, Montpellier, France.

Seeds were germinated on wet filter paper and, after 4 days, seedlings were transplanted into the custom-made 'rhizo-pots', one plant per pot. The special rhizo-pot was designed based on the root phenotyping concept, which was validated in our previous work (Shi et al., 2018) and the prototype was pre-tested in the system. The bottom and three sides of the box are made of black PVC in order to prevent the roots from being exposed to light. The front side is tilted 30 degrees allowing the roots to be visualized effectively. A NIR filter which allows the spectrum above 750 nm to pass through is inserted at this side. The plants were transplanted close to the NIR filter, and the root images were taken only from this side. The size of the box is 35 x 25 x 40 cm (LxBxH; Figure 1). The boxes were filled with about 7 kg of black peat soil (Graberde, Plantaflor, Germany). The top surface of the boxes were covered with a black mesh to improve image quality and reduce water evaporation. All the rhizo-pots were placed in carriers and entered the conveyor belt-based automated plant phenotyping system. The system is located at the IPK in a climatized greenhouse and plants were grown under controlled long-day conditions with 25/20 °C and 16/8 h day/night, as descripted by Junker et al. (2015).

All the hybrids and inbred lines used for the first case study were grown only under well-watered conditions (60% field capacity (FC)). The FC was determined on a gravimetric basis as described by Junker et al. (2015). Briefly, soil water content corresponding to 100% field capacity was determined by weighing soil-filled pots (0.3L) after watering to full saturation (100% FC) and weighing them after drying the soil completely (20 days at 70 °C). The weight corresponding to 60% or 35% field capacity was then calculated accordingly. For the second case study, the five inbred lines were grown under well-watered (WW) and drought (D) conditions within the same experiment. The plants of the well-watered inbred lines B73, PHT77, P148, and N22 were the same in both studies. Water supply was maintained by automated weighing and watering towards target weight and was stopped at 13 days after transplanting (DAT) to induce drought stress and was kept to 35% FC. Five soil moisture sensors (Decagon 5TE, UMS, Germany) were inserted in the soil at a depth of 10 cm for each genotype under different treatment to record the water content in the pot. All plants were fertilized with Hakaphos Blau (Compo Expert, Germany) 150 ml/pot at 11 DAT. The hybrids and WW plants were fertilized two times more at 21 DAT and 27 DAT.

In order to further evaluate the newly integrated root phenotyping system, additional plants of two inbred lines B73 and N22 (each with seven replicates) were cultivated simultaneously with the plants of the two case studies and sampled at 19 DAT. These two lines have contrasting root biomass as shown in our previous work (Shi et al., 2018): B73 has a relatively large root biomass while N22 has a small root biomass. At the end of the experiment, roots of B73 and N22 were dug out, washed, and placed in a 28 x 40 cm transparent tray filled with distilled water. The roots were scanned at 400 dpi on an Epson Expression 10000 XL scanner (Seiko Epson).

The V stage (the number of visible leaf collars) and leaf number were counted manually after 13 DAT on a weekly basis. At 40 DAT, shoots were cut from the base and the fresh and dry weight (oven-dry at 70˚C for one week) were determined.

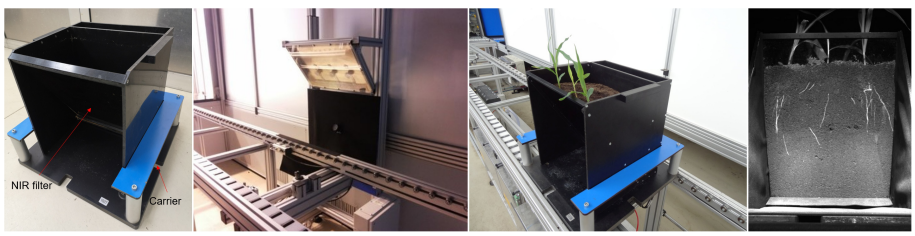

FIGURE 1
Custom-made 'rhizo-pot' for simultaneous root and shoot imaging. NIR filter: long pass near infrared filter plate allows only light above 750nm to pass through. The root images are taken by a NIR-sensitive camera directed at right angles to the NIR filter plate upon illumination with NIR (850 nm) emitting diodes.

Imaging acquisition and analysis

After transplanting, visible light (RGB) and static fluorescence (FLUOR) top view and side view images of shoots, as well as near infra-red (NIR) images of roots, were taken on a daily basis from 4 to 40 DAT (4 to 39 DAT for roots). Due to technical failures, time points were missing at 9 (only for root), 30, and 35 to 39 DAT. Root images were taken by a CMO Mono sensor with 12 Mp resolution (UI-5200SE-M-GL Rev.4, iDS, Germany) which was integrated into the system. During imaging, an LED (LZ4-00R408 peak: 850 nm, range 835-875 nm) panel was used for NIR illumination.

To extract image-based shoot traits, the Integrated Analysis Platform (IAP) software (version 2.0; Klukas et al., 2014) was used with a customized analysis pipeline. From the very elaborate output of the image analysis with 445 phenotypic traits, the shoot traits 'estimated shoot biovolume (px^3)' (ESV; biomass-related), 'projected leaf area (px^2)' (PLA; biomass-related), 'estimated plant height (px)' (EPH; architecture-related), and the 'brown to green ratio' (colour-related) were selected and presented. They are based on visible light and from a combined view, top view, side view, and side view, respectively.

The scanned roots from B73 and N22 were analysed by WinRhizo Pro ver. 2013c (Regent Instruments). Root images derived from the phenotyping facility were pre-processed and analysed by the semi-automated Root Image Analysis (saRIA) software (Narisetti et al., 2019). It supports efficient image segmentation on soil-root images, while user input for selecting the best combination of algorithmic parameters is required. Noisy regions could be manually removed as well (Narisetti et al., 2019). The root traits 'total root length (px)' (TRL), 'total root surface area (px^2)' (TRSA), 'total root volume (px^3)' (TRV), and 'average root diameter (px)' (RD) were used for further analysis. The NIR root images from B73 and N22 at 19 DAT, which were used for validation, were additionally analysed by the SmartRoot software (Lobet et al., 2011). The root trait values extracted from images acquired after 29 DAT were not considered for statistical analysis as they were regarded as unreliable due to the increasing density of the root system and the progressive merging and overlapping of roots. Nevertheless, values derived from images taken at two time points, 34 and 39 DAT, were included in the figures, but only for illustrative purposes (shaded grey in the figures).

For the first case study, mid-parent heterosis (MPH in %) was calculated as the difference between hybrid performance (F1) and the mean value of the two parents [MP=(P1+P2)/2] for each trait at all time points as Eq.1.

$$\mathrm{MPH} = \frac{(\mathrm{F1} - \mathrm{MP})}{\mathrm{MP}} \times 100 \qquad \text{(Eq. 1)}$$

To evaluate the drought tolerance of the lines, the biomass ratio was assessed by comparing the biomass under drought (D) with the biomass under well-watered (WW) conditions. The calculation was done as follows (Eq.2-Eq.5; Fischer and Maurer, 1978; Correia et al., 2022). Shoot DW ratio was calculated based on the data at the end of the experiment, while the estimated shoot biovolume (ESV), total root length (TRL), and total root volume (TRV) were derived from the daily acquired images. Mean values were calculated for each day of the growth period after drought was imposed at 13 DAT.

$$\text{Shoot DW ratio} = \frac{\text{shoot DW}_\mathrm{D}}{\text{shoot DW}_\mathrm{WW}} \qquad \text{(Eq. 2)}$$

$$\text{ESV ratio} = \frac{\mathrm{ESV_D}}{\mathrm{ESV_{WW}}} \qquad \text{(Eq. 3)}$$

$$\text{TRL ratio} = \frac{\mathrm{TRL_D}}{\mathrm{TRL_{WW}}} \qquad \text{(Eq. 4)}$$

$$\text{TRV ratio} = \frac{\mathrm{TRV_D}}{\mathrm{TRV_{WW}}} \qquad \text{(Eq. 5)}$$

Statistical analysis

The manually measured traits were analysed by an analysis of variance (ANOVA) or t-test using GENSTAT software ver. 16.0. Correlations between traits were analysed using the Pearson product moment correlation. The data visualization for phenotyping data was performed using the R software (R Core Team, 2019). Significant differences between the treatments for each day and trait were determined by one-way ANOVA at a significance level of 0.05.

Results

Validation of the root phenotyping implementation

Two genotypes contrasting in root biomass, B73 and N22, each analysed with seven replicates, were sampled at 19 days after transplanting (DAT) and used to validate the root phenotyping setup in our phenotyping platform. To this end, roots were dug out manually, washed, scanned, and root morphological traits were analysed using the WinRhizo (SC) software to generate ground truth data. The high-throughput phenotyping images were processed with 'SmartRoot' (SR) and 'Semi-automated Root Image Analysis' (saRIA).

The correlations between root dry weight (RDW) and root traits obtained by different software tools are shown in Table 1. There were high positive correlations among all three root traits: total root length (TRL), total root surface area (TRSA), and total root volume (TRV). The TRV obtained by scanning the root system displayed the highest correlation with RDW (r = 0.99). TRV reflected RDW better than TRL, regardless which software was used. Notably, the traits obtained by the saRIA software showed higher correlation with RDW than the traits obtained by the SmartRoot software which required manually tracing the roots. Therefore, the saRIA software was used to analyse root traits in the two case studies performed.

TABLE 1 Correlations between RDW (root dry weight), root traits TRL (total root length), TRSA (total root surface area), and total root volume (TRV) analysed by different software (n=14).

	SC-TRL	SC-TRSA	SC-TRV	SR-TRL	SR-TRSA	SR-TRV	saRIA-TRL	saRIA-TRSA	saRIA-TRV
RDW	0.967	0.985	0.99	0.915	0.941	0.959	0.939	0.953	0.963
SC-TRL	–	0.993	0.974	0.922	0.933	0.937	0.942	0.950	0.947
SC-TRSA		–	0.994	0.932	0.949	0.958	0.947	0.958	0.961
SC-TRV			–	0.929	0.952	0.965	0.939	0.954	0.962
SR-TRL				–	0.992	0.966	0.944	0.955	0.948
SR-TRSA					–	0.990	0.956	0.966	0.968
SR-TRV						–	0.963	0.972	0.982
saRIA-TRL							–	0.993	0.987
saRIA-TRSA								–	0.995
saRIA-TRV									–

SC (WinRhizo), SR (SmartRoot), and saRIA (Semi-automated Root Image Analysis) refer to the used software. The values denote correlation coefficient (R) between the traits analysed by Pearson correlation. The correlations were all statistically highly significant at $p< 0.001$.

Dynamic shoot and root growth of hybrid and inbred maize genotypes.

Manually measured shoot traits

At the end of the experiment, most hybrids (B73xUH007, N22xUH007, P148xUH007, and PHT77xUH007) had a significantly higher plant height (PH) and shoot dry weight (DW) compared with the corresponding female parental inbred lines (B73, N22, P148, and PHT77) or the male tester UH007 (Figure 2 and Supplementary Figure 1). The only exception was the DW difference between N22xUH007 and UH007. The manually measured traits V stage and leaf number, both representing the development of the maize plants, increased over time. At 13 DAT, the hybrids were further developed, displaying a higher V stage and leaf number than the female inbred lines. Significant differences in V stage between UH007 and the hybrids were detectable starting at 26 DAT (P148xUH007). For leaf number, B73xUH007 and P148xUH007 had significantly more leaves than UH007 at 13 DAT and all the hybrids had a higher leaf number than UH007 at 40 DAT, similar to the other female inbred lines. Among the inbred lines, N22 displayed significantly lower shoot DW and a lower plant height compared with B73, PHT77, and UH007. During the whole growth period, N22 developed fewer leaves than the other inbred lines, which could be observed as early as 13 DAT.

Image-derived shoot and root phenotypic traits

Similar tendencies of the manually measured traits were also observed for the image-derived shoot traits. Estimated shoot biovolume (ESV), estimated plant height (EPH), and projected leaf area (PLA) from 4 to 40 DAT are shown in Figures 3A, B and Supplementary Figure 2, respectively. Due to a technical failure at 30 DAT, no imaging and watering was performed on this particular day. There were also no images between 35-39 DAT, but watering was carried out every second day during this period. Both hybrid and inbred lines showed continuous ESV, PLA, and PH increases over time. There was more variation at the later stages, most likely caused by losing some old leaves and/or greater overlap of leaves. As mentioned by Scharr et al. (2016), with the growth of plants, leaves tend to overlap which could result in less accurate estimates of the leaf area due to partial occlusion.

The traits TRL, TRV, and TRSA were extracted from the root images acquired by the NIR camera and their changes over time (from 4-29 DAT) were analysed (Figures 4A, B and Supplementary Figure 3, respectively). In concordance with shoot growth, the hybrid lines displayed higher TRL values compared to the inbred lines almost throughout the whole growth period. This tendency could be observed already during the early growth phase at 4 DAT (Table 2). At 29 DAT, the hybrids B73xUH007, N22xUH007, P148xUH007, and PHT77xUH007 had a 1.6, 4.2, 2.5, and 1.6 times greater TRL than their respective parental inbred lines B73, N22, P148, and PHT77. Among the inbred lines, B73, PHT77, and UH007 had similar TRL, and they were substantially higher compared with N22 (Figure 4A). Roots of N22 were not only shorter, but also displayed a limited volume, which reflected a smaller root system. TRV showed a similar tendency as TRL regarding the growth pattern of hybrids and inbred lines, except that UH007 had the highest TRV among all inbred lines, which was even higher than the hybrid N22xUH007. This mainly resulted from the bigger RD, as show in Supplementary Figure 3.

The mean mid-parent heterosis (MPH) for the hybrids was calculated based on the imaging-derived traits of both shoots and roots (Figure 5). Generally, the MPH of all traits varied dynamically over time with higher MPH values at the early stage. TRL, TRV, and TRSA especially displayed high MPH at 4 DAT, though with quite high variation. The highest MPH for EPH was found at 5 DAT which reached 144%. The MPH of ESV and PLA showed the highest value several days later, in the period of 9 to 10 DAT, and both reached

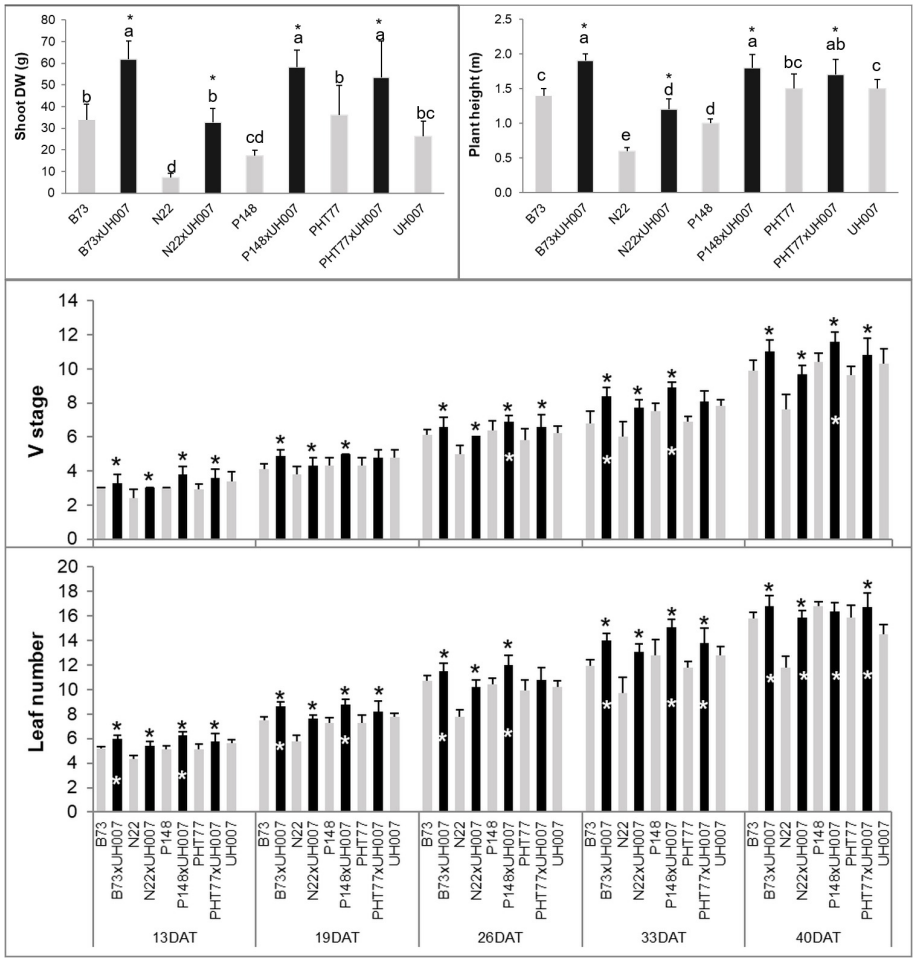

FIGURE 2
Manually measured plant height and shoot dry weight (DW) at the end of the experiment, V stage, and leaf number over time of hybrid and inbred lines. DAT: days after transplanting. Bars indicate means ± SD (n = 9). A black * indicates significant differences between the hybrid and the female parent inbred lines, while a white * indicates significant differences between the hybrid and the male parent inbred line UH007 compared by t-test ($p<0.05$). Different letters indicate statistically significant differences among all the lines ($p<0.05$) determined by ANOVA and Tukey's HSD test.

more than 200%. It seems that heterosis was manifested earlier in roots than in shoots, while the degree of heterosis was lower in roots compared to shoots. The range of MPH for TRL and TRV (4-29 DAT) was 70-146%, and 28-144%, while MPH for ESV and PLA (4-40 DAT) it ranged between 73-217% and 81-224%, respectively.

Shoot and root growth dynamics under drought stress

The inbred lines B73, N22, P148, PHT77, and S052 were evaluated for their phenotypic response to drought. Drought stress was induced by stopping the water supply starting from 13 DAT. Due to the large soil volume in the rhizo-pot, the soil moisture level dropped down progressively as shown either by soil VWC measured with soil sensors (Figure 6) or by the calculated field capacity (FC; Supplementary Figure 4). Both methods showed the same tendency that only at a late stage, after 33 DAT, did the FC of the soil in the pots of B73 and PHT77 decrease to 35%. For P148 and S052, the FC dropped to 40% during the last two days, while the pots of N22 still had about 45% FC at the end of the experiment (Supplementary Figure 4).

Manually measured shoot traits

Drought stress significantly decreased PH and shoot DW of B73, PHT77, and S052. Although P148 displayed a decreased PH, the DW did not differ significantly between well-watered and drought-stressed plants. Both PH and shoot DW were unaffected by the drought treatment in N22, likely due to a lower stress intensity with a relatively high FC (higher than the intended 35%) even at the late growth stages (Figure 7). The V stage and leaf number of B73 and PHT77 were affected by the drought from 33 DAT, while only at 40 DAT, a substantial effect was observed on P148 and S052. Similar to PH and shoot DW results, the V stage and leaf number did not differ between the two treatments in N22 (Figure 7).

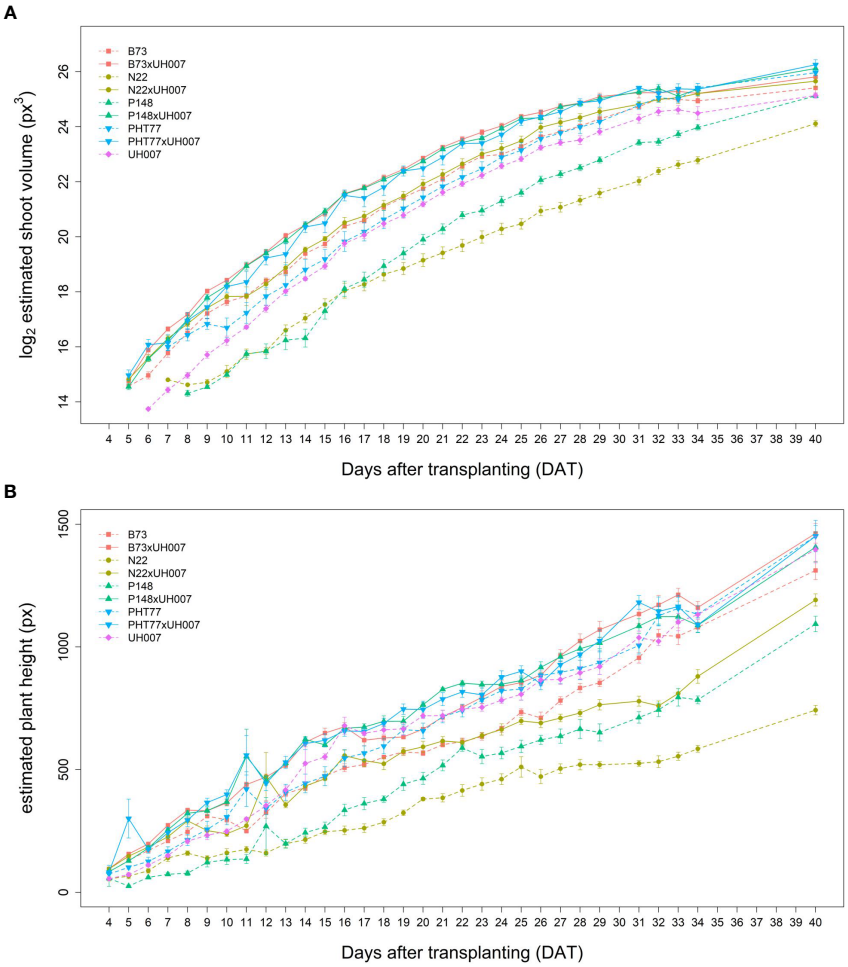

FIGURE 3
Estimated shoot biovolume (ESV) **(A)** and estimated plant height (EPH) **(B)** derived from the images of hybrid and inbred maize plants over time. Data are shown as means of nine replicates and the error bars denote ± SE.

Image-derived shoot and root phenotypic traits

It took several days for plants to show detectable phenotypic changes after the drought stress was imposed. Starting from 29 DAT, a significant difference in ESV appeared between well-watered and drought-treated plants (Table 2). Drought tended to reduce PH for all the tested inbred lines over time, although significant differences were not detectable until 32 DAT. The ESV and EPH at 40 DAT were 2.3 and 1.35 times higher, respectively, under well-watered conditions compared with drought treatment (Figures 8A, B). B73 and PHT77 were most severely affected by the drought stress. Their ESV and PLA decreased about ten days after drought imposition, while there was no significant difference detectable in N22 at that time (Figure 8A; Supplementary Figure 5). Most colour-related shoot traits, such as the brown to green ratio (Supplementary Figure 6), showed no obvious changes due to the drought stress.

Root growth of all tested lines was substantially affected by the drought stress (Figures 9A, B and Supplementary Figure 7). Water deficit significantly decreased TRV compared to well-watered plants, and this was evident from 24 DAT, about 10 days after the watering was stopped (Figure 9B and Table 2). TRL showed a trend toward higher TRL in the drought-treated plants, although the differences between 18 and 23 DAT were not significant (Figure 9A). Subsequently, the TRL of most drought-treated plants stagnated or decreased over time and was on average 10% lower than that of the well-watered plants at 29 DAT. RD of all the lines were decreased under drought stress (Supplementary Figure 7).

Drought stress reduced the shoot DW for all tested inbred lines (Figure 10A). Among the lines, B73 was most severely affected by the drought treatment and gained only 45.3% of shoot biomass of the corresponding well-watered plants, while N22 was least affected (79.5%). After one week of drought stress, the ESV ratio between drought and well-watered plants dropped below a value of 1 for all lines. The value continuously decreased over time and reached on average about 0.5 at 40 DAT (Figure 10B). There was variation in the degree of reduction in the five inbred lines. Starting from 32 DAT, the observed tendency became stable. Consistent with the end-point results at 40 DAT, the ESV ratios for B73, PHT77, and S052 were lower than for P148 and N22, indicating a stronger effect on those lines. Root growth was affected by the water deficit as well, as shown

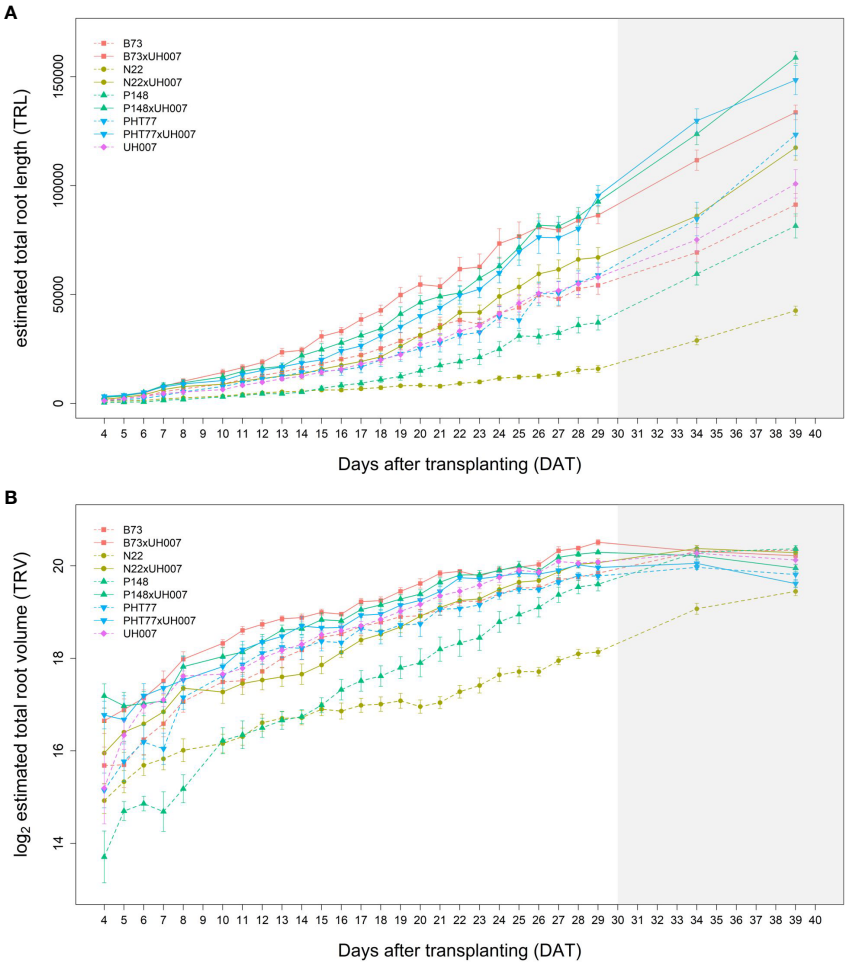

FIGURE 4
Estimated total root length (TRL) **(A)** and total root volume (TRV) **(B)** of hybrid and inbred maize plants over time extracted from NIR-images by saRIA (semi-automated Root Image Analysis) software. Data are shown as means of nine replicates and the error bars denote ± SE. The grey area marks time points with data of low reliability due to the increasing density of roots and their progressive merging and overlapping. Values derived from images taken at 34 and 39 DAT are included only for illustration.

TABLE 2 Statistical analysis by using ANOVA (analysis of variance) between hybrid and inbred lines, as well as well-watered (WW) and drought-treated (D) maize plants.

	Hybrid vs. Inbred				WW vs. D			
DAT	ESV	EPH	TRL	TRV	ESV	EPH	TRL	TRV
4	– [a]	*	***	***	NS [b]	NS	NS	NS
5	–	*	***	***	NS	NS	NS	NS
6	***	***	***	***	NS	NS	NS	NS
7	***	***	***	***	NS	NS	NS	NS
8	***	***	***	***	NS	NS	NS	NS
9	***	***	***	***	NS	NS	NS	NS
10	***	**	***	***	NS	NS	NS	NS
11	***	**	***	***	NS	NS	NS	NS
12	***	*	***	***	NS	NS	NS	NS
13	***	***	***	***	NS	NS	NS	NS

(Continued)

TABLE 2 Continued

	Hybrid vs. Inbred				WW vs. D			
DAT	ESV	EPH	TRL	TRV	ESV	EPH	TRL	TRV
14	***	***	***	***	NS	NS	NS	NS
15	***	***	***	***	NS	NS	NS	NS
16	***	**	***	***	NS	NS	NS	NS
17	***	***	***	***	NS	NS	NS	NS
18	***	***	***	***	NS	NS	NS	NS
19	***	***	***	***	NS	NS	NS	NS
20	***	***	***	***	NS	NS	NS	NS
21	***	***	***	***	NS	NS	NS	NS
22	***	***	***	***	NS	NS	NS	NS
23	***	***	***	***	NS	NS	NS	NS
24	***	***	***	***	NS	NS	NS	*
25	***	***	***	***	NS	NS	NS	*
26	***	***	***	***	NS	NS	NS	**
27	***	***	***	***	NS	NS	NS	***
28	***	***	***	***	NS	NS	NS	***
29	***	***	***	***	*	NS	NS	***
31	***	***			*	NS		
32	***	**			***	*		
33	***	**			**	*		
34	***	*			***	**		
35	–	–			–	–		
39	–	–			–	–		
40	***	**			***	***		

*indicates p< 0.5, **p<0.1, and ***p< 0.01. Analysis results of values derived from root images taken from 30 to 39 DAT are not shown due to the increasing density of roots and their progressive merging and overlapping.
[a]denotes no data, [b]denotes no significant difference.
ESV, estimated shoot biovolume; EPH, estimated plant height; TRL, total root length; TRV, total root volume; NS-no significant difference.

in Figures 10C, D. The TRV ratio decreased over time, and it appears there were genotypic differences between the lines. After ten days of water deficit, the TRV of S052 was much less reduced than the TRV of the other lines (Figure 10C). The ratio of TRL showed a different pattern. The ratio was above 1 for all lines during more than half of the drought stress period from 15 to 25 DAT. This increased root length (ratio >1) lasted for about ten days, and then decreased to an average value of 0.83 at 29 DAT (except for S052). Notably, for S052 the TRL increased for a period of 14 days (15 to 29 DAT), while for N22 it only increased for 7 days (15 to 22 DAT; Figure 10D).

Discussion

Although diverse high-throughput phenotyping facilities have been developed in recent years, platforms capable of simultaneously assessing both the root and the shoot of plants are rare. It has been reported that the growth and structure of the belowground and aboveground parts of plants affect each other and, hitherto, this relationship has been particularly investigated in trees by ecologists (Parsons et al., 1994; Wang et al., 2023). However, also in annual plants like maize, effects of aerial conditions such as solar radiation can affect both shoot and root growth and can cause shifts in the root/shoot ratio (Guo et al., 2021). As reported by Su et al. (2019), the growth of plant shoots is closely associated with the size of the root system. They found nitrogen efficient maize hybrids had deeper and bigger roots and higher grain yield than nitrogen inefficient lines at low nitrogen application rates, although the mechanism of the interaction between shoots and roots is still unclear. Therefore, further studies with suitable phenotyping facilities are necessary to examine root and shoot traits in a single framework.

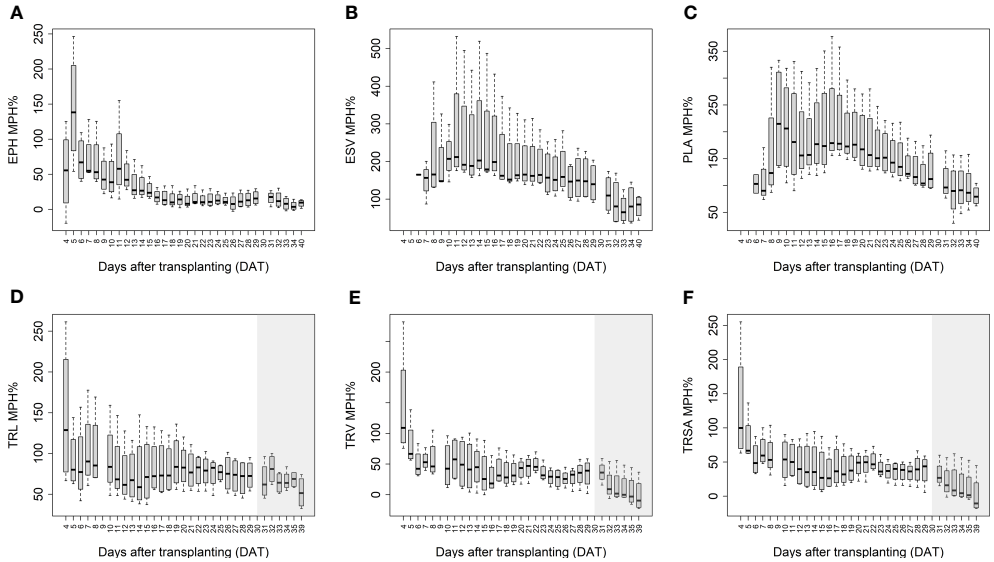

FIGURE 5
Mean mid-parent heterosis (MPH) for estimated plant height (EPH) **(A)**, estimated shoot biovolume (ESV) **(B)**, projected leaf area (PLA) **(C)**, total root length (TRL) **(D)**, total root volume (TRV) **(E)**, and total root surface area (TRSA) **(F)** across hybrids by using image-derived traits. The grey area marks time points with data of low reliability due to the increasing density of roots and their progressive merging and overlapping. Values derived from images taken at 34 and 39 DAT are included only for illustration.

Integrated root phenotyping

The non-invasive high-throughput shoot phenotyping platform at IPK has been utilized in many research studies for diverse models and crop plants (Junker et al., 2015; Muraya et al., 2017; Knoch et al., 2020; Dodig et al., 2021). As realized by many researchers, crop species with optimised root systems are essential for future food security and key to improving agricultural productivity and sustainability (Li A. et al., 2022). In order to enhance our understanding of the root system, in particularly the dynamics of root growth and development, a root phenotyping concept was developed (Shi et al., 2018) and root phenotyping units were established and integrated in the existing phenotyping platform for large plants. In this work, we present the upgraded facility and the use of the root phenotyping units to evaluate jointly shoot and root growth in two case studies.

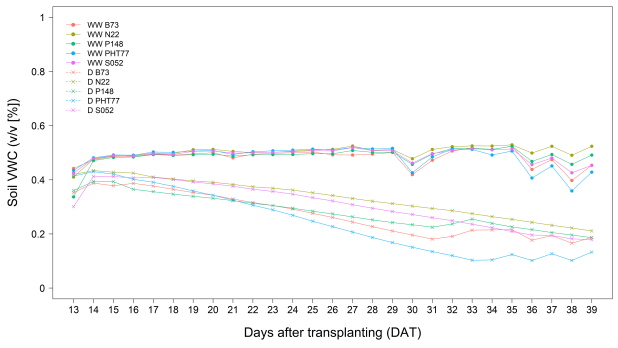

FIGURE 6
Soil volumetric water content (VWC (v/v [%])) determined by a soil sensor in well-watered (WW) and drought-treated (D) pots. The values denote the mean of five replicates of each line.

The high positive correlations between root DW and image-derived traits such as TRL and TRV indicate that our root phenotyping facility is well suited to monitor root growth (Table 1). The root analysis software saRIA (Narisetti et al., 2019) was utilized to analyse the root images obtained by the automated high-throughput phenotyping system. This upgraded system now enables simultaneous non-invasive analysis of root and shoot traits of the same plants in a particular phenotyping experiment.

Shoot and root growth dynamics in maize hybrid and inbred lines

Hybrids often display superior phenotypes due to their vigorous nature (van Dijk et al., 2016), a phenomenon widely known as heterosis. The superior performance of F1 hybrids compared to their parental inbreds has been known for decades, although the underlying genetic and regulatory mechanisms remain largely unclear (Paschold et al., 2010). Heterosis studies rely on morphological and physiological analyses of inbred lines and corresponding hybrids. So far, most related research has focused either on shoot or root traits independently using separate approaches.

In the present study, the dynamics of vegetative shoot and root growth were investigated in a selection of maize hybrid and inbred lines. Growth-related image-derived shoot and root traits were analysed during the early vegetative growth phase, from 4 to 40 DAT. The phenotyping results indicated an early establishment of heterosis in the tested hybrids. EPH, TRL, and TRV were higher in hybrids than in their corresponding parental inbred lines as early as 4 DAT, the first day when shoot and root images were taken (Table 2). At the end of the growth period, EPH and shoot DW in

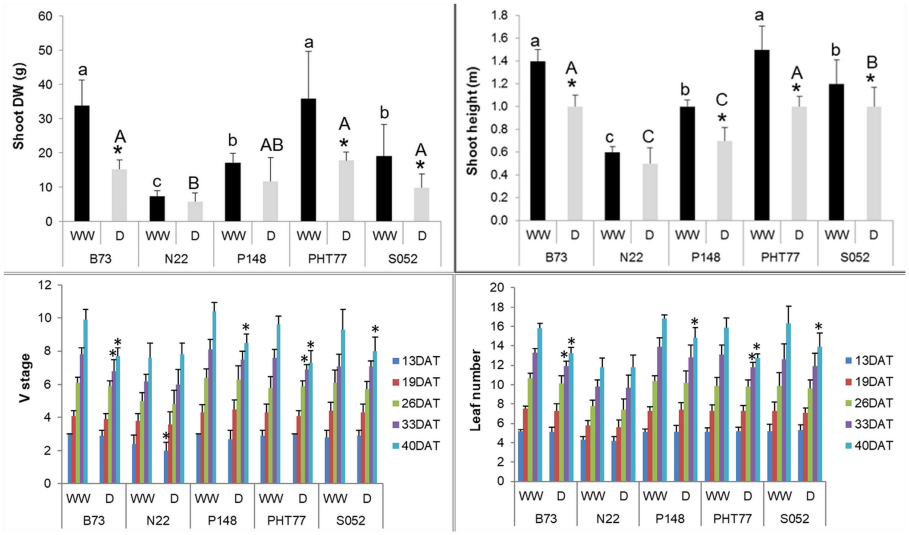

FIGURE 7
Manually measured shoot height and shoot dry weight (DW) at the end of the experiment, V stage, and leaf number over time. DAT: days after transplanting. Bars indicate means ± SD (n = 9). * indicates significant differences between well-watered (WW) and drought-treated (D) plants ($p<0.05$). Different letters indicate statistically significant differences among the genotypes under well-watered (small letters) or drought (capital letters) condition ($p<0.05$).

hybrids were on average 20% and 55% higher than in their parental inbred lines, respectively. These findings are consistent with the results of previous studies, which showed the superiority of hybrids (Hauck et al., 2014; Zhou et al., 2018). The range of MPH for ESV (73-217%) and PLA (81-224%) was similar to that reported by Tollenaar et al. (2004). In their study, they reported MPH values from 138% to 214% for dry matter accumulation and 92% to 204% for leaf area at the 14-leaf stage, respectively. Thanks to the better performance with superior biomass and higher seed yield, hybrid maize varieties have been predominantly grown worldwide since the 1960s (Li C. et al., 2022). Further increasing yield potential and yield stability through heterosis remains a major goal of maize breeding (Duvick, 2005; Li C. et al., 2022). The advances in high-throughput phenotyping facilities will assist and fasten this process by supporting the gain of fundamental genetic and mechanistic knowledge.

In addition to the aboveground parts, heterosis is also observable in the belowground organs of plants. In accordance with Hoecker et al. (2006), the primary root length, number of seminal roots, and the lateral root density can display substantial heterosis. They demonstrated that heterosis manifests in the very early stages of root development a few days after germination. We observed in our study that hybrids displayed high MPH values as early as 4 DAT (8 days after germination), with on average 67% and 70% higher TRL and TRV values than the inbred lines, respectively (Figure 5). Compared to conventional methods of quantifying trait expression at one particular time point (usually using destructive techniques), heterosis in shoots and roots can be assessed here in a dynamic manner by a non-invasive, fast, and high-throughput procedure. We observed that heterosis occurred earlier in roots than in shoots and decreased over time in both organs.

The ability to compare heterosis for both shoot and root simultaneously, even under various conditions, will help researchers to further explore the developmental and physiological mechanisms associated with heterosis and to jointly study the genetic basis of heterosis for both organ systems, which are highly interdependent.

Shoot and root growth dynamics in maize in response to drought

Drought stress is one of the most serious adverse environmental factors limiting crop productivity and a major threat to world food security (Boyer et al., 2013; Berdugo et al., 2020). Due to global climate change, the frequency and duration of drought periods will most likely increase (Trenberth et al., 2014). Therefore, it is of the utmost importance to understand how plants respond and adapt to water deficit in order to support solutions to this problem and enhance the sustainability of agricultural production.

In the present study, drought stress was induced at 13 DAT and drought symptoms such as leaf wilting and rolling could be observed in B73 and PHT77 at the growth stages V6-V10. The effect of drought was reflected by decreases in PLA and ESV, as well as in the final shoot DW. Plants generally decline the number and area of leaves in response to drought stress. This was confirmed by our manually measured parameters and image-derived shoot phenotypic traits (Figures 7, 8). To cope with drought, plants induce protective mechanisms against water deficit. In addition to stomatal closure, assimilates are often re-allocated from the shoot to the root, thereby enhancing root growth and extension into deeper soil layers (Rich and Watt, 2013; Xu et al., 2015). Roots have the

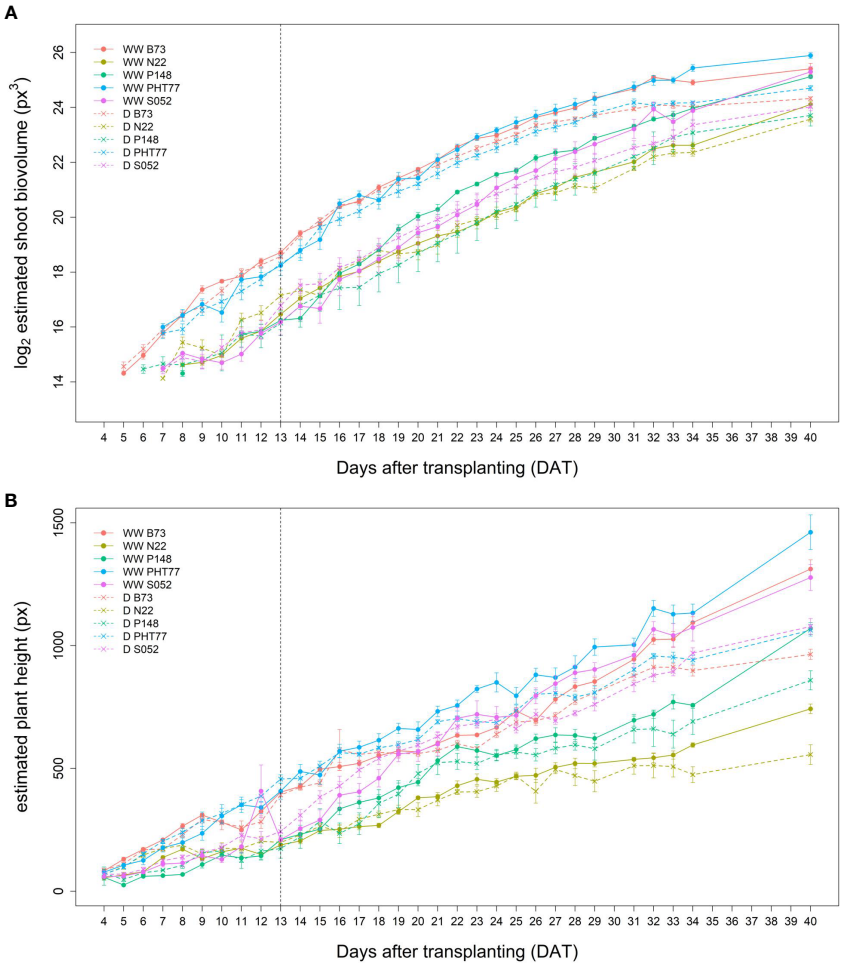

FIGURE 8
Estimated shoot biovolume (ESV) **(A)** and estimated plant height (EPH) **(B)** derived from the images of well-watered (WW) and drought-treated (D) plants over time. Data are shown as means of nine replications and the error bars denote ± SE. The vertical dashed line denotes the starting time of imposing drought stress at 13 DAT.

ability to plasticly change their spatial distribution in the soil in response to drought stress (Orman-Ligeza et al., 2018; Orosa-Puente et al., 2018; von Wangenheim et al., 2020). The degree of plasticity, however, is trait and genotype dependent. As mentioned by Tracy et al. (2020), phenotypes in roots and shoots are expressed differently depending on environmental conditions. Our results show that roots respond faster to drought than shoots as significant differences between drought and WW treatments occurred 10 days after drought imposition in roots, while in shoots significant differences could only be observed 4 days later (Table 2). Drought affected not only root biomass, which was represented by TRV, but also modified the morphology of root with changes in other traits, such as TRL, and also the root diameter.

Notably, there was a tendency for TRL to increase shortly after the onset of drought stress, although the difference was not significant. Sharp and Davies (1979) showed that a mild degree of water stress resulted in a higher root elongation rate compared to well-watered maize. The rate of root growth probably depends on the degree and the duration of the stress. Under extreme water deficit, root growth will be inhibited in many species (Rich and Watt, 2013; Kou et al., 2022). It is therefore highly important to assess the dynamics of root growth changes over time and under different conditions to gain deeper insights into the responsible mechanisms. Addressing only single time points will be inappropriate. Our high-throughput phenotyping platforms supports such measurements and thus the elucidation of the responses of plant organs to environmental cues and the adaptation to stress conditions.

The biomass ratio between well-watered and drought-treated plants provides a parameter to compare different genotypes with respect to their response to drought (Harb et al., 2010; Correia et al., 2022). Among the five inbred lines tested here, B73 exhibited the lowest ESV ratio at most time points. This suggests that B73 was most severely affected by drought, which is in line with the study of Chen et al. (2012), who classified B73 as a drought-sensitive line. The estimated TRL and TRV ratios suggested that S052 produced more roots, likely through enhanced lateral root growth and this effect lasted also longer than in the other lines. This might partly

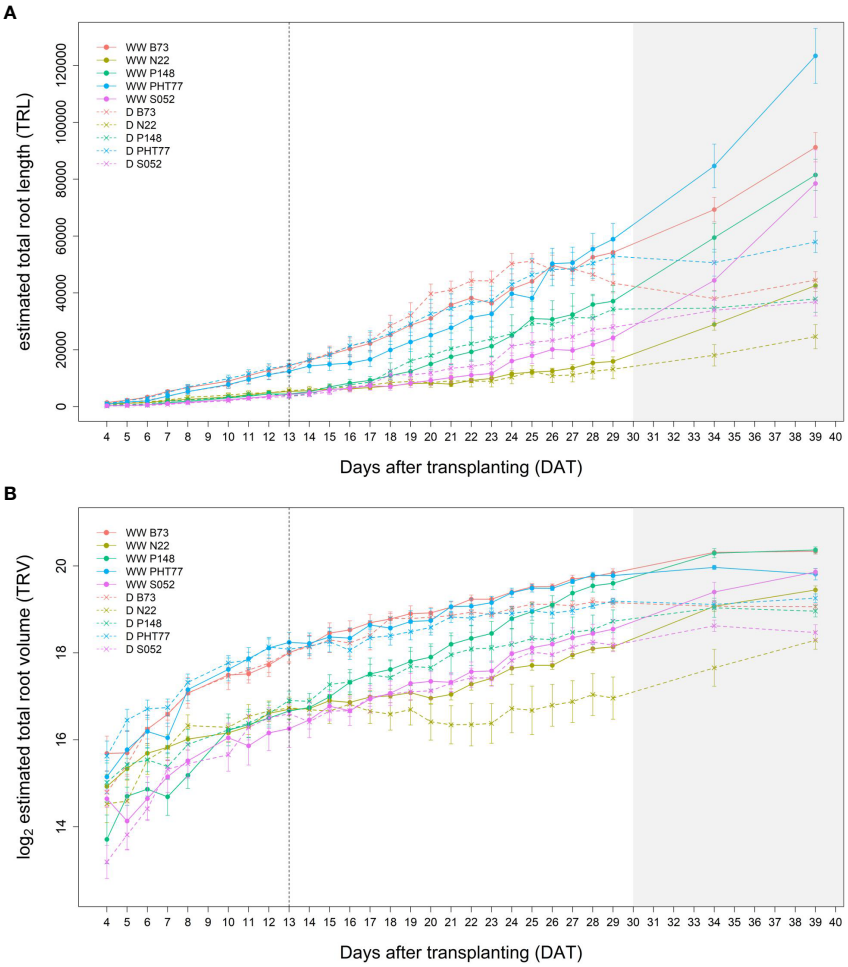

FIGURE 9
Estimated total root length (TRL) **(A)** and total root volume (TRV) **(B)** of well-watered (WW) and drought-treated (D) plants over time extracted from the NIR-images by saRIA (semi-automated Root Image Analysis) software. Data are shown as means of nine replications and the error bars denote ± SE. The vertical dashed line denotes the starting time of imposing drought stress at 13 DAT. The grey area marks time points with data of low reliability due to the increasing density of roots and their progressive merging and overlapping (particularly in the WW plants). Values derived from images taken at 34 and 39 DAT are included only for illustration.

result from the relatively small shoot biomass (and transpiration) and the lower water consumption of the plants of this line (Figure 10), which caused a longer time period to reach water deficit than for other genotypes.

In future, some features of the phenotyping installation need to be taken into account when it is used to assess genotypic difference in responses to drought: due to the relatively large volume of the rhizo-pots compared to regular growth pots, soil moisture levels will decrease more slowly. This is closer to the natural drought scenarios in the field, where gradual changes in water availability occur rather than abrupt changes (Poorter et al., 2012). Soil drying in the rhizo-pots occurs due to the water consumption by the plants and the evaporation from the soil surface. While the latter is rather uniform (also due to the use of the soil cover), the former is affected by the size of the plants and by their physiological states, in particular their rates of transpiration. The impact of small plant size was evident for the line N22, which did not suffer from the drought stress as much as the other lines, since the FC was still 40% at the end of the experiment (Supplementary Figure 4). This is probably the main reason why the reduction of shoot mass was least compared to the other genotypes. A similar tendency could be observed for many other measured traits. Also, most colour-related traits did not differ after water deprivation, which might also be caused by the weak stress imposed in the system. If the different water consumption of plant lines under investigation (mainly due to different plant sizes) cannot be avoided by an appropriate selection of the population under investigation, we suggest adjusting the drought regime imposed to all plants to that of the plants with the lowest water consumption. This could be achieved by programming a gradual decrease of the watering target weight, which is gauged to the weakest water consumer, rather than a complete stop of watering. To avoid a too long period to reach considerable water stress levels, the soil moisture level in the rhizo-pot used in the initial phase of the experiment should be carefully adjusted.

Plant productivity is the results of integrating processes occurring in both the root and the shoot systems. Therefore, a

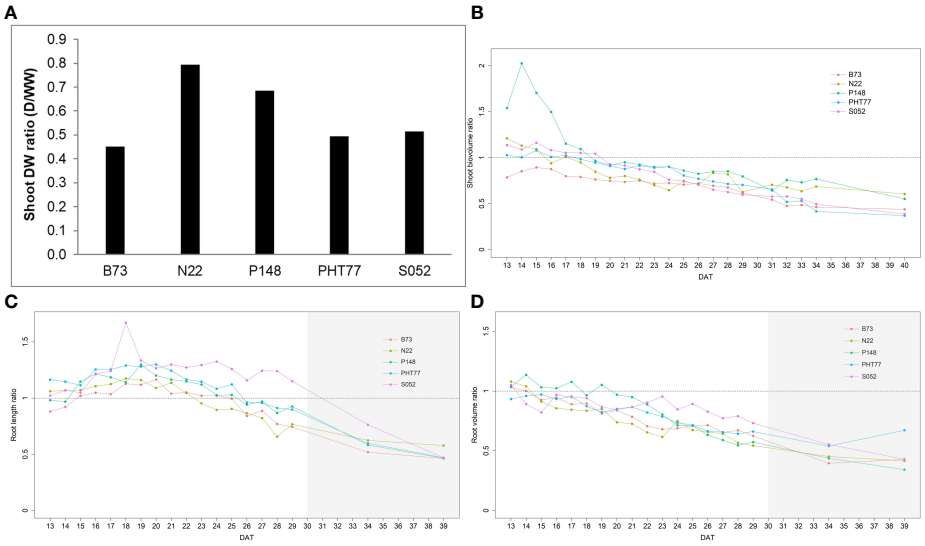

FIGURE 10
Shoot DW ratio (shoot DW under drought/shoot DW under well-watered) of the five inbred lines at the end of the experiment at 40 DAT **(A)**. Estimated shoot biovolume ratio (ESV ratio) over time after drought imposition at 13 DAT **(B)**. Estimated total root length (TRL) and total root volume ratio (TRV) over time **(C, D)**. The mean values of nine replicates under each treatment were used to calculate the ratio. The dashed line denotes 1 which means the trait had the same value in the drought and the well-watered (WW) conditions. DAT: days after transplanting. The grey area marks time points with data of low reliability due to the increasing density of roots and their progressive merging and overlapping (particularly in the WW plants). Values derived from images taken at 34 and 39 DAT are included only for illustration.

deeper understanding of the effects of different stresses such as water deficit or nutrient limitation on roots and shoots is of great value for cultivar selection, the improvement of crop models, and low-input agriculture (Hadir et al., 2020). Our observations confirm that the root phenotyping upgrade of the platform supports experiments to assess the dynamic phenotypic changes of both shoots and roots (and thus the relations of these two important organ systems) caused by genetic variation and/or induced by environmental triggers such as drought stress.

Conclusion

With the latest updates, the IPK automated high-throughput phenotyping platform for large plants is capable of capturing images from both shoots and roots. Consequently, the dynamic growth patterns among various genotypes in up to 396 carriers/plants, as well as the response to different environmental scenarios, can be analysed in a single experiment.

This study illustrates the applicability and importance of this system. Combing growth-related shoot and root traits helps us to better interpret the difference between hybrid and inbred lines. Moreover, it sheds some light on the hidden parts of plants and illustrated the early response of roots to drought. Genotypic differences in adaptation were identified in the five inbred lines. The assessment of dynamic growth from more diverse lines with different degrees of drought resilience will be helpful to explore the underlying mechanisms and to obtain more information about the shoot–root relationships in response to drought. The integrated shoot and root phenotyping platform can also be applied to investigate other stress responses or nutrient deficiency scenarios for large plant species.

Data availability statement

The raw data supporting the conclusions of this article will be made available by the authors, without undue reservation.

Author contributions

TA and AJ designed the experiment. RS and CS performed the experiment. RS and DK analysed the data. RS drafted the manuscript with input from CS, DK, and TA. TA and AJ supervised the project. All authors contributed to the article and approved the submitted version.

Funding

This work was supported in the German Plant-Phenotyping Network (DPPN) and the European Plant Phenotyping Network project EPPN2020, funded by the German Federal Ministry of Education and Research (BMBF), project identification number 031A053, and by the European Commission, H2020-INFRAIA 2016-1, grant agreement number 731013, respectively. Costs for open access publishing were partially funded by the Deutsche Forschungsgemeinschaft (DFG, German Research Foundation, grant 491250510).

Acknowledgments

We thank Ingo Mücke, Gunda Wehrstedt, Iris Fischer, and Marion Michaelis for excellent technical assistance. We are grateful to Albrecht Melchinger (University of Hohenheim, Germany), Alain Charcosset and Cyril Bauland (INRA(E), Moulon, France), and Claude Welcker (INRA(E), LEPSE, Montpellier, France) for the provision of seed material of the studied maize lines and hybrids.

Conflict of interest

Author AJ is employed by the company Syngenta Seeds GmbH, Germany.

The remaining authors declare that the research was conducted in the absence of any commercial or financial relationships that could be construed as a potential conflict of interest.

Publisher's note

Supplementary material

The Supplementary Material for this article can be found online at: https://www.frontiersin.org/articles/10.3389/fpls.2023.1233553/full#supplementary-material

References

Berdugo, M., Delgado-Baquerizo, M., Soliveres, S., Hernández-Clemente, R., Zhao, Y., Gaitán, J. J., et al. (2020). Global ecosystem thresholds driven by aridity. *Science* 367, 787–790. doi: 10.1126/science.aay5958

Boyer, J. S., Byrne, P., Cassman, K. G., Cooper, M., Delmer, D., Greene, T., et al. (2013). The U.S. drought of 2012 in perspective: A call to action. *Global Food Secur.* 2, 139–143. doi: 10.1016/j.gfs.2013.08.002

Chen, J., Xu, W., Velten, J., Xin, Z., and Stout, J. (2012). Characterization of maize inbred lines for drought and heat tolerance. *J. Soil Water Conserv.* 67, 354–364. doi: 10.2489/jswc.67.5.354

Correia, P. M. P., Cairo Westergaard, J., Bernardes Da Silva, A., Roitsch, T., Carmo-Silva, E., and Marques Da Silva, J. (2022). High-throughput phenotyping of physiological traits for wheat resilience to high temperature and drought stress. *J. Exp. Bot.* 73, 5235–5251. doi: 10.1093/jxb/erac160

Costa, C., Schurr, U., Loreto, F., Menesatti, P., and Carpentier, S. (2019). Plant phenotyping research trends, a science mapping approach. *Front. Plant Sci.* 9. doi: 10.3389/fpls.2018.01933

De Diego, N., and Spíchal, L. (2022). Presence and future of plant phenotyping approaches in biostimulant research and development. *J. Exp. Bot.* 73, 5199–5212. doi: 10.1093/jxb/erac275

Dodig, D., Božinović, S., Nikolić, A., Zorić, M., Vančetović, J., Ignjatović-Micić, D., et al. (2021). Dynamics of maize vegetative growth and drought adaptability using image-based phenotyping under controlled conditions. *Front. Plant Sci.* 12. doi: 10.3389/fpls.2021.652116

Downie, H., Holden, N., Otten, W., Spiers, A. J., Valentine, T. A., and Dupuy, L. X. (2012). Transparent soil for imaging the rhizosphere. *PloS One* 7, e44276. doi: 10.1371/journal.pone.0044276

Duvick, D. N. (2005). "The Contribution of Breeding to Yield Advances in maize (Zea mays L.)," in *Advances in Agronomy* (United States: Elsevier), 83–145. doi: 10.1016/S0065-2113(05)86002-X

Fischer, R., and Maurer, R. (1978). Drought resistance in spring wheat cultivars. I. Grain yield responses. *Aust. J. Agric. Res.* 29, 897. doi: 10.1071/AR9780897

Giehl, R. F. H., Gruber, B. D., and Von Wirén, N. (2014). It's time to make changes: modulation of root system architecture by nutrient signals. *J. Exp. Bot.* 65, 769–778. doi: 10.1093/jxb/ert421

Gioia, T., Galinski, A., Lenz, H., Müller, C., Lentz, J., Heinz, K., et al. (2017). GrowScreen-PaGe, a non-invasive, high-throughput phenotyping system based on germination paper to quantify crop phenotypic diversity and plasticity of root traits under varying nutrient supply. *Funct. Plant Biol.* 44, 76. doi: 10.3390/agriculture11010021

Guo, X., Yang, Y., Liu, H., Liu, G., Liu, W., Wang, Y., et al. (2021). Effects of solar radiation on root and shoot growth of maize and the quantitative relationship between them. *Crop Sci.* 61, 1414–1425. doi: 10.1002/csc2.20416

Hadir, S., Gaiser, T., Hüging, H., Athmann, M., Pfarr, D., Kemper, R., et al. (2020). Sugar beet shoot and root phenotypic plasticity to nitrogen, phosphorus, potassium and lime omission. *Agriculture* 11, 21. doi: 10.3390/agriculture11010021

Harb, A., Krishnan, A., Ambavaram, M. M. R., and Pereira, A. (2010). Molecular and physiological analysis of drought stress in arabidopsis reveals early responses leading to acclimation in plant growth. *Plant Physiol.* 154, 1254–1271. doi: 10.1104/pp.110.161752

Hauck, A. L., Johnson, G. R., Mikel, M. A., Mahone, G. S., Morales, A. J., Rocheford, T. R., et al. (2014). Generation means analysis of elite ex-plant variety protection commercial inbreds: a new public maize genetics resource. *Crop Sci.* 54, 174–189. doi: 10.2135/cropsci2013.03.0172

Hauck, A. L., Novais, J., Grift, T. E., and Bohn, M. O. (2015). Characterization of mature maize (Zea mays L.) root system architecture and complexity in a diverse set of Ex-PVP inbreds and hybrids. *SpringerPlus* 4, 424. doi: 10.1186/s40064-015-1187-0

Hoecker, N., Keller, B., Piepho, H.-P., and Hochholdinger, F. (2006). Manifestation of heterosis during early maize (Zea mays L.) root development. *Theor. Appl. Genet.* 112, 421–429. doi: 10.1007/s00122-005-0139-4

Iyer-Pascuzzi, A. S., Symonova, O., Mileyko, Y., Hao, Y., Belcher, H., Harer, J., et al. (2010). Imaging and analysis platform for automatic phenotyping and trait ranking of plant root systems. *Plant Physiol.* 152, 1148–1157. doi: 10.1104/pp.109.150748

Janni, M., Coppede, N., Bettelli, M., Briglia, N., Petrozza, A., Summerer, S., et al. (2019). In vivo phenotyping for the early detection of drought stress in tomato. *Plant Phenomics* 2019, 6168209. doi: 10.34133/2019/6168209

Janni, M., and Pieruschka, R. (2022). Plant phenotyping for a sustainable future. *J. Exp. Bot.* 73, 5085–5088. doi: 10.1093/jxb/erac286

Jeudy, C., Adrian, M., Baussard, C., Bernard, C., Bernaud, E., Bourion, V., et al. (2016). RhizoTubes as a new tool for high throughput imaging of plant root development and architecture: test, comparison with pot grown plants and validation. *Plant Methods* 12, 31. doi: 10.1186/s13007-016-0131-9

Jia, Z., Giehl, R. F. H., Meyer, R. C., Altmann, T., and Von Wirén, N. (2019). Natural variation of BSK3 tunes brassinosteroid signaling to regulate root foraging under low nitrogen. *Nat. Commun.* 10, 2378. doi: 10.1038/s41467-019-10331-9

Junker, A., Muraya, M. M., Weigelt-Fischer, K., Arana-Ceballos, F., Klukas, C., Melchinger, A. E., et al. (2015). Optimizing experimental procedures for quantitative evaluation of crop plant performance in high throughput phenotyping systems. *Front. Plant Sci.* 5. doi: 10.3389/fpls.2014.00770

Klukas, C., Chen, D., and Pape, J.-M. (2014). Integrated analysis platform: an open-source information system for high-throughput plant phenotyping. *Plant Physiol.* 165, 506–518. doi: 10.1104/pp.113.233932

Knoch, D., Abbadi, A., Grandke, F., Meyer, R. C., Samans, B., Werner, C. R., et al. (2020). Strong temporal dynamics of QTL action on plant growth progression revealed through high-throughput phenotyping in canola. *Plant Biotechnol. J.* 18, 68–82. doi: 10.1111/pbi.13171

Kou, X., Han, W., and Kang, J. (2022). Responses of root system architecture to water stress at multiple levels: A meta-analysis of trials under controlled conditions. *Front. Plant Sci.* 13. doi: 10.3389/fpls.2022.1085409

Langstroff, A., Heuermann, M. C., Stahl, A., and Junker, A. (2022). Opportunities and limits of controlled-environment plant phenotyping for climate response traits. *Theor. Appl. Genet.* 135, 1–16. doi: 10.1007/s00122-021-03892-1

Li, C., Guan, H., Jing, X., Li, Y., Wang, B., Li, Y., et al. (2022c). Genomic insights into historical improvement of heterotic groups during modern hybrid maize breeding. *Nat. Plants* 8, 750–763. doi: 10.1038/s41477-022-01190-2

Li, A., Zhu, L., Xu, W., Liu, L., and Teng, G. (2022a). Recent advances in methods for in *situ* root phenotyping. *PeerJ* 10, e13638. doi: 10.7717/peerj.13638

Lobet, G., Pagès, L., and Draye, X. (2011). A novel image-analysis toolbox enabling quantitative analysis of root system architecture. *Plant Physiol.* 157, 29–39. doi: 10.1104/pp.111.179895

López-Bucio, J., Cruz-Ramírez, A., and Herrera-Estrella, L. (2003). The role of nutrient availability in regulating root architecture. *Curr. Opin. Plant Biol.* 6, 280–287. doi: 10.1016/S1369-5266(03)00035-9

Lozano, Y. M., Aguilar-Trigueros, C. A., Flaig, I. C., and Rillig, M. C. (2020). Root trait responses to drought are more heterogeneous than leaf trait responses. *Funct. Ecol.* 34, 2224–2235. doi: 10.1111/1365-2435.13656

Muraya, M. M., Chu, J., Zhao, Y., Junker, A., Klukas, C., Reif, J. C., et al. (2017). Genetic variation of growth dynamics in maize (*Zea mays* L.) revealed through automated non-invasive phenotyping. *Plant J.* 89, 366–380. doi: 10.1111/tpj.13390

Nagel, K. A., Putz, A., Gilmer, F., Heinz, K., Fischbach, A., Pfeifer, J., et al. (2012). GROWSCREEN-Rhizo is a novel phenotyping robot enabling simultaneous measurements of root and shoot growth for plants grown in soil-filled rhizotrons. *Funct. Plant Biol.* 39, 891. doi: 10.1071/FP12023

Narisetti, N., Henke, M., Seiler, C., Shi, R., Junker, A., Altmann, T., et al. (2019). Semi-automated root image analysis (saRIA). *Sci. Rep.* 9, 19674. doi: 10.1038/s41598-019-55876-3

Neumann, K., Klukas, C., Friedel, S., Rischbeck, P., Chen, D., Entzian, A., et al. (2015). Dissecting spatiotemporal biomass accumulation in barley under different water regimes using high-throughput image analysis: Biomass accumulation in barley. *Plant Cell Environ.* 38, 1980–1996. doi: 10.1111/pce.12516

Orman-Ligeza, B., Morris, E. C., Parizot, B., Lavigne, T., Babé, A., Ligeza, A., et al. (2018). The xerobranching response represses lateral root formation when roots are not in contact with water. *Curr. Biol.* 28, 3165–3173.e5. doi: 10.1016/j.cub.2018.07.074

Orosa-Puente, B., Leftley, N., Von Wangenheim, D., Banda, J., Srivastava, A. K., Hill, K., et al. (2018). Root branching toward water involves posttranslational modification of transcription factor ARF7. *Science* 362, 1407–1410. doi: 10.1126/science.aau3956

Pandey, B. K., Huang, G., Bhosale, R., Hartman, S., Sturrock, C. J., Jose, L., et al. (2021). Plant roots sense soil compaction through restricted ethylene diffusion. *Science* 371, 276–280. doi: 10.1126/science.abf3013

Parsons, W. F. J., Knight, D. H., and Miller, S. L. (1994). Root gap dynamics in lodgepole pine forest: nitrogen transformations in gaps of different size. *Ecol. Appl.* 4, 354–362. doi: 10.2307/1941939

Paschold, A., Marcon, C., Hoecker, N., and Hochholdinger, F. (2010). Molecular dissection of heterosis manifestation during early maize root development. *Theor Appl Genet* 120, 383–388. doi: 10.1007/s00122-009-1082-6

Poorter, H., B Hler, J., van Dusschoten, D., Climent, J., and Postma, J. A. (2012). Pot size matters: a meta-analysis of the effects of rooting volume on plant growth. *Funct Plant Biol* 39, 839–850. doi: 10.1071/FP12049

R Core Team. (2019). *R: A language and environment for statistical computing* Vienna, Austria: R Foundation for Computing.

Ren, W., Zhao, L., Liang, J., Wang, L., Chen, L., Li, P., et al. (2022). Genome-wide dissection of changes in maize root system architecture during modern breeding. *Nat. Plants* 8, 1408–1422. doi: 10.1038/s41477-022-01274-z

Rich, S. M., and Watt, M. (2013). Soil conditions and cereal root system architecture: review and considerations for linking Darwin and Weaver. *J. Exp. Bot.* 64, 1193–1208. doi: 10.1093/jxb/ert043

Rincent, R., Nicolas, S., Bouchet, S., Altmann, T., Brunel, D., Revilla, P., et al. (2014). Dent and Flint maize diversity panels reveal important genetic potential for increasing biomass production. *Theor. Appl. Genet.* 127, 2313–2331. doi: 10.1007/s00122-014-2379-7

Scharr, H., Minervini, M., French, A. P., Klukas, C., Kramer, D. M., Liu, X., et al. (2016). Leaf segmentation in plant phenotyping: a collation study. *Mach. Vision Appl.* 27, 585–606. doi: 10.1007/s00138-015-0737-3

Sharp, R. E., and Davies, W. J. (1979). Solute regulation and growth by roots and shoots of water-stressed maize plants. *Planta* 147, 43–49. doi: 10.1007/BF00384589

Shi, R., Junker, A., Seiler, C., and Altmann, T. (2018). Phenotyping roots in darkness: disturbance-free root imaging with near infrared illumination. *Funct. Plant Biol.* 45, 400–411. doi: 10.1071/FP17262

Su, W., Kamran, M., Xie, J., Meng, X., Han, Q., Liu, T., et al. (2019). Shoot and root traits of summer maize hybrid varieties with higher grain yields and higher nitrogen use efficiency at low nitrogen application rates. *PeerJ* 7, e7294. doi: 10.7717/peerj.7294

Tollenaar, M., Ahmadzadeh, A., and Lee, E. A. (2004). Physiological basis of heterosis for grain yield in maize. *Crop Sci.* 44, 2086–2094. doi: 10.2135/cropsci2004.2086

Tracy, S. R., Nagel, K. A., Postma, J. A., Fassbender, H., Wasson, A., and Watt, M. (2020). Crop improvement from phenotyping roots: highlights reveal expanding opportunities. *Trends Plant Sci.* 25, 105–118. doi: 10.1016/j.tplants.2019.10.015

Trenberth, K. E., Dai, A., van der Schrier, G., Jones, P. D., Barichivich, J., Briffa, K. R., et al. (2014). Global warming and changes in drought. *Nat. Clim. Change* 4, 17–22. doi: 10.1038/nclimate2067

Uga, Y., Sugimoto, K., Ogawa, S., Rane, J., Ishitani, M., Hara, N., et al. (2013). Control of root system architecture by DEEPER ROOTING 1 increases rice yield under drought conditions. *Nat. Genet.* 45, 1097–1102. doi: 10.1038/ng.2725

van Dijk, P. J., Rigola, D., and Schauer, S. E. (2016). Plant breeding: surprisingly, less sex is better. *Curr. Biol.* 26, R122–R124. doi: 10.1016/j.cub.2015.12.010

von Wangenheim, D., Banda, J., Schmitz, A., Boland, J., Bishopp, A., Maizel, A., et al. (2020). Early developmental plasticity of lateral roots in response to asymmetric water availability. *Nat. Plants* 6, 73–77. doi: 10.1038/s41477-019-0580-z

Walter, A., Liebisch, F., and Hund, A. (2015). Plant phenotyping: from bean weighing to image analysis. *Plant Methods* 11, 14. doi: 10.1186/s13007-015-0056-8

Wang, H., Qin, J., Hu, Y., and Guo, C. (2023). Asymmetric growth of belowground and aboveground tree organs and their architectural relationships: a review. *Can. J. For. Res.* 53, 315–327. doi: 10.1139/cjfr-2022-0216

Wu, X., Feng, H., Wu, D., Yan, S., Zhang, P., Wang, W., et al. (2021). Using high-throughput multiple optical phenotyping to decipher the genetic architecture of maize drought tolerance. *Genome Biol.* 22, 185. doi: 10.1186/s13059-021-02377-0

Xu, W., Cui, K., Xu, A., Nie, L., Huang, J., and Peng, S. (2015). Drought stress condition increases root to shoot ratio via alteration of carbohydrate partitioning and enzymatic activity in rice seedlings. *Acta Physiol. Plant* 37, 9. doi: 10.1007/s11738-014-1760-0

Zhou, Z., Zhang, C., Lu, X., Wang, L., Hao, Z., Li, M., et al. (2018). Dissecting the genetic basis underlying combining ability of plant height related traits in maize. *Front. Plant Sci.* 9. doi: 10.3389/fpls.2018.01117

frontiers | Frontiers in Plant Science

TYPE Policy and Practice Reviews
PUBLISHED 04 September 2023
DOI 10.3389/fpls.2023.1235175

OPEN ACCESS

EDITED BY
Salvatore Ceccarelli,
Bioversity International (Italy), Italy

REVIEWED BY
Micaela Colley,
Organic Seed Alliance, United States
Stuart Smyth,
University of Saskatchewan, Canada

*CORRESPONDENCE
Maria Gerullis
mkg66@cornell.edu

RECEIVED 05 June 2023
ACCEPTED 07 August 2023
PUBLISHED 04 September 2023

CITATION
Gerullis M, Pieruschka R, Fahrner S, Hartl L, Schurr U and Heckelei T (2023) From genes to policy: mission-oriented governance of plant-breeding research and technologies.
Front. Plant Sci. 14:1235175.
doi: 10.3389/fpls.2023.1235175

From genes to policy: mission-oriented governance of plant-breeding research and technologies

Maria Gerullis[1,2*], Roland Pieruschka[3], Sven Fahrner[3], Lorenz Hartl[4], Ulrich Schurr[3] and Thomas Heckelei[2]

[1]Dyson School of Applied Economics and Management, Cornell University, Ithaca, NY, United States, [2]Institute for Food and Resource Economics, University of Bonn, Bonn, Germany, [3]Plant Sciences, Institute of Bio- and Geosciences 2, Jülich Research Centre, Jülich, Germany, [4]Wheat and Oat Breeding Research, Institute for Crop Science and Plant Breeding, Bavarian State Research Center for Agriculture, Freising, Germany

Mission-oriented governance of research focuses on inspirational, yet attainable goals and targets the sustainable development goals through innovation pathways. We disentangle its implications for plant breeding research and thus impacting the sustainability transformation of agricultural systems, as it requires improved crop varieties and management practices. Speedy success in plant breeding is vital to lower the use of chemical fertilizers and pesticides, increase crop resilience to climate stresses and reduce postharvest losses. A key question is how this success may come about? So far plant breeding research has ignored wider social systems feedbacks, but governance also failed to deliver a set of systemic breeding goals providing directionality and organization to research policy of the same. To address these challenges, we propose a heuristic illustrating the core elements needed for governing plant breeding research: Genetics, Environment, Management and Social system (GxExMxS) are the core elements for defining directions for future breeding. We illustrate this based on historic cases in context of current developments in plant phenotyping technologies and derive implications for governing research infrastructures and breeding programs. As part of mission-oriented governance we deem long-term investments into human resources and experimental set-ups for agricultural systems necessary to ensure a symbiotic relationship for private and public breeding actors and recommend fostering collaboration between social and natural sciences for working towards transdisciplinary collaboration.

KEYWORDS

research policy, governance, sustainability goals, plant phenotyping, automated phenotyping technologies

1 Introduction

With Horizon Europe there is a €95.5 billion program fostering mission-oriented research and innovation in Europe (Mazzucato, 2019), entailing a new approach to research and its governance aiming to achieving the sustainable development goals (SDGs; Mazzucato, 2018). Mission orientation calls for a changed role of state and public organizations. Public organizations are supposed to act entrepreneurial, meaning they need to actively set innovation pathways and create markets, instead of only intervening in failed markets (Mazzucato, 2013). This implies a change in governance of research centered around specific, inspirational, yet, attainable goals, called missions (Mazzucato, 2018). Similar to the Apollo mission, putting a man on the moon, mission-oriented governance in Europe sets out with missions on, for example, climate-resilient regions (DGRI (Directorate General Research and Innovation), 2020b), beating cancer (DGRI (Directorate General Research and Innovation), 2020c), or healthy soils (DGRI (Directorate General Research and Innovation), 2020a). Mission goals need to be supported and brought about aided by appropriately governed research and innovation activities. We call these new efforts of governance 'mission-oriented governance'. The different mission goals are developed such that they prioritize those systemic transformations with the best leverage towards reaching the SDGs (Sachs et al., 2019).

Achieving SDGs, demands that systemic transformation occurs in (1) education, gender, and inequality; (2) health, well-being, and demography; (3) energy decarbonization and sustainable industry; (4) sustainable food, land, water, and oceans; (5) sustainable cities and communities; and (6) digital revolution for sustainable development (Sachs et al., 2019). The agricultural sector is touched by all of these transformations: Be it through land-use efficiency, developing more productive plants, reducing food waste, impacts of unequal supply of education in rural areas, or applications of biotechnology in medicine amongst many others. Mission-orientated governance aims to facilitate these transformations from current agricultural production into sustainable agricultural systems (Sachs et al., 2019).

Core to sustainable agriculture is plants with improved properties and management practices allowing circularity and decoupling negative impacts (Pretty, 2018; Sachs et al., 2019). Currently plant production and breeding focus on increased yields, which needs to be extended to include other sustainability aspects, such as lower use of chemical fertilizers and pesticides, crop resilience to climate stress, and reduced postharvest losses (Qaim, 2020). Hence, plant breeding needs to provide the scaffold for efficient use of resources like water, nutrients, and minimization of pollutants in plant production. Targeted improvements of plants through plant breeding, however, are bound by evolving social and technological systems in research accelerating plant breeding.

Our objective is to propose a governance heuristic illustrating core elements needed for governing plant breeding research, such that its mission-oriented governance can achieve overall sustainability goals. Genetics (G), environment (E), management (M), and social system feedbacks (S) influence plant breeding outcomes. Symbolized by GxExMxS (as governance heuristic) we motivate, that holistic and systemic considerations need enter the creation of mission-oriented policy targets for plant improvements.

Yet, mission-oriented governance of agriculture creates a tension between how economists traditionally give policy advice on research and innovations in agriculture – with the state as intervening in failing markets (Alston and Pardey, 1996) - and a kind of governance centering around actively creating pathways of innovation. Hence, policy advice on mission-oriented governance focuses on a) directionality, b) dynamic evaluation, c) organization, and d) risk-and-reward sharing amongst public and private actors (Mazzucato, 2016). Directionality addresses how one may pick concrete targets and evaluation measures of effectiveness, which are broad enough to not stymie bottom-up exploration, discovery, and learning of involved actors within breeding contexts. Organizational challenges are related to building research infrastructures (RIs) advancing plant breeding providing sufficient absorptive capacity and long-run patience for high-risk undertakings, yet remain agile and innovative from within. This entails tackling how one can foster risk-and-reward sharing amongst public and private actors when RIs promise overall benefits. We adopt this approach in the following for research policy advice on mission-oriented governance of new approaches and technologies for phenotyping.

Phenotyping is the current bottleneck in developing advanced quantitative approaches to breeding needed for successfully creating improved crops (Pieruschka and Schurr, 2019). Developing ways for non-invasive high-throughput phenotyping and quantitative analytics is necessary for developing these new processes and tools for creating sustainable plant attributes. The European research infrastructure on plant phenotyping (EMPHASIS), currently being implemented, provides services like access to plant phenotyping facilities, competencies and data. Since 2002 the European Strategy Forum on Research Infrastructures (ESFRI) put forward the establishment of RIs integrated across Europe. RIs are public organizations that are supposed to provide access and other services to physical and virtual infrastructures for researchers across the EU (e.g. experimental facilities, biological samples, scientific data) and integrate national towards pan-European and global efforts (ESFRI (European Strategy Forum on Research Infrastructures), 2021). The RIs can develop their pan-European strategies towards providing research services and adapting RIs' governance such that SDGs can be met in long-term. Accordingly, mission-oriented governance of plant breeding research – private and public - is supposed to support and bring forward breakthroughs in plant breeding research, and the EMPHASIS RI will be a vital part in implementing this strategy.

In the following, we first introduce the 'nuts and bolts of plant breeding (section 2.1), then introduce what we mean by sustainability for agricultural systems (section 2.2) and how plant breeding in the past promoted and failed in achieving these goals. We highlight historic cases illustrating how genetics (G), environment (E), management (M), and social system (S) influenced plant breeding outcomes in the past (section 2). Symbolized by GxExMxS we motivate, that holistic and systemic considerations need enter the creation of mission-oriented policy targets for plant improvements (section 3). Then we introduce new

modes and technologies of phenotyping, which will change and accelerate plant breeding processes (section 4.1). We discuss related economic implications for variety development in governing individual breeding programs (section 5.1) and point at potential challenges and bottlenecks in reaching sustainability goals (section 5.2). We then illustrate what mission-orientation under the premise of sustainability means for the governance of RIs developing phenotyping technologies and potential threats to their effectiveness (section 5.3 and 5.4) before concluding.

2 From genes to institutions – history and governance of plant breeding towards sustainability

In the following, we first describe basic terms for plant breeding. Then we illustrate the role plant breeding plays for the sustainability of societies and how we use the term sustainability for this paper. We then illustrate with historic cases what role phenotyping played in plant breeding and how modern advances in phenotyping technologies evolved from past challenges in sustaining societies.

2.1 Key terms in plant breeding

Phenotyping is observing the appearance of a plant and evaluating its products (Fiorani and Schurr, 2013). It is vital for plant breeding being concerned with selecting amongst different candidates those variants of plants showing superior attributes, also called traits (Becker, 2011). Breeding processes usually aim at a dedicated breeding target, a combination of superior attributes. Breeding targets are for example improving yield, resistance to pathogens, or having a certain quality, such as baking qualities. All observable measures, as they appear in a plant, are termed phenotype. The phenotype, however, is connected to the genotype.

A genotype is the genetic material of an organism and hence carries the hereditary information recorded in the organism's genome. Changes in the genotype lead to changes in the plant's phenotype dynamically interacting with its environment (Pieruschka and Schurr, 2019). Breeders usually denote this relationship between genotype (G) and phenotype (P) by using the formula P=GxExM with E for environment and M for the management of the plant. In practice plant scientists measure phenotypic traits under different conditions of environment and management (ExM) and connect these insights to the genetic makeup of the plant (G) (Becker, 2011). Plant scientists are usually more interested in how functional properties (like photosynthesis, transpiration, nutrient uptake) or structural properties (like shoot and root architecture, leaf size) of the plant are affected by the environment.

When looking at the genetic setup, bringing about phenotypes, researchers usually discern traits into complex (quantitative) and simple (qualitative) ones (Acquaah, 2007). Flowering time is an example of a simple trait, determined only by a few genes. Whereas, nutrient uptake or yield signify complex genetic traits being spread out over multiple loci on the genome. Plant phenotyping is particularly important to quantify the diversity of phenotypic traits and understand in which social and ecological contexts which genetic setup translates to which phenotypes.

Yield exemplifies how the different actors in the breeding system all have different perceptions and understanding of complex traits. Basic research in biology and plant science contributes to improving yield, by looking at the multitude of plant physiological traits influencing yield. For example, scientists try to understand how photosynthesis works in C3 compared to C4 plants telling us the range of yield in- or decrease in crops reacting to increased levels in CO2 in the atmosphere (Kebeish et al., 2007). These insights serve as theoretic background for pre-breeders.

Pre-breeders make some of these insights from basic research utilizable for breeding. They transfer knowledge about how single plants work to small populations of crops or introduce new genetic resources, for example from wild relatives to more adapted breeding material. They breed crops having advantageous new traits and bring about a yield level comparable to adapted varieties of a specific pedo-climatic region. Varieties are groups of homogenous, distinguishable plants of the same crop (Becker, 2011). Introducing new traits to a gene pool of already adapted varieties demands a lot of effort in pre-breeding (Gerullis et al., 2021). It is usually undertaken by partnerships between academia and industry (Moore, 2015; Gerullis et al., 2021). Figure 1 shows the different steps of breeding and pre-breeding. Pre-breeders usually focus on selecting for those plants containing targeted traits into a better adapted genetic background with higher yields. This process usually takes years in practice (Gerullis et al., 2021), as complex traits need specific combinations of genes, being spread over the genome, whilst crossing-in new traits abates these efforts. Once new traits have entered an adapted gene pool, applied breeders can take these materials and cross them in with their breeding material (Figure 1 box 1, 5 to 7). They create new varieties containing these new traits, aiming for best performance of all other important traits (higher average yields and qualities) by even better adapting these to a specific region. While applied breeders still include grain yield, seed weight, and resistances when they refer to yield, multipliers and farmers usually talk about yield in terms of tons per hectare.

Developing genetic markers for different traits necessitates characterizing genetic diversity (Figure 1 box 1). Phenotyping provides here the necessary information to correlate genetic information with observations on how these genotypes perform under different environmental and management conditions, and how well different traits are inherited (Figure 1 box 2 to 4). Phenotyping is basis for developing of molecular markers and genomics-based selection (Cooper et al., 2014). Automated systems in laboratory and field promise an increase in speed and precision in generating data and thereby accelerating pre-breeding and breeding processes.

Breeding outputs, namely varieties with improved properties, usually focus on improving yields, but also include other qualities, such as flowering colors, baking qualities, resistances to pests, nutrient content, or edibility. These are important to the remaining supply chain of agricultural and other plant-based products. It can take a decade or more to make a new variety of a crop. (Becker, 2011)

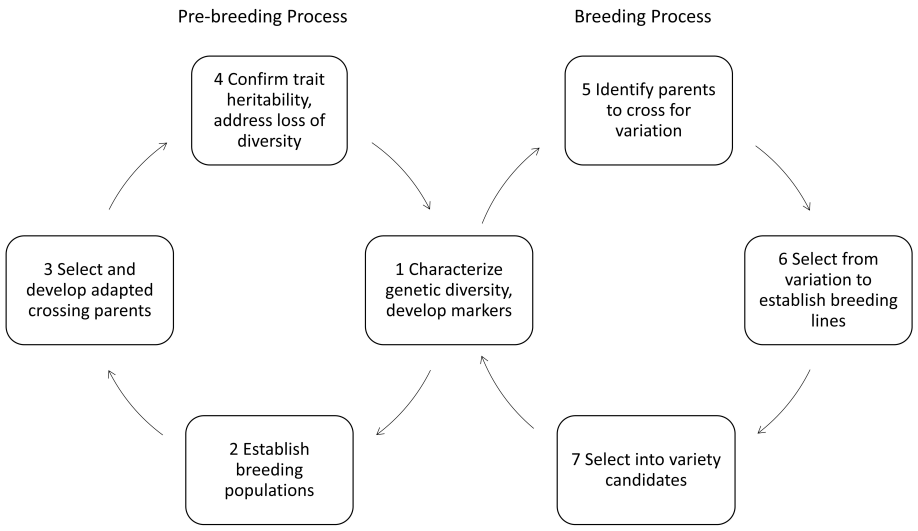

FIGURE 1
Pre-breeding and breeding processes adopted and extended from Watt et al. (2020).

Plant breeding maintains and increases global productivity in agricultural products, see Laidig et al. (2017) for the contribution of breeding progress to yields and qualities in German winter wheat. Due to changes in the environment, breeders need to constantly adapt to changing conditions, and therefore maintaining the same yield level facing ever-changing pests can already be considered an improvement (see Olmstead and Rhode, 2008). Yet, as we are going to see in the following plants' efficiency in resource use, their attributes in nutrient cycling and the systemic position cropping takes within the agricultural system determines how sustainable the overall system will be.

2.2 Sustainability by plant breeding?

In this section, we define what we mean by sustainable agricultural systems to clarify towards which goals we are heading, if we transform agriculture with mission-oriented governance. For this paper sustainability means that we can ensure the survival and thriving of humanity over an infinite time horizon. Doing so means living within the ecological boundaries of our planet (Rockström et al., 2009) while providing the social means to do so for all – as laid out by the SDGs (Raworth, 2017). Sustainable agricultural systems are social-ecological-technical systems (McGinnis and Ostrom, 2014) in which social, ecological, and technical processes produce food and fiber for the nourishment and fulfillment of the needs of humanity, while staying within the ecological boundaries of our planet (Rockström et al., 2017).

Sustainability of agricultural practices is in question if the current performance cannot be kept up in the long term. Some farming practices may lead to decreasing yields over shorter or longer periods and are as such intrinsically unsustainable. Whereas some are easily recognized in a short time (e.g. onion monoculture, Aragona and Orr, 2011) others involving soil erosion or accumulating salt may not be recognized by the individual farmer (see ancient Mesopotamian agriculture in Jacobsen and Adams, 1958; Gibson, 1974). Additionally, farming practices relying on resources that are not replenished as fast as they are being used are also non-sustainable. Phosphorus use for fertilizer or water use for irrigation are examples of it. The task of breeding in this context is to provide varieties that allow those agricultural systems avoiding such unsustainable practices.

Whether changes of traits by breeding are an 'improvement' depends on the boundaries of and the specific social-ecological context of the system considered. For example, if we breed plants for a cropping system with higher input of phosphorus, then this has implications not only for crop management but the whole supply chain of inputs related to it. Higher yields may directly impact the nutritional and income status of those growing the crops, yet phosphorus may need to be mined and economic and social conditions of those handling the resource on its way to the farm are impacted (Yiin et al., 2016; Nesme et al., 2018). If we, however, breed new traits into crops to use the phosphorous in the ground more effectively and have a lower phosphate extraction rate (van de Wiel et al., 2016), maybe some transportation of resources around the globe can be saved and additional extraction activities need not take place (Schipanski and Bennett, 2012). As we can see from this example, what to consider and how different changes in varieties affect sustainability depends on the context.

The overall direction of breeding goals for future cropping systems should consider context-specific resource-use efficiency, stability, or more generally, sustainability of farm and food system outcomes. Improving the ratio of relevant output to resources used such as land, water, energy, biodiversity, and other environmental pressures.

The adoption of high-yielding crops by farmers challenges plant breeders when it comes to incorporating other beneficial traits into their breeding programs. Farmers predominantly adopting crops with high potential yield (Lassoued and Smyth, 2023) favors varieties that promise just this at the expense of other

characteristics like resistance to pathogens. Plant breeders face the dilemma of balancing expected yield enhancement with incorporating traits such as disease resistance, or other qualities (Gerullis et al., 2021). Incorporating new traits into breeding programs may initially lead to lower yields compared to 'elite' varieties, and yields have to be regained for example through backcrossing. This prolongs the breeding process and increases cost. Consequently, breeders must find innovative ways to address these challenges, striving to strike a balance between high yield potential and other traits, ensuring the long-term resilience and sustainability of agricultural systemsCrop traits shape crop production and we need to give plant breeding proper consideration in its role towards achieving the mission targets ahead. Hence, we point at new directions that may open up with new technologies and approaches to phenotyping in breeding research to navigate towards the SDGs more effectively. Yet, phenotyping technologies will not solve all challenges in bringing about sustainability and should not be treated as a panacea, as we elaborate in the following section.

2.3 Origins of phenotyping - or how to adapt genes to fit environmental conditions

Early forms of phenotyping were already employed in the rudimentary forms of plant breeding appearing when sedentism emerged. Having domesticated plants meant a vital step towards sustaining large-scale societies where agriculture serves using and bundling energy – sunlight – such that human societies can use it for better survival and thriving (Bätzing, 2020). As crops pose very specific demands on climate, soils, pathogens to survive, it is decisive to know which crop functions well in which environment to reliably secure nutrition and allow humans to pursue other purposes. Domesticating wild plant species into early crops through plain eye-sight, intuitive judgment and trial and error was thereby a form of mending the first plant-based biological technologies[1] (Maisels, 1993; Becker, 2011).

Aggregating plants, through mass selection into landraces, can be counted as a process of cultural learning (Henrich and McElreath, 2003). Adapting plants, like the wild relatives of cereals, throughout domestication to the pedo-climatic conditions of the Fertile Crescent (Maisels, 1993; Brown et al., 2009), is a process of cumulative cultural evolution (Henrich and McElreath, 2003). The most important information of these early days of agriculture was enclosed in the genetic information of saved seed and could be propagated to the next generation by simple mass selection (Purugganan and Fuller, 2009). The accumulation of advantageous traits took several intermediate stages before certain crops were prominent over wider regions (Brown et al., 2009; Smith et al., 2019).

2.3.1 The advent of scientific plant breeding

The advent of scientific plant breeding in the late 19th century stimulated more targeted breeding practices compared to the formerly used mass selection (Kloppenburg, 2004; Harwood, 2015). Breeders started to incorporate experimental designs (Mendel, 1866; Wieland, 2004). They generated scientific insights on-farm management and included the first mental models of the influences of genes on farm outputs (Brandl and Glenna, 2017). Breeders selected for more homogenous plant types (Kloppenburg, 2004; Wieland, 2004) and adopted more explicit and precise approaches to the underlying causalities assumed between plant physiological traits and farm outputs. They developed different forms of breeding and introduced the concepts of varieties, as uniform and stably performing groups of plants outperforming landraces in their yield by far (Becker, 2011). Meanwhile, crop genetic diversity reduced in richness (van de Wouw et al., 2010).

Approaching the management of crops with scientific methods emerged together with the different disciplines within the agricultural sciences (Wieland, 2004). They targeted higher yields by adding synthetic fertilizer and crop protection agents tested with experimental designs. Aiming for control of the natural environment in fields, by suppressing pathogens and weeds (Wieland, 2004). Coinciding, use of machinery increased, labor intensity decreased and productivity of western agricultural systems increased immensely (Olmstead and Rhode, 2008; Pardey et al., 2010). These scientific developments meant adding "M" to the basic formula of breeding, GxExM. This evolution in the agricultural sciences invoked the impression that the impact of the environment "E" was controllable by management practices (Wieland, 2004). Yet, pests constantly diminished the gains just realized by more targeted breeding (Olmstead and Rhode, 2008).

Discovering semi-dwarfed varieties, capable of producing comparatively higher yields, denoted a breakthrough in plant breeding (Pingali, 2012). Scientists, like Norman Borlaug, were capable of reversing a trait (long stems in cereals) brought about by natural selection in crops (Denison, 2012). Instead of further fueling individual competition between plants, dwarfing genes lead to plants putting their energy in higher grain yields and low stems, producing even greater outputs if fertilized (Denison, 2012). Developments in breeding went hand in hand with farm management advancements.

2.3.2 Genotyping and biotechnology – answers to the pest problem?

Genotyping technologies invented in the 1980s allowed a deeper look into the genome. Breeders and pre-breeding scientists use these technologies to associate specific phenotypic traits, like a certain degree of susceptibility to a pathogen, with different mostly simple traits in the genome of crops (Eathington et al., 2007). Several genotyping techniques have been invented over the last two decades and have dramatically improved in terms of cost, speed, and accuracy for detecting correlations amongst gene loci and their phenotypic performance in different environments. While modern genotyping technologies permit to find those places in massive amounts of genetic data which bring about complex traits, limited data in phenotypes across different environments is available and

1 The same is also true for the even earlier domestication of animal species.

hinders scientists to leverage their full potential. The data limitation in phenotypic information poses a bottleneck to advancing insight on how different genotypes perform in different environments (Fiorani and Schurr, 2013; Pieruschka and Schurr, 2019).

Explicitly taking genetic information into account for breeding opened up possibilities for modification. Pairing chemical mechanisms of pesticides with plant physiological traits, rooted in genetic modification (GM), was used to fight pests. Herbicide tolerance means that GM plants will survive a broad-spectrum herbicide where other weeds die (Kishore et al., 1992). Insect resistances for example induced through parts of Bacillus thuringiensis (Bt) genes lead to plants producing insecticidal proteins (Ranjekar et al., 2003). Yet, these alleged solutions to pressing pests are in vain from an evolutionary perspective, as the mechanisms employed to fend off pests are overcome by evolved resistances against these (Tabashnik, 2008; Carroll et al., 2014).

Denison et al. (2003) states that we merely enter an arms race between host plants and pests, but not resolving underlying problems. These cases of GMs[2] represent low-hanging fruit in genetic modification and may even be misdirected in how they approach agricultural systems as a whole in face of natural selection. What seems successful at first produces no long-lasting improvements of agricultural systems. Natural selection caught up with human inventions, as these traits were used in big monocultural setups and pathogens had plenty of room for developing resistances to the employed chemical mechanisms (Denison, 2012; Søgaard Jørgensen et al., 2020). Consequently, the targeted plant protection starts to fail (Gassmann et al., 2011; see Tabashnik and Carrière, 2017 for an overview). In these cases, GMs add nothing new than what the application of pesticides and the co-evolving resistant weeds already did in conventional agriculture (Varah et al., 2020).

From an evolutionary perspective, Denison (2012) argues that humans are less likely to improve on those traits natural selection has been optimizing for millennia, but chances for improvement lie in redirecting natural selection. As plants face trade-offs in how they use their energy, some traits, stemming from increases in individual plant fitness, but unnecessary to human use, can be reversed for improvements towards human needs. Denison (2012) puts forward that for pests, there is no way of winning at the individual level, as plants and pathogens have been in these co-evolutionary cycles for long enough that natural selection developed plenty of strategies implemented in individual organisms to circumvent them. We can only hope to prolong a cycle in the arms race long enough to come up with new ideas of adaptation.

There is, however, a set of strategies aimed at changing agricultural practices on a collective level. When looking at pests from the perspective of an ecosystem, another set of possibilities opens up. Interrupting a pathogens propagation mechanism, for example by eradicating intermediate hosts (Olmstead and Rhode, 2002) as done with mulberries to eradicate black rust in wheat. These strategies alter a crop's environment on a higher level. Strategies like these cannot be considered a mere change in management practices of an individual farmer, as they involve targeted collective action by farmers, extension services, and other interest groups on landscape level. The entailed social dilemmas, where incentive structures for individual costs and collective benefits diverge, can be quite complex, but have been achieved before with successful governance– see Olmstead and Rhode (2008) for more examples of historic accounts from the United States.

The principles and elements of agroecology as suggested by the FAO (FAO, 2018) target integration of social and ecological aspects for design and management of agricultural systems at a higher level (ecosystem level). Yet, Denison (2012) warns of false mimicry of whole ecosystems as it may lead to suboptimal outcomes compared to competitively tested systems. Competitive selection pressures of natural selection are not as effective on ecosystem level, as they are on individual (plant) level, as ecosystems usually do not compete for space against each other, opposed to individuals in ecosystems (Denison, 2012). Pest management is such an example, as any pest management strategy is counteracted by individual adaptations of pests. Yet, within an agroecosystem with homogenous conditions where a single strategy is being scaled up, pests are going to have an easier time for counteraction. Hence pest management strategies that employ diversity as a principle, for example refugia or crop mixtures with susceptible plants (Mallet and Porter, 1992; Tabashnik, 1994), need to be considered.

Independent of detailed strategies in governing agricultural practices, pest management is a good example to show, that aside of the fit between genetics, biological environment, and direct farm management practices, the social system and its governance on a higher-level needs consideration when developing targets for innovations in breeding. This will allow for achieving relevant individual and whole system-level outcomes (Carroll et al., 2014).

3 A governance heuristic for sustainability in plant breeding

Successful breeding demands very high R&D costs, which led to considerable concentration of firms in commercial seed markets (Deconinck, 2020) and the need for wise decision making in how and where public spending is directed. We can learn three things from the cases presented: One, not all traits are created with equal ease. We need to account for this in policy such that hard-to-get traits are developed by public monies, as private actors may be more likely to produce the low-hanging fruits. Two, the direction of genetic development is not open towards all possibilities. We need to account for what traits have been brought about by natural selection and where there is still room for development towards human needs. Three, the pest management examples highlighted above show that interactions of social-ecological dynamics lead to co-evolutionary cycles influencing cropping long-term. Short-term successes must not be overrated, as second-order effects on collective level may turn out to hamper overall systemic performance. We may

2 Usually termed as first generation GMOs, not to be confused with second generation GMOs who were altered for farming output traits like nutrient profiles of plants or third generation GMOs used for medical uses like insulin production.

need to find ways of slowing down arms races on wider systemic levels to have enough time for developing new adaptions.

While words like "social system" or "governance" may strike plant breeders and most crop scientists as a vague notion irrelevant to their work, we want to prevent exactly that and add an "S" for social system to the mental model of breeding and create a new heuristic for plant breeding governance:

GxExMxS

As explained, cropping outcomes rely on interaction of genetics (G), biological environment (E), directly applied management practices (M), and influences from the collective level implemented through governing the social system. Comparable to ecological environments higher-level social systems are complex in themselves. They are usually being structured by institutions (Ostrom, 2006) and entail all prescriptions bringing about individual-level behavioral patterns – usually subcategorized in rules, norms, and strategies, opposed to the laymen notion of an institution being an organization like a ministry. The management practices pointed out above are classical examples of strategies – describing what activities specific actors (e.g. farmers) perform. Norms and rules are usually brought about by different forms of governance systems, like cooperation organizations, lobby groups, or law-making bodies; they specify the conditions and sanctioning mechanisms under which individual strategies may or must (not) be enacted. Incentive alignment between individual strategies and the rules and norms brought about by the governance systems on all scales is key to structuring future breeding and farming systems.

We suggest the GxExMxS formula, see Table 1, as a governance heuristic to those people in policy advice and governance specific to plant breeding contexts. It should serve as a gentle reminder of not putting considerations of collective level activities in agricultural systems aside too quickly. For example, when EU project funds are being granted to researchers, funders should have some notion how activities scale up as this will influence the effectiveness of implementing innovations from plant breeding. Meanwhile, we want to encourage economists, who are traditionally good at considering markets and other institutions of governance, to more explicitly include notions of interactions between genetics and environment together with individual management and system-level outcomes.

4 Phenotyping technologies

In the following section, we define and introduce automated phenotyping technologies and delineate underlying scarcities these breeding technologies may alleviate and point out bottlenecks they may bring about.

4.1 Overview of technologies in early research and development stages

Non-invasive high-throughput phenotyping technologies measure plant growth, structure, and composition with a specific precision in an automated manner, without destroying organs or canopy of the observed plant (Fiorani and Schurr, 2013). Being non-invasive, the new technologies enable observing plant traits without interrupting plant growth. Basic sensors and data processing may also be employed in farming, but plant breeding and pre-breeding pose different demands on these technologies, as they need to process smaller batches and have more heterogeneous tasks to fulfill (Watt et al., 2020). Sensor-based vision goes beyond the spectrum visible to humans' eyes and even below ground, making it possible to observe new traits, only passively accounted for in breeding so far.

Researchers involved in breeding encounter scarcities in phenotypic data due to limited time and person-power. Precision and depth of data are usually an issue in collecting phenotypic data, depending on the physiological plant traits or farming outputs researchers are looking for. For example, daily images of the same plants throughout their growth period can be interlinked mathematically with genotypic information and daily climate data, for inferring how different genotypes may react to various weather conditions. Usually, multiple people need to score these attributes, by hand and eye inspection, while the source of data changes, once the person leaves the field, as plants continue growing. Main advantages of the new technologies are that one can see more, see faster, more precisely and there is no primary data loss.

For plant scientists there is a plethora of automated phenotyping technologies in different stages of development. Table 2 presents an overview of the heterogeneity of phenotyping systems available for (pre)-breeding. All breeders must have some form of implicit or explicit notion about what and how inputs and efforts connect with their (pre)-breeding outputs, called mental models (Kieras and Bovair, 1984). Depending on their technical possibilities for inquiry, breeders use a variety of physical infrastructures for phenotyping: a) controlled conditions, like greenhouses or climate chambers, used alongside b) lean fields using minimal phenotyping equipment, like drones or robots or c) intensive fields using highly equipped for monitoring plants and environments. All physical infrastructure is complemented with d) information systems and e) modeling tools for processing sensor data.

TABLE 1 Governance heuristic for plant breeding research.

Definitions of GxExMxS	
G	"Genetics" – stands for changes on genetic/plant level.
E	"Environment" – denotes biotic (e.g. pathogens) and abiotic (e.g. soil and climate) environment of an agricultural system. It means those parts of the biophysical surroundings of locations where agricultural production or breeding takes place.
M	"Management" – means those activities undertaken by actors directly influencing plant growth in fields and controlled environments.
S	"Social" – implies the wider social system influencing management activities from the collective level but also co-evolving with the wider biophysical environment.

TABLE 2 Overview of phenotyping technology types.

Infrastructure category	Object of interest	Basic characteristics	Operational modes	Limitations/ challenges	Examples
Mental Model	Design of experiment	Denotes the functional and heuristic connections between breeding inputs and outputs	Present in all forms of breeding and pre-breeding practice: Implicit knowledge Explicit knowledge	Bound by computational capacity and information storage	• Breeder's eye • Experimental designs and idea funnel
Controlled Conditions	Mostly single plants in pots (up to containers)	• Plant growth: plants are grown in growth chambers, greenhouse • Environment: well controlled environment • Capacity: 100-1000s plans per experiment • Experimental duration: days to weeks	Quantitative plant measurement using: Carrier system for plants PtS • Conveyor belts • Robotic systems Carrier system for sensors StP • Gantry systems Sensor: • Optical sensors (visible light (RGB), near infrared, multispectral, hyperspectral, thermal, fluorescence imaging, tomographic systems)	Often only small to medium sized plants possible	• WIWAM xy; • GrowScreen-Rhizo-1 • Phenotron Lemnatec
Intensive Field	Canopies in plots	• Plant growth: micro-plots usually in natural soil • Environment: Environmental monitoring (Semi-controlled conditions) • Capacity: 100-1000s plots per experiment • Experimental duration: Usually a growth season	Quantitative plant measurements: Carrier systems for sensors: • Fixed (e.g. towers, gantry systems) • Ground based mobile (e.g. phenomobiles) • Airborne mobile (e.g. drones) Sensors: • Optical sensors (visible light (RGB), near infrared, multispectral, hyperspectral, thermal, fluorescence imaging,)	Heterogeneous environment	• Breed-FACE • Pheno3C • Field Scanalyzer Rothamsted
Lean Field	Canopies in plots	• Plant growth: micro-plots usually in natural soil • Environment: Basic environmental monitoring • Capacity: 100s – 1000s of microplots multiple field sites • Experimental duration: Usually one or more growth seasons	Quantitative plant measurements Sensor carrier: • Ground based mobile (e.g. phenomobiles) • Airborne mobile (e.g. drones) Sensors: • Optical sensors (visible light (RGB), near infrared, multispectral, hyperspectral, thermal, fluorescence imaging,)	Heterogeneous environment	• Projects with networks of field trials (DROPS)
Modelling	Plants in silico (= virtual representation of phenotypes under different conditions)	• Virtual tools: –integrated in phenotyping pipelines (experimental design, image analysis) –interfacing with phenotyping pipelines (develop, validate in silico models)	In silico plant modelling • Process based models (e.g. simulate growth) • Functional structural plant models (e.g. plant architecture and physiology) • Statistical models • Models in phenotyping pipelines (e.g. trait quantification, dissection)	Need for experimental data	• Collection of models: https://www.quantitative-plant.org/
Phenotyping Information Systems	Data (all kinds of data, images and outcome measures)	• methods and interfaces for interoperability of datasets • manage, share, reuse and visualize heterogeneous, high-throughput plant phenotyping data stemming from different sources	Local information systems • Data base as part of a physical infrastructure for storage, visualisation data etc. • Data integration and reusability standardisation (data models, metadata)	Implementation of standards	• Data standards: MIAPPE (https://www.miappe.org/) BrAPI (https://brapi.org/)

Source: based on Morisse et al. (2018) for updated list of examples from EU Infrastructure for plant phenotyping – EMPHASIS - see https://emphasis.plant-phenotyping.eu/phenotyping-landscape/infrastructure-map.

4.2 Controlled environments and enhanced vision traits

Controlled environments, in greenhouses and climate chambers, serve to investigate genetic variability in measured plant traits as a response to well-defined environmental conditions (Table 2). Researchers and breeders need to know the functional connection of how individual genes interact with each other as part of a plant and their environments. Most platforms can phenotype shoots throughout their growth period observing plant response when simulating biotic and/or abiotic environments, like temperature, water, nutrient availability, pathogens, etc. (example: PhenoTron in Table 2).

Predominantly for controlled conditions the platform upon which the sensor system is mounted is fixed and plants are automatically moved to sensors creating observations (Table 2; Yang et al., 2020). Yet, there are also large installations where plants grow in fixed carriers and are being moved towards sensor systems – e.g., GrowScreen-Rhizo 1 (Nagel et al., 2012). Sensor systems are usually defined by noninvasive imaging measuring time series of dynamic processes such as plant growth. Depending on the trait of interest an entire electromagnetic spectrum can be used for different modes of imaging (Fiorani et al., 2012) usually in fully or semi-automated systems. With the current state of the art, most installations can process plants only until a certain stage in their growth – or only smaller crops and some platforms only permit to scan single plants, which decreases speed of inspection (Fiorani and Schurr, 2013).

Some platforms are capable of phenotyping roots below ground. While breeders have inspected above ground for thousands of years, to judge a plant's quality, seeing it below ground opens up new possibilities to research. Now breeders can select for below-ground traits in a targeted manner. There are a few success stories demonstrating targeted selection of root traits (Watt et al., 2020). Being able to observe root setup without destroying them or their soil habitat over the growth period in an automated manner allows for data improving the speed in selection for root traits. This is essential for traits like water or nutrient use efficiency. These observations allow disentangling the role of root structures and their functional properties such as uptake of nutrients, biotic interactions within the rhizosphere (Watt et al., 2006). This brings about insights on genotype-to-phenotype relationships including those related to soil environments. (e.g. flood or drought stress, interactions between microorganisms and roots. We may be able to select entirely new trait types in applied breeding based on roots, where so far only shoot observations were used (Ober et al., 2021). So far, however, simultaneous measures of roots and shoots show that relationships between both are unpredictable, particularly for plant growth traits, like biomass (Nagel et al., 2015). Having more data available will likely give rise to disentangling these relationships.

Applying results from pre-breeding to practical breeding depends on how well genotypes predict intended outcomes, like yield, under field conditions. Yet, there are significant differences between controlled and field conditions in the target environments (Poorter et al., 2012) for example regarding light intensities or room for root expansion. It is impossible to fully simulate outdoor environmental conditions in experimental setups due to their complex dynamics (Kumar et al., 2015). Moreover, insight can usually only be gathered for smaller time spells in growth phases of a plant and rarely spans from seedling to harvest. Therefore, correlations between controlled environments and field conditions are generally fairly low (Kumar et al., 2015; Watt et al., 2020). Controlled environments allow predictions and heritability assessments of yield components where it may not be possible to assess those under field conditions. This allows directly developing insights for plants grown under controlled conditions, as needed for horticulture and vertical farming. However, phenotyping under field conditions is needed to see the performance of farming outcomes of different genotypes of crops farmed in large outdoor spaces.

4.3 Field environments and faster data generation

Field phenotyping serves testing plants – or rather their genotypes – under real environmental conditions. Testing plants in as many different environments of future potential relevance reveals the range of environments in which plant candidates perform well. This information can already be used for crop model simulations to scale up the variety's 'spatial reach' (Grassini et al., 2015; Ersoz et al., 2020).

The range of technologies applicable for usage in the field is wide (Araus and Cairns, 2014; Table 2). Ensuring adaptability to differences in agricultural practice technologies range from rather low-tech field-bikes, with sensors mounted between two manually pushed wheels, robots looking like moving photobooths for cereals, or drones scanning fields. Most technology combinations of platforms and sensors currently tried out are mobile devices where the sensor is carried to the plants for imaging and can be distinguished by scanning single plants or multiple plots at a time. Some technologies are being developed for specific crops – like grapevines or sugar beet canopies – and therefore have limited flexibility in their technical setup (Schemenner and Tatikonda, 2005).

There are trade-offs involved at the technical level. Drones have the advantage of being faster at scanning a whole field than any human, yet resolution in their data is still limited (Burud et al., 2017). Drones do not need to navigate driving lanes or muddy fields nor do they compact soils. Yet, drones have trouble flying in adverse conditions with wind and rain (Chapman et al., 2014). Automated wheel-driven robots can easily produce high-resolution images of individual plants but still, take a lot longer than their human counterparts at scanning a whole field (Vijayarangan et al., 2018).

4.4 Socio-technological bottlenecks – data processing and management as the missing link

Scientists and breeders need to have actionable insights they can directly translate into their breeding practice. The knowledge about causal relationships between different factors and the phenotype is key to know what material to use next for breeding actual varieties. Scientists need to communicate these insights for breeders to use. Their experimental set-ups should enhance our understanding of relevant traits and their functional interactions of GxExMxS. Machine Learning is capable of compressing the high-dimensional 'big data' obtained and to produce predictions of phenotypical traits from genetic and environmental features (Minervini et al., 2015, Tsaftaris et al., 2016). To be able to employ machine learning, breeders need training or hire services/employees with the required new skills.

Another challenge is managing data for reusability. In pre-breeding, genotype-to-phenotype data in different environments is scarce, as a low number of candidate plants or seeds contain specific traits limiting repeated measurements. Meta-analyses could support robust insights on quantitative and qualitative traits (Watt et al., 2020). There are challenges involved in facilitating these studies: Data needs to be a) accessible, b) standardized/interoperable and c) worded in a common language (ontology), (d) findable (FAIR principle; Wilkinson et al., 2016) for describing what is being measured to make data comparable and re-usable across experiments. For meaningful comparison across different environmental contexts, pedo-climatic conditions, pathogen pressures, and other plant growth conditions need to be recorded systematically. Reusable data and replicable results are hard to gain under constantly changing environmental conditions (Massonnet et al., 2010). Ensuring FAIR data needs a collective effort by scientists and breeding practitioners complying with these principles. Several initiatives already exist aiming to harmonize experimental data from phenotyping, like the International Wheat Information System (http://www.wheatis.org/) or MIAPPE (https://www.miappe.org/).

5 The future of governing phenotyping technologies in plant breeding

High throughput phenotyping can contribute to sustainable intensification on different scales by shaping and accelerating crop improvements. Automation will influence individual breeding programs as they produce varieties with better traits than before. RIs provide the socio-technical environment and concrete demand-driven services to achieve this.

5.1 Implications for managing applied breeding programs

Breeding programs produce varieties for farmers to use. Private businesses try to recoup their research and development investments through sales of varieties or licenses for multiplication. Breeders are usually faced with the two-fold problem of creating variation of trait expressions in candidate variants and then selecting effectively and efficiently from the variation created for combinations leading to improved farm outputs. The number of varieties admitted for sale and income generated from sales or licenses can be seen as their current measure of success. Yet, these numbers need to be interpreted as relative to the inputs used by a breeding firm. (Gerullis et al., 2021).

Inputs - limiting factors to practical breeders' operations - are nursery space, different locations for having a variety of environments available to test breeding lines under different conditions, genetic variation in their material, and skilled or unskilled person-power producing and evaluating the depth and breadth of data created through the mentioned factors of production. Breeders employ social strategies to work around the physical limits of their firm. Some breeders share and exchange information, nursery space in different locations, and material with their colleagues or co-produce new genetic traits with scientists in pre-breeding programs (Gerullis et al., 2021). Even small breeding programs can be quite successful as such (Brandl, 2018) if they manage their input to output ratio well and produce well-working varieties for different ecological niches.

Adopting high throughput phenotyping as an applied breeder leading a breeding program only makes sense if the technologies alleviate the resource scarcities mentioned and if they help outperform the return on investments necessary for the technologies of the breeding process currently in use. Those firms will be the most successful in employing the technologies that can leverage them for developing wider phenotypic variation and/or then employing the technologies for increased selection pressure, thereby accelerating the breeding process (Brandl, 2018).

Breeders' mental models of the functional connection between crop physiological traits, genotypic information, and the phenotypic observations of varieties and farming outputs under different environments (biological and social) determine what breeders use in their breeding process. It is vital to know for a breeder how and when to inspect signs of a disease, for example, fusarium head blight in late growth stages shows a whitening of wheat ears, to look for resistance of the same (Champeil et al., 2004). They need to know how candidate variants perform under different disease pressures and then relate observable farm outcomes, like toxin levels in wheat harvests if they are susceptible to fusarium.

Sensors employed in high throughput phenotyping can enhance vision beyond plain eye-sight, opening up possibilities for completely new breeding input traits, so far ignored (Watt et al., 2020). Yet, for bringing about improved varieties, breeders' mental models, depicting causal connections in terms of structure and processes of the plant system (Kieras and Bovair, 1984), are decisive. For example, if a higher-level goal for breeding is to boost plant productivity by introducing crop varieties paired with specific variants of mycorrhizae (Brito et al., 2021), then the tricky part for the pre-breeder is figuring out which plant physiological attributes an applied breeder needs to look out for to bring about improved farm outputs. Breeders need to know what patterns to look for in the images of root structures they gather and what these different patterns mean to formulate expectations of how crops work and how they can gain improvements. Additionally, opportunities arise where interactions of multiple factors come into play. For example, if different root structural patterns allow for a narrower planting on the same space, an increase in yield through interspecies cooperation (e.g. micro-organisms and plants) and variation in field arrangements (Grahmann et al., 2021) allows a push and pull pest control, then all three factors may be combined (Denison, 2012). Both examples need new ways of phenotyping and the integration of experimental meta-data into experimental set-ups of applied breeders.

Automation – once established – can bring about more comparable and precise measures of phenotypes across locations. In handicraft breeding, personnel have to hand-inspect and rate every variant plot for multiple time slots throughout growing

seasons (Reynolds et al., 2019). There are differences in how individuals rate plots. Breeders usually compensate this by knowing their staffs' style of judgment and triangulating the results for important diseases. Human staff will usually correct their ratings for environmental conditions. Some diseases may not be visible well if another disease already infected big parts of a plant or if only low disease pressure is present. Automated phenotyping and the corresponding image processing algorithms could, once machine learning models employed are trained to compensate for these problems, aid in inspecting and rating over multiple locations saving person power and time (Reynolds et al., 2019). Paired with decision support systems for breeders, which pre-process the data, there is potential for accelerating breeders' work in this approach if robotics and data management systems can be maintained and adapted easily (Kuriakose et al., 2020). Yet, the additional data in terms of quality and quantity created needs to be processed, standardized and interoperable to work effectively (van Dijk et al., 2021).

5.2 Bottlenecks in breeding programs and opportunities for new service industries

Depending on their pre-existing socio-technological infrastructures, private breeders face different trade-offs when considering investing in automated phenotyping technologies. The cost and risks of investing in robotics-based phenotyping may be immense for a small breeding firm currently equipped with just the minimum technical setup for instance in wheat breeding – nursery fields, skilled and unskilled labor, and a rudimentary computer system where they store and manage data from plant inspections. The firm would need to invest, in the robot (s) itself, the highly skilled robotics personnel to implement, maintain and improve it and more personnel skilled in computer science for implementing, maintaining, and improving data and knowledge management and analysis (Reynolds et al., 2019). With shifting to new systems, firms run the risk that the new technology will cost more than it adds in value. Similar considerations struck breeding programs 35 years ago when they faced the integration of molecular genetics with plant physiology (Reece and Haribabu, 2007). Some breeding firms outsourced genotyping their seeds and a service industry appeared (Shkolnykova, 2020). This outsourcing generally worked better for some breeding programs, where the initially chosen interdisciplinary collaboration between molecular biologists and applied plant breeders was problematic (Reece, 2007; Reece and Haribabu, 2007). Today, smaller breeding programs use genotyping services to scan for specific markers, targeted genetic sequences, of intended breeding input traits and base their selection on the results. Using services for genetic markers in breeding accelerates breeding already.

Having more data from an automated phenotyping process will only increase value-added if the software for processing the new data types enables breeders to integrate their hypotheses into building new ideotypes, i.e. targeted ideal phenotypes. Software needs to be flexible enough to accommodate new insights when new traits are developed (Xu and Crouch, 2008). They need to contain graphical user interfaces, which allow for ample flexibility for the set-up of data processing through the breeder, without having to have a computer science degree (Galitz, 2007). It is important that breeders can individually fine-tune analyses and try out assumptions for different functional models between trait expressions and outcomes. Breeders need to be able to arrange their experimental designs for crossing and selecting according to their wishes. Breeders need to learn how to explicitly transform the "breeders' eye" (Brandl, 2018) into heuristic computer models. Open question is whether breeders will actively engage in pre-breeding and try to develop different ideotypes, or go for merely applying what pre-breeding research serves to them as new ideotypes and use trial and error in application.

There is ample opportunity for specialized services to develop alongside new breeding technologies. Effortless usage and maintenance of robots and data infrastructures may be provided well by businesses, who arrange their activities around co-producing services for multiple breeders. We specifically say co-production, as these services demand a collective and dynamic learning process, based on research by universities and research institutes, then tailored to different localized social contexts, biological environments, and crops. In other sectors, like banking, the co-creation of technologies with heterogeneous small actors has brought about decentralized organizational structures and kept market concentration at bay (Hannan and McDowell, 1990). Considering how heterogeneous and locally adapted breeding needs to be to produce varieties fit for prevailing environmental conditions, long-run cooperative networks of firms may outperform single players in achieving this goal. Multiple firms may pool resources and share risks in developing software, data management services, and robots focusing on ease of use and flexibility for individual ideas and specific conditions. This way, a diversified approach of adopting the new technologies seems possible for breeders even if they currently possess low-tech infrastructure. As the case of German winter wheat shows (Brandl, 2018), cooperative breeding strategies have led to German wheat breeders outperforming the global competition over the last 100 years in terms of yields (Brandl et al., 2014). Going for co-production may in the long-term better hedge our bets for societal goals of sustainability overall, as we maintain flexibility and adaptiveness to localized conditions.

Accelerating the breeding process through increased selection pressure may bring about a trade-off over nursery space for short-term variety development and maintaining genetic resources in adapted breeding material (Gerullis et al., 2021). If automated phenotyping provides more precise predictions compared to current selection schemes, breeders will be quicker with selection decisions for dropping material. Meaning that breeders run the risk of dropping material earlier in the breeding process than before, possibly losing too much valuable variation in genotypes. Private incentives led to underinvestment in crop genetic resources in the past already in the USA (Day-Rubenstein et al., 2005). Hence, monitoring and evaluating *in-situ* genetic resources from breeders and their released varieties will be vital to ensure long-term functioning of seed production and needs to be developed alongside the new technologies. In the next section, we will go deeper into how public RIs can support these strategies and promote overall sustainability goals.

5.3 Implications for policy: threats and opportunities to effective research infrastructure governance

RIs provide resources and services for research communities conducting research and fostering innovation (ESFRI (European Strategy Forum on Research Infrastructures), 2020). From a mission-oriented perspective, a RI around plant phenotyping serves as an accelerator for developing agricultural systems adapted to existing or upcoming challenges. Developing these sustainable agricultural systems demands governance connecting scientists and all relevant stakeholders, providing physical and mental space to rigorously test different system configurations against each other. Principles of mission-oriented governance (Mazzucato and Li, 2021) necessitate a) defining overall but also intermediate goals, b) entertaining a widespread portfolio of project set-ups so that failures become acceptable, c) involving actors and investment across different scientific disciplines, private and public sectors, d) joined governance, yet, strategic division of labor among involved research sections with well-defined responsibilities for coordination and monitoring.

We put forward GxExMxS as rule of thumb for thinking about how efficiencies in land use, water, energy, ecological impacts due to changes in nitrogen, phosphorous, and carbon cycling are brought about, at different levels initiated and/or complemented by changes in traits of crops. Research programs under the Horizon Europe missions should integrate relevant stakeholders having expertise in different topics. RIs are supposed to function as an organization providing services such as access to facilities, data, resources and could function as an important element stimulating cross-disciplinary interaction and research towards common goals. With their cross-cutting capabilities to reach many different actor groups, RIs are key in shaping how governmental monies spill over to private industry (Mazzucato and Li, 2021). They can deploy mission-oriented organizations, to crowd-in private investment and use knowledge governance for public values, by putting in play conditionalities of public interest (Mazzucato, 2018; Mazzucato and Li, 2021).

Aside from immediate breeding outcomes, the performance on-farm and beyond must be considered as well, potentially already during pre-breeding. High-throughput installations need to be accessible to create high-quality, reusable data sets to yield reliable results for crop model predictions and integration into simulation models over larger spatial scales including different pedo-climatic zones. Basic research on crop improvement needs rigorous testing of different technical systems' performance, necessitating flexibility in where and how different sensors are used. This demands modular installations, sensors, and platforms. Scientific testing and optimization must not stop until new system configurations outperform the best running systems in use on farms, to provide proper proof of concept ready for wider application. On the level of research, this includes from biological insights of symbiotic interactions amongst crops and other organisms to technical inventions developing enhanced vision with machines.

EU funding of RIs together with other fiscal incentive schemes for agricultural research aims at developing innovations for the Green New Deal (Mazzucato and McPherson, 2019) and achieving sustainable development goals with mission-oriented governance (Sachs et al., 2019). The goal is to crowd-in those individuals and organizations, who are willing to innovate for achieving these goals and co-creating new markets for and through sustainable innovations. RIs play a role as enabling scaffold in these overall European goals.

Yet, treating RIs merely as enabling organizations is not enough. Supporting the overall directionality of missions like healthier soils or adaptation to climate change (European Strategy Forum on Research Infrastructures, 2016; ESFRI (European Strategy Forum on Research Infrastructures), 2020) effectively not only requires the development of technological features, like steering software for robots, but collective learning across sectors and disciplines to achieve goals like the SDGs. As reaching the SDGs requires deep structural changes across all sectors of society (Sachs et al., 2019), they include social cooperation problems across multiple scales and amongst different stakeholders discussed in section 2.3. Leading actors in RIs may need to adopt institutional navigation as they pursue the SDG policy goals against a backdrop of complex, polycentric governance, where multiple decision-makers engage in different forms of organization to manage cooperation problems present in agriculture (Lubell and Morrison, 2021).

Facilitating a research environment with learning and high explorative capacity best fits for tackling the mission's challenges (Mazzucato, 2015; Lubell and Morrison, 2021). High explorative capacity within these organizational structures may be achieved through a social environment where RI staff can welcome uncertainties and long-term competencies are developed (Mazzucato, 2015). Additionally, staff need to be proactive and entrepreneurial in their role of leading researchers and other actors using the infrastructure and its outputs (Table 2 for examples).

In fiscal terms, this necessitates long-term investment in equipment and human resources (Mazzucato, 2016). In RIs for breeding and agricultural purposes, long-term experimentation is important (e.g. considering breeding cycles taking 10 years and more, Gerullis et al., 2021). Experimental set-ups need to go beyond the usual 3-year project term and limited field space to bring about useful and accurate long-term results. With the current set-up of phenotyping networks in Europe (see Figure 2 for the Emphasis RI) it is possible to leverage multiple locations and installations distributed across Europe even though individual scientists may not have the same access to specialized installations at their home institutions.

There is a necessity to keep a good portion of scientific expertise within the RI as it needs maintenance and building up expertise for smooth workflows (ESFRI (European Strategy Forum on Research Infrastructures), 2020; Knowles et al., 2021). Long-term human resource development must be applied to scientists in the same way it is usually done in private businesses. While high-throughput phenotyping will need the same level of highly trained scientific staff, it will ease the shortage in person-power of technical staff for phenotyping large amounts of plant materials. Yet, technical

FIGURE 2
Overview of network for automated phenotyping technologies within research infrastructure.

knowledge on installations being run needs to be maintained over time as well and allowed to evolve further.

Individual scientists need to find an environment fostering collaboration across a wide range of disciplines and working cultures, who need to find new and transdisciplinary ways of solving research challenges (Brown et al., 2015). Transdisciplinary research needs disciplinary specialists *and* generalists who function as boundary actors between these different disciplines (Poteete et al., 2011). Hiring and maintaining the right set of people will determine success or failure of these infrastructures. Evaluation criteria for scientists working in research facilities connected to infrastructures determine the type of individuals joining different projects (Brown et al., 2015), research venues, and the success in using technological installations over longer time horizons. From climate change science we can learn that team science is key in solving complex challenges at hand and one can safely assume that sustainable agriculture is similar (Ledford, 2015; Cundill et al., 2019). Likewise, integration of social sciences is vital for tackling research challenges such as social system feedbacks (Viseu, 2015). For example, having a few social scientists that "speak plant" may help elicit unknown areas of knowledge between what breeders have been selecting for with "breeders eye" (Timmermann, 2009) – i.e. implicit knowledge on how breeding input traits translate into farm output traits in plants – and what pre-breeding scientists can see with their new sensors for enhanced vision. Such insights have potential to improve the effectiveness in implementing new breeding strategies, farming practices complementing newly bred plants, and extension services.

On an organizational level, polycentric governance of plant breeding requires RIs to build cooperative relationships amongst different actor groups to ensure effective research towards reaching mission goals (Lubell and Morrison, 2021). Scientists need to co-produce with farmers, breeders, agri-business, and citizens what sustainable traits in crops are and how they manifest in the food and

fiber supply chain. Note though that each of these groups needs separate consideration in transdisciplinary approaches (Max-Neef, 2005).

Integrating farmers and food processors into the trait development process may also be of advantage when fruit attributes like thicker skins can enhance shelf life, for example in horticultural breeding. This could be done in a business-to-business context. An option would be to actively build platforms for public and private research cooperation by supporting start-up incubators with a focus on plant breeding (Shkolnykova, 2021) or to target participation of food processors in trait development as in the EMPHASIS RI context withthe Agroserv project (https://emphasis.plant-phenotyping.eu/european-infrastructures/cluster-projects/agroserv). Another option is integrating crop producers in participatory breeding processes (see Ceccarelli and Grando, 2020 for an overview) or in an extension service context, where extension employees survey the needs of the producers to allow plant breeders to make use of the knowledge on demanded traits.

Integrating non-scientific actor groups early on spells-out issues usually leading to unforeseen transition risks and lack of adoption (Mazzucato and McPherson, 2019). An example is the considerable societal resistance in Europe towards GMs and their ban from most agricultural use thereafter (Directive 2001/18/EC). Incorporating a dialogue with stakeholders and the public may lower transition risks and can be used as an opportunity for collective learning and diffusing innovations in public interest. Using and including governmental organizations already in place, such as agricultural extension services should be tried early on in development and testing processes, as it provides a notion of feasibility of traits in farm management practices.

How private businesses are integrated into a phenotyping network providing public services for research will greatly influence the effectiveness of delivering research insights. 'Toxic actors' can have detrimental effects on whole research venues and hamper their effectiveness in delivering research outcomes (Lubell and Morrison, 2021). Conflicts of interest may arise around data and material sharing, or specific methodological insights that constitute trade secrets. Mitigating these problems relies partially on a shift in mindset and ethics, towards more sharing attitudes and balancing incentive structures towards long-term goals over short-term revenues. A recent example within the EU RIs is the ENVRIplus project, which developed ethical guidelines for RIs (Capua et al., 2018) explicitly mentioning reciprocity amongst their guiding values. Including private actors may enhance testing capacities and promote insights if data is shared in a FAIR manner and symbiotic relationships are fostered (Mazzucato, 2016). Public value creation must be in focus of those taking care of research contracts over new projects for effective long-term risk and reward sharing (Mazzucato, 2016). Risk and reward sharing needs to be implemented such that they maintain an open innovation culture, which reinvests into further research. For example, in the RI Cluster project, CORBEL, governing guidelines for industry collaborations are provided to support this (Abuja et al., 2019).

Overall, the success of RIs will depend on how well its staff strategizes over knowledge, relationships, and decisions for implementation toward mission goals (Lubell and Morrison, 2021).

6 Conclusions

Mission-oriented governance for research is supposed to be implemented for plant breeding research to fulfill the SDGs and facilitate green growth. Improving crops through plant breeding will be vital for reaching the SDGs associated with agriculture. Crop breeding research shall bring about varieties enabling the necessary transformations to agricultural systems. High throughput technologies for phenotyping are meant to accelerate the plant breeding process and enhance breeders' vision of breeding materials, leveraging innovation pathways. Yet, against the backdrop of complex agricultural systems and polycentric research venues, and agricultural governance, the question remains how to reach these ambitious goals.

We propose a governance heuristic illustrating how mission-oriented governance can work for plant breeding research. We show the current state-of-the-art of phenotyping technologies and draw, based on historic examples from plant breeding, implications for their introduction to individual breeding programs and RIs.

Our core result is that plant breeding is not only about the interaction of genetics (G), environment (E), and farm management practices (M), but that activities at collective level (S) are crucial for the sustainability performance at lower levels of the system. Hence, we propose GxExMxS as a guiding rule of thumb for future governance of plant breeding. This heuristic needs to be interpreted in specific context of application, e.g. when a funder wants to decide if a research project for plant breeding may be justified they may ask how novel plant traits lead to results on a higher level in the social-ecological system.

Additionally, we want to caution that novel phenotyping technologies alone will not bring about sustainable agricultural systems. Integrating robotics, sensors, and information systems meaningfully is necessary to elevate mental models of breeders, scientists, and other actors contributing to crop breeding. This implies a high heterogeneity in potential adoption of these technologies in breeding programs. Concurrently, RIs need to care how they institutionally navigate their role as facilitator and promoter of research to reach mission goals.

Author contributions

MG is first author and wrote the first draft of the manuscript, conceptualized the paper. TH contributed to structure. SF, RP, LH and US edited sections of the manuscript. All authors contributed to the article and approved the submitted version.

Funding

MG, TH and US are partially funded by the Deutsche Forschungsgemeinschaft (DFG, German Research Foundation) under Germany's Excellence Strategy - EXC 2070 – 390732324-PhenoRob. MG is also funded at Cornell University under the USDA Project number 1218256. US, SF, RP are supported by the

EU funded project EMPHASIS-GO under Grant Agreement No. 101079772, the project AgroServ under the Grant Agreement No. 101058020, the project PHENET under the Grant Agreement No. 101094587. LH receives funding from Bavarian State Ministry for Food, Agriculture, and Forestry. This work was supported by the Open Access Publication Fund of the University of Bonn and Cornell University.

Acknowledgments

MG gratefully acknowledges the conversations she has had on this paper with Marlene Prinz, Ford Denison, Yoko Kusunose, Michael Cox and her colleagues from the Early Career Network of the International Association for the Study of the Commons; Hita Unnikrishnan and Eve Whittaker.

Conflict of interest

The authors declare that the research was conducted in the absence of any commercial or financial relationships that could be construed as a potential conflict of interest.

Publisher's note

References

Abuja, P. M., Carapina, T., de Kort, M., Raess, M., Chris Tieken, C., and Wagstaff, N. (2019). *Industry Collaboration Best Practice Guide*. Available at: https://zenodo.org/record/2615365.

Acquaah, G. (2007). *Principles of plant genetics and breeding* (Malden, MA, USA: Blackwell Publishing).

Alston, J. M., and Pardey, P. G. (1996). *Making science pay: The economics of agricultural R&D policy*.

Aragona, F. B., and Orr, B. (2011). Agricultural intensification, monocultures, and economic failure: The case of onion production in the tipajara watershed on the eastern slope of the Bolivian Andes. *J. Sustain. Agric.* 35 (5), 467–492. doi: 10.1080/10440046.2011.579832

Araus, J. L., and Cairns, J. E. (2014). Field high-throughput phenotyping: the new crop breeding frontier. *Trends Plant Sci.* 19 (1), 52–61. doi: 10.1016/j.tplants.2013.09.008

Bätzing, W. (2020). *Das Landleben* (München: C.H.Beck).

Becker, H. (2011). *Pflanzenzüchtung* (Stuttgart, Germany: UTB).

Brandl, B. (2018). *Wissenschaft, Technologieentwicklung und die Spielarten des Kapitalismus: Analyse der Entwicklung von Saatgut in USA und Deutschland* (Wiesbaden, Germany: Springer).

Brandl, B., and Glenna, L. L. (2017). Intellectual property and agricultural science and innovation in Germany and the United States. *Science Technology Hum. Values* 42 (4), 622–656. doi: 10.1177/0162243916675954

Brandl, B., Paula, K., and Gill, B. (2014). Spielarten des Wissenskapitalismus - die Kommodifizierung von Saatgut in den USA und in Deutschland. *Leviathan* 42 (4), 539–572. doi: 10.5771/0340-0425-2014-4-539

Brito, I., Carvalho, M., and Goss, M. J. (2021). Managing the functional diversity of arbuscular mycorrhizal fungi for the sustainable intensification of crop production. *PLANTS PEOPLE PLANET* 3 (5), 491–505. doi: 10.1002/ppp3.10212

Brown, R. R., Deletic, A., and Wong, T. H. (2015). Interdisciplinarity: how to catalyse collaboration. *Nat. News* 525 (7569), 315. doi: 10.1038/525315a

Brown, T. A., Jones, M. K., Powell, W., and Allaby, R. G. (2009). The complex origins of domesticated crops in the fertile crescent. *Trends Ecol. Evol.* 24 (2), 103–109. doi: 10.1016/j.tree.2008.09.008

Burud, I., Lange, G., Lillemo, M., Bleken, E., Grimstad, L., and From, P. J. (2017). Exploring robots and uavs as phenotyping tools in plant breeding. *IFAC PapersOnLine* 50 (1), 11479–11484. doi: 10.1016/j.ifacol.2017.08.1591

Capua, G. D., Peppoloni, S., Haslinger, F., and Marti, M. (2018). *ENVRIplus deliverable: D13.3 ethical guidelines for RIs*. Available at: https://www.researchgate.net/publication/333653440_D133_-_Ethical_Guidelines_for_RIs.

Carroll, S. P., Jørgensen, P. S., Kinnison, M. T., Bergstrom, C. T., Denison, R. F., Gluckman, P., et al. (2014). Applying evolutionary biology to address global challenges. *Science* 346 (6207), 1245993. doi: 10.1126/science.1245993

Ceccarelli, S., and Grando, S. (2020). Participatory plant breeding: Who did it, who does it and where? *Exp. Agric.* 56 (1), 1–11. doi: 10.1017/S0014479719000127

Champeil, A., Dore, T., and Fourbet, J. (2004). Fusarium head blight: epidemiological origin of the effects of cultural practices on head blight attacks and the production of mycotoxins by fusarium in wheat grains. *Plant Sci.* 166 (6), 1389–1415. doi: 10.1016/j.plantsci.2004.02.004

Chapman, S., Merz, T., Chan, A., Jackway, P., Hrabar, S., Dreccer, M. F., et al. (2014). Pheno-copter: A low-altitude, autonomous remote-sensing robotic helicopter for high-throughput field-based phenotyping. *Agronomy* 4 (2), 279–301. doi: 10.3390/agronomy4020279

Cooper, M., Messina, C. D., Podlich, D., Totir, L. R., Baumgarten, A., Neil, J., et al. (2014). Predicting the future of plant breeding: complementing empirical evaluation with genetic prediction. *Crop Pasture Sci.* 65 (4), 311–336. doi: 10.1071/CP14007

Cundill, G., Currie-Alder, B., and Leone, M. (2019). The future is collaborative. *Nat. Climate Change* 9, 343–347. doi: 10.1038/s41558-019-0447-3

Day-Rubenstein, K. A., Heisey, P. W., Shoemaker, R. A., Sullivan, J., and Frisvold, G. B. (2005). *Crop genetic resources: An economic appraisal*. USDA ERS, Vol. 1476-2016-121016). 47.

Deconinck, K. (2020). Concentration in seed and biotech markets: Extent, causes, and impacts. *Annu. Rev. Resource Economics* 12 (1), 129–147. doi: 10.1146/annurev-resource-102319-100751

Denison, R. F. F. (2012). *Darwinian Agriculture: How understanding evolution can improve agriculture* (Princeton: Princeton University Press).

Denison, R. F., Kiers, E. T., and West, S. A. (2003). Darwinian agriculture: when can humans find solutions beyond the reach of natural selection? *Q. Rev. Biol.* 78 (2), 145–168. doi: 10.1086/374951

DGRI (Directorate General Research and Innovation) (2020a). *Caring for soil is caring for life: Ensure 75 of soils are healthy by 2030 for food, people, nature and climate - report of the mission board for soil health and food* (Brussel, Belgium: Mission Board for Soil health and food).

DGRI (Directorate General Research and Innovation) (2020b). *A climate resilient Europe: Prepare Europe for climate disruptions and accelerate the transformation to a climate resilient and just Europe by 2030* (Brussel, Belgium: Mission Board on Adaptation to Climate Change, including Societal Transformation).

DGRI (Directorate General Research and Innovation) (2020c). *Proposed mission: Conquering cancer, mission possible* (Brussel, Belgium: Mission Board on Cancer).

Eathington, S. R., Crosbie, T. M., Edwards, M. D., Reiter, R. S., and Bull, J. K. (2007). Molecular markers in a commercial breeding program. *Crop Sci.* 47 (3), 154–163. doi: 10.2135/cropsci2007.04.0015IPBS

Ersoz, E. S., Martin, N. F., and Stapleton, A. E. (2020). On to the next chapter for crop breeding: Convergence with data science. *Crop Sci.* 60 (2), 639–655. doi: 10.1002/csc2.20054

ESFRI (European Strategy Forum on Research Infrastructures) (2020). *Making science happen: A new ambition for research infrastructures in the European research area: ESFRI white paper 2020* (Brussel, Belgium: European Strategy Forum on Research Infrastructures).

European Strategy Forum on Research Infrastructures (2016). *Strategy report on research infrastructures: Roadmap 2016*.

ESFRI (European Strategy Forum on Research Infrastructures) (2021). *Strategy report on research infrastructures: Roadmap 2021 public guide* (Brussels: European Strategy Forum on Research Infrastructures).

FAO (2018). *The 10 elements of agroecology: guiding the transition to sustainable food and agricultural systems*. Rome, Italy: FAO.

Fiorani, F., Rascher, U., Jahnke, S., and Schurr, U. (2012). Imaging plants dynamics in heterogenic environments. *Curr. Opin. Biotechnol.* 23 (2), 227–235. doi: 10.1016/j.copbio.2011.12.010

Fiorani, F., and Schurr, U. (2013). Future scenarios for plant phenotyping. *Annu. Rev. Plant Biol.* 64, 267–291. doi: 10.1146/annurev-arplant-050312-120137

Galitz, W. O. (2007). *The essential guide to user interface design: an introduction to GUI design principles and techniques* (NEW YORK • CHICHESTER • WEINHEIM • BRISBANE • SINGAPORE • TORONTO: John Wiley & Sons).

Gassmann, A. J., Petzold-Maxwell, J. L., Keweshan, R. S., and Dunbar, M. W. (2011). Field-evolved resistance to bt maize by western corn rootworm. *PloS One* 6 (7), e22629. doi: 10.1371/journal.pone.0022629

Gerullis, M. K., Heckelei, T., and Rasch, S. (2021). Toward understanding the governance of varietal and genetic diversity. *Ecol. Soc.* 26 (2). doi: 10.5751/ES-12333-260228

Gibson, M. (1974). *Violation of fallow and engineered disaster in mesopotamian civilization. No. 25* (Tucson, AZ, USA: University of Arizona Press).

Grahmann, K., Reckling, M., Hernandez-Ochoa, I., and Ewert, F. (2021). An agricultural diversification trial by patchy field arrangements at the landscape level: The landscape living lab "patchcrop". *Aspects Appl. Biol.* 146, 385–391.

Grassini, P., van Bussel, L. G., van Wart, J., Wolf, J., Claessens, L., Yang, H., et al. (2015). How good is good enough? Data requirements for reliable crop yield simulations and yield-gap analysis. *Field Crops Res.* 177, 49–63. doi: 10.1016/j.fcr.2015.03.004

Hannan, T. H., and McDowell, J. M. (1990). The impact of technology adoption on market structure. *Rev. Economics Stat* 72 (1), 164–168. doi: 10.2307/2109755

Harwood, J. (2015). "Did mendelism transform plant breeding? genetic theory and breeding practice 1900–1945," in *New perspectives on the history of life sciences and agriculture* (Cham: Springer), 345–370.

Henrich, J., and McElreath, R. (2003). The evolution of cultural evolution. *Evolutionary Anthropol Issues News Rev.* 12 (3), 123–135. doi: 10.1002/evan.10110

Jacobsen, T., and Adams, R. M. (1958). Salt and silt in ancient Mesopotamian agriculture. *Science* 128 (3334), 1251–1258.

Kebeish, R., Niessen, M., Thiruveedhi, K., Bari, R., Hirsch, H. J., Rosenkranz, R, et al. (2007). Chloroplastic photorespiratory bypass increases photosynthesis and biomass production in arabidopsis thaliana. *Nat. Biotechnol.* 25 (5), 593–599. doi: 10.1038/nbt1299

Kieras, D. E., and Bovair, S. (1984). The role of a mental model in learning to operate a device. *Cogn. Sci.* 8 (3), 255–273. doi: 10.1207/s15516709cog0803_3

Kishore, G. M., Padgette, S. R., and Fraley, R. T. (1992). History of herbicide-tolerant crops, methods of development and current state of the art: Emphasis on glyphosate tolerance. *Weed Technol.* 6 (3), 626–634. doi: 10.1017/S0890037X00035934

Kloppenburg, J. R. (2004). "First the seed: The political economy of plant biotechnology 1942-2000," in *Science and technology in society*, *2nd ed* (Madison, Wis: University of Wisconsin Press).

Knowles, R., Mateen, B. A., and Yehudi, Y. (2021). We need to talk about the lack of investment in digital research infrastructure. *Nat. Comput. Sci.* 1 (3), 169–171. doi: 10.1038/s43588-021-00048-5

Kumar, J., Pratap, A., and Kumar, S. (2015). *Phenomics in crop plants: Trends, options and limitations* (New Delhi: Springer India).

Kuriakose, S. V., Pushker, R., and Hyde, E. M. (2020). *Data-driven decisions for accelerated plant breeding* (Cham: Springer International Publishing), 89–119.

Laidig, F., Piepho, H. P., Rentel, D., Drobek, T., Meyer, U., and Huesken, A. (2017). Breeding progress, environmental variation and correlation of winter wheat yield and quality traits in German official variety trials and on-farm during 1983-2014. TAG. Theoretical and applied genetics. *Theoretische und angewandte Genetik* 130 (1), 223–245. doi: 10.1007/s00122-016-2810-3

Lassoued, R., and Smyth, S. (2023). Decision factors influencing new variety adoption in western Canada by the seed industry. *Can. J. Plant Science.* 103 (2), 214–227. doi: 10.1139/cjps-2022-0204

Ledford, H. (2015). Team science. *Nature* 525, 308–311. doi: 10.1038/525308a

Lubell, M., and Morrison, T. H. (2021). Institutional navigation for polycentric sustainability governance. *Nat. Sustainability* 4, 1–8. doi: 10.1038/s41893-021-00707-5

Maisels, C. K. (1993). *The emergence of civilization: From hunting and gathering to agriculture, cities, and the state of the near east. 1st ed* (London, UK: Routledge).

Mallet, J., and Porter, P. (1992). Preventing insect adaptation to insect-resistant crops: are seed mixtures or refugia the best strategy? *Proc. R. Soc. London. Ser. B: Biol. Sci.* 250 (1328), 165–169. doi: 10.1098/rspb.1992.0145

Massonnet, C., Vile, D., Fabre, J., Hannah, M. A., Caldana, C., Lisec, J., et al. (2010). Probing the reproducibility of leaf growth and molecular phenotypes: a comparison of three arabidopsis accessions cultivated in ten laboratories. *Plant Physiol.* 152 (4), 2142–2157. doi: 10.1104/pp.109.148338

Max-Neef, M. A. (2005). Foundations of transdisciplinarity. *Ecol. Economics* 53 (1), 5–16. doi: 10.1016/j.ecolecon.2005.01.014

Mazzucato, M. (2013). *The entrepreneurial state: Debunking public vs. private myths in risk and innovation* (London, United-Kingdom: Anthem Press).

Mazzucato, M. (2015). *Building the entrepreneurial state: A new framework for envisioning and evaluating a mission-oriented public sector: Working paper no. 824.* Annandale-on-Hudson, NY: Levy Economics Institute.

Mazzucato, M. (2016). From market fixing to market-creating: a new framework for innovation policy. *Industry Innovation* 23 (2), 140–156. doi: 10.1080/13662716.2016.1146124

Mazzucato, M. (2018). *Mission-oriented research & innovation in the European Union: A problem-solving approach to fuel innovation-led growth* (Brussel, Belgium: European Commission Directorate-General for Research and Innovation).

Mazzucato, M. (2019). *Governing missions: Governing missions in the European Union* (Brussel, Belgium: European Commission Directorate-General for Research and Innovation).

Mazzucato, M., and Li, H. L. (2021). A market shaping approach for the biopharmaceutical industry: Governing innovation towards the public interest. *J. law Med. ethics: J. Am. Soc. Law Med. Ethics* 49 (1), 39–49. doi: 10.1017/jme.2021.8

Mazzucato, M., and McPherson, M. (2019). *What the green revolution can learn from the IT revolution: A green entrepreneurial state*, Policy brief 08. (London, UK: UCL Institute for Innovation and Public Purpose).

McGinnis, M. D., and Ostrom, E. (2014). Social-ecological system framework: initial changes and continuing challenges. *Ecol. Soc.* 19 (2). doi: 10.5751/ES-06387-190230

Mendel, G. (1866). "Versuche über Pflanzen-hybriden. Verhandlungen des naturforschenden Vereines in Brünn," in *Classic papers in genetics*, vol. 4. (Brünn, Germany: Prentice-Hall), 3–47.

Minervini, M., Scharr, H., and Tsaftaris, S. A. (2015). Image analysis: The new bottleneck in plant phenotyping [applications corner]. *IEEE Signal Process. Magazine* 32 (4), 126–131.

Moore, G. (2015). Strategic pre-breeding for wheat improvement. *Nat. Plants* 1 (15018). doi: 10.1038/nplants.2015.18

Morisse, M., Wells, D., Alary, P.-E., Pieruschka, R., and Dhondt, S. (2018). EMPHASIS-PREP Deliverable 2.1: Criteria list for infrastructure. *Zenodo*. doi: 10.5281/zenodo.3765459

Nagel, K. A., Bonnett, D., Furbank, R., Walter, A., Schurr, U., and Watt, M. (2015). Simultaneous effects of leaf irradiance and soil moisture on growth and root system architecture of novel wheat genotypes: Implications for phenotyping. *J. Exp. Bot.* 66 (18), 5441–5452. doi: 10.1093/jxb/erv290

Nagel, K. A., Putz, A., Gilmer, F., Heinz, K., Fischbach, A., Pfeifer, J, et al. (2012). Growscreen-rhizo is a novel phenotyping robot enabling simultaneous measurements of root and shoot growth for plants grown in soil-filled rhizotrons. *Funct. Plant Biol.* 39 (11), 891–904. doi: 10.1071/FP12023

Nesme, T., Metson, G. S., and Bennett, E. M. (2018). Global phosphorus flows through agricultural trade. *Global Environ. Change* 50, 133–141. doi: 10.1016/j.gloenvcha.2018.04.004

Ober, E. S., Alahmad, S., Cockram, J., Forestan, C., Hickey, L. T., Kant, J., et al. (2021). Wheat root systems as a breeding target for climate resilience. *Theor. Appl. Genet.* 134, 1–18. doi: 10.1007/s00122-021-03819-w

Olmstead, A., and Rhode, P. (2002). *The red queen and the hard reds: Productivity growth in American wheat 1800-1940* (Cambridge, MA: National Bureau of Economic Research).

Olmstead, A. L., and Rhode, P. W. (2008). *Creating abundance: Biological innovation and American agricultural development 1700–1960* (New York, USA: Cambridge University Press).

Ostrom, E. (2006). *Understanding institutional diversity* (Princeton, NJ: Princeton University Press).

Pardey, P. G., Alston, J. M., and Ruttan, V. W. (2010). "The economics of innovation and technical change in agriculture. In Handbook of the economics of innovation," in *Handbooks in economics*. Eds. B. H. Hall and N. Rosenberg (Amsterdam: North Holland), 939–984.

Pieruschka, R., and Schurr, U. (2019). Plant phenotyping: Past, present, and future. *Plant Phenomics* 2019, 1–6. doi: 10.1155/2019/7507131

Pingali, P. L. (2012). Green revolution: Impacts, limits, and the path ahead. *Proc. Natl. Acad. Sci.* 109 (31), 12302–12308. doi: 10.1073/pnas.0912953109

Poorter, H., Bühler, J., van Dusschoten, D., Climent, J., and Postma, J. A. (2012). Pot size matters: a meta-analysis of the effects of rooting volume on plant growth. *Funct. Plant Biol.* 39 (11), 839–850. doi: 10.1071/FP12049

Poteete, A. R., Janssen, M. A., and Ostrom, E. (2011). Working together: Collective action, the commons, and multiple methods in practice. *J. Artif. Societies Soc. Simulation* 14 (3), 2.

Pretty, J. (2018). Intensification for redesigned and sustainable agricultural systems. *Science* 362 (6417), 1–7. doi: 10.1126/science.aav0294

Purugganan, M. D., and Fuller, D. Q. (2009). The nature of selection during plant domestication. *Nature* 457 (7231), 843–848. doi: 10.1038/nature07895

Qaim, M. (2020). Role of new plant breeding technologies for food security and sustainable agriculturaldevelopment. *Appl. Economic Perspect. Policy* 42 (2), 129–150.

Ranjekar, P. K., Patankar, A., Gupta, V., Bhatnagar, R., Bentur, J., and Kumar, P. A. (2003). Genetic engineering of crop plants for insect resistance. *Curr. Sci.* 84 (3), 321–329.

Raworth, K. (2017). *Doughnut economics: Seven ways to think like a 21st-century economist* (White River Junction, Vermont: Chelsea Green Publishing).

Reece, J. D. (2007). What enables innovation in the private sector? Lessons from the development of salt-tolerant hybrid rice. *J. Int. Dev.* 19 (6), 853–863. doi: 10.1002/jid.1397

Reece, J. D., and Haribabu, E. (2007). Genes to feed the world: The weakest link? *Food Policy* 32 (4), 459–479. doi: 10.1016/j.foodpol.2006.10.003

Reynolds, D., Baret, F., Welcker, C., Bostrom, A., Ball, J., Cellini, F., et al. (2019). What is cost-efficient phenotyping? Optimizing costs for different scenarios. *Plant Sci.* 282, 14–22. The 4th International Plant Phenotyping Symposium. doi: 10.1016/j.plantsci.2018.06.015

Rockström, J., Steffen, W., Noone, K., Persson, °A, Chapin, F. S. III, Lambin, E., et al. (2009). Planetary boundaries: Exploring the safe operating space for humanity. *Ecol. Soc.* 14 (2), 472–475. doi: 10.1038/461472a

Rockström, J., Williams, J., Daily, G., Noble, A., Matthews, N., Gordon, L., et al. (2017). Sustainable intensification of agriculture for human prosperity and global sustainability. *Ambio* 46 (1), 4–17. doi: 10.1007/s13280-016-0793-6

Sachs, J. D., Schmidt-Traub, G., Mazzucato, M., Messner, D., Nakicenovic, N., and Rockström, J. (2019). Six transformations to achieve the sustainable development goals. *Nat. Sustainability* 2 (9), 805–814. doi: 10.1038/s41893-019-0352-9

Schipanski, M. E., and Bennett, E. M. (2012). The influence of agricultural trade and livestock production on the global phosphorus cycle. *Ecosystems* 15 (2), 256–268. doi: 10.1007/s10021-011-9507-x

Schmenner, R. W., and Tatikonda, M. V. (2005). Manufacturing process flexibility revisited. *InternationalJournal Operations Production Manage.*

Shkolnykova, M. (2020). *Firm innovation and industry transformation. the case of German biotechnology* (Bremen, Germany: Universität Bremen).

Smith, O., Nicholson, W. V., Kistler, L., Mace, E., Clapham, A., Rose, P., et al. (2019). A domestication history of dynamic adaptation and genomic deterioration in sorghum. *Nat. Plants* 5 (4), 369–379. doi: 10.1038/s41477-019-0397-9

Søgaard Jørgensen, P., Folke, C., Henriksson, P. J., Malmros, K., Troell, M., and Zorzet, A. (2020). Coevolutionary governance of antibiotic and pesticide resistance. *Trends Ecol. Evol.* 35 (6), 484–494. doi: 10.1016/j.tree.2020.01.011

Tabashnik, B. E. (1994). Delaying insect adaptation to transgenic plants: seed mixtures and refugia reconsidered. *Proc. R. Soc. London. Ser. B: Biol. Sci.* 255 (1342), 7–12. doi: 10.1098/rspb.1994.0002

Tabashnik, B. E. (2008). Delaying insect resistance to transgenic crops. *Proc. Natl. Acad. Sci. United States America* 105 (49), 19029–19030. doi: 10.1073/pnas.0810763106

Tabashnik, B., and Carrière, Y. (2017). Surge in insect resistance to transgenic crops and prospects for sustainability. *Nat. Biotechnol.* 35, 926–935. doi: 10.1038/nbt.3974

Timmermann, M. (2009). *Der Züchterblick: Erfahrung, Wissen und Entscheidung in der Getreidezüchtung* (Aachen, Germany: Shaker Verlag).

Tsaftaris, S. A., Minervini, M., and Scharr, H. (2016). Machine learning for plant phenotyping needs image processing. *Trends Plant Sci.* 21 (12), 989–991. doi: 10.1016/j.tplants.2016.10.002

van de Wiel, C. C., van der Linden, C. G., and Scholten, O. E. (2016). Improving phosphorus use efficiency in agriculture: opportunities for breeding. *Euphytica* 207 (1), 1–22. doi: 10.1007/s10681-015-1572-3

van de Wouw, M., van Hintum, T., Kik, C., van Treuren, R., and Visser, B. (2010). Genetic diversity trends in twentieth century crop cultivars: a meta analysis. *TAG. Theor. Appl. Genet.* 120 (6), 1241–1252. doi: 10.1007/s00122-009-1252-6

van Dijk, A. D. J., Kootstra, G., Kruijer, W., and de Ridder, D. (2021). Machine learning in plant science and plant breeding. *iScience* 24 (1), 101890.

Varah, A., Ahodo, K., Coutts, S. R., Hicks, H. L., Comont, D., Crook, L., et al. (2020). The costs of human-induced evolution in an agricultural system. *Nat. sustainability* 3 (1), 63–71. doi: 10.1038/s41893-019-0450-8

Vijayarangan, S., Sodhi, P., Kini, P., Bourne, J., Du, S., Sun, H., et al. (2018). "High-throughput robotic phenotyping of energy sorghum crops," in *Field and service robotics* (Cham: Springer), 99–113.

Viseu, A. (2015). Integration of social science into research is crucial. *Nat. News* 525 (7569), 291. doi: 10.1038/525291a

Watt, M., Fiorani, F., Usadel, B., Rascher, U., Muller, O., and Schurr, U. (2020). Phenotyping: New windows into the plant for breeders. *Annu. Rev. Plant Biol.* 71, 689–712. doi: 10.1146/annurev-arplant-042916-041124

Watt, M., Silk, W. K., and Passioura, J. B. (2006). Rates of root and organism growth, soil conditions, and temporal and spatial development of the rhizosphere. *Ann. Bot.* 97 (5), 839–855. doi: 10.1093/aob/mcl028

Wieland, T. (2004). *Wir beherrschen den pflanzlichen Organismus besser,…: Wissenschaftliche Pflanzenzüchtung in Deutschland 1889-1945* (München, Deutschland: Deutsches Museum).

Wilkinson, M. D., Dumontier, M., Aalbersberg, I. J. J., Appleton, G., Axton, M., Baak, A., et al. (2016). The fair guiding principles for scientific data management and stewardship. *Sci. Data* 3 (1). doi: 10.1038/sdata.2016.18

Xu, Y., and Crouch, J. H. (2008). Marker-assisted selection in plant breeding: From publications to practice. *Crop Sci.* 48 (2), 391–407. doi: 10.2135/cropsci2007.04.0191

Yang, W., Feng, H., Zhang, X., Zhang, J., Doonan, J. H., Batchelor, W. D., et al. (2020). Crop phenomics and high-throughput phenotyping: Past decades, current challenges, and future perspectives. *Mol. Plant* 13 (2), 187–214. doi: 10.1016/j.molp.2020.01.008

Yiin, J. H., Daniels, R. D., Kubale, T. L., Dunn, K. L., and Stayner, L. T. (2016). A study update of mortality in workers at a phosphate fertilizer production facility. *Am. J. Ind. Med.* 59 (1), 12–22. doi: 10.1002/ajim.22542

frontiers | Frontiers in Plant Science

TYPE Original Research
PUBLISHED 30 October 2023
DOI 10.3389/fpls.2023.1253706

OPEN ACCESS

EDITED BY
Ulrich Schurr,
Helmholtz Association of German Research Centres (HZ), Germany

REVIEWED BY
Juliano Lino Ferreira,
Embrapa Pecuária Sul, Brazil
Asrat Asfaw,
International Institute of Tropical Agriculture (IITA), Nigeria

*CORRESPONDENCE
Tiago de Souza Marçal
tiago.marcal@ufla.br
Vinicius Samuel Martins
viniciusmartins93@outlook.com

RECEIVED 06 July 2023
ACCEPTED 25 September 2023
PUBLISHED 30 October 2023

CITATION
Martins VS, Andrade MHML, Padua LN, Miguel LA, Fernandes Filho CC, Guedes ML, Nunes JAR, Hoffmann L Jr, Zotarelli L, Resende MFRd Jr, Carneiro PCS and Marçal TdS (2023) Evaluating the impact of modeling the family effect for clonal selection in potato-breeding programs. *Front. Plant Sci.* 14:1253706. doi: 10.3389/fpls.2023.1253706

Evaluating the impact of modeling the family effect for clonal selection in potato-breeding programs

Vinicius Samuel Martins[1]*, Mario Henrique Murad Leite Andrade[2], Leticia Novais Padua[1], Luciana Aparecida Miguel[1], Claudio Carlos Fernandes Filho[3], Marcio Lisboa Guedes[4], Jose Airton Rodrigues Nunes[1], Leo Hoffmann Jr[5], Lincoln Zotarelli[5], Márcio Fernando Ribeiro de Resende Jr[5], Pedro Crescêncio Souza Carneiro[6] and Tiago de Souza Marçal[1]*

[1]Departamento de Biologia, Universidade Federal de Lavras, Lavras, Brazil, [2]School of Food and Agriculture, University of Maine, Orono, ME, United States, [3]Centro de Tecnologia Canavieira (CTC), Piracicaba, Brazil, [4]Rede Interuniversitária para o Desenvolvimento do Setor Sucroenergético (RIDESA), Universidade Federal de Goiás, Goiânia, Brazil, [5]Department of Horticultural Sciences, Institute of Food and Agricultural Sciences, University of Florida, Gainesville, FL, United States, [6]Departamento de Biologia, Universidade Federal de Viçosa, Viçosa, Brazil

Because of its wide distribution, high yield potential, and short cycle, the potato has become essential for global food security. However, the complexity of tetrasomic inheritance, the high level of heterozygosity of the parents, the low multiplication rate of tubers, and the genotype-by-environment interactions impose severe challenges on tetraploid potato–breeding programs. The initial stages of selection take place in experiments with low selection accuracy for many of the quantitative traits of interest, for example, tuber yield. The goal of this study was to investigate the contribution of incorporating a family effect in the estimation of the total genotypic effect and selection of clones in the initial stage of a potato-breeding program. The evaluation included single trials (STs) and multi-environment trials (METs). A total of 1,280 clones from 67 full-sib families from the potato-breeding program at Universidade Federal de Lavras were evaluated for the traits total tuber yield and specific gravity. These clones were distributed in six evaluated trials that varied according to the heat stress level: without heat stress, moderate heat stress, and high heat stress. To verify the importance of the family effect, models with and without the family effect were compared for the analysis of ST and MET data for both traits. The models that included the family effect were better adjusted in the ST and MET data analyses for both traits, except when the family effect was not significant. Furthermore, the inclusion of the family effect increased the selective efficiency of clones in both ST and MET analyses via an increase in the accuracy of the total genotypic value. These same models also allowed the prediction of clone effects more realistically, as the variance components associated with family and clone effects within a family were not confounded. Thus, clonal selection based on the total genotypic value, combining the effects of family and clones within a family,

proved to be a good alternative for potato-breeding programs that can accommodate the logistic and data tracking required in the breeding program.

KEYWORDS

Solanum tuberosum L., nested structure, accuracy, G×E interactions, autotetraploid genetics, tuber yield

1 Introduction

Potato is the third most important crop for human consumption worldwide, playing a central role in global food security. Potato has a wide adaptation and higher yield compared with cereal crops (FAO, 2020). It will certainly continue to have an essential role in food security in the coming years, particularly regarding population growth (Devaux et al., 2014; FAO, 2020; Devaux et al., 2021). The world's average potato production has grown at a rate of 2% per year for the past 20 years, with an average yield of 21.0 Mg ha^{-1}, which represents only 13% of the potential yield (Kunkel and Campbell, 1987; FAO, 2021). The gap in production between average and potential yield presents the potential for increasing global potato production. This potential can be exploited through technological innovations in the potato production system, using new and improved cultivars, and optimizing agricultural practices. Within the framework of genetic improvement, tuber yield can be increased through an accurate selection of clones more tolerant to biotic and abiotic stresses, and more efficient in the use of resources, such as water and nitrogen, meeting the demand for an increasingly sustainable global production system (Foley et al., 2011; Birch et al., 2012; Obidiegwu et al., 2015; Dahal et al., 2019; Devaux et al., 2021).

Tetraploid potato–breeding programs generate thousands of seedlings annually (Stich and Van Inghelandt, 2018). Larger populations are required to increase the probability of selecting superior clones because potato breeders must deal with the complexity of tetrassomic segregation, heterosis, and high level of heterozygosity of parents (Meyer et al., 1998; Gopal, 2015). A small number of seed potatoes are available in the early stages of a potato-breeding program (Haynes et al., 2012; Stich and Van Inghelandt, 2018), which restricts the use of repetitions and the number of plants per plot (Haynes et al., 2012; Paget et al., 2017). In this context, the use of unreplicated designs, such as the augmented block design (ABD) (Federer, 1956), has been frequent (Andrade et al., 2020; Fernandes Filho et al., 2021). Partially replicated design (P-REP) (Cullis et al., 2006) is an efficient alternative in the initial stages of potato breeding (Paget et al., 2017). Furthermore, P-REP can be increased (Williams et al., 2011; Williams et al., 2014), i.e., a proportion of candidates can be replicated in each location, which allows the study of genotype-by-environment interaction (G×E) even with limited seed.

The G×E heavily influences quantitative traits of economic importance in potatoes. Currently, up to 40 traits can be selected in potato-breeding programs (Bradshaw, 2017), where the low correlation of the main traits between the environments results in a considerable loss of genetic gain (Andrade et al., 2021). This effect is significant for potato-breeding programs in tropical and subtropical regions as the crop is grown in different seasons throughout the year (winter, fall, and summer). Therefore, one goal of this program is the development of heat-tolerant clones by assessing promisor clones in contrasting seasons to determine their ability to withstand heat stress (Fernandes Filho et al., 2021; Patiño-Torres et al., 2021). Mixed model methodologies have an important role in connecting these different experiments and estimating parameters that are useful for the selection process (Henderson et al., 1959; Smith et al., 2001; Smith et al., 2015).

The limited number of repetitions, presence of G×E, and low heritability result in low selection accuracy in the early stages of a potato-breeding program. This implies low genetic progress over the selection cycles once accuracy is directly proportional to expected gains with selection (Cobb et al., 2019). Using a genetic relationship matrix has been demonstrated to increase the accuracy of estimated breeding values for traits with low heritability. This approach leverage information from all relatives (half and full-sibs, parents, etc.) to accurately estimate the breeding values of candidates (Slater et al., 2014a). However, in estimating non-additive effects, such as dominance, you need a balanced mating design to capture general and specific combining ability (Amadeu et al., 2020; Voss-Fels et al., 2021; Yadav et al., 2021).

The prediction of the total genotypic value (additive + non-additive effects) for complex quantitative traits, such as tuber yield, in the initial stage of the potato-breeding programs, relies on the use of genomic resources (Stich and Van Inghelandt, 2018; Amadeu et al., 2020; Voss-Fels et al., 2021; Wilson et al., 2021; Yadav et al., 2021). Nevertheless, early-stage genotyping is more expensive than phenotyping, making unfeasible use of genomic selection in some research, especially in stages where many candidates were evaluated (Stich and Van Inghelandt, 2018; Wilson et al., 2021; Bradshaw, 2022). Alternatively, Piepho et al. (2008) argued that the use of models with nested structure (Family/Clone = Family + Family + Clone) could be advantageous. These models account implicitly for the kinship relationship. Furthermore, using this structure allows us to predict the total genotypic value more easily, without the need for a kinship matrix, which can be valuable in cases where the mating design does not allow an accurate estimation of the specific combining ability.

The dominance effect can be estimated with a kinship matrix using complete mating design or using genomics. A third alternative is the modeling of the family effect. Although the

nested structure appears naturally in the initial stage of potato-breeding programs because seedlings are derived from different crosses (usually bi-parental), the family effect has been neglected (Fernandes Filho et al., 2021), mainly due to the easiness of mass selection in the early stages of selection. Therefore, it is hypothesized that using nested structure models can increase the selective efficiency of clones, both in single-trial (ST) and multi-environment–trial (MET) selection schemes.

Thus, this work aims to investigate the impact of the family effect and the selection accuracy of clones in the initial stage of a tetraploid potato–breeding program in ST and MET clonal selection schemes.

2 Materials and methods

2.1 Field trials

2.1.1 Experimental designs and crop management

A total of six trials from the potato-breeding program at the Universidade Federal de Lavras (PROBATATA-UFLA) were installed at the Center for Scientific and Technological Development, City Lavras, Minas Gerais State, Brazil (21°12′19.8″ S, 44°58′48.8″W), located at 919 m American Sign Language (ASL), and soil was classified as red-yellow latosol.

The details of each trial are shown in Table 1. Four trials were designed in an ABD (Federer, 1956), and two trials a P-REP with p_N around 20% were employed (Cullis et al., 2006).

Each plot consisted of five plants spaced 0.30 m between plants and 0.80 m between rows. Crop management practices for all the trials were done according to the recommendations for the state of Minas Gerais, in which 1.5 Mg ha^{-1} of 08-28-16 fertilizer blend (N–P_2O_5–K_2O) was applied during the planting. Side dress fertilizer application was performed with 0.30 Mg ha^{-1} 20-00-20 (N–P_2O_5–K_2O). All the trials were irrigated using a sprinkler irrigation system, according to the need of the crop and the incidence of rainfall through the seasons.

2.1.2 Levels of heat stress

The trials were evaluated in three seasons with different levels of heat stress: without heat stress (WHS), moderate heat stress (MHS), and high heat stress (HHS) (Figure 1). The trials WHS (season from May to September), MHS (February to May), and HHS (November to February) were carried out during winter, fall, and summer seasons, respectively (Figure 1; Table 1).

The compensated mean temperatures (TMEAN, °C) were obtained using the expression TMEAN = (T9am + 2T9pm + TMAX + TMIN)/5, where T9am, T9pm, TMAX, and TMIN are the air temperature at 9 a.m., 9 p.m., maximum, and minimum, respectively (INMET, 2022).

2.1.3 Phenotyping

Two traits were evaluated in each trial: total tuber yield (TTY – Mg ha^{-1}) and specific gravity (SG). Total tuber yield was estimated by the weight of all tubers harvested in 1.2 m^2 for each plot. The SG was estimated by the expression SG = tuber mass in air/(tuber mass in the air – tuber mass in water), where tuber mass in air and tuber mass in water were measured from fresh samples of tubers, ranging from 2.0 kg and 2.5 kg, using a hydrostatic scale (Schippers, 1976).

2.2 Statistical analysis

A nested genetic treatment structure was evaluated. The clones were obtained from different clonal families. Thus, it is possible to access family and clone within-family effects from the data.

For the analysis, in which c clones were sampled from s clonal families and evaluated together with p checks, the general form of the linear mixed model is presented in Equation (1). This model is suitable for both ST or MET data. For MET data analysis, appropriate (co)variance structures should be used to model the vectors of the family ($\mathbf{u}_s$) and clone within-family ($\mathbf{u}_c$) effects, aiming to account for the G×E:

$$\mathbf{y} = \mathbf{1}\boldsymbol{\mu} + \mathbf{X}_o\boldsymbol{\tau}_o + \mathbf{Z}_s\mathbf{u}_s + \mathbf{Z}_c\mathbf{u}_c + \mathbf{Z}_b\mathbf{u}_b + \mathbf{e} \quad (1)$$

TABLE 1 Trials characterization, size, and number of blocks, family, clone, check, and percentage of plots replicate.

Trial†	Year	Design‡	Number of levels					p_N§
			Block	Family	Clone	Check	Plot	
POP1(WHS)	2013	ABD	48	24	477	3	621	22.71
POP2(WHS)	2017	ABD	20	31	491	2	531	7.16
POP2(MHS)	2017	ABD	20	31	491	2	531	7.16
POP2(HHS)	2018	ABD	20	31	491	2	531	7.16
POP3(WHS)	2021	P-REP	20	12	304	4	400	23.00
POP3(HHS)	2021	P-REP	20	12	312	3	400	21.25

†The trial identification: POP1(WHS), POP2(WHS), POP2(MHS), POP2(HHS), POP3(WHS), and POP3(HHS), where the codes POP1, POP2, and POP3 identify different clonal populations and codes WHS, MHS, and HHS identify three different seasons, varying in the function of stress level: without heat stress (WHS) moderate heat stress (MHS), and high heat stress (HHS).
‡Experimental designs: augmented block design (ABD) and partially replicated design (P-REP).
§p_N: percentage of plots experimental units occupied by replicated clones, given by the expression. $p_N = (N - N_{treat})/N$, where N is the number of plots and N_{treat} is the number of treatments.

10.3389/fpls.2023.1253706

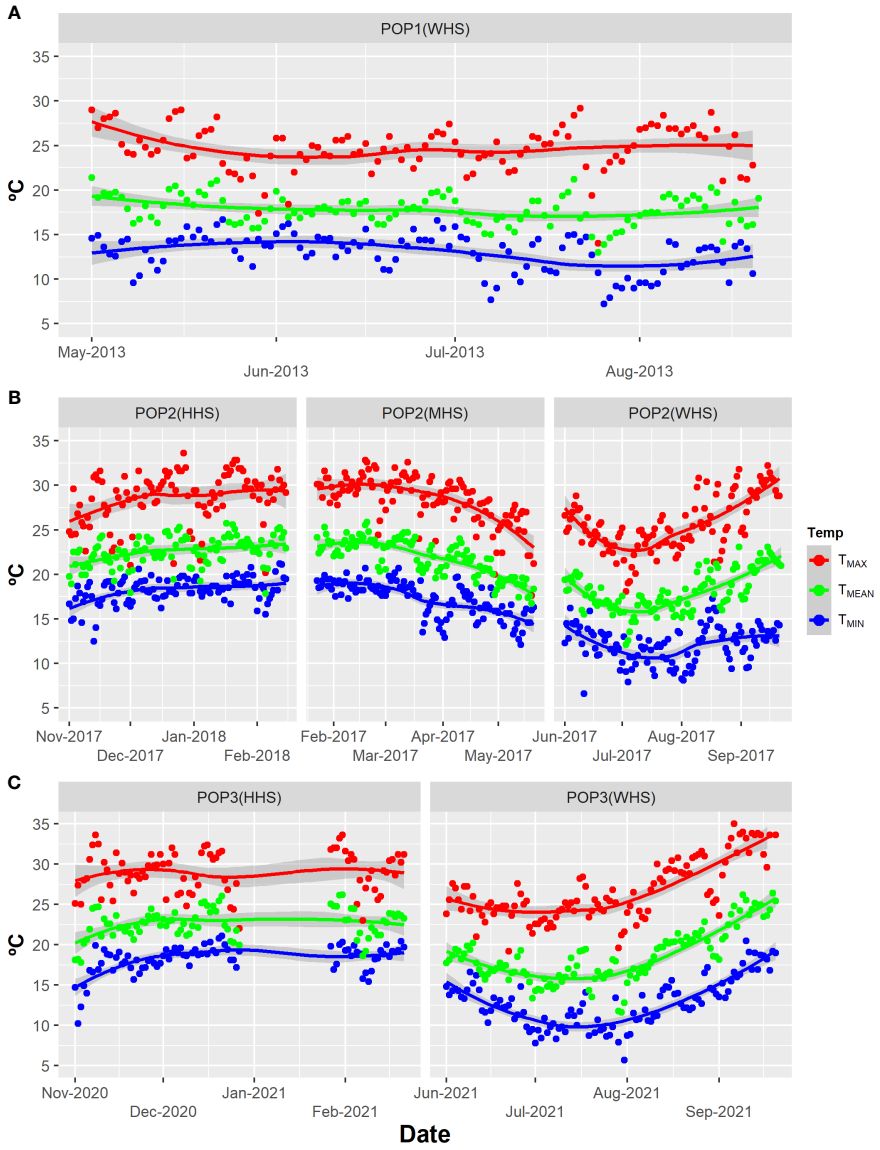

FIGURE 1
Temp: Maximum temperature (T_{MAX}), minimum temperature (T_{MIN}), and compensated mean temperature (T_{MEAN}) in degrees Celsius for all trials: **(A)** POP1(WHS), ranging from May to August of 2013; **(B)** POP2(WHS), ranging from June to September 2017; POP2(MHS), ranging from February to May 2017; POP2(HHS), ranging from November 2017 to February 2018; POP3(WHS), ranging from June to September 2021; and **(C)** POP3(HHS), ranging from November 2020 to February 2021 for Lavras, Minas Gerais State, Brazil (INMET, 2022). Seasons varying in terms of stress level: without heat stress (WHS) moderate heat stress (MHS), and high heat stress (HHS) from 2013 to 2021.

where $\mathbf{y}^{(N\times 1)}$ is the vector of phenotypic observations, where N is the number of plots for ST data or plots by seasons for MET data; $\mathbf{1}^{(N\times 1)}$ is a vector in which all elements are unity; $\boldsymbol{\mu}^{(1\times 1)}$ is the intercept; $\boldsymbol{\tau}_o^{(o\times 1)}$ is the vector of fixed effects, composed of check, environment, and check by environment interaction effects (the environment and check by environment interaction effects were only used in MET data analysis), associated with matrix the design $\mathbf{X}_o^{(N\times o)}$ (assuming full rank), where o is the number of fixed effects; $\mathbf{u}_s^{(s\times 1)}$ is the vector of random effects of family associated with the design matrix $\mathbf{Z}_s^{(N\times s)}$, where s is the number of families for ST data or families by seasons for MET data; $\mathbf{u}_c^{(cs\times 1)}$ is the vector of random genotypic effects of clone within-family associated with the design matrix $\mathbf{Z}_c^{(N\times cs)}$, where c is the number of clone within-family for ST data or clone within-family by seasons for MET data; $\mathbf{u}_b^{(b\times 1)}$ is the vector of random effects of block associated with the design matrix $\mathbf{Z}_b^{(N\times b)}$, where b is the number of blocks for ST data or blocks by seasons for MET data; and $\mathbf{e}^{(N\times 1)}$ is the vector of random errors.

We assume that the $\mathbf{u}_c$, $\mathbf{u}_s$, $\mathbf{u}_b$, and $\mathbf{e}$ vectors of random effects are mutually independent and distributed as multivariate Gaussian, with zero means and (co)variance matrices $\text{var}(\mathbf{u}_c) = \mathbf{G}_c$, $\text{var}(\mathbf{u}_s) = \mathbf{G}_s$, $\text{var}(\mathbf{u}_b) = \mathbf{G}_b$, and $\text{var}(\mathbf{e}) = \mathbf{R}$. The structures of these (co) variance matrices are shown in Table 2 for ST (STMpF and STMwF) and MET (METMpF and METMwF) data analysis models, including or not the family effect, respectively. For STMwF and METMwF models, the vector of clone effects was

TABLE 2 Summary of models fitted: single-trial model without family effect (STMwF), single-trial model plus family effect (STMpF), multi-environment–trial model without family effect (METMwF), and multi-environment–trial model plus family effect (METMpF).

(Co)variance matrix	Single-trial analysis		Multi-environment–trial analysis	
	STMwF	STMpF	METMwF	METMpF
$\mathbf{G}_b$	$\sigma_b^2\ \mathbf{I}_b$	$\sigma_b^2\ \mathbf{I}_b$	$\oplus_{j=1}^{t}\ \sigma_{bj}^2\ \mathbf{I}_{bj}$	$\oplus_{j=1}^{t}\ \sigma_{bj}^2\ \mathbf{I}_{bj}$
$\mathbf{G}_s$		$\sigma_s^2\ \mathbf{I}_s$		$\mathbf{G}_{ts}\otimes\mathbf{I}_s$
$\mathbf{G}_c$	$\sigma_{c'}^2\ \mathbf{I}_c\otimes\mathbf{I}_s$	$\sigma_c^2\ \mathbf{I}_c\otimes\mathbf{I}_s$	$\mathbf{G}_{tc'}\otimes\mathbf{I}_c\otimes\mathbf{I}_s$	$\mathbf{G}_{tc}\otimes\mathbf{I}_c\otimes\mathbf{I}_s$
$\mathbf{R}$	$\sigma^2\ \mathbf{I}_N$	$\sigma^2\ \mathbf{I}_N$	$\oplus_{j=1}^{t}\ \sigma_j^2\ \mathbf{I}_{Nj}$	$\oplus_{j=1}^{t}\ \sigma_j^2\ \mathbf{I}_{Nj}$

$\mathbf{G}_b$, $\mathbf{G}_s$, $\mathbf{G}_c$, and $\mathbf{R}$: (co)variance matrices associated with the block, family, clone within-family, and error effects, respectively; $\mathbf{G}_{ts}$, $\mathbf{G}_{tc'}$, and $\mathbf{G}_{tc}$: unstructured (co)variance matrices used to accommodate the G×E interaction for the family, clone, and clone within-family effects, respectively; $\sigma_b^2, \sigma_{bj}^2,\ \sigma_s^2,\ \sigma_{c'}^2, \sigma_c^2,\ \sigma^2$, and σ_j^2: variance components associated with the block, block in each trial, family, clone, clone within-family, error, and error in each trial effects, respectively; $\mathbf{I}_b$, $\mathbf{I}_{bj}$, $\mathbf{I}_s$, $\mathbf{I}_c$, $\mathbf{I}_N$ e, and $\mathbf{I}_{Nj}$: identity matrices associated with the block, block in each trial, family, clone within-family, error, and error in each trial effects, respectively; ⊗: Kronecker product operator; ⊕: direct sum operator.

called $\mathbf{u}_{c'}$. For the MET data analysis, the heterogeneity of variances of block and error effects was accommodated by the direct sum operation (⊕), whereas the heterogeneity of the variances and covariances of the G×E interaction for family and clone within-family effects was accommodated by the direct product operation (⊗). The (co)variance matrices of environments for family and clone within-family effects were modeled by an unstructured matrix with $t(t + 1)/2$ covariance parameters, where t is the number of trials.

The covariance parameters of models shown in Table 2 were estimated by the residual maximum likelihood (REML) method (Patterson and Thompson, 1971) and best linear unbiased predictions (BLUP) of the random effects by Henderson's mixed model equations (Henderson et al., 1959) through the software Echidna Mixed Models (Gilmour, 2021) version 1.61. The graphic plots and other analyses discussed in the following sections were performed using the R software (R Core Team, 2021) and R packages base and ggplot2 (Wickham, 2016).

2.2.1 Single-trial analysis

From the linear mixed model for STMpF presented in Table 2, the vector of random total genotypic effects of clones can be predicted for ST analysis ($\mathbf{u}_{gST}$) by combining the vectors of family ($\mathbf{u}_s$) and clone within-family ($\mathbf{u}_c$) effects as presented in Equation (2). The (co)variance structure of the $\mathbf{u}_{gST}$ vector is given by the composite symmetry (CS) form as shown in Equation (3):

$$\mathbf{u}_{gST} = (\mathbf{1}_c \otimes \mathbf{I}_s)\,\mathbf{u}_s + \mathbf{u}_c \tag{2}$$

$$\text{var}(\mathbf{u}_{gST}) = (\sigma_s^2\mathbf{J}_c + \sigma_s^2\mathbf{I}_c) \otimes \mathbf{I}_s \tag{3}$$

where $\mathbf{1}_c$ is a vector in which all elements are unity, $\mathbf{J}_c$ is a matrix in which all elements are unity, and σ_s^2 and σ_c^2 are variance components of family and clone within-family effects, respectively.

The simple reparameterization of Equation (3), for correlation scale, allows obtaining ρ_S correlation by Equation (4). This correlation ranges from 0 to 1 (assuming $\sigma_s^2 > 0$ and $\sigma_c^2 > 0$) and measures the proportion of total genetic variance due to variation among families.

$$\rho_S = \frac{\sigma_s^2}{\sigma_s^2 + \sigma_c^2} \tag{4}$$

The vector of clone effects ($\mathbf{u}_{c'}$) from STMwF model was also predicted. However, for STMwF, both the variance component and the BLUP of clones are confounded with family effect. Thus, the comparison between STMpF and STMwF models in terms to accuracy of total genotypic values of clones is inadequate if $\sigma_s^2 > 0$ (Supplementary Information, Note S1). In this context, the STMpF and STMwF models were compared using the Akaike information criterion (AIC) presented in Equation (5) (Akaike, 1974) and through the correspondence of the top 20% best clones by Czekanowski coefficient (Qiao et al., 2000) [CC, Equation (6)], as well as ranking concordance through the Spearman correlation coefficient (r_S) between $\mathbf{u}_{c'}$ and $\mathbf{u}_{gST}$. Furthermore, the variance components of the STMwF and STMpF models were tested using the likelihood ratio test (LRT) shown in Equation (7):

$$\text{AIC} = -2\ell + 2p \tag{5}$$

$$\text{CC} = a/(a + b) \tag{6}$$

$$\text{LRT} = -2\ln(\ell_1/\ell_2) \tag{7}$$

where ℓ is the maximum point of residual log-likelihood function, p is the number of variance parameters, a is the number of coincident clones by both selection strategies, b is the number of divergent clones by both selection strategies, ℓ_1 is the maximum point of residual log-likelihood function from reduced model (without the effect tested), and ℓ_2 is the maximum point of residual log-likelihood function from complete model.

Although the variance component σ_c^2 represents the average within-families genotypic variance, the BLUP of the clone within-family effect is coded to the overall mean and adjusted for the family structure, which allows for comparison of clones from different families (Supplementary Information, Note S1). Thus, we also compared the selection by $\mathbf{u}_c$ and $\mathbf{u}_{gST}$ vectors through the correspondence of the top 20% best clones by Czekanowski coefficient [Equation (6)], as well as ranking concordance through the Spearman correlation coefficient (r_S).

10.3389/fpls.2023.1253706

To facilitate the visualization of the results, the variance components of the STMwF and STMpF models have been presented at percentage of total variation (sum of all variance components of ST analysis of the STMwF or STMpF model). To compare the efficiency of the selection strategies based on total genotypic ($\mathbf{u}_{gST}$) and clone within-family ($\mathbf{u}_c$) effects from STMpF, we assessed the efficiency through the accuracy ratio of respective effects.

2.2.2 Multi-environment–trial analysis

The models METMwF and METMpF are extensions of the models STMwF and STMpF for MET data, respectively (Table 2). Similarly, to what was done for the STMpF model, the vector of total genotypic effects may also be predicted for the MET analysis using the METMpF model, combining the vectors of family ($\mathbf{u}_s$) and clone within-family ($\mathbf{u}_c$) effects as presented in Equation (8). However, unlike Equation (2), Equation (8) capitalizes the G×E. The (co)variance structure of vector $\mathbf{u}_{gMET}$ is given by multivariate compound symmetry form as shown in Equation (9):

$$\mathbf{u}_{gMET} = (\mathbf{1}_c \otimes \mathbf{I}_s \otimes \mathbf{I}_t)\mathbf{us} + \mathbf{u}_c \tag{8}$$

$$\text{var}(\mathbf{u}_{gMET}) = (\mathbf{G}_{ts} \otimes \mathbf{J}_c + \mathbf{G}_{tc} \otimes \mathbf{I}_c) \otimes \mathbf{I}_s \tag{9}$$

where $\mathbf{I}_t$ is an identity matrix of trials and $\mathbf{G}_{ts}$ and $\mathbf{G}_{tc}$ are (co) variance matrices of trials for family and clone within-family effects.

A similar vector to the vector $\mathbf{u}_{gMET}$ may also be predicted from the METMwF model, which was called $\mathbf{u}_{c'}$. However, because of the reasons highlighted in Section 2.2.1, the models METMpF and METMwF models were compared using the AIC presented in Equation (5) (Akaike, 1974) and through the correspondence of the top 20% best clones by Czekanowski's coefficient (CC) (Qiao et al., 2000) [Equation (6)], as well as ranking concordance through the Spearman correlation coefficient (r_S) based on FAI-BLUP index score (Rocha et al., 2018), between the strategies ($\mathbf{u}_{gMET}$ vs. $\mathbf{u}_{c'}$).

Because of the difficulty of performing the LRT test for parameters of the unstructured matrices ($\mathbf{G}_{tc'}$, $\mathbf{G}_{ts}$, and $\mathbf{G}_{tc}$), two 95% confidence intervals were used for parameters of the METMwF and METMpF models. The first one, based on Chi-Square distribution (SAS Institute, 2016), used the variance components for family and clones within-family. The second is based on the Normal distribution (Meyer, 2008) for the correlations between pairs of environments for family and clone within-family effects (Supplementary Information, Note S2).

The genotypic correlations between the environment pairs for clone ($\rho_{G_{c'}}$), family (ρ_{G_s}), and clone within-family (ρ_{G_c}) effects were estimated from parameters of matrices $\mathbf{G}_{tc'}$, v$\mathbf{G}_{ts}$, and $\mathbf{G}_{tc}$, using the expressions (10), (11), and (12):

$$\rho_{G_{c'ij}} = \frac{\sigma_{c'_{ij}}}{\sqrt{\sigma^2_{c'_i} \times \sigma^2_{c'_j}}} \tag{10}$$

$$\rho_{G_{sij}} = \frac{\sigma_{s_{ij}}}{\sqrt{\sigma^2_{s_i} \times \sigma^2_{s_j}}} \tag{11}$$

$$\rho_{G_{cij}} = \frac{\sigma_{c_{ij}}}{\sqrt{\sigma^2_{c_i} \times \sigma^2_{c_j}}} \tag{12}$$

where $\sigma_{c'_{ij}}$, $\sigma_{s_{ij}}$, and $\sigma_{c_{ij}}$ are covariances between environments pairs i and j for clone, family, and clone within-family effects; $\sigma^2_{c'_i}$ and $\sigma^2_{c'_j}$ are variance components of environments i and j for clone effect; $\sigma^2_{s_i}$ and $\sigma^2_{s_j}$ are variance components of environments i and j for family effect; and $\sigma^2_{c_i}$ and $\sigma^2_{c_j}$ are variance components of environments i and j for clone within-family effect.

The visualization of the results and the variance components of the models METMwF and METMpF were presented in percentage of total variation for each trial (sum of all variance components for each trial of the MET analysis of the model METMwF or METMpF). To compare the effectiveness of the selection strategies based on total genotypic ($\mathbf{u}_{gMET}$) and clone within-family ($\mathbf{u}_c$) effects from METMpF, we assessed the effectiveness through the accuracy ratio of respective effects.

Finally, we used the FAI-BLUP index (Rocha et al., 2018), to rank the clones based on predicted BLUPs of MET data for both strategies ($\mathbf{u}_{gMET}$ vs. $\mathbf{u}_c$). The two selection strategies have been compared as described before. Conducted the exploratory factor analysis, with Factor Analysis (FA) and Principal Component Analysis (PCA). PCA was used to extract the factorial loads from the genetic correlation matrix, obtained by the predicted values (BLUPs). The analysis used is varimax criterion (Kaiser, 1958) for the analytic rotation and the calculation of the factor scores of the weighted least squares method (Bartlett, 1938). Thus, PCA and FA were performed on the set of BLUP mean for six variables from population 2, three seasons (POP2HHS, POP2MHS, and POP2WHS), and two traits (TTY and SG) of each vector $\mathbf{u}_c$, $\mathbf{u}_{c'}$, and $\mathbf{u}_{gMET}$. They were estimated from multi-environment–trial model without the family effect (METMwF) and multi-environment–trial model plus the family effect (METMpF).

2.2.3 Accuracy of family, clone within-family, total genotypic effects, and relative efficiency

The accuracy of family ($r_{\hat{s}s}$), clone within-family ($r_{\hat{c}c}$), total genotypic effects ($r_{\hat{g}g}$), and relative efficiency (RE) were obtained by expressions (13), (14), (15), and (16) for both ST and MET data analysis:

$$\text{r}_{\hat{s}s} = \sqrt{1 - \frac{v_s}{\sigma^2_s}} \tag{13}$$

$$\text{r}_{\hat{c}c} = \sqrt{1 - \frac{v_c}{\sigma^2_c}} \tag{14}$$

$$\text{r}_{\hat{g}g} = \sqrt{1 - \frac{v_g}{\sigma^2_s + \sigma^2_c}} \tag{15}$$

$$RE = \frac{\text{r}_{\hat{g}g}}{\text{r}_{\hat{c}c}} \tag{16}$$

where v_s, v_c, and v_g are the average prediction error variance of family, clone within-family, and total genotypic effects, respectively.

10.3389/fpls.2023.1253706

The RE was used to measure the difference between the proposed models to ST and MET data.

3 Results

3.1 Comparison of the STMwF and STMpF models

The inclusion of the family effect improved the goodness of fit of the models in all trials, on which the STMpF model showed lower AIC than the STMwF, and the only exception was for TTY from POP3(WHS) (Table 3). In addition, the inclusion of family effect also increased the log-likelihood (ℓ) in all trials for both traits. Only for the TTY trait in the POP3(WHS) trial did this increment does not exceed 1.92 units (critical point for the detection of significant σ_s^2 effect) (Table 3). These results are reinforced by the results of the LRT test (Table 4) and indicate the presence of genetic variability between families in most trials.

Clone ($\sigma_{c'}^2$, STMwF) and clone within-family (σ_c^2, STMpF) variances were significant in all trials for both traits (Table 4; Supplementary Material, Table S2), revealing the existence of genetic variability among clones. The contribution of clone within-family variance (C) to the total phenotypic variance was always lower than the clone effect (C′) (Table 4). However, the magnitude of the difference between C′ and C was directly proportional to the contribution of family variance to the total genetic variation (ρ_S). The amplitude of ρ_S for the SG trait (0.09 and 0.35) exceeded the amplitude for the TTY trait (0.03 and 0.26) (Table 4).

CC and Spearman's correlation coefficient (r_S) were used as comparison criterion for both selection strategies tested ($\mathbf{u}_{c'}$ vs. $\mathbf{u}_{gST}$ and $\mathbf{u}_c$ vs. $\mathbf{u}_{gST}$). It was observed that, regardless of the selection strategy

TABLE 3 Log-likelihood residual (ℓ) and Akaike information criterion (AIC) for single-trial model without family effect (STMwF) and single-trial model plus family effect (STMpF), for all trials and traits.

Trait‡	Model	Trial†	ℓ	AIC
TTY	STMwF	POP1(WHS)	−1,826.81	3,659.63
		POP2(WHS)	−1,459.44	2,924.89
		POP2(MHS)	−1,584.44	3,174.88
		POP2(HHS)	−1,191.74	2,389.47
		POP3(WHS)	−1,031.07	2,068.14
		POP3(HHS)	−1,155.63	2,317.27
	STMpF	POP1(WHS)	−1,820.36	3,648.72
		POP2(WHS)	−1,450.92	2,909.84
		POP2(MHS)	−1,581.43	3,170.85
		POP2(HHS)	−1,189.63	2,387.26
		POP3(WHS)	−1,030.43	2,068.85
		POP3(HHS)	−1,149.94	2,307.87
SG	STMwF	POP1(WHS)	2,587.78	−5,169.57
		POP2(WHS)	2,200.75	−4,395.51
		POP2(MHS)	2,262.34	−4,518.68
		POP2(HHS)	1,822.53	−3,639.06
		POP3(WHS)	1,278.39	−2,550.77
		POP3(HHS)	1,591.35	−3,176.70
	STMpF	POP1(WHS)	2,613.73	−5,219.45
		POP2(WHS)	2,209.84	−4,411.68
		POP2(MHS)	2,276.28	−4,544.56
		POP2(HHS)	1,833.07	−3,658.15
		POP3(WHS)	1,281.73	−2,555.45
		POP3(HHS)	1,594.28	−3,180.55

‡Total tuber yield (TTY; Mg ha^{-1}) and specific gravity (SG).

†The trial identification: POP1(WHS), POP2(WHS), POP2(MHS), POP2(HHS), POP3(WHS), and POP3(HHS), where the codes POP1, POP2, and POP3 identify the different clonal populations and the codes WHS, MHS, and HHS identify three different seasons, varying in function of stress level: without heat stress (WHS) moderate heat stress (MHS), and high heat stress (HHS).

10.3389/fpls.2023.1253706

TABLE 4 Contribution (%) of the variances of block, clone (C′), family (F), clone within-family (C), and residuals (Res.) for the phenotypic variance of the traits total tuber yield (TTY; Mg ha^{-1}) and specific gravity (SG) estimated from single-trial model without family effect (STMwF) and single-trial model plus family effect (STMpF) in different seasons.

Trait	Trial†	STMwF			STMpF				
		Block	Clone (C′)	Res.	Block	Family (F)	Clone (C)	Res.	ρ_S ‡
TTY	POP1(WHS)	2.67^{ns}	40.97**	56.35	2.05^{ns}	7.18**	34.42**	56.35	0.17
	POP2(WHS)	7.88**	47.78**	44.34	5.50**	11.56**	35.56*	47.38	0.26
	POP2(MHS)	3.88**	37.74*	58.38	3.77**	4.43**	32.62*	59.18	0.12
	POP2(HHS)	0.22^{ns}	69.55**	30.23	0.19^{ns}	4.38*	65.25**	30.18	0.06
	POP3(WHS)	7.13**	77.27**	15.61	7.26**	2.32^{ns}	74.90**	15.52	0.03
	POP3(HHS)	1.09^{ns}	68.44**	30.47	1.61^{ns}	8.76**	59.62**	30.01	0.13
SG	POP1(WHS)	9.83**	69.87**	20.30	7.69**	18.56**	53.15**	20.60	0.26
	POP2(WHS)	12.76**	35.00*	52.24	5.03^{ns}	15.11**	28.43*	51.43	0.35
	POP2(MHS)	2.26*	43.40*	54.34	2.10^{ns}	13.60**	29.94*	54.36	0.31
	POP2(HHS)	3.91**	56.78**	39.31	3.57*	12.97**	44.10**	39.36	0.23
	POP3(WHS)	3.29*	57.63**	39.09	3.42*	6.75**	49.88**	39.96	0.12
	POP3(HHS)	8.01**	58.58**	33.41	7.97**	5.04**	52.42**	34.56	0.09

†The trial identification: POP1(WHS), POP2(WHS), POP2(MHS), POP2(HHS), POP3(WHS), and POP3(HHS), where the codes POP1, POP2, and POP3 identify the different clonal populations and the codes WHS, MHS, and HHS identify three different seasons, varying in function of stress level: without heat stress (WHS) moderate heat stress (MHS), and high heat stress (HHS).
‡ρ_S correlation: measures the proportion of total genetic variance due to variation among families.
Significance by the likelihood-ratio test (LRT): p-value< 0.01 "**" and 0.05 "*" and p-value > 0.05 not significant "ns".

and trait, both coefficients showed an inverse relationship with ρ_S, suggesting that an increase in genetic variability among families reduces the similarity of the $\mathbf{u}_{c'}$ and $\mathbf{u}_c$ vectors with the $\mathbf{u}_{gST}$ vector in the ranking of clones. Furthermore, the magnitude of the correlations of the CC and r_S coefficients with ρ_S was higher for the TTY (−0.82 and −0.78) compared with that for the SG (−0.72 and −0.71) (Figure 2).

In general, both CC and r_S showed lower magnitude for the second selection strategy with family effect ($\mathbf{u}_c$ vs. $\mathbf{u}_{gST}$), which

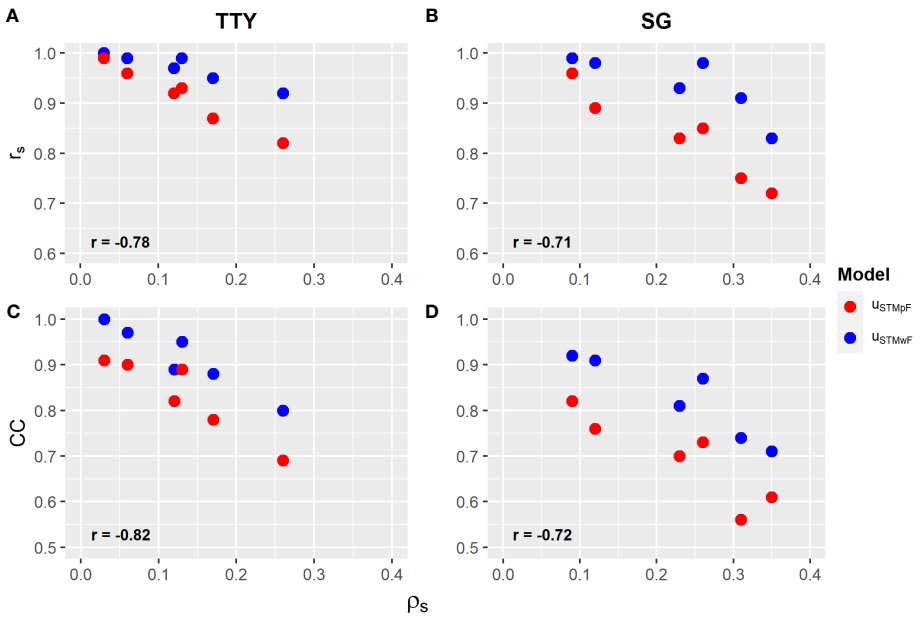

FIGURE 2
(A, B) Spearman correlation coefficient (r_S), and **(C, D)** Czekanowski coefficient (CC) (Supplementary Material, Tables S3, S4) between the proportion of total genetic variance of families (ρ_S) (Table 4) for the vector of clone effects of models from the single trial without family (u_{STMwF}) and plus family effect (u_{STMpF}) to the total tuber yield (TTY; Mg ha^{-1}) and specific gravity (SG). Labels in bold are correlations between selective efficiency and ρ_S.

suggests a greater agreement of the $\mathbf{u}_{c'}$ vector without family effect with $\mathbf{u}_{gST}$ in the clone ranking (Figure 2; Supplementary Material, Tables S4, S5). Furthermore, independent of the selection strategy, an increment in CC and r_S can be observed with increasing heat stress for both traits in POP2 and POP3, except for the TTY in population POP3 (Supplementary Material, Tables S4, S5).

3.2 Relative efficiency of selection based on total genotypic effect of clone for ST analysis

Regardless of the trait, selection based on the vector of total genotypic effects of clone ($\mathbf{u}_{gST}$) was found to be greater than the selection based on the vector of clone effects within family ($\mathbf{u}_c$) (Table 5). The efficiency was directly proportional to ρ_S, showing that the increment in genetic variability among families increases the selective efficiency of clones. The correlation between efficiency and ρ_S was higher for SG (0.88) when compared with that for TTY (0.72) (Figure 3).

On average, the accuracies $r_{\hat{s}s}$, $r_{\hat{c}c}$, and $r_{\hat{g}g}$ were higher for SG (0.80, 0.70, and 0.78, respectively) compared with that for TTY (0.71, 0.69 and 0.74), respectively. The difference between the accuracies $r_{\hat{g}g}$ and $r_{\hat{c}c}$ was higher for SG (0.78 and 0.70) than that for TTY (0.74 and 0.69), which resulted in higher average selective efficiency for the SG (11%) compared with that for TTY (7%) (Table 5).

3.3 Comparison of the METMwF and METMpF models

Variance component associated with family effect in the trial POP3(WHS) was not significant by the LRT test for TTY (Table 4) and, thus, was not included in the MET analysis. The family effect (METMpF) did not improve the goodness of fit compared with the METMwF model for POP3 (Table S5); thus, the MET analysis results were presented only for POP2 (Table 6).

The variance estimates associated with the effects of clone ($\sigma^2_{c'}$, METMwF), family (σ^2_s, METMpF), and clone within-family (σ^2_c, METMpF), as well as their respective contributions to the phenotypic variance, were similar to those obtained in the ST analyses in all trials and traits. The variance components associated with clone, family, and clone within-family were higher than zero in all scenarios (Table S6), confirming the results found in the ST analyses (Tables 4, 6; Supplementary Material, Tables S6, S7). It is worth noting that the values of ρ_S were also like those obtained in the ST analyses (Tables 4, 6).

Overall, variation was observed in the estimates of variance components $\sigma^2_{c'}$, σ^2_s, and σ^2_c across the different seasons for both traits, indicating that populations that have G×E can be attributed to the interaction of a simple nature (Supplementary Material, Table S8). Genetic correlation between seasons for the effects of clone, family, and clone within-family was positive in all scenarios for SG, with values higher than 0.50 in most cases. This suggests a low contribution of complex type G×E for this trait. In contrast, most genetic correlation estimates for TTY were lower than 0.50,

TABLE 5 Accuracy of the family ($r_{\hat{s}s}$), clone within-family (.), and total genotypic ($r_{\hat{g}g}$) effects for traits total tuber yield (TTY; Mg ha^{-1}) and specific gravity (SG) estimated from single-trial model plus family effect (STMpF) in different seasons.

Trait	Trial†	$r_{\hat{s}s}$	$r_{\hat{c}c}$	$r_{\hat{g}g}$	Efficiency‡
TTY	POP1(WHS)	0.74	0.60	0.67	1.12
	POP2(WHS)	0.76	0.64	0.71	1.11
	POP2(MHS)	0.63	0.58	0.63	1.09
	POP2(HHS)	0.60	0.81	0.83	1.02
	POP3(WHS)		0.90§		
	POP3(HHS)	0.81	0.81	0.84	1.02
	Average	0.71	0.69	0.74	1.07
SG	POP1(WHS)	0.87	0.82	0.87	1.06
	POP2(WHS)	0.80	0.58	0.71	1.22
	POP2(MHS)	0.82	0.58	0.71	1.22
	POP2(HHS)	0.79	0.70	0.78	1.11
	POP3(WHS)	0.77	0.75	0.78	1.04
	POP3(HHS)	0.73	0.78	0.80	1.03
	Average	0.80	0.70	0.78	1.11

†The trial identification: POP1(WHS), POP2(WHS), POP2(MHS), POP2(HHS), POP3(WHS), and POP3(HHS), where the codes POP1, POP2, and POP3 identify the different clonal populations and the codes WHS, MHS, and HHS identify three different seasons, varying in function of stress level: without heat stress (WHS) moderate heat stress (MHS), and high heat stress (HHS).

‡Relative efficiency: $r_{\hat{g}g}/r_{\hat{c}c}$ ratio.

§Not included in estimate of average accuracy.

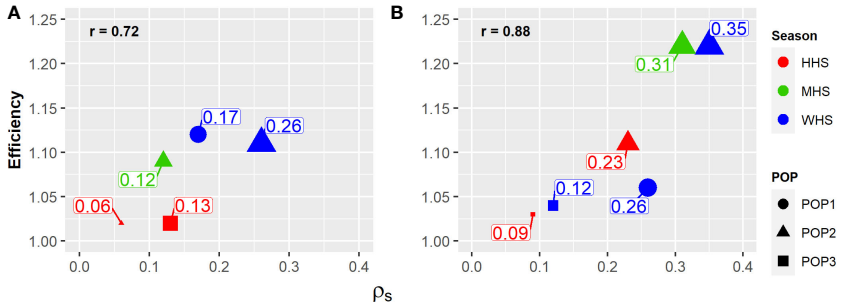

FIGURE 3
Family effect response (ρ_S) (size) on the selective accuracy of potato clones (relative efficiency) in the function of heat stress level (color): without heat stress (WHS), moderate heat stress (MHS), and high heat stress (HHS), in three populations evaluated (shape): POP1, POP2, and POP3. **(A)** Total tuber yield (TTY; Mg ha^{-1}) and **(B)** specific gravity (SG).

suggesting a greater contribution of the complex G×E (Supplementary Material, Tables S6, S7).

Regardless of the model and trait, the variance component estimates associated the effects of clone ($\sigma^2_{c'}$) and clone within-family (σ^2_c) were always higher in the higher heat stress season (HHS) when compared with that in the no heat stress season (WHS), indicating an increase in genetic variability under extreme heat stress (Supplementary Material, Table S1). The variance component associated with family effect (σ^2_s) showed a behavior inversely proportional to the increase of heat stress for the TTY trait, reducing about 50% with the increment of heat stress [11.32 (WHS), 7.32 (MHS), and 3.64 (HHS)] (Supplementary Material, Table S3). Furthermore, regardless of the model adopted, we recorded reductions of 42% and 3% in the average of the clones in the POP2 population for the traits TTY and SG under HHS, respectively (Supplementary Material, Table S3). It is worth noting that, considering the period from the beginning of tuberization (about 30 days after planting) until harvest, the average daily temperature exceeded 20°C on 64% of the days in the MHS season and 88% of the days in the HHS season (88%) (Figure 1).

The exploratory factor analysis showed mean communality of 0.91, 0.91, and 0.87 for the respective vectors $\mathbf{u}_{c'}$, $\mathbf{u}_c$, and $\mathbf{u}_{gMET}$, respectively, indicating that the three factors were sufficient to explain more than 87% of the relationship between seasons. Regardless of the effect, Factor 1 represented the three seasons for SG, Factor 2 represented the WHS and MHS seasons for TTY, and Factor 3 represented only the HHS season (Supplementary Material, Table S8).

After obtaining the FAI-BLUP index scores, which included both traits and all seasons, the Czarnowski's coefficients (CC) and Spearman's correlation (r_S) were utilized to compare the two selection strategies tested ($\mathbf{u}_{c'}$ vs. $\mathbf{u}_{gMET}$ and $\mathbf{u}_c$ vs. $\mathbf{u}_{gMET}$). Similarly, to what was observed for the ST analysis, both CC and r_S showed lower magnitude for the second selection strategy ($\mathbf{u}_c$ vs. $\mathbf{u}_{gMET}$), which suggests closer concordance of the vector $\mathbf{u}_{c'}$ with $\mathbf{u}_{gMET}$ in the ranking of the clones (Table 7).

3.4 Relative efficiency of selection based on the total genotypic effect of clone for MET analysis

Similar to the ST results, independent of trait or season, the selection based on the vector of genotypic effect of clones in the

TABLE 6 Contribution (%) of the variances of blocks, clones (C′), families (F), clone within-family (C), and residuals (Res.) for the phenotypic variance of the traits total tuber yield (TTY; Mg ha^{-1}) and specific gravity (SG) estimated from multi-environment–trial model without family effect (METMwF) and multi-environment–trial model plus family effect (METMpF) in different seasons.

Trait	Trial†	METMwF			METMpF				
		Block	Clone (C′)	Res.	Block	Family (F)	Clone (C)	Res.	ρ_S ‡
TTY	POP2(WHS)	8.75$^+$	48.17$^+$	43.09$^+$	5.80$^+$	11.26$^+$	36.45$^+$	46.48$^+$	0.24
	POP2(MHS)	3.22$^+$	38.34$^+$	58.44$^+$	3.00$^+$	4.81$^+$	33.08$^+$	59.11$^+$	0.13
	POP2(HHS)	0.00$^\#$	70.02$^+$	29.98$^+$	0.00$^\#$	4.38$^+$	65.70$^+$	29.92$^+$	0.06
SG	POP2(WHS)	12.63$^+$	33.33$^+$	54.04$^+$	6.37$^+$	13.50$^+$	28.03$^+$	52.10$^+$	0.33
	POP2(MHS)	1.53$^+$	43.06$^+$	55.41$^+$	1.52$^+$	13.79$^+$	29.70$^+$	54.99$^+$	0.32
	POP2(HHS)	3.81$^+$	56.31$^+$	39.88$^+$	3.47$^+$	12.71$^+$	44.13$^+$	39.69$^+$	0.22

†The trial identification: POP2WHS, POP2MHS, and POP2HHS, where the code POP2 identify the clonal population and codes WHS, MHS, and HHS identify three different seasons, varying in function of stress level: without heat stress WHS, moderate heat stress MHS, and high heat stress HHS.
‡ ρS correlation: measures the proportion of total genetic variance due to variation among families.
$^+$Variance component does not intercept the zero by 95% Chi-Squared confidence intervals.
$^\#$Variance component intercept the zero by 95% Chi-Squared confidence intervals.

TABLE 7 Czekanowski's coefficient (CC) and Spearman's correlation (r_S) between the FAI-BLUP index score vectors of different strategies ($\cup_{c'}$ vs. $\cup_{gMET}$ and $\cup_c$ vs. $\cup_{gMET}$), for traits total tuber yield (TTY; Mg ha^{-1}) and specific gravity (SG).

Strategies†	CC	r_S
$\mathbf{u}_{c'}$ vs. $\mathbf{u}_{gMET}$	0.94	0.98
$\mathbf{u}_c$ vs. $\mathbf{u}_{gMET}$	0.82	0.92

†$\mathbf{u}_{c'}$ is the vector of clone effects from multi-environment–trial model without family effect (METMwF), $\mathbf{u}_c$ is the vector of clone's effects from multi-environment–trial model with family effect (METMpF), and $\mathbf{u}_{gMET}$ is the vector of total genotypic effects of clones from METMpF.

MET ($\mathbf{u}_{gMET}$) was higher than the selection based on the vector of clone within-family in the MET ($\mathbf{u}_c$) (Table 8). It is worth noting that, because of the relationship between the season's pairs, the accuracy associated with the within-family clone effect was increased in all seasons for both traits, although the accuracy associated the family effect was maintained or was increased (Table 8).

For the TTY trait, efficiency estimates were progressively reduced with increasing heat stress levels [1.09 (WHS), 1.06 (MHS), and 1.02 (HHS)], although, for the SG trait, efficiencies were similar in all seasons. On average, the accuracies $r_{\hat{s}s}$, $r_{\hat{c}c}$, and $r_{\hat{g}g}$ were higher for the SG trait (0.82, 0.70, and 0.78) in comparison with the TTY trait (0.70, 0.71, and 0.75), respectively. Furthermore, the magnitude of the difference between the accuracies $r_{\hat{g}g}$ and $r_{\hat{c}c}$ was higher for the SG trait (0.78 and 0.70) detriment of TTY (0.75 and 0.71), which resulted in higher average selective efficiency for the SG trait (12%) when compared to the TTY trait (6%) (Table 8).

4 Discussion

4.1 ST analyses

The results presented here indicate that adjusting for the structure created by family effects can improve the estimation of genetic values. However, it is important to highlight that phenotyping individual data in the early stages of the process may not be compatible with certain breeding pipelines. For example, in certain programs, the first-year evaluation takes place in the field, with mass selection, and using single-hill trials (one seed potato). In this case, the extra phenotyping and modeling of the data would incur additional resources, and the feasibility of such change needs to be evaluated on a case-by-case basis. One technology that potentially can be used to facilitate data collection in the early stages of the program would be the use of aerial images for phenotyping tubers that are dug out of the ground but left in the field (Matias et al., 2020). In contrast, in cases where the early stages are already established with larger plots and randomization of clones, the inclusion of the family effect in the quantitative genetics model would come at no additional effort in data collection.

The genetic progress obtained through conventional potato breeding is slow due to the complexity of the tetrassomic inheritance, the elevated level of heterozygosity of the genitors, and the large number of traits to be assessed (~40) (Haynes et al., 2012; Slater et al., 2014b; Gopal, 2015; Bradshaw, 2017). Potato-breeding programs generate thousands of seedlings annually to overcome these challenges (Stich and Van Inghelandt, 2018). Furthermore, initial stage of potato breeding has low availability of seeds because of the slow tuber multiplication rates, which restricts the use of repetitions and plot size (Paget et al., 2017). These factors contribute to lower experimental precision and selection accuracy.

Typically, the clones being evaluated come from various families, which are often created through biparental crossings. Therefore, the selection process involves making comparisons not only between clones from the same family but also between those from different families. Thus, the effect of clones, and its variance component, are confounded with the family effect. To address this problem and achieve higher selection accuracy, is the use of a nested model, on which the effect of clones is nested within the family effect (Family/Clone = Family + Family + Clone). According to Piepho et al. (2008), models with this structure can be advantageous as they

TABLE 8 Accuracy of family ($r_{\hat{s}s}$), clone within-family ($r_{\hat{c}c}$), and total genotypic ($r_{\hat{g}g}$) effects for traits total tuber yield (TTY; Mg ha^{-1}) and specific gravity (SG) estimated from multi-environment–trial model plus family effect (METMpF) in different seasons.

Trait	Trial†	$r_{\hat{s}s}$	$r_{\hat{c}c}$	$r_{\hat{g}g}$	Efficiency‡
TTY	POP2(WHS)	0.76	0.67	0.73	1.09
	POP2(MHS)	0.68	0.65	0.69	1.06
	POP2(HHS)	0.65	0.82	0.84	1.02
	Average	0.70	0.71	0.75	1.06
SG	POP2(WHS)	0.80	0.67	0.75	1.12
	POP2(MHS)	0.84	0.69	0.78	1.13
	POP2(HHS)	0.82	0.73	0.80	1.10
	Average	0.82	0.70	0.78	1.12

†The trial identification: POP2(WHS), POP2(MHS), POP2(HHS), where the code POP2 identify the clonal population and codes WHS, MHS, and HHS identify three different seasons, varying in function of stress level: without heat stress (WHS) moderate heat stress (MHS), and high heat stress (HHS).
‡Relative efficiency: $r_{\hat{g}g}/r_{\hat{c}c}$ ratio.

implicitly account for the genetic relatedness of clones. It is important to highlight that including the family effect enhances the model performance due to a better representation of the families, once the clones within a family work as repetitions.

Resende et al. (2016) conducted a study on the effectiveness of the nested structure in a dry bean breeding program using progenies from various populations. They emphasized the significance of the population effect, as the use of the nested model resulted in 20 times more repetitions for each population compared to the progenies. Resulted from an increase in the selective efficiency of progenies. Some papers that considered the effect of populations are reported on bean (Resende et al., 2016; Paula et al., 2020) and soybean (Pereira et al., 2017; Volpato et al., 2018) crops. Thus, the nested structure allows obtaining a more accurate BLUP of the family, which enables a more reliable selection of the best clones. In addition, it allows for the selection of the best families, which enables the evaluation of a greater number of clones per family and increased plot size, thereby increasing the probability of obtaining superior clones.

The utilization of a nested structure presents a significant advantage in providing precise estimations of genetic parameters. This is because the variance components within and between families are not confounded, which can happen in models that do not take family effects into account (Supplementary Material, Note S1). In the former, the heritability of clones is overestimated due to the variance component of family, whereas, in the nested models, the family structure gives a better estimate of the clone effect (Supplementary Material, Note S1). The effects of clone and clone within-family are only equivalent when the variance component of families is zero or close to zero. Pereira et al. (2017) indicates that incorporating the population effect into the estimation of genetic and non-genetic components in soybean breeding data offers a more accurate and realistic methodology.

Higher accuracy was observed using the vector of total genotypic effects ($\mathbf{u}_{gST}$), obtained by combining the vectors of family effects ($\mathbf{u}_s$) and clone within-family ($\mathbf{u}_c$), and it was directly proportional to the contribution of the variance component associated with family in the total genetic variation (ρ_S). Resende et al. (2016) in a simulation study showed that the selection accuracy increases in function of the increased contribution of the between-population variance component to the total genetic variation. Therefore, although, in potato breeding, the genetic variance between families is lower than the genetic variance within families, the inclusion of the effect of family can increase the selection accuracy because the heritability of families has been, in general, higher than the heritability of clone within-family (Diniz et al., 2006; Melo et al., 2011). Greater average RE recorded for the SG trait is associated with the higher mean accuracy for the effect of families (0.80) and the higher ρ_S mean (0.23).

The utilization of the family effect in potato breeding, which models the nested effect of clones within the family, has been shown to be advantageous. This methodology has led to an improvement in the accuracy of predicting the genotypic values of clones and has achieved a greater degree of RE for the two traits that were studied. The increase in accuracy achieved by the nested model does not reflect increased costs in cases where the data are already recorded. We expect that animal modeling properly accounting for additive and dominance effects would also result in more efficient results. However, the results showed that family effect inclusion is a simpler approach, mainly in cases where the mating design is not complete.

4.2 MET analyses

Understanding and effectively managing the G×E interaction is essential for achieving long-term improvements in plant breeding programs because the success of a new cultivar depends on its improved performance on different traits (e.g., TTY and SG) while also presenting good adaptability and stability. The G×E assumes a particular importance for potato breeding, mainly under tropical conditions, because heat stress limits yield and quality in the hottest periods of the year (Fleisher et al., 2017; Fernandes Filho et al., 2021; Patiño-Torres et al., 2021).

Potato crop generally presents better performance in regions with temperate climate, with average temperatures between 5°C and 21°C (Haverkort and Verhagen, 2008). With temperature exceeding 21°C, heat stress significantly reduces tuber yield and quality, due to a series of physiological changes, including an increase in tuber disorders (e.g., internal heat necrosis, knobs, and tuber chain), reduced plant growth, increased respiration rate, greater allocation of dry biomass to leaves at the expense of the tubers, and the reduction in photosynthetic pigments (Lambert et al., 2006; Haverkort and Verhagen, 2008; Hancock et al., 2014; Rykaczewska, 2015; Patiño-Torres et al., 2021). Thus, the selection of heat-tolerant clones is vital to increase potato tuber yield and quality.

Brazil potato season is carried out in three distinct seasons: dry (January to March), winter (April to July), and water (August to December) seasons. Temperatures above the critical threshold, 21°C, are commonly recorded in the dry and water seasons (Andrade et al., 2021). Fernandes Filho et al. (2021) classified these seasons according to their level of heat stress: MHS, WHS, and HHS. One of the major limiting factors for Brazilian potato yield is the use of cultivars that are poorly adapted for tropical conditions and hot temperatures.

The Universidade Federal de Lavras's potato-breeding program has worked intensively developing heat-tolerant clones (Benites and Pinto, 2011; Figueiredo et al., 2015; Fernandes Filho et al., 2021; Patiño-Torres et al., 2021). To determine which clones, have high heat tolerance, they are tested under varying levels of heat stress. Only clones that perform well under mild and high temperatures are selected (Benites and Pinto, 2011; Rykaczewska, 2015; Fernandes Filho et al., 2021; Patiño-Torres et al., 2021). Furthermore, Andrade et al. (2021) reported that environments with a higher level of heat stress showed a greater capacity to differentiate clones according to their performance.

The strategy mentioned above for selecting heat-tolerant clones requires clones to be evaluated in two or more contrasting environments regarding heat stress. According to Smith et al. (2001), to better evaluate G×E, it is more realistic to use models that consider variance heterogeneity and genetic covariances when analyzing MET data. Cullis et al. (1998) and Smith et al. (2001) reported a significant reduction in the log-likelihood REML when homogenous variance was assumed for the G×E. In multiplicative

models for MET data, the interaction of simple nature is accounted by the heterogeneity of genetic variances along the environments, whereas the complex interaction is accounted by the heterogeneity of genetic correlations between pairs of environments (Crossa et al., 2004; Eeuwijk et al., 2016). According to Eeuwijk et al. (2016), when the genetic correlations between two environments are high, it means that there is a smaller percentage of complex interaction involved.

MET data analysis can be carry out in one or two stages (Cullis et al., 1998; Smith et al., 2001; Smith et al., 2015; Gogel et al., 2018). Although the two-stage analysis is often employed, under unbalance (varying number of genotypes between environments or varying number of repetitions between and within environments), a common condition in the early stage of potato-breeding programs, the MET data analysis in one stage is more efficient (Cullis et al., 1998; Smith et al., 2001; Paget et al., 2017; Gogel et al., 2018).

Although the analysis of MET data is advantageous because of the advantage of the interrelationship between environments, it is increasing selective accuracy and allows a better interpretation of the G×E interaction (Smith et al., 2001; Kelly et al., 2007). The family effect, naturally present in the initial stage of potato-breeding programs, has also been neglected in this type of analysis (Fernandes Filho et al., 2021). However, one can combine the advantages cited above with those described in Section 4.1. Making MET analysis a powerful tool for clone selection in the early stages of potato-breeding programs, especially under tropical conditions, it is opportune to highlight that the recovery of inter-environmental information was more pronounced for the effect of clones within-family because of the higher magnitude of genetic correlations between seasons. This corroborates with the lower magnitude of the selective efficiency in MET analysis comparison to ST analysis. Selective efficiency for the TTY trait progressively reduced with increasing heat stress levels, whereas the selective efficiency for the SG trait was maintained practically constant. These results ratify the importance of environments with higher heat stress levels to discriminate potato clones for the TTY trait, as well as the greater contribution of the family effect to the selection of superior clones for the SG trait.

The unstructured model can be used in cases when only a few trials are included, due to the smaller number of parameters that need to be estimated, avoiding the use of factor analysis (Smith et al., 2001; Melo et al., 2020; Fernandes Filho et al., 2021). However, the use of the unstructured model implies the prediction of genotypic effects for each trial (Kelly et al., 2007; Eeuwijk et al., 2016; Melo et al., 2020; Fernandes Filho et al., 2021). Hence, it is desirable to use a selection index to capture the G×E interaction and to combine MET analyses realized for multiple traits (Kelly et al., 2007; Melo et al., 2020; Fernandes Filho et al., 2021).

There are many options for selection indexes (Mendes et al., 2009; Rocha et al., 2018; Yan and Frégeau-Reid, 2018; Melo et al., 2020). Among the different indexes, the FAI-BLUP index stands out, because it can incorporate data from various environments and traits without the need for weights. It also avoids issues with multicollinearity and makes it easier to understand the G×E interaction through exploratory factor analysis (Rocha et al., 2018; Oliveira et al., 2019). In the present study, factor analysis showed a superior performance in summarizing the relationships among environments (WHS, MHS, and HHS) and traits (TTY and SG) for each effect ($\mathbf{u}_{c'}$, $\mathbf{u}_{c}$, and $\mathbf{u}_{gMET}$). In addition, the factor analysis showed that the SG trait had a lower level of interaction because all seasons were grouped under Factor 1. On the other hand, the TTY trait had a higher level of interaction as the WHS and HHS seasons were grouped under distinct factors. Thus, including the effect of families in the MET analysis is a helpful strategy to increase the accuracy of superior clone selection.

Finally, the inclusion of the family effect increased the selective efficiency of clones in ST and MET selection on schemes through an increment in the accuracy of the total genotypic value. On average, the selective efficiency of clones was 11% and 7% for ST and 12% and 6% in MET for the traits SG and TTY, respectively. An expressive reduction of the family effect under heat stress for TTY and of lower magnitude for SG was observed.

Thus, the results of the present work suggest that the inclusion of the family effect in clone selection models, in the initial stage of potato-breeding programs, is desirable because it contributes to increasing the selective efficiency of clones without generating additional costs, especially for the SG trait.

Data availability statement

The original contributions presented in the study are included in the article/Supplementary Material. Further inquiries can be directed to the corresponding authors.

Author contributions

VM: Conceptualization, Data curation, Formal Analysis, Investigation, Methodology, Project administration, Writing – original draft, Writing – review & editing. MA: Supervision, Writing – review & editing. LP: Data curation, Writing – review & editing. LM: Data curation, Writing – review & editing. CF: Data curation, Writing – review & editing. MG: Data curation, Writing – review & editing. JN: Supervision, Writing – review & editing. LJ: Supervision, Writing – review & editing. LZ: Supervision, Writing – review & editing. MR: Supervision, Writing – review & editing. PC: Supervision, Writing – review & editing. TM: Conceptualization, Formal Analysis, Investigation, Methodology, Project administration, Supervision, Validation, Writing – original draft, Writing – review & editing.

Funding

This work was partially supported by the Brazilian funding agencies: Conselho Nacional de Desenvolvimento Científico e Tecnológico (CNPq), Fundação de Amparo à Pesquisa do Estado de Minas Gerais (FAPEMIG), Coordenação de Aperfeiçoamento de Pessoal de Nível Superior (CAPES).

Conflict of interest

The authors declare that the research was conducted in the absence of any commercial or financial relationships that could be construed as a potential conflict of interest.

Publisher's note

All claims expressed in this article are solely those of the authors and do not necessarily represent those of their affiliated organizations, or those of the publisher, the editors and the reviewers. Any product that may be evaluated in this article, or claim that may be made by its manufacturer, is not guaranteed or endorsed by the publisher.

Supplementary material

The Supplementary Material for this article can be found online at: https://www.frontiersin.org/articles/10.3389/fpls.2023.1253706/full#supplementary-material

References

Akaike, H. (1974). A new look at the statistical model identification. *IEEE Trans. Automat Contr* 19, 716–723. doi: 10.1109/TAC.1974.1100705

Amadeu, R. R., Ferrão, L. F. V., Oliveira, I., de, B., Benevenuto, J., Endelman, J. B., et al. (2020). Impact of dominance effects on autotetraploid genomic prediction. *Crop Sci.* 60, 656–665. doi: 10.1002/csc2.20075

Andrade, M. H. M. L., Fernandes Filho, C. C., Fernandes, M. O., Bastos, A. J. R., Guedes, M. L., Marçal, T., et al. (2020). Accounting for spatial trends to increase the selection efficiency in potato breeding. *Crop Sci.* 60, 2354–2372. doi: 10.1002/csc2.20226

Andrade, M. H. M. L., Patiño-Torres, A. J., Cavallin, I. C., Guedes, M. L., Carvalho, R. P., Gonçalves, F. M. A., et al. (2021). Stability of potato clones resistant to potato virus Y under subtropical conditions. *Crop Breed Appl. Biotechnol.* 21, 1–9. doi: 10.1590/1984-70332021v21n1a8

Bartlett, M. S. (1938). Methods of estimating mental factors. *Nature* 141, 609–610.

Benites, F. R. G., and Pinto, C. A. B. P. (2011). Genetic gains for heat tolerance in potato in three cycles of recurrent selection. *Crop Breed Appl. Biotechnol.* 11, 133–140. doi: 10.1590/S1984-70332011000200005

Birch, P. R. J., Bryan, G., Fenton, B., Gilroy, E. M., Hein, I., Jones, J. T., et al. (2012). Crops that feed the world 8: Potato: are the trends of increased global production sustainable? *Food Secur* 4, 477–508. doi: 10.1007/s12571-012-0220-1

Bradshaw, J. E. (2017). Review and analysis of limitations in ways to improve conventional potato breeding. *Potato Res.* 60, 171–193. doi: 10.1007/s11540-017-9346-z

Bradshaw, J. E. (2022). A brief history of the impact of potato genetics on the breeding of tetraploid potato cultivars for tuber propagation. *Potato Res.* 65, 461–501. doi: 10.1007/s11540-021-09517-w

Cobb, J. N., Juma, R. U., Biswas, P. S., Arbelaez, J. D., Rutkoski, J., Atlin, G., et al. (2019). Enhancing the rate of genetic gain in public-sector plant breeding programs: lessons from the breeder's equation. *Theor. Appl. Genet.* 132, 627–645. doi: 10.1007/s00122-019-03317-0

Crossa, J., Yang, R.-C., and Cornelius, P. L. (2004). Studying crossover genotype × environment interaction using linear-bilinear models and mixed models. *J. Agric. Biol. Environ. Stat.* 9, 362–380. doi: 10.1198/108571104X4423

Cullis, B., Gogel, B., Verbyla, A., and Thompson, R. (1998). Spatial analysis of multi-environment early generation variety trials. *Biometrics* 54, 1. doi: 10.2307/2533991

Cullis, B. R., Smith, A. B., and Coombes, N. E. (2006). On the design of early generation variety trials with correlated data. *J. Agric. Biol. Environ. Stat.* 11, 381–393. doi: 10.1198/108571106X154443

Dahal, K., Li, X.-Q., Tai, H., Creelman, A., and Bizimungu, B. (2019). Improving potato stress tolerance and tuber yield under a climate change scenario – A current overview. *Front. Plant Sci.* 10. doi: 10.3389/fpls.2019.00563

Devaux, A., Goffart, J.-P., Kromann, P., Andrade-Piedra, J., Polar, V., and Hareau, G. (2021). The potato of the future: opportunities and challenges in sustainable agri-food systems. *Potato Res.* 64, 681–720. doi: 10.1007/s11540-021-09501-4

Devaux, A., Kromann, P., and Ortiz, O. (2014). Potatoes for sustainable global food security. *Potato Res.* 57, 185–199. doi: 10.1007/s11540-014-9265-1

Diniz, M. C. D. R., Pinto, C. A. B. P., and de Lambert, E. S. (2006). Sample size for family evaluation in potato breeding programs. *Cienc Agrotecnologia.* 30, 277–282. doi: 10.1590/S1413-70542006000200013

Eeuwijk, F. A., Bustos-Korts, D. V., and Malosetti, M. (2016). What should students in plant breeding know about the statistical aspects of genotype × Environment interactions? *Crop Sci.* 56, 2119–2140. doi: 10.2135/cropsci2015.06.0375

FAO. (2020). *Food balance sheet* (Food and Agriculture Organization of the United Nations). Available at: www.fao.org/faostat/en/#data/FBS (Accessed July 01, 2023).

FAO. (2021). (Food and Agriculture Organization of the United Nations. FAOSTAT). Available at: www.fao.org/faostat/en/#data/QCL (Accessed July 01, 2023).

Federer, W. T. (1956). "Augmented (or hoonuiaku) designs," in *Biometrics unit technical reports*, vol. 33. Available at: https://ecommons.cornell.edu/server/api/core/bitstreams/7e626471-05ad-4f2b-858e-be100a513b5e/content

Fernandes Filho, C. C., Andrade, M. H. M. L., Souza Marçal, T., Fernandes, M. O., Bastos, A. J. R., Guedes, M. L., et al. (2021). Selection of potato clones for heat tolerance and resistance to potato viruses X and Y for processing purposes. *Crop Sci.* 61, 552–565. doi: 10.1002/csc2.20361

Figueiredo, I. C. R., Pinto, C. A. B. P., Ribeiro, G. H. M. R., de O., L., Lyra, D. H., and Moreira, C. M. (2015). Efficiency of selection in early generations of potato families with a view toward heat tolerance. *Crop Breed Appl. Biotechnol.* 15, 210–217. doi: 10.1590/1984-70332015v15n4a37

Fleisher, D. H., Condori, B., Quiroz, R., Alva, A., Asseng, S., Barreda, C., et al. (2017). A potato model intercomparison across varying climates and productivity levels. *Glob Chang Biol.* 23, 1258–1281. doi: 10.1111/gcb.13411

Foley, J. A., Ramankutty, N., Brauman, K. A., Cassidy, E. S., Gerber, J. S., Johnston, M., et al. (2011). Solutions for a cultivated planet. *Nature* 478, 337–342. doi: 10.1038/nature10452

Gilmour, A. R. (2021). *Echidna mixed model software*. Available at: www.echidnamms.org/ (Accessed March 05, 2021).

Gogel, B., Smith, A., and Cullis, B. (2018). Comparison of a one- and two-stage mixed model analysis of Australia's National Variety Trial Southern Region wheat data. *Euphytica* 214, 44. doi: 10.1007/s10681-018-2116-4

Gopal, J. (2015). Challenges and way-forward in selection of superior parents, crosses, and clones in potato breeding. *Potato Res.* 58, 165–188. doi: 10.1007/s11540-015-9292-6

Hancock, R. D., Morris, W. L., Ducreux, L. J. M., Morris, J. A., Usman, M., Verrall, S. R., et al. (2014). Physiological, biochemical, and molecular responses of the potato (*Solanum tuberosum* L.) plant to moderately elevated temperature. *Plant Cell Environ.* 37, 439–450. doi: 10.1111/pce.12168

Haverkort, A. J., and Verhagen, A. (2008). Climate change and its repercussions for the potato supply chain. *Potato Res.* 51, 223–237. doi: 10.1007/s11540-008-9107-0

Haynes, K. G., Gergela, D. M., Hutchinson, C. M., Yencho, G. C., Clough, M. E., Henninger, M. R., et al. (2012). Early generation selection at multiple locations may identify potato parents that produce more widely adapted progeny. *Euphytica* 186, 573–583. doi: 10.1007/s10681-012-0685-1

Henderson, C. R., Kempthorne, O., Searle, S. R., and von Krosigk, C. M. (1959). The estimation of environmental and genetic trends from records subject to culling. *Biometrics* 15, 192. doi: 10.2307/2527669

INMET. (2022). *Instituto Nacional de Meteorologia* (INMET). Available at: www.gov.br/agricultura/pt-br/assuntos/inmet (Accessed July 04, 2022).

Kaiser, H. F. (1958). The varimax criterion for analytic rotation in factor analysis. *Psychometrika* 23, 187–200. doi: 10.1007/BF02289233

Kelly, A. M., Smith, A. B., Eccleston, J. A., and Cullis, B. R. (2007). The accuracy of varietal selection using factor analytic models for multi-environment plant breeding trials. *Crop Sci.* 47, 1063–1070. doi: 10.2135/cropsci2006.08.0540

Kunkel, R., and Campbell, G. S. (1987). Maximum potential potato yield in the Columbia Basin, USA: Model and measured values. *Am. Potato J.* 64, 355–366. doi: 10.1007/BF02853597

Lambert, E. S., Pinto, C. A. B. P., and Menezes, C. B. (2006). Potato improvement for tropical conditions: I. Analysis of stability. *Crop Breed Appl. Biotechnol.* 6, 129–135. doi: 10.12702/1984-7033.v06n02a03

Matias, F. I., Caraza-Harter, M. V., and Endelman, J. B. (2020). FIELDimageR: An R package to analyze orthomosaic images from agricultural field trials. *TPPJ* 3:e20005. doi: 10.1002/ppj2.20005

Melo, D. S., Pinto, C. A. B. P., Peixouto, L. S., Neder, D. G., and de Assis, J. C. (2011). Early selection of full-sib potato families. *Cienc. Agrotecnologia* 35, 1101–1109. doi: 10.1590/S1413-70542011000600009

Melo, V. L., de Marçal, T. S., de Rocha, J. R. A. S. C., dos Anjos, R. S. R., Carneiro, P. C. S., and de Carneiro, J. E. S. (2020). Modeling (co)variance structures for genetic and non-genetic effects in the selection of common bean progenies. *Euphytica* 216, 77. doi: 10.1007/s10681-020-02607-9

Mendes, F. F., Ramalho, M. A. P., and de Abreu, Â.F.B. (2009). Selection index for choosing segregating populations in common bean. *Pesqui Agropecu Bras.* 44, 1312–1318. doi: 10.1590/S0100-204X2009001000015

Meyer, K. (2008). Likelihood calculations to evaluate experimental designs to estimate genetic variances. *Heredity (Edinb)* 101, 212–221. doi: 10.1038/hdy.2008.46

Meyer, R. C., Milbourne, D., Hackett, C. A., Bradshaw, J. E., McNichol, J. W., and Waugh, R. (1998). Linkage analysis in tetraploid potato and association of markers with quantitative resistance to late blight (Phytophthora infestans). *Mol. Gen. Genet.* 259, 150–160. doi: 10.1007/s004380050800

Obidiegwu, J. E., Bryan, G. J., Jones, H. G., and Prashar, A. (2015). Coping with drought: stress and adaptive responses in potato and perspectives for improvement. *Front. Plant Sci.* 6. doi: 10.3389/fpls.2015.00542

Oliveira, I. C. M., Marçal, T., de, S., da Bernardino, K. C., de Ribeiro, P. C. O., da Parrella, R. A. C., et al. (2019). Combining ability of biomass sorghum lines for agroindustrial characters and multitrait selection of photosensitive hybrids for energy cogeneration. *Crop Sci.* 59, 1554–1566. doi: 10.2135/cropsci2018.11.0693

Paget, M. F., Alspach, P. A., Anderson, J. A. D., Genet, R. A., Braam, W. F., and Apiolaza, L. A. (2017). Replicate allocation to improve selection efficiency in the early stages of a potato breeding scheme. *Euphytica* 213, 221. doi: 10.1007/s10681-017-2004-3

Patiño-Torres, A. J., Andrade, M. H. M. L., Guedes, M. L., Cavallin, I. C., Pinto, C. A. B. P., Souza, J. C., et al. (2021). Performance of superior potato clones under high and mild temperatures in tropical climate. *Agron. J.* 113, 2349–2360. doi: 10.1002/agj2.20704

Patterson, H. D., and Thompson, R. (1971). Recovery of inter-block information when block sizes are unequal. *Biometrika* 58, 545–554. doi: 10.1093/biomet/58.3.545

Paula, R. G., Pereira, G. S., Paula, I. G., Carneiro, A. L. N., Carneiro, P. C. S., dos Anjos, R. S. R., et al. (2020). Multipopulation recurrent selection: An approach with generation and population effects in selection of self-pollinated progenies. *Agron. J.* 112, 4602–4612. doi: 10.1002/agj2.20422

Pereira, F. C., Bruzi, A. T., de Matos, J. W., Rezende, B. A., Prado, L. C., and Nunes, J. A. R. (2017). Implications of the population effect in the selection of soybean progeny. *Plant Breed* 136, 679–687. doi: 10.1111/pbr.12512

Piepho, H. P., Möhring, J., Melchinger, A. E., and Büchse, A. (2008). BLUP for phenotypic selection in plant breeding and variety testing. *Euphytica* 161, 209–228. doi: 10.1007/s10681-007-9449-8

Qiao, C. G., Basford, K. E., DeLacy, I. H., and Cooper, M. (2000). Evaluation of experimental designs and spatial analyses in wheat breeding trials. *Theor. Appl. Genet.* 100, 9–16. doi: 10.1007/s001220050002

R Core Team. (2021). *R: A language and environment for statistical computing* (Vienna, Austria: R Foundation for Statistical Computing). Available at: www.Rproject.org/.

Resende, M. D. V., Ramalho, M. A. P., Carneiro, P. C. S., Carneiro, J. E. S., Batista, L. G., and Gois, I. B. (2016). Selection index with parents, populations, progenies, and generations effects in autogamous plant breeding. *Crop Sci.* 56, 530–546. doi: 10.2135/cropsci2015.05.0303

Rocha, J. R., do, A. S., de, C., MaChado, J. C., and Carneiro, P. C. S. (2018). Multitrait index based on factor analysis and ideotype-design: proposal and application on elephant grass breeding for bioenergy. *GCB Bioenergy* 10, 52–60. doi: 10.1111/gcbb.12443

Rykaczewska, K. (2015). The effect of high temperature occurring in subsequent stages of plant development on potato yield and tuber physiological defects. *Am. J. Potato Res.* 92, 339–349. doi: 10.1007/s12230-015-9436-x

SAS Institute Inc. (2016). "SAS/STAT® 14.2 user's guide," in *Software* (Cary, NC: SAS Institute Inc).

Schippers, P. A. (1976). The relationship between specific gravity and percentage dry matter in potato tubers. *Am. Potato J.* 53, 111–122. doi: 10.1007/BF02854115

Slater, A. T., Cogan, N. O., Hayes, B. J., Schultz, L., Dale, M. F. B., Bryan, G. J., et al. (2014b). Improving breeding efficiency in potato using molecular and quantitative genetics. *Theor. Appl. Genet.* 127, 2279–2292. doi: 10.1007/s00122-014-2386-8

Slater, A. T., Wilson, G. M., Cogan, N. O. I., Forster, J. W., and Hayes, B. J. (2014a). Improving the analysis of low heritability complex traits for enhanced genetic gain in potato. *Theor. Appl. Genet.* 127, 809–820. doi: 10.1007/s00122-013-2258-7

Smith, A., Cullis, B., and Thompson, R. (2001). Analyzing variety by environment data using multiplicative mixed models and adjustments for spatial field trend. *Biometrics* 57, 1138–1147. doi: 10.1111/j.0006-341X.2001.01138.x

Smith, A. B., Ganesalingam, A., Kuchel, H., and Cullis, B. R. (2015). Factor analytic mixed models for the provision of grower information from national crop variety testing programs. *Theor. Appl. Genet.* 128, 55–72. doi: 10.1007/s00122-014-2412-x

Stich, B., and Van Inghelandt, D. (2018). Prospects and potential uses of genomic prediction of key performance traits in tetraploid potato. *Front. Plant Sci.* 9. doi: 10.3389/fpls.2018.00159

Volpato, L., Simiqueli, G. F., Alves, R. S., Rocha, J. R., do, A. S., de, C., et al. (2018). Selection of inbred soybean progeny (*Glycine max*): an approach with population effect. *Plant Breed* 137, 865–872. doi: 10.1111/pbr.12648

Voss-Fels, K. P., Wei, X., Ross, E. M., Frisch, M., Aitken, K. S., Cooper, M., et al. (2021). Strategies and considerations for implementing genomic selection to improve traits with additive and non-additive genetic architectures in sugarcane breeding. *Theor. Appl. Genet.* 134, 1493–1511. doi: 10.1007/s00122-021-03785-3

Wickham, H. (2016). "ggplot2," in *Data analysis* (Cham: Springer), 189–201. doi: 10.1007/978-3-319-24277-4_9

Williams, E. R., John, J. A., and Whitaker, D. (2014). Construction of more flexible and efficient P-rep designs. *Aust. N Z J. Stat.* 56, 89–96. doi: 10.1111/anzs.12068

Williams, E., Piepho, H.-P., and Whitaker, D. (2011). Augmented p-rep designs. *Biom J.* 53, 19–27. doi: 10.1002/bimj.201000102

Wilson, S., Zheng, C., Maliepaard, C., Mulder, H. A., Visser, R. G. F., van der Burgt, A., et al. (2021). Understanding the effectiveness of genomic prediction in tetraploid potato. *Front. Plant Sci.* 12. doi: 10.3389/fpls.2021.672417

Yadav, S., Wei, X., Joyce, P., Atkin, F., Deomano, E., Sun, Y., et al. (2021). Improved genomic prediction of clonal performance in sugarcane by exploiting non-additive genetic effects. *Theor. Appl. Genet.* 134, 2235–2252. doi: 10.1007/s00122-021-03822-1

Yan, W., and Frégeau-Reid, J. (2018). Genotype by yield*Trait (GYT) biplot: a novel approach for genotype selection based on multiple traits. *Sci. Rep.* 8, 8242. doi: 10.1038/s41598-018-26688-8

frontiers | Frontiers in Plant Science

TYPE Original Research
PUBLISHED 14 November 2023
DOI 10.3389/fpls.2023.1244384

OPEN ACCESS

EDITED BY
Gregorio Egea,
University of Seville, Spain

REVIEWED BY
Sergio Vélez,
Wageningen University and Research, Netherlands
Léo Pichon,
Montpellier SupAgro, France

*CORRESPONDENCE
Meltem Cantürk
cantuerk@igg.uni-bonn.de

RECEIVED 23 June 2023
ACCEPTED 19 October 2023
PUBLISHED 14 November 2023

CITATION
Cantürk M, Zabawa L, Pavlic D, Dreier A, Klingbeil L and Kuhlmann H (2023) UAV-based individual plant detection and geometric parameter extraction in vineyards.
Front. Plant Sci. 14:1244384.
doi: 10.3389/fpls.2023.1244384

UAV-based individual plant detection and geometric parameter extraction in vineyards

Meltem Cantürk*, Laura Zabawa, Diana Pavlic, Ansgar Dreier, Lasse Klingbeil and Heiner Kuhlmann

Institute of Geodesy and Geoinformation, University of Bonn, Bonn, Germany

Accurately characterizing vineyard parameters is crucial for precise vineyard management and breeding purposes. Various macroscopic vineyard parameters are required to make informed management decisions, such as pesticide application, defoliation strategies, and determining optimal sugar content in each berry by assessing biomass. In this paper, we present a novel approach that utilizes point cloud data to detect trunk positions and extract macroscopic vineyard characteristics, including plant height, canopy width, and canopy volume. Our approach relies solely on geometric features and is compatible with different training systems and data collected using various 3D sensors. To evaluate the effectiveness and robustness of our proposed approach, we conducted extensive experiments on multiple grapevine rows trained in two different systems. Our method provides more comprehensive canopy characteristics than traditional manual measurements, which are not representative throughout the row. The experimental results demonstrate the accuracy and efficiency of our method in extracting vital macroscopic vineyard characteristics, providing valuable insights for yield monitoring, grape quality optimization, and strategic interventions to enhance vineyard productivity and sustainability.

KEYWORDS

precision viticulture, grapevine detection, vineyard canopy characteristics, 3D vineyard structure, UAV-based point cloud

1 Introduction

Enhancing and optimizing the productivity and quality of grapevine crops is a primary goal for winegrowers, making vineyard management decisions significant (Moreno and Andújar, 2023). A key factor in achieving this lies in obtaining precise and detailed information about the overall structure of vineyards, which encompasses plant arrangements and geometric canopy attributes. This information plays a pivotal role in making well-informed decisions that are essential for tasks like pruning, applying

pesticides, and maximizing yield (De Castro et al., 2018). Plant-wise canopy characteristics offer insights into plant vigor, which is crucial for informed decisions during the growth season. Despite the challenge of measuring these attributes across the entire vineyard, such as estimating per-plant volumes, their inspection can provide valuable information. This, in turn, has the potential to significantly impact the precise application of sprayed substances, enhancing overall vineyard management strategies (Caruso et al., 2017).

Key geometric parameters of grapevine crops, such as canopy structure, height, width, volume, and leaf area, are closely connected to plant growth, health, and potential yield. These factors allow breeders to identify and efficiently manage distinct vineyard areas, optimizing their cultivation strategies (Moreno and Andújar, 2023). Estimation of these parameters is traditionally performed by human operators collecting manual measurements about the canopy characteristics. However, as this task is labor intensive, these parameters are typically extrapolated from a small sub-section of the vineyard, preventing farmers from making optimal decisions at the individual plant level (Zabawa et al., 2020). Thus, automating the identification and accurate mapping of individual vine rows and trunks becomes crucial for precisely evaluating the vineyard's state (Jurado et al., 2020; Biglia et al., 2022). Recently, Unmanned Aerial Vehicles (UAVs) have been commonly used for this task due to their efficient data acquisition, simplicity, and cost-effectiveness (Matese and Di Gennaro, 2015). UAVs can quickly cover large vineyard areas and capture high-resolution images at low altitudes, offering advantages over ground-based, satellite, and aircraft systems (Ferro and Catania, 2023).

Although some grapevine parameters can be extracted from single images, a complete 3D vineyard model is more effective for investigating conditions under the canopy and deriving traits like biomass, canopy volume, and vine-row width and height (Weiss and Baret, 2017; Pádua et al., 2018; Pádua et al., 2019; Tsouros et al., 2019; Di Gennaro and Matese, 2020; Ferro and Catania, 2023). For an accurate 3D vineyard model, different sensor modalities can be used, including LiDAR sensors, Terrestrial Laser Scanners (TLS), and RGB cameras combined with structure from motion (SfM) algorithm (Remondino and El-Hakim, 2006). LiDAR and SfM point clouds have distinct characteristics that impact their suitability for vineyard plant phenotyping, and several studies compared the accuracy of the two point clouds. In one study (Madec et al., 2017), both UAV-based SfM and ground-based LiDAR showed comparable accuracy in wheat crop height determination, while another (Petrović et al., 2022) showed SfM point cloud superior accuracy in representing grapevine canopies due to its higher data density capture based on ground sampling distance. The affordability of RGB cameras compared to LiDAR has sparked interest, leading to numerous studies utilizing SfM-derived point clouds to estimate vineyard parameters (De Castro et al., 2018; Matese and Di Gennaro, 2018; Jurado et al., 2020; Pádua et al., 2020).

Accurately determining the location of individual plants within a vineyard is crucial for precision vineyard management tasks like selective harvesting, accurate spraying, fertilization and weeding, and effective crop management (Milella et al., 2019). In a related study, Milella et al. (2019) proposed an algorithm using an affordable RGB-D sensor on an agricultural vehicle to estimate per-plant canopy volume via k-means clustering of a reconstructed 3D vine row. However, this method requires knowing the exact plant count (k) and spacing, which is unfeasible for larger vineyards where the number of plants and their spacing can vary significantly between vineyards. Additionally, they segmented images into grape bunches, leaves, and trunks but they did not explore individual trunk detection and only tested on a single vine row. In another study, Jurado et al. (2020) described an automatic method for identifying and locating individual grapevine trunks, posts, and missing plants based on spatial segmentation without using prior knowledge of the number of plants and the distance between plants. However, this method cannot provide the canopy parameters of the vineyard but just the individual plants' locations within a point cloud. Both of these research efforts highlight the challenges of accurately estimating vineyard parameters, particularly when dealing with large-scale vineyards. While they contribute valuable methods for plant detection and identification, they each have limitations regarding the information they can provide about the vineyard as a whole.

Several studies investigated the estimation of geometric canopy characteristics. Mathews and Jensen (2013) utilized the SfM technique to construct a 3D vineyard point cloud to estimate the vine leaf area index (LAI). Furthermore, Weiss and Baret (2017) developed an algorithm that utilizes dense point clouds derived from an SfM algorithm to estimate crucial vineyard structural attributes like row orientation, height, width, and spacing. Similarly, Comba et al. (2018) introduced an unsupervised algorithm for vineyard detection and evaluation of vine-row attributes such as vine rows orientation and inter-rows spacing based on the 3D point cloud. Subsequently, Comba et al. (2019) extended the utilization of 3D point clouds by integrating multispectral and thermal images with RGB data to perform a comprehensive characterization of vineyard vigor. Mesas-Carrascosa et al. (2020) classified 3D point cloud into vegetation and soil using RGB information through color vegetation indices (CVIs) and calculated the height of vines with respect to the classified soil. In a distinct approach, Di Gennaro and Matese (2020) implemented the 2.5D-surface and 3D-alpha shape approaches to build an unsupervised and integrated procedure for biomass estimation and missing plant detection in a vineyard. All the above approaches estimate a subset of the necessary parameters for vineyard management. To the best of our knowledge, no single automatic pipeline capable of concurrently estimating a large set of vine canopy traits from 3D point clouds has been proposed in the literature.

The contribution of this paper is a pipeline to determine single plant locations in a vineyard from UAV-derived point clouds. Additionally, we extract geometric parameters like plant height, width, and volume along the row with a high spatial resolution, making it possible to assign the values to the detected single plants. We demonstrate the method's capability with several datasets generated with an SfM approach using UAV imagery. We also analyze which flight parameters are suitable for the task. Finally, we show the results derived from UAV-based LiDAR data without

changing any parameters of the pipeline. This demonstrates that our pipeline significantly reduces the need for manual parameter tuning and can be successfully applied to different 3D sensors.

2 Materials and methods

2.1 Study site and data acquisition

The study area is located in the experimental vineyard plots of JKI Geilweilerhof in Siebeldingen, Germany. The institute aims to breed new cultivars resistant to grapevine disease, weather-related stress factors, and high-quality wine production. The vineyard plot was composed of 23 rows, comprising 14 rows trained in the semi-minimal pruned hedge (SMPH) system and 9 rows in the vertical shoot positioning (VSP) system, as illustrated in Figure 1. Our investigation focused on assessing the accuracy of the proposed method within two distinct training systems, both characterized by irregular vine spacing.

The VSP system has been commonly used in traditional grape cultivation in Germany due to its suitability for cool climates. However, this system requires labor-intensive tasks like winter pruning and wire

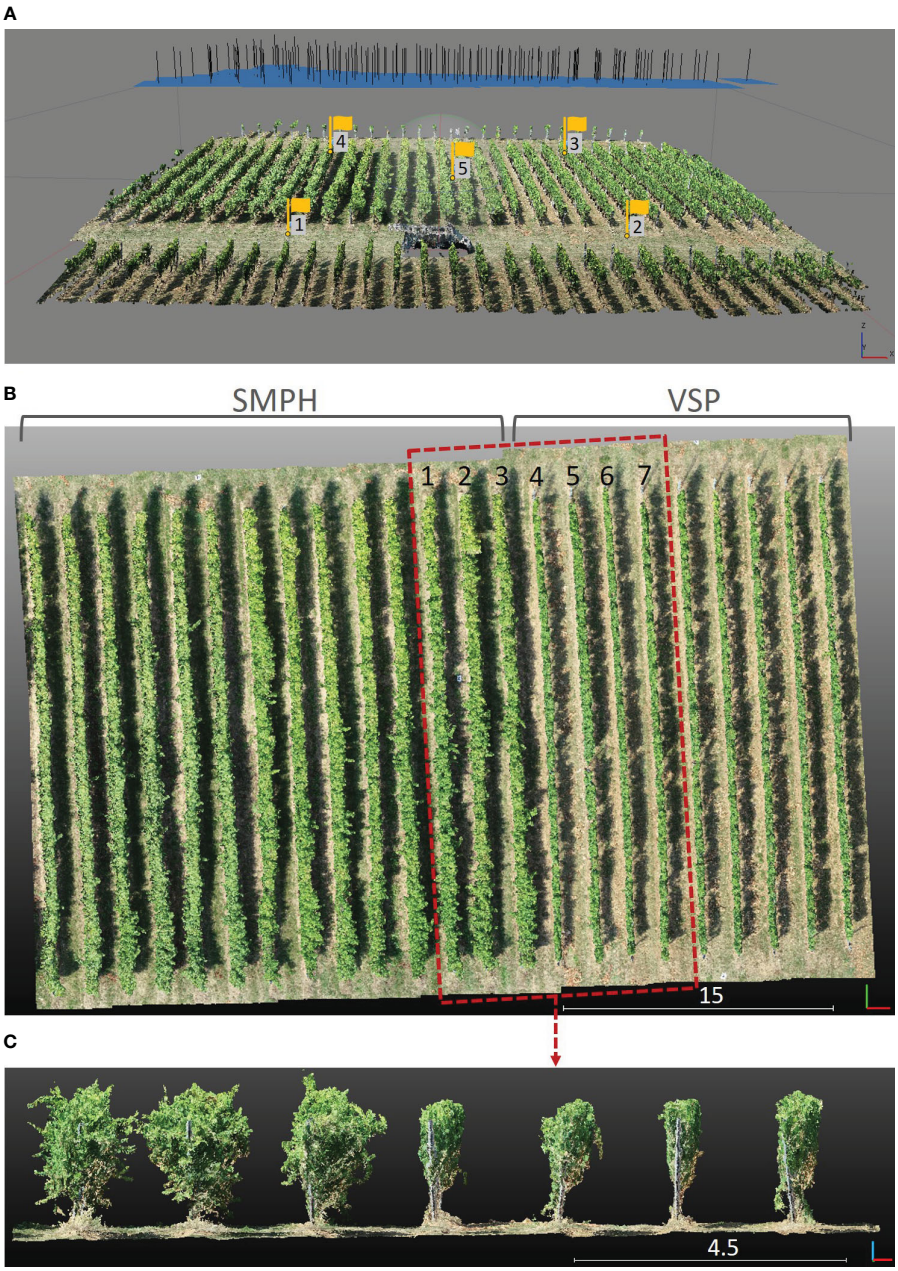

FIGURE 1
(A) The camera positions at the moment of image acquisition and reconstructed 3D point cloud. The 5 yellow flags represent the GCPs. **(B)** Top view of the reconstructed 3D point cloud. The area in the red rectangle was selected as a subset. **(C)** Side view of the subset that comprises 3 rows of the SMPH training system (left) and 4 rows of the VSP training system (right).

positioning, leading to high labor costs. To address this challenge and reduce manual labor expenses, a new training method called SMPH was introduced. SMPH aims to optimize grapevine growth and canopy development while minimizing the need for time-consuming pruning and maintenance activities (Kraus et al., 2018). The SMPH pruning system for grapevines results in notable physiological and morphological changes compared to the traditional VSP trellis. VSP has a single main branch that grows over several years, and the rest gets removed after each growth period. Every year, the other branches regrow. The grapes are mostly positioned near the bottom of the canopy where they are rarely occluded (Zabawa et al., 2019). On the other hand, SMPH allows branches to remain in the trellis after the growing season, creating a more voluminous canopy with older wood and smaller leaves that bud earlier in spring than the VSP. Moreover, it changes the grape cluster structure, producing smaller berries on longer stalks in looser clusters (Pennington, 2019). Two different training systems can be seen in detail in Figure 1C. This distinction highlights the variety of cultivation practices employed within the vineyard, enriching the scope of our study.

This study used two different setups for data collection and generating the vineyard point cloud. The first setting is based on a DJI Phantom 4 Pro quadcopter UAV, equipped with an onboard RGB camera. Three flights were conducted over one plot (49° 13'10.4" N, 8°02'33.5" E) with different heights and camera angles. The flight parameters of the UAV measurements can be seen in Table 1. To obtain the absolute coordinates of the 3D point cloud, 5 ground control points (GCPs) have been measured using the Leica GS18 GNSS RTK system, with 2-3 cm accuracy in position and height. The camera positions at the time of image acquisition at 15 m height and with a nadir angle can be seen in Figure 1A. The point cloud was reconstructed using images with a combination of three different flight parameters and individually with the images belonging to each flight number. This first study setting utilized the SfM technique in Agisoft Metashape Professional (version 1.7.4) to generate 3D point clouds. Aerial images acquired with three different flight parameter settings are aligned using the software automatically identifying features from each image (Che et al., 2020; Wu et al., 2022). For each flight, GCPs were used to get a georeferenced dense point cloud. Since the UAV was equipped with an RGB camera, the result was a 3D point cloud including RGB information. The area in the red rectangle in Figure 1B was manually selected as a subset to investigate the impact of different flight parameters on the extracted plant parameters. The subset included three rows (1, 2, and 3) trained in SMPH, and four rows (4, 5, 6, and 7) trained in VSP. As a result, we obtained four different point clouds, one of them being the *combined* dataset, while the others were associated with their respective flight parameters: *tilted_20m*, *nadir_20m*, and *nadir_15m*.

TABLE 1 Flight parameters of the UAV measurements.

	tilted_20m	*nadir_20m*	*nadir_15m*
Flight height	20 m	20 m	15 m
Camera angle	65°	Nadir	Nadir
Number of images	88	76	153

The second experimental setup for this study is based on a DJI Matrice 600 Pro UAV equipped with a Riegl miniVUX-2UAV laser scanner with a 200kHz pulse repetition rate and a 15 mm accuracy at 50 m distance. Furthermore, the platform has pose estimation sensors onboard, including the Inertial Measurement Unit (IMU) Applanix APX-20 and GNSS antenna Applanix AV14. For this second setting, we used another vineyard plot (49°13'03" N, 8°02'49.5" E). The resulting georeferenced LiDAR point cloud had horizontal accuracy below 0.05 m and vertical accuracy under 0.10 m.

2.2 Point cloud processing pipeline

We proposed a pipeline to extract different phenotypic traits of the vineyard such as plant height, canopy width, and canopy volume as well as individual plant (trunk) positions. The pipeline included three main steps; (i) point cloud separation into the ground (*GroundPCl*) and plant (*PlantPCl*), (ii) individual row segmentation, and (iii) extraction of row parameters. The study workflow is shown in Figure 2. Furthermore, the study utilized the software Matlab 2022b for point cloud processing and CloudCompare 2.12 for point cloud visualization.

2.2.1 Ground-plant separation and height normalization

To extract plant parameters, the point cloud was separated into ground and plant using the Cloth Simulation Filtering (CSF) algorithm (Zhang et al., 2016) in CloudCompare and defined as *Ground PCl* and *Plant PCl*. The CSF algorithm is well-suited for rugged and sloping terrains (Liu et al., 2021). Since the vineyard was located in a sloped area, we used the CSF algorithm to separate ground and plant. The algorithm inverts the point cloud and then covers the inverted surface with a simulated cloth. Using the interactions between the cloth nodes and the corresponding points, the point cloud can be separated into the ground and non-ground points. The main two parameters we tuned in this algorithm are grid resolution *GR* and distance threshold *DT*. *GR* represents the horizontal distance between two neighboring particles in the simulated cloth to cover the terrain. As the *GR* decreases, the level of detail in the resulting digital terrain model becomes more refined. The *DT* determines whether the points are classified as ground or non-ground based on their distances from the cloth grid. Fewer ground points are obtained with a smaller *DT* value, while more points are separated as plants. We chose a grid resolution *GR* of 0.3 m and a distance threshold *DT* of 0.3 m as the parameter settings. The 0.3 m *GR* allowed for capturing sufficient details in the point cloud while maintaining computational efficiency. Similarly, the 0.3 m *DT* was suitable for accurately separating the ground and plant points, minimizing the likelihood of misclassification. The qualitative result can be seen in Figure 3A.

In the point cloud, the z-value of each point was the ellipsoidal height. Since we were interested in plant height which is the vertical distance between the ground level and the uppermost boundary of the primary photosynthetic tissues of a plant (excluding inflorescences) (Perez-Harguindeguy et al., 2016), the separated *PlantPCl* was normalized in height by subtracting the ground point

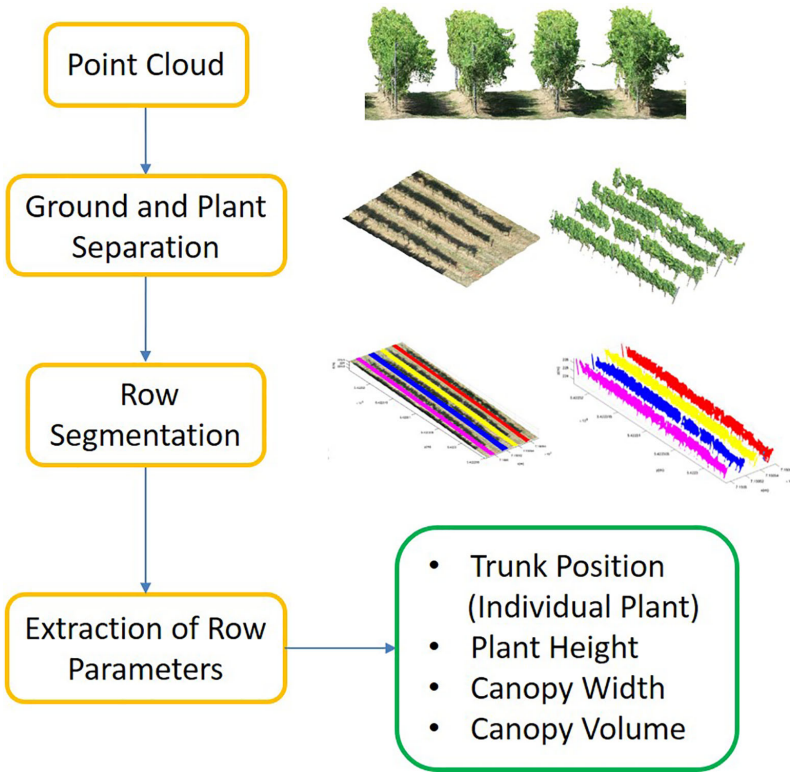

FIGURE 2
Flowchart of the general framework for row parameter extraction.

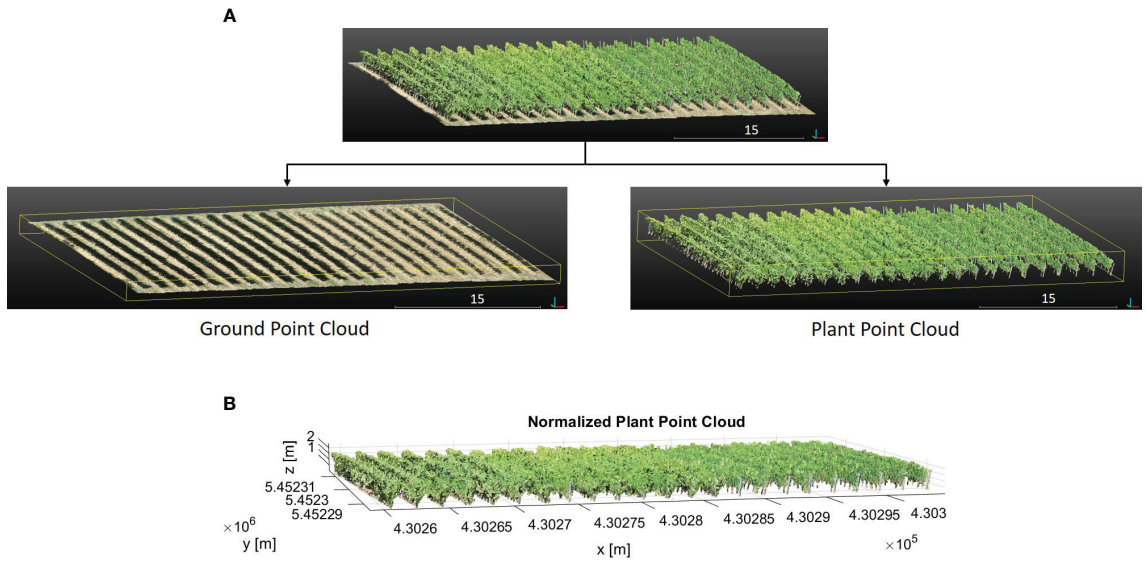

FIGURE 3
(A) The segmentation of the whole point cloud into plant and ground. **(B)** The height-normalized *PlantPCl*.

elevation from all plant points to estimate plant height. By substituting the z-value of each plant point with the computed height difference, the height-normalized *PlantPCl* was obtained (Figure 3B).

2.2.2 Row segmentation

We segmented the *PlantPCl* and *GroundPCl* into individual rows to extract plant parameters row-wise. Our pipeline for row segmentation consisted of two steps: segmentation of the *PlantPCl* into rows and defining a bounding box in 3D space to represent the spatial location of each segmented row to effectively segment the *GroundPCl* into rows as well. The flowchart of the proposed method for row segmentation can be seen in Figure 4.

First, we downsampled the *PlantPCl* to reduce the computational complexity and processing time of the algorithm using a 3D grid box with the size of (0.1 x 0.1 x 0.1 m). Second, we reduced the dimension to 2D by removing the z component. Assuming that the single rows do not overlap, we then applied the Density-based Spatial Clustering of Applications with Noise (DBSCAN) algorithm in the xy-plane. This algorithm was proposed by Ester et al. (1996) and is a density-based clustering algorithm intended to find clusters of any shape. DBSCAN relies on two main parameters: ϵ, the radius distance for point neighbors (Euclidean distance in our case), and P_{min}, the minimum points needed to form a cluster (Amiruzzaman et al., 2022). We selected the parameters of the DBSCAN algorithm empirically based on the characteristics of the point cloud and the desired clustering outcome. After performing some preliminary experiments, we empirically set ϵ to 0.35 m, corresponding to the average inter-point distance in the downsampled *PlantPCl*, capturing closely located point clusters effectively. P_{min} was set to 40 to identify clusters with a sufficient number of points while excluding noise, based on the point density distribution in the point cloud. This value was chosen based on the point density distribution in the downsampled point cloud, making it independent of the input point cloud density.

The initial result of the DBSCAN algorithm can be seen in Figure 5. Each row cluster is shown with a different color. However, these clusters may not be consistent due to gaps or missing plants. To address this issue, we improved the results by incorporating cluster centroids and leveraging the assumption that rows are linear. To achieve this, we fit a 2D line to the row clusters, allowing us to estimate the row orientation. Then, we rotated the point cloud with the row orientation angle θ parallel to the y-axis. After rotation, we calculated the centroids of the clusters and determined their similarity based on Euclidean distances d along the x-axis (Figure 5). Clusters with closely spaced centroids were merged into the same row, while clusters with larger centroid distances were considered separate rows. In our refinement method for row segmentation, we set the d between the centroids of clusters as 1 m by analyzing the datasets to address the issue of disjoint rows merging.

To segment the *GroundPCl* into rows, we used 3D bounding boxes that represent the spatial location of each segmented plant row. As explained before, since the rows had an orientation, it became challenging to compute the skewed boundaries of the bounding boxes. Therefore, we defined the 3D bounding boxes after obtaining the rotated rows. We used the maximum boundaries of the *PlantPCl* in the x and y direction and the boundaries of the *GroundPCl* for the z-direction to calculate the boundaries of the bounding boxes. To segment the *GroundPCl* into rows, we rotated it using the angle θ and used 3D bounding boxes for clustering.

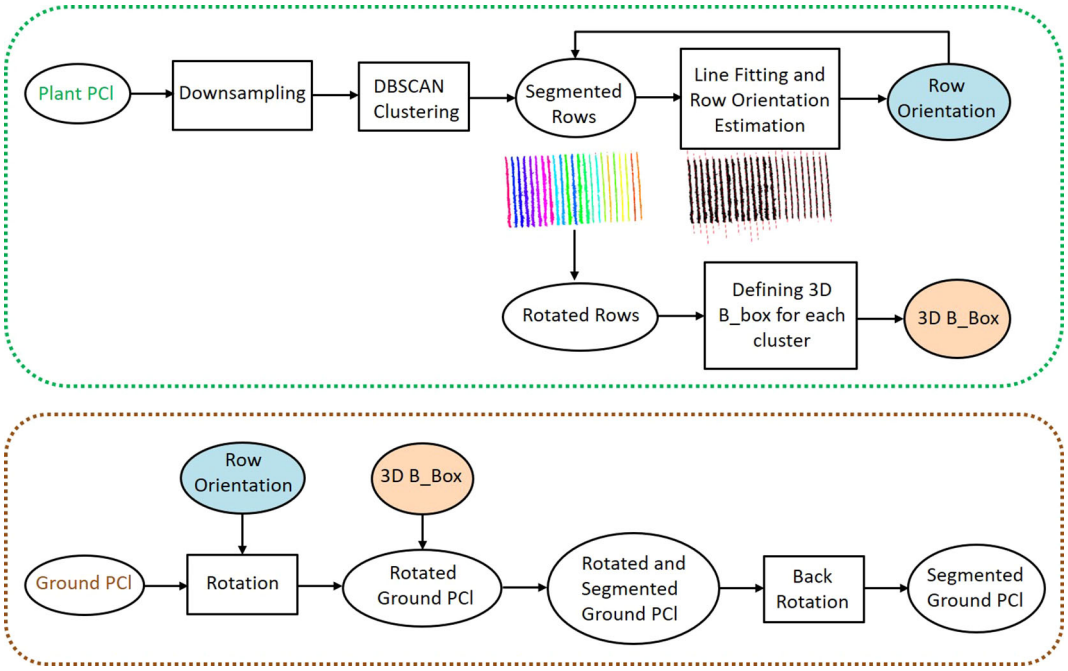

FIGURE 4
The proposed pipeline for the individual row segmentation.

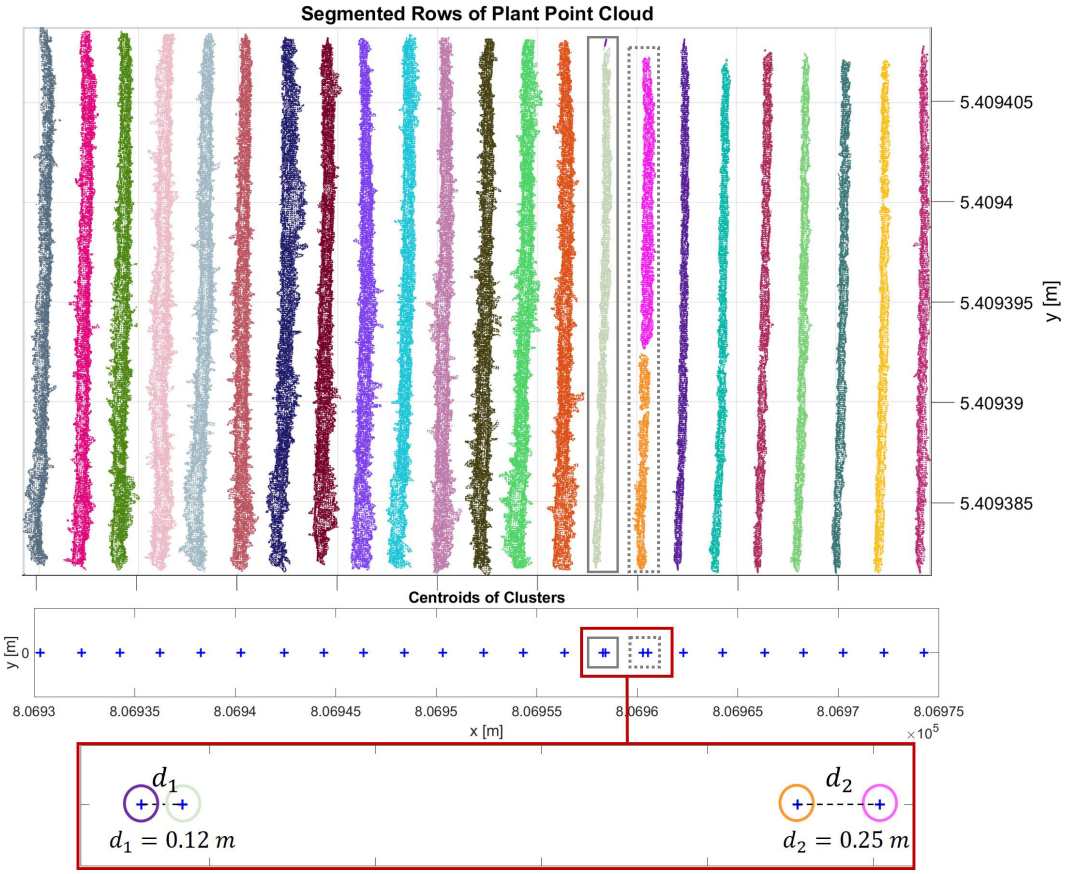

FIGURE 5
Initial result of the DBSCAN algorithm. Each row cluster is shown with a different color. Each centroid of the cluster is represented with a blue cross. In the grey rectangle (left), a whole row and a metal post in the row are clustered separately and are colored greenish-grey and purple, respectively. In the grey dashed rectangle (right), the row is segmented into two clusters due to the gap in the canopy. The clusters are shown in pink and orange colors. These centroids are analyzed more closely in the red frame. The distance between these pairs in grey and grey dashed rectangles respectively is less than the threshold value, therefore they are merged into the same cluster.

2.2.3 Row parameters extraction

2.2.3.1 Trunk position

Identifying trunks under the canopy in vineyards with complex geometric structures is challenging. In our investigation in the *PlantPCl*, we observed that the thin structure of the majority of trunks was hard to reconstruct accurately due to the occlusions caused by the leaves, as can be seen in Figure 6A. On the other hand, the bottom part of the trunks was reconstructed better in the *GroundPCl* (Figure 6B). Furthermore, Figure 6B shows that the ground approximates a planar surface; in contrast, the trunks were observed with a different geometry clearly distinguished from the ground. We used geometric features to detect trunks in the *GroundPCl* to address this issue.

We proposed a pipeline for trunk detection in vineyards, leveraging features derived from the local neighborhood. To enhance computational efficiency, reduce noise, and improve feature stability, we downsampled the segmented row of the *GroundPCl* using a 3D grid box with dimensions of (0.05 x 0.05 x 0.05 m). This downsampling ensured a manageable density of points for subsequent calculations. Feature calculation involved two steps: computing the covariance matrix for the points within a local neighborhood around each point, defined by a specified radius R to analyze the variability of the point cloud in different directions, and determining eigenvalues of the matrix that provides insight into the principal axes of variability. The corresponding eigenvalues were sorted as $\lambda_1 \geq \lambda_2 \geq \lambda_3 \geq 0$. After conducting several experiments, we determined that the sphericity feature $S_\lambda = \lambda_3/\lambda_1$ outperformed other features for trunk identification in the *GroundPCl*. For the sphericity feature calculation, we set the radius R to 0.25 m for the nearest neighbor search, as it effectively captured the approximate trunk diameter.

We performed three steps to identify trunk candidates and estimate their 3D positions. Firstly, the sphericity values of each point in the segmented ground row were sorted into a histogram. We determined a threshold that helps us identify trunk candidates using Otsu's method (Otsu, 1979). These candidates were the points with sphericity values exceeding the threshold (Figure 7A). Since trunk candidates stored many points for each trunk, the points belonging to the same trunk must be clustered. To achieve this, the DBSCAN algorithm was used to cluster the trunk candidates. The chosen parameters for the DBSCAN were 0.10 m and 5 for ϵ and P_{min}, respectively. These parameter choices aided in effectively grouping the trunk candidates into meaningful clusters. Figure 7B illustrates the trunk candidates clusters, each represented by a

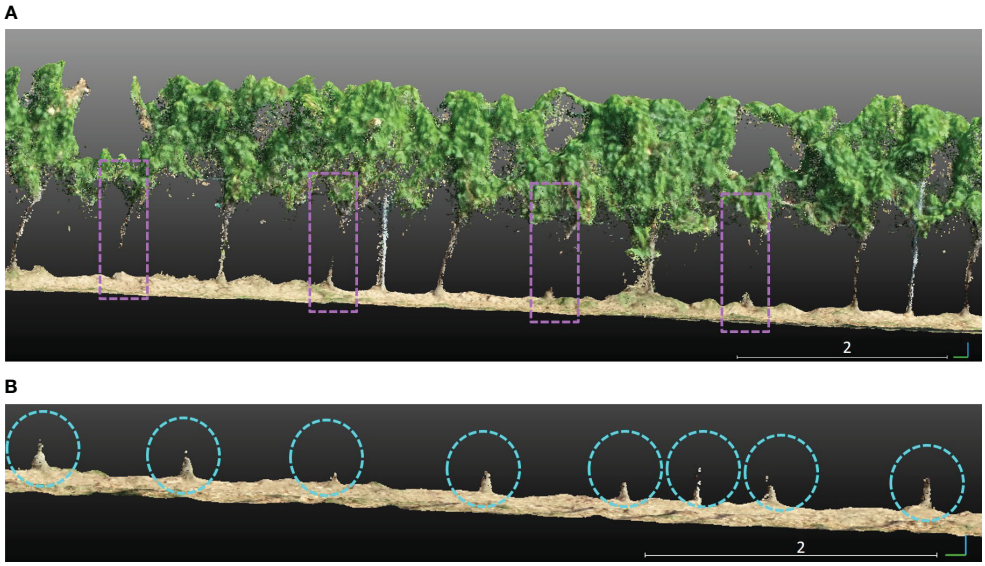

FIGURE 6
(A) Trunks that are not reconstructed well in the segmented plant row are shown in purple rectangles. **(B)** The trunks in a segmented ground row are encircled with cyan circles.

distinct color. Finally, to estimate the position of each trunk, we calculated the 3D centroid of each cluster. By following these steps, we effectively identified trunk candidates and estimated their respective 3D positions in each segmented ground row, enabling a comprehensive analysis of the trunks in the given dataset (Figure 7C).

2.2.3.2 Canopy characteristics

Canopy geometric parameters were extracted for each row of the *PlantPCl* with a high spatial resolution along the row. Our approach involved segmenting each row into 3D bounding boxes of equal length along the y-axis according to the methodology described in Escolà et al. (2017); Cabrera-Pérez et al. (2023), and Escolà et al. (2023). Segments, represented by yellow bounding boxes, were visually depicted along a single row in Figure 8A. Furthermore, a top and close-up view of the segments was presented in Figure 8B. Each parameter was computed in each segment along the row. By doing this, we can achieve a detailed analysis of parameters along a row by adjusting the number of segments. Therefore, any desired resolution of the parameter

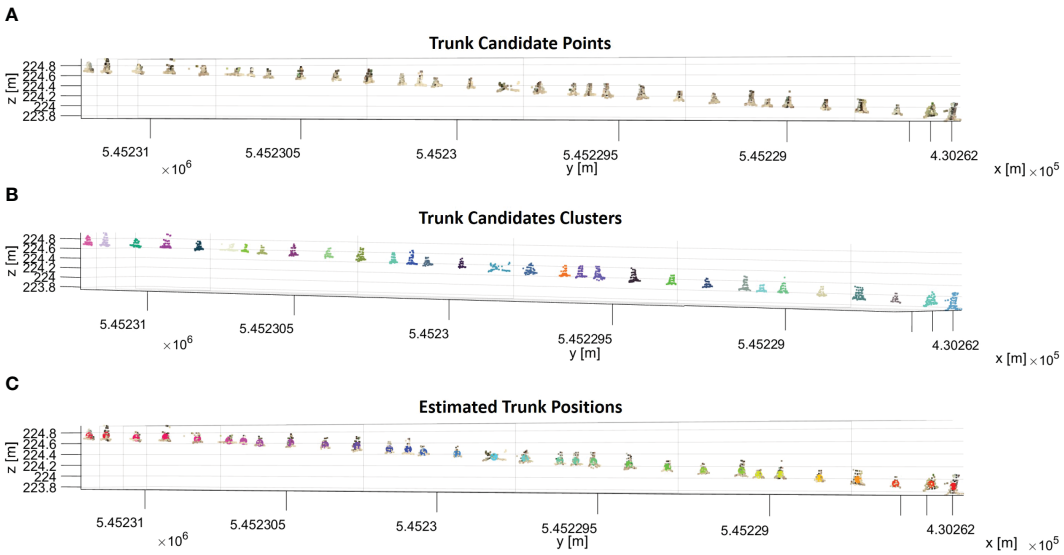

FIGURE 7
(A) Trunk candidate points that have a sphericity value larger than the sphericity threshold in a segmented ground row. **(B)** Trunk candidates are segmented into clusters with the DBSCAN algorithm, and each cluster of trunk candidates is shown in a different color. **(C)** The calculated centroid of each cluster is shown in different colors with trunk candidates.

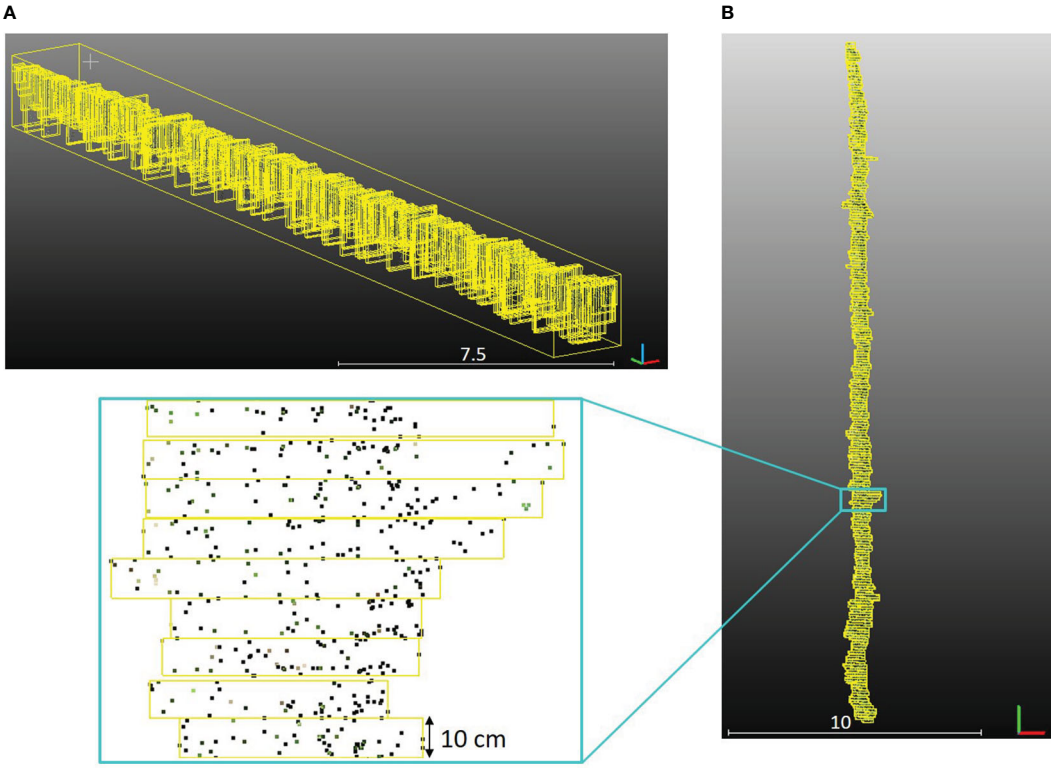

FIGURE 8
(A) Segments of the one row in the *PlantPCl* that were enclosed with a yellow bounding box in 3D space. **(B)** Top view of the segments along the row.

estimation along the row can be achieved. To ensure a high level of detail, we chose the number of segments to be 250. This decision resulted in a consistent segment length of 10 cm along the row. Comprehensive information and visualizations regarding each plant parameter along each row were provided through detailed diagrams and histograms. In the following, we described the parameters extracted by our pipeline.

Plant Height: The shortest distance from the ground to the highest point of the canopy in the z-axis is defined as plant height (Perez-Harguindeguy et al., 2016). We used a method based on the 90th percentile of normalized heights, as shown in a prior study (Becirevic et al., 2019), which highlighted the reliability of the UAV-based crop height extraction. We also visually inspected the data to ensure our choice of percentile was appropriate. By calculating the mean of the z-values within the 90th percentile of the normalized height, we obtained height estimations for each segment.

Canopy Width: Assuming that each row in the *PlantPCl* was positioned on the xy-plane and aligned parallel to the y-axis following the rotation and ground projection, we can define the canopy width as a distance perpendicular to the y-axis. In our pipeline, we calculated the canopy width as the difference between the mean of the y-values within the 90th percentile and the mean of the y-values within the 10th percentile, following the procedure already described for the plant height. In this way, we obtained a more accurate estimation of the canopy width while excluding extremes.

Canopy Volume: The canopy volume is a reliable indicator of the overall health and vigor of plants (Arnó et al., 2013; Caruso et al., 2017; Escolà et al., 2017). The estimated vine canopy volume becomes particularly valuable in assessing vigor, especially where a single measure, such as height and width, is insufficient to understand canopy geometry. To calculate the canopy volume we employed the alpha shape algorithm (Edelsbrunner et al., 1983), which generates a bounding volume encompassing a set of plant points. However, to accurately calculate the canopy volume, it was necessary to discard pieces of trunks or single branches that were occasionally present in the *PlantPCl*, as illustrated in Figure 9A. As explained before, since the trunks were not reconstructed well, the number of trunk points was significantly lower than the canopy points in the *PlantPCl*. To address this, we applied the Statistical Outlier Removal (SOR) filter to eliminate these points within the row. As a result, we obtained a filtered *PlantPCl* that excludes trunk or branch pieces, as illustrated in Figure 9B. After filtering, the alpha shape approach was employed with different alpha radius α. The parameter α is the sphere's radius that sweeps over the points to create the alpha shape and is used to tighten or loosen the object. The approach, in theory, uses an optimal alpha value to approximate bounding volume; however, finding an optimal value is extremely difficult (Yan et al., 2019). Therefore, we empirically chose an alpha radius representing the canopy's concave structures without creating disconnected objects. Through empirical observations in our study, we determined the value of α as 0.3 m for the alpha shape object when calculating the canopy volume (Figure 9C).

Canopy Lower Bound: The filtered *PlantPCl*, which excludes the trunks, holds significant importance in facilitating a comprehensive analysis of the canopy structure. In the filtered

FIGURE 9
(A) Side view of the segmented row in *PlantPCl*. **(B)** Filtered point cloud. Trunk and branch pieces are removed with the SOR filter. **(C)** The alpha shape object of the row.

PlantPCl, we can define the canopy lower bound as the lowest point that belongs to the canopy on the z-axis. In our pipeline, the canopy lower bound was estimated as the mean of the z-values within the 10th percentile. Thus, by incorporating this canopy characteristic, we obtain valuable insights into the vertical structure of the canopy, enabling a more detailed examination of the vegetation distribution and its variability along the row.

2.3 Evaluation method

2.3.1 Row segmentation

To evaluate the accuracy of the segmented plant rows, the point clouds of the segmented rows were compared with the manually segmented rows. The evaluation involved comparing the number of points in the segmented row with the number of points in the corresponding manually segmented row. Segmentation accuracy was calculated for each row considering the overlap between the segmented row and the ground truth one. Furthermore, we took into account the training system associated with each row. This analysis provided insights into the performance of the segmentation method across different training systems.

2.3.2 Trunk position

Our study focused on accurately estimating the positions of individual trunks within vineyard rows. We evaluated the accuracy of our estimations by comparing them to ground truth data which is manually selected trunks in the point cloud. To determine the accuracy of our estimates, we defined a 15 cm search radius and checked if any ground truth trunks were within this radius. Then the confusion matrix was calculated based on the presence or absence of ground truth trunks. The evaluation of our estimated trunk positions involved calculating true positives (TP), false positives (FP), and false negatives (FN). We computed precision, recall, and F1 scores for each dataset to assess the performance of trunk detection. Precision focuses on the quality of the detected trunks, measuring the extent to which the identified trunks are valid. On the other hand, recall, in our case, quantifies the capability to accurately identify actual trunks, emphasizing the detection rate. To obtain a comprehensive evaluation, we utilized the F1 score, which offers a balanced assessment of the overall performance, considering both recall and precision.

Furthermore, we conducted an additional experiment to investigate the impact of different flight parameters on the trunk detection method. To do so, we applied our method to three distinct datasets, *tilted_20m*, *nadir_20m*, and *nadir_15m*, and subsequently compared the obtained results.

2.3.3 Canopy characteristics

In previous studies (De Castro et al., 2018; Di Gennaro and Matese, 2020; Mesas-Carrascosa et al., 2020), UAV-based canopy geometric parameter estimation has demonstrated higher accuracy compared to ground truth measurements; however, the validity of such comparisons is highly dependent on the specific sample positions, rendering them less meaningful. For instance, ground truth volume measurements are highly subjective and depend on the specific person taking the measure (Colaço et al., 2017; Qi et al., 2021). These measurements are also time-consuming, with the additional limitation of not accounting for canopy gaps. Furthermore, certain studies have indicated that manual measurements tend to overestimate canopy thickness by approximately 30% when compared to LiDAR-based measurements (Gil et al., 2014). Therefore, considering these challenges, we rely on the proven reliability of parameter estimation methods, as demonstrated in previous research, and do not directly compare our estimates with reference measures.

3 Results and discussion

3.1 Row segmentation

The final result of row segmentation is visually represented in Figure 10. Figure 10A illustrates the segmentation results for the *PlantPCl*. The rows are color-coded, with each row represented by a different color. Our segmentation method accurately separates the *PlantPCl* into distinct rows, therefore we can have a clear understanding of the spatial distribution and arrangement of the plants within the vineyard. By employing our proposed method, we successfully address the challenges posed by gaps or missing plants in the canopy, resulting in accurate and consistent row segmentation. Similarly, Figure 10B shows the segmentation result for the *GroundPCl*. The ground points are assigned different colors based on the rows they belong to. This segmentation allows for a comprehensive analysis of the ground characteristics along each row, which is interesting for individual trunk detection.

As a result, the row segmentation method demonstrated outstanding accuracy in all datasets, achieving a flawless segmentation rate of 100%, in line with existing research (Jurado

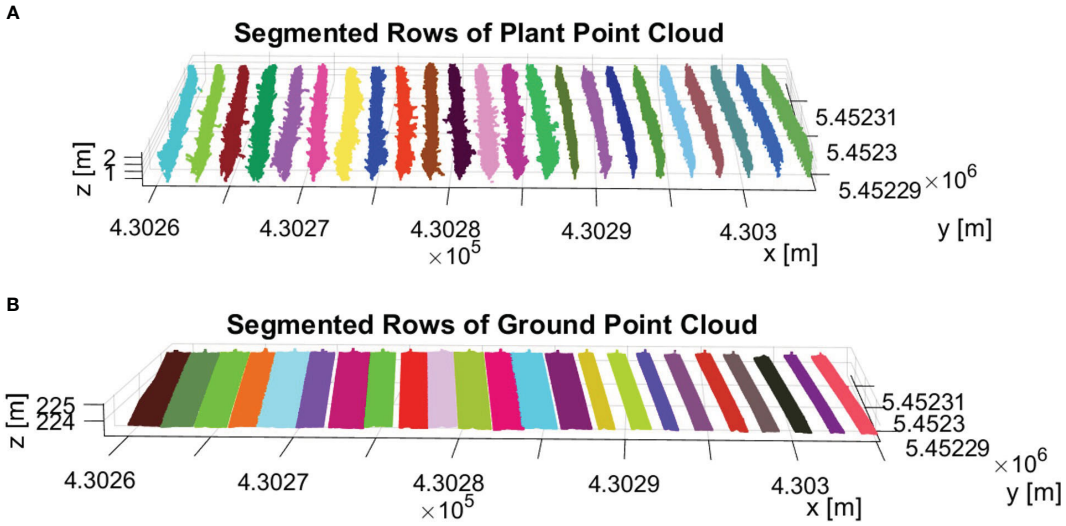

FIGURE 10
Result of row segmentation. The rows are color-coded, with each row represented by a different color. **(A)** Segmented rows of *PlantPCl*. **(B)** Segmented rows of *GroundPCl*.

et al., 2020; Moreno and Andújar, 2023). Notably, our analysis revealed that the training systems had no noticeable effect on the performance of the row segmentation method. Furthermore, the comparison of different flight parameters revealed no impact on the accuracy of row segmentation.

3.2 Row parameters extraction

3.2.1 Trunk position

We presented the estimated trunk positions and ground truth data in Figure 11, where blue dots represent estimated trunks and black circles represent ground truth trunks. Table 2 shows the corresponding numerical evaluation. In *combined* dataset, trunk positions in the SMPH training system were estimated with a higher F1 score of 76% compared to 59% F1 score in the VSP training system. It can be seen in Figure 11 that trunks were not detected well in rows number 4, 5, and 6. This is because, in this specific dataset, these trunks belonging to these rows were not properly reconstructed by the SfM pipeline due to the occlusions caused by the canopy.

The evaluation revealed that the highest F1 score of 91% was achieved in *nadir_20m* dataset with the VSP training system. This is because, in the VSP case, the canopy volume is much lower so that a larger portion of the trunk is visible from the camera, which results in a higher precision on all datasets for our pipeline. Considering both training systems, the highest F1 score was achieved with the *tilted_20m* dataset, indicating that the trunks were detected better in this dataset. Specifically, we observed that the more inclined camera angle outperformed the nadir angle in effectively detecting plants under the canopy. This confirms existing research on both maize (Che et al., 2020) and grapevines (García-Fernández et al., 2021) where a more inclined camera angle was more effective for the point cloud reconstruction. However, in existing works, no assessment of the trunk detection performances was investigated.

The lowest F1 score of 59% was achieved in the *combined* dataset. Although being reconstructed using images captured from different camera angles and flight heights, the *combined* dataset did not yield an improvement in performance. Interestingly, the individual datasets displayed significantly higher recall rates when compared to the *combined* dataset. These findings suggest that the variability in data introduced by the different flight parameters did not enhance the overall detection outcome. Based on these results, it is evident that selecting a specific flight parameter set, rather than combining data captured using different flight parameters, provided superior trunk detection performances.

We can see from the results that there is no substantial difference in terms of F1 score between the *nadir_20m* and *nadir_15m* datasets. These datasets were both captured from a nadir angle but at varying flight heights, enabling us to assess the influence of flight height on plant detection directly. Notably, we discovered that higher flight height can still yield accurate results with lower data density but a larger field of view, potentially shortening data collection time.

Although existing research achieved high accuracy for grapevine detection, some conditions were assumed regarding either plant distributions (Milella et al., 2019; Pádua et al., 2020) or the absence of the canopy (Jurado et al., 2020; Di Gennaro et al., 2023). Instead, in our work, we assess the trunk detection performances without any assumptions about the vineyard conditions. In fact, we tested our pipeline with different training systems, irregular plant spacing, and the presence of a fully developed canopy, achieving a precision of 92%. It is important to note that, although in our case most plants within the vineyard were effectively reconstructed, the thin-structured trunks located under the canopy posed a challenging scenario for accurate trunk detection. Our research findings highlight the impact of camera angle and flight height when designing aerial imaging surveys for plant detection within vineyards. By optimizing these parameters, researchers and practitioners can substantially improve performances in individual trunk identification.

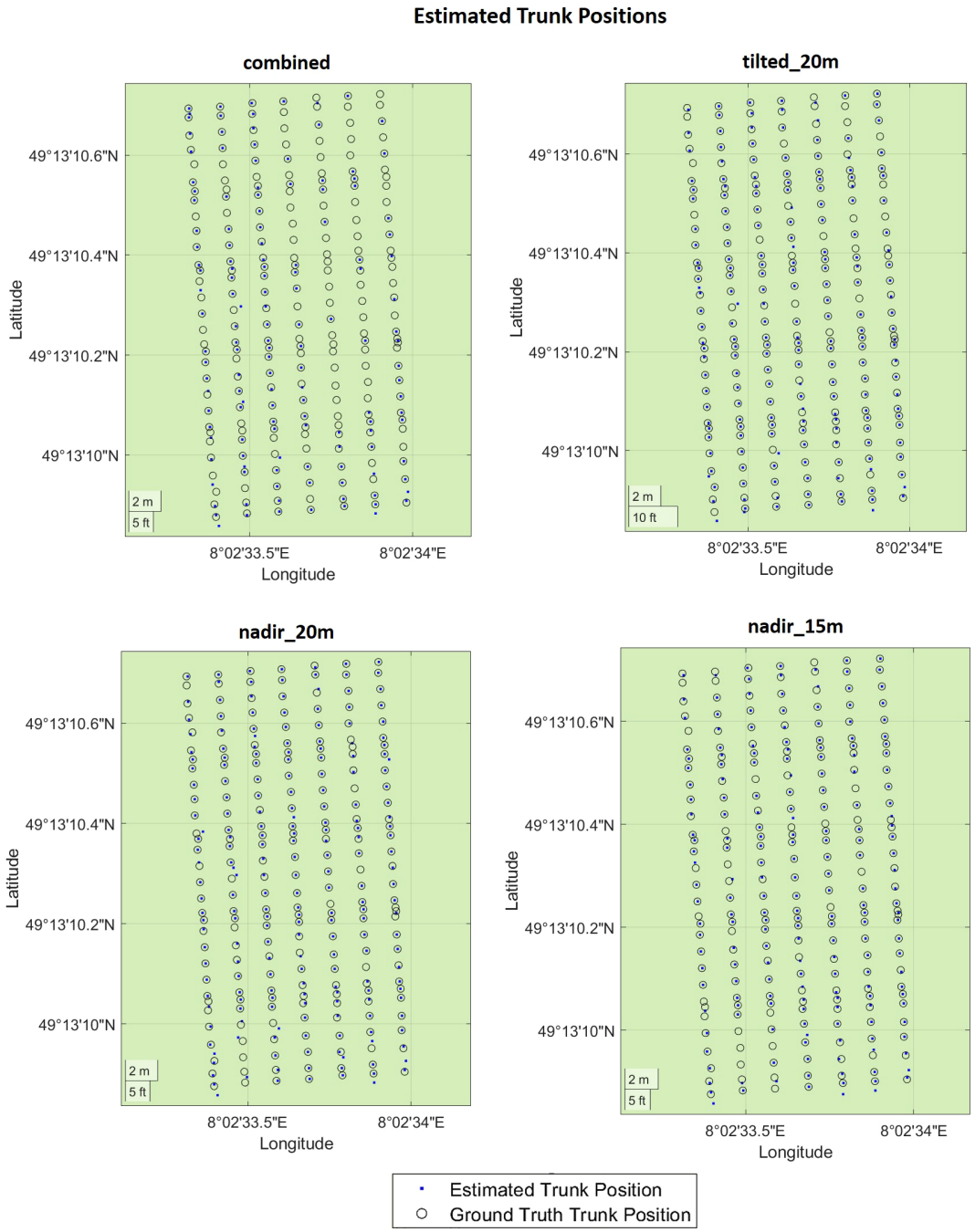

FIGURE 11
Evaluation of the trunk positions in geographic coordinates. The estimated trunk positions are colored in blue. The black circles represent the ground truth trunk positions.

3.2.2 Canopy characteristics

In Figures 12 and 13, we show the distribution of the canopy characteristics along a subset of rows using our segment-based approach. Figure 12 provides valuable and comprehensive insights into the canopy characteristics and trunk positions in Row-5 trained in the VSP system. The side view and top view of the row are shown in Figures 12A, B, respectively. It allows us to observe the changes in canopy geometry along the row, beginning from point *P* to the end of the row, with the highlighted regions of interest indicating areas where the canopy structure undergoes abrupt variations.

By analyzing the estimated plant height and the lower canopy bound in Figure 12C, we gain a deeper understanding of the vertical structure of the plants. The blue points representing the estimated trunk positions allowed us to relate the plant positions to the respective canopy structures. The proposed method for height estimation provided us with not only height estimation but also identification of

10.3389/fpls.2023.1244384

TABLE 2 Evaluation of detected trunks.

	Training system	TP	FP	FN	Precision	Recall	F1 score
combined	SMPH	66	14	27	83%	71%	76%
	VSP	54	5	70	92%	44%	59%
tilted_20m	SMPH	83	9	10	90%	89%	90%
	VSP	101	10	23	91%	81%	86%
nadir_20m	SMPH	73	19	20	79%	78%	79%
	VSP	111	11	13	91%	90%	91%
nadir_15m	SMPH	67	11	26	86%	72%	78%
	VSP	109	12	15	90%	88%	89%

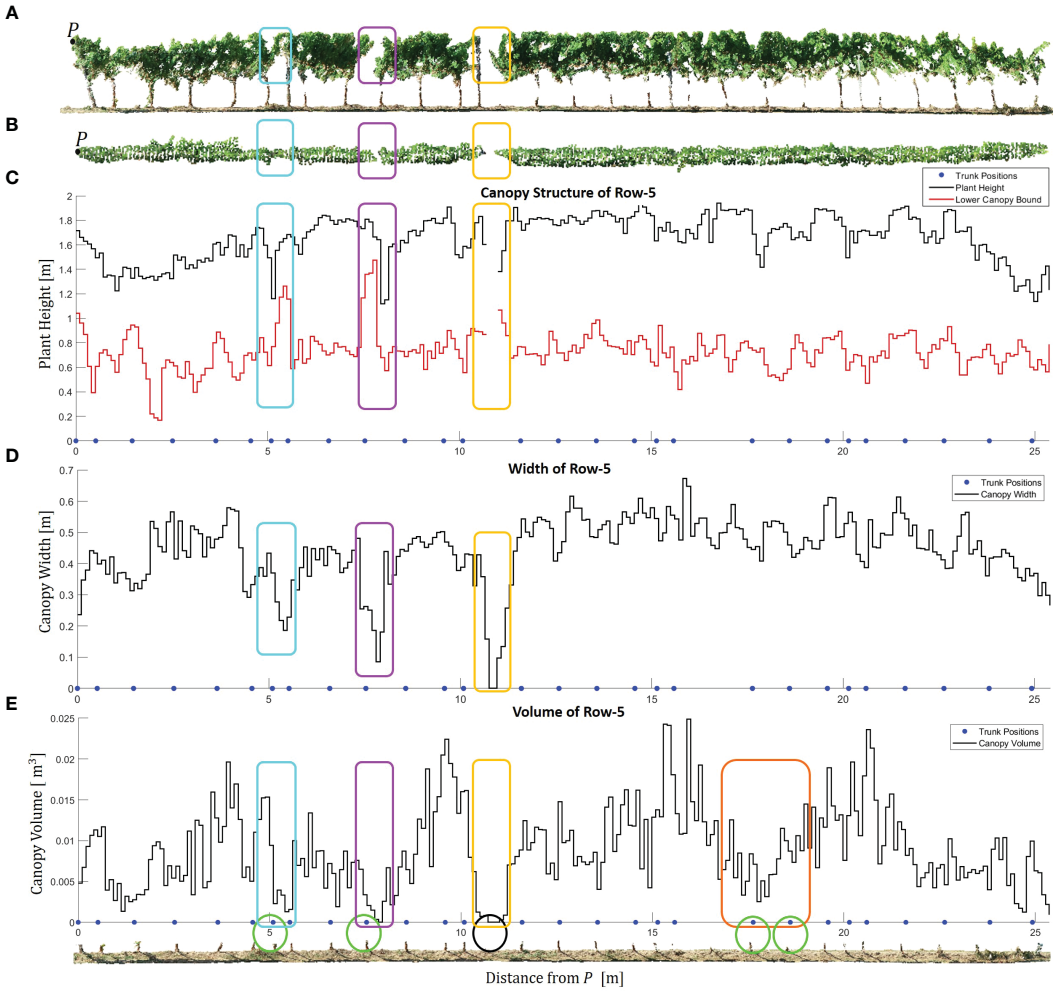

FIGURE 12
Canopy characteristics of Row-5. **(A)** Side view of the row. Point *P* marks the starting point of the row, representing the location with the minimum y-coordinate. The cyan, magenta, yellow, and orange rectangles highlight significant regions of interest where the canopy geometry changes abruptly. **(B)** Top view of the row. **(C)** Estimated plant height and lower canopy bound along the row. The blue points indicate the estimated positions of the trunks. **(D)** Estimated canopy width along the row. **(E)** Estimated canopy volume along the row. The circles within the *GroundPCl* of Row-5 indicate the positions of the estimated trunks related to abrupt changes in the canopy.

the missing plants along the row. We observed an interruption and sharp fall in the graph in the absence of plants as can be seen in yellow rectangles. The absence of the related trunk in the black circle in *GroundPCl* proved our analysis as can be seen in Figure 12E. Furthermore, the estimated canopy width in Figure 12D revealed variations in the lateral extent of the canopy along Row-5. In particular, we observed sudden declines in the graph, highlighted with magenta, cyan, and yellow frames in Figure 12D. It is clear that the canopy width has decreased in these frames, as can be seen in Figure 12B.

The graph of the estimated canopy volume in Figure 12E provided a quantitative measure of the three-dimensional extent of the canopy, reflecting the overall vegetative vigor and biomass accumulation. This specific alpha radius selection allowed for accurately representing concave structures within the canopy while avoiding creating disconnected or fragmented objects. While no significant change was observed in plant height and width, there was a significant decrease in canopy volume as can be seen in the orange frame. Therefore, when combined with plant height and canopy width, canopy volume provided a holistic perspective on the vineyard's canopy architecture, allowing for a more accurate assessment of its health and growth dynamics (Escolà et al., 2017).

We further focused on the comparison between the results for two training systems, VSP and SMPH. Figure 13 shows the histogram of row parameters for two exemplary rows that are Row-1 (trained in the SMPH system) and Row-5 (trained in the VSP system). The expected difference in plant height, canopy width, and volume explained in Section 2.1 could be precisely detected between the two training systems. As shown in Figure 13, the mean height, width, and volume of Row-1 are much larger than Row-5, as in the SMPH system the canopy volume is typically denser than in VSP. Although we show histograms just for two rows, we also computed the mean of the row parameters trained with the SMPH and VSP system separately for each dataset. In this way, we investigated both the differences in row parameters for the two training systems and the influence of the different flight settings, as shown in Table 3. Similarly to the Row-1/Row-5 results, we observed that the mean plant height, canopy width, and canopy volume of the rows trained in the SMPH system were higher than those trained in the VSP system for all datasets. Our results found no significant differences in plant height and canopy width across *tilted_20m*, *nadir_20m*, and *nadir_15m* datasets in two training systems. However, a relatively lower canopy volume was observed in the SMPH training system within the *nadir_15m* dataset. The reason for this may be the lower flight altitudes can yield a higher spatial resolution, which makes the system more sensitive to small canopy variations potentially causing an underestimation of canopy volume.

One of the notable advantages of our method is its flexibility in achieving the desired resolution of parameter calculations. By adjusting the number of segments, we can readily modify the resolution along the row. Compared to other methods that fix the segment length *a priori* (Escolà et al., 2017; Cabrera-Pérez et al., 2023), we can precisely analyze and evaluate the plant's characteristics and variations along the row at the desired level of detail. One example of this is given in Table 3, where the canopy volume is computed with a segment length of 1 m instead of 10 cm to give a more reasonable value. Overall, our approach provides a robust and adaptable framework for obtaining essential plant parameters, offering valuable insights into the spatial distribution and properties of the plant along the row.

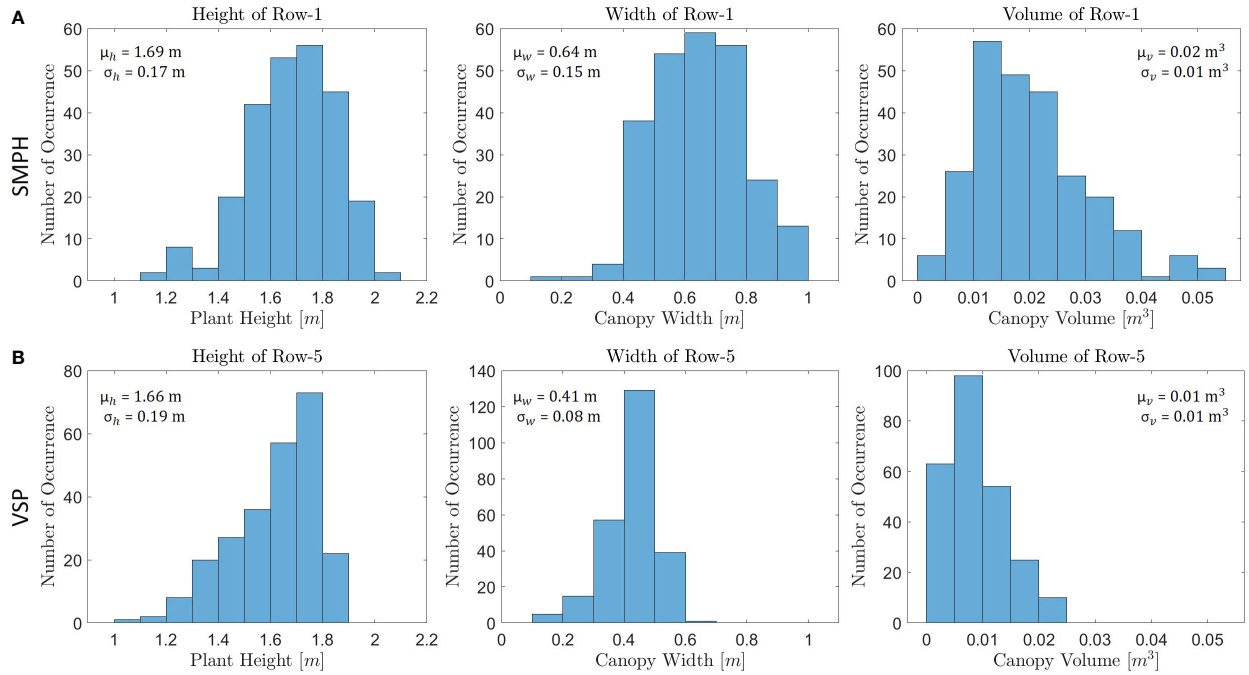

FIGURE 13
A comparison was conducted between **(A)** Row-1 in the SMPH training system and **(B)** Row-5 in the VSP training system in terms of their training systems, using histograms to analyze the row parameters.

10.3389/fpls.2023.1244384

TABLE 3 Row parameters in different datasets.

Parameters:	Plant height [*m*]				Canopy width [*m*]				Canopy volume [m^3]			
	SMPH		VSP		SMPH		VSP		SMPH		VSP	
Training system:	Mean	SD	Mean	SD	Mean	SD	Mean	SD	Mean	SD	Mean	SD
combined	1.72	0.04	1.66	0.03	0.66	0.03	0.35	0.05	0.61	0.03	0.23	0.02
tilted_20m	1.71	0.03	1.61	0.02	0.69	0.03	0.36	0.04	0.59	0.03	0.24	0.02
nadir_20m	1.70	0.06	1.58	0.01	0.70	0.03	0.36	0.05	0.55	0.02	0.23	0.02
nadir_15m	1.71	0.04	1.58	0.01	0.71	0.03	0.37	0.05	0.46	0.02	0.21	0.01

3.3 Algorithm application on LiDAR dataset

We successfully applied our pipeline to the vineyard's LiDAR point cloud dataset. Figure 14 shows the qualitative results of row segmentation and trunk detection algorithm. We utilized the same set of parameters used in the image-based datasets for all components within the pipeline. Remarkably, our method effectively segmented the point cloud into rows with 100% accuracy. Figure 14A shows the qualitative result of row segmentation. Notably, our trunk detection algorithm also succeeded in identifying trunks, achieving an F1 score of 77%. Figure 14B shows the detected trunks with red spheres. This experiment demonstrated that our algorithm can generalize effectively

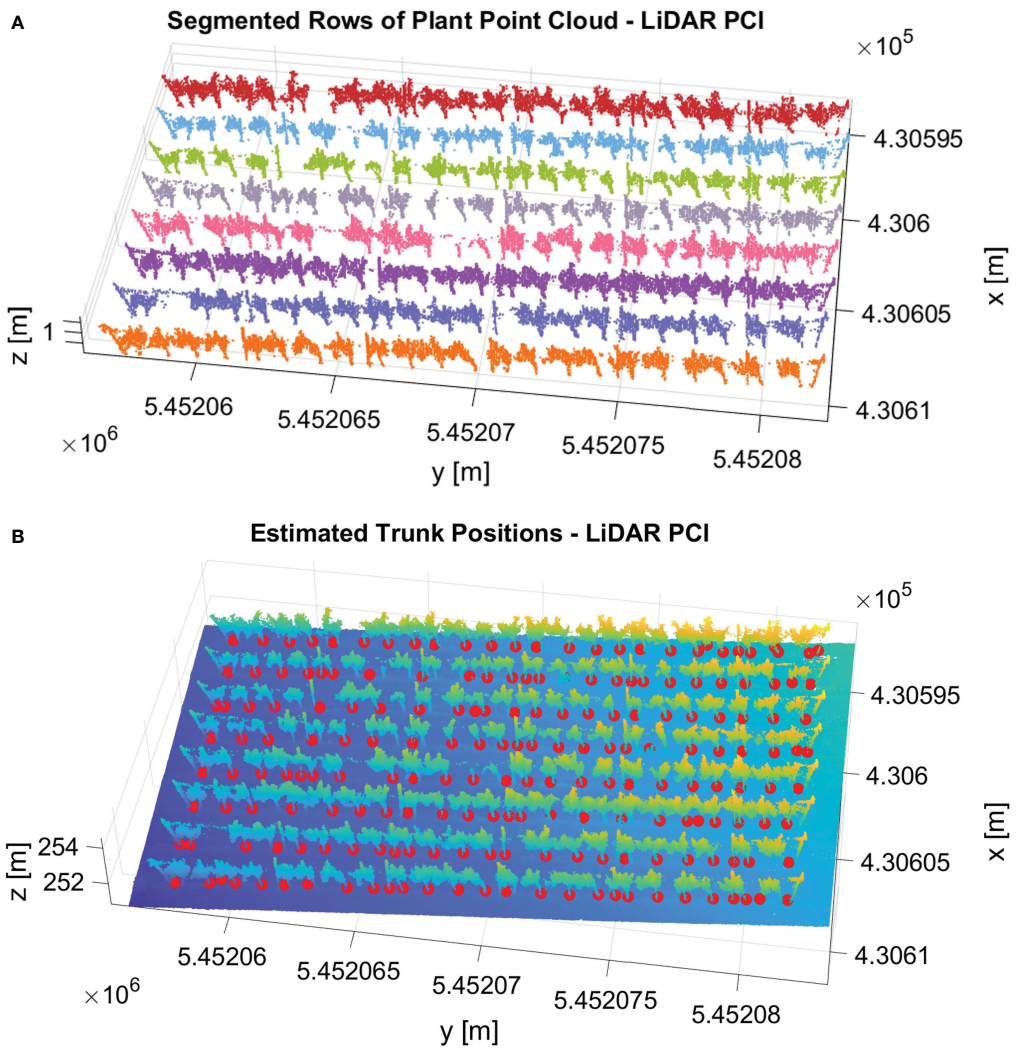

FIGURE 14
Results of our pipeline in the vineyard's LiDAR point cloud dataset. **(A)** The row segmentation output. Each segmented row is represented with a different color. **(B)** The result of the trunk detection algorithm. The detected trunks are shown with red spheres.

to different sensor settings with accurate results without parameter tuning.

4 Conclusion

The determination of the geometric properties and the identification of the individual plants were the main focus of this work, and the results presented demonstrate the potential of using a 3D plant model derived from RGB images acquired with a UAV for achieving these objectives in the vineyard. The extraction of single rows was performed. Consequently, for each row, we derived the plant positions as well as detailed row parameters, including the plant height, canopy width, and canopy volume. In contrast to many other approaches, we provided detailed information and visualizations of the height, width, and volume in the form of diagrams and histograms, giving essential clues on the distribution of these factors along the row. These extracted parameters have the potential to enhance vineyard productivity, improve grape quality, and contribute to the long-term sustainability of vineyard operations. This detailed geometric analysis of the canopy offers valuable insights for vineyard managers and breeders, assisting them in crucial tasks such as pruning, agrochemical spraying, and optimizing yields. Additionally, the influences of different flight parameters on the extracted plant parameters have been investigated. The whole pipeline is independent of the terrain slope and does not require assumptions like plant or row spacing. We investigated all these parameters in detail and had reference data for the segmented rows and estimated trunk positions for the evaluation. The vine rows were segmented with a high accuracy of 100% in the vineyard plot independent of the training systems and different flight parameter settings. We could also identify the trunk positions with a precision of 92%. Furthermore, we applied our algorithm to the LiDAR point cloud and showed accurate results regarding row segmentation and trunk detection. This experiment demonstrates that our algorithm can generalize to different sensor settings with good performances without the need for parameter tuning.

Data availability statement

The raw data supporting the conclusions of this article will be made available by the authors, without undue reservation.

Author contributions

MC designed and conducted the analyses. LK and HK helped to initiate the work. The development of the method was done by MC, guided by LZ and LK. LK helped to co-design the experiments. DP and AD collected and preprocessed the data. LZ contributed to the data preparation. MC, LZ, and LK contributed to the writing of the manuscript. All authors contributed to the article and approved the submitted version.

Funding

The author(s) declare financial support was received for the research, authorship, and/or publication of this article. This work was partially funded by the Deutsche Forschungsgemeinschaft (DFG, German Research Foundation) under Germany's Excellence Strategy – EXC 2070 – 390732324 and partially supported by funds of the Federal Ministry of Food and Agriculture (BMEL) based on a decision of the Parliament of the Federal Republic of Germany via the Federal Office for Agriculture and Food (BLE) under the innovation support program in the framework PhytoMo (project number 2818718C19).

Conflict of interest

The authors declare that the research was conducted in the absence of any commercial or financial relationships that could be construed as a potential conflict of interest.

Publisher's note

References

Amiruzzaman, M., Rahman, R., Islam, M. R., and Nor, R. M. (2022). Logical analysis of built-in dbscan functions in popular data science programming languages. *MIST Int. J. Sci. Technol.* 10, 25–32. doi: 10.47981/j.mijst.10(01)2022.349(25-32)

Arnó, J., Escolà, A., Valles, J. M., Llorens, J., Sanz, R., Masip, J., et al. (2013). Leaf area index estimation in vineyards using a ground-based lidar scanner. *Precis. Agric.* 14, 290–306. doi: 10.1007/s11119-012-9295-0

Becirevic, D., Klingbeil, L., Honecker, A., Schumann, H., Rascher, U., Léon, J., et al. (2019). On the derivation of crop heights from multitemporal uav based imagery. *ISPRS Ann. Photogramm. Remote Sens. Spatial Inf. Sci.* 4, 95–102. doi: 10.5194/isprs-annals-IV-2-W5-95-2019

Biglia, A., Zaman, S., Gay, P., Aimonino, D. R., and Comba, L. (2022). 3d point cloud density-based segmentation for vine rows detection and localisation. *Comput. Electron. Agric.* 199, 107166. doi: 10.1016/j.compag.2022.107166

Cabrera-Pérez, C., Llorens, J., Escola, A., Royo-Esnal, A., and Recasens, J. (2023). Organic mulches as an alternative for under-vine weed management in mediterranean irrigated vineyards: Impact on agronomic performance. *Eur. J. Agron.* 145, 126798. doi: 10.1016/j.eja.2023.126798

Caruso, G., Tozzini, L., Rallo, G., Primicerio, J., Moriondo, M., Palai, G., et al. (2017). Estimating biophysical and geometrical parameters of grapevine canopies ('sangiovese') by an unmanned aerial vehicle (uav) and vis-nir cameras. *Vitis* 56, 63–70. doi: 10.5073/vitis.2017.56.63-70

Che, Y., Wang, Q., Xie, Z., Zhou, L., Li, S., Hui, F., et al. (2020). Estimation of maize plant height and leaf area index dynamics using an unmanned aerial vehicle with oblique and nadir photography. *Ann. Bot.* 126, 765–773. doi: 10.1093/aob/mcaa097

Colaço, A. F., Trevisan, R. G., Molin, J. P., Rosell-Polo, J. R., and Escolà, A. (2017). A method to obtain orange crop geometry information using a mobile terrestrial laser scanner and 3d modeling. *Remote Sens.* 9, 763. doi: 10.3390/rs9080763

Comba, L., Biglia, A., Aimonino, D. R., Barge, P., Tortia, C., and Gay, P. (2019). "2d and 3d data fusion for crop monitoring in precision agriculture," in *2019 IEEE International workshop on metrology for agriculture and forestry (MetroAgriFor)*. (Portici, Italy: IEEE). 62–67.

Comba, L., Biglia, A., Aimonino, D. R., and Gay, P. (2018). Unsupervised detection of vineyards by 3d point-cloud uav photogrammetry for precision agriculture. *Comput. Electron. Agric.* 155, 84–95. doi: 10.1016/j.compag.2018.10.005

De Castro, A. I., Jiménez-Brenes, F. M., Torres-Sánchez, J., Peña, J. M., Borra-Serrano, I., and López- Granados, F. (2018). 3-d characterization of vineyards using a novel uav imagery-based obia procedure for precision viticulture applications. *Remote Sens.* 10, 584. doi: 10.3390/rs10040584

Di Gennaro, S. F., and Matese, A. (2020). Evaluation of novel precision viticulture tool for canopy biomass estimation and missing plant detection based on 2.5 d and 3d approaches using rgb images acquired by uav platform. *Plant Methods* 16, 1–12. doi: 10.1186/s13007-020-00632-2

Di Gennaro, S. F., Vannini, G. L., Berton, A., Dainelli, R., Toscano, P., and Matese, A. (2023). Missing plant detection in vineyards using uav angled rgb imagery acquired in dormant period. *Drones* 7, 349. doi: 10.3390/drones7060349

Edelsbrunner, H., Kirkpatrick, D., and Seidel, R. (1983). On the shape of a set of points in the plane. *IEEE Trans. Inf. Theory* 29, 551–559. doi: 10.1109/TIT.1983.1056714

Escolà, A., Martínez-Casasnovas, J. A., Rufat, J., Arnó, J., Arbonés, A., Sebé, F., et al. (2017). Mobile terrestrial laser scanner applications in precision fruticulture/horticulture and tools to extract information from canopy point clouds. *Precis. Agric.* 18, 111–132. doi: 10.1007/s11119-016-9474-5

Escolà, A., Peña, J. M., López-Granados, F., Rosell-Polo, J. R., de Castro, A. I., Gregorio, E., et al. (2023). Mobile terrestrial laser scanner vs. uav photogrammetry to estimate woody crop canopy parameters–part 1: methodology and comparison in vineyards. *Comput. Electron. Agric.* 212, 108109. doi: 10.1016/j.compag.2023.108083

Ester, M., Kriegel, H. P., Sander, J., and Xu, X. (1996). A density-based algorithm for discovering clusters in large spatial databases with noise. *In kdd* 96, 226–231.

Ferro, M. V., and Catania, P. (2023). Technologies and innovative methods for precision viticulture: a comprehensive review. *Horticulturae* 9, 399. doi: 10.3390/horticulturae9030399

García-Fernández, M., Sanz-Ablanedo, E., Pereira-Obaya, D., and Rodríguez-Pérez, J. R. (2021). Vineyard pruning weight prediction using 3d point clouds generated from uav imagery and structure from motion photogrammetry. *Agronomy* 11, 2489. doi: 10.3390/agronomy11122489

Gil, E., Arnó, J., Llorens, J., Sanz, R., Llop, J., Rosell-Polo, J. R., et al. (2014). Advanced technologies for the improvement of spray application techniques in spanish viticulture: an overview. *Sensors* 14, 691–708. doi: 10.3390/s140100691

Jurado, J. M., Pádua, L., Feito, F. R., and Sousa, J. J. (2020). Automatic grapevine trunk detection on uav-based point cloud. *Remote Sens.* 12, 3043. doi: 10.3390/rs12183043

Kraus, C., Pennington, T., Herzog, K., Hecht, A., Fischer, M., Voegele, R. T., et al. (2018). Effects of canopy architecture and microclimate on grapevine health in two training systems. *Vitis* 57, 53–60. doi: 10.5073/vitis.2018.57.53-60

Liu, X., Wang, Y., Kang, F., Yue, Y., and Zheng, Y. (2021). Canopy parameter estimation of citrus grandis var. longanyou based on lidar 3d point clouds. *Remote Sens.* 13, 1859. doi: 10.3390/rs13091859

Madec, S., Baret, F., De Solan, B., Thomas, S., Dutartre, D., Jezequel, S., et al. (2017). High-throughput phenotyping of plant height: comparing unmanned aerial vehicles and ground lidar estimates. *Front. Plant Sci.* 8, 2002. doi: 10.3389/fpls.2017.02002

Matese, A., and Di Gennaro, S. F. (2015). Technology in precision viticulture: A state of the art review. *Int. J. Wine Res.* 7, 69–81. doi: 10.2147/IJWR.S69405

Matese, A., and Di Gennaro, S. F. (2018). Practical applications of a multisensor uav platform based on multispectral, thermal and rgb high resolution images in precision viticulture. *Agriculture* 8, 116. doi: 10.3390/agriculture8070116

Mathews, A. J., and Jensen, J. L. (2013). Visualizing and quantifying vineyard canopy lai using an unmanned aerial vehicle (uav) collected high density structure from motion point cloud. *Remote Sens.* 5, 2164–2183. doi: 10.3390/rs5052164

Mesas-Carrascosa, F.-J., de Castro, A. I., Torres-Sánchez, J., Triviño-Tarradas, P., Jiménez-Brenes, F. M., García-Ferrer, A., et al. (2020). Classification of 3d point clouds using color vegetation indices for precision viticulture and digitizing applications. *Remote Sens.* 12, 317. doi: 10.3390/rs12020317

Milella, A., Marani, R., Petitti, A., and Reina, G. (2019). In-field high throughput grapevine phenotyping with a consumer-grade depth camera. *Comput. Electron. Agric.* 156, 293–306. doi: 10.1016/j.compag.2018.11.026

Moreno, H., and Andújar, D. (2023). Proximal sensing for geometric characterization of vines: A review of the latest advances. *Comput. Electron. Agric.* 210, 107901. doi: 10.1016/j.compag.2023.107901

Otsu, N. (1979). "A threshold selection method from gray-level histograms," in *IEEE transactions on systems, man, and cybernetics*. (IEEE) Vol. 9. 62–66. doi: 10.1109/TSMC.1979.4310076

Pádua, L., Adão, T., Sousa, A., Peres, E., and Sousa, J. J. (2020). Individual grapevine analysis in a multi-temporal context using uav-based multi-sensor imagery. *Remote Sens.* 12, 139. doi: 10.3390/rs12010139

Pádua, L., Marques, P., Adão, T., Guimãraes, N., Sousa, A., Peres, E., et al. (2019). Vineyard variability analysis through uav-based vigour maps to assess climate change impacts. *Agronomy* 9, 581. doi: 10.3390/agronomy9100581

Pádua, L., Marques, P., Hruška, J., Adão, T., Peres, E., Morais, R., et al. (2018). Multi-temporal vineyard monitoring through uav-based rgb imagery. *Remote Sens.* 10, 1907. doi: 10.3390/rs10121907

Pennington, T. (2019). *Natural pest suppression in vineyards under innovative management. doctoral thesis*. (Universitätsstraβe 1 56070 Koblenz Germany: Universität Koblenz-Landau, Campus Landau, Universitätsbibliothek).

Perez-Harguindeguy, N., Diaz, S., Garnier, E., Lavorel, S., Poorter, H., Jaureguiberry, P., et al. (2016). Corrigendum to: New handbook for standardised measurement of plant functional traits worldwide. *Aust. J. Bot.* 64, 715–716. doi: 10.1071/BT12225_CO

Petrović, I., Sečnik, M., Hočevar, M., and Berk, P. (2022). Vine canopy reconstruction and assessment with terrestrial lidar and aerial imaging. *Remote Sens.* 14. doi: 10.3390/rs14225894

Qi, Y., Dong, X., Chen, P., Lee, K.-H., Lan, Y., Lu, X., et al. (2021). Canopy volume extraction of citrus reticulate blanco cv. shatangju trees using uav image-based point cloud deep learning. *Remote Sens.* 13, 3437. doi: 10.3390/rs13173437

Remondino, F., and El-Hakim, S. (2006). Image-based 3d modelling: a review. *Photogramm. Rec.* 21, 269–291. doi: 10.1111/j.1477-9730.2006.00383.x

Tsouros, D. C., Bibi, S., and Sarigiannidis, P. G. (2019). A review on uav-based applications for precision agriculture. *Information* 10, 349. doi: 10.3390/info10110349

Weiss, M., and Baret, F. (2017). Using 3d point clouds derived from uav rgb imagery to describe vineyard 3d macro-structure. *Remote Sens.* 9, 111. doi: 10.3390/rs9020111

Wu, J., Wen, S., Lan, Y., Yin, X., Zhang, J., and Ge, Y. (2022). Estimation of cotton canopy parameters based on unmanned aerial vehicle (uav) oblique photography. *Plant Methods* 18, 129. doi: 10.1186/s13007-022-00966-z

Yan, Z., Liu, R., Cheng, L., Zhou, X., Ruan, X., and Xiao, Y. (2019). A concave hull methodology for calculating the crown volume of individual trees based on vehicle-borne lidar data. *Remote Sens.* 11, 623. doi: 10.3390/rs11060623

Zabawa, L., Kicherer, A., Klingbeil, L., Milioto, A., Topfer, R., Kuhlmann, H., et al. (2019). "Detection of single grapevine berries in images using fully convolutional neural networks," in *Proceedings of the IEEE/CVF conference on computer vision and pattern recognition workshops*. (Long Beach, California, USA: IEEE).

Zabawa, L., Kicherer, A., Klingbeil, L., Töpfer, R., Kuhlmann, H., and Roscher, R. (2020). Counting of grapevine berries in images via semantic segmentation using convolutional neural networks. *ISPRS J. Photogramm. Remote Sens.* 164, 73–83. doi: 10.1016/j.isprsjprs.2020.04.002

Zhang, W., Qi, J., Wan, P., Wang, H., Xie, D., Wang, X., et al. (2016). An easy-to-use airborne lidar data filtering method based on cloth simulation. *Remote Sens.* 8, 501. doi: 10.3390/rs8060501

frontiers | Frontiers in Plant Science

TYPE Original Research
PUBLISHED 20 November 2023
DOI 10.3389/fpls.2023.1204791

OPEN ACCESS

EDITED BY
Jennifer Clarke,
University of Nebraska-Lincoln,
United States

REVIEWED BY
Kang Yu,
Technical University of Munich, Germany
Qingfeng Song,
Chinese Academy of Sciences (CAS), China
Nisha Pillai,
Mississippi State University, United States

*CORRESPONDENCE
Benoit Mercatoris
benoit.mercatoris@uliege.be

RECEIVED 14 April 2023
ACCEPTED 30 October 2023
PUBLISHED 20 November 2023

CITATION
Carlier A, Dandrifosse S, Dumont B and Mercatoris B (2023) Comparing CNNs and PLSr for estimating wheat organs biophysical variables using proximal sensing.
Front. Plant Sci. 14:1204791.
doi: 10.3389/fpls.2023.1204791

Comparing CNNs and PLSr for estimating wheat organs biophysical variables using proximal sensing

Alexis Carlier[1], Sébastien Dandrifosse[1], Benjamin Dumont[2] and Benoit Mercatoris[1]*

[1]Biosystems Dynamics and Exchanges, TERRA Teaching and Research Center, Gembloux Agro-Bio Tech, University of Liège, Gembloux, Belgium, [2]Plant Sciences, TERRA Teaching and Research Center, Gembloux Agro-Bio Tech, University of Liège, Gembloux, Belgium

Estimation of biophysical vegetation variables is of interest for diverse applications, such as monitoring of crop growth and health or yield prediction. However, remote estimation of these variables remains challenging due to the inherent complexity of plant architecture, biology and surrounding environment, and the need for features engineering. Recent advancements in deep learning, particularly convolutional neural networks (CNN), offer promising solutions to address this challenge. Unfortunately, the limited availability of labeled data has hindered the exploration of CNNs for regression tasks, especially in the frame of crop phenotyping. In this study, the effectiveness of various CNN models in predicting wheat dry matter, nitrogen uptake, and nitrogen concentration from RGB and multispectral images taken from tillering to maturity was examined. To overcome the scarcity of labeled data, a training pipeline was devised. This pipeline involves transfer learning, pseudo-labeling of unlabeled data and temporal relationship correction. The results demonstrated that CNN models significantly benefit from the pseudolabeling method, while the machine learning approach employing a PLSr did not show comparable performance. Among the models evaluated, EfficientNetB4 achieved the highest accuracy for predicting above-ground biomass, with an R^2 value of 0.92. In contrast, Resnet50 demonstrated superior performance in predicting LAI, nitrogen uptake, and nitrogen concentration, with R^2 values of 0.82, 0.73, and 0.80, respectively. Moreover, the study explored multi-output models to predict the distribution of dry matter and nitrogen uptake between stem, inferior leaves, flag leaf, and ear. The findings indicate that CNNs hold promise as accessible and promising tools for phenotyping quantitative biophysical variables of crops. However, further research is required to harness their full potential.

KEYWORDS

phenotyping, close-range sensing, wheat, CNN, biophysical variables, multi-task, PLSr

1 Introduction

Biophysical vegetation variables are critical indicators of plant growth and health, providing essential information for understanding complex plant-environment interactions (Hawkesford and Riche, 2020; Lemaire and Ciampitti, 2020). Among these variables, Leaf Area Index (LAI), Aboveground Biomass (AGB), and Nitrogen Uptake (Nupt) stand out as key parameters that aid in crop monitoring and yield prediction. Additionally, they play a pivotal role in unraveling the underlying physiological processes that govern the intricate associations between final yield, genotype, and the surrounding environment. As concerns about climate change and the human food security continue to intensify, the accurate assessment of vegetation variables becomes increasingly crucial (Hickey et al., 2019). Timely and reliable information on crop growth and health can help optimize agricultural practices, enhance resource utilization, and help breeders and researchers improve crops.

Recent developments in phenotyping systems, utilizing multiple remote sensing platforms such as satellites, drones, and ground platforms equipped with various sensors (e.g., RGB, spectral data, thermal, LiDAR, etc…), have led to an improvement in the high-throughput and non-destructive screening of crops (Reynolds et al., 2020; Araus et al., 2022; Sun et al., 2022). These technologies have enabled the collection of large volumes of image data, facilitating the rapid, non-invasive, and detailed acquisition of plant phenotyping traits throughout the entire crop lifecycle (Verrelst et al., 2019). Remote sensing, which has lower spatial resolution, can capture the canopy in its entirety in a fast way. In contrast, proximal sensing provides more precise measurements at the organ level and might better handle the impact of unwanted factors (Deery et al., 2014). Ground-based phenotyping systems equipped with multiple sensors can acquire high-resolution data, facilitating improved identification of plant organs, diseases, or yellow and green plant parts (Carlier et al., 2022; Dandrifosse, 2022; Serouart et al., 2022; Tanner et al., 2022; Xu and Li, 2022). The integration of big data and machine/deep learning techniques further enhances the potential for precision phenotyping, enabling more accurate and efficient analyses of crop characteristics for enhanced agricultural management and breeding practices (Verrelst et al., 2019).

The assessment of such biophysical variables using remote sensing and proximal sensing methods requires a comprehensive understanding of agronomy, image and data analysis, given the inherent complexity of these traits and their susceptibility to various influencing factors. Usual methods for estimating AGB and LAI rely on crop architecture, vegetation indices, radiative transfer models, or a combination of these models (Tilly et al., 2015; Brocks and Bareth, 2018; Yue et al., 2019; Raj et al., 2021; Schiefer et al., 2021; Wan et al., 2021). Such methods are also widely used for assessing crop nitrogen status (Berger et al., 2020).

The algorithm pipeline commonly used in plant phenotyping comprises several stages, which involve feature extraction through image analysis methods, including color information collection, thresholding, edge detection, or/and pattern recognition. While these methods can be effective, their reliance on handcrafted features and hyperparameter tuning often results in a lack of robustness. This limitation becomes particularly evident when dealing with complex environmental conditions, such as the presence of soil, weeds, and biotic and abiotic stresses, as well as variations in plant characteristics like growth stage and canopy architecture. Thus, many phenotyping studies focus solely on local areas or specific agricultural practices, leading to limitations in the broader applicability and generalization of proposed models (Chao et al., 2019).

These challenges can lead to suboptimal performance and reduced accuracy in plant phenotyping tasks (Kamilaris and Prenafeta-Boldú, 2018; Nabwire et al., 2021). Yet, it becomes paramount to design studies that effectively capture the diversity present within crop populations and account for the variability of growing conditions. By doing so, we could unlock valuable insights into the intricate interactions shaping these biophysical variables, fostering more robust and adaptable solutions for the future (Hawkesford and Riche, 2020). To address these issues, researchers have been exploring the potential of deep learning and artificial intelligence techniques also in agricultural applications. These approaches have shown promising results in overcoming the limitations of traditional methods by automatically learning relevant features and adaptively adjusting to diverse conditions.

By leveraging advanced machine learning algorithms, such as deep neural networks and convolutional neural networks (CNNs), plant phenotyping can benefit from improved accuracy and generalization across varying scenarios (Singh et al., 2018; Kattenborn et al., 2021; Arya et al., 2022). These methods excel in handling complex datasets and can effectively capture intricate patterns and relationships in plant-related data. Additionally, they reduce the need for manual feature engineering and parameter tuning, leading to more efficient and reliable analyses. For instance, when predicting wheat biomass during early growth stages, CNNs demonstrated less susceptibility to plant density variations compared to alternative methods (Ma et al., 2019). Moreover, these innovative approaches enhance the ability to accurately estimate traits and unlock the extraction of more advanced parameters, such as crop growth rate, particularly when applied to time-series data (Buxbaum et al., 2022). Furthermore, their remarkable ability to solve highly complex patterns makes them ideal for multi-output purposes, enabling the production of multi-trait outputs using a single model (Pound et al., 2017; Nguyen et al., 2023).

The accessibility of ready-to-use libraries, datasets, and emerging methodologies like transfer learning has enabled the application of sophisticated algorithms to crop characterization. The ever-growing availability of neural networks architectures and hyperparameters can present a challenge when it comes to selecting or designing the most suitable architecture. While some authors have successfully created their own neural architectures that perform comparably to well-known ones in terms of accuracy (Li et al., 2021), it is still highly recommended to use established and widely recognized architectures. Nonetheless, ensuring the accuracy and robustness of these models is crucial, and their training and validation with large ground-truth datasets remain essential. This becomes particularly challenging when dealing with biophysical variables, such as AGB, which require a significant amount of human labor and destructive measurements to construct a dataset (Jiang and Li, 2020). This could explain why regression CNN is not yet widely adopted.

To address the need for data, several methods have been proposed to train robust models with a limited amount of labeled data. One approach is to use pre-trained models with transfer learning, which has been successful in estimating forage biomass (Castro et al., 2020; de Oliveira et al., 2021). However, when dealing with multispectral images, pre-trained models that are generally trained on RGB images may not perform well. Another approach is to use data augmentation to artificially increase the dataset size by applying transformations to the images. Advanced data augmentation methods, such as generative adversarial networks (GANs), have been used to improve wheat yield estimation (Zhang et al., 2022). Yet, phenotyping users often acquire large amounts of unlabeled data that still can be used to train a part of a CNN. Semi-supervised learning methods could be used to pre-trained the convolutional parts of CNN from unlabeled datasets (Zbontar et al., 2021). Additionally, one can predict labels for unlabeled data and subsequently insert them into the training dataset if they meet certain criteria; this technique is known as pseudo-labeling (Lee, 2013).

The use of CNNs in various domains has shown promise, and their potential in agriculture for regression purposes needs more investigation. The current study investigate the use of CNN for estimating biophysical variables such as AGB, LAI, nitrogen concentration, and nitrogen uptake from proximal images of wheat. While some studies have already shown some good examples of the use of CNNs for biomass or LAI prediction (Ma et al., 2019; Li et al., 2021; Sapkota et al., 2022; Schreiber et al., 2022; Zheng et al., 2022), many questions remain unanswered. These unanswered questions encompass identifying the optimal CNN architectures for achieving superior performance in estimating LAI, above-ground biomass, nitrogen uptake, and nitrogen concentration for wheat organs utilizing RGB and multispectral close-range images. Additionally, addressing the challenges related to insufficient training data and devising an effective training pipeline is imperative. Furthermore, there is a need to evaluate the effectiveness of multi-output models in assessing dry matter and nitrogen uptake partitioning, as well as nitrogen concentration partitioning in various wheat organs. Lastly, the best-performing CNN methods will be compared to a traditional machine learning approach, a Partial Least Squares regression (PLSr), using feature engineering.

2 Materials and methods

2.1 Experimental design

Data were acquired on winter wheat trials during four years in the Hesbaye area, Belgium (50 33'50" N and 4 42'00" E). Experimental microplots measuring 1.95 m × 6 m were sown with an inter-row spacing of 0.14 m, on homogeneous deep silt loamy soil in a temperate climate. The microplots were fertilized with 27% ammonium nitrate during the tillering, stem elongation and flag leaf stage corresponding to the BBCH 28, 30 and 39 growth stages, respectively. The trials were of two types: (i) trials testing different fertilization fractioning, noted as F and detailed in Table S1 and in Table S2, (ii) trials composed of different fertilization fractioning combined with different fungicide application programs, noted as FP and detailed in Table S3. These abbreviations, along with the year of experimentation, are used in the trial names presented in Table 1.

2.1.1 Reference measurements

Manual measurements were conducted on major phenological growth stages (Table 1), which mainly consisted of tillering, stem elongation, flag leaf, flowering, grain development, and maturity stages. The F trials involved five treatments, while the FP trials involved seven treatments, with three and four replicates conducted, respectively. Fresh AGB was sampled from the three central rows of the microplot over a length of 0.50 m. In the laboratory, the samples were manually separated into ear, stem, flag leaf (L1) and inferior leaves (Linf) groups. Each part was subsequently dried to determine

TABLE 1 Field trial details.

Trial name	Cultivar	BBCH growth stages of samples	No. image acquisitions dates	Sensor	Sowing (grains/m^2)	Sowing date (dd/mm/yyyy)
19-F	Safari	30, 32, 39, 65, 77, 89	11	RGB	250	23/10/2018
20-FP	LG Vertikal	39, 65, 89	11	RGB + MS	250	07/11/2019
20-F	Mentor	32, 39, 65, 75, 89	15	RGB + MS	250	05/11/2019
21-FP	LG Vertikal	39, 65, 89	16	RGB + MS	300	27/10/2020
21-F	Mentor	30, 32, 39, 65, 75, 89	15	RGB + MS	275	20/10/2020
22-F	Mentor	30, 65, 89	13	RGB + MS	300	28/10/2021
22-FP	Bennington	30, 32, 39, 65, 75, 89	17	RGB + MS	300	28/10/2021

In 2019, there was only one RGB camera, whereas the other years there were two RGB cameras and one multispectral (MS) camera.

the associated dry matter (DM) expressed in t/ha. The nitrogen concentration (%N) was then measured using the Dumas method, and nitrogen uptake (Nupt) was calculated by multiplying the DM by the corresponding %N, expressed in kgN/ha. Organs DM and Nuptake values of organs were expressed as relative values, representing the partitioning of DM and N uptake among each organ. These relative values indicate the proportion of each organ in relation to the total plant values. Additionally, the Nitrogen Nutrition Index (NNI) was computed using the traditional approach described in (Justes, 1994).

To determine LAI, plants were sampled by taking one row measuring 0.50 m in length. The leaves were separated from the stems, weighed, spread on a white paper using a transparent adhesive sheet, and scanned. An Otsu segmentation method was employed to isolate the leaves from the white background (Otsu, 1979). The leaf surface area was calculated by summing the areas of the scanned paper sheets multiplied by the proportion of pixels segmented as leaf. Since this protocol was time-consuming, only five microplots with contrasting fertilization were selected for manual LAI measurements at each collection date. These LAI values were correlated with the associated fresh masses by means of a linear regression to predict the LAI of the other microplots. Each correlation had a really high correlation above 0.9, thus validate this method as a reference.

2.1.2 Image acquisitions

To capture nadir frames of wheat microplots, a phenotyping platform was designed (Figure 1). In 2019, a single RGB camera was utilized, while a sensor pod combining two types of cameras was employed in 2020, 2021, and 2022. The sensor pod comprised of two close-up RGB cameras dedicated to stereovision. These RGB cameras were GO-5000C-USB cameras from JAI A/S in Copenhagen, Denmark, and featured a 2560 × 2048 CMOS sensor. Additionally, a multispectral camera, the Micro-MCA from Tetracam Inc. in Gainesville, FL, USA, was used. It had six 1280 × 1024 pixel CMOS sensors, each of them equipped with narrow filter centered respectively at 490, 550, 680, 720, 800, and 900 nm. To avoid shadows from the rest of the platform in the images, both cameras were installed on a cantilever beam. The height of the cameras was adjusted at each acquisition date to maintain a consistent distance between the cameras and the top of the canopy. The height was about 1 m in 2019 and 1.6 m for the other years. Two to four images were taken per microplots for both cameras.

The RGB images were recorded using a color depth of 12-bit per pixel in 2019, 2020 and 2021, which were then converted to 8-bit to match the following algorithms. The multispectral grey scale images were converted from 10 to 8-bit, in accordance with the constructor recommendations. In 2019, the RGB camera auto-exposure algorithm was used. Then, a custom exposure algorithm was developed to limit the number of saturated pixels to less than 1%. The multispectral auto-exposure algorithm was based on a master-slaves principle. The 800 nm filter served as the master and its exposure time was determined automatically using the manufacturer algorithm. The exposure time of each slave filters was then defined as a ratio of the master time. These ratios were adjusted across the season to avoid saturated pixels.

The cropping seasons were thoroughly covered, with multiple image acquisitions from tillering to maturity (Figure 2). Nevertheless, some unforeseen events occurred, such as the COVID-19 pandemic and a violent storm in 2021, which disrupted data acquisition.

The multispectral images underwent two pre-processing steps. The first step involved image registration to correct for shifts between the gray-scale images caused by the proximity to the canopy and the physical lenses gap. The considered method proposed by Dandrifosse et al. (2021) employs a b-spline approach to achieve pixel-wise alignment. The second step involved correcting the multispectral images for different light conditions during acquisition, using the method described by Dandrifosse et al. (2022). A laboratory calibration was performed to convert the digital numbers of the images to Bi-directional Reflectance Factor (BRF), known as reflectance, using an Incident Light Spectrometer, specifically an AvaSpec-ULS2048 from Avantes, Apeldoorn, The Netherlands.

2.2 Partial Least Squares regression approach

A conventional machine learning approach was tested to confront the CNN models presented below. As machine learning

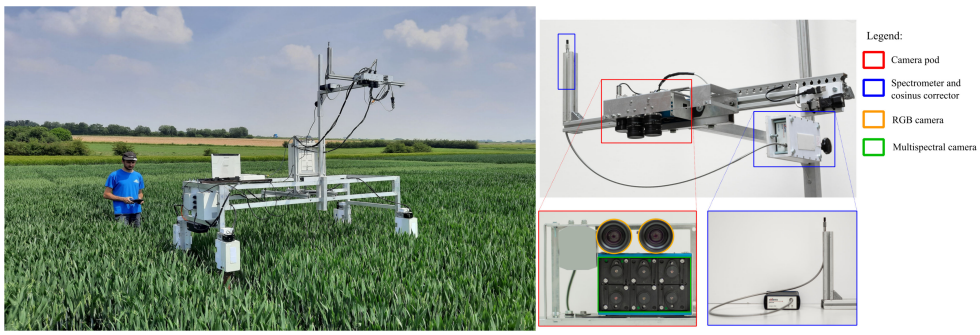

FIGURE 1
Experimental setup. A ground mobile platform (on the left) was equipped with a camera pod (on the right) comprising two high-resolution RGB cameras, a multispectral camera, and an incident light spectrometer, all positioned at a height of 1.6m above the canopy.

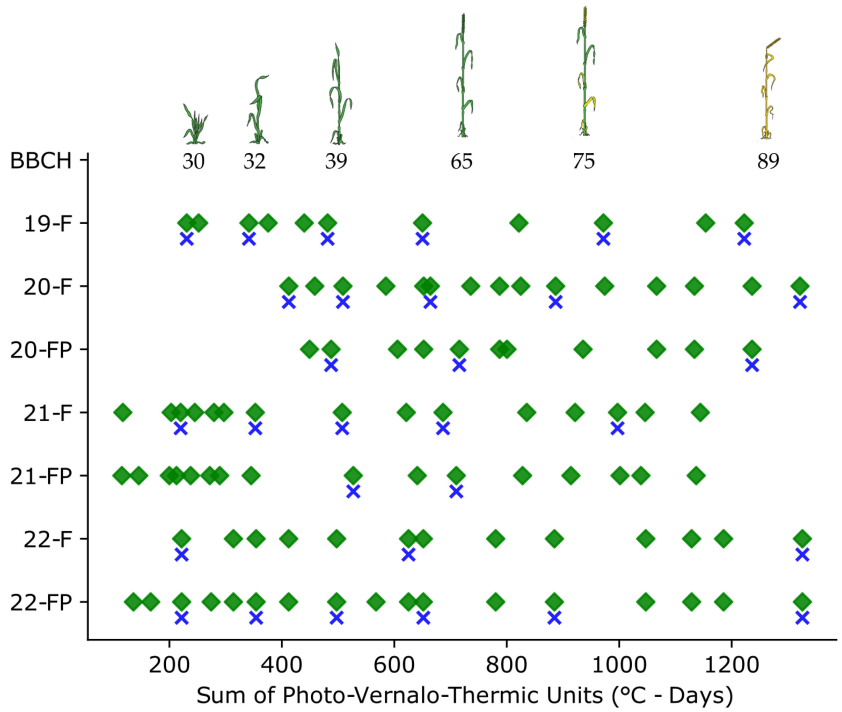

FIGURE 2
Overview of the data acquisitions during the cropping seasons. Green diamonds represent the image acquisitions, and the blue crosses the agronomic samples.

algorithms require relevant image features to be extracted, additional processes were applied after performing the pre-processing steps as described in the previous section. Firstly, a stereovision process was used to extract plant height information using the 95th percentile of the height map (Dandrifosse et al., 2020). Secondly, the plant ratio was computed as the proportion of plants in the scene, using a simple threshold method on the 800 nm image as detailed in Dandrifosse et al. (2022). Finally, twelve vegetation indices (see Table S7) were computed using the six BRFs.

A Partial Least Squares regression (PLSr) model was trained and validated using these twenty features for DM, %N and Nupt of the entire plant. It is worth noting that PLSr has previously exhibited good performance in analogous studies (Freitas Moreira et al., 2021). To fine-tune the model, a sequential backward feature selection approach was employed similar to (Song et al., 2022). This method involved generating all possible feature subsets of size n - 1, where n represents the total number of features. Each subset was rigorously assessed using a 5-fold cross-validation technique on the training dataset. The feature to be removed at each step was determined based on the subset's performance, with the least contributing feature being eliminated. This iterative process continued until the maximum R^2 value was achieved. It is important to mention that the training data did not encompass the 2019 dataset, primarily due to the limited availability of only one RGB camera during that period. Furthermore, the efficacy of the pseudo-labeling strategy, as described in Section 2.3.3 was also explored for PLSr. This training was performed using the PLSr default parameters from the Scikit-Learn 1.3 Python library (Pedregosa et al., 2011).

2.3 CNN training

2.3.1 Architecture

Three CNN architectures available in the python library Tensorflow 2.4. and Keras 2.4 were tested in this study. They were Resnet50 (He et al., 2015) and EfficientNetB0 and B4 (Tan and Le, 2020). They represent the actual state-of-the-art CNN models with different properties (i.e., architecture and number of parameters) and purposes. Resnet 50 was already used for biomass prediction by (Zheng et al., 2022) and EfficientNet is a cutting-edge neural network architecture with a remarkable ability to seamlessly scale from smaller to larger sizes while maintaining good efficiency.

The CNN architectures were customized to perform two tasks: (i) a single-output model to estimate LAI, DM, %N and Nupt of the whole plant respectively; and (ii) a multi-output model to estimate DM, %N, or Nupt of each wheat organ, also referred as partitioning model in the rest of this paper. Multi-output, also known as multi-task model have already been successfully used in phenotyping by (Nguyen et al., 2023) to predict a set of traits using a single model. Whereas a multivariate model deals with multiple dependent variables and aims to model their relationships, a multi-output model is a machine learning model designed to predict multiple output variables simultaneously. A linear activation function was considered for the last neuron of each single-output model. Regarding the multi-output models, four output neurons were considered, one for each organ. A linear activation function was used for the estimation of %N whereas the softmax activation function were used for the relative values of DM and Nupt, i.e., the proportion, in order to keep the values between 0 and 1. All models were initialized with weights from the ImageNet dataset (Deng et al., 2009).

The CNN architectures were originally designed for three-channel images, but the multispectral images used in this study had six channels. To accommodate this, a 2D convolutional layer with three filters and a kernel size of (1,1) was added at the beginning of each model when using multispectral images. It allowed to provide a three channels input required for the selected CNN models with pre-trained weights.

2.3.2 Dataset configuration

The study used a dataset consisting of 1809 RGB images and 1391 multispectral images with their corresponding reference measurements. These numbers correspond to the multiplication of dates, samples, replicates, and images per microplots. Each image was associated with a specific combination of agronomic variables. From this dataset, two treatments from F trials (Tables S1, S2), and one treatment from FP trials (Table S3) were selected for the validation dataset that included 424 RGB images and 341 multispectral images.

In addition to the images acquired on the same days as the manual sampling, each trial was monitored continuously throughout the season, as illustrated in Figure 2. All those acquisitions yielded a dataset comprising 16 812 RGB images and 14 491 multispectral images. To prepare the data for the CNN models, some pre-processing steps were taken.

The first pre-processing step involved determining the image size, which is a trade-off between retaining as much information as possible and limiting the computing time and resources required. Additionally, when using pre-trained models, it is recommended to set the input image size to match the size used during initial training. Therefore, all images were resized to 224 x 224 for the ResNet50 and EfficientNetB0 models, and to 380 x 380 for the EfficientNetB4 model. It is worth noting that the images were previously cropped into a square to avoid distortion.

In addition to image resizing, the pixel scaling was also adjusted for each model. For the RGB images, pixel scaling was adapted according to the Keras documentation and the requirements of each model. For the multispectral images, Bi-directional Reflectance Factor (BRF) values were first normalized between 0 and 1. Next, the data was standardized based on the mean and standard deviation of the training dataset as advice by Tensorflow. To further enhance the dataset, data augmentation techniques, namely random flip up/down and right/left, were applied. These techniques increase the diversity of the dataset, which can improve the generalization performance of the models.

2.3.3 Training pipeline

In the field of phenotyping, researchers often encounter a substantial amount of unlabeled data. However, these data hold untapped potential for enhancing the performance of machine learning models. In this study, a pseudo-labeling method was employed to leverage the unlabeled data effectively. Pseudo-labeling involves predicting the labels of unlabeled data using a model that demonstrates acceptable performance. These predicted labels, known as pseudo-labels, can then be incorporated into the training dataset, subject to a predefined confidence threshold. For classification tasks, this confidence threshold is based on class probabilities. Nevertheless, regression tasks utilize a linear activation function, leading to the absence of probabilities. To overcome this challenge, this research proposes a novel approach. The predicted biophysical variables from each microplot were plotted against time to generate a crop growth curve. This curve characterizes the growth pattern of the crop over time and can be harnessed to rectify the predicted values.

Based on this idea, a well-defined pipeline was constructed (see Figure 3). The pipeline entailed utilizing CNN models pre-trained on ImageNet through transfer learning. The initial training phase involved training the CNN models for 40 epochs with a learning rate of 1×10^{-3}. During this process, only the last layer, specifically the linear dense layer, was trained, while keeping the remaining layers frozen.

Following this, a fine-tuning stage was conducted for 10 epochs, with a reduced learning rate of 1×10^{-5}. During fine-tuning, the last convolutional layer block was unfrozen and retrained, leading to the creation of Model 1.

Next, Model 1 was utilized to generate predicted labels (Ypred) for the complete training dataset. These predicted labels were then plotted against the Photo-Vernalo-Thermic Units (°C-days) (Duchene et al., 2021). A cubic B-Spline for LAI and a cubic polynomial function for the other variables was fitted with a high smoothing condition. These curves are traditionally used in biophysical variables modeling (van Eeuwijk et al., 2019). Basic correction conditions were also implemented to help that fitting, such as setting organ values to 0 when they were not present at specific times. The outcome of this process yielded a fitted curve from which "corrected" pseudo-labels (Ypseu) could be extracted.

Last, pre-trained CNNs from ImageNet were trained on the corrected pseudo-labels (Ypseu) for 30 epochs, using a learning rate of 1×10^{-5}. This resulted in the development of Model 2, which was thus trained on a much larger dataset compared to Model 1.

The Mean Square Error (MSE) loss function and Adam optimizer were used in all models. However, in the case of multi-output model for %N, the MSE calculation was limited to true labels above 0. This means that if an organ was not yet visible (e.g., the ear during tillering growth stage), the loss function did not take it into account, which prevented it from interfering with the loss function. Additionally, a weight was applied to the loss calculation when working with relative multi-output models. Specifically, the flag leaf pool weights were multiplied by twenty to ensure consistency with the order of magnitude of the other organ pools. This helped to balance the contributions of different organ pools and prevent one pool from dominating the loss calculation. All models were trained on an NVidia Tesla V100 GPUs.

To evaluate the performance of all models, two metrics were used: the determination coefficient (R^2) and the root mean square error (RMSE).

3 Results

3.1 Variations of winter wheat biophysical variables

The descriptive statistics reveal significant variations in the four biophysical variables across the different growth stages: biomass ranging from 0.51 to 27.89 T/ha, LAI from 0.69 to 8.66, nitrogen concentration from 0.61 to 4.76%, and nitrogen uptake from 13.49

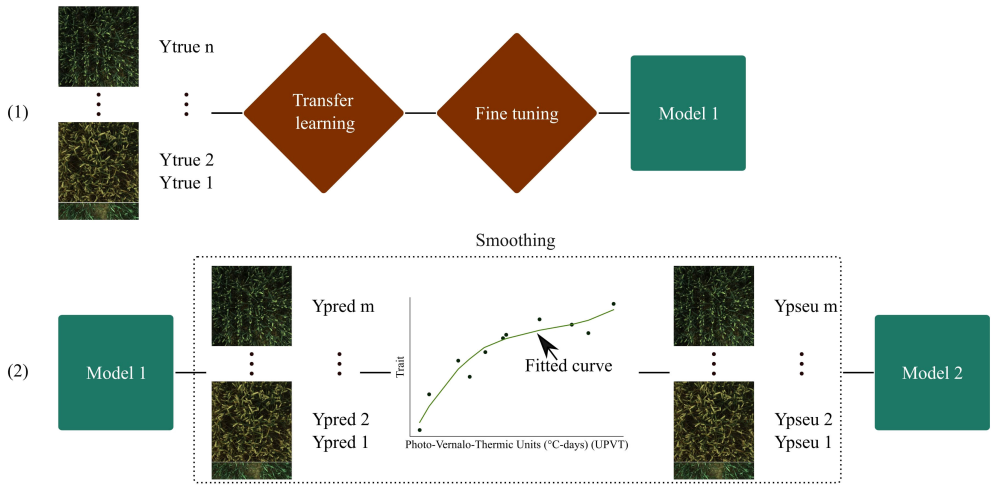

FIGURE 3
Proposed training pipeline. (1) is the training with transfer learning, and (2) is the training with pseudo-labels. Ytrue corresponds to the reference measurements. Ypred are predicted labels. A curve is fitted to provide the Ypseu which represent the corrected pseudo-labels. n and m correspond to the number of reference measurements and the total number of images respectively.

to 338.59 kg N/ha (Table 2). This wide variability in the datasets was attributed to diverse factors, including variations in growing stages, repeated measurements over multiple years, and heterogeneous treatments, particularly variations in nitrogen inputs. The analysis, specifically employing ANOVA, indicates that most of these biophysical variables exhibit significant differences among treatments (Table S4). Both the training and validation datasets exhibit similar statistics, which validates the appropriateness of the dataset splitting method. Furthermore, correlations between these variables were examined, and the results show that biomass demonstrated a Pearson correlation of -0.27, -0.71, and 0.87 with LAI, nitrogen concentration, and nitrogen uptake, respectively. The correlation between nitrogen concentration and nitrogen uptake was found to be -0.44.

3.2 Plant biophysical variable modeling

This study evaluated various models for predicting plant biophysical variables. The EfficientNetB4 model trained on pseudo-labels demonstrated the highest performance for DM, achieving an R^2 of 0.92 and a low RMSE of 1.50 on the validation dataset (Table 3). In contrast, the PLSr model had an R^2 of 0.77 and a higher RMSE of 2.58, indicating weaker predictive ability.

Regarding LAI, the ResNet50 model trained on pseudo-labels yielded the best R^2 of 0.82 (Table 4). For nitrogen concentration prediction using multispectral images, the ResNet50 model achieved an R^2 of 0.80 (Table 5) and an R^2 of 0.73 for Nitrogen uptake (Table 6).

The other CNN models investigated in this study exhibited robust and comparable performance levels when subjected to the pseudo-labeling pipeline during training. The utilization of pseudo-labels played a pivotal role in mitigating disparities between the outcomes observed on the validation and training datasets. It is worth noting that the PLSr model did not yield any discernible advantages from the pseudo-labeling technique, consistently falling short of the CNN models in terms of performance. One noteworthy observation is that this pseudo-labeling method appeared to exacerbate the disparities between the performance of the training and validation sets. Furthermore, the results of the backward feature

TABLE 2 Descriptive statistics of dry matter (T/ha), LAI, N concentration (%) and N uptake (kg N/ha).

Dataset	Statistic	Dry matter (T/ha)	LAI	N concentration (%)	N uptake (kg N/ha)
Training	mean	10.44	3.40	1.81	152.31
	std	6.15	1.65	0.85	77.37
	min	0.51	0.72	0.61	13.49
	max	23.07	8.66	4.76	338.59
Validation	mean	10.32	3.28	1.76	145.21
	std	6.00	1.45	0.80	66.86
	min	0.51	0.69	0.87	16.26
	max	27.89	7.35	4.09	307.14

TABLE 3 Model performances for DM of the plant.

Model	Data	RMSE train	R^2 train	RMSE val	R^2 val
EfficientNetB0	Ytrue	1.76	0.91	2.11	0.83
EfficientNetB0	Ypseu	0.91	0.95	1.66	0.91
EfficientNetB4	Ytrue	1.38	0.93	1.89	0.86
EfficientNetB4	Ypseu	1.09	0.96	1.50	**0.92**
Resnet50	Ytrue	0.78	0.98	1.87	0.89
Resnet50	Ypseu	1.05	0.97	1.64	0.90
PLSr	Ytrue	2.49	0.80	2.55	0.78
PLSr	Ypseu	1.32	0.92	2.58	0.77

selection analysis, as depicted in Figures S1 to S4, indicated that the augmentation of the dataset via this approach led to an increased requirement for features to achieve optimal performance levels.

Throughout the growing season, the models successfully assessed the variables, as evidenced by Figures 4 and 5. However, there were some outliers that significantly deviated from the ideal 1:1 relationship between predicted and true values. Additionally, a saturation effect was observed, where the models struggled to accurately predict the maximum values of each variable, leading to a lack of detail in certain growing seasons. These observations provide valuable insights for further refining the modeling approach and improving predictive accuracy.

3.3 Organs biophysical variable modeling

The utilization of multi-output models yielded diverse outcomes regarding the proportion of dry matter and nitrogen uptake, as indicated in Table S5. Table 7 displays the performance of the multiplication of both the single output models and the multi-output models for dry matter and nitrogen uptake, and solely the multi-output model for nitrogen concentration.

Among the models evaluated, EfficientNetB0 demonstrated superior performance for predicting nitrogen uptake, achieving commendable R^2 values of 0.7, 0.59, 0.69, and 0.86 for stem, inferior leaves, flag leaf, and ear, respectively. ResNet50 exhibited R^2 values of 0.87, 0.62, 0.38, and 0.94 for dry matter, and 0.50, 0.76, 0.69, and -1.07 for nitrogen concentration, indicating its effectiveness in certain cases.

Analyzing individual organs, the ear and stems exhibited higher prediction accuracy by the models, while the flag leaf showed comparatively poorer prediction, depending on the specific model employed. Concerning the %N models, the stem and inferior leaf pools were accurately predicted, but the prediction performance for the ear was notably inadequate.

Interestingly, while the pseudo-labeling method led to reduced performance for the multi-output models (Table S5), its combination with the single output models, which significantly benefit from pseudo-labels, did not have a substantial impact on the prediction of DM and %N for each organ. This suggests that the pseudo-labeling approach is effective in enhancing the single output models but may require further optimization for multi-output models.

The Figure 6 presents the predicted partitioning of wheat dry matter and nitrogen uptake over the growing season for a single microplot. It offers a nice alternative to provide valuable insight about the partitioning of the matter within the plant. Moreover, both RGB and multispectral models successfully detected the emergence of new organs, such as the flag leaf and ear. Notably, the dry matter model showed an earlier appearance of ears compared to the nitrogen uptake model in this specific example.

TABLE 4 Model performances for LAI.

Model	Data	RMSE train	R^2 train	RMSE val	R^2 val
EfficientNetB0	Ytrue	1.06	0.69	1.18	0.57
EfficientNetB0	Ypseu	0.72	0.86	0.80	0.80
EfficientNetB4	Ytrue	0.68	0.86	0.78	0.80
EfficientNetB4	Ypseu	0.67	0.87	0.78	0.81
Resnet50	Ytrue	0.27	0.98	0.79	0.79
Resnet50	Ypseu	0.66	0.98	0.78	**0.82**
PLSr	Ytrue	0.77	0.75	0.83	0.75
PLSr	Ypseu	0.28	0.95	0.91	0.69

TABLE 5 Model performances for %N of the plant.

Model	Data	RMSE train	R^2 train	RMSE val	R^2 val
EfficientNetB0	Ytrue	0.37	0.74	0.36	0.72
EfficientNetB0	Ypseu	0.24	0.90	0.30	0.79
EfficientNetB4	Ytrue	0.33	0.75	0.32	0.55
EfficientNetB4	Ypseu	0.23	0.89	0.31	0.73
ResNet50	Ytrue	0.14	0.97	0.32	0.78
ResNet50	Ypseu	0.24	0.90	0.30	**0.80**
PLSr	Ytrue	0.49	0.59	0.43	0.54
PLSr	Ypseu	0.20	0.88	0.44	0.51

TABLE 6 Model performances for Nupt of the plant.

Model	Data	RMSE train	R^2 train	RMSE val	R^2 val
EfficientNetB0	Ytrue	42.42	0.65	37.97	0.66
EfficientNetB0	Ypseu	28.84	0.84	34.38	0.72
EfficientNetB4	Ytrue	37.46	0.70	43.39	0.47
EfficientNetB4	Ypseu	25.33	0.87	34.05	0.69
ResNet50	Ytrue	14.24	0.96	37.27	0.68
ResNet50	Ypseu	26.69	0.86	33.89	**0.73**
PLSr	Ytrue	39.72	0.65	39.89	0.70
PLSr	Ypseu	17.78	0.88	42.81	0.66

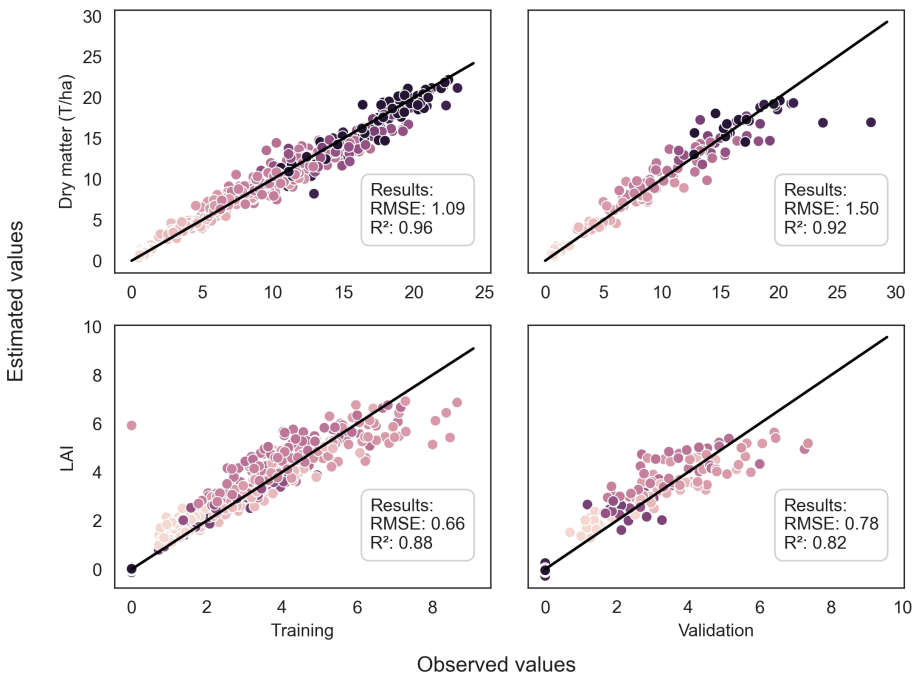

FIGURE 4
Comparison between observed and predicted values of DM of the whole plant and LAI for both training and validation datasets, using the EfficientNetB4 model for DM and the ResNet50 model for LAI. The dots are color-coded according to the stages in the season, with darker dots indicating later stages. The dark line represents the 1:1 line.

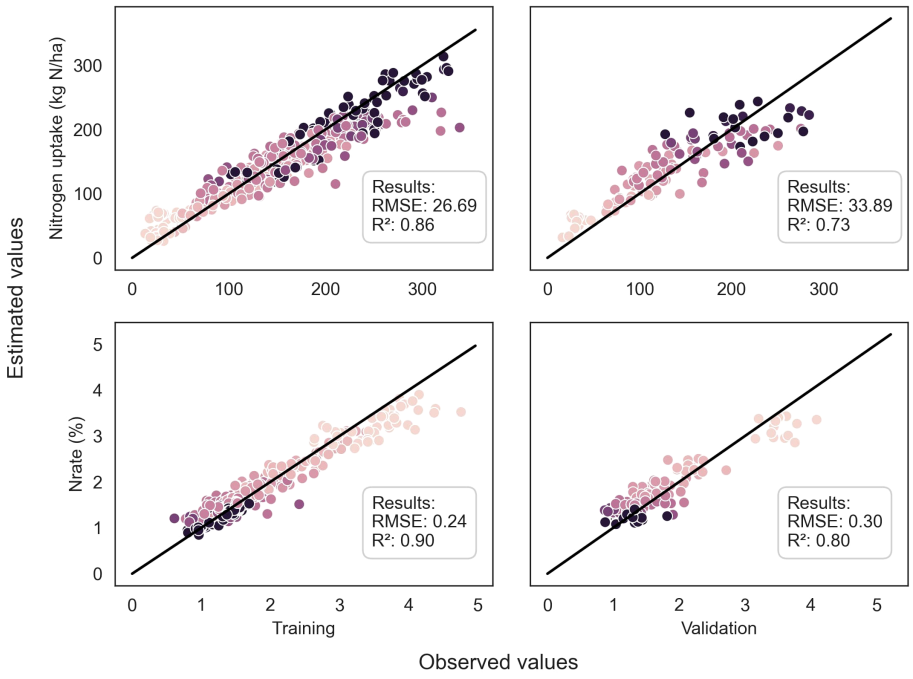

FIGURE 5
Comparison between observed and predicted values of %N and Nupt of the whole plant for both training and validation datasets, using the ResNet50 model. The dots are color-coded according to the stages in the season, with darker dots indicating later stages. The dark line represents the 1:1 line.

4 Discussion

4.1 Convolutional neural networks as an effective approach for predicting biophysical variables

This study presents a comprehensive investigation into the potential of recent CNNs in accurately predicting biophysical vegetation variables, such as dry matter, leaf area index, and nitrogen uptake and concentration. The research demonstrate that our CNN-based approach stands as one of the most advanced methods for this task, even though direct performance comparisons with prior studies are hindered by the limited availability of benchmark datasets.

In this study, CNN models outperformed a PLSr approach, consistent with previous research findings (Ma et al., 2019; Castro et al., 2020). Thus, CNN stands out as a potent tool in this context due to its ability to autonomously extract features, eliminating the need for manual feature extraction. It demonstrates remarkable adaptability in handling the evolving features of crops throughout the growing season, including changes in physiology and color. This adaptability negates the necessity for fine-tuning models to specific

TABLE 7 R^2 of the different multi-outputs models to predict nitrogen uptake, dry matter and nitrogen concentration of each organ.

Model	Data	Dataset	Nuptake				DM				%N			
			Stem	Linf	L1	Ear	Stem	Linf	L1	Ear	Stem	Linf	L1	Ear
EfficienNetB0	Ypseu	train	0.84	0.78	0.77	0.92	0.91	0.49	0.08	0.97	0.71	0.86	-0.08	-2.18
	Ytrue	train	0.72	0.67	0.7	0.91	0.90	0.49	0.17	0.96	0.60	0.75	0.60	-1.09
EfficienNetB4	Ypseu	train	0.54	0.02	0.65	0.75	0.90	0.53	-0.11	0.96	0.67	0.75	-0.10	-1.95
	Ytrue	train	0.6	0.48	-0.47	0.7	0.92	0.65	0.57	0.97	0.38	0.56	0.10	-2.46
ResNet50	Ypseu	train	0.8	0.75	0.76	0.93	0.88	0.51	0.15	0.94	0.73	0.87	-0.05	-2.10
	Ytrue	train	0.84	0.78	0.8	0.96	0.93	0.76	0.67	0.98	0.86	0.93	0.95	0.52
EfficienNetB0	Ypseu	val	0.7	0.59	0.69	0.86	0.83	0.28	-0.09	0.95	0.54	0.84	-0.43	-2.64
	Ytrue	val	0.63	0.47	0.54	0.86	0.82	0.34	-0.16	0.93	0.47	0.69	0.58	-1.72
EfficienNetB4	Ypseu	val	0.51	-0.2	0.52	0.66	0.83	0.38	-0.15	0.94	0.59	0.73	-0.46	-2.11
	Ytrue	val	0.41	0.3	-1.66	0.65	0.84	0.55	0.14	0.94	0.10	0.55	0.13	-3.91
ResNet50	Ypseu	val	0.64	0.52	0.64	0.85	0.87	0.57	0.22	0.94	0.48	0.84	-0.45	-3.17
	Ytrue	val	0.67	0.56	0.66	0.86	0.87	0.62	0.38	0.94	0.50	0.76	0.69	-1.07

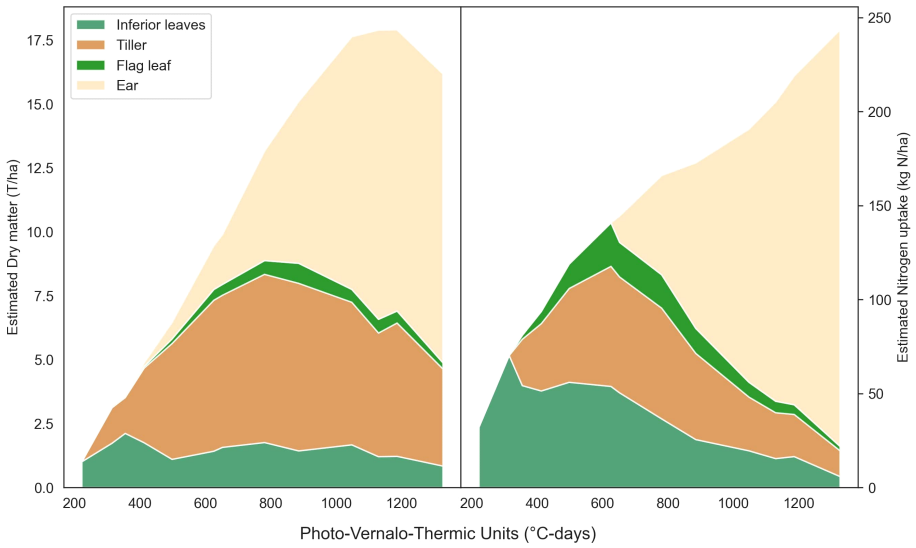

FIGURE 6
Predicted partitioning of dry matter and nitrogen uptake throughout the season for a microplot from the 22-F trial. This results from the use of the multi-output ResNet50 (Table S5) multiplied by the single output ResNet50 (Table 3).

growth stages or cultivars, as highlighted by previous machine learning research (Yue et al., 2019). These studies commonly adopt a strategy of employing one model for each growth stage, alongside a single overarching model that typically yields less satisfactory results (Wang et al., 2022a). Nevertheless, it would remain intriguing to explore the performance of the presented CNN models on new cultivars, which may exhibit distinct characteristics.

Moreover, the results pertaining to nitrogen concentration are particularly intriguing. One might expect that CNNs would prioritize features related to plant architecture, which would be more closely associated with nitrogen uptake. However, the observed medium correlation (-0.44) between nitrogen concentration and uptake tends to limit this assumption, suggesting that the CNNs might have also identified some kind of vegetation indices contributing to the predictions. Despite these remarkable outcomes, interpreting the specific features extracted by CNNs remains challenging. To enhance our understanding of the underlying mechanisms and improve model interpretability, ongoing research is dedicated to developing techniques for explaining CNN predictions. One such approach, Grad-CAM (Selvaraju et al., 2020), shows promise in providing insights into the regions of the image that significantly influence the model's decisions.

Among the CNN architectures explored, ResNet50 exhibited high performance, consistent with similar studies (Castro et al., 2020). Notably, EfficientNet also yielded promising results, especially for DM prediction of the entire plant. However, it is worth considering that the advantage of EfficientNetB4 might be attributed to its capacity to capture finer details in larger images. Interestingly, recent research has shown that performance gains may saturate beyond a certain image size (Li et al., 2021). This behavior could be dependent on the architecture, as EfficientNet is explicitly designed for scalable optimization on specific datasets (Tan and Le, 2020).

In contrast, the machine learning approach utilizing PLSr and feature fusion from the multi-sensor system consistently delivered inferior performance when compared to CNN models. Nevertheless, it is important to underscore that this method still achieved commendable results, boasting an R^2 value exceeding 0.6, which aligns with the findings reported in Yue et al. (2019).

An intriguing aspect arising from the backward feature selection analysis was the observed increase in the number of selected features between Ytrue and Ypseu, signifying the heightened demand for features in constructing models with a larger dataset (See Supplementary Material). Additionally, both sets of features exhibited substantial similarities, affirming their efficacy in modeling agronomical parameters. Among these features, plant height emerged as the most frequently utilized, followed by plant ratio and MCARI index. Furthermore, it is noteworthy that DM and Nuptake shared three out of four features, a logical outcome given that Nuptake was derived from DM. Other features selected for nitrogen-related analysis included well-established indices such as MCARI, mNDB, and GR.

However, it is essential to exercise caution when drawing overarching conclusions solely based on this method. Notably, the selection of these features can be intricate, as they may exhibit seasonal variations, as documented in (Yue et al., 2019; Wang et al., 2022a, b). It is conceivable that more advanced methods may yield superior results, as suggested in (Wang et al., 2021).

4.2 The significance of the amount of ground truth data in deep learning for regression of biophysical variables

Deep learning techniques, especially in regression tasks involving biophysical variables, encounter a substantial challenge

due to the scarcity of sufficient training datasets. The limited availability of labeled data necessitates the development of innovative approaches to overcome this issue. A training pipeline was devised in this study, which capitalizes on the abundance of unlabeled data commonly found in highthroughput phenotyping installations. This method represents a practical approach to leverage unlabeled data, leading to optimized performance of CNN models in phenotyping applications.

The pseudo-labeling method emerged as an effective strategy to mitigate overfitting of the model. As a result, the performance gap between the training and validation datasets was reduced, signifying enhanced generalization. To perform such data correction, a polynomial cubic curve was chosen for its simplicity in representing biophysical curves and ease of fitting. Finer curves more related to plant growth pattern, such as P-splines or logistic curves, could have been used, but the fitting process may prove difficult (van Eeuwijk et al., 2019). These finer curves often require more frequent measurements (one to two per week) for accurate fitting (Roth et al., 2020), a frequency that our data did not meet. To address potential bias, correcting conditions were introduced, particularly essential for organ models. For example, when an organ was absent at a specific time (t), the corresponding pseudo-label was set to 0, a correction that, while seemingly straightforward, significantly contributed to the accuracy of representations. The effectiveness of traditional machine learning might also be a good option to generate pseudo-labels in the case of fewer ground truth data.

During the research, we also examined more advanced data augmentation techniques, such as 90° rotation and color space transformations without success. It is crucial to exercise caution when employing such methods, as their indiscriminate application may adversely affect model performance, as observed in certain models in (Castro et al., 2020). Conversely, (Ma et al., 2019) reported clear performance improvements with these methods. The discrepancy in results may be attributed to the risk of the model becoming overly reliant on specific features, such as wheat lines in the case of image rotation. Hence, prudent consideration of data augmentation is warranted based on the specific characteristics of the dataset and model.

4.3 Limitations and perspectives

An effective approach for evaluating model performance is to combine their predictions into a single other variable. In this study, we used DM and %N of the plant, predicted from their respective models, to calculate the Nitrogen Nutrition Index (NNI). The R^2 values for the training and validation datasets were 0.71 and 0.33, respectively, suggesting the potential utility of this method for measuring NNI as well. Although the dataset contains a substantial amount of heterogeneous ground truth data, the performance of the models may raise questions due to its limited size in terms of crop architecture and color, which only includes a few genotypes. The observed patterns in predicted values in Figures 5 and 4 appeared scattered, resembling a cloud rather than forming a clear line, and some outliers were evident, indicating room for improvement in the models. Overfitting was also observed, particularly with ResNet50, which frequently achieved R^2 values above 0.95 for the training dataset. To address this, a prudent approach would be to initially use small architectures and acquire more data. Despite the need for improvements concerning trait saturation and accuracy within specific growth stages Figure 4, the models' potential is significant. They can be employed to compute advanced traits, such as growth rate and spot ideotypes using temporal curves, as demonstrated in a recent study (Roth et al., 2022).

By leveraging diverse and large-scale datasets, CNNs can yield more robust and precise models, reducing the need for heavily relying on study-specific feature engineering. Therefore, the phenotyping community should prioritize the development of extensive and well-annotated datasets for essential phenotyping challenges, such as the Global Wheat Head Detection (GWHD) dataset (David et al., 2021). Additionally, exploring alternative solutions, such as self-supervised learning (Zbontar et al., 2021) or generating synthetic data using Functional-Structural Plant Models (FSPM) (Gao et al., 2023), can further enhance model training and performance.

Research on the allocation of major plant elements, such as sink/source regulation processes and their relationship with grain nitrogen content, heavily relies on dry matter and nitrogen uptake partitioning (Martre et al., 2003; Gaju et al., 2014). The multi-output models proposed in this study have shown promising results (Table 7), with good performance in most cases. However, certain organs exhibited poor performance, such as %N of the ear, which may be attributed to the lack of visible traits that could account for it, like a greener ear. The subpar performance of DM and Nupt for flag leaf could be mainly attributed to the multi-output proportion model's poor performance for this organ (Table S5), despite assigning it a higher weight in the loss function. Additional images specifically featuring flag leaves might be needed to improve its representation, as the ear rapidly develops behind them.

This multi-output model exemplifies the potential of such approaches for plant phenotyping. While this study employed a simple approach by sharing a common loss function, the benefits of multi-output learning can be substantial. For instance, a single model assessing both dry matter and leaf area index can significantly reduce computational costs and processing time, while maintaining high accuracy for both tasks. In fact, when tasks share complementary information, they can act as regularizers for each other, enhancing prediction performance (Standley et al., 2020). However, combining complex associations between tasks, such as classification and regression tasks, requires careful consideration of model architecture, loss function, and training strategy to achieve optimal performance. Ongoing research in this area is actively being pursued (Vafaeikia et al., 2020; Vandenhende et al., 2020).

The ability of the models to autonomously discover the appearance of new organs, such as ears and flag leaves, is particularly intriguing and opens exciting new research avenues too. This suggests the feasibility of developing growth stage

estimation models per RGB image in a similar manner. Such models could be further utilized for various purposes, such as optimizing crop models (Yang et al., 2021).

5 Conclusions

In this study, a robust training pipeline that leverages unlabeled data through the innovative combination of pseudo-labeling and temporal relationship correction were developed and implemented. The results demonstrate the significant advantages of employing CNN models over a PLSr approach, as they achieve superior performance without the need for labor-intensive feature engineering. Notably, EfficientNetB4 was better in predicting above-ground biomass, while ResNet50 exhibited superior performances in predicting LAI, nitrogen uptake, and nitrogen concentration. Additionally, our exploration of multi-output models provided valuable insights into the distribution of dry matter and nitrogen uptake among different plant organs, enriching our understanding of plant biophysical characteristics.

While CNN models show great promise, it is evident that further investigation is required to fully unlock their potential. This research effectively demonstrates the capabilities of CNNs in predicting biophysical vegetation variables and offers valuable insights into addressing limitations and future perspectives in plant phenotyping. Moving forward, data sharing within the phenotyping community will be critical to optimize model performance. Access to large and diverse datasets, such as the Global Wheat Head Detection dataset, is indispensable for advancing phenotyping research and enhancing the performances of CNN models. By fostering data sharing and continued research efforts, CNNs can continue to revolutionize plant phenotyping and make profound contributions to agricultural and environmental sciences.

Data availability statement

The raw data supporting the conclusions of this article will be made available by the authors, without undue reservation.

Author contributions

AC and SD performed experiments and data collection; AC build the models, performed the statistical analysis, interpreted the results, and prepared the first draft. BD and BM contributed to the result interpretation and supervised the project. All authors revised the manuscript. All authors contributed to the article and approved the submitted version.

Funding

This research was funded by the Agriculture, Natural Resources and Environment Research Direction of the Public Service of Wallonia (Belgium), project D65-1412/S1 PHENWHEAT, and the National Fund of Belgium F.R.S-FNRS (FRIA grant).

Acknowledgments

Computational resources have been provided by the Consortium des Équipements de Calcul Intensif (CÉCI), funded by the Fonds de la Recherche Scientifique de Belgique (F.R.S.-FNRS) under Grant No. 2.5020.11 and by the Walloon Region. The authors thank the research and teaching support units Agriculture Is Life of TERRA Teaching and Research Centre, Liege` University for giving access to the field trials. The authors are grateful to Jerome Heens, Jesse Jap, Franc¸oise Thys and Gauthier Lepage for their help. The authors also thank CRA-W/Agromet.be for the meteorological data.

Conflict of interest

The authors declare that the research was conducted in the absence of any commercial or financial relationships that could be construed as a potential conflict of interest.

Publisher's note

Supplementary material

The Supplementary Material for this article can be found online at: https://www.frontiersin.org/articles/10.3389/fpls.2023.1204791/full#supplementary-material

SUPPLEMENTARY TABLE 1
Fertilization trial (F) in 2020, 2021 and 2022.

SUPPLEMENTARY TABLE 2
Fertilization trial (F) in 2019.

SUPPLEMENTARY TABLE 3
Trials composed of different fertilization fractioning combined with different fungicide application programs (FP) in 2020, 2021 and 2022.

SUPPLEMENTARY TABLE 4
Dry matter, LAI, nitrogen concentration and nitrogen uptake of the whole plant used in this study. Data are means +/- the standard deviation (n=3 or 4 repetitions). Significance of treatment effects were analyzed using a one-way ANOVA (*: $P \leq 0.05$; **: $P \leq 0.01$; **: $P \leq 0.001$).

SUPPLEMENTARY TABLE 5
R^2 of the different models to predict DM and Nupt proportion of each organ.

SUPPLEMENTARY TABLE 6
Pearson correlation table of the agronomic data

SUPPLEMENTARY TABLE 7
Vegetation indices selected in this study.

SUPPLEMENTARY FIGURE 1
Backward feature selection with PLSr for DM Estimation: On the left, selected features for estimating DM from Ytrue include Plant Ratio, 95th Percentile of Height, MCARI, and BRF 490. On the right, the selected features for estimating DM from Ypseu comprise Plant Ratio, 95th Percentile of Height, MCARI, and BRF 550.

SUPPLEMENTARY FIGURE 2
Backward feature selection with PLSr for LAI Estimation: On the left, selected features fo estimating LAI from Ytrue include SR, GNDVI, MCARI, CIgree, BRF 900 and BRF 720. On the right, the selected features for estimating LAI from Ypseu comprise NDRE, SR, GNDVI, CIgreen, CIrede and BRF 550.

SUPPLEMENTARY FIGURE 3
Backward feature selection with PLSr for Nuptake Estimation: On the left, selected features for estimating Nuptake from Ytrue include Plant Ratio, 95th percentile of height and MCARI. On the right, the selected features for estimating Nuptake from Ypseu comprise Plant Ratio, 95th percentile of height, GR, MCARI, mNDB and BRF 550.

SUPPLEMENTARY FIGURE 4
Backward feature selection with PLSr for Nrate Estimation: On the left, selected features for estimating Nrate from Ytrue include 95th percentile of height and MCARI. On the right, the selected features for estimating Nrate from Ypseu comprise 95th percentile of height, GR and mNDB.

References

Araus, J. L., Buchaillot, M. L., and Kefauver, S. C. (2022). "High Throughput Field Phenotyping," in *Wheat Improvement*. Eds. M. P. Reynolds and H.-J. Braun (Cham: Springer International Publishing), 495–512. doi: 10.1007/978-3-030-90673-327

Arya, S., Sandhu, K. S., Singh, J., and kumar, S. (2022). Deep learning: As the new frontier in high-throughput plant phenotyping. *Euphytica* 218, 47. doi: 10.1007/s10681-022-02992-3

Berger, K., Verrelst, J., Féret, J.-B., Wang, Z., Wocher, M., Strathmann, M., et al. (2020). Crop nitrogen monitoring: Recent progress and principal developments in the context of imaging spectroscopy missions. *Remote Sens. Environ.* 242, 111758. doi: 10.1016/j.rse.2020.111758

Brocks, S., and Bareth, G. (2018). Estimating barley biomass with crop surface models from oblique RGB imagery. *Remote Sens.* 10, 268. doi: 10.3390/rs10020268

Buxbaum, N., Lieth, J. H., and Earles, M. (2022). Non-destructive plant biomass monitoring with high spatio-temporal resolution *via* proximal RGB-D imagery and end-to-end deep learning. *Front. Plant Sci.* 13. doi: 10.3389/fpls.2022.758818

Carlier, A., Dandrifosse, S., Dumont, B., and Mercatoris, B. (2022). Wheat ear segmentation based on a multisensor system and superpixel classification. *Plant Phenomics* 2022. doi: 10.34133/2022/9841985

Castro, W., Marcato Junior, J., Polidoro, C., Osco, L. P., Gonc¸alves, W., Rodrigues, L., et al. (2020). Deep learning applied to phenotyping of biomass in forages with UAV-based RGB imagery. *Sensors* 20, 4802. doi: 10.3390/s20174802

Chao, Z., Liu, N., Zhang, P., Ying, T., and Song, K. (2019). Estimation methods developing with remote sensing information for energy crop biomass: a comparative review. *Biomass Bioenergy* 122, 414–425. doi: 10.1016/j.biombioe.2019.02.002

Dandrifosse, S. (2022). Dynamics of wheat organs by close-range multimodal machine vision. Ph.D. thesis, ULiège. GxABT - Liège Université. *Gembloux Agro-Bio Tech Gembloux Belgium*.

Dandrifosse, S., Bouvry, A., Leemans, V., Dumont, B., and Mercatoris, B. (2020). Imaging wheat canopy through stereo vision: overcoming the challenges of the laboratory to field transition for morphological features extraction. *Front. Plant Sci.* 11. doi: 10.3389/fpls.2020.00096

Dandrifosse, S., Carlier, A., Dumont, B., and Mercatoris, B. (2021). Registration and fusion of closeRange multimodal wheat images in field conditions. *Remote Sens.* 13, 1380. doi: 10.3390/rs13071380

Dandrifosse, S., Carlier, A., Dumont, B., and Mercatoris, B. (2022). In-field wheat reflectance: how to reach the organ scale? *Sensors* 22, 3342. doi: 10.3390/s22093342

David, E., Serouart, M., Smith, D., Madec, S., Velumani, K., Liu, S., et al. (2021). Global Wheat Head Detection 2021: an improved dataset for benchmarking wheat head detection methods. *Plant Phenomics* 2021. doi: 10.34133/2021/9846158

Deery, D., Jimenez-Berni, J., Jones, H., Sirault, X., and Furbank, R. (2014). Proximal remote sensing buggies and potential applications for field-based phenotyping. *Agronomy* 4, 349–379. doi: 10.3390/agronomy4030349

Deng, J., Dong, W., Socher, R., Li, L.-J., Li, K., and Fei-Fei, L. (2009). "ImageNet: A large-scale hierarchical image database," in *2009 IEEE Conference on Computer Vision and Pattern Recognition*. IEEE. 248–255. doi: 10.1109/CVPR.2009.5206848

de Oliveira, G. S., Marcato Junior, J., Polidoro, C., Osco, L. P., Siqueira, H., Rodrigues, L., et al. (2021). Convolutional neural networks to estimate dry matter yield in a Guineagrass breeding program using UAV remote sensing. *Sensors* 21, 3971. doi: 10.3390/s21123971

Duchene, O., Dumont, B., Cattani, D. J., Fagnant, L., Schlautman, B., DeHaan, L. R., et al. (2021). Processbased analysis of Thinopyrum intermedium phenological development highlights the importance of dual induction for reproductive growth and agronomic performance. *Agric. For. Meteorol*, 301–302. doi: 10.1016/j.agrformet.2021.108341

Freitas Moreira, F., Rojas de Oliveira, H., Lopez, M. A., Abughali, B. J., Gomes, G., Cherkauer, K. A., et al. (2021). High-throughput phenotyping and random regression models reveal temporal genetic control of soybean biomass production. *Front. Plant Sci.* 12. doi: 10.3389/fpls.2021.715983

Gaju, O., Allard, V., Martre, P., Le Gouis, J., Moreau, D., Bogard, M., et al. (2014). Nitrogen partitioning and remobilization in relation to leaf senescence, grain yield and grain nitrogen concentration in wheat cultivars. *Field Crops Res.* 155, 213–223. doi: 10.1016/j.fcr.2013.09.003

Gao, Y., Li, Y., Jiang, R., Zhan, X., Lu, H., Guo, W., et al. (2023). Enhancing green fraction estimation in rice and wheat crops: A self-supervised deep learning semantic segmentation approach. *Plant Phenomics* 5, 64. doi: 10.34133/plantphenomics.0064

Hawkesford, M., and Riche, A. (2020). Impacts of G x E x M on nitrogen use efficiency in wheat and future prospects. *Front. Plant Sci.* 11. doi: 10.3389/fpls.2020.01157

He, K., Zhang, X., Ren, S., and Sun, J. (2015). *Deep Residual Learning for Image Recognition*. doi: 10.48550/arXiv.1512.03385

Hickey, L. T., Hafeez, A. N., Robinson, H., Jackson, S. A., Leal-Bertioli, S. C. M., et al. (2019). Breeding crops to feed 10 billion. *Nat. Biotechnol.* 37, 744–754. doi: 10.1038/s41587-019-0152-9

Jiang, Y., and Li, C. (2020). Convolutional neural networks for image-based high-throughput plant phenotyping: a review. *Plant Phenomics*, 1–22. doi: 10.34133/2020/4152816

Justes, E. (1994). Determination of a critical nitrogen dilution curve for winter wheat crops. *Ann. Bot.* 74, 397–407. doi: 10.1006/anbo.1994.1133

Kamilaris, A., and Prenafeta-Boldú, F. X. (2018). Deep learning in agriculture: A survey. *Comput. Electron. Agric.* 147, 70–90. doi: 10.1016/j.compag.2018.02.016

Kattenborn, T., Leitloff, J., Schiefer, F., and Hinz, S. (2021). Review on Convolutional Neural Networks (CNN) in vegetation remote sensing. *ISPRS J. Photogrammetry Remote Sens.* 173, 24–49. doi: 10.1016/j.isprsjprs.2020.12.010

Lee, D.-H. (2013). Pseudo-label : the simple and efficient semi-supervised learning method for deep neural networks. *ICML 2013 Workshop Challenges Representation Learn. (WREPL)*.

Lemaire, G., and Ciampitti, I. (2020). Crop mass and N status as prerequisite covariables for unraveling nitrogen use efficiency across genotype-by-environment-by-management scenarios: a review. *Plants* 9, 1309. doi: 10.3390/plants9101309

Li, Y., Liu, H., Ma, J., and Zhang, L. (2021). Estimation of leaf area index for winter wheat at early stages based on convolutional neural networks. *Comput. Electron. Agric.* 190, 106480. doi: 10.1016/j.compag.2021.106480

Ma, J., Li, Y., Chen, Y., Du, K., Zheng, F., Zhang, L., et al. (2019). Estimating above ground biomass of winter wheat at early growth stages using digital images and deep convolutional neural network. *Eur. J. Agron.* 103, 117–129. doi: 10.1016/j.eja.2018.12.004

Martre, P., Porter, J. R., Jamieson, P. D., and Tribo¨ı, E. (2003). Modeling grain nitrogen accumulation and protein composition to understand the sink/source regulations of nitrogen remobilization for wheat. *Plant Physiol.* 133, 1959–1967. doi: 10.1104/pp.103.030585

Nabwire, S., Suh, H.-K., Kim, M. S., Baek, I., and Cho, B.-K. (2021). Review: application of artificial intelligence in phenomics. *Sensors* 21, 4363. doi: 10.3390/s21134363

Nguyen, C., Sagan, V., Bhadra, S., and Moose, S. (2023). UAV multisensory data fusion and multi-task deep learning for high-throughput maize phenotyping. *Sensors* 23, 1827. doi: 10.3390/s23041827

Otsu, N. (1979). A threshold selection method from gray-level histograms. *IEEE Trans. Systems Man Cybernetics* 9, 62–66. doi: 10.1109/TSMC.1979.4310076

Pedregosa, F., Varoquaux, G., Gramfort, A., Michel, V., Thirion, B., Grisel, O., et al. (2011). Scikit-learn: machine learning in python. *J. Mach. Learn. Res.* 12, 2825–2830. doi: 10.48550/arXiv.1201.0490

Pound, M. P., Atkinson, J. A., Wells, D. M., Pridmore, T. P., and French, A. P. (2017). "Deep learning for multi-task plant phenotyping," in *2017 IEEE International Conference on Computer Vision Workshops (ICCVW)*, 2055–2063. doi: 10.1109/ICCVW.2017.241

Raj, R., Walker, J. P., Pingale, R., Nandan, R., Naik, B., and Jagarlapudi, A. (2021). Leaf area index estimation using top-of-canopy airborne RGB images. *Int. J. Appl. Earth Observation Geoinformation* 96, 102282. doi: 10.1016/j.jag.2020.102282

Reynolds, M., Chapman, S., Crespo-Herrera, L., Molero, G., Mondal, S., Pequeno, D. N., et al. (2020). Breeder friendly phenotyping. *Plant Sci.* 295, 110396. doi: 10.1016/j.plantsci.2019.110396

Roth, L., Barendregt, C., Bétrix, C.-A., Hund, A., and Walter, A. (2022). High-throughput field phenotyping of soybean: spotting an ideotype. *Remote Sens. Environ.* 269, 112797. doi: 10.1016/j.rse.2021

Roth, L., Camenzind, M., Aasen, H., Kronenberg, L., Barendregt, C., Camp, K.-H., et al. (2020). Repeated multiview imaging for estimating seedling tiller counts of wheat genotypes using drones. *Plant Phenomics* 2020. doi: 10.34133/2020/3729715

Sapkota, B., Popescu, S., Rajan, N., Leon, R., Reberg-Horton, C., Mirsky, S., et al. (2022). Use of synthetic images for training a deep learning model for weed detection and biomass estimation in cotton. *Sci. Rep.* 12. doi: 10.1038/s41598-022-23399-z

Schiefer, F., Schmidtlein, S., and Kattenborn, T. (2021). The retrieval of plant functional traits from canopy spectra through RTM-inversions and statistical models are both critically affected by plant phenology. *Ecol. Indic.* 121. doi: 10.1016/j.ecolind.2020.107062

Schreiber, L., Atkinson Amorim, J., Guimãraes, L., Motta Matos, D., Maciel da Costa, C., and Parraga, A. (2022). Above-ground biomass wheat estimation: deep learning with UAV-based RGB images. *Appl. Artif. Intell.* doi: 10.1080/08839514.2022.2055392

Selvaraju, R. R., Cogswell, M., Das, A., Vedantam, R., Parikh, D., and Batra, D. (2020). Grad-CAM: visual explanations from deep networks *via* gradient-based localization. *Int. J. Comput. Vision* 128, 336–359. doi: 10.1007/s11263-019-01228-7

Serouart, M., Madec, S., David, E., Velumani, K., Lopez Lozano, R., Weiss, M., et al. (2022). SegVeg: segmenting RGB images into green and senescent vegetation by combining deep and shallow methods. *Plant Phenomics* 2022. doi: 10.34133/2022/9803570

Singh, A. K., Ganapathysubramanian, B., Sarkar, S., and Singh, A. (2018). Deep learning for plant stress phenotyping: trends and future perspectives. *Trends Plant Sci.* 23, 883–898. doi: 10.1016/j.tplants.2018.07.004

Song, X., Yang, G., Xu, X., Zhang, D., Yang, C., and Feng, H. (2022). Winter wheat nitrogen estimation based on ground-level and UAV-mounted sensors. *Sensors* 22. doi: 10.3390/s22020549

Standley, T., Zamir, A. R., Chen, D., Guibas, L., Malik, J., and Savarese, S. (2020). Which tasks should be learned together in multi-task learning? doi: 10.48550/arXiv.1905.07553

Sun, D., Robbins, K., Morales, N., Shu, Q., and Cen, H. (2022). Advances in optical phenotyping of cereal crops. *Trends Plant Sci.* 27, 191–208. doi: 10.1016/j.tplants.2021.07.015

Tan, M., and Le, Q. V. (2020). EfficientNet: rethinking model scaling for convolutional neural networks. doi: 10.48550/arXiv.1905.11946

Tanner, F., Tonn, S., de Wit, J., Van den Ackerveken, G., Berger, B., and Plett, D. (2022). Sensorbased phenotyping of above-ground plant-pathogen interactions. *Plant Methods* 18, 35. doi: 10.1186/s13007-022-00853-7

Tilly, N., Aasen, H., and Bareth, G. (2015). Fusion of plant height and vegetation indices for the estimation of barley biomass. *Remote Sens.* 7, 11449–11480. doi: 10.3390/rs70911449

Vafaeikia, P., Namdar, K., and Khalvati, F. (2020). A brief review of deep multi-task learning and auxiliary task learning. doi: 10.48550/arXiv.2007.01126

Vandenhende, S., Georgoulis, S., Proesmans, M., Dai, D., and Gool, L. (2020). Revisiting multi-task learning in the deep learning era. *ArXiv*. doi: 10.1109/TPAMI.2021.3054719

van Eeuwijk, F. A., Bustos-Korts, D., Millet, E. J., Boer, M. P., Kruijer, W., Thompson, A., et al. (2019). Modelling strategies for assessing and increasing the effectiveness of new phenotyping techniques in plant breeding. *Plant Sci.* 282, 23–39. doi: 10.1016/j.plantsci.2018.06.018

Verrelst, J., Malenovsky, ´, Z., van der Tol, C., Camps-Valls, G., Gastellu-Etchegorry, J.-P., Lewis, P., et al. (2019). Quantifying vegetation biophysical variables from imaging spectroscopy data: a review on retrieval methods. *Surveys Geophysics* 40, 589–629. doi: 10.1007/s10712-018-9478-y

Wan, L., Zhang, J., Dong, X., Du, X., Zhu, J., Sun, D., et al. (2021). Unmanned aerial vehicle-based field phenotyping of crop biomass using growth traits retrieved from PROSAIL model. *Comput. Electron. Agric.* 187, 106304. doi: 10.1016/j.compag.2021.106304

Wang, Z., Lu, Y., Zhao, G., Sun, C., Zhang, F., and He, S. (2022b). Sugarcane biomass prediction with multi-mode remote sensing data using deep archetypal analysis and integrated learning. *Remote Sens.* 14, 4944. doi: 10.3390/rs14194944

Wang, W., Wu, Y., Zhang, Q., Zheng, H., Yao, X., Zhu, Y., et al. (2021). AAVI: A novel approach to estimating leaf nitrogen concentration in rice from unmanned aerial vehicle multispectral imagery at early and middle growth stages. *IEEE J. Selected Topics Appl. Earth Observations Remote Sens.* 14, 6716–6728. doi: 10.1109/JSTARS.2021.3086580

Wang, F., Yang, M., Ma, L., Zhang, T., Qin, W., Li, W., et al. (2022a). Estimation of above-ground biomass of winter wheat based on consumer-grade multi-spectral UAV. *Remote Sens.* 14, 1251. doi: 10.3390/rs14051251

Xu, R., and Li, C. (2022). A review of high-throughput field phenotyping systems: focusing on ground robots. *Plant Phenomics* 2022. doi: 10.34133/2022/9760269

Yang, K.-W., Chapman, S., Carpenter, N., Hammer, G., McLean, G., Zheng, B., et al. (2021). Integrating crop growth models with remote sensing for predicting biomass yield of sorghum. *silico Plants* 3, diab001. doi: 10.1093/insilicoplants/diab001

Yue, J., Yang, G., Tian, Q., Feng, H., Xu, K., and Zhou, C. (2019). Estimate of winter-wheat above-ground biomass based on UAV ultrahigh-ground-resolution image textures and vegetation indices. *ISPRS J. Photogrammetry Remote Sens.* 150, 226–244. doi: 10.1016/j.isprsjprs.2019.02.022

Zbontar, J., Jing, L., Misra, I., LeCun, Y., and Deny, S. (2021). Barlow twins: self-supervised learning *via* redundancy reduction. doi: 10.48550/arXiv.2103.03230

Zhang, J., Tian, H., Wang, P., Tansey, K., Zhang, S., and Li, H. (2022). Improving wheat yield estimates using data augmentation models and remotely sensed biophysical indices within deep neural networks in the Guanzhong Plain, PR China. *Comput. Electron. Agric.* 192, 106616. doi: 10.1016/j.compag.2021.106616

Zheng, C., Abd-Elrahman, A., Whitaker, V. M., and Dalid, C. (2022). Deep learning for strawberry canopy delineation and biomass prediction from high-resolution images. *Plant Phenomics* 2022. doi: 10.34133/2022/9850486

frontiers | Frontiers in Plant Science

TYPE Original Research
PUBLISHED 08 January 2024
DOI 10.3389/fpls.2023.1304751

OPEN ACCESS

EDITED BY
Elias Kaiser,
Wageningen University and Research,
Netherlands

REVIEWED BY
Lea Hallik,
University of Tartu, Estonia
Dimitrios Fanourakis,
Technological Educational Institute of Crete,
Greece

*CORRESPONDENCE
Oliver Knopf
o.knopf@fz-juelich.de

RECEIVED 29 September 2023
ACCEPTED 05 December 2023
PUBLISHED 08 January 2024

CITATION
Knopf O, Castro A, Bendig J, Pude R, Kleist E, Poorter H, Rascher U and Muller O (2024) Field phenotyping of ten wheat cultivars under elevated CO_2 shows seasonal differences in chlorophyll fluorescence, plant height and vegetation indices.
Front. Plant Sci. 14:1304751.
doi: 10.3389/fpls.2023.1304751

Field phenotyping of ten wheat cultivars under elevated CO_2 shows seasonal differences in chlorophyll fluorescence, plant height and vegetation indices

Oliver Knopf [1*], Antony Castro [1], Juliane Bendig [1], Ralf Pude [2], Einhard Kleist [1], Hendrik Poorter [1,3], Uwe Rascher [1] and Onno Muller [1]

[1]Institute of Bio- and Geosciences: Plant Sciences (IBG-2), Forschungszentrum Jülich GmbH, Jülich, Germany, [2]INRES-Renewable Resources, University of Bonn, Rheinbach, Germany, [3]Department of Natural Sciences, Macquarie University, North Ryde, NSW, Australia

In the context of climate change and global sustainable development goals, future wheat cultivation has to master various challenges at a time, including the rising atmospheric carbon dioxide concentration ([CO_2]). To investigate growth and photosynthesis dynamics under the effects of ambient (~434 ppm) and elevated [CO_2] (~622 ppm), a Free-Air CO_2 Enrichment (FACE) facility was combined with an automated phenotyping platform and an array of sensors. Ten modern winter wheat cultivars (*Triticum aestivum* L.) were monitored over a vegetation period using a Light-induced Fluorescence Transient (LIFT) sensor, ground-based RGB cameras and a UAV equipped with an RGB and multispectral camera. The LIFT sensor enabled a fast quantification of the photosynthetic performance by measuring the operating efficiency of Photosystem II (F_q'/F_m') and the kinetics of electron transport, i.e. the reoxidation rates F_{r1}' and F_{r2}'. Our results suggest that elevated [CO_2] significantly increased F_q'/F_m' and plant height during the vegetative growth phase. As the plants transitioned to the senescence phase, a pronounced decline in F_q'/F_m' was observed under elevated [CO_2]. This was also reflected in the reoxidation rates F_{r1}' and F_{r2}'. A large majority of the cultivars showed a decrease in the harvest index, suggesting a different resource allocation and indicating a potential plateau in yield progression under e[CO_2]. Our results indicate that the rise in atmospheric [CO_2] has significant effects on the cultivation of winter wheat with strong manifestation during early and late growth.

KEYWORDS

CO_2, wheat, fluorescence, phenotyping, climate change, senescence, chlorophyll, FACE (Free-Air CO_2 Enrichment)

1 Introduction

Since the industrial age, the atmospheric CO_2 concentration ([CO_2]) has increased by 50%, from 280 ppm at the end of the 19th century to 418 ppm in 2022 (Keeling et al., 1976; IPCC, 2021a; NOAA ESRL, 2023). Current climate scenarios predict a further increase to an expected level of 550 ppm CO_2 by 2060 (IPCC, 2021b), resulting in significant global climatic changes, including rising air temperatures and changing precipitation patterns (IPCC, 2021a). The complex and variable responses of crops to elevated CO_2 concentrations complicate crop management and breeding strategies, making it increasingly difficult to meet the food demands of a growing population (FAO, 2011; OECD and FAO, 2012).

Understanding genotype, environment, and management (GxExM) interactions and developing resource-efficient, climate-resilient crops are among the top priorities for plant scientists and breeders (Beres et al., 2020; Cooper et al., 2021). Plant breeding has evolved over the years by incorporating new tools and technologies, but the main objectives remain unchanged - improving crop productivity by selecting heritable traits (Reynolds and Braun, 2022). Given the dynamic nature of the effects resulting from increased atmospheric CO_2, crops will need to adapt to an increasingly different growing environment within a few breeding cycles. Wheat plays a crucial role as the third most important staple crop, providing one-fifth of the global caloric intake. It also is a major source of income for many small-scale farmers, and therefore also a significant contributor to global economic development (FAO, 2021).

Since CO_2 is a key molecule in the plants' carbon assimilation process, increased atmospheric CO_2 levels may also lead to notable increases in photosynthesis (Long et al., 2004). Improving the effectiveness at which crops capture and convert H_2O, CO_2 and light energy into substance, i.e. photosynthetic efficiency, is regarded as a key pathway to achieving our sustainable development goals and is expected to play a significant role in the Fourth Green Revolution (Long et al., 2015). The fundamental prerequisite is a better understanding of the light-use efficiency of crops under dynamic light conditions and their interactions with the environment. Studying the highly dynamic photosynthesis process under such conditions presents a challenge to overcome. To address this knowledge gap, a number of elaborate growth chamber experiments, open-top chambers and free-air CO_2 enrichment (FACE) emerged after the publication of the Brundtland report in 1987 (United Nations, 1987). FACE experiments mimic future atmospheric CO_2 conditions under actual field conditions. Among the most important findings of these experiments is the capability of elevated CO_2 concentrations (e[CO_2]) to boost photosynthetic assimilation rates and increase the productivity of C_3 and C_4 plants (Ainsworth and Long, 2004; Ainsworth and Long, 2021; Gardi et al., 2022). Despite these advances, it remains unclear whether we can fully capture and describe the physiologically relevant dynamic features of field photosynthesis in sufficient detail. Therefore, Murchie et al. (2018) emphasise the need for extensive field data collection at different time points over the growing season.

In response to the growing need for a more holistic quantitative assessment of plants, the last decade has seen a surge in advanced phenotyping platforms, as highlighted by Cendrero-Mateo et al. (2017). These incorporate automated imaging, robotics, and machine learning to analyse plant growth, physiology, and morphology on a large scale. Recent sensor advancements in remote sensing and field phenotyping have shifted the focus from individual plants to canopy and field-level observations. These non-invasive methods enable quicker, more accurate measurements of plant traits, greatly benefiting breeding and genetic studies.

RGB imagery and Chlorophyll Fluorescence (ChlF) acquisition methods have shown great promise in studying the impact of abiotic and biotic stress on various plant species and crops (Rebetzke et al., 2019; Fu et al., 2022; Pieruschka and Schurr, 2022). ChlF is a measurable optical signal resulting from the competing light energy pathways in plants where light is either (a) utilised in photosynthesis (photochemistry), (b) transferred to other pigments, (c) dissipated in the form of heat (NPQ) or (d) re-emit as a byproduct with a longer wavelength in the form of fluorescence. ChlF can be quantified using active instruments containing an excitation light source and a fluorometer (Maxwell and Johnson, 2000; Baker and Rosenqvist, 2004; Baker, 2008). Pulse-amplitude modulation (PAM) fluorometry is commonly used for active ChlF measurements, but its limitations, such as short-distance applicability, hinder large-scale open field studies with high throughput. To address these challenges, the Light-induced fluorescence transient device (LIFT) has emerged as a promising alternative to actively quantify ChlF traits, including the PSII operating light-use efficiency of light-adapted plants (F_q'/F_m') (Osmond et al., 2017; Keller, 2018). Previous work has suggested that LIFT can be useful for uncovering genetic variation in response to environmental stress (Zendonadi dos Santos et al., 2021).

Several studies investigated the effect of e[CO_2] on photosynthetic assimilation (Lauriks et al., 2021) and efficiency (Javaid et al., 2022) at different stages of development in diverse

Abbreviations: ChlF, Chlorophyll fluorescence; DEM, Digital elevation model (ppm); DOY, Day of the year, sequential day number starting with day 1 on January 1st(ppm); a[CO_2], Ambient carbon dioxide concentration; e[CO_2], Elevated carbon dioxide concentration; EVI, Enhanced Vegetation Index; ExG, Excess Green Index; FACE, Free-air CO_2 enrichment; F_m', Maximal chlorophyll fluorescence yield from light-adapted plants; F_{r1}', Reoxidation efficiency of Q_A^- up to ~0.65 ms after F_m' is reached, i.e., the kinetics of electron transfer from Q_A to PQ pool from light-adapted plants; F_{r2}', Reoxidation efficiency of Q_A^- up to ~6.64 ms after F_{r1}', i.e., the kinetics of electron transfer from PQ pool to PSI from light-adapted plants; FRR, Fast repetition rate; F_q'/F_m', Photosystem II operating efficiency of light-adapted plants; GNSS, Global navigation satellite systems; GxExM, Genotype x environment x management interaction; LIFT, Light-induced fluorescence transient; NDVI, Normalised difference vegetation index; OSAVI, Optimised Soil-Adjusted Vegetation Index; PAM, Pulse-amplitude modulation; PAR, Photosynthetically active radiation(µmol·s^{-1}); PSI/PSII, Photosystem I/Photosystem II; ppm, Parts per million; Q_A, Primary Quinone electron acceptor in photosystem II; RE, Relative error; RGB, RGB colour space; ROI, Region of interest; R_{QA}, Rexoiddation sequence of Q_A; S_{QA}, Saturation sequence of Q_A; SP1, Senescence period 1, i.e. DOY 168 – DOY 176; SP2, Senescence period 2, i.e. DOY 176 – DOY 193; UAV, Unmanned aerial vehicle; VI, Vegetation index.

plant species yielding various outcomes – a large number of them were devoted to understanding long term effects of tree species and grasslands. A growth chamber experiment with *Acacia logifolia* showed increased photosynthetic assimilation per unit leaf area under e[CO_2], mainly at the beginning of the growing period. As the growing period progressed, relative differences in assimilation under a[CO_2] and e[CO_2] got smaller and finally dropped significantly (p = .001) towards the end of the experiment (Javaid et al., 2022). Potential alterations of the photosynthetic efficiency under e[CO_2] could be substantially relevant to global agricultural production. Most previous studies on the effect of CO_2 enrichment on senescence reported either no changes or a delay in plant senescence (Curtis et al., 1989; Taylor et al., 2008). On the other hand, there are also studies which reported a slightly earlier flowering and senescence under e[CO_2], often associated with the underlying concept that e[CO_2] boosted photosynthesis; this ramped up sugar accumulation, depleting chloroplast nitrogen reserves faster and thus directly affecting the C/N balance resulting in oxidative stress (Agüera and De la Haba, 2018; Zani et al., 2020). A greenhouse experiment from Marc and Gifford (1984) investigated the floral initiation of wheat under e[CO_2] and did not show an apparent effect on the crop. Bresson et al. (2018) suggest that senescence is not only driven by environmental factors but also genotypic properties, as well as the development of the plant. In turn, each of these factors can affect the onset, intensity and rate of progression of senescence. These previously observed species-dependent responses urge the need to study photosynthesis and the seasonal dynamics of crops under elevated CO_2 closer.

This study introduces a pioneering approach by combining a LIFT instrument to monitor photosynthesis with an automated field phenotyping platform. This unique combination enables investigating winter wheat growth under elevated [CO_2] in a typical agricultural field environment.

Our study aimed to employ novel techniques to gather a comprehensive dataset, enhancing our understanding of how e[CO_2] influences the photosynthetic dynamics and growth patterns of winter wheat across its various developmental stages. In particular, we wanted to (1) provide a comprehensive description of the combination of a FACE system with an automated field phenotyping platform, emphasising its capabilities and contributions to the research, (2) assess the final biomass and various yield parameters across cultivars, (3) investigate seasonal growth dynamics by the help of UAV data, and (4) evaluate the seasonal variation in ChlF-related traits and the influence of abiotic factors, in response to ambient and elevated [CO_2].

2 Materials and methods

2.1 Plant material and crop management

Ten modern winter wheat (*Triticum aestivum* L.) cultivars, released between 2014 and 2020 (Appendix Table A1), were evaluated within the 'BigBaking project'. These cultivars, provided by nine European breeders, are commonly used in Germany. The selection targeted high-yielding cultivars with genotypic diversity from different quality groups to validate recent breeding efforts and to assess their resilience to climate change. Additionally, these cultivars served for subsequent baking quality and proteomics analysis to explore the relationship between yield and grain quality under e[CO_2]. The cultivars were grown in plots sized 2 x 3 m with a sowing density of 330 kernels per m^{-2} and a row distance of 0.11 m. Winter wheat was sown on October 22nd 2020, with three replicate plots per treatment and in a complete randomised plot design. Plants emerged on November 2nd 2020 and were harvested on August 12th 2021. A total of 160 kg N per ha^{-1} liquid nitrogen fertilisers were applied in three doses of 60/60/40 kg per ha^{-1} on March 24th, April 20th and June 7th 2021. The field was managed following standard agricultural practices for the region and was monitored regularly to prevent damage from pests and pathogens. Significant crop management events were summarised together with phenological stages in Table 1.

2.2 Study site, experimental design, and phenotyping platform

The study was conducted at Campus Klein-Altendorf, the experimental field site of the University Bonn, near Rheinbach, Germany (50°37' 29.3196" N 6°59'12.9834 "E, elevation: 177 m). Over the past 64 years, the mean annual temperature has been 9.6° C, and the mean annual precipitation was 603 mm $year^{-1}$. Situated in the Lower Rhine Bay, the region is influenced by the Atlantic climate with prevailing westerly winds. The soil is classified as a Haplic Luvisol developed from loess with high clay content and high soil fertility (Pätzold and Pude, n.d).

To elevate the atmospheric CO_2 concentration (e[CO_2]), a Free-Air Carbon Dioxide Enrichment (FACE) experiment was set up. This so-called BreedFACE facility is a mobile system and, therefore, allows for a three-year crop rotation system with winter barley (*Hordeum vulgare*) as a pre- and follow-crop (Muller et al., 2018; Quiros-Vargas et al., 2021; Soares et al., 2021). Eight ~7.25 m long steel pipes were joined together to form an octagonal structure of 18.5 m diameter (~254 m^2). This sub-construction could be adjusted to the canopy height and was used to attach smaller poly-vinyl-chlorid pipes with tiny holes every 20 cm where pure CO_2 was released. The amount of released CO_2 was adjusted in real-time depending on the wind direction, wind speed and the actual CO_2 concentration. Those factors were measured at a centrally positioned environment station together with the photosynthetic active radiation (model LI-190R, Li-COR Inc., Lincoln, NE, USA, licor.com/env/products/light/quantum), air temperature and air humidity. The target [CO_2] was set to 600 ppm and measured using different CO_2 sensors (HMP110, GMP343 and GMT221, Vaisala Oyj, Vantaa, Finland, vaisala.com). Over the growing season, the sensors were adjusted so they were always slightly above the canopy, i.e. a minimum of 0.2 m higher (Figure 1).

CO_2 feeding started with plant emergence in November 2020, was paused for two weeks for safety reasons over New Year and was elevated with a few minor interruptions as long as we could perform measurements with detectable photosynthesis activity. This was the case until July 12th, 2021. As day length increased throughout the

TABLE 1 Important cultivation measures and relevant phenological stages.

Event Management	Phenological stage	Date	Day of Year
Sowing		22-Oct-20	296
	Emergence	02-Nov-20*	307
Herbicide treatment (Malibu)		04-Nov-20	309
Start of CO_2 enrichment		13-Nov-20	318
	Leaf development	16-Nov-20*	321
1st fertiliser application (AHL 30% N)		24-Mar-21	83
Growth regulator (CCC, Moddus)		25-Mar-21	84
	Canopy closure	30-Mar-21*	89
	Stem elongation	15-Apr-21*	105
2nd fertiliser application (AHL 30% N)		20-Apr-21	110
Fungicide and growth regulator (Input, Moddus)		23-Apr-21	113
3rd fertiliser application (AHL 30% N)		07-May-21	127
Fungicide treatment (Ascra Xpro)		21-May-21	141
	Heading	31-May-21*	151
Fungicide and insecticide (Protendo, Solzil, Karate)		08-Jun-21	159
	Anthesis	14-Jun-21*	165
	Ripening	28-Jun-21*	179
End of CO_2 enrichment		12-Jul-21	193
Harvest	Grain maturity	12-Aug-21	224

*indicates the time point where a majority of the cultivars reached that stage.

season, the CO_2 feeding period was adapted, ranging from 9 hours per day during the early vegetation period up to 13 hours per day later in the year.

The BreedFACE facility is complemented by the FieldSnake (see Figures 1B, C), a semi-automated mobile phenotyping platform (prototype developed by Lommers Tuinbouwmachines, Bergeijk, The Netherlands and the Forschungszentrum Jülich, Jülich, NRW, Germany). Integral part of the FieldSnake is a movable measurement platform that is attached to a bridge, adjustable in height (1.5 – 3.5 m) and capable of carrying various phenotyping sensors up to a payload of 100 kg. The 20-meter-wide bridge is supported by compartments on each side (i.e. engine and steering) running on caterpillars.

Under human surveillance, the FieldSnake is capable of navigating autonomously over the experimental field at a speed of about 2-3 km/h with the help of three Global Navigation Satellite System (GNSS) antennas, two of them positioned at the outer edges of the machine and one directly on the measurement platform. The GNSS signal is supplemented by the German SAPOS reference service (https://sapos.de/) to optimise the accuracy of the navigation to centimetres. The data acquisition pattern was set beforehand in an iOS-based mobile application (HariPilot, Hari Tech KFT, Pötréte, Hungary, https://hari-tech.hu/) and could be checked and adapted on an iPad among other settings, e.g. the traverse speed of the measurement platform (0.05 – 0.18 m/s), measurement height, acquisition mode (scanning or stationary). Positioning data were logged every second, together with other relevant parameters and transmitted to a server.

2.3 LIFT and PhenoCam data acquisition

A Light-Induced Fluorescence Transient device (model LIFT-REM 1.0, Soliense Inc., Shoreham, NY, USA; https://soliense.com/LIFT_Terrestrial.php) was employed to monitor variations in ChlF. The active probing method first described by Kolber et al. (1998) induces chlorophyll fluorescence by emitting a series of sub-saturating excitation light impulses at a fast repetition rate (FRR). Multiple lenses focus the light of a blue (λ 450 nm) light-emitting diode (LED) to a 40 mm light beam at a distance of 0.6 m. By the FRR method, the capacity of Electron Transport to Photosystem II (PSII) is exceeded, causing reaction centres to close. Thereby, resulting changes in the plants' fluorescence signal can be measured within microseconds by an avalanche photodiode in combination with an

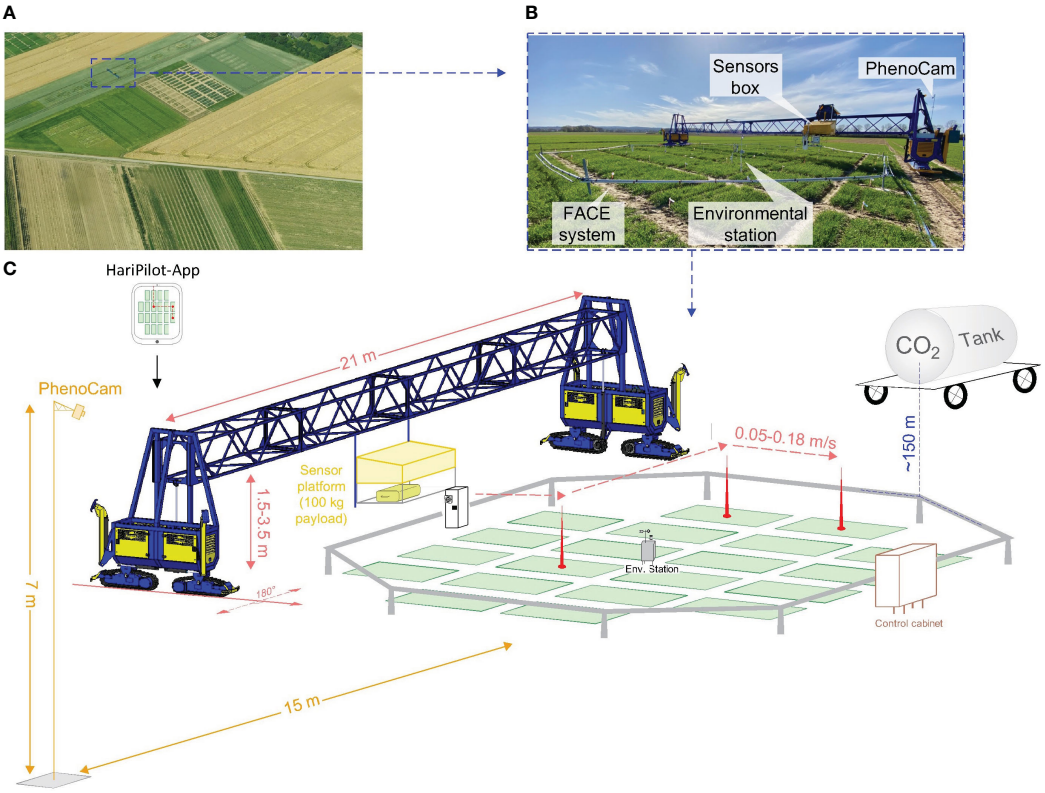

FIGURE 1
The Free-Air CO_2 Enrichment (BreedFACE) experiment and the automated multipurpose phenotyping platform. **(A)** Aerial view of the BreedFACE field at Campus Klein-Altendorf, Rheinbach, Germany. **(B)** Ground-level photograph of the automated 'FieldSnake' phenotyping platform (shown in blue) alongside the FACE system. **(C)** A detailed illustration of the setup, highlighting the structural components such as the octagonal ring structure surrounding the winter wheat plots, the control cabinet, the CO_2 supply tank, the environmental station, and PhenoCam alongside with the 'FieldSnake'.

optical interference filter (685 nm ± 10 nm) that separates the red ChlF from the rest of the light. The device was programmed to progressively saturate the plastoquinone A pool (S_{QA} sequence) within 300 ms. Following the maximum ChlF (F_m'), a 127 ms long relaxation sequence (R_{QA}) with exponentially increasing breaks between the flashlets allows Q_A to reoxidate (Osmond et al., 2017). This saturation-relaxation-measurement protocol ultimately results in a transient of which kinetics can be calculated (Appendix Figure A1). The PSII operating efficiency for light-adapted plants (F_q'/F_m') has been found to exhibit a high correlation with F_v'/F_m' measurements obtained using pulse amplitude modulation (PAM) techniques (Wyber et al., 2017). F_{r1}' and F_{r2}' are parameters used to characterise the electron transport kinetics of light-adapted plants during the R_{QA} sequence, as described by Zendonadi dos Santos et al. (2021). These parameters are obtained through log-log-transformed regression analysis of the slope of the transient, and they correspond to two specific time intervals of the measurement protocol, i.e. t_1 0.82-1.44 ms and t_2 1.56-8.08 ms. Within these intervals, electron transfer occurs from Q_A to the PQ pool and, to some extent, from the PQ pool to PSI.

To closely follow the senescence period, a permanent setup of two identical RGB cameras (model SD500BN, StarDot Technologies, Buena Park, CA, USA) was set up at a fixed distance from the ring (15 m) to ensure continuous measurements of phenological changes (PhenoCams). They were mounted on a tower of 7 m in height and acquired daily images from June 13th till the harvest on August 12th, 2021 (Figure 1).

2.4 Field measurements

2.4.1 LIFT measurements

During the vegetation period, nine LIFT measurements were conducted bi-weekly under clear-sky conditions (see Appendix: Table A2), starting with canopy closure from late March (DOY 89) to mid-July (DOY 193). Therefore, the 15 kg heavy LIFT instrument capable of measuring ChlF up to a distance of 3 m was mounted to the FieldSnake platform, levelled by a gimbal pointing downward (Nadir) at a fixed measurement distance of ~0.6 m above the canopy. The platform's height was adjusted to match the average canopy height of the plants grown at a[CO_2] and e[CO_2]. Scanning at approximately 10 cm s^{-1} along crop rows, over 1'200 point measurements were acquired across the BreedFACE field, with around 20 measurements per plot.

2.4.2 Manual height measurements

Canopy height was assessed manually six times throughout the vegetation period by measuring the vertical distance from the tip of

the plant closest to the ruler to the soil level. These measurements were performed using a folding ruler at three random locations across the plots.

2.4.3 UAV data acquistion

A total of twelve flight campaigns covered key growth stages of the crop from November 2020 to July 2021 (Figure 3). Flights were mostly conducted under clear-sky conditions around midday (see Appendix: Table A2). To obtain RGB and multispectral data, a Sony ILCE-7RM3 respectively a MicaSense dual camera system (AgEagle Sensor Systems Inc., Wichita, KS, USA) were mounted to an Unmanned Aerial Vehicle (UAV, DJI Matrice Pro 600, SZ DJI Technology Co., Ltd., Shenzhen, China) as described in Chakhvashvili et al. (2022). Geotagging was performed using onboard equipment. Flights were conducted at a 20 m altitude, resulting in 0.001-0.002 m pixel size.

2.4.4 Harvest and post-processing

The above-ground biomass was determined at the harvest on August 12th 2022. A special combine harvester (model Quantum Plus, Wintersteiger AG, Ried, Austria) allowed for a core harvest of 1.5 x 2 m and separated grains from the shoot. The straw was immediately collected and weighed. Straw sub-samples were taken, weighed, and dried for 72 h in a drying oven at 70°C before being weighed again to calculate the vegetative dry matter. Grain samples underwent additional cleaning, and their weight, along with the thousand-grain weight, was measured before conducting subsequent analysis.

2.5 Data processing and statistics

2.5.1 LIFT and FieldSnake data processing

Data were mainly processed using R (Version 2022.02.2 + 485, R Core Team, 2013). After processing the acquired LIFT raw data, the data was linked to spatial data logged by the FieldSnake using timestamps from both systems. The combination of data allowed to correct for the sensor mounting offset, enabling further spatial data cleaning in QGIS (Version 3.24.2), e.g. excluding measurements in border areas (30 cm).

2.5.2 UAV data processing

Digital elevation models (DEMs) were generated from RGB imagery and orthomosaics from multispectral imagery using AgiSoft Metashape (Version 2.0.1). Nine panels with varying reflectance factors were used for processing multispectral images to top of canopy reflectance (Chakhvashvili et al., 2022). We chose to analyse the Normalised Difference Vegetation Index (NDVI), a commonly used index for assessing vegetation health and cover. The Enhanced Vegetation Index (EVI), which offers refinements of the NDVI such as atmospheric correction and improved performance in densely vegetated areas, as well as the Optimised Soil-Adjusted Vegetation Index (OSAVI), which is used to minimise the impact of soil background (Table 2).

Plant height was extracted by subtracting DEMs from a respective growth stage from a DEM of bare soil (Bendig et al., 2014). Plot-level information was extracted using the zonal statistics function exact_extract (Baston, 2022). Data were further analysed and visualised in R.

2.5.3 PhenoCam data processing

Within each image retrieved from the PhenoCam, a region of interest (ROI) with multiple points of interest was set for the cores of all plots. Values retrieved from the images were then normalised (Richardson et al., 2018) in order to calculate the excess green index (ExG, Table 2), which was used to describe plant senescence on a canopy level. The data was then fitted with a log-regression model for the time intervals between the LIFT measurements during the senescence period, i.e. senescence period 1 being DOY 168 – DOY 176 and senescence period 2 from DOY 176 to DOY 193 where the dependent PSII operating efficiency was log-transformed.

3 Results

3.1 Abiotic environmental parameters

At the experimental site, the mean temperature during the growing period (October 2020 - August 2021) was 10.1°C and thus half a degree warmer than the observed long-term average. While November 2020 was a rather cold month (-2.2°C), the months of February and June were relatively warm, with monthly mean temperatures deviating by +2.4°C and +3.2°C, respectively, compared to the long-term average. The annual precipitation reached 707 mm, representing a 17.3% increase compared to the recorded long-term average. This increase was mainly driven by heavy rainfall events in January and July 2021, during which more than twice the average amount of rainfall was recorded. With an annual sum of 1054 kWh m^{-2}, the global radiation was slightly lower compared to the long-term measured global radiation of 1093.0 kWh m^{-2} per year.

Regarding the CO_2 concentrations, the mean ambient CO_2 concentration during operating hours was 434 ± 24 ppm in control plots and elevated by 43% to a mean concentration of 622 ± 57 ppm CO_2 in the FACE system. During operating hours, the CO_2 target concentration of 550 ppm and higher was reached 93% of the time at the ring's centre (see Appendix: Figure A2).

3.2 Yield parameters

Given that intermediate destructive harvests were not feasible due to the limited number of replicates, plant height served as a proxy for seasonal biomass accumulation in this study. Following the start of the flight campaign in November 2020, a significant (p<.001) difference in plant height for winter wheat grown under e[CO_2] was observed in January 2021 (DOY 14), with a mean difference of 1.43 cm ± .09 cm (Figure 2). This significant increase in plant height gradually continued throughout the entire vegetation period and peaked on June 11th, 2021 (DOY 162), with a mean difference of 19.11 cm ± 5.82 cm. However, on August 4th, 2021 (DOY 216), just before the harvest, a decline in canopy height was observed for plants grown under e[CO_2].

To validate the UAV data, manual measurements were taken on six days from May 22nd, 2021 (DOY 142), to July 23rd, 2021 (DOY 204). These measurements confirmed the trend observed from the UAV data and showed a high correlation (ρ = .89, R^2 = .79) with similar statistically significant differences. However, the difference in height between winter wheat cultivars treated with e[CO_2] and the control was smaller. The maximum mean difference was measured on June 16th, 2021 (DOY 167), with plants under e[CO_2] being 8.49 ± 3.08 cm taller, and a smaller decrease in mean height difference after that date to 7.07 ± 2.38 cm was recorded on July 23rd, 2021 (DOY 204). A more detailed look at the data revealed that while there were cultivar-specific variations in the extent of height increase, the overall trend — an increase in height in response to elevated CO_2 levels — was consistently observed across all ten cultivars.

The relative difference in biomass was determined by the absolute weight at the end of the vegetation period, where significant CO_2 effects were observed with notable increases in plants grown under e[CO_2] compared to those grown under a [CO_2]. Winter wheat cultivars grown under e[CO_2] exhibited a significant (p<.001) increase in vegetative biomass, i.e. straw only (VDM, see Table 3). The mean vegetative biomass for plants grown under a[CO_2] was 776.03 ± 59.16 g per m^2, while plants grown under e[CO_2] showed a 21.73% boost in vegetative biomass accumulation, reaching 936.86 ± 88.46 g per m^2 (excluding two samples from Moschus due to a combine harvester processing failure). In terms of vegetative biomass, the cultivar Apostel displayed the strongest CO_2 effect size of.28, with a 32.9% increase. In contrast to that, KWS Emerick experienced the smallest biomass increase of 16.3% under e[CO_2].

For grain yield (GDM), generally, smaller effect sizes were observed, but a significant treatment effect (p<.001) was documented. Harvesting the core area of the plots resulted in an average grain yield of 1017.23 ± 66.9 g per m^2 for cultivars grown under a[CO_2] and a mean yield increase of 7.6%, equivalent to 1094.59 ± 102.65 g per m^2, for cultivars grown under e[CO_2]. Although grain yield was generally positively affected by e[CO_2], the response varied significantly among cultivars. Campesino exhibited a significant increase (p<.001) of 20.8% under e[CO_2], while many other cultivars demonstrated weaker and non-significant responses.

Hyvega was the only cultivar that experienced a 2.5% decrease in grain yield under e[CO_2]. Differences were also observed in Total Dry Matter (see TDM, Table 3), with an average increase of 13.10% in cultivar biomass under e[CO_2]. Four cultivars showed a significant (p<.001) increase in biomass, with the highest increase of 19.95% observed in the cultivar Campesino.

The Harvest Index (HI, see Table 3) generally decreased, except for the cultivar Campesino, where the ratio between grain yield and vegetative mass remained consistent and was equally boosted under e[CO_2]. The most significant shift in biomass accumulation was observed in Hyvega, where the HI decreased significantly (p<.05) by 9.79% under e[CO_2].

The thousand-grain weight (TGW, see Table 3) decreased by 5.06%, with significant changes observed in six cultivars. Only KWS Emerick maintained its grain weight but, in turn, showed a slight decrease in the number of grains per m^2. The number of grains increased in all other cultivars, with an average increase of 12.87% for cultivars grown under e[CO_2]. Campesino displayed the most significant increase, with a 29.47% difference (see TGW, Table 3).

3.3 Phenology

The vegetation indices (VIs) obtained from the UAV-MicaSense setup revealed a comparable trend across all three indices throughout the observation period (Figure 2). Before the canopy closure on March 30th 2021, both the Enhanced Vegetation Index (EVI) and the Optimised Soil-Adjusted Vegetation Index (OSAVI) exhibited similarly low values, indicating a sparse and young vegetation cover. In contrast, the Normalised Difference Vegetation Index (NDVI) displayed increased values during the

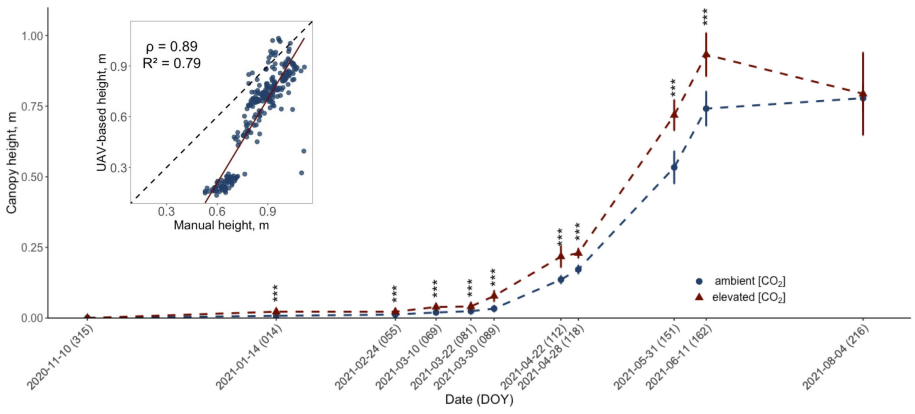

FIGURE 2
Development of the UAV-retrieved canopy height (m) for ten modern winter wheat cultivars (*Triticum aestivum* L.) grown under ambient (~434 ppm) and elevated (~622 ppm) [CO_2] throughout the 2020/2021 vegetation period. The data for each treatment group is pooled across cultivars. Plants were cultivated in the BreedFACE experimental field at Campus Klein-Altendorf, Rheinbach, Germany. Error bars indicate the standard deviation of the mean height. Statistical significance was assessed using Welch's Two Sample t-test, p< 0.001 *** (n = 30). The insert in the figure shows the correlation between manual and UAV-based measurements, with the correlation coefficient (ρ) and coefficient of determination (R^2).

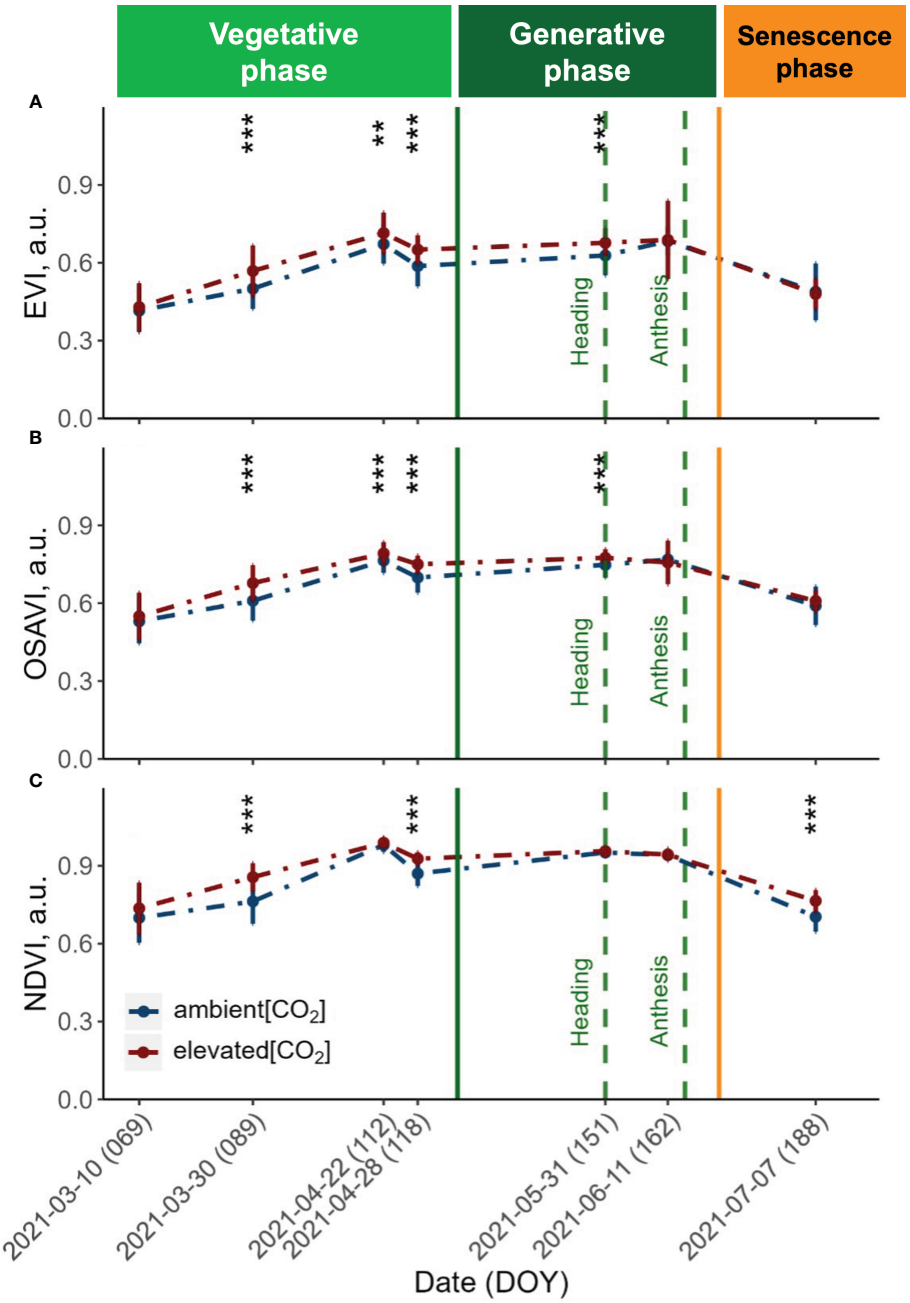

FIGURE 3
Seasonal dynamics of the **(A)** Enhanced Vegetation Index (EVI), **(B)** Optimised Soil-Adjusted Vegetation Index (OSAVI) and **(C)** Normalised Difference Vegetation Index (NDVI) derived from UAV with a Mica-Sense camera. Pooled data of ten modern winter wheat cultivars (*Triticum aestivum* L.) grown under ambient (~434 ppm) and elevated (~622 ppm) [CO_2] measured throughout the vegetation period 2020/2021. Plants were grown in the BreedFACE experimental field at Campus Klein-Altendorf, Rheinbach, Germany. Error bars indicate the standard deviation from the mean. ** p<.01 *** p<001.

first flight campaign and continued to show consistently higher values over the entire vegetation period.

At canopy closure (DOY 89), all three VIs were significantly increased under e[CO_2] (p<.001). This rise is indicative of an increase in vegetation biomass and greenness, reflecting the maturation and densification of the plant canopy. The values continued to rise until reaching their peak on April 22nd 2021, reflecting optimal vegetation health and productivity. Following this peak, a drop in all three VIs was observed, but values remained significantly higher (p<.001) for plants grown under e[CO_2] until shortly after heading. At this stage, the NDVI did not exhibit any significant differences (p = 0.05) for plants grown under e[CO_2]. Towards the end of the vegetation period, the three VIs displayed distinct patterns. While the EVI exhibited a trend of slightly decreased values under e[CO_2], the NDVI showed the opposite effect, with values increasing under e[CO_2].

TABLE 2 Visible (VI_{RGB}) and near-infrared vegetation indices (VI_{NIR}) used in this study.

VI	Name	Formula	Reference
ExG	Excess Green Index	$ExG = 2\star\frac{Green}{Red+Green+Blue} - \frac{Blue}{Red+Green+Blue} - \frac{Red}{Red+Green+Blue}$	(Sonnentag et al., 2012)
EVI	Enhanced Vegetation Index	$EVI = 2.5\star\frac{NIR - Red}{NIR + 6\ x\ Red - 7.5\ x\ Blue + 1}$	(Huete et al., 2002)
OSAVI	Optimised Soil-Adjusted Vegetation Index	$OSAVI = \frac{NIR - Red}{NIR + Red + 0.16}$	(Rondeaux et al., 1996)
NDVI	Normalised Difference Vegetation Index	$NDVI = \frac{NIR - Red}{NIR + Red}$	(Peñuelas et al., 1994)

TABLE 3 Relative change of various yield parameters.

Cultivar	VDM	GDM	TDM	HI	TGW	GN
Apostel	32.9 %***	6.2 %	17.3 %*	-9.7 %*	-7.8 %**	15.9 %*
Asory	26.3 %**	11.0 %	17.3 %**	-5.4 %	-7.7 %**	20.2 %**
Campesino	18.8 %*	20.8 %***	20.0 %**	0.8 %	-6.5 %*	29.5 %***
Foxx	17.9 %*	5.7 %	11.1 %	-4.9 %	-6.5 %*	12.7 %*
Hyvega	23.4 %**	-2.5 %	8.1 %	-9.8 %*	-8.1 %**	6.2 %
Informer	18.4 %*	6.7 %	11.7 %	-4.5 %	-2.9 %	9.9 %
KWS Emerick	16.3 %*	0.2 %	7.1 %	-6.3 %	0.7 %	-0.4 %
LG Initial	19.2 %*	6.0 %	11.6 %	-4.8 %	-7.4 %*	14.5 %*
Moschus	21.7 %*	4.4 %	11.2 %	-7.4 %**	-3.2 %	7.9 %
RGT Reform	22.3 %**	10.6 %*	15.6 %**	-4.4 %	-1.3 %	12.3 %*
Mean	21.7 %	6.9 %	13.1 %	-5.6 %	-5.1 %	12.9 %
Observations	60	62	60	60	62	62
Cultivar	0.138	**0.002**	**0.017**	0.171	**<0.001**	**<0.001**
e[CO_2]	**<0.001**	**<0.001**	**<0.001**	**0.027**	**<0.001**	**<0.001**
Cult. x e[CO2]	0.97	0.252	0.201	**0.045**	0.208	0.063

Relative change of Vegetative Dry Matter (VDM), Grain Dry Matter (GDM), Total Dry Matter (TDM), Harvest Index (HI), Thousand-Grain Weight (TGW) and Number of Grains (GN) of plants grown under elevated CO_2 and compared to ambient CO_2. A two-way ANOVA was conducted to examine the effects of cultivars and elevated CO_2 on yield components with Bonferroni-adjusted p-values shown below. Stars indicate statistically significant differences in the main effects analysed by pairwise comparisons, * p <.05 ** p<.01 *** p<.001.
Bold values are significant at p < .05.

Figure 4 presents a temporal high-resolution view of the plant senescence progression obtained by PhenoCams. Data retrieved from the PhenoCams indicate that the Excess Green index (ExG) was generally higher under e[CO_2]. Whereas senescence duration is prolonged in cultivars like Apostel and Foxx, the onset is delayed in other cultivars such as Hyvega or RGT Reform and then progresses faster. In most cultivars, the e[CO_2] treatment led to a further delay of senescence, which is also compensated in several cultivars by a faster progression rate and, in some cultivars, resulted in an even stronger degradation of chlorophyll according to the ExG index. According to PhenoCam data, plants grown under a[CO_2] exhibited a higher senescence rate, i.e. the slope of the curve was steeper under a[CO_2] in the second senescence period (Figure 5A).

The correlation between the LIFT-retrieved PSII operating efficiency and the PhenoCam-retrieved senescence rate was investigated at two independent time points during the senescence (DOY 168 and DOY 176). The findings show a significant negative relationship between the senescence rate and F_q'/F_m' at both time intervals. Plants grown under e[CO_2] exhibited a correlation coefficient of -0.91, while plants grown under a[CO_2] had a correlation coefficient of -0.85. These results suggest that an increase in senescence rate leads to a decrease in F_q'/F_m' or vice versa (Figure 5B).

3.4 Chlorophyll fluorescence traits

Canopy closure in late March (DOY 89) marked the time point where it was possible to conduct consistent and reliable LIFT measurements. At this early vegetative growth stage, we observed consistently high PSII operating efficiencies (F_q'/F_m') across cultivars (Figure 6A). All cultivars grown under e[CO_2] had higher F_q'/F_m' values compared to plants grown under a[CO_2]. At this time, the

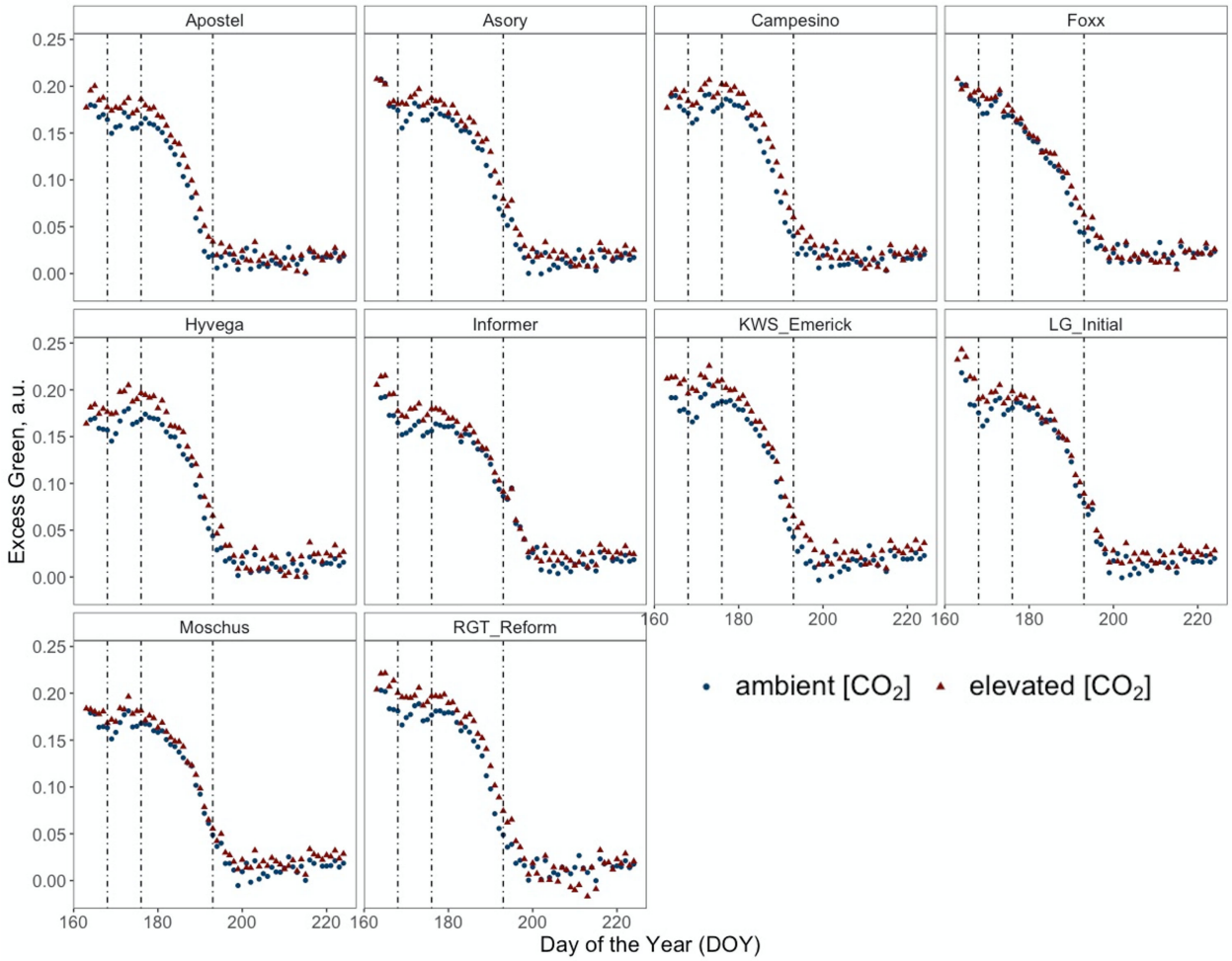

FIGURE 4
Normalised Excess Green index (ExG) retrieved from RGB images of PhenoCams monitoring the experiment during the senescence period from DOY 167 to DOY 225 of ten modern winter wheat cultivars (*Triticum aestivum* L.) grown under ambient (~434 ppm) and elevated (~622 ppm) [CO_2] measured throughout the vegetation period 2020/2021. Plants were grown in the BreedFACE experimental field at Campus Klein-Altendorf, Rheinbach, Germany. Each dot represents the mean value of three plots (n = 3), and vertical lines indicate LIFT measurement dates and different senescence periods.

retrieved values showed the highest absolute and relative differences between elevated and a[CO_2]. Measured F_q'/F_m' was more than 20% higher under e[CO_2] in cultivars such as Informer (M = 21.05%, RE = 1.60), Foxx (M = 20.34%, RE = 1.68) and Campesino (M = 20.16%, RE = 1.36). In order to investigate the effect of the three different growth periods, i.e. vegetative period (DOY< 125), generative period (DOY 125 - 160) and senescence period (DOY > 160) on the response variable (Fq'/F_m'), a two-way ANOVA was conducted. The results showed no significant main effect of the CO_2 treatment ($F(1, 538) = .49$, $p = .484$), but a highly significant main effect of the three different growth periods ($F(2, 538) = 364.89$, $p<.001$) and a highly significant interaction effect between CO_2 and the growing period ($F(2, 538) = 29.32$, $p<.001$). The simple main effects were analysed to further investigate the nature of this interaction. The analysis of the main effects on F_q'/F_m' revealed a significant treatment effect ($F(1, 184) = 53.91$, $p<.001$) for the vegetative growth period. While mean values for the vegetative period were higher under e[CO_2] (.531 ± .077) compared to a[CO_2] (.484 ± .079), this changed during the generative period. There, winter wheat plants tended to have a higher mean F_q'/F_m' under ambient conditions (M = .491 ± .081 vs M = .505 ± .079). During the generative growth period, the analysis indicated no significant treatment effect ($F(1, 183) = .42$, p = .517). During the senescence period, mean values have dropped significantly to M = .394 ± .0969 for wheat cultivars grown under e[CO_2] compared to M = 0.415 ± .0805 at a[CO_2]. The simple main effects analysis of F_q'/F_m' did reveal a trend towards lower values under e[CO_2] with a marginally significant treatment effect ($F(1, 171) = 3.71$, $p = .056$) due to larger variance during this final growth stage. On DOY 176, Campesino grown under e[CO_2] had a by 30.66% lower mean F_q'/F_m' (RE = 2.19) than plants grown at ambient conditions. Overall, the results suggest that the CO_2 treatment affected the operating efficiency of PSII predominantly during vegetative growth with reduced effect during later growth stages.

F_{r1}' and F_{r2}' show a comparable trend (Figures 6B, C) that consistently opposes the behaviour observed in F_q'/F_m', resulting in a moderate to strong negative correlation (r -.58, respectively r =

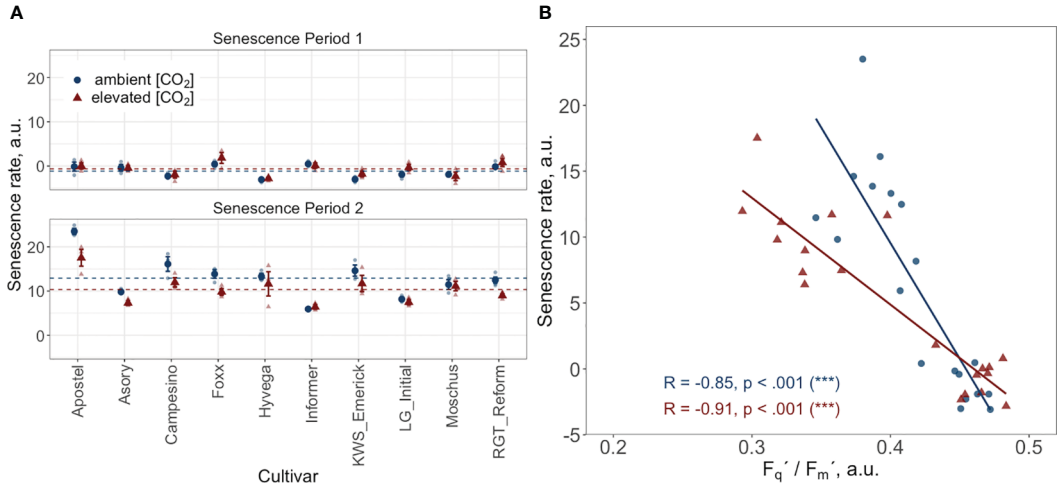

FIGURE 5
(A) Senescence rate during two periods: period 1 spans from the start of the grain filling phase, DOY 168 to DOY 176, and period 2 covers DOY 176 to DOY 193. Data points represent the mean senescence rate for each cultivar, with error bars indicating the standard error. Dashed horizontal lines indicate the overall mean senescence rate across all cultivars for the treatment and control groups during their respective periods. **(B)** Correlation between the PhenoCam-retrieved senescence rate and the LIFT-retrieved PSII operating efficiency (F_q'/F_m') at two time points (DOY 168 and DOY 176) during the senescence phase. Data points represent the mean value per cultivar. Both datasets come from ten modern Winter wheat cultivars (*Triticum aestivum* L.) grown under ambient (~434 ppm) and elevated (~622 ppm) [CO_2] in the BreedFACE experimental field at Campus Klein-Altendorf, Rheinbach, Germany, during the 2020/2021 vegetation period.

-.97). Specifically, at the beginning of the vegetation period, both F_{r1}' and F_{r2}' demonstrate higher values under a[CO_2] conditions compared to e[CO_2], with the difference between the two being more pronounced in the case of F_{r2}'. As the seasons advanced, both F_{r1}' and F_{r2}' showed a declining trend. But while F_{r2}' values increased again before heading, F_{r1}' was decoupled, and values did not rise again before anthesis. Also for F_{r1}' and F_{r2}', a significant growth period effect ($F(2,538) = 79.65$, $p < 0.001$; $F(2,538) = 364.89$, $p < .001$) and interaction effect was documented ($F(2,538) = 12.15$, $p < .001$; $F(2,538) = 29.32$, $p < .001$). The analysis of the simple main effects resulted in no significant treatment effect for F_{r1}' but in significant treatment effects for F_{r2}' during the vegetative growth period ($F(1,184) = 56.70$, $p < .001$) and during senescence ($F(1,171) = 14.00$, $p < .001$). The development of F_{r2}' included a more pronounced difference between treatments at the beginning of the season, a decline in mid-season, and an increase after heading, particularly under a[CO_2].

4 Discussion

4.1 Abiotic environmental parameters

According to the German Meteorological Service (DWD), 2021 was an ambivalent year, generally following the long-term trends with slightly increased temperatures (Imbery et al., 2021). During the experiment, the vegetative growth period featured more favourable environmental conditions compared to the grain-filling phase, which faced a drought and heat period. The climatic conditions observed in 2021, characterised by increased temperatures, periods of drought, and episodes of heavy rainfall, align with future climate prediction models, increasing the relevance of our e[CO_2] dataset for future projection scenarios.

The here described FACE setup has shown to be an effective experimental setup to increase the CO_2 concentration in a winter wheat field. The system also managed to increase the [CO_2] during cold and windy winter conditions. Outside the FACE operating hours, especially in the early morning hours, we recorded a substantial accumulation of the CO_2 concentration in all sensors placed in the elevated and ambient CO_2 ring. On windless summer nights, these values often exceeded thresholds of 1000 ppm. This effect could also be observed in various eddy-covariance stations (TERENO, https://ddp.tereno.net). The accumulation of CO_2 can be explained by plant respiration mechanisms, which tend to increase with biomass accumulation over the season, peaking shortly before ear emergence and are generally higher during wind-still, warm nights with reduced air circulation (Ney and Graf, 2018; Pearman and Garratt, 2022). Additionally, soil respiration mechanisms of microorganisms releasing CO_2 back into the atmosphere during the night contribute to the effect and may also lead to slightly increased values under e[CO_2] (Lipson et al., 2005). Since the effect was observed in either treatment and mainly during the night when photosystems were idle, we presume that this effect had a neglectable influence on crop development in this study.

FACE experiments are constrained by their capacity for homogenous CO_2 distribution, limiting the experimental area and leading to CO_2 fluctuations. Although fluctuations in [CO_2] are also present in natural environments, they are substantially greater in a FACE system. Allen et al. (2020) noted that these fluctuations can cause a reduced photosynthetic activity which can lead to an underestimation in yield, suggesting a yield data correction factor of 1.5. Furthermore, the authors argue that until the effects of fluctuating vs. constant elevated CO_2 are better understood, modelling plant growth and yield will remain uncertain. The

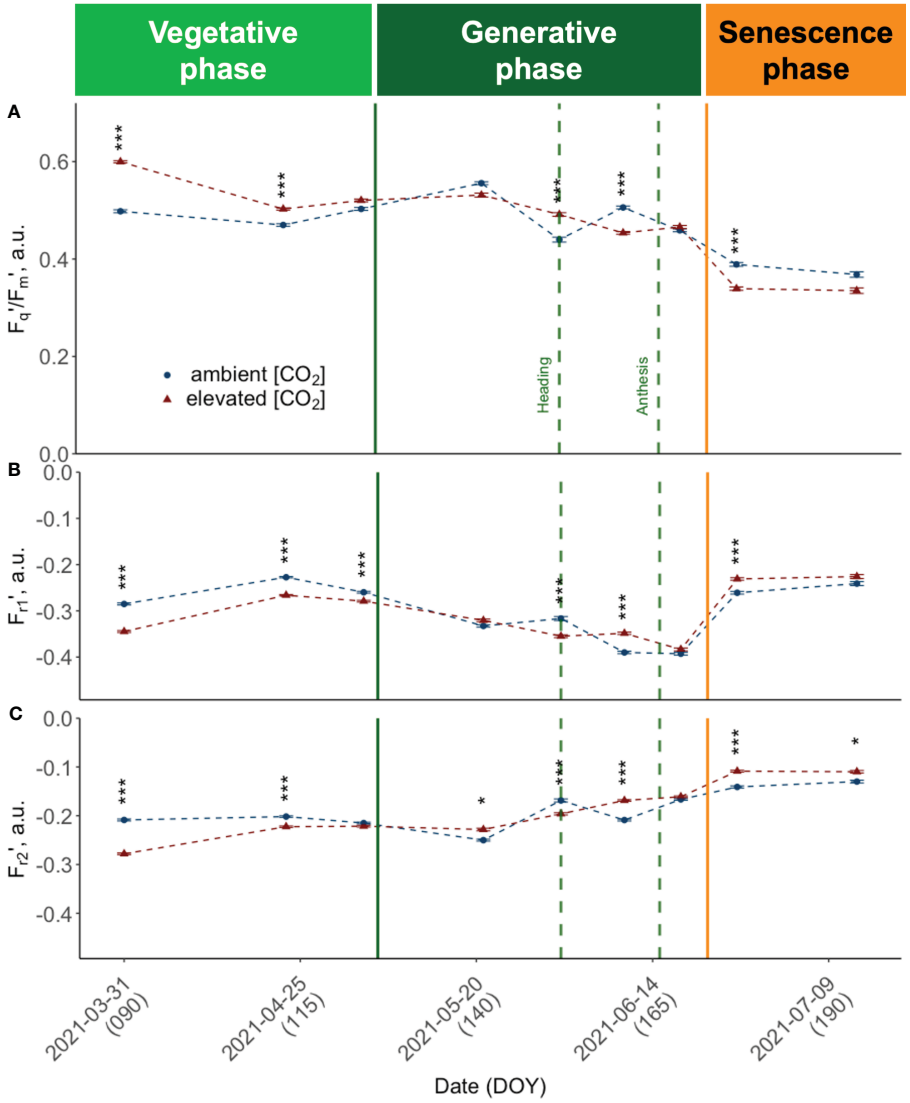

FIGURE 6
Seasonal dynamics of chlorophyll fluorescence traits, pooled data of ten modern light-adapted winter wheat (*Triticum aestivum* L.) cultivars grown under ambient (~434 ppm) and elevated (~622 ppm) [CO_2]. **(A)** PSII operating efficiency (F_q'/F_m') and **(B)** F_{r1}' representing the kinetics of electron transfer from QA to PQ pool, up to ~0.65 ms after F_m' is reached, i.e., F_{r1}' the kinetics of electron transfer from Q_A to PQ pool from light-adapted plants and **(C)** F_{r2}' the kinetics of electron transfer from PQ pool to PSI up to 6.64 ms after initiation of the measurement protocol. The data was collected using a LIFT-REM device in 2021 at the BreedFACE experimental field at Campus Klein-Altendorf, Rheinbach, Germany. Cultivar independent comparison, error bars indicate the SE, Bonferroni adjusted t-test, ns = not significant, *** p< 0.001 (n = 30, total number of measurements = 8'901). * p <.05.

extent of these fluctuations can be largely managed through the design and technology of the FACE system. To ensure best possible results, the here presented FACE ring structure was limited to 18.5 m in diameter. The ability to achieve homogenous CO_2 fumigation is further dependent on factors such as wind speed, direction and air temperature, which were carefully considered and accounted for in the design and execution of the experiment.

Despite the technical and financial challenges of CO_2 fumigation, the target concentration was generally maintained at a high level. Although the scalability of FACE experiments is limited by these challenges, they offer the most accurate simulation of natural conditions and are therefore indispensable for understanding plant and ecosystem responses to future climatic conditions.

4.2 Yield parameters

Since 2021 has been a year with rather challenging weather conditions, and where extreme precipitation events led to increased lodging and harvest losses, our grain yields were compared to a multi-regional state cultivar trial. Despite the weather conditions, cultivars grown in the present study are in range with the state trial and obtained grain yields for plants grown at a[CO_2] were marginally higher (+2.8%) (NRW Chamber of Agriculture, 2021).

The observed substantial increase in straw biomass under e [CO_2] aligns with the prevailing favourable environmental conditions during the vegetative growth phase. This increase, coupled with the observed rise in photosynthetic efficiency, could

contribute to more sustainable and multifunctional agricultural practice, where increased straw biomass not only contributes to carbon sequestration, e.g. carbon farming, but potentially also offers valuable ecosystem services or serves as a valuable industrial raw material. While the increase in photosynthetic efficiency correlates with biomass accumulation, it may not fully capture the complexity of the processes contributing to biomass accumulation. However, the synergy between the increased photosynthetic efficiency and the boosted growth in the early vegetative stage may be linked to clarify the potential shift in resource allocation as indicated by the Harvest Index (HI). Interestingly, Campesino was the only cultivar that maintained its grain-to-shoot biomass ratio. This cultivar belongs to the quality group B and is characterised by its low crude protein content. Moschus, an Elite-cultivar characterised by high crude protein content, had the highest decrease in the HI. Similar decreases in the HI have previously been reported in a meta-analysis on barley grown under elevated [CO_2] (Gardi et al., 2022). The observed shift in the resource allocation for the large majority of the cultivars, favouring vegetative growth over investments into reproductive organs, is potentially based on the down-regulation of RuBisCo activity and electron transport under e[CO_2] (Ainsworth et al., 2004). LIFT measurements performed during the grain filling phase showed an apparent down-regulation of the PSII operating efficiency in Moschus. In contrast, Campesino could maintain higher F_q'/F_m' during our last measurements under e[CO_2]. Whether the higher CO_2 concentration and the related change in the resource allocation of crops also led to an impairment of the crop quality needs further investigation.

Although a handful of FACE studies investigated the yield response of spring wheat, only very few studies explicitly focused on winter wheat. Dier et al. (2018) conducted a two-year FACE study with a single cultivar and observed an 18% increase in vegetative biomass and 17% in grain yield. In another experiment dealing with two winter wheat cultivars, conducted by Bunce (2012), no significant grain yield increase was detectable. The results obtained in our study indicated an above-average increase in vegetative dry matter for most of the cultivars. However, the mean grain yield was lower than in previous studies, except for the cultivars Asory and Campesino. The substantial relative increase in grain yield under e[CO_2] observed for these two cultivars could potentially be attributed to genetic factors such as the integration of a rye translocation genome T1AL.1RS/T1RS.A1, which has previously been described to cope well with dry conditions during the grain filling stage (Dr. B. Hackauf, personal communication). The below-average grain yield increase could be attributed to the anthropogenic-caused rise in temperature, which is suggested to offset growth enhancements driven by e[CO_2] as described in a recent meta-analysis (Helman and Bonfil, 2022). Disparities in reported biomass accumulation of other FACE studies can also be attributed to our selection of cultivars characterised by a very high yield, presumably reaching their maximum yield potential. The phenomenon known as yield plateauing may account for the non-environmentally caused limited increase under e[CO_2]. Also, past studies often include fewer cultivars, typically with older release years. The diversity of these findings highlights the importance of studying cultivar-specific responses to e[CO_2] and stresses the importance of genetic diversity in developing climate-resilient crops.

Both manual and UAV-based data demonstrated increased height for plants grown under e[CO_2]. Intriguingly, this growth stimulation occurred early in the season and was maintained throughout the entire growth period, exhibiting only marginal variations. This trend indicates that the examined cultivars are especially prone to e[CO_2] during early growth and that the investments made during that time were decisive for later development. Towards the end of the vegetation period, however, a decline of plant height was observed for plants grown under e[CO_2], which may be linked to the observed phenomenon of earlier senescence, which was also noticeable in the EVI and in ChlF traits (see section 4.3 and 4.4). While a strong correlation was observed between manual plant height measurements and UAV-retrieved data, we also observed an increasing discrepancy between the two methods. The offset between the two methods can primarily be attributed to differences in the measurement technique. While manual measurements allowed for a simple determination of a plant's tip, identifying the relatively small tips, i.e. ears, from a nadir perspective in UAV imagery with a resolution of several centimetres is challenging. The increasing disparities can also be attributed to observed alterations during the senescence phase. While ears maintained their height, leaves were shrinking and changing their angle, i.e., more downwards, leading to a potential decline in canopy height. Furthermore, during the processing of the UAV data, a 95% confidence interval was set to exclude extremes, e.g. overreaching plants. Similar observations were previously reported by Bareth et al. (2016). Although UAV-retrieved measurements seem to result in a slightly lower accuracy, they allow for large area assessments and thus are by far more time efficient.

4.3 Phenology

The potential to boost the vegetative growth by e[CO_2] was also demonstrated by the significantly higher VI values (p<.001) observed under e[CO_2] after canopy closure. As the vegetation period advanced, the EVI and OSAVI clearly responded to the disparities between a[CO_2] and e[CO_2] and were maintained up to anthesis. After that, we observed a noticeable decrease in VIs and photosynthetic performance measured by ChlF traits. This decline in photosynthetic activity is a result of the transition from the generative phase to the senescence phase, which is marked by a progressive browning of the vegetation. During the senescence period, the response was different for the different VIs. While EVI values for plants grown under e[CO_2] slightly dropped below the values of plants grown under a[CO_2], the NDVI values were maintained, suggesting that e[CO_2] either extended the vegetation's productive phase or mitigated the effects of senescence. On the other hand, the NDVI already showed rising values during the first flight campaign, suggesting that the increasing CO_2 levels continued to have a consistent and prolonged influence on the plant height and biomass accumulation throughout the observation period and followed a similar trend as the ExG throughout the senescence period. The persistent increases in vegetation indices relative to ambient CO_2 conditions indicate that the NDVI was generally less

sensitive to increases in biomass, which has previously been documented (Baret and Guyot, 1991; Mutanga and Skidmore, 2004).

Often described as the final stage of a plant's life cycle, senescence is an essential upcycling process where resources such as RuBisCo are reallocated within the plant to maximise reproductive success (Pyung et al., 2007). The visible degreening process or degradation of pigments results from oxidative stress, caused by an imbalance of the C/N ratio and is accompanied by reduced enzymatic activity, resulting in an increased H_2O_2 production (Agüera and De la Haba, 2018). To monitor senescence dynamics at the canopy level, temporally high-resolved data was recorded with PhenoCams. The ExG index, derived from the PhenoCam data, notably revealed a less pronounced senescence rate under e[CO_2]. However, the declining ExG values may not solely be attributed to wilting leaves and chlorophyll degradation but also to an architectural change in the plants. This phenomenon is also evident in the UAV data (DOY 216), showing differences in canopy height between a[CO_2] and e[CO_2]. Even though one of the earliest visible signs of senescence is the breakdown of chlorophyll, leaf yellowing is not a good indicator of the early stages since it occurs when the process has proceeded for some time (Diaz et al., 2005). Bertheloot et al. (2008) described that senescence in winter wheat progresses from the bottom to the top of the canopy, influenced by the quantity of available protein in the vegetative organs. The instruments used in our study, PhenoCams and LIFT, captured this phenomenon differently due to their viewing angles. Specifically, PhenoCams, which capture the canopy from a side view, primarily focus on the upper leaves. In contrast, LIFT takes a nadir (top-down) view, giving it a more comprehensive look into the deeper layers of the canopy. This is crucial for understanding the differential effects of e[CO_2] on the plant. Under e[CO_2], the lower leaves, presumably richer in protein, show an earlier decrease in F_q'/F_m'. This suggests that resources are being reallocated to the upper leaves, allowing them to maintain higher photosynthetic activity for a longer period. Therefore, the combination of both systems under e[CO_2] reflect not just current photosynthetic efficiency but also the plant's adaptive resource allocation strategy in response to e[CO_2].

4.4 Chlorophyll fluorescence traits

Regardless of the treatment, the obtained F_q'/F_m' parameter generally followed the expected trend of a high photosynthetic efficiency during the beginning of the vegetation period, followed by a decline over the vegetation period. This decline can be attributed to the natural ageing process of the plants, which consequently also leads to a continuous reduction of carbon fixation per unit leaf area throughout the growing season. Further examination of the data showed that all ChlF traits followed a consistent trend across varieties until the grain-filling stage. After DOY 170, however, the responses became strongly cultivar-specific.

The results of this study indicate that ChlF traits of plants grown under e[CO_2] differed from those grown under ambient conditions. While under e[CO_2], F_q'/F_m' was significantly increased during the vegetative period, it showed a more substantial decline towards the end of the vegetation period. Conversely, there was no discernible trend during the mid-season.

In this context, understanding the relationship between photosynthesis and sink capacity is critical. Existing research suggests that a plant's ability to utilise excess assimilates produced under e[CO_2] is likely driven by its sink capacity. Variations in the observed ChlF traits across different growth stages could reflect differences in sink strengths. Early in the growing season, resources are allocated primarily towards the developing stem and leaf tissues. The observed rapid growth under e[CO_2] likely stimulated the production of NADPH and ATP, which are essential for efficient electron transport, thereby promoting photosynthetic efficiency. The gap between F_q'/F_m' under ambient and e[CO_2] then narrows, possibly due to increased sink-driven respiration or potential acclimation effects (Lauriks et al., 2021).

However, as the plants approach heading and anthesis, the focus of resource allocation shifts from leaves to reproductive structures, such as developing inflorescence and grains, which serve as strong sinks. Although the timing of anthesis across different cultivars was relatively consistent and not significantly altered by e[CO_2], the accelerated growth and increased carbohydrate production during the vegetative phase might indirectly lead to a more pronounced decline in F_q'/F_m' under e[CO_2] conditions. The increased F_{r1}' and F_{r2}' values during the senescence phase suggest a slowing down of reoxidation rates under e[CO_2], possibly due to a shift in resource allocation. Fewer electrons from PSII could be available for downstream processes like the Calvin cycle, leading to this deceleration in reoxidation rates. The strong correlation between F_{r1}' and F_{r2}' with F_q'/F_m' indicates that e[CO_2] likely influences the efficiency of the Calvin cycle, contributing to the observed changes in photosynthetic efficiency.

Correlation analysis of the ChlF traits and environmental factors revealed distinct correlations during different growth stages. During the vegetative growth phase, there is a positive correlation between temperature and F_q'/F_m' (r = .50), while the reoxidation efficiencies F_{r1}' and F_{r2}' exhibit a negative correlation (r = -.70 respectively r = -.44). The observed pattern in the vegetative phase could indicate that winter wheat optimises F_q'/F_m' under e[CO_2], particularly at higher temperatures during the initial growth stages. A meta-analysis by Poorter et al. (2021) highlighted that the internal water-use efficiency of C_3 plants tends to be significantly higher under e[CO_2]. This could explain why winter wheat grown under e[CO_2] maintained a relatively higher F_q'/F_m', particularly during dry days.

When transitioning into the generative growth phase, a strong positive correlation exists between F_{r2}' and both temperature (r = .64) and PAR (r = .80), indicating increased electron transfer kinetics from the PQ pool to PSI. This may suggest an enhancement of reproductive growth processes. In the senescence growth phase, F_q'/F_m' is again positively correlated with temperature (r = .71) and PAR (r = .50), implying an augmented light-associated plant efficiency during the transition to senescence. In contrast, F_{r1}' and F_{r2}' exhibit a negative correlation with these factors during this phase (r_{Temp} = -.87 and r_{PAR} = -.60, respectively r_{Temp} = -.60 and r_{PAR} = -.40). These observations underline the intricate and dynamic interactions between photosynthetic efficiency, electron transfer kinetics, and environmental variables across the growth stages.

5 Conclusions

We demonstrated that a future increase in the atmospheric CO_2 concentration, to an expected level of the second half of this century, significantly impacts the growth dynamics and development of modern winter wheat cultivars. Early vegetation stages particularly benefit from enhanced growth under e[CO_2], a crucial phase where plants establish the foundation for subsequent development. However, e[CO_2] also appears to alter the senescence process. This dual impact results in a changed resource allocation strategy, as evidenced by changes in yield parameters like the harvest index.

The observed variations in photosynthetic efficiency, quantified as F_q'/F_m', reflect a complex interplay of environmental conditions, developmental stages, and potentially genetic factors. This suggests that plants' ability to exploit additional resources under e[CO_2] may be constrained by varying sink capacities throughout the growth cycle. Such insights could guide targeted management interventions, such as the application of growth regulators or breeding programs aimed at optimising genetic composition for resilience under changing climatic conditions. Importantly, these findings were made possible by integrating an automated phenotyping platform in a FACE system in combination with an array of sensors. Platforms like this offer invaluable data for the assessment of climate-resilient crop cultivars. Moreover, continuous photosynthetic measurements could serve as a monitoring tool for assessing the impact of environmental stressors. This knowledge could then be applied to fine-tune crop management practices, enhancing yield while minimising the input, thereby contributing to broader efforts to make farming systems more sustainable.

Data availability statement

The original contributions presented in the study are included in the article/Supplementary Material, further inquiries can be directed to the corresponding author.

Author contributions

OK: Conceptualization, Data curation, Formal analysis, Investigation, Methodology, Project administration, Software, Visualization, Writing – original draft, Writing – review & editing. AC: Data curation, Formal analysis, Investigation, Writing – review & editing. JB: Data curation, Formal analysis, Investigation, Methodology, Software, Writing – review & editing. RP: Project administration, Resources, Writing – review & editing. EK: Conceptualization, Data curation, Formal analysis, Investigation, Methodology, Resources, Validation, Writing – review & editing. HP: Conceptualization, Methodology, Supervision, Validation, Writing – review & editing. UR: Conceptualization, Funding acquisition, Methodology, Project administration, Resources, Supervision, Writing – review & editing. OM: Conceptualization, Funding acquisition, Methodology, Project administration, Resources, Supervision, Validation, Writing – review & editing.

Funding

The author(s) declare financial support was received for the research, authorship, and/or publication of this article. This work has been supported by funds of the German Federal Ministry of Food and Agriculture (BMEL project number 2818404A18) based on a decision of the Parliament of the Federal Republic of Germany via the Federal Office for Agriculture and Food (BLE) under the innovation support programme. Additionally, this work has been funded by the Deutsche Forschungsgemeinschaft (DFG, German Research Foundation) under Germany's Excellence Strategy – EXC 2070 – 390732324. Open access to this article is funded by the Deutsche Forschungsgemeinschaft (DFG, German Research Foundation) – 491111487.

Acknowledgments

The authors express their gratitude for the invaluable support and technical assistance provided by Dr. Juan Quiros, Kevin Warstat, Angelina Steier, Michael Quarten, Nils Müller, David Lenzen, Sandra Markwitz, Lars Zinken, Ilgaz Askin, Dr. Nícolas Zendonadi dos Santos, Patrick Hostnik, and Dr. Zbigniew S. Kolber, as well as the supporting personnel from IBG-2. We would also like to extend our thanks to the partners of the 'BigBaking' project: LfL Bavarian State Research Center for Agriculture, Karlsruher Institute for Technology, Saatzucht Josef Breun GmbH & Co. KG, SECOBRA Saatzucht GmbH, Strube Research GmbH & Co. KG, Saatzucht Bauer GmbH & Co KG, Saatzucht Streng-Engelen GmbH & Co. KG, and the GFPi for the coordination. Special thanks are due to Dr. Manuel Geyer, Dr. Lorenz Hartel, Dr. Katharina Scherf, and Christine Kämper for their invaluable contributions.

Conflict of interest

Authors OK, AC, JB, EK, HP, UR, and OM were employed by Forschungszentrum Jülich GmbH.

The remaining author declares that the research was conducted in the absence of any commercial or financial relationships that could be construed as a potential conflict of interest.

Publisher's note

Supplementary material

The Supplementary Material for this article can be found online at: https://www.frontiersin.org/articles/10.3389/fpls.2023.1304751/full#supplementary-material

References

Agüera, E., and De la Haba, P. (2018). Leaf senescence in response to elevated atmospheric CO2 concentration and low nitrogen supply. *Biol. Plantarum* 62 (3), 401–408. doi: 10.1007/s10535-018-0798-z

Ainsworth, E. A., and Long, S. P. (2004). What have we learned from 15 years of free-air CO2 enrichment (FACE)? A meta-analytic review of the responses of photosynthesis, canopy properties and plant production to rising CO2. *New Phytol.* 165 (2), 351–372. doi: 10.1111/j.1469-8137.2004.01224.x

Ainsworth, E. A., and Long, S. P. (2021). 30 years of free-air carbon dioxide enrichment (FACE): What have we learned about future crop productivity and its potential for adaptation? *Global Change Biol.* 27 (1), 27–49. doi: 10.1111/gcb.15375

Ainsworth, E. A., Rogers, A., Nelson, R., and Long, S. P. (2004). Testing the "source-sink" hypothesis of down-regulation of photosynthesis in elevated [CO2] in the field with single gene substitutions in Glycine max. *Agric. For. Meteorology* 122 (1–2), 85–94. doi: 10.1016/j.agrformet.2003.09.002

Allen, L. H., Kimball, B. A., Bunce, J. A., Yoshimoto, M., Harazono, Y., Baker, J. T., et al. (2020). Fluctuations of CO2 in Free-Air CO2 Enrichment (FACE) depress plant photosynthesis, growth, and yield. *Agric. For. Meteorology* 284 (January), 107899. doi: 10.1016/j.agrformet.2020.107899

Baker, N. R. (2008). Chlorophyll fluorescence: A probe of photosynthesis *in vivo*. *Annu. Rev. Plant Biol.* 59 (1), 89–113. doi: 10.1146/annurev.arplant.59.032607.092759

Baker, N. R., and Rosenqvist, E. (2004). Applications of chlorophyll fluorescence can improve crop production strategies: An examination of future possibilities. *J. Exp. Bot.* 55 (403), 1607–1621. doi: 10.1093/jxb/erh196

Baret, F., and Guyot, G. (1991). Potentials and limits of vegetation indices for LAI and APAR assessment. *Remote Sens. Environ.* 35 (2–3), 161–173. doi: 10.1016/0034-4257(91)90009-U

Bareth, G., Bendig, J., Tilly, N., Hoffmeister, D., Aasen, H., and Bolten, A. (2016). A comparison of UAV- and TLS-derived plant height for crop monitoring: Using polygon grids for the analysis of crop surface models (CSMs). *Photogrammetrie Fernerkundung Geoinformation* 2016 (2), 85–94. doi: 10.1127/pfg/2016/0289

Baston, D. (2022). *Fast Extraction from Raster Datasets using Polygons in R package version 0.8.2*. Available at: https://cran.r-project.org/package=exactextractr.

Bendig, J., Bolten, A., Bennertz, S., Broscheit, J., Eichfuss, S., and Bareth, G. (2014). Estimating biomass of barley using crop surface models (CSMs) derived from UAV-based RGB imaging. *Remote Sens.* 6 (11), 10395–10412. doi: 10.3390/rs61110395

Beres, B. L., Hatfield, J. L., Kirkegaard, J. A., Eigenbrode, S. D., Pan, W. L., Lollato, R. P., et al. (2020). Toward a better understanding of genotype × Environment × Management interactions—A global wheat initiative agronomic research strategy. *Front. Plant Sci.* 11 (June). doi: 10.3389/fpls.2020.00828

Bertheloot, J., Martre, P., and Andrieu, B. (2008). Dynamics of Light and Nitrogen Distribution during Grain Filling within Wheat Canopy. *Plant Physiol.* 148 (3), 1707–1720. doi: 10.1104/pp.108.124156

Bresson, J., Bieker, S., Riester, L., Doll, J., and Zentgraf, U. (2018). A guideline for leaf senescence analyses: From quantification to physiological and molecular investigations. *J. Exp. Bot.* 69 (4), 769–786. doi: 10.1093/jxb/erx246

Bunce, J. A. (2012). Responses of cotton and wheat photosynthesis and growth to cyclic variation in carbon dioxide concentration. *Photosynthetica* 50 (3), 395–400. doi: 10.1007/s11099-012-0041-7

Cendrero-Mateo, M. P., Muller, O., Albrecht, H., Burkart, A., Gatzke, S., Janssen, B., et al. (2017). Field phenotyping: concepts and examples to quantify dynamic plant traits across scales in the field. *Terrestrial Ecosystem Res. Infrastructures* , 53–80. doi: 10.1201/9781315368252-4

Chakhvashvili, E., Siegmann, B., Muller, O., Verrelst, J., Bendig, J., Kraska, T., et al. (2022). Retrieval of crop variables from proximal multispectral UAV image data using PROSAIL in maize canopy. *Remote Sens.* 14 (5). doi: 10.3390/rs14051247

Cooper, M., Voss-Fels, K. P., Messina, C. D., Tang, T., and Hammer, G. L. (2021). Tackling G × E × M interactions to close on-farm yield-gaps: creating novel pathways for crop improvement by predicting contributions of genetics and management to crop productivity. *Theor. Appl. Genet.* 134 (6), 1625–1644. doi: 10.1007/s00122-021-03812-3

Curtis, P. S., Drake, B. G., Leadley, P. W., Arp, W. J., Whigham, D. F., and Environmental, S. (1989). Oecologia exposed to elevated CO2 concentrations on an estuarine marsh. *Oecologia* 78 (t 989), 20–26. doi: 10.1007/BF00377193

Diaz, C., Purdy, S., Christ, A., Morot-Gaudry, J.-F., Wingler, A., and Masclaux-Daubresse, C. (2005). Characterization of markers to determine the extent and variability of leaf senescence in arabidopsis. A metabolic profiling approach 1. *Plant Physiol.* 138, 898–908. doi: 10.1104/pp.105.060764

Dier, M., Sickora, J., Erbs, M., Weigel, H. J., Zörb, C., and Manderscheid, R. (2018). Decreased wheat grain yield stimulation by free air CO2 enrichment under N deficiency is strongly related to decreased radiation use efficiency enhancement. *Eur. J. Agron.* 101 (February), 38–48. doi: 10.1016/j.eja.2018.08.007

FAO (2011). *Save and Grow. A policymaker's guide to sustainable intensification of smallholder crop production* (Rome: Food and Agriculture Organization of the United Nations). Available at: http://www.fao.org/docrep/014/i2215e/i2215e.pdf.

FAO (2021). *World Food and Agriculture – Statistical Yearbook 2021* (Rome: FAO). doi: 10.4060/cb4477en

Fu, P., Montes, C. M., Siebers, M. H., Gomez-Casanovas, N., Mcgrath, J. M., Ainsworth, E. A., et al. (2022). Advances in field-based high-throughput photosynthetic phenotyping. *J. Exp. Bot.* 73 (10), 3157–3172. doi: 10.1093/jxb/erac077

Gardi, M. W., Haussmann, B. I. G., Malik, W. A., and Högy, P. (2022). Effects of elevated atmospheric CO2 and its interaction with temperature and nitrogen on yield of barley (Hordeum vulgare L.): a meta-analysis. *Plant Soil* 0123456789), 535–550. doi: 10.1007/s11104-022-05386-5

Helman, D., and Bonfil, D. J. (2022). Six decades of warming and drought in the world's top wheat-producing countries offset the benefits of rising CO2 to yield. *Sci. Rep.* 12 (1), 1–11. doi: 10.1038/s41598-022-11423-1

Huete, A., Didan, K., Miura, T., Rodriguez, E. P., Gao, X., and Ferreira, L. G. (2002). Overview of the radiometric and biophysical performance of the MODIS vegetation indices. *Remote Sens. Environ.* 83 (1–2), 195–213. doi: 10.1016/S0034-4257(02)00096-2

Imbery, F., Friedrich, K., Kaspar, F., Fleckenstein, R., Lengfeld, K., Daßler, J., et al. (2021). *Klimatologische Einordnung des Jahres 2021*. Available at: https://www.dwd.de/DE/presse/pressemitteilungen/DE/2021/20211230_deutschlandwetter_jahr2021_news.html.

IPCC (2021a). "Climate change 2021: the physical science basis," in *Contribution of Working Group I to the Sixth Assessment Report of the Intergovernmental Panel on Climate Change*. Eds. V. Masson-Delmotte, P. Zhai, A. Pirani, S. L. Connors, C. Péan, S. Berger, N. Caud and Y. Chen (Cambridge, United Kingdom and New York, NY, USA: Cambridge University Press), 3949. Available at: https://www.ipcc.ch/report/ar6/wg1/downloads/report/IPCC_AR6_WGI_Full_Report.pdf.

IPCC (2021b). *Summary for Policymakers. Climate Change 2021: The Physical Science Basis*. Available at: https://www.ipcc.ch/report/ar6/wg1/.

Javaid, M. M., Wang, X., Florentine, S. K., Ashraf, M., Mahmood, A., Li, F. M., et al. (2022). Effects on Photosynthetic Response and Biomass Productivity of Acacia longifolia ssp. longifolia Under Elevated CO2 and Water-Limited Regimes. *Front. Plant Sci.* 13 (March). doi: 10.3389/fpls.2022.817730

Keeling, C. D., Bacastow, R. B., and Bainbridge, A. E. (1976). Atmospheric carbon dioxide variations at Mauna Loa Observatory, Hawaii. *Tellus* 28 (6), 538–551. doi: 10.3402/tellusa.v28i6.11322

Keller, B. (2018). *Analyzing photosynthetic performance in natural fluctuating environment using light-induced fluorescence transient (LIFT) method in high-throughput*. Available at: http://hss.ulb.uni-bonn.de/2018/5284/5284.pdf.

Kolber, Z. S., Prášil, O., and Falkowski, P. G. (1998). Measurements of variable chlorophyll fluorescence using fast repetition rate techniques: Defining methodology and experimental protocols. *Biochim. Biophys. Acta - Bioenergetics* 1367 (1–3), 88–106. doi: 10.1016/S0005-2728(98)00135-2

Lauriks, F., Salomón, R. L., De Roo, L., and Steppe, K. (2021). Leaf and tree responses of young European aspen trees to elevated atmospheric CO2 concentration vary over the season. *Tree Physiol.* 41 (10), 1877–1892. doi: 10.1093/treephys/tpab048

Lipson, D. A., Wilson, R. F., and Oechel, W. C. (2005). Effects of elevated atmospheric CO2 on soil microbial biomass, activity, and diversity in a chaparral ecosystem. *Appl. Environ. Microbiol.* 71 (12), 8573–8580. doi: 10.1128/AEM.71.12.8573-8580.2005

Long, S. P., Ainsworth, E. A., Rogers, A., and Ort, D. R. (2004). Rising atmospheric carbon dioxide: plants FACE the future. *Annu. Rev. Plant Biol.* 55 (1), 591–628. doi: 10.1146/annurev.arplant.55.031903.141610

Long, S. P., Marshall-Colon, A., and Zhu, X. G. (2015). Meeting the global food demand of the future by engineering crop photosynthesis and yield potential. *Cell* 161 (1), 56–66. doi: 10.1016/j.cell.2015.03.019

Marc, J., and Gifford, R. M. (1984). Floral initiation in wheat, sunflower, and sorghum under carbon dioxide enrichment. *Can. J. Bot.* 62 (1), 9–14. doi: 10.1139/b84-002

Maxwell, K., and Johnson, G. N. (2000). Chlorophyll fluorescence - A practical guide. *J. Exp. Bot.* 51 (345), 659–668. doi: 10.1093/jxb/51.345.659

Muller, O., Keller, B., Zimmermann, L., Jedmowski, C., Kleist, E., Pingle, V., et al. (2018). "Field phenotyping and an example of proximal sensing of photosynthesis under elevated CO2," in *International Geoscience and Remote Sensing Symposium (IGARSS)*, , 2018-July. 8252–8254. doi: 10.1109/IGARSS.2018.8517301

Murchie, E. H., Kefauver, S., Araus, J. L., Muller, O., Rascher, U., Flood, P. J., et al. (2018). Measuring the dynamic photosynthome. *Ann. Bot.* 122 (2), 207–220. doi: 10.1093/aob/mcy087

Mutanga, O., and Skidmore, A. K. (2004). Narrow band vegetation indices overcome the saturation problem in biomass estimation. *Int. J. Remote Sens.* 25 (19), 3999–4014. doi: 10.1080/01431160310001654923

Ney, P., and Graf, A. (2018). High-resolution vertical profile measurements for carbon dioxide and water vapour concentrations within and above crop canopies. *Boundary-Layer Meteorology* 166 (3), 449–473. doi: 10.1007/s10546-017-0316-4

NOAA ESRL (2023). *Global Monitoring Laboratory - Carbon Cycle Greenhouse Gases*. Available at: https://gml.noaa.gov/ccgg/trends/data.html.

NRW Chamber of Agriculture (2021). *Landessortenversuch 2021 NRW*. Available at: https://www.landwirtschaftskammer.de/landwirtschaft/ackerbau/getreide/winterweizen/winterweizen-sv-2021.htm.

OECD and FAO (2012). *OECD-FAO Agricultural Outlook 2012* (Rome). doi: 10.1787/agr_outlook-2012-en

Osmond, B., Chow, W. S., Wyber, R., Zavafer, A., Keller, B., Pogson, B. J., et al. (2017). Relative functional and optical absorption cross-sections of PSII and other photosynthetic parameters monitored *in situ*, at a distance with a time resolution of a few seconds, using a prototype light induced fluorescence transient (LIFT) device. *Funct. Plant Biol.* 44 (10), 985–1006. doi: 10.1071/FP17024

Pätzold, S., and Pude, R. *Soil Characteristics CKA*. Available at: https://www.aussenlabore.uni-bonn.de/cka/de/standort/copy_of_standortbeschreibung.

Pearman, G. I., and Garratt, J. R. (2022). Carbon dioxide measurements above a wheat crop. II CO2 flux density and the effects of diffuse radiation. *Agric. For. Meteorology* 320 (April), 108944. doi: 10.1016/j.agrformet.2022.108944

Peñuelas, J., Gamon, J. A., Fredeen, A. L., Merino, J., and Field, C. B. (1994). Reflectance indices associated with physiological changes in nitrogen- and water-limited sunflower leaves. *Remote Sens. Environ.* 48 (2), 135–146. doi: 10.1016/0034-4257(94)90136-8

Pieruschka, R., and Schurr, U. (2022). "Origins and drivers of crop phenotyping," in *Advances in plant phenotyping for more sustainable crop production*, *1st ed*. Ed. A. Walter (Philadelphia, PA: Burleigh Dodds Science Publishing), 3–28. doi: 10.19103/AS.2022.0102.01

Poorter, H., Knopf, O., Wright, I. J., Temme, A. A., Hogewoning, S. W., Graf, A., et al. (2021). A meta-analysis of responses of C3 plants to atmospheric CO2: dose–response curves for 85 traits ranging from the molecular to the whole-plant level. *New Phytol.* 233. doi: 10.1111/nph.17802

Pyung, O. L., Hyo, J. K., and Hong, G. N. (2007). Leaf senescence. *Annu. Rev. Plant Biol.* 58, 115–136. doi: 10.1146/annurev.arplant.57.032905.105316

Quiros-Vargas, J., Caldeira, R. D., dos Santos, N. Z., Zimmermann, L., Siegmann, B., Kraska, T., et al. (2021). "Response of bean (Phaseolus vulgaris L.) to elevated $[\mathbf{CO_{2}}]$ in yield, biomass and chlorophyll fluorescence," in *2021 IEEE International Geoscience and Remote Sensing Symposium IGARSS*. 5861–5864. doi: 10.1109/igarss47720.2021.9554347

R Core Team (2013). *R: A language and environment for statistical computing* (Vienna, Austria: R Foundation for Statistical Computing). Available at: http://www.r-project.org/.

Rebetzke, G. J., Jimenez-Berni, J., Fischer, R. A., Deery, D. M., and Smith, D. J. (2019). Review: High-throughput phenotyping to enhance the use of crop genetic resources. *Plant Sci.* 282 (June), 40–48. doi: 10.1016/j.plantsci.2018.06.017

Reynolds, M. P., and Braun, H.-J. (2022). *Wheat Improvement. Wheat Improvement* (Cham, Switzerland). doi: 10.1007/978-3-030-90673-3_1

Richardson, A. D., Hufkens, K., Milliman, T., Aubrecht, D. M., Chen, M., Gray, J. M., et al. (2018). Tracking vegetation phenology across diverse North American biomes using PhenoCam imagery. *Sci. Data* 5, 1–24. doi: 10.1038/sdata.2018.28

Rondeaux, G., Steven, M., and Baret, F. (1996). Optimization of soil-adjusted vegetation indices. *Remote Sens. Environ.* 55 (2), 95–107. doi: 10.1016/0034-4257(95)00186-7

Soares, J. C., Zimmermann, L., Zendonadi dos Santos, N., Muller, O., Pintado, M., and Vasconcelos, M. W. (2021). Genotypic variation in the response of soybean to elevated CO2. *Plant-Environment Interact.* 2 (6), 263–276. doi: 10.1002/pei3.10065

Sonnentag, O., Hufkens, K., Teshera-Sterne, C., Young, A. M., Friedl, M., Braswell, B. H., et al. (2012). Digital repeat photography for phenological research in forest ecosystems. *Agric. For. Meteorology* 152 (1), 159–177. doi: 10.1016/j.agrformet.2011.09.009

Taylor, G., Tallis, M. J., Giardina, C. P., Percy, K. E., Miglietta, F., Gupta, P. S., et al. (2008). Future atmospheric CO2 leads to delayed autumnal senescence. *Global Change Biol.* 14 (2), 264–275. doi: 10.1111/j.1365-2486.2007.01473.x

United Nations (1987). *Report of the World Commission on Environment and Development*. Available at: http://digitallibrary.un.org/record/139811.

Wyber, R., Malenovský, Z., Ashcroft, M. B., Osmond, B., and Robinson, S. A. (2017). Do daily and seasonal trends in leaf solar induced fluorescence reflect changes in photosynthesis, growth or light exposure? *Remote Sens.* 9 (6). doi: 10.3390/rs9060604

Zani, D., Crowther, T. W., Mo, L., Renner, S. S., and Zohner, C. M. (2020). Increased growing-season productivity drives earlier autumn leaf senescence in temperate trees. *Science* 370 (6520), 1066–1071. doi: 10.1126/science.abd8911

Zendonadi dos Santos, N., Piepho, H., Condorelli, G. E., Groli, E. L., Newcomb, M., Ward, R., et al. (2021). High-throughput field phenotyping reveals genetic variation in photosynthetic traits in durum wheat under drought. *Plant Cell Environ.* 1–21. doi: 10.1111/pce.14136

frontiers | Frontiers in Plant Science

TYPE Original Research
PUBLISHED 21 February 2024
DOI 10.3389/fpls.2023.1305292

OPEN ACCESS

EDITED BY
Philipp Von Gillhaussen,
Interantional Plant Phenotyping Network (IPPN), Germany

REVIEWED BY
Germano Gomes,
Flemish Institute for Biotechnology, Belgium
Muqing Zhang,
Guangxi University, China

*CORRESPONDENCE
Carmela Rosaria Guadagno
cguadagn@uwyo.edu

†These authors have contributed equally to this work

RECEIVED 01 October 2023
ACCEPTED 21 December 2023
PUBLISHED 21 February 2024

CITATION
Renó V, Cardellicchio A, Romanjenko BC and Guadagno CR (2024) AI-assisted image analysis and physiological validation for progressive drought detection in a diverse panel of *Gossypium hirsutum* L.. *Front. Plant Sci.* 14:1305292. doi: 10.3389/fpls.2023.1305292

AI-assisted image analysis and physiological validation for progressive drought detection in a diverse panel of *Gossypium hirsutum* L.

Vito Renó[1†], Angelo Cardellicchio[1†], Benjamin Conrad Romanjenko[2] and Carmela Rosaria Guadagno[2,3*]

[1]Institute of Intelligent Industrial Technologies and Systems for Advanced Manufacturing, National Research Council of Italy (CNR STIIMA), Bari, Italy, [2]Department of Botany, University of Wyoming, Laramie, WY, United States, [3]Science Initiative, University of Wyoming, Laramie, WY, United States

Introduction: Drought detection, spanning from early stress to severe conditions, plays a crucial role in maintaining productivity, facilitating recovery, and preventing plant mortality. While handheld thermal cameras have been widely employed to track changes in leaf water content and stomatal conductance, research on thermal image classification remains limited due mainly to low resolution and blurry images produced by handheld cameras.

Methods: In this study, we introduce a computer vision pipeline to enhance the significance of leaf-level thermal images across 27 distinct cotton genotypes cultivated in a greenhouse under progressive drought conditions. Our approach involved employing a customized software pipeline to process raw thermal images, generating leaf masks, and extracting a range of statistically relevant thermal features (e.g., min and max temperature, median value, quartiles, etc.). These features were then utilized to develop machine learning algorithms capable of assessing leaf hydration status and distinguishing between well-watered (WW) and dry-down (DD) conditions.

Results: Two different classifiers were trained to predict the plant treatment—random forest and multilayer perceptron neural networks—finding 75% and 78% accuracy in the treatment prediction, respectively. Furthermore, we evaluated the predicted versus true labels based on classic physiological indicators of drought in plants, including volumetric soil water content, leaf water potential, and chlorophyll *a* fluorescence, to provide more insights and possible explanations about the classification outputs.

Discussion: Interestingly, mislabeled leaves mostly exhibited notable responses in fluorescence, water uptake from the soil, and/or leaf hydration status. Our findings emphasize the potential of AI-assisted thermal image analysis in

enhancing the informative value of common heterogeneous datasets for drought detection. This application suggests widening the experimental settings to be used with deep learning models, designing future investigations into the genotypic variation in plant drought response and potential optimization of water management in agricultural settings.

KEYWORDS

thermal imaging, drought, plant phenotyping, machine learning, leaf classification, artificial intelligence

Introduction

Climate change is exerting a profound impact on global crop production, primarily driven by the escalating variability in precipitation patterns and the increased occurrence of droughts (IPCC, 2022). These shifts in water availability have far-reaching consequences, affecting the productivity, quantity, and quality of all agricultural crops, including those essential for anthropic use.

One such crop is *Gossypium hirsutum* L., important for its significant contributions to fiber production, seed oil extraction, and livestock fodder. Thriving in arid environments where water resources are already limited, this species necessitates a substantial volume of annual water (60–120 cm) to support its robust growth (Wegier et al., 2016; Khan et al., 2020). With 25 million tons of fiber produced per year and an economic impact exceeding 600 billion dollars, cotton plays a pivotal role in supplying over 80% of the global natural fiber demand, underscoring its critical importance to both individuals and global economies (Townsend, 2020). In recent years, the production of this crop has been decreasing due to more severe weather events (Meyer et al., 2023), and projections suggest that the world cotton production may struggle to meet the burgeoning demand in the next decades (Li et al., 2021). However, a silver lining is represented by the substantial genetic diversity inherent within this species constituting an unprecedented avenue for the selection, breeding, and cultivation of varieties that are inherently better equipped to endure and thrive amidst increasing climatic pressures.

Plant phenotyping consistently applies image processing (IP) techniques (either classical or modern ones to data acquired from visible, infrared, and hyperspectral cameras, showing the potential to enable for non-destructive, high-throughput detection and selection of desirable traits across different temporal and spatial scales (Zhao et al., 2019). Thermal imaging, also known as infrared thermography, is a powerful and non-invasive technique that has found widespread relevance in recent years to assess canopy temperature and their responses to both abiotic and biotic stressors, from salt stress, heat, and drought stress to bacterial and fungal infections (Pineda et al., 2021). The analysis of canopy temperatures has been connected to traditional physiological measurements—leaf water potential, gas exchange, and chlorophyll *a* fluorescence (Cohen et al., 2005; Casari et al., 2019)—and utilized to screen for genotypic variation across several species (Casari et al., 2019; Bhandari et al., 2021; Ferguson et al., 2021). The processing of thermal images usually starts by separating the canopy impression from the background pixels that may include soil particles and other structures. This initial pixel exclusion process can be completed through a variety of different approaches: manual isolation of the canopy and leaf via polygon selection, gray scaling, image segmentation, two-means clustering, and bimodal peak detection (Mohanty et al., 2016; Prakash et al., 2021; Stutsel et al., 2021; Sakurai et al., 2023). Despite the utilized methodology, the postprocessing times for the analysis of thermal images are usually long and often affected by the low resolution of the images (Kohin and Butler, 2004).

To cope with the constraints imposed by traditional IP methods, over the last few years, the scientific community has largely adopted machine learning (ML) and, particularly, deep learning (DL) techniques to deal with data acquired by plant phenotyping platforms or, more in general, from high-throughput measurements (Solimani et al., 2023). These algorithms can also represent a great opportunity to implement the postprocessing of thermal images captured with handheld cameras and indeed increase their final throughput. ML algorithms have already been used to analyze thermal images, specifically to enhance stomatal count, surface recognition, and crop disease classification (Cho et al., 2018; Ferguson et al., 2021; Pignon et al., 2021; Batchuluun et al., 2022). Three different ML algorithms, namely, random forest, multivariate linear regression, and gradient boosting, were previously used to correlate thermal data—acquired by thermal IR images—to environmental drivers, such as solar radiation, air temperature, relative humidity, and wind speed, to assess the relationship between the stomatal conductance in crop canopies and changes in environmental factors (Zhao et al., 2021). Another approach consisted of two models based on variations for decision trees used to define a relationship between the regression of thermal indexes for droughted and well-watered scenarios of vineyard crops (Gutiérrez et al., 2018). DL approaches have also been proposed by developing a custom architecture based on convolutional neural networks (CNNs) to classify five different crop diseases and defects (e.g., blast, bacteria leaf blight, leaf folder) (Batchuluun et al., 2022).

In that case, the model was first trained on the Paddy crop dataset and then refined on a new empirical dataset consisting of 4,720 images. The results were further investigated by using class activation maps to highlight the parts of the image that were considered relevant by the network to achieve the classification result. Finally, indexes of classification, such as the crop water stress index (CWSI), have been computed to distinguish between droughted and well-watered crops. Despite these significant IP applications to thermal images and the correlations to different physiological indicators from various crops, models that use thermal crop response to water stress across extreme genotypes using deep learning are scarce (Berni et al., 2009; Pratap et al., 2019).

Here, we provide an evaluation of the response of different genotypes to different levels of water limitations, from mild to severe drought. First, we screened a panel of 27 geographically different genotypes (Supplementary Figure S2) in the species *Gossypium* for their response to water limitation using a handheld IR camera. These imaging data were used as the basis to develop a hybrid IP/ML processing software pipeline, which used IP techniques to extract the region of interest from each leaf and then feed a statistically enhanced ML algorithm to predict the leaf water status, as either well-watered (WW) or subjected to dry-down (DD) at two different times during the complete water withholding (mild and severe drought). Finally, we coupled additional leaf-level physiological measurements, such as water potential and chlorophyll *a* fluorescence to the IP/ML analysis, providing a meaningful interpretation of the modeled results.

Materials and methods

Plant materials

A panel of 27 different genotypes was utilized for the experiment, and all seeds were obtained from the USDA Germplasm Collection. Genotypes originate from Australia, China, Guatemala, Mexico, Trinidad and Tobago, and the USA, covering all four zones that have the highest production of cotton in the world (Wendel et al., 2009). Aside from being geographically diverse, the selected genotypes also span a large range in leaf size, plant and leaf architecture, and coloration (Figure 1). This extreme genotypic variation inevitably affects the physiology of these genotypes, including their water status and their ability to maintain leaf turgor despite water limitations (e.g., large versus small leaves, significantly impacting transpiration rates) making the panel of choice perfectly suited for testing our pipeline, due to expected great variation in the thermal features of the leaves under progressive drought.

Growth conditions

The cotton panel was grown in a greenhouse research bay of the Plant Growth & Phenotyping Facility at the University of Wyoming (Laramie, Wyoming, USA) for a total of 122 days from seed to seed, planting to harvesting, during the winter of 2022–2023. The cotton panel, 27 genotypes × 3 replicates each, was grown following a random block design, and the greenhouse environmental conditions were controlled by state-of-the-art climate control systems (Argus, British Columbia, Canada). Temperature was set to 27°C ± 3°C/26°C ± 3°C (day/night), and relative humidity was between 10% and 30%. Additional lighting was given by a four-channel Heliospectra growth light system (Heliospectra AB, Gothenburg, Sweden). The intensity of the Elixia LED channels was set as follows: 450 nm (blue) at 500 units, 660 nm (red) at 500 units, 735 nm (far-red) at 500 units, and the white 5,700K LED channel at 1,000 units. All intensities are reported as 0–1,000 units corresponding to 0%–100% of max LED output as for the Heliospectra manual. The photoperiod was 14/10 (D/N), 0600h–0800h; the highest recorded photosynthetically active radiation (PAR) was 1,600 µmol photons m^{-2} s^{-1} with the sensor located in the middle of the canopy. Aside from the OMNI sensors from Argus, the environmental conditions were also tracked using CR1000 Data Logger (Campbell Scientific Inc. Logan, UT, United States) monitoring: air temperature and relative humidity HMP45AC (VAISALA, Vantaa, Finland); PAR, LI-COR Quantum (LI-COR, Lincoln, NE, United States); and soil moisture, Delmhorst GB-1 (Delmhorst Instrument Co., Towaco, NJ, United States). Sensors were spaced across the entire area covered by canopy in the ~40-m/420-ft^2 greenhouse bay.

Experimental design

One seed per pot (10 quarts/11 L in volume) was sown in a substrate made up of sand (80% v/v; Premium Play Sand, Quickrete, Atlanta, GA), fritted clay (10% v/v; Greens Grade, Buffalo Grove, IL), and organic soil mix (10% v/v; Miracle-Gro moisture control Potting Mix, Marysville, OH) amended with ½ tablespoon of Osmocote 16–6–12 fertilizer (Scotts, Marysville, OH). Sown seeds were covered and placed centrally in the pot at a depth of ~½ inch/1.2 cm and covered in vermiculite to aid in the germination. Plants were hand-watered with reverse osmosis (RO) water daily to maintain soil field capacity and a soil water potential close to saturation until 105 days after sowing (DAS) when all genotypes and replicates had at least 50% of opened flowers (Figure 2). At 106 DAS, two randomly chosen replicates for each genotype were subjected to complete water withholding for the rest of the experiment forming the dry-down cohort of plants (DD), while one replicate per genotype was maintained at the daily watering regime in the well-watered (WW) cohort. All physiological measurements occurred at two points in time, at 110 DAS (mild drought) and 121 DAS (severe drought), after 4 and 14 days of uninterrupted progressive drought, respectively.

Leaf-level physiological measurements

On measurement days, chlorophyll *a* fluorescence was measured on two separate fully developed leaves of the mid-canopy with a handheld fluorometer (FluorPen FP100, Photon System Instruments, Drásov, Czech Republic). Measurements of photosystem II efficiency were taken using a saturation pulse that

10.3389/fpls.2023.1305292

FIGURE 1
In-vivo pictures of extreme genotypes in the cotton panel. Striking examples of plant architecture, leaf types, and coloration differences in the experimental panel. Red/dark green medium size leaf for *Red Dwarf Harrison* **(A)**; large, with low venation leaves in *TX_180* **(B)**; inverted margins for the leaves of *Cup Leaf* **(C)**; trilobate morphology for *Gumbo* leaves **(D)**; pale green and short overall plant size for *Virescent nankeen* **(E)**; and short-overall plant size and okra-like leaves for *Pronto* **(F)**. All plants were WW and imaged on the same day (70 DAS).

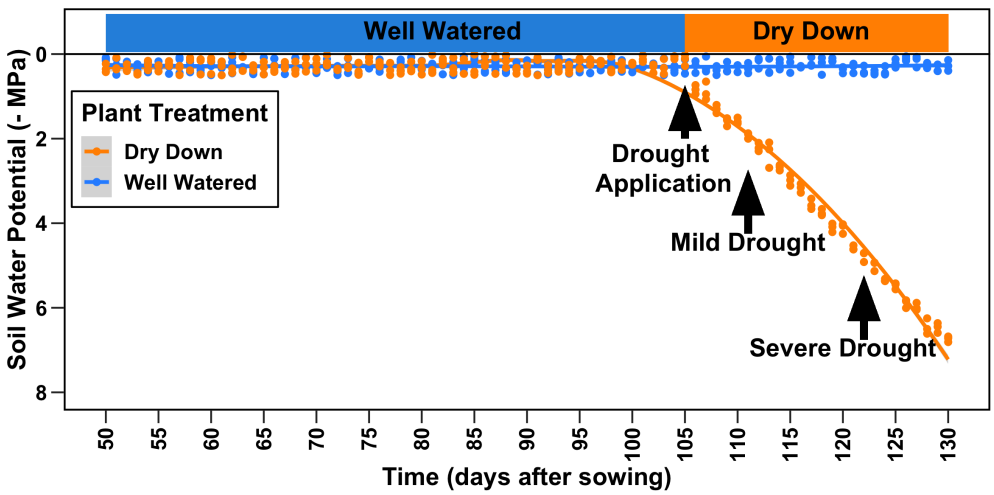

FIGURE 2
Experimental design. A panel of 27 diverse genotypes of cotton was grown for a total of 122 days after sowing (DAS). All plants were watered at saturation until 105 DAS when drought was applied as complete water withholding for a subset of plants (dry-drown). All data presented in the manuscript were collected at 110 DAS (mild drought) and 121 DAS (severe drought).

was applied (1,500 µmol photons m^{-2} s^{-1}) to measure *Fv/Fm* or *Fv'/Fm'* on dark- or light-acclimated leaves, respectively (Murchie and Lawson, 2013). During the same measurement days, one fully developed leaf per plant was also harvested and used to measure leaf water potential (PMS Instrument Company, Albany, OR, United States). Soil moisture measurements were also taken using a HydroSense II (Campbell Scientific Inc., Logan, UT, United States). Leaf water potential, chlorophyl *a* fluorescence, and soil moisture measurements were taken over a 24-h time course during the hours of 10:00–12:00 h, 16:00–18:00 h, and 22:00–24:00 h. After the start of the dry-down, all physiological measurements were taken during the hours of 04:00–06:00 h (predawn) and 11:00–13:00 h (midday).

Thermal imagery collection

Thermal images were taken using a handheld FLIR Thermal Camera T560, 640 × 480 pixel resolution, wide angle lens $f = 10$ mm (FLIR Systems Inc., Wilsonville, OR, United States). Fully developed leaves near the top of the canopy were chosen for imaging, and one leaf per replicate plant across all genotypes and treatment was imaged at the same time as the other leaf-level physiological measurements. A white paper backdrop was placed directly behind the leaf, and an image was taken holding the camera objective facing both the leaf and backdrop to allow for a full frontal view of the images (Figure 3). Image parameters were set using leaf emissivity, 0.95, and with focus regulation (Buitrago et al., 2016). A total of 648 images was made up from two images per leaf, from three replicate plants for 27 genotypes at two times of the day (predawn and midday) and at two drought treatments. After initial QC, the final dataset used for the ML analysis was a balanced dataset of 419 images between WW and DD. All thermal images were converted to *CSV* format using FLIR Thermal Studio.

Data analysis

Physiological data were processed using Excel and R 4.3.1 (R Core Team, 2013) with packages dplyr (Wickham et al., 2023) and tidyverse (Wickham et al., 2019). The presented graphs were generated using the packages ggplot2 (Wickham, 2016) and ggrepel (Slowikowski, 2023).

Hybrid IP/ML software pipeline for thermal data

The hybrid IP/ML pipeline used in this work is summarized in Figure S2, and it includes the following computational steps.

1. *Data parsing*: First, raw format data exported by the FLIR thermal camera were parsed by a specific software routine to store the data in an interoperable format such as comma-separated value (CSV) files. Each one of these files held two separate representations, that is, a thermal representation, where each pixel represented a thermal value stored as a floating point number, and an RGB value, used for visualization purposes.

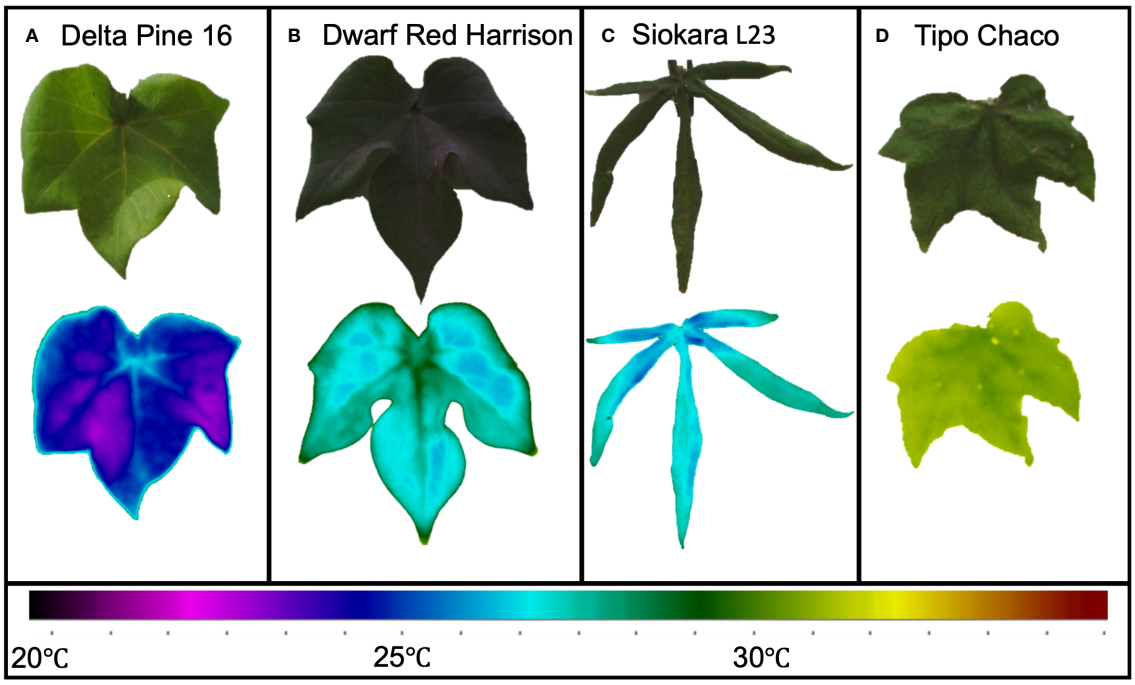

FIGURE 3
Leaf thermal variation in extreme cotton genotypes. Bright green, large leaf from *Delta Pine 16* **(A)**; red/dark green medium size leaf from *Red Dwarf Harrison* **(B)**; okra-like leaf from *Siokara L23* **(C)**, and dark green medium to large leaf from *Tipo Chaco* **(D)**.

2. *Data preprocessing*: After the parsing step, a preprocessing step aimed at obtaining a high-pass-filtered version of the raw thermal image, as well as its gradient, was performed. To this end, the fast Fourier transform (FFT) of the raw thermal image was first computed (Figure 4A). Then, a binary mask was computed to keep all the FFT pixels whose value was less than the continuous component, considered as the central, brighter, pixel (Figure 4B). Then, the inverse transform was applied, as shown in Figure 4C. Finally, the gradient of the filtered image was computed (Figure 4D) and used to compute the leaf mask in the next step.

3. *Leaf mask computation*: The computation of the leaf mask is performed starting from the gradient obtained during the preprocessing step. First, the first quartile q_1 and the third quartile q_3 of the values of the gradient image are computed. Then, the interquartile range $IQR = q_3 - q_1$ is the used to compute a threshold $thr_{dw} = q_1 - 1.5 \cdot IQR$. Let δ be the gradient image; a binary mask M is then obtained according to the following binarization logic:

$$M(i,j) = \begin{cases} 1, & if \quad \delta(i,\ j) \ \vee \delta(i,j) < thr_{dw} \\ 0, & otherwise \end{cases}$$

To enhance the mask M, the morphological operations of dilation, hole filling, and erosion, followed by a blob analysis, were performed, computing the connected components of the image. The final mask M is then selected as the region with the greatest number of contiguous pixels turned on. Some examples of leaf masks for different genotypes are shown in Figure 5. The pixel values in the region highlighted by the leaf masks are used to compute thermal features. As such, the temperature values are first statistically filtered removing the outliers, hence making the algorithm robust to small leaf mask misalignments. Then, a set of eight statistical thermal indicators are computed from raw thermal values, that is, mean, standard deviation, median, 25th and 75th percentiles, interquartile range, max, min, and temperature range.

The IP/ML software pipeline was developed and tested, and all the AI applications were run on a machine equipped with an Intel Core i9-11900K, 32 GB of RAM, and an Nvidia GeForce RTX 3080 GPU with 10 GB of RAM. The software was developed in Python 3.10, and the Scikit Image (Van der Walt et al., 2014) and Scikit Learn (Pedregosa et al., 2011) libraries were used.

Results and discussion

Statistical analyses

The first step was to use the IP preprocessing techniques (Figure S1) to extract all the leaf masks from the raw thermal data along with the associated features. The algorithms used at this stage are non-parametric, meaning that they automatically tune the parameters after a preprocessing step of each thermal image, so that the leaf mask can be estimated (Figure 6) and the thermal

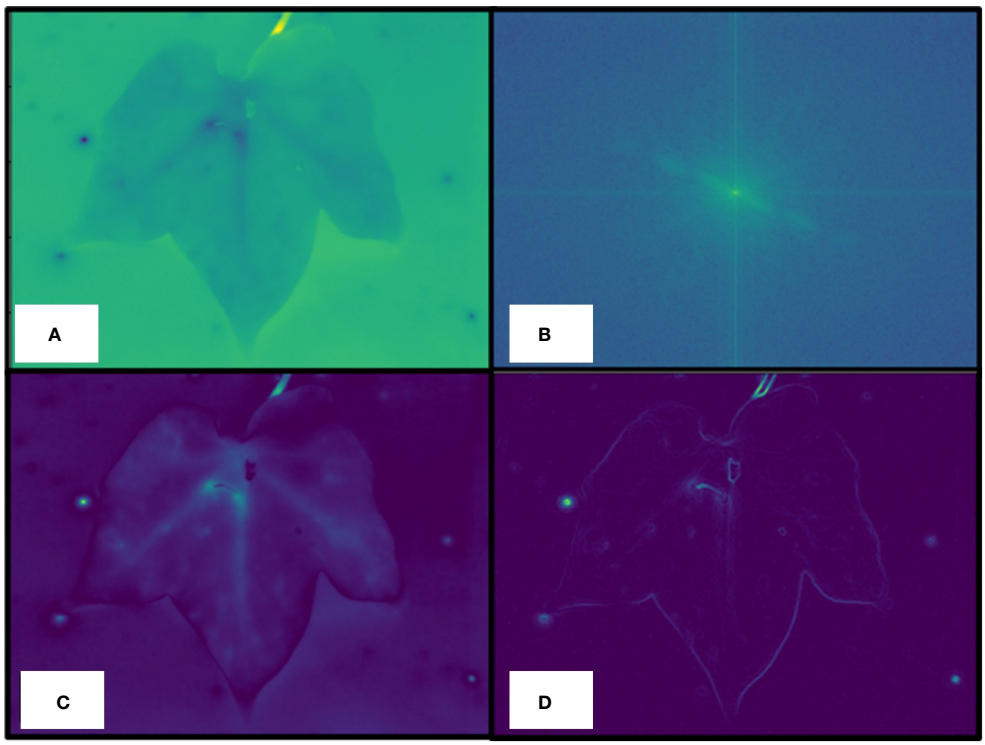

FIGURE 4
Data preprocessing details. Raw thermal image **(A)**, a fast Fourier transform (FFT) of the raw thermal image is computed to keep all the FFT pixels whose value is less than the continuous component, considered as the central, brighter, pixel **(B)**, inverse transform application **(C)**, computed gradient of the filtered image **(D)** used to compute the actual leaf mask.

10.3389/fpls.2023.1305292

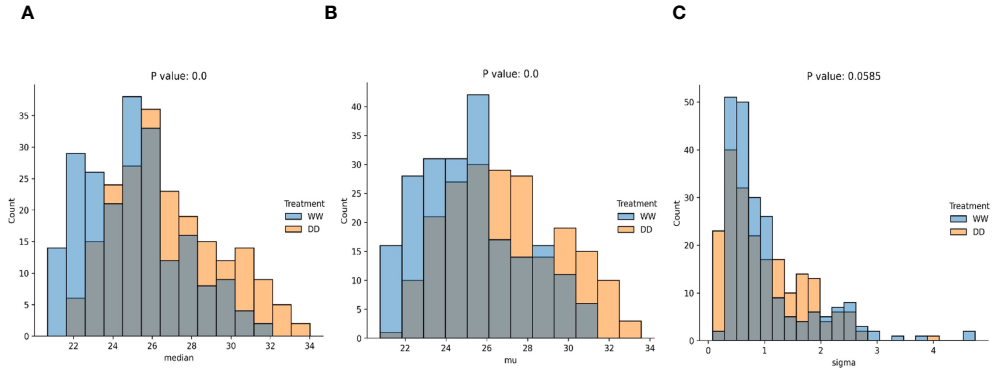

FIGURE 5
Statistical comparisons of data distributions (significant). Statistical comparison using the KS test of the median **(A)**, mean **(B)**, and variance **(C)** computed over the distributions of WW and DD leaves.

features are extracted almost in real time. This step was mandatory for providing the baseline data to be used for the next steps of the pipeline.

The thermal features extracted from this initial data parsing step were then used as the basis for the ML processing software pipeline. For this, a first exploratory analysis was performed using a two-sample Kolmogorov–Smirnoff test on single features. This led to a comparison between well-watered leaves and droughted ones, aiming at identifying those features that were not sampled from the same statistical distribution. In other words, this test allowed the evaluation of features that were likely to be used to discriminate between WW and DD leaves.

As no assumptions were made on the distribution for WW and DD leaves, two non-parametric distributions were anticipated. A comparison was performed using the median, mean, standard deviation, range, and interquartile range of each distribution (Figures 5, 7). Median (Figure 5A), mean (Figure 5B), and standard deviation (Figure 5C) were statistically compared for the two distributions, and they all showed an extremely low p-value, below the standard threshold $\alpha = 0.05$. As a consequence, the null hypothesis stating that data come from the same distribution could be rejected for these variables. When the data range and the interquartile range (IQR) were statistically compared (Figures 5A, B), the p-value was not lower than the standard threshold α, with $p = 0.00764$ and $p = 0.0753$, respectively. Hence, in this case, the null hypothesis could not be rejected, and we could not conclude that these quantities were drawn from different data distributions. From this statistical evaluation, we can assume that features related to the median, mean, and standard deviation of the values for the thermal features of the leaves can be effectively used to distinguish between WW and DD leaves. However, the range of the features and the interquartile range cannot be confidently considered during the evaluation since it cannot be concluded whether they are drawn from different distributions.

Machine learning algorithms

A complete comparison between two different processing software pipelines was performed. Specifically, two different classifiers were trained to predict the plant treatment (DD or WW), that is, random forest (RF) and multilayer perceptron (MLP). The dataset used for the ML algorithms training, test, and validation was composed of 419 samples, 212 of them for WW leaves and 207 for DD leaves. Each sample is obtained by joining the automatically computed thermal features with the respective plant treatment (DD or WW), removing all the non-discriminating features from the dataset. The dataset subset split strategy was as follows: 75% of the samples (314) to compute the T subset (for the training and test) and 25% of the samples (105) to compute the V subset (for the validation). Each one of the ML algorithms was inserted in a pipeline, which first scaled each feature to match a normal distribution $N(0, 1)$, namely, a distribution with zero-average and unitary standard deviation. A feature selection procedure was then performed using the mutual information criterion. Finally, the T subset was used to train and test the classifier using a random search for hyperparameter optimization and a K-fold cross-validation with $k = 10$. A summary of the results for optimization is shown in Table 1 for both the RF and MLP pipelines.

The resulting classification report (computed on the V subset) for the RF classifier showed weighted average values for precision and recall of 78% and 71%, respectively (Table 2). Overall, the weighted accuracy on a total support of 105 leaves across all genotypes was approximately 75%, meaning that the classifier was incorrect in predicting 25% of the original images during validation. Comparing the true labels of the leaves against the predicted labels using the RF classifier, 40 WW and 38 DD leaves across all genotypes were correctly predicted, while a total of 27 leaves were miscategorized (Figure 8A).

The MLP classifier showed slight overall improvements: the classifier achieved improved recall on DD leaves and precision on WW leaves, at the cost of lower values of precision and recall for DD and WW leaves, respectively (Table 3). However, there was an improvement in terms of the overall accuracy, increasing to 78%. It is important to highlight that for this second classifier, the data support was changed, although not significantly, due to the random generation process for the validation dataset used to ensure the generalization properties of the classifier. The higher overall

10.3389/fpls.2023.1305292

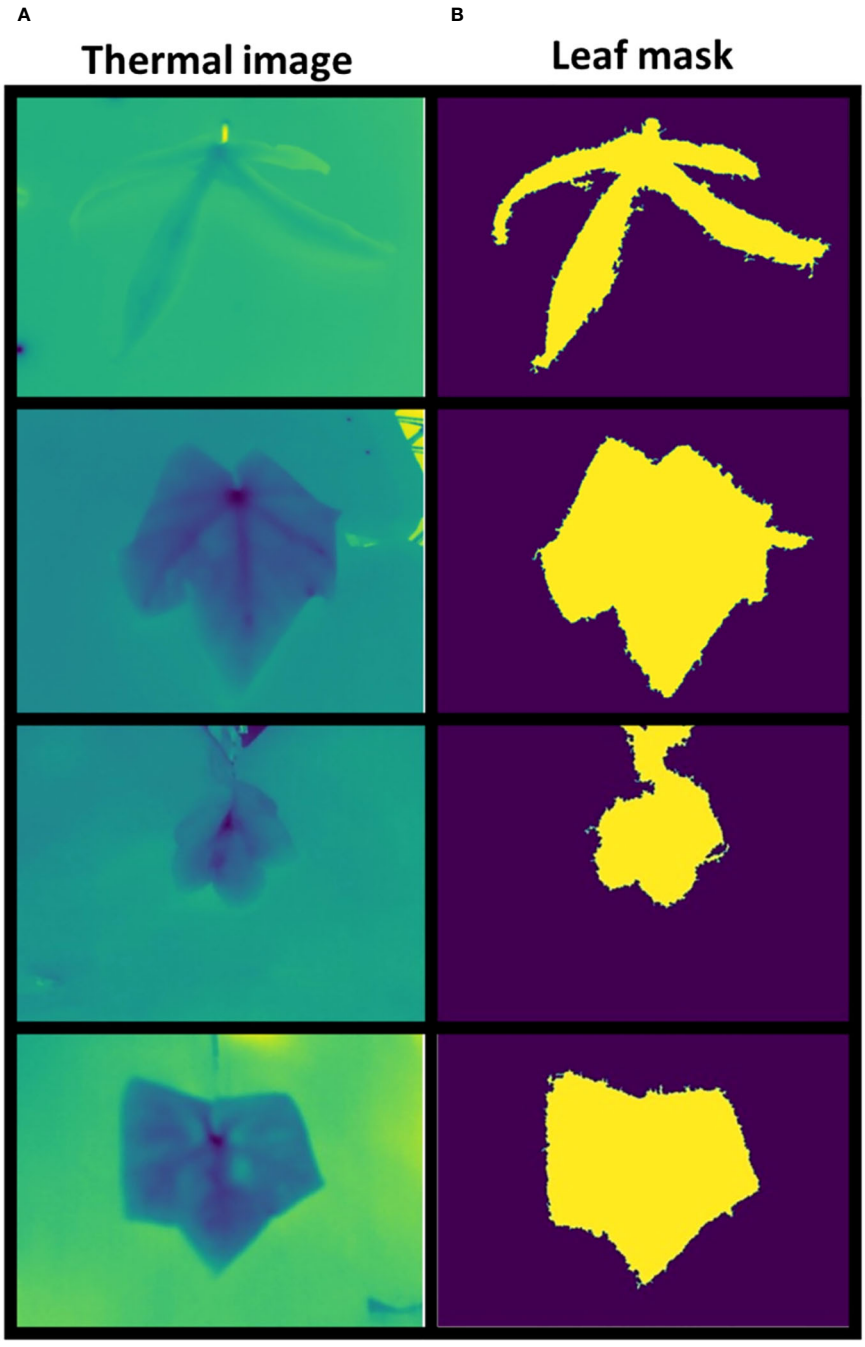

FIGURE 6
Leaf mask comparison. Examples of thermal images **(A)** and correspondent computed masks **(B)**.

accuracy of the MLP approach was reflected in the confusion matrix showing that the correct predictions across all 27 genotypes increased for both treatments (Figure 8B). Specifically, the MLP correctly categorized a total of 82 leaves between WW (37) and DD (45), compared with the 78 total of the RF classifier.

Both the RF and MLP classifiers resulted in an accuracy greater than 70%, considering support data (105 leaves) pooled from 27 different genotypes for both WW and DD treatments, in mild and severe drought, corresponding to 4 and 14 days after the beginning of the progressive water withholding (Figure 2).

Testing the physiological soundness of the AI analysis

Since the presented ML pipelines were built using the data from the entire panel of *Gossypium* under different degrees of water limitation, the accuracy results of the classifications can be considered in line with previous results (Solimani et al., 2023). The great genotypic diversity of the experimental cotton panel inevitably caused extreme variability in leaf size, plant and leaf architecture, and coloration (Figure 1). These diverse genotypes

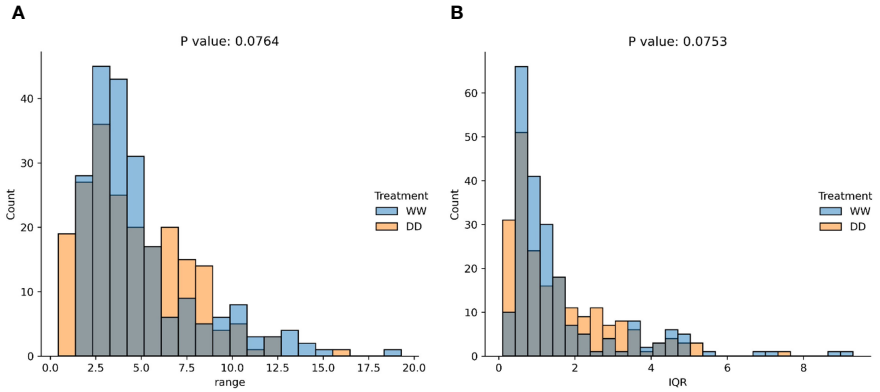

FIGURE 7
Statistical comparisons of data distributions (non-significant). Statistical comparison using the KS test of the data range **(A)** and interquartile range (IQR) **(B)** computed over the distributions of WW and DD leaves.

TABLE 1 Hyperparameters selected for random forest and multilayer perceptron processing software pipelines.

Processing pipeline	Hyperparameter	Value	Description
RF pipeline (feature selection + random forest)	K	3	Number of the most relevant features selected according to the mutual information criterion
	Minimum samples per leaf	5	Minimum number of samples to determine whether a node of each tree in the decision forest can be marked as a terminal one (i.e., a leaf)
	Max depth	5	Maximum depth of each tree in the decision forest
MLP pipeline (feature selection + multilayer perceptron)	K	7	Number of the most relevant features selected according to the mutual information criterion
	Solver	ADAM	Optimization algorithm used during backpropagation
	Learning rate	Constant	Learning rate schedule used during backpropagation. In this case, constant means that no adaptive scheduling is used.
	Hidden layer sizes	50	Number of neurons used in the hidden layer of the multilayer perceptron

TABLE 2 Classification report for the random forest.

Class	Precision	Recall	F1 score	Weighted accuracy	Support
DD	0.78	0.71	0.74	0.75	51
WW	0.71	0.78	0.74	0.74	54

have already been reported to be indeed affected by their physiology resulting in a large spectrum of water status and drought response (Wendel et al., 2009; Wendel et al., 2010; Sreedasyam and Schmutz, 2019). This variability was clearly visible in the range of leaf temperatures captured already in WW conditions (Figure 3). For instance, the Delta Pine16 genotype showed a leaf temperature mean almost 5°C lower than *Tipo Chaco* in the same WW conditions, while two morphologically dissimilar genotypes, namely, *Dwarf Red Harrison* and *Siokara L23*—one with dark red/green, medium-size leaves and one with green, okra-like type of leaves—showed very similar leaf temperatures. It is known that leaf temperature is affected by changes in the microclimate at the canopy level and this can be somewhat variable in greenhouse conditions based on the spatial locations of the pots and on the time of the day (Beverly et al., 2020). However, drawing significant relationships between leaf temperature per se and genotypic variation was not the scope of the current work, and the diverse experimental panel was used as a robust testbed for the development of the novel IP/ML software pipeline for thermal data.

To understand the misclassifications from the ML classifiers, we more closely analyzed the environmental and the volumetric soil water content associated with each image (Supplementary Table S3). First, we confirmed that the applied drought treatments caused a reduction of volumetric soil water content (%) for the DD plants compared with the WW, and this reduction was more evident under severe drought (Figure S4). As expected, the 27 genotypes responded differently to the progressive drought, with the most water-efficient genotypes like *Cup Leaf*, *L23*, and

10.3389/fpls.2023.1305292

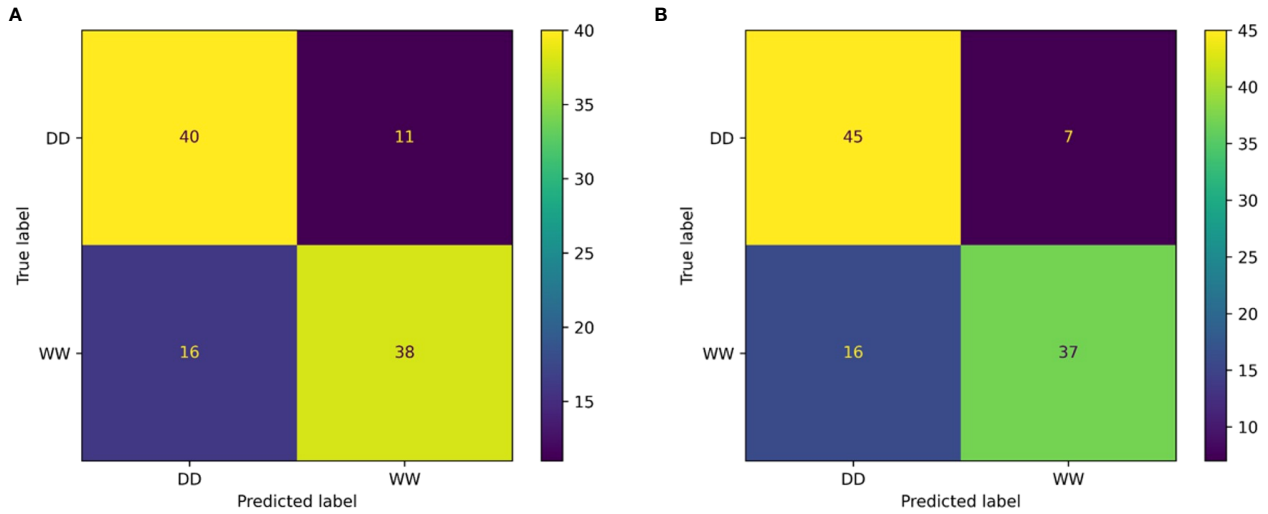

FIGURE 8
Confusion matrix outcomes. Confusion matrix for the random forest **(A)** and the multilayer perceptron **(B)** classifiers.

TABLE 3 Classification report for the multilayer perceptron.

Class	Precision	Recall	F1 score	Weighted accuracy	Support
DD	0.74	0.87	0.80	0.79	52
WW	0.84	0.70	0.76	0.78	53

Lorinator, maintaining their leaf water potential closer to the WW value even under drought conditions (Figure 9). When comparing soil moisture and the efficiency of PSII from chlorophyll *a* fluorescence values for a random subset from all classified images, we found that the leaves wrongly classified by the ML pipeline also showed an outlier behavior in either one or both traits under both mild and severe drought conditions (Figure 10, Figure S4). For instance, under mild drought, the mislabeled genotypes (*TM1*, *Lorinator*, and *Durango*) were the ones that did not significantly decrease their soil moisture although they were sitting in the DD cohort of the panel, most likely due to microclimate variations in the greenhouse. The same validation with soil moisture was revealed for mislabeled plants under severe drought as well, and it similarly applied for plants sitting in the WW cohort, such as *Tipo Chaco* that for the true label of WW resulted in a predicted label of DD for the image pipeline (Figure 8B). While soil moisture seems to

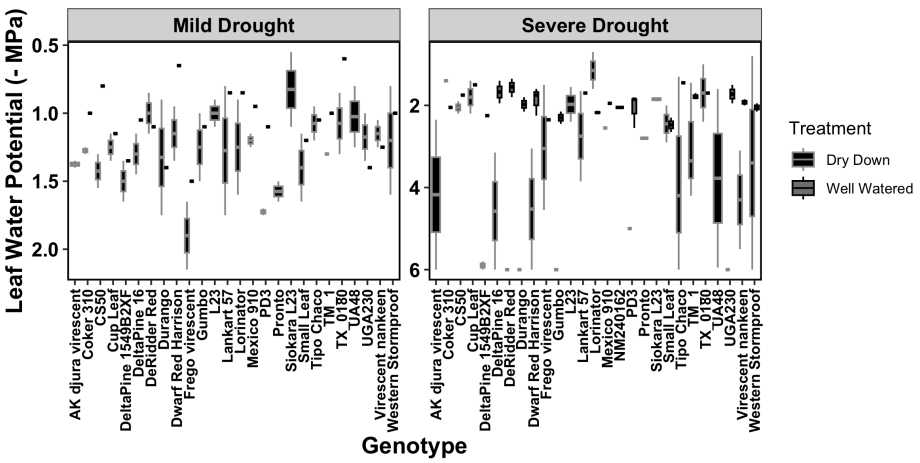

FIGURE 9
Leaf water potential across the 27 experimental genotypes. The distribution of leaf water potentials is observed across genotypes in both mild and severe drought. The well-watered plants (WW) are represented in gray and the plants under dry-down (DD) in black.

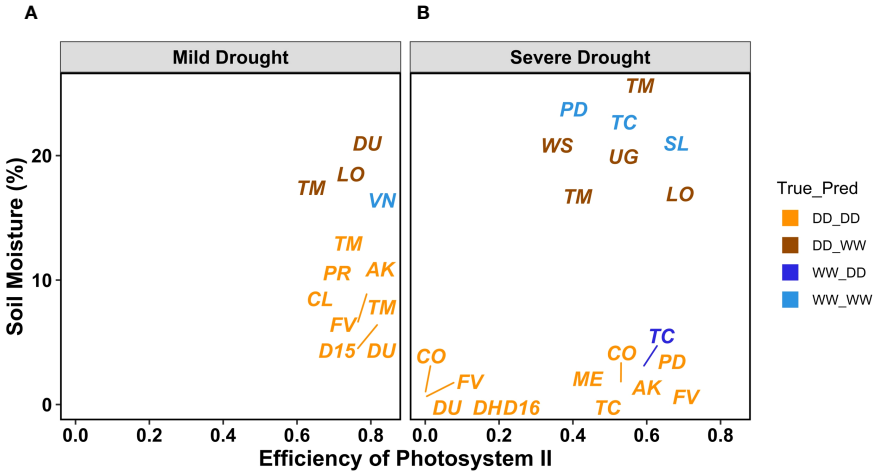

FIGURE 10
PSII efficiency and soil moisture as volumetric soil water content values for MLP outcomes. Labels refer to the true label compared with the MLP classification DD_DD (orange), DD_WW (brown), WW_DD (blue), and WW_WW (electric blue). A randomly chosen subset of leaves with the corresponding PSII efficiency and soil moisture from all genotypes and for both mild **(A)** and severe drought **(B)**.

be sufficiently explanatory for the mislabeled leaves, the efficiency of PSII seems to be less correlated to the ML outcomes. While the randomly chosen DD leaves in severe drought showed high PSII efficiency, such as expected from their still relatively high soil moisture, the mislabeled *Tipo Chaco* sitting in the WW cohort was misclassified as DD by the ML pipelines even if it maintained a PSII efficiency of 0.55 (Figure 10B). Chlorophyll *a* fluorescence as the efficiency of PSII has previously been shown to follow drought response dynamics across different species (Guadagno et al., 2017), and this mismatch between soil moisture value and fluorescence might be due to a particular resistance of the photosynthetic machinery of this specific genotype to severe drought, which is not the focus of the presented work. This analysis of the software pipeline outcomes indicated soil moisture as a highly possible driver of the misclassification and the efficiency of PSII evidently being a less but still correlated physiological trait. From the physiological ground truthing, thermal imaging and the classifiers had lower than 25% and 22% mislabeled leaves (Supplementary Table S3) considering that the actual label was not meaningful of the actual treatment and/or physiological status of the plant.

Conclusions

Our work confirmed the efficiency of thermal imaging data in detecting water limitations and the invaluable assistance of AI analysis in increasing the throughput of handheld IR cameras (Kamarudin and Ismail, 2022). Our results are suggestive of increased efficiency in the postprocessing of thermal data time even when extreme genotypic variation is present. In the utilized experimental panel, the spectrum of thermal features for different genotypes was in fact extremely variable even for WW samples. The presented classification becomes more meaningful considering that the support data for the ML application were coming from leaves exposed to two different levels of water limitation—aside from the WW control—triggering a large variety of physiological interplays across the 27 genotypes. Our leaf-level experimental approach coupled other physiological measurements to the thermal imaging, allowed us for further testing of the ML results. We found that mislabeled leaves also had a significantly different behavior in other means of plant water status such as soil water potential and content to partly account model errors. Overall, our study confirms that AI can be an incredible resource to optimize the throughput of handheld thermal cameras despite genotypic variation, extreme morphological and temperature features, and over a large combination of G × E, allowing for more generalized applications in water management across different geographical agricultural scenarios. In the future, we auspicate for the development of more targeted designs aimed to dissect the temporal progression of water limitation across different genotypes and its correlation with peculiar leaf venation types and architectures. Higher accuracy in thermal image classification will allow for the development of more complex ML pipelines, representing an essential aid in breeding and water management efforts,especially for globally relevant crop species like cotton.

Data availability statement

The original contributions presented in the study are included in the article/Supplementary Material. Further inquiries can be directed to the corresponding author.

Author contributions

VR: Conceptualization, Formal analysis, Methodology, Software, Visualization, Writing – original draft, Writing – review & editing, Investigation. AC: Formal analysis, Methodology, Software, Visualization, Writing – original draft, Investigation.

BR: Data curation, Formal analysis, Investigation, Methodology, Visualization, Writing – original draft. CG: Conceptualization, Funding acquisition, Methodology, Project administration, Resources, Supervision, Validation, Visualization, Writing – original draft, Writing – review & editing.

Funding

The author(s) declare financial support was received for the research, authorship, and/or publication of this article. This research was supported by the National Science Foundation (NSF Research PGR#2102120) and by the NIFA AG2PI Collaborative (Award # 2021-70412-35233 Department of Agriculture (USDA).

Acknowledgments

We are grateful to the laboratory assistants at the University of Wyoming, Jade Whiting, Isaiah Spiegelberg, Sarah Doyle, and Reese Milburn for their significant contribution to the experiment, from plant care to the leaf-level data collection, data entry, and thermal image preprocessing.

Conflict of interest

The authors declare that the research was conducted in the absence of any commercial or financial relationships that could be construed as a potential conflict of interest.

Publisher's note

Supplementary material

The Supplementary Material for this article can be found online at: https://www.frontiersin.org/articles/10.3389/fpls.2023.1305292/full#supplementary-material

SUPPLEMENTARY FIGURE S1
The processing image pipeline. Building blocks of the developed pipeline used in this work includes four computational steps: CSV parsing, pre-process, leaf mask computing, and thermal stats computing.

SUPPLEMENTARY FIGURE S2
Genotypes included in the experimental panel. All 27 genotypes included in the cotton experimental panel and their correspondent abbreviations used in during the experiment.

SUPPLEMENTARY TABLE S3
Single measurements of volumetric soil water content across all collected images.

SUPPLEMENTARY FIGURE S4
Volumetric soil water content across the 27 experimental genotypes. Distribution of leaf water potentials are observed across genotypes in both mild and severe drought. The well-watered plants (WW) are represented in grey and the plants under dry down (DD) in black.

References

Batchuluun, G., Nam, S. H., and Park, K. R. (2022). Deep learning-based plant classification and crop disease classification by thermal camera. *J. King Saud Univ. - Comput. Inf. Sci.* 34 (10, Part B), 10474–10486. doi: 10.1016/j.jksuci.2022.11.003

Berni, J. A. J., Zarco-Tejada, P. J., Sepulcre-Cant´o, G., Fereres, E., and Villalobos, F. (2009). Mapping canopy conductance and CWSI in olive orchards using high resolution thermal remote sensing imagery. *Remote Sens. Environ.* 113 (11), 2380–2388.

Beverly, D. P., Guadagno, C. R., and Ewers, B. E. (2020). Biophysically informed imaging acquisition of plant water status. *Front. Forests Global Change* 3. doi: 10.3389/ffgc.2020.589493

Bhandari, M., Xue, Q., Liu, S., Stewart, B. A., Rudd, J. C., Pokhrel, P., et al. (2021). Thermal imaging to evaluate wheat genotypes under dryland conditions. *Agrosystems Geosciences Environ.* 4 (2), e20152. doi: 10.1002/agg2.20152

Buitrago, M. F., Groen, T. A., Hecker, C. A., and Skidmore, A. K. (2016). Changes in thermal infrared spectra of plants caused by temperature and water stress. *ISPRS J. Photogrammetry Remote Sens.* 111, 22–31. doi: 10.1016/j.isprsjprs.2015.11.003

Casari, R. A. C. N., Paiva, D. S., Silva, V. N. B., Ferreira, T. M. M., Souza Junior, M. T., Oliveira, N. G., et al. (2019). Using thermography to confirm genotypic variation for drought response in maize. *Int. J. Mol. Sci.* 20 (9), 2273. doi: 10.3390/ijms20092273

Cho, Y., Bianchi-Berthouze, N., Marquardt, N., and Julier, S. J. (2018). "Deep thermal imaging: proximate material type recognition in the wild through deep learning of spatial surface temperature patterns," in *Proceedings of the 2018 CHI conference on human factors in computing systems*. 1–13, ACM.

Cohen, Y., Alchanatis, V., Meron, M., Saranga, Y., and Tsipris, J. (2005). Estimation of leaf water potential by thermal imagery and spatial analysis*. *J. Exp. Bot.* 56 (417), 1843–1852. doi: 10.1093/jxb/eri174

Ferguson, J. N., Fernandes, S. B., Monier, B., Miller, N. D., Allen, D., Dmitrieva, A., et al. (2021). Machine learning-enabled phenotyping for GWAS and TWAS of WUE traits in 869 field-grown sorghum accessions. *Plant Physiol.* 187 (3), 1481–1500. doi: 10.1093/plphys/kiab346

Guadagno, C. R., Ewers, B. E., Speckman, H. N., Aston, T. L., Huhn, B. J., DeVore, S., et al. (2017). Dead or alive? Using membrane failure and chlorophyll a fluorescence to predict plant mortality from drought. *Plant Physiol.* 175 (1), 223–234. doi: 10.1104/pp.16.00581

Gutiérrez, S., Diago, M. P., Fernández-Novales, J., and Tardaguila, J. (2018). Vineyard water status assessment using on-the-go thermal imaging and machine learning. *PLoS One* 13 (2), e0192037.

IPCC (2022). *Climate change 2022: impacts, adaptation, and vulnerability. contribution of working group ii to the sixth assessment report of the intergovernmental panel on climate change*. Eds. H.-O. Pörtner, D. C. Roberts, M. Tignor, E. S. Poloczanska, K. Mintenbeck, A. Alegría, et al. (Cambridge, UK and New York, NY, USA: Cambridge University Press), 3056. doi: 10.1017/9781009325844

Kamarudin, M. H., and Ismail, Z. H. (2022). IOP conf. Ser. *Earth Environ. Sci.* 1091, 01204.

Khan, M. A., Wahid, A., Ahmad, M., Tahir, M. T., Ahmed, M., Ahmad, S., et al. (2020). "World cotton production and consumption: an overview," in *Cotton Production and Uses: Agronomy, Crop Protection, and Postharvest Technologies*. Eds. S. Ahmad and M. Hasanuzzaman (Singapore: Springer), 1–7. doi: 10.1007/978-981-15-1472-2_1

Kohin, M., and Butler, N. R. (2004). Performance limits of uncooled VOx microbolometer focal plane arrays. *Infrared Technol. Appl. XXX* 5406, 447–453. doi: 10.1117/12.542482

Li, N., Yao, N., Li, Y., Chen, J., Liu, D., Biswas, A., et al. (2021). A meta- analysis of the possible impact of climate change on global cotton yield based on crop simulation approaches. *Agric. Syst.* 193, 103221. doi: 10.1016/j.agsy.2021.103221

Meyer, L., Dew, T., Grace, M., Lanclos, K., MacDonald, S., and Soley, G. *The world and united states cotton outlook*. Available at: https://www.usda.gov/sites/default/files/documents/2023AOF-cotton-outlook.pdf

Mohanty, S. P., Hughes, D. P., and Salathé, M. (2016). Using deep learning for image-based plant disease detection. *Front. Plant Sci.* 7, 1419. doi: 10.3389/fpls.2016.01419

Murchie, E., and Lawson, T. (2013). Chlorophyll fluorescence analysis: a guide to good practice and understanding some new applications. *J. Exp. Bot.* 64, 3983–3998. doi: 10.1093/jxb/ert208

Pedregosa, F., Varoquaux, G., Gramfort, A., Michel, V., Thirion, B., Grisel, O., et al. (2011). Scikit-learn: machine learning in python. *J. Mach. Learn. Res.* 12, 2825–2830.

Pignon, C. P., Fernandes, S. B., Valluru, R., Bandillo, N., Lozano, R., Buckler, E., et al. (2021). Phenotyping stomatal closure by thermal imaging for GWAS and TWAS of water use efficiency-related genes. *Plant Physiol.* 187 (4), 2544–2562. doi: 10.1093/plphys/kiab395

Pineda, M., Barón, M., and Pérez-Bueno, M.-L. (2021). Thermal imaging for plant stress detection and phenotyping. *Remote Sens.* 13 (1), 68. doi: 10.3390/rs13010068

Prakash, P. T., Banan, D., Paul, R. E., Feldman, M. J., Xie, D., Freyfogle, L., et al. (2021). Correlation and co-localization of QTL for stomatal density, canopy temperature, and productivity with and without drought stress in Setaria. *J. Exp. Bot.* 72 (13), 5024–5037. doi: 10.1093/jxb/erab166

Pratap, A., Gupta, S., Nair, R. M., Gupta, SK., Schafleitner, R., Basu, P. S., et al. (2019). Using plant phenomics to exploit the gains ofgenomics. *Agronomy* 9 (3), 126. doi: 10.3390/agronomy9030126

R Core Team. (2013). *R: A language and environment for statistical computing*.

Sakurai, K., Toda, Y., Hamazaki, K., Ohmori, Y., Yamasaki, Y., Takahashi, H., et al. (2023). Random regression for modeling soybean plant response to irrigation changes using time-series multispectral data. *Front. Plant Sci.* 14. doi: 10.3389/fpls.2023.1201806

Slowikowski, K. (2023). *ggrepel: Automatically Position Non-Overlapping Text Labels with 'ggplot2'. R package version 0.9.3*.

Solimani, F., Cardellicchio, A., Nitti, M., Lako, A., Dimauro, G., and Renò, V. (2023). A systematic review of effective hardware and software factors affecting high-throughput plant phenotyping. *Information* 14 (4), 214.

Sreedasyam, A., and Schmutz, J. (2019). "Dynamic transcriptional landscape of polyploid plants," in *Plant and Animal Genome*(San Deigo, CA).

Stutsel, B., Johansen, K., Malbéteau, Y. M., and McCabe, M. F. (2021). Detecting plant stress using thermal and optical imagery from an unoccupied aerial vehicle. *Front. Plant Sci.* 12. doi: 10.3389/fpls.2021.734944

Townsend, T. (2020). "1B - World natural fibre production and employment," in *Handbook of Natural Fibres*, *2nd ed*. Eds. R. M. Kozłowski and M. Mackiewicz-Talarczyk (Delhi: Woodhand publishing) 15–36. doi: 10.1016/B978-0-12-818398-4.00002-5

Van der Walt, S., Schönberger, J. L., Nunez-Iglesias, J., Boulogne, F., Warner, J. D., Yager, N., et al. (2014). scikit-image: image processing in Python. *PeerJ* 2, e453.

Wegier, A., Alavez, V., and Piñero, D. (2016). "Cotton: traditional and modern uses," in *Ethnobotany of Mexico: Interactions of People and Plants in Mesoamerica*. Eds. R. Lira, A. Casas and J. Blancas (New York: Springer), 439–456. doi: 10.1007/978-1-4614-6669-7_18

Wendel, J. F., Brubaker, C., Alvares, I., Cronn, R., and Stewart, J. M. (2009). "Evolution and natural history of the cotton genus," in *Genetics and Genomics of Cotton*. Ed. A. H. Paterson (New York, NY: Springer US (Plant Genetics and Genomics: Crops and Models), 3–22. doi: 10.1007/978-0-387-70810-2_1

Wendel, J. F., Brubaker, C. L., and Seelanan, T. (2010). "The origin and evolution of gossypium," in *Physiology of Cotton*. Ed. J. Stewart, et al (Dordrecht: Springer Netherlands), 1–18. doi: 10.1007/978-90-481-3195-2_1

Wickham, H. (2016). *ggplot2: Elegant Graphics for Data Analysis* (New York: Springer-Verlag).

Wickham, H., Averick, M., Bryan, J., Chang, W., McGowan, L. D., François, R., et al. (2019). Welcome to the tidyverse. *J. Open Source Software* 4, 1686. doi: 10.21105/joss.01686

Wickham, H., Francois, R., Henry, L., Müller, K., and Vaughan, D. (2023). *dplyr: A Grammar of Data Manipulation. R package version 1.1.2*. Available at: https://cran.r-project.org/web/packages/ggrepel/ggrepel.pdf

Zhao, C., Zhang, Y., Du, J., Guo, X., Wen, W., Gu, S., et al. (2019). Crop phenomics: Current status and perspectives. *Front. Plant Sci.* 10, 714.

Zhao, L., Wang, L., Li, J., Bai, G., Shi, Y., and Ge, Y. (2021). "Toward accurate estimating of crop leaf stomatal conductance combining thermal IR imaging, weather variables, and machine learning," in *Autonomous air and ground sensing systems for agricultural optimization and phenotyping VI*, vol. 11747, 98–105. Available at: https://plantstomata.wordpress.com/2021/11/29/estimating-of-crop-leaf-stomatal-conductance-combining-thermal-ir-imaging-weather-variables-and-machine-learning/

Frontiers in
Plant Science

Cultivates the science of plant biology and its applications

The most cited plant science journal, which advances our understanding of plant biology for sustainable food security, functional ecosystems and human health.

Discover the latest Research Topics

See more →

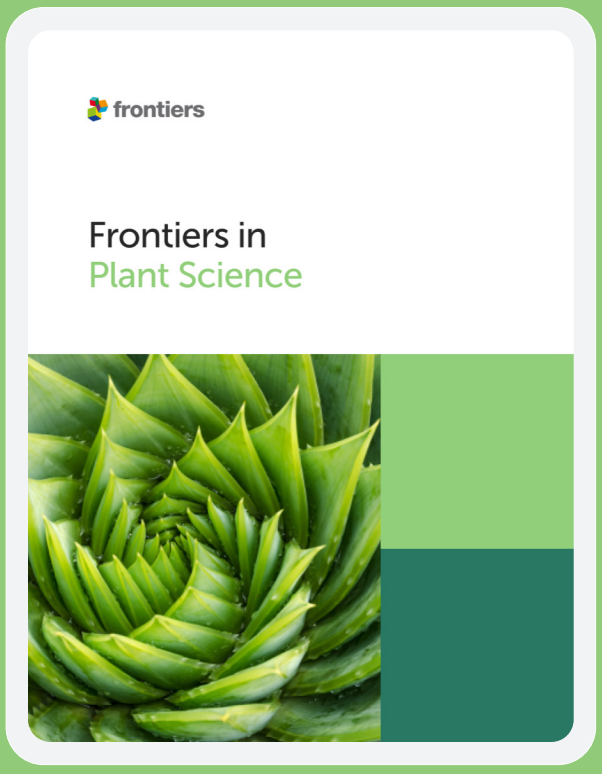

Frontiers

Avenue du Tribunal-Fédéral 34
1005 Lausanne, Switzerland
frontiersin.org

Contact us

+41 (0)21 510 17 00
frontiersin.org/about/contact